UNIVERSITY OF ICELAND

Ph.D. Thesis

in CHEMISTRY

Building Smart Materials by Tuning the Self-assembly Modes in Supramolecular Gels

Sreejith Sudhakaran Jayabhavan

February 2025

FACULTY OF PHYSICAL SCIENCES

Building Smart Materials by Tuning the Self-assembly Modes in Supramolecular Gels

Sreejith Sudhakaran Jayabhavan

Dissertation submitted in partial fulfillment of a
Philosophiae Doctor degree in Chemistry

Advisor
Prof. Krishna Kumar Damodaran

Ph.D. Committee
Prof. Guðmundur Gunnar Haraldsson
Prof. Már Másson

Opponents
Dr. Gareth O. Lloyd
Dr. Stefán Jónsson

Faculty of Physical Sciences
School of Engineering and Natural Sciences
University of Iceland
Reykjavik, Feb 2025

Building Smart Materials by Tuning the Self-assembly Modes in Supramolecular Gels

Dissertation submitted in partial fulfillment of a *Ph.D* degree in Chemistry

Faculty of Physical Sciences
School of Engineering and Natural Sciences
University of Iceland
Dunhagi 3
107 Reykjavik
Iceland

Telephone: 525 4000

Bibliographic information:
Sreejith Sudhakaran Jayabhavan, 2024, *Building Smart Materials by Tuning the Self-assembly Modes in Supramolecular Gels*, PhD dissertation, Faculty of Physical Sciences, University of Iceland, 429 pp.

Author ORCID: 0000-0002-1557-1354
ISBN: 978-9935-9826-2-9

Abstract

The astounding capacity of nature to self-assemble is a fundamental principle that is seen at many different scales, ranging from micro to macromolecular structures. The study of self-assembly continues to be a vibrant area of research, but understanding self-assembly in nature is a challenging task because of its dynamic nature. Therefore, studying the role of such interactions provides valuable insights into designing smart materials. This doctoral work aimed to study the role of various non-bonding interactions and the spatial arrangement of the functional groups in dictating the self-assembly modes in individual and multi-component low molecular weight gels (LMWGs). The primary focus was on LMWGs with functionalities such as amide, urea, thiourea, and carbamate moieties with extended hydrogen bonding capability, which could result in gel fibrils with intriguing properties. Furthermore, antibacterial agents and drug-mimicking moieties were incorporated in addition to the above functionalities, and the applications of LMWGs in sensing, antibacterial studies, and gel phase crystallization were investigated. LMWGs were designed and synthesized, and the structure-property correlation was studied using rheology, scanning electron microscopy, circular dichroism, FT-IR, UV-visible spectroscopy, and X-ray diffraction techniques. The gelation properties in the presence of metal salts were investigated, which showed that the presence of metal salts leads to the making/breaking of gels. The interactions of polymorphic drugs in gels with drug-mimicking and non-mimicking functionalities were examined to evaluate the specific role of functionalities in the crystal growth of active pharmaceutical ingredients (APIs). The self-assembly in the multi-component gels based on chiral or enantiomeric compounds was studied in detail and the specific co-assembly modes in mixed enantiomeric gels was confirmed by various analytical techniques. In general, the doctoral thesis aimed at understanding the crucial role of particular functionalities or substituents in tuning the gelation properties in individual and enantiomeric multi-component systems. This doctoral thesis gives a detailed outlook towards tuning the self-assembly in both individual and multi-component gels via various internal and external factors, which will help us to predict the mechanism of supramolecular gel formation and design LMWGs with tunable properties.

Útdráttur

Náttúran sýnir í eðli sínu ótrúlega hæfileika til að raða, setja eða hvarfa sjálfkrafa saman grunneiningar til að mynda smásameindir, fjölliður svo og risasameindir. Rannsóknir og þekking á náttúrulegum ferlum í sjálfkrafa hvörfum grunneininga til fjölliðumyndunar er krefjandi og heillandi viðfangsefni, sér í lagi þar sem lífheimurinn hannar og býr til „snjallefni“ á einfaldan hátt. Í þessu rannsóknaverkefni til doktorsprófs voru rannsökuð gel efnasambönd með lága sameindamassa (LMWG). Hlutverk ýmissa ótengdra þátta og víxlverkana milli virkra efnahópa voru rannsakaðir með það markmið að ákvarða hvaða þættir stjórna sjálfkrafa byggingu sameindanna í gelunum. Valin voru fjölþátta kerfi með tveimur virkum hópum og aðallega litið til virkni eftirfarandi hópa: amíð, þvagefni, thíoþvagefni og karbamat vegna eiginleika virku hópanna og hæfileika til að mynda vetnistengi í trefjakenndum gelum. Áhrif efna eins og salta/jóna, bakteríudrepandi efna og lífrænna lyfjaefna voru einnig rannsökuð með tilliti til bakteríudrepandi virkni, gelmyndunar, og breytinga á kristöllun trefjanna í gelforminu. Mismunandi LMWG gel voru hönnuð og smíðuð og uppbygging eða byggingaeiginleikar þessara gela rannsökuð og greind með togþolsmælingum, seigju, og styrkleika gelsins, rafeindasmásjá, ljósbrotseiginleikum, FT-IR, litrófsmælingum á útfjólubláa og sýnilega sviðinu og röntgen kristal greiningu. Áhrif málmsalta á gelin voru rannsökuð, bæði við myndun þeirra og niðurbrot. Víxlverkun lífvirkra efna og efna er líkja eftir lyfjavirkum sameindum var rannsökuð til að öðlast skilning á hlutverki virku hópanna við kristöllun lyfvirkra efna (API). Hlutverk og áhrif handhverfuhreinna efna við sjálfvirka byggingu fjölþátta kerfa við gelmyndun var rannsökuð og greind. Sértæk samsetning í blöndum af handhverfu gelunum var staðfest með ýmsum greiningaraðferðum svo og afgerandi hlutverk tiltekinna virkra hópa til að stýra byggingareiginleikum þessara gela. Rannsóknaverkefnið svaraði ýmsum spurningum varðandi gelmyndun og getur leitt til betri og skilvirkari aðferðafræði við hönnun og myndun LMWG með fyrirsjáanlega eiginleika.

Dedication

The thesis is dedicated to my mother and all the wonderful teachers I have come across who inspired me with a passion towards chemistry.

Preface

The term supramolecular chemistry was first coined by Jean-Marie Lehn in the 1970s, who is also known as the father of supramolecular chemistry. Supramolecular chemistry can be defined as the interactions between small molecules to self-assemble into molecular assemblies. However, predicting the nature of the self-assembly is a challenging task due to the dynamic nature of the non-covalent interactions such as hydrogen bonding, π—π stacking, electrostatic attraction, van der Waals force, hydrophilic/hydrophobic interaction, and coordination bonding. The supramolecular gels establish a solid-like nanoscale network that encompasses a liquid-like continuous phase, converting the molecular-scale information into material performance. Understanding the molecular self-assembly of supramolecular gels helps us to design LMWGs with tunable properties. We can study the role of specific interactions in gel formation by varying the functionalities/substituents of the LMWGs that play a major role in gelation.

In this doctoral work, we primarily focused on evaluating the role of the position and spatial orientation of the functional groups in dictating the self-assembly modes in LMWGs. We have mainly divided the project into four sections: (a) to analyze the role of functionality in individual gels, (b) to study the spatial arrangement and position of the functional groups, (c) to analyze the role of functionality in the self-assembly of multi-component gels, and (d) to analyze the role of functionalities or linker core on the self-assembly of multi-component gels based on enantiomers. This thesis comprises published articles and manuscripts either in the final stage or prepared for submission to a peer-reviewed publication. The article's references are cited directly inside the publications, complying with the journal's citation style.

In the first part, we studied self-assembly in single-component-based gels by analyzing the role of specific functionality. We have designed and synthesized bis(pyridyl-*N*-oxide urea) and mono-/bis-pyridyl-*N*-oxide amides. The modification of parent pyridyl urea compounds to pyridyl-*N*-oxide compounds induced hydrogelation, and similar results were also obtained upon modifying the parent bis(pyridyl)amides to their corresponding mono-/bis-pyridyl-*N*-oxide amides. X-ray diffraction analysis provided valuable insights into the solid-state interactions and non-bonding interactions of the *N*-oxide based gelators. We have studied the sensing ability of these parent and modified *N*-oxide compounds towards salts/ions. The results showed that the modified compounds (*N*-oxides) displayed enhanced gel strength in the presence of certain salts, and salts induced gelation was observed with concentration below the minimum gelator concentration of the corresponding gelators, but aluminum chloride and transition metal salts disrupted the gel network. We then studied the role of hydrogen bond functionalities in LMWGs by replacing the urea moiety to a thiourea moiety and studied the gelation properties. We further investigated whether the metal salts could induce gelation and the results indicated that selective gelation was observed for bis(pyridyl)thiourea compounds with various copper salts (1:2 metal-to-ligand ratio). The coordination-driven self-assembly was studied using multiple techniques, such as UV-visible spectroscopy and X-ray diffraction.

In the second part, we studied the spatial arrangement and position of the functionality in a series of bis(urea) compounds that mimicked the drug metronidazole and its structural isomer isometronidazole. Compounds formed gel in nitrobenzene and used the gel as a medium for crystallization of polymorphic drug metronidazole, which resulted in market crystal habit modification with the metronidazole mimicking gels, which highlights the specific position of functionality in influencing the crystal habit outcome. The nitroimidazole-based drug metronidazole is known for its antibacterial activity against anaerobic bacteria. We have incorporated carbamate functionality along with pyridyl functional groups and their corresponding *N*-oxide derivatives to synthesize potential ligands active against aerobic bacteria. However, the ligands were inactive, which envisaged us to build complexes of these ligands with transition metal salts such as silver(I) nitrate and cadmium chloride. Antibacterial studies revealed the ability of these complexes to kill both gram-positive and gram-negative bacteria. Interestingly, hydrogelation was observed with only 3-pyridyl-based *N*-oxide moiety, showing the importance of the position of functional groups in dictating gelation properties.

In the third part, we have studied the self-assembly process in chiral multi-component gels based on donor-acceptor pairs. We used computational studies to predict the electronic distribution in individual chiral molecules. We have analyzed the gelation of all the individual chiral compounds, enantiomeric mixed compounds, and mixed chiral compounds based on donor and acceptor moieties. We found that mixed chiral donor-acceptor gels were stronger but had lower thermal stability than other gels. The study highlighted that charge transfer interactions played a significant role in the self-assembly of mixed chiral donor-acceptor gels.

In the last part, we have analyzed the effect of functionality or linkers in the self-assembly of multi-component gels based on enantiomers. We have divided this part into three sections. Initially, we examined the role of the flexibility of the gelator core on the self-assembly modes of multi-component gels based on enantiomeric compounds of biphenyl bis(amides). We then focused on examining how functional side groups influence the gelation properties of multi-component systems based on enantiomeric compounds of biphenyl bis(amides) of alanine and phenylalanine methyl ester. The anion-sensing ability of these gels was examined and showed that the gels based on alanine functionality collapsed, while gels with a hydrophobic phenyl group did not show any profound effect with the salts. Various characterization techniques, such as X-ray diffraction, rheology, circular dichroism, and anion sensing experiments, were used to understand the self-assembly modes and properties of the multi-component gels. In the next section, we have evaluated the nature and effect of the linker functionality on the self-assembly modes in enantiomeric multi-component gels. The mixed enantiomeric gels based on the linker with flexible groups (methylene group) formed weaker gel compared to the individual enantiomeric gels. However, the linkers with methine groups or in the absence of methylene groups showed enhanced gel strength, presumably due to a different self-assembly mode. Therefore, we monitored the self-assembly modes in these multi-component gels and showed that the transformation of self-assembly (orthogonal self-assembly to specific co-assembly) can be achieved in enantiomeric multi-component gels by modifying the linker functionalities. We believe that all these findings could provide valuable information about the self-assembly process in multi-component gels based on enantiomers and will contribute to society towards the design and synthesis of various multi-component-based supramolecular architectures with tunable properties based on specific applications.

Table of Contents

List of Figures

List of Schemes

List of Publications

The thesis is based on the following original publication.

1. Crystal Habit Modification of Metronidazole by Supramolecular Gels with Complementary Functionality, Sreejith Sudhakaran Jayabhavan, J. W. Steed, and Krishna K. Damodaran, *Cryst. Growth Des*. **2021**, *21*, 9, 5383–5393.
2. Making and Breaking of Gels: Stimuli-Responsive Properties of Bis(Pyridyl-*N*-oxide Urea) Gelators, Sreejith Sudhakaran Jayabhavan, Dipankar Ghosh and Krishna K. Damodaran, *Molecules*, **2021**, *26*(21), 6420
3. Stimuli-responsive Properties of Supramolecular Gels based on Pyridyl-*N*-oxide Amides, S. S. Jayabhavan, B. Kristinsson, D. Ghosh, C. Breton and Krishna K. Damodaran, *Gels* **2023**, *9*(2), 89.
4. The Role of Functional Groups in Tuning the Self-Assembly Modes and Physical Properties of Multicomponent Gels, S. S Jayabhavan, G. Kuppadakkath and Krishna K. Damodaran, *ChemPlusChem*, **2023**, e202300302
5. Analysing the self-assembly modes in chiral multi-component gels based on donor and acceptor moieties, S. S. Jayabhavan, H. Myneni, M. Riedel and Krishna K. Damodaran, *Supramol. Chem*. **2024**, 1-13.
6. Flexibility of Linkers: An Important Factor in Tuning the Gelation Properties in Multicomponent Based Gels, S. S. Jayabhavan, and Krishna K. Damodaran (Manuscript ready, preparing for submission).
7. Evaluating the Self-Assembly and Antibacterial Activity of Tailored Supramolecular Gels, S. S. Jayabhavan, Arthi Chandramouli, Jayakumar Rangasamy and Krishna K. Damodaran (Manuscript ready, preparing for submission).
8. Selective Gelation of Bis(Pyridyl)Thiourea by Copper(II) Salts, S. S. Jayabhavan, and Krishna K. Damodaran (Manuscript under final preparation).

Conference and second-author publication

1. An Insight Into the Gelation Properties in Multi-Component Gels, Sreejith Sudhakaran Jayabhavan, Dipankar Ghosh, and Krishna Kumar Damodaran* *The Nordic Rheology Conference*, **2022**, *30*, 91.
2. The Supramolecular Gels Based on C_3-Symmetric Amides: Application in Anion-Sensing and Removal of Dyes from Water, Geethanjali K., S. S. Jayabhavan, and Krishna K. Damodaran, *Molecules*, **2024**, *29*, 9, 2149.

Abbreviations

CD	Circular dichroism
CLSM	Confocal laser scanning microscopy
DMF	N,N'-Dimethylformamide
DMSO	Dimethyl sulfoxide
DVB	Divinyl benzene
EG	Ethylene glycol
EtOH	Ethanol
EtOAc	Ethyl acetate
FT-IR	Fourier-transform infrared
G'	Storage modulus
G''	Loss modulus
GdL	Glucono-δ-lactone
GPC	Gel phase crystallization
HCl	Hydrochloric acid
HT	High tension
HRMAS	High resolution magic angle spinning
LMWG	Low molecular weight gelator
LVR	Linear viscoelastic region
mCPBA	*meta*-Chloroperoxybenzoic acid
MeOH	Methanol
MGC	Minimum gelator concentration
NMR	Nuclear magnetic resonance
OBz	Benzyl ester
OEt	Ethyl ester
OMe	Methyl ester
PG	Polymeric gel
PTA	Phosphotungstic acid
PXRD	Powder X-ray diffraction
SANS	Small-angle neutron scattering
SAXS	Small-angle X-ray scattering
SCXRD	Single crystal X-ray diffraction
SDS	Sodium dodecyl sulphate
SEM	Scanning electron microscopy
SSD	Silver sulfadiazine
TBABr	Tetrabutylammonium bromide
TEM	Transmission electron microscopy
TFA	Trifluoroacetic acid

TGA	Thermogravimetric analysis
THF	Tetrahydrofuran
TLC	Thin layer chromatography
T_{gel}	Sol-gel transition temperature
UV–vis	Ultraviolet–visible
1D	One-dimensional
2D	Two-dimensional
3D	Three-dimensional

Acknowledgements

I would like to express my deepest gratitude to the following individuals and organizations who have contributed to the completion of my PhD thesis:

First and foremost, I would like to thank my supervisor, Prof. Krishna Kumar Damodaran, for the guidance, mentorship, and unwavering support throughout my PhD journey. Your expertise, patience, and encouragement have been invaluable to me, and I am grateful for the opportunity to have worked under your direction.

I would also like to acknowledge the contributions of my thesis committee members, Prof. Guðmundur Gunnar Haraldsson and Prof. Már Másson, for their valuable feedback and insights that have helped shape my research. I also thank my distinguished opponents, Dr. Gareth O. Lloyd and Dr. Stefán Jónsson, for finding time from their busy schedule and willing to review this dissertation and my work. Your input has been instrumental in refining my ideas and improving the quality of my work.

I want to extend my gratitude to all my colleagues and previous and current lab members, Dr Dipankar Ghosh, Mr. Shubham Sharma, Mrs. Geethanjali Kuppadakkath, Mr. Adin Karaman, and Mr. Baldur Kristinsson, for collaboration, and support. Working alongside such a talented and dedicated team has been a pleasure. I appreciate the many late nights and weekends we spent discussing our research and sharing our ideas. I am grateful to Dr. Sigríður Jónsdóttir and Dr. Gunnar Widtefeldt Reginsson for helping with NMR and mass spectroscopy, Svana Hafdís Stefánsdóttir, Sverrir Guðmundsson and Óskar Rudolf Kettler for helping with chemicals and laboratory equipment. I would also like to thank all the academic and technical staff: Dr. Fridrik Magnus from the University of Iceland (for powder X-ray), Birgir Jóhannesson from Tæknisetur (SEM), and the Biochemistry department for the circular dichroism studies.

This work would not have been possible without the help of our national and international collaborators, Dr. Hemanadhan Myneni and Prof. Morris Riedel (Faculty of Industrial Engineering, Mechanical Engineering, and Computer Science, University of Iceland), Prof. Jonathan Steed and Dr. Matthew T. Mulvee (Durham University, U.K), and Prof. Jayakumar Rangasamy (Amrita School of Nanosciences and Molecular Medicine, Kochi) for the research collaboration. I would like to acknowledge the financial support provided by the University of Iceland for the doctoral research grant for my PhD research. I also acknowledge the Teaching Assistantship grant, Rannis Iceland, and Aðalsteinn Kristjánsson Memorial grant. Their funding has enabled me to pursue my research goals and has been instrumental in the completion of my thesis.

I would like to thank my family for their love, encouragement, and sacrifices. Finally, I would like to acknowledge the contributions of the University of Iceland community, including various departments and the University staff, for providing me with the resources, facilities, and opportunities necessary to complete my PhD. Thank you all again for your support, guidance, and encouragement. I hope that my research will make a positive impact and contribute to the advancement of knowledge in this area.

1 Introduction

Self-assembly is an intriguing process in which individual components naturally converge into an organized structure.[1] Self-assembly process has numerous opportunities for generating materials with intriguing properties, and the structures may undergo modification independently, which leads to dynamic systems that could adapt to the changing conditions, thereby improving efficiency and functionality. This natural mechanism is essential in biology and chemistry, regulating interactions at the atomic level, cellular replication, and the folding of DNA, RNA, and proteins.[2] Over the past three decades, materials scientists have sought to harness nature's self-assembly principles to develop artificial materials with hierarchical structures and customized properties to produce useful devices.[3-6]

1.1 Supramolecular materials

Supramolecular self-assembly is applicable in various fields, such as drug delivery, sensors, catalysis, and optoelectronic devices. The discipline of supramolecular chemistry emerged in the 1970s, with the investigation of non-covalent interactions and molecular recognition by Jean-Marie Lehn, Donald J. Cram, and Charles J. Pedersen.[7, 8] Their research established the foundation for comprehending how molecules might aggregate into more complex forms. Supramolecular self-assembly is the process wherein molecules independently assemble into organized architectures via non-covalent interactions, such as hydrogen bonding, electrostatic forces, van der Waals interactions, and π—π stacking. The energy of the non-covalent interactions (0.5-50 kcal/mol) is lower than the conventional covalent bonds (60-120 kcal/mol).[9] Since these non-covalent interactions are not covalent in nature, they exhibit a dynamic nature such that the material undergoes reversible processes based on external stimuli. The most commonly observed non-covalent interactions are hydrogen bonding, ionic bonds, hydrophobic and van der Waals interaction. The hydrogen bonding interactions are stronger than the dipole interaction and π—π stacking, and the van der Waals interactions energy is the least.[10-12] These non-covalent interactions are responsible for the self-assembly of individual molecules into smart supramolecular materials, starting from basic dimer structures to more complex nanostructures or larger macroscopic materials with intriguing properties.[13]

1.1.1 Self-assembly based on non-covalent interactions

In 1997, Stupp and coworkers showed the first examples of self-assembling supramolecular materials in the form of nanostructure lattices, specifically mushroom-shaped aggregates that spontaneously organize into films with polar arrangements.[14] These aggregates demonstrate nonlinear optical properties and distinct hydrophobic/hydrophilic surfaces. Supramolecular materials comprise several molecules linked by non-covalent interactions, leading to ordered structures that display distinctive physical and chemical properties. Despite their relative weakness in strength compared to covalent interactions, non-covalent interactions are crucial in crystal engineering, anion transport, anion-sensing, anion-recognition chemistry,

protein folding, enzyme inhibition, and drug-receptor interactions.[15-18] Supramolecular materials find applications in drug delivery, sensors, nanotechnology, gas storage, and catalysis.[19-22]

Supramolecular materials are mainly categorized into supramolecular polymers, self-assembled monolayers (SAMs), molecular rotors, metal-organic frameworks (MOFs), supramolecular host-guest systems, supramolecular assemblies in organic electronics, biological supramolecular structures, nanostructured materials, and supramolecular gels.[13, 23] Supramolecular gels fall under the category of smart supramolecular systems because the self-assembly process mainly depends on the nature of the non-covalent interactions.[24-26] These materials display various potential applications in various fields, such as sensors, pharmaceuticals, cosmetics, food industry, crystal growth media, and scaffolds in biomedical engineering.[27-34] We are interested in supramolecular gels, where the self-assembly process depends on various experimental conditions and the molecular structure of the building blocks[35-38] The gel network can respond to changes in the environment, such as temperature, pH, or solvent composition (*Scheme 1.1*) and a detailed description of supramolecular gels are provided in the following sections.

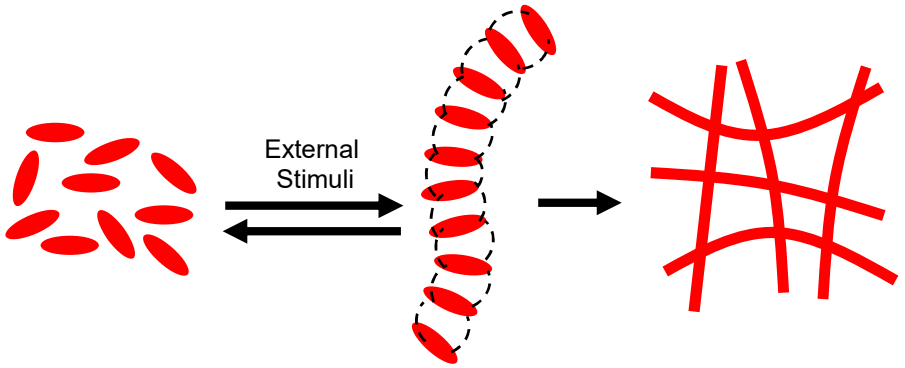

Scheme 1.1 Effect of external stimuli on the self-assembly via non-covalent interactions

1.1.2 Supramolecular gels (History and classification)

Gels are fascinating materials surrounding us in everyday life as cosmetics, food, and medicines that exist in semi-solid phases and show both solid and liquid properties. Supramolecular gels self-assemble themselves spontaneously into well-defined structures due to intermolecular interactions. Supramolecular gels are formed through non-covalent interactions, and they consist of small organic molecules or polymers that self-assemble into a three-dimensional network, trapping a solvent within the structure and leading to a gel-like consistency. One of the earliest gels was based on calcium stearate, which was made by mixing animal fat with limestone.[39, 40] Later, lithium 12-hydroxystearate (HSA) became more popular as a lubricant, and even today, the choice of 12-HAS is of major interest. [41, 42] Thus, the history of lubricants shows that gels had much earlier origins. In the 1990s, considerable advancements were made in the identification of small molecules capable of functioning as gelators.

Gels are classified into several categories based on the nature of interactions, molecular weight, and solvent medium.[43] Based on the nature of the interaction or type of aggregation, gels are classified into polymeric gels (PGs) and supramolecular gels (*Scheme 1.2*). The 3-D network in polymeric gels is held together via strong covalent interactions, while supramolecular gels are governed by weak non-covalent interactions. The primary disadvantage of cross-linked PGs is the establishment of covalent bonds, leading to the formation of irreversible systems. Supramolecular gels derived from small organic molecules, generally with a molecular weight under 3000 amu/molecule, are categorized as low molecular weight gelators (LMWGs).[44] Conversely, supramolecular gels are created by weak non-covalent interactions, providing flexibility and tunable gel state characteristics. Gelation is commonly identified by the simple 'inversion test' for supramolecular gels, wherein the material remains stationary against gravity.

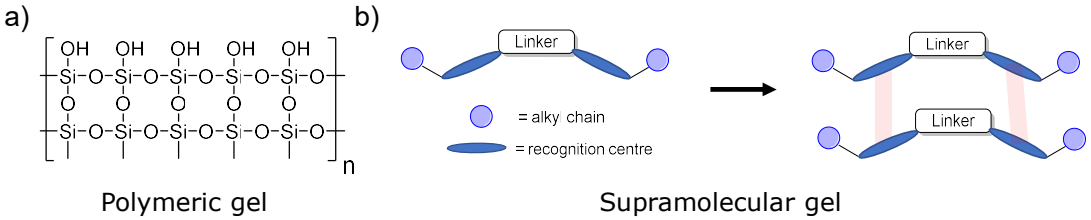

Scheme 1.2 Types of gels based on the nature of interaction.

Supramolecular gels typically comprise 1.0–5.0 wt/v% of the gelator, and 95.0–99.0 wt/v% of the solvent, which gets trapped inside a three-dimensional gel network (*Scheme 1.3*). Supramolecular gels self-assemble themselves spontaneously into well-defined structures due to intermolecular interactions. Supramolecular gels are formed through non-covalent interactions, and they consist of small organic molecules or polymers that self-assemble into a three-dimensional network, trapping a solvent within the structure and leading to a gel-like consistency. LMWGs are categorized as hydrogels or organogels based on the type of solvent utilized. The self-assembly can be tuned via the choice of solvent and the structure of the gelator. Hydrogels contain water as a solvent, while organogels consist of organic solvents.[45]

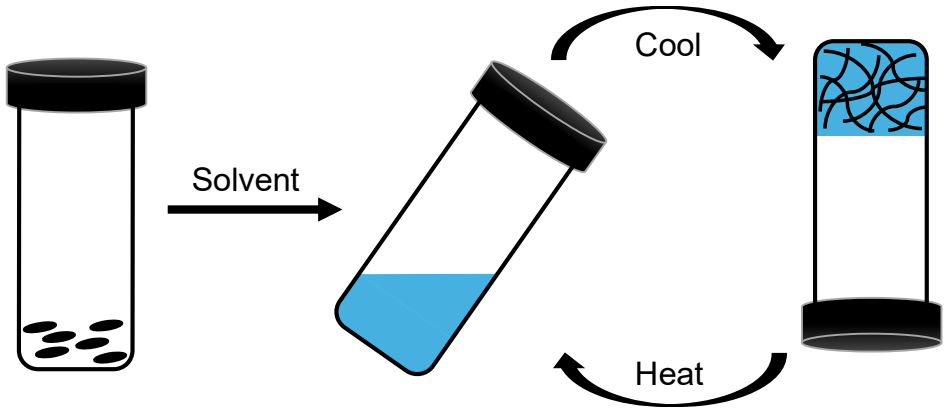

Scheme 1.3 Supramolecular gel formation.

The majority of gelators were identified accidentally rather than via intentional design; nevertheless, there has been a growing development of straightforward design tools to facilitate this process.[46, 47] The progress in supramolecular chemistry has enhanced the understanding of self-assembly, facilitating the explanation of why specific molecules form gels. For instance, 'one-dimensional' non-covalent interactions are recognized as one of the prominent factors for gel network formation, and efforts have been undertaken to correlate these interactions with the possibility of gel formation.[46] Recently, computational techniques have been widely employed to comprehend and/or anticipate the presence of gel-forming systems in LMWGs.[48, 49] The self-assembly process depends on various experimental conditions such as choice of solvents, sonication, pH, gelator structure, and temperature.[35-38] These factors play a major role in the dynamic nature of the supramolecular gels, which facilitates their stimuli-responsive behavior.[50-53] The design of the molecular building blocks is a critical factor which influences the self-assembly process.[54-56] Incorporating specific functional groups (e.g., hydrogen bonding moieties, π—π stacking, charged groups) enables the formation of desired non-covalent interactions. The nature and spatial orientation of these functional groups play an important role in the self-assembly process and efforts have been made to design LMWGs using multi-functional ligands because the rigidity/flexibility of the functionality influences the conformational freedom associated with the molecular structure.

Multi-functional ligands are molecules capable of binding to different entities or have multiple functionalities within a singular structure. In supramolecular self-assembly, multi-functional ligands are essential for the design and development of complex assemblies via non-covalent interactions.[57] Multi-functional ligands may contain several binding sites, enabling interaction with multiple substrates or components. These ligands could facilitate hydrogen bonding, π—π interaction, van der Waals interaction, halogen bonding and metal coordination that promotes the supramolecular architecture. Such interactions may result in the development of distinct structures, including two-dimensional or three-dimensional networks. Multi-functional ligands are viable to chemical modification resulting in the introduction of several functional groups that interact with multiple targets.[58] Examples of such functionalities are urea, amide, phenyl, pyridyl, thiourea, carbamates, and *N*-oxides. This tunability enables researchers to engineer ligands that can react to external changes (pH, temperature), which can be used for various applications (e.g., sensing, drug administration).[37, 59] Numerous supramolecular assemblies constructed with multi-functional ligands display dynamic properties that can undergo reversible transformations.[60-62] For example, the presence of multi-functional ligands in individual and multi-component gels can lead to enhanced mechanical and thermal strength, elasticity, and responsiveness.[59, 63] This property is crucial for tuning the gel state properties, which will aid their applications in various fields such as drug delivery, catalysis, and cell culture.[64-66]

1.1.3 LMWGs based on individual and multi-component systems

Supramolecular gels are formed from individual or multi-component building blocks in the presence of a suitable solvent. A single type of small molecule that can self-assemble into three-dimensional networks to form a gel is called an individual low molecular weight gelators (LMWGs). The gelation mechanism is much simpler in this case, where the individual LMWGs are first dissolved in a particular solvent via sonication or heat. It is then cooled or applied with an external stimulus like a change in pH, addition of salts, or heat or light that triggers self-assembly.[44] This results in the formation of molecular-level self-

assembly, which aggregates to form one-dimensional (1-D) fibers. The molecular level assembly is governed by non-covalent interactions such as hydrogen bonding, π-π stacking, van der Waals forces, and hydrophobic interactions. Finally, the fibers are entangled to form the actual gel network, which is three-dimensional in nature. The final properties of the gel mainly depend on the nature of the functional groups present in the gelator, the solubility of the gelator in the solvent of choice, and other external factors like pH, temperature, and the presence of salts/ions.[67] The majority of current gelators are synthetically produced by accident or by modifying an existing gelator.[68]

LMWGs with two or more components are classified as multi-component gels. Multi-component supramolecular self-assembly, commonly found in natural systems, can produce complex structures due to thermodynamic favorability. Multi-component self-assembly is a strategy utilized to produce sophisticated gels that may show properties which are not obtained with the individual components.[69] Self-assembled materials can be readily synthesized from various components by combining multiple molecules in a solvent; this represents a significant advantage of the supramolecular approach to materials science. Consequently, there has been significant interest in multi-component gels. Buerkle and Rowan subsequently devised a classification system for these gels, which offers simplicity and advantages for conceptual application.[35] Three primary categories of multi-component gels have been examined (*Figure 1.1*). The initial class necessitates all components to access the gel, which means no individual component alone creates a gel. A second class employs two or more gelators that may self-assemble, while the final class comprises one or more gelators and non-gelling additives that might influence the assembly process of the gelator, hence affecting the properties of the gel. Multi-component supramolecular gels offer a facile way to change the ratio of the multiple components that were added and tune the gel state properties.

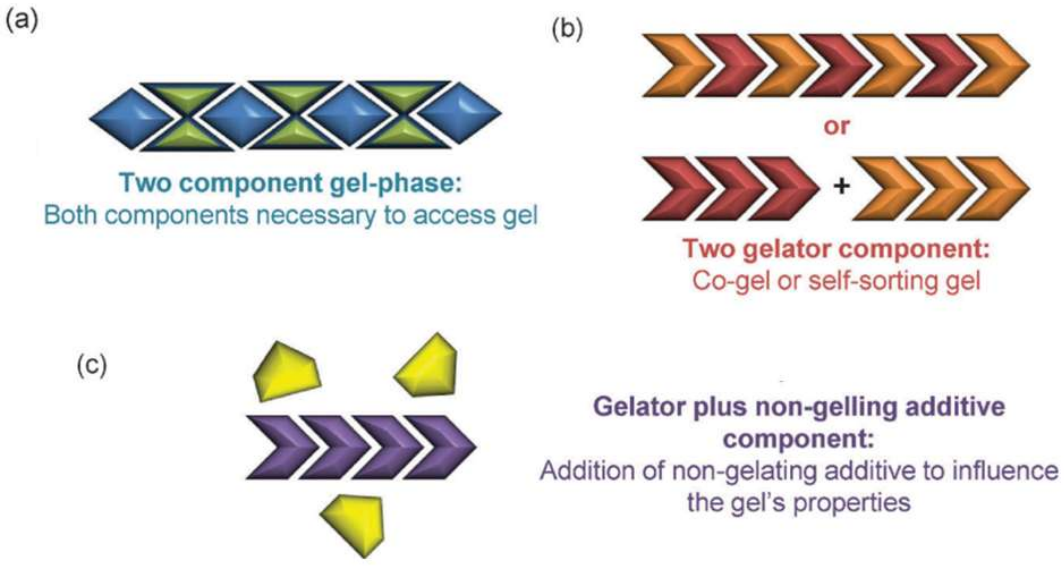

Figure 1.1 Types of multi-component supramolecular gels.[35]

1.2 Self-assembly process in LMWGs based on individual components

The first low molecular weight hydrogelator in the academic literature was lithium urate, reported in 1841 by Lipowitz.[70] Another example of an LMWG that originated over 100 years ago is Dibenzoylcystine, which was first reported in 1892 by Brenzinger (*Scheme 1.4*).[71] One of the influential academic works on LMWGs was published by Terech and Weiss on specific organogelators like fatty acid derivatives and steroid derivatives, highlighting their structural organization, gelation properties, and microscopic characteristics.[72] Since then, the LMWGs based on individual systems have been studied in detail to find the key elements that govern the gelation mechanism and relevant application of these systems in various fields.

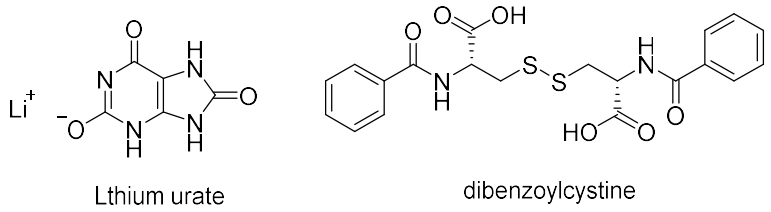

Scheme 1.4 LMWGs with origin dating back over 100 years.

LMWGs[43, 73-80] provide enhanced control over the self-assembly processes, which can be turned on/off by external stimuli such as anions, heat, light, and sound. This will help us study the self-assembly process from the molecular scale to the network level since the gel network formation is affected by the stimuli-responsive nature. For example, at the molecular level, it can alter the nature of molecular interactions; at the fiber level, it can enhance or deprive the fiber formation; and at the network level, it can alter gel characteristics such as color or nature (swelling or shrinkage).

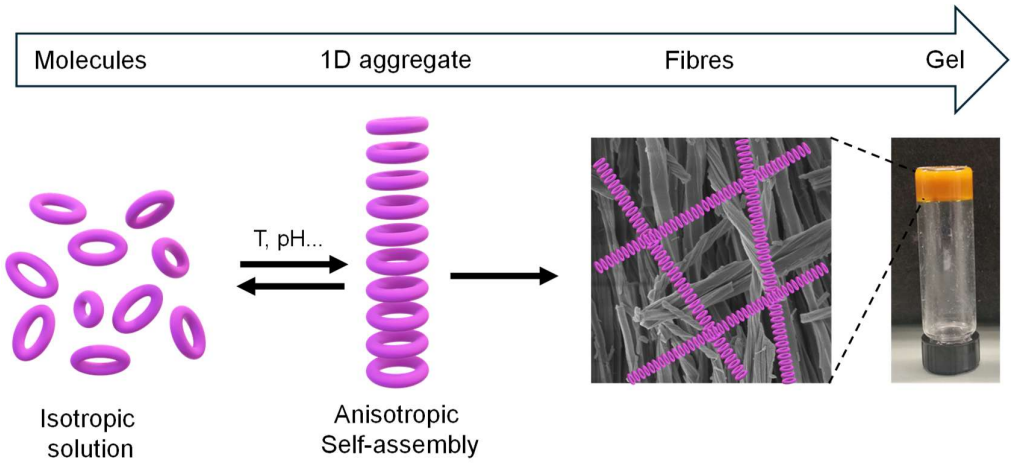

Scheme 1.5 Schematic illustration of the assembly of low-molecular-weight gelators (LMWGs) from an isotropic solution into anisotropic self-assembled structures, which then hierarchically organize to produce a gel-phase material.[81]

In LMWGs, the molecular-level aggregation originates through several non-covalent interactions among gelator molecules, including hydrogen bonding, π—π interactions, van der Waals forces, and halogen bonding. Molecular interactions govern the nanostructure, and it is recognized that molecular aggregation frequently results in 1-D chains. The 1-D chains subsequently interact with one another, resulting in the formation of fibrils. Finally, the fibers are entangled to form the gel network (*Scheme 1.5*).[76] The ability of bis(urea) systems to form the primary α-tape structure is an example of the formation of fibrils from 1-D chains, which finally entangle to form secondary and tertiary structures (*Scheme 1.6)*.[82]

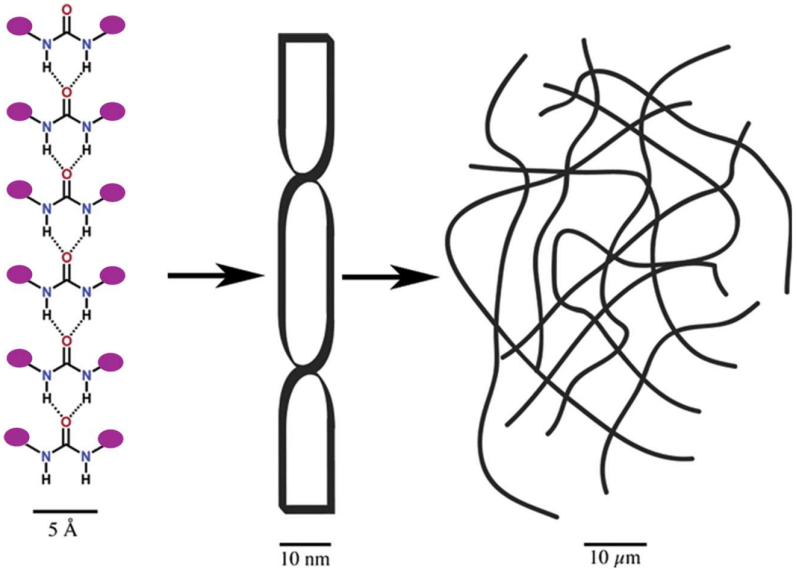

Scheme 1.6 Self-assembly of urea-based gelators to form primary, secondary and tertiary structures.[82]

A delicate balance between solvophilic and solvophobic interaction is crucial for effective gelation. Smith's group has demonstrated the impact of the type of solvent on the self-assembly of gel-phase materials. It provides insights into the role of solvents in modulating the structural and macroscopic properties of the assembled superstructures.[83] LMWGs are often discovered via serendipity,[68] therefore, the design of LMWG is essential to create gels with specific properties tailored to particular applications.

Gels derived from LMWGs are typically formed by cooling a solution of the LMWG in the corresponding solvent, resulting in a supersaturated solution. Various triggers can be applied, including heat-cool cycles, solvent-switch, pH alteration, and addition of salts/ions. The choice of a gelation trigger influences the resulting networks, which in turn impact the characteristics of the bulk gel. Supersaturation induces a swift organization of gelator molecules into elongated fibers, generally measuring 5.0-100.0 nm in diameter.[81] These fibers then aggregate to form a fibrous three-dimensional entangled network, transforming the liquid into a supramolecular gel. LMWG comprises an entangled fibrous network of gelator molecules maintained by specific intermolecular interactions among the gelator molecules.[81] By programming the self-assembly properties of molecular building blocks through molecular shape and intermolecular interactions, one can influence the formation of a gel network. LMWGs can undergo significant changes in their physical or chemical properties in the presence of external stimuli.[84] This adaptability of LMWGs makes them

smart materials that can perform specific functions or adapt to their environment. The behavior of a gel in response to varying environmental conditions offers valuable insight into its molecular interactions and structural integrity.[85] Examining the gel's behavior across varying temperatures can clarify the characteristics of hydrophobic interactions or hydrogen bonding within the gel network.[86] Observing the swelling or contraction of the gel in response to pH variations can provide insights into ionic interactions and the existence of certain types of functional groups.[87] Assessing the alterations in the gel's mechanical properties under stress provides insights into the molecular structural arrangement and connectivity.

1.2.1 Factors influencing the properties of LMWGs

LMWGs are a class of "smart" stimuli-responsive materials that exhibit a dramatic change in their properties in response to the application of an environmental stimulus, such as salts/ions, sound, light, gelator structure, heat, voltage, magnetic field, mechanical stress, and pH.[50-53, 88-92] It is crucial to understand the role of each type of stimuli in influencing the gelation process, to study the mechanism of gelation.

Anion-responsive supramolecular gels are soft materials that can alter their physical properties in the presence of specific anions.[93-97] The design of these gels will require precise choice of functional groups capable of selectively binding to target anions, along with a consideration of the gel architecture to guarantee stability and responsiveness. Consequently, anions are crucial in dictating the gel-state properties, resulting in significant research efforts focused on anion-responsive supramolecular gels. The self-assembly of the low molecular weight gelators based on amino acids can be triggered using salts/ions, and Hofmeister series can be correlated to understand the effect of ions on the self-assembly. A century ago, Franz Hofmeister made a series called 'Hofmeister series,' which refers to the arrangement of anions or cations in order of their ability to decrease (kosmotropes) or increase (chaotropes) the solubility of proteins.[98, 99]

In 2014, Miravet and colleagues developed a bolaamphiphilic hydrogelator based on an L-valine derivative and studied the effect of guanidium ions on the gelation process (*Figure 1.2*). The self-assembly of this gelator was driven by hydrophobic effects, hydrogen bonding,

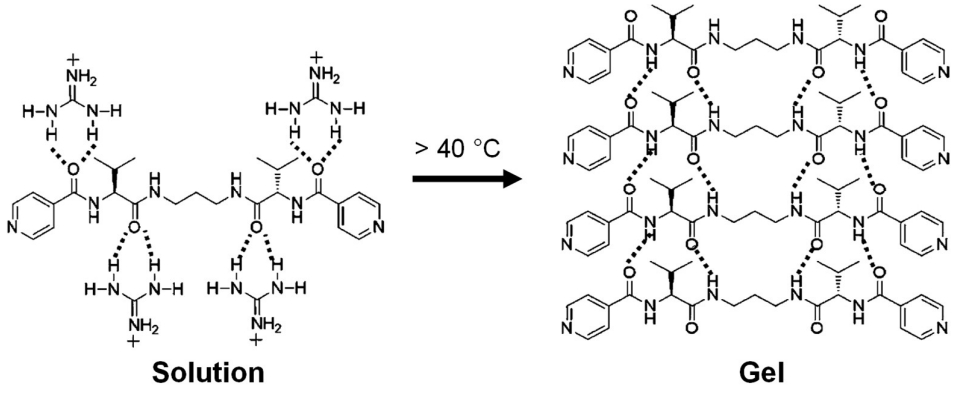

Figure 1.2 Heat-triggered gelation by releasing guanidinium ions above 40.0 °C.[100]

and π–π interactions. When a chaotropic ion is present, the solubility of the gel is enhanced. Guanidium chloride, based on its behavior, is reported in protein science to be chaotropic. It is mostly used as a denaturant for proteins, as it disrupts proteins and facilitates their unfolding. Guanidinium ions can form hydrogen bonds with amide and urea groups. However, when the temperature was increased, the guanidinium cation was released, which induced self-assembly and formed a viscoelastic gel (*Figure 1.2*). The hydrogel remains stable at room temperature for at least 48 hours.[100]

Steed and colleagues developed an anion-responsive organogelator based on pyridinylmethyl urea, which formed a strong gel in aromatic solvents. However, in the presence of inorganic salts, the gel was weakened or destroyed due to metal ions and anions, causing the collapse of the urea α-tape motif. The metallogels exhibited a lower elastic modulus than organogel alone, and the sol-gel transition was triggered by adding tetrabutylammonium bromide (BTABr) (*Figure 1.3*).[101]

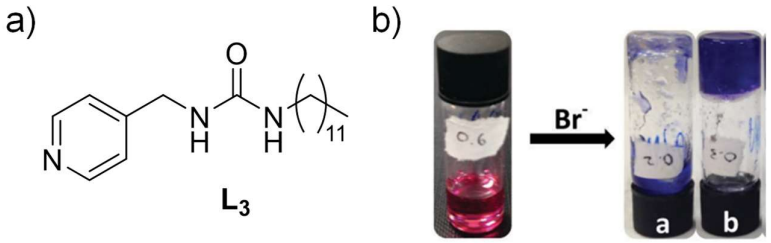

Figure 1.3 a) chemical structure of the gelator L3 and b) addition of TBABr and sonication to a 2:1 solution of L3 and cobalt(II) nitrate in nitrobenzene. Equivalents of TBABr added: a) 0.2, b) 0.3.[101]

Ultrasound, defined as high-frequency pressure waves exceeding 20.0 kHz, is frequently employed in supramolecular chemistry to cross the energy barriers, facilitating the regulation of self-assembly and gelation processes.[102-105] Ulijn and colleagues employed ultrasonic sound to regulate the self-assembly of peptides, align the nanostructures, and ultimately affect the gelation process (*Figure 1.4*).[106]

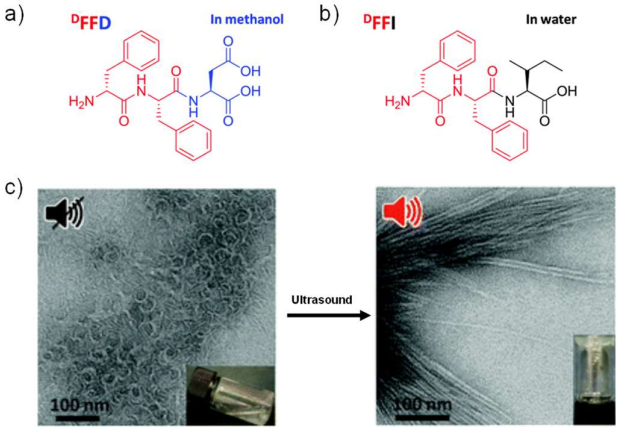

Figure 1.4 a) Chemical structures of tri-peptide derivatives of ^{D}FFD (D-phenylalanine–L-phenylalanine–L-aspartic acid), b) ^{D}FFI (D-phenylalanine–L-phenylalanine–L-isoleucine, and c) TEM images of ^{D}FFD in methanol before and after ultrasound exposure.[106]

The utilization of light as a stimulus in supramolecular gels serves as a non-invasive stimulus while offering superior spatial and temporal resolution.[107] Azobenzene is undoubtedly the most studied example in photoinduced configurational isomerization.[108] Hughes and colleagues examined the reactivity and gelation ability of an azobenzene-appended organogelator (C_8-Azo-TPC), which contains a photo responsive unit and a benzoyl chloride group to facilitate functionalization. Upon exposure to light, alterations in the characteristics of the gel were examined at the molecular level and also observed macroscopically. The *in situ* change between gel and solution under light irradiation in highly organized self-assemblies is particularly intriguing. Upon activation of UV light, both moduli significantly decrease, causing G′ and G″ to converge (both moduli < 100 Pa) (*Figure 1.5*).[109]

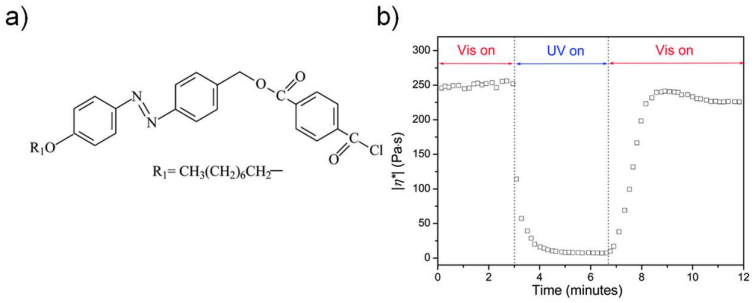

Figure 1.5 a) Chemical structures C_8-Azo-TPC and b) Real-time photorheology measured over alternating UV (365 nm, 200 mW cm^{-2}) and visible (38 mW cm^{-2}) light irradiation for C_8-Azo-TPC in n-dodecane (1.0 wt/v%) at 20 °C. The data were obtained at a constant frequency of 5 rad s^{-1} and a strain of 1.0%.[109]

The structure of the gelators is critical in supramolecular gelation, affecting the formation, stability, and characteristics of the resultant gels.[110, 111] The self-assembly of the gelators depends on the specific arrangement of the functional groups.[112] The strength of the gelator can be tuned by having rigidity or flexibility in the gelator structure.[113] Damodaran and coworkers studied the role of specific non-covalent interactions in the self-assembly process of LMWGs by altering the non-covalent interactions responsible for gel formation through structural modification of the gelator/nongelator. This was achieved by modifying pyridyl moieties of bis(pyridyl) urea-based hydrogelator (4–BPU) and the isomer (3–BPU) to pyridyl *N*–oxide compounds (L_1 and L_2, respectively).[114] (*Figure 1.6*).

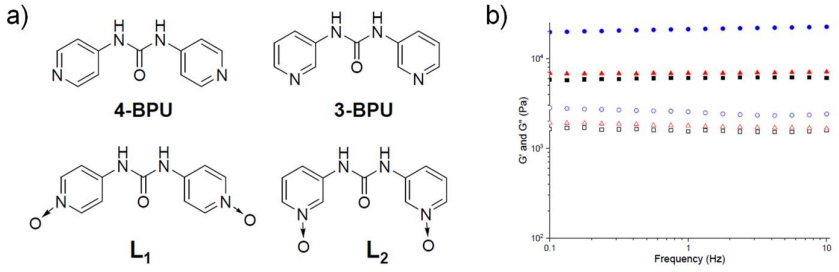

*Figure 1.6 a) Chemical structures of compounds and b) Frequency sweep experiments performed on **4–BPU**, **L1** and **L2** gels at 1.0 wt/v% in water at 25.0 °C at a constant strain of 0.05%. Color codes: G', **4–BPU** (black solid square), G", **4–BPU** (black hollow square), G', **L1** (red solid triangle), G", **L1** (red hollow triangle), G', **L2** (blue solid circle), G", **L2** (blue hollow circle).*[114]

The study showed that introducing *N*–oxide moieties had a significant effect on the gelation properties, resulting in better mechanical and thermal stabilities and different morphologies of the gel network

The gelation mechanism has been studied using various analytical techniques, including spectroscopic, microscopic, and X-ray diffraction.[115-120] It has been shown that X-ray diffraction methods are one of the most promising tools for comprehending the structure of the gelator and its aggregation behavior.[121-126] The dynamic nature of the non-covalent interactions, however, makes it challenging to anticipate the gel structure or regulate the gel state features, resulting in low molecular order throughout the gel state. Consequently, understanding the molecular self-assembly in supramolecular gels is a tough task, however, analyzing the self-assembly will help us in the design of LMWGs with intriguing properties.[33, 68, 82, 127-129] One promising method to analyze the effect of a specific interaction in gel formation is to evaluate the role of specific functional groups in gel network formation.

1.2.2 Role of functionality on the self-assembly process in individual gels

Functional groups play a crucial role in the self-assembly process of supramolecular gels.[110, 130, 131] They influence the gelation properties and the overall gel network through various non-covalent interactions.[114, 132] Polar functional groups such as hydroxyl, amides, urea, amino, and acid groups are observed to form hydrogen bonds, which are essential for the self-assembly of gelators into a three-dimensional network. On the other hand, non-polar functional groups such as alkyl/alkenyl/alkynyl promote self-assembly via aggregation due to hydrophobic interactions. Aromatic groups can engage in π-π stacking interactions, which help stabilize the gel network, and the Van der Waals forces and electrostatic interaction can also affect the self-assembly in the gelation process. The nature and spatial position of functional groups also play a major role in gel formation. Thus, the design of a multi-functional molecule as the LMWGs must be performed with careful consideration of all of these components.

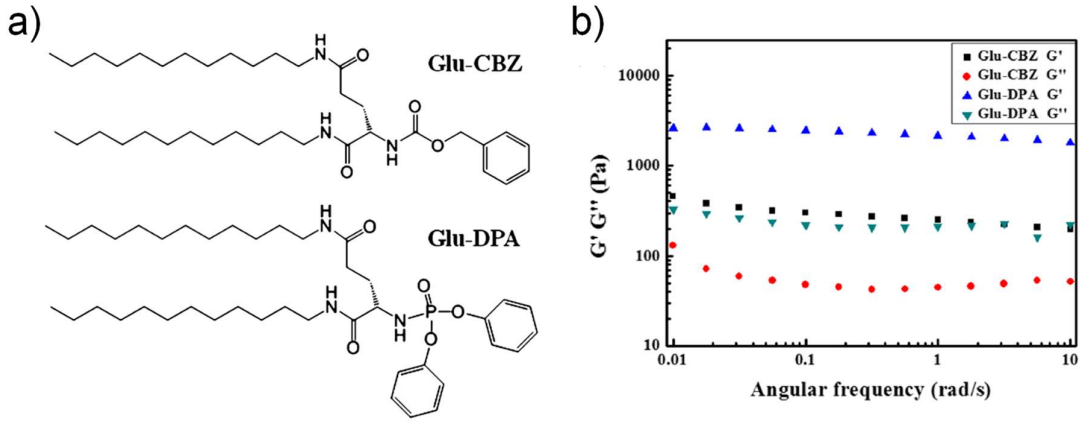

Figure 1.7 a) Chemical structures of compounds Glu-CBZ and Glu-DPA and b) angular frequency sweep comparison of gels formed in styrene at a concentration of 2.0 wt/v%.[133]

Wang and coworkers explored the impact of gelator structures on the self-assembly mechanisms and the gel properties. Two gelators, Glu-CBZ and Glu-DPA, (*Figure 1.7)* were synthesized, and the effect of the carbobenzoxy group and diphenyl phosphate group on

gelation was studied.[133] The results indicated that the gels of Glu-CBZ possess superior network integrity and thermal stability, whereas the gels of Glu-DPA exhibited enhanced rheological properties (*Figure 1.7)*. The increase in the benzene ring provided a stronger intermolecular force in the dynamic process, but it led to a steric hindrance effect in the static process.

A better understanding of the role of functional groups can be obtained by altering the functional groups of molecules with known supramolecular architecture. Zinchuan *et al*. synthesized a cholesterol-based dendrimer gelator from the parent terminal alkyne gelator, and demonstrated that the modified compounds formed gels in polar solvents, whereas the parent compound only generated gels in nonpolar solvents (*Scheme 1.7*).[134] On top of that, the BisDEC gel system showed intriguing self-healing and self-supporting properties (*Figure 1.8*).

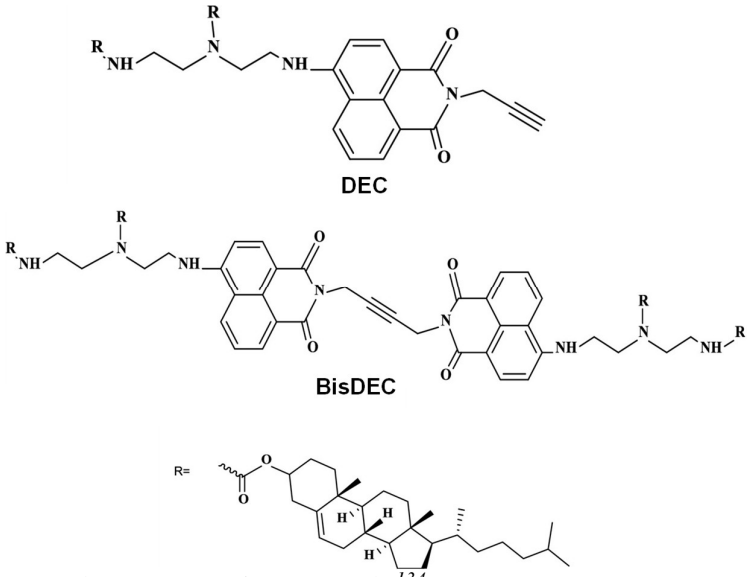

Scheme 1.7 Chemical structures of compounds.[134]

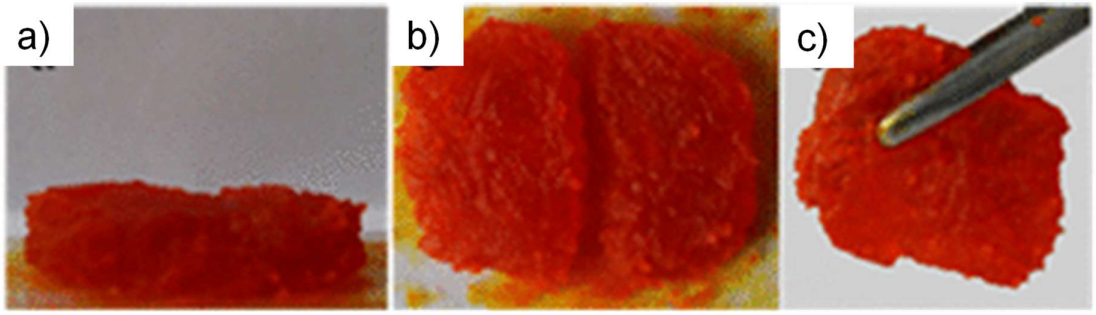

Figure 1.8 BisDEC gel (4 wt %) in cyclohexanol a) gel block, b) gel after being cut in half, and c) healing gel.[134]

Damodaran and coworkers showed that the tris(pyridyl-*N*-oxide) gelator obtained by modifying trimesic amide-based LMWG can be used as a crystallizing medium for copper(II) isonicotinate–*N*-oxide complex.[135] The gelation characteristics of the parent and modified gelators were compared to assess the significance of specific interactions.The role

of functional groups in adjusting gelation qualities through the modification of pyridyl groups in *N*–(4–pyridyl)isonicotinamide to *N*-oxide groups (*Figure 1.9*) was reported by the same group.[132] The compounds containing *N*–oxide groups provide numerous advantages over the parent pyridyl-*N* atom due to the additional lone pairs in the *N*-oxide moiety, perhaps resulting in improved interactions with solvent or guest molecules.

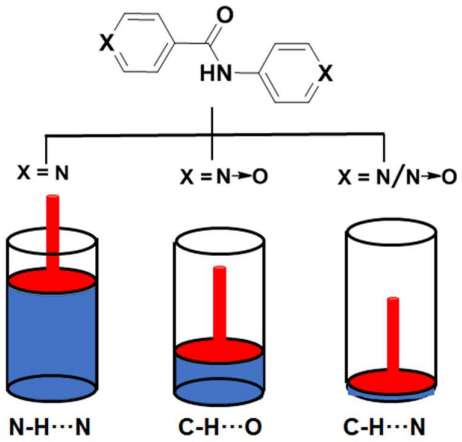

Figure 1.9 Effect of modification of functional group on the mechanical strength.[132]

Thus, understanding the role of functionality, along with the nature of non-covalent interactions, may aid researchers in designing advanced materials derived from LMWGs. The ability to form a 1-D hydrogen-bonded chain is regarded as a fundamental essential interaction in the formation of gel networks in LMWGs.[68, 82, 136, 137] Similarly, metal binding can enhance the gelation by cross-linking, altering the pH, also via increasing ionic strength.[59] Hence, metallogels demonstrate unique characteristics and capabilities.

1.2.3 Metal-based LMWGs

Metallogels represent one of the most swiftly advancing areas of functional materials nowadays. The integration of metal ions into gels imparts novel features to the system, such as catalytic and redox activity, conductivity, luminescence, and magnetism.[116, 138-140] The integration of metal centers into supramolecular gels is anticipated to produce multi-functional metallogels. Lee *et al*. reported the stimuli-responsive metallogel through counter-anion exchange in aqueous media.[141] The addition of $AgBF_4$ to the compounds formed gel in aqueous solution due to the formation of hexagonal columnar structures. The gel-sol transition was observed by the addition of F^- or $C_2F_5COO^-$ ions due to counter-anion exchange (*Figure 1.10*). Mitra *et al.* reported a bromide-responsive metallogel based on a triazole derivative with cobalt(II) acetate. A solution of 3, 5-diamino-1,2,4-triazole (DAT) in dimethylformamide (DMF) was mixed with a solution of cobalt(II) acetate.[142] The gel was disrupted and subsequently transformed into a sol upon the addition of bromide ions. The sol was converted to a gel upon the introduction of silver(I) nitrate. The disintegration of the gel network was attributed to the presence of a bulky cation and a bromide anion, which disrupted the hydrogen-bonded network (*Figure 1.11*). Silver(I) nitrate successfully scavenged the bromide anion, resulting in the formation of silver(I) halide, which reinstated the hydrogen-bonded network and the gel state.

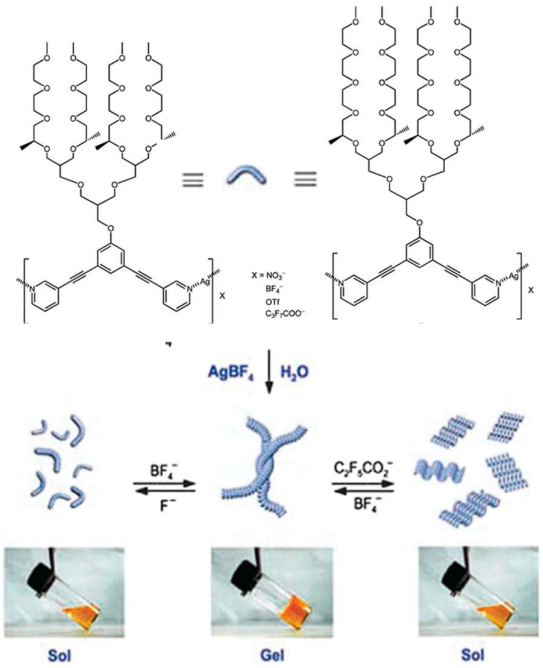

Figure 1.10 Schematic representation of reversible conversion between folded and unfolded conformations of a coordination chain upon counter-anion exchange.[141]

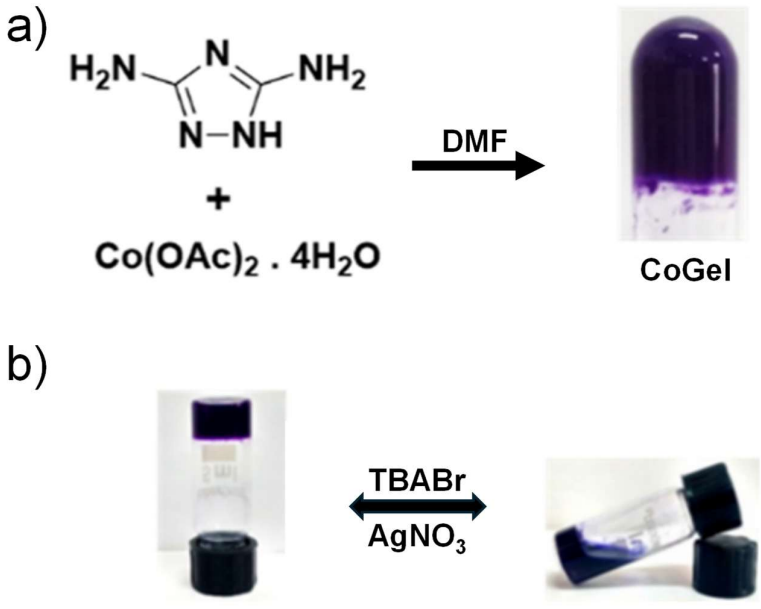

Figure 1.11 a) CoGel formation and b) reversible gel-to-sol transformation.[142]

Employing a tripodal ligand, Jung *et al*. synthesized a Cd(II)-coordinated metallogel and subsequently investigated its catalytic efficacy in the Knoevenagel condensation reaction (*Figure 1.12*).[143] The morphologies of the metallogels were examined using SEM and X-ray techniques, revealing fibrillar structures composed of a one-dimensional coordination

polymer on an octahedral Cd(II) center. The xerogel 3/Cd demonstrated significant activity in the condensation of benzaldehyde with various active methylene substrates, including malononitrile, ethyl cyanoacetate, and cyano-acetic acid tert-butyl ester, with the reaction predominantly taking place on the xerogel's surface. Moreover, the xerogel was readily recovered through straightforward filtration and reused without loss of catalytic activity.

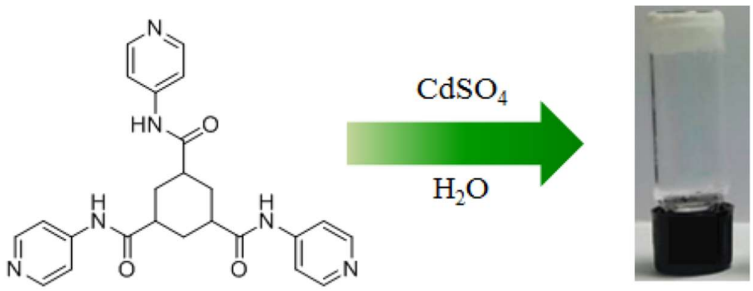

Figure 1.12 Synthesis of 3/Cd metallogel.[143]

Damodaran and coworkers reported the selective gelation properties of *N*-(4-pyridyl)nicotinamide (4PNA) with copper(II) salts. The gelation mechanism was attributed to hydrogen bonding interactions between the gelator amide groups and coordinated anions. The study demonstrates the selective gelation of copper(II) salts over other metal salts due to the Jahn–Teller distorted nature of copper(II). X-ray powder diffraction analysis suggests that the copper(II) acetate complex is the primary gelator due to its 1-D hydrogen-bonded chain structure (*Figure 1.13*).[125]

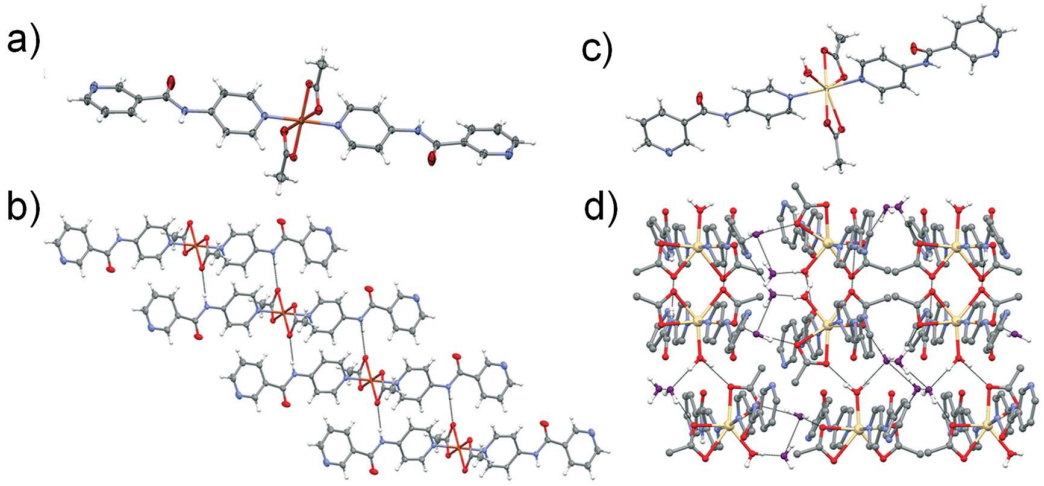

Figure 1.13 a) Molecular structure of [Cu(4PNA)$_2$(OAc)$_2$] b) corresponding 1-D hydrogen-bonded chain observed in the solid state, c) Molecular structure of [Cd(4PNA)$_2$(OAc)$_2$(H$_2$O)]·2H$_2$O (uncoordinated water molecules are not shown) and, d) the corresponding 2D hydrogen-bonded chain observed in the solid state (uncoordinated water molecules are shown in purple).[125]

Significantly, in contrast to conventional supramolecular gels, metallogels are responsive to a broader spectrum of physical and chemical stimuli. Numerous stimulus-responsive metallogel systems have been effectively engineered and constructed to respond to diverse

external stimuli, such as temperature, light, sound, mechanical force, magnetic fields, electric fields, pH, and chemicals. Overall, the future of supramolecular metallogels looks promising, with ongoing research likely to unlock new applications and improve upon existing technologies.

1.3 Self-assembly process in LMWGs based on multi-component gels

The nature of complexity in multi-component systems depends on the number of entities that can be made of two or more components.[144] Two-component systems are simple to design and characterize, cost-effective, and more manageable in controlling their interactions.[145] In multi-component gels based on two components, the two components interact to form an advanced network structure. The two components may interact by hydrogen bonding, π-π stacking, or van der Waals forces. The selection of components can markedly affect the characteristics of the gel. The self-assembly of the two components is directed by molecular interactions that result in the creation of fibrous structures.[146] These structures then entangle to create a three-dimensional network capable of entrapping solvents, thereby yielding a gel. The concentration of the components, temperature, and solvent type are critical factors in the gelation process. In multi-component systems, the interaction between the components can provide synergistic effects, resulting in gelation, or it displays novel properties not seen with the individual components. Multi-component gels possess several applications, including drug delivery, tissue engineering, and serving as scaffolds in materials research. Their tunable characteristics render them appropriate for various applications.[147]

1.3.1 Multi-component gels

Multi-component gel refers to situations in which a gel is made by combining more than one gelator, a gelator and a non-gelator, or even a combination of two non-gelators.[35] We are interested in the self-assembly of a two-component-based multi-component system. Self-assembled multi-component gels by mixing gelators display intriguing properties that are not achieved by individual components. The first non-covalent two-component system was based on a host-guest complex. In 1993, Hanabusa and colleagues utilized complementary hydrogen bonds between two orthogonal building blocks derived from barbituric acid and pyrimidine to create a compound that subsequently assembled into tape-like supramolecular structures, forming a gel (*Figure 1.14*).[148]

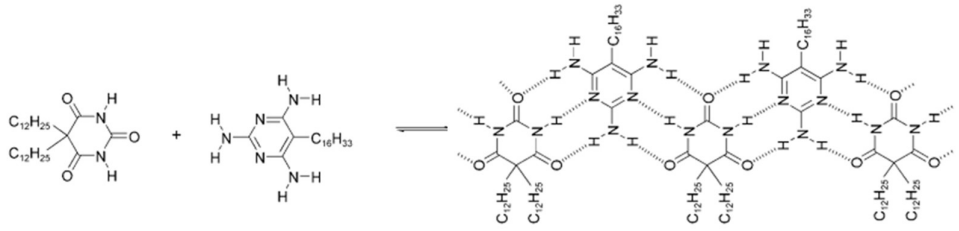

Figure 1.14 Hydrogen bonding interaction between barbituric acid and pyrimidine subunits.[85]

Smith and coworkers developed multi-component gels utilizing the fundamental interaction between dendritic peptide carboxylic acids and apolar amines, resulting in a persistent acid-base complex in organic solvents. The resultant complex exhibits altered solubility, prompting further assembly into nanofibers due to hydrogen bond interactions among the peptide groups (*Figure 1.15*).[149]

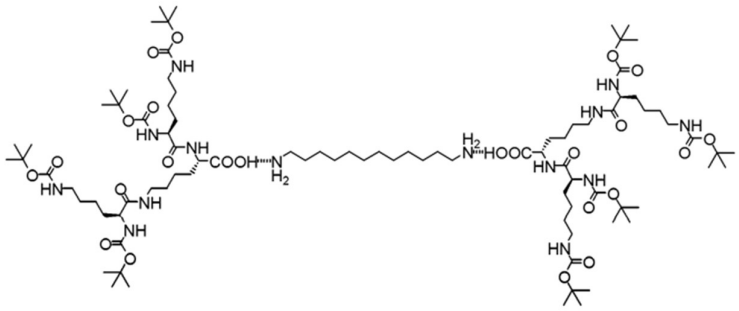

Figure 1.15 Hydrogen bonding interaction between dendritic branch and diaminododecane to form two-component gel.[149]

The most studied area of multi-component supramolecular gels involves mixing two components that do not gel independently but form gels when combined. Bhattacharya *et al*. studied by mixing water-insoluble fatty acids with water-soluble amines, such that they observed that stearic ($C_{18}H_{37}COOH$) and eicosanoic ($C_{20}H_{41}COOH$) acids could generate hydrogels with various primary diamines, including methylated diethylenetriamine, 3,3'-iminobis(propylamine), and *N*,*N*'-bis(3-aminopropyl)-ethylenediamine (*Scheme 1.8*).[150] The combination of the two components in ratios from 2.5:1 to 15:1 of the amine to carboxylic acid produced aqueous soluble complexes upon heating, and it gelled upon cooling to ambient temperature. The hydrophobicity of the fatty acid component plays a major role in the stability of the gel; fatty acids with an alkyl chain length shorter than 16 did not form gels.

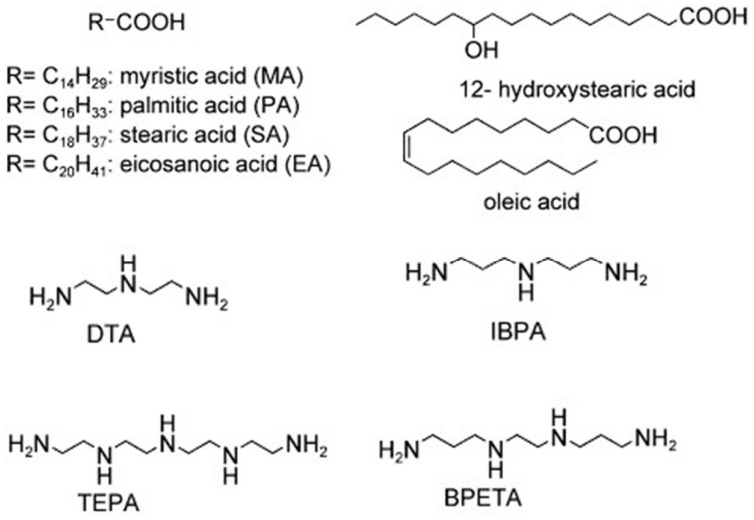

Scheme 1.8 Structures and abbreviations of various acids and amines used for gelation.[150]

The second type of multi-component supramolecular gels entails the combination of two low molecular weight gelators. One of the advantages of multi-component systems based on mixing two gelators is that the self-assembly process can be compared by correlating the non–covalent interactions between individual and the mixed gelator molecules.[69] Moffat and Smith investigated the combination of two gelators in a 9:1 ratio of styrene to divinylbenzene.[151] The gel with the amide functionality showed much greater thermal stability compared to the one with carbamate functionality, with its T_{gel} approximately 30.0 °C higher at a concentration of 20.0 mM. The varying alkyl end-groups in the two systems may also influence the difference in thermal strength. Scanning electron microscopy (SEM) of dried gel samples revealed that the fibers of the stronger gel are considerably smaller, with a diameter of approximately 20.0 nm, compared to the other weaker gel, with a diameter of around 80.0 nm. Combining the equimolar proportions of both gelators yields a self-sorting gel. SEM studies effectively illustrate the existence of both big fibers (about 50–125 nm in diameter) and small fibers (approximately 25.0 nm in diameter) (*Figure 1.16*). Notably, this mixed gel displays a T_{gel} comparable to the stronger gel, which aligns with the observation that the former weaker gel does not interfere with the ability of the stronger gel to establish a robust network that governs the thermomechanical properties of the system.

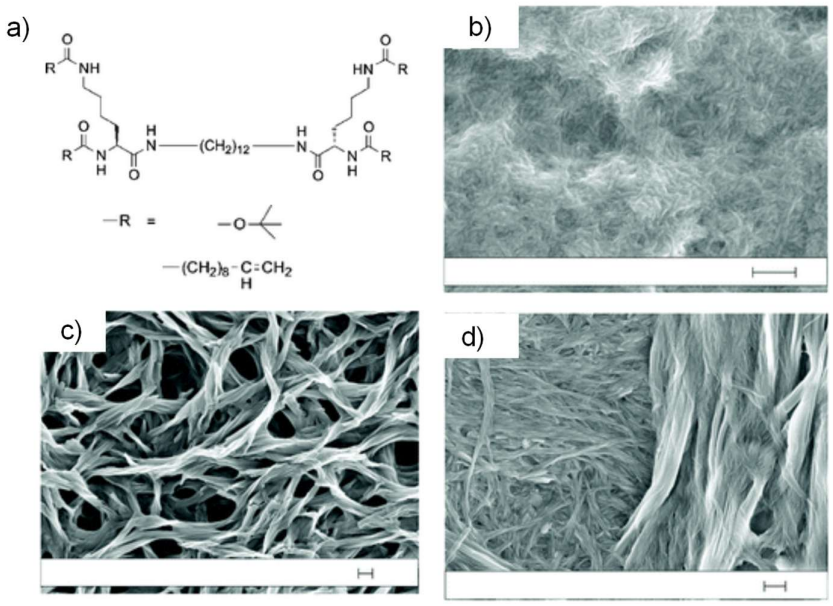

Figure 1.16 a) Chemical structures of amide and carbamate gelators. SEM image of dried gels from styrene-DVB (9: 1) of b) amide gelator scale bar: 200 nm, c) carbamate gelator scale bar: 300 nm, and d) equimolar mixture of both gelators, scale bar: 200 nm.[151]

Finally, multi-component supramolecular gels are also made from one gelator when combined with non-gelating molecules. Fuhrhop *et al*. demonstrated that hydrogelator *N*-octyl-D-gluconamide can be stabilized in the short term with phosphotungstic acid (PTA) and for a minimum of five months with the charged surfactant sodium dodecylsulfate (SDS).[152] The authors proposed that the micelles produced by the SDS solubilized any crystal nuclei that emerged prior to the onset of macroscale crystallization. Nevertheless, the authors observe that at 2.0 wt/v%, gels can only be generated with a molar ratio of up to 2.5:1 gelator to SDS ratio. The inclusion of any additional SDS leads to gel dissolution.

These examples showed how the nature of components can influence the gel-state properties in two component-based multi-component gels. The interaction of both components is a major factor that dictates the self-assembly in multi-component gels.

1.3.2 Types of Self-assembly

Self-assembly in multi-component gels is a process wherein two or more molecules or particles spontaneously arrange into organized systems, occurring across multiple scales, from the molecular level to bigger structures.[153] Self-assembly in a two-component system is a dynamic mechanism that facilitates the formation of diverse structures and materials with unique properties which are not obtained from its individual components. When mixed, the combined effect of two substances facilitates self-recognition at the molecular level, enabling similar molecules to either aggregate into 'self-sorted' fibers or interact to yield well-ordered fibers comprising both gelators (specific co-assembly).[154, 155] Two distinct classes of self-assembly were thus observed: co-assembled system, in which the molecules interact to create architectures comprising both components and self-sorting system, where the molecules independently assemble into separate, potentially interpenetrating structures. The creation of co-assembled system is the predominant category of dual-component systems.[35] Such systems can be created by combining two components with analogous binding motifs and minimal structural differences. This process enables access to a diverse array of characteristics that cannot be achieved using only one of the two components. In some cases, molecules interact randomly, which can be called random co-assembly, which may or may not show the properties of self-sorted or specifically co-assembled structures (*Figure 1.17*). The application of various self-assembly techniques expands the potential to create novel materials with finely tuned features. Self-assembly in multi-component gels is governed by various factors, such as the structural relation with both the components, hydrogen bonding, hydrophobic interactions, ionic interactions, π-π stacking interactions, pH, light, and electric and magnetic fields.

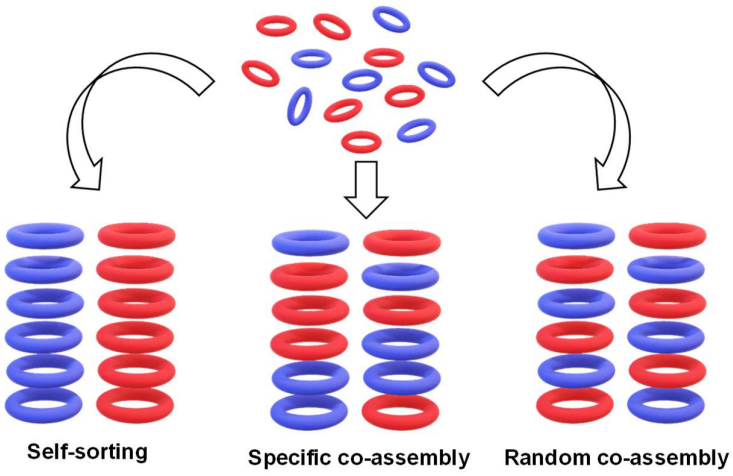

Figure 1.17 Self-assembly modes in multi-component gels.

Nilsson and coworkers showed that the rippled *β*-sheet materials formed via coassembled enantiomeric amphipathic peptides were resistant to proteolytic degradation; however, the *β*-sheet formed from self-assembled L-peptides was disrupted by common proteases (*Figure*

1.18).[156] Moreover, the coassembled gel (D- and L-Ac-(FKFE)$_2$-NH$_2$) also showed enhanced mechanical strength in comparison with the self-assembled L-Ac-(FKFE)$_2$-NH$_2$.

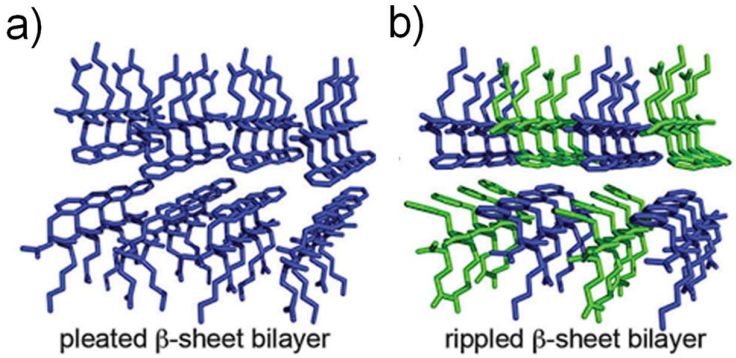

Figure 1.18 a) Pleated β-sheet fibrils composed of L-Ac-(FKFE)$_2$-NH$_2$ and b) Rippled β-sheet fibrils composed of coassembled enantiomeric D- and L-Ac-(FKFE)$_2$-NH$_2$ peptides.[156]

Hamachi and colleagues utilized confocal laser scanning microscopy (CLSM) to study the self-sorted network within a hydrogel based on peptides.[157] Two gelators and their fluorescent equivalents were combined and subjected to a heating-cooling cycle. The gelator pairs self-assemble orthogonally, which ensured that the green and red fibers did not overlap but rather became entangled (*Figure 1.19*). CD spectra further corroborated the self-sorting phenomenon; a 1:1 mixture of them exhibits behavior analogous to the simple summation of their individual spectra.

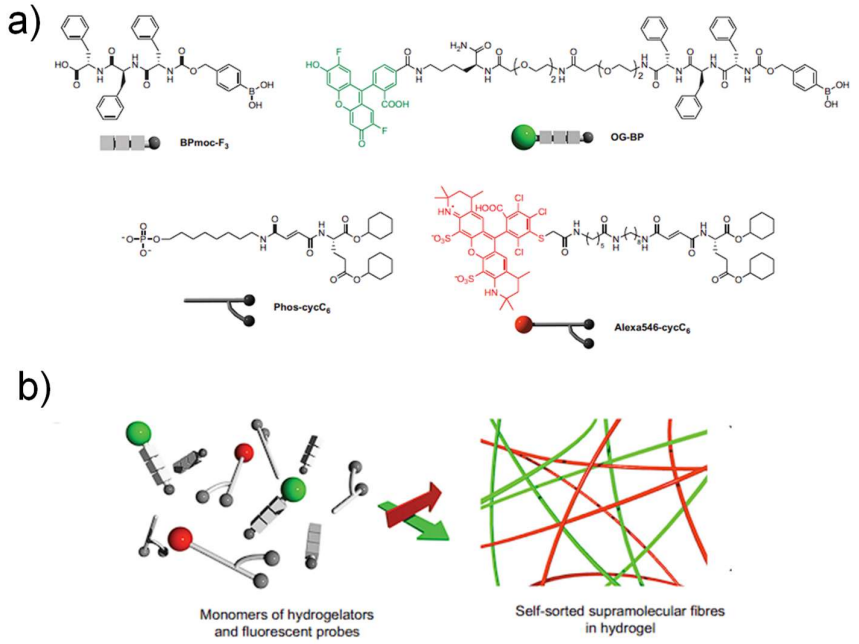

Figure 1.19 a) Molecular structures of the hydrogelators (BPmoc-F$_3$ and Phos-cycC$_6$) and fluorescent probes (OG-BP and Alexa546-cycC$_6$) and b) Schematic representation of the self-sorting phenomenon.[157]

Towar *et al*. reported peptide-based multichromophoric hydrogelator systems.[158] The self-sorting and co-assembly can be influenced by altering the kinetics of acidification. The hydrolysis of glucono-δ-lactone (GdL) facilitated a gradual decrease in pH that enabled the sequential activation of peptide components into predominantly self-sorted nanostructures due to minor pKa variations, whereas the addition of HCl results in a rapid formation of randomly co-assembled structures, which can reorganize upon aging.

1.3.3 Factors affecting self-assembly

Predicting the self-assembly modes is challenging because the self-assembly modes of individual gelators, for example, the formation of a self-sorted or co-assembled network, depend on the molecular structure and various parameters such as the gelation condition, mutual interaction, pH, external entity, and temperature.[35-38] Thus, understanding the role of the self-assembly modes in multi-component gels will help us generate functional materials with tunable properties.[37] It is crucial to study the factors that govern the self-assembly in multi-component gels. Multi-component gels obtained by mixing individual compounds that could form a gel of its own provide a better platform to study the self-assembly process in multi-component gels by correlating the gelation state properties of the individual and mixed gels.[35-38]

Smith's group has studied multi-component gels based on two LMWGs, DBS-$CONHNH_2$ and Nap-FF, which facilitate gel formation induced by glucono-δ-lactone (GdL) or calcium chloride ($CaCl_2$).[159] The selection of triggers influenced the self-assembly of Nap-FF, resulting in distinct nanoscale networks and rheological properties. GdL-triggering induced molecular-level self-sorting and network-level co-assembly, whereas $CaCl_2$-triggering resulted in both molecular-level and network-level self-sorting (*Figure 1.20*).

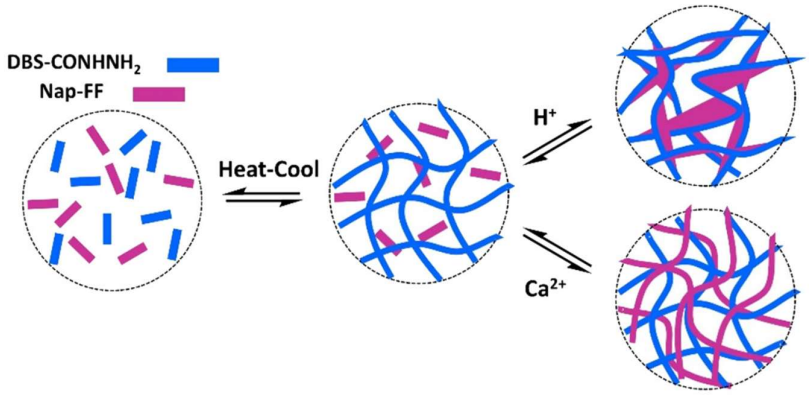

Figure 1.20 Schematic representation of multi-component assembly triggered by a heat/cool cycle to assemble DBS-$CONHNH_2$ combined with either H^+ or Ca^{2+} to assemble Nap-FF, with the choice of trigger leading to different outcomes.[159]

The self-assembly mechanisms of multi-component gels can be controlled by introducing an external agent because of their stimuli-responsive properties.[35-38] Recent research by Steed and colleagues presented another intriguing instance of combining a non-gelator with a gelator. They demonstrated that the supramolecular gel medium may be utilized to crystallize non-gelling species. For instance, the bisurea gelator and the crystallization

substrate carbamazepine, which serves as an anticonvulsant.[160] The two components (1.0 wt/v%) were dissolved in toluene by slow heating, resulting in a gel upon cooling, with carbamazepine crystals visible emerging after 8–12 hours. The comparison of the mechanical properties of the gel, with and without 1.0 wt/v% drug, indicates that the external entity did not affect the storage modulus but significantly increased the yield stress (*Figure 1.21*). The authors proposed that this effect may result from a reinforcing effect of the drug's crystals on the gelling network. The utilization of a supramolecular gel as the crystallization medium presents a distinct advantage over a regular polymer gel, as the reversible characteristics of the supramolecular gel facilitate the easy release of the crystal. The authors demonstrate that this is achievable by the incorporation of acetate anions, which are recognized for their ability to disrupt bisurea gelators.

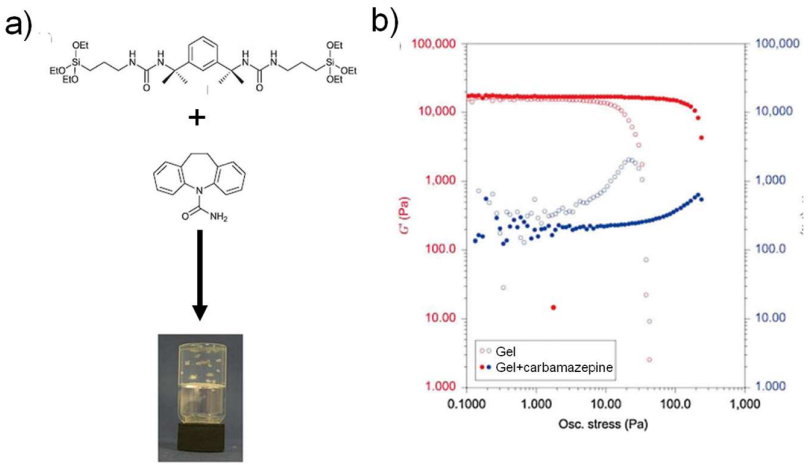

Figure 1.21 a) Gel phase crystallization of carbamazepine and b) Oscillatory sweep experiments of the gelator with and without the presence of the carbamazepine.[160]

The self-assembly mechanism can also be influenced by controlling the pH. Adam and co-workers have shown that self-sorting or co-assembly modes can be achieved by varying the hydrophobicity using the pH switch method.[161, 162] Adam's group illustrated the ability to alter the composition and characteristics of multi-component gels via pH change, resulting in diverse morphologies and complex structures (*Figure 1.22*).[162]

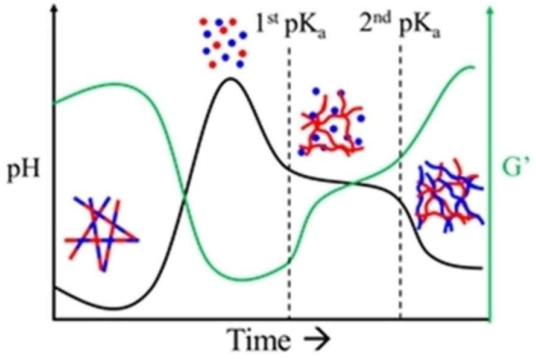

Figure 1.22 Switching from co-assembled to self-sorted fibers via change in pH.[162]

The self-sorted network was observed via two steps as the process was influenced by the pKa of the individual components (*Figure 1.22*). Their study investigated the transition from co-assembled to self-sorted systems, demonstrating alterations in microstructure, stiffness, and composition influenced by the annealing process. The self-assembly in multi-component systems was thus observed to be influenced by the nature of non-covalent interactions, pH, and foreign particles, however, the self-assembly can be controlled to a certain extent by the structure of the gelling components.[35-38]

1.3.4 Structurally non-similar components

Self-sorting behavior is mostly observed when structurally non-similar components are mixed. However, mixing donor and acceptor species tends to form co-assembly. Self-assembly driven by charge transfer interactions has been extensively investigated due to its promising applications in organic photovoltaics, sensing, ferroelectricity, and semiconductors.[163-165] Charge-transfer complexation has been employed in the development of several supramolecular architectures, including organogels, rotaxanes, catenanes, and liquid crystalline solids.[166-168] The self-assembly in the donor-acceptor pair occurs due to the charge transfer (CT) interaction between the highest occupied molecular orbital (HOMO) of the donor to the lowest unoccupied molecular orbital (LUMO) of the acceptor.[169]

The choice of non-similar components is mostly seen with the donor-acceptor system since the molecules interact via a charge transfer mechanism rather than their structural similarity. Charge-transfer interactions that produced gelation in multi-component systems comprising bile acids and trinitrofluorenone had first been documented in 1999 by Maitra's group, who demonstrated that the configuration of the donor unit on the bile acid backbone was pivotal to the gelation process.[167] The location of the pyrene unit on the bile acid appeared to be critical for gel formation (*Figure 1.23*).

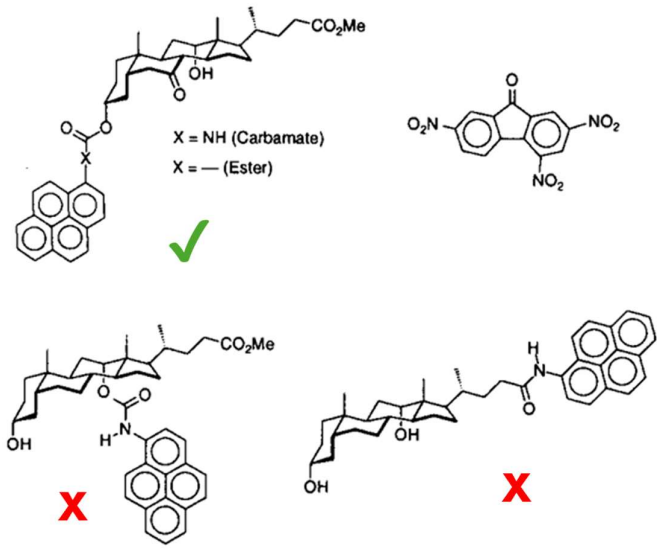

Figure 1.23 Green tick refers to pyrene based bile acid, which forms gel with trinitrofluorenone, but the red cross mark refers to molecules that failed to form gel with trinitrofluorenone.[167]

Das and Ghosh indicated that a naphthalene-based gelator (donor moiety) can be combined with a naphthalene diimide-based gelator.[170] The gels produced from the individual components were transparent and pale yellow, respectively. The development of a charge transfer complex upon mixing demonstrated specific co-assembly, yielding a deep red gel. A distinct mixture was designed with an anticipation of self-sorting to occur. The gel appeared pale yellow, indicating a lack of charge transfer, revealing self-sorting (*Figure 1.24*).

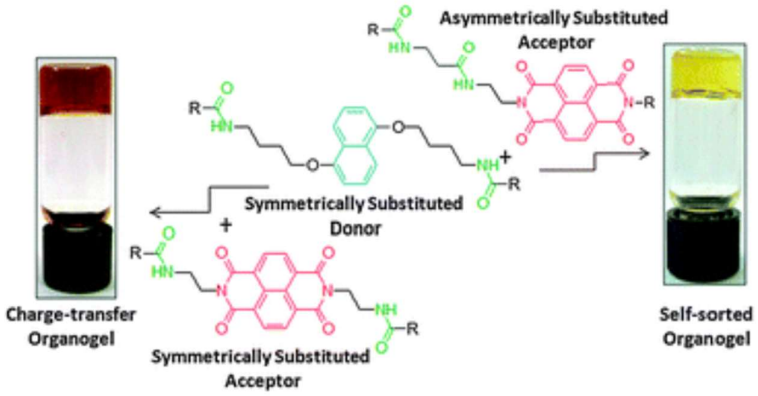

Figure 1.24 Gel formation by mixing naphthalene-diimide (NDI) acceptor and dialkoxy-naphthalene (DAN) donor-based moieties.[170]

Zhibo Li's group studied the effects of conjugated aromatic core in the donor and acceptor, which influenced the co-assembly via CT interactions.[171] The size of the aromatic core from the acceptors was found to have a significant impact on the fiber width of the organogels. The larger the aromatic core, the higher the π-π interaction and the corresponding CT gel formed fibers with less width (*Figure 1.25*).

Figure 1.25 Yellow block represents donor moiety, and blue blocks represent acceptor moieties, dense fiber formation with less width when the size of the blue block was large.[171]

The self-sorting phenomena between donor and acceptor moieties are crucial, potentially resulting in distinct bundles of fibers exhibiting *p*-type and *n*-type features for efficient electron transfer and charge carrier transport. Ghosh *et al*. documented a variety of bis-amide functionalized donor and acceptor moieties and examined the influence of spacer length on self-assembly and gelation.[172] When the distance between the bis-amide is inconsistent, the donor-acceptor (D-A) pair experiences self-sorting, as evidenced by π-π stacking and hydrogen bonding interactions between the amide functionalities of D-D or A-A.

1.3.5 Structure similar components (enantiomers)

Structural similarity is a fundamental feature that significantly influences the interactions among individual components in multi-component gels. A combination of enantiomeric gels can facilitate self-recognition at the molecular level, owing to the structural similarity of the components, leading to gels with enhanced packing and advantageous features not accessed by individual enantiomeric gels.[69, 156, 173-192] Multi-component gels with such structurally similar components will mostly favor co-assembly[63, 161, 173-177, 193-196]; however, if the individual components display favorable interaction among themselves, self-sorting will be observed.[187, 189, 197, 198] In rare cases, co-assembled and self-sorted fibers are formed in multi-component based enantiomeric gels.[69, 190, 191] Damodaran and coworkers showed enhanced thermal and mechanical strength with the mixed enantiomeric gels compared to the enantiomeric or racemic gels in a bis(urea) system tagged with phenylalanine methyl ester (*Figure 1.26*).[69] The increase in the mixed gel strength was attributed to the enhanced intermolecular forces between the racemate and the enantiomer and the combination of self-sorted and co-assembled enantiomers in the mixed gel.

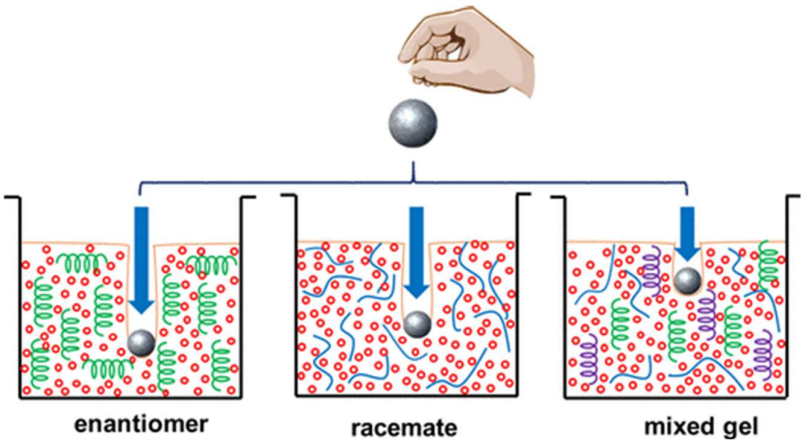

Figure 1.26 Demonstrating the enhanced mechanical strength of the mixed gel in comparison with the racemate and enantiomeric gels.[69]

The same group has also shown that mixing components leads to specific co-assembly in multi-component gels based on enantiomers and reported the first structural evidence of co-assembled gelators using X-ray diffraction analysis in equimolar mixed enantiomeric gels (*Figure 1.27*).[175]

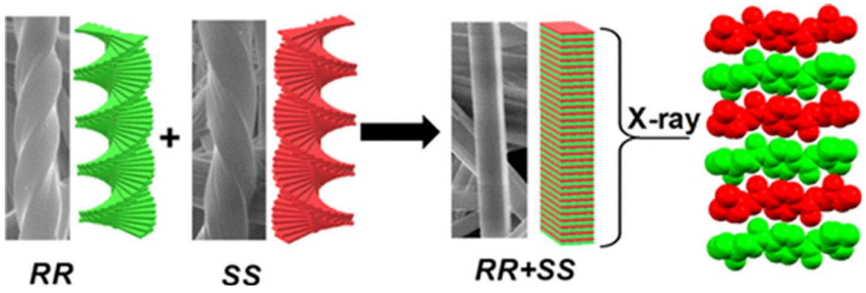

Figure 1.27 Self-assembly in mixing enantiomeric gels to form the mixed gels with the specifically co-assembled network, supported by SEM and SC-XRD analysis.[175]

Banerjee *et al*. studied the self-assembly in an equimolar mixture of an N-terminally protected amino acid Fmoc-(L/D)Glu and (L/D)Lys (Glu: Glutamic acid, Lys: lysine) that formed hydrogels via co-assembly by utilizing acid–base type interaction (electrostatic interaction), hydrogen bonding and aromatic π–π stacking interactions (*Scheme 1.9*).[187] However, on mixing all four components, i.e., [(Fmoc-(L)Glu + (L)Lys) + (Fmoc-(D)Glu + (D)Lys)] also formed hydrogels. Self-sorting was observed with almost equal amounts of left- and right-handed helical nanofibers, as confirmed by AFM images.

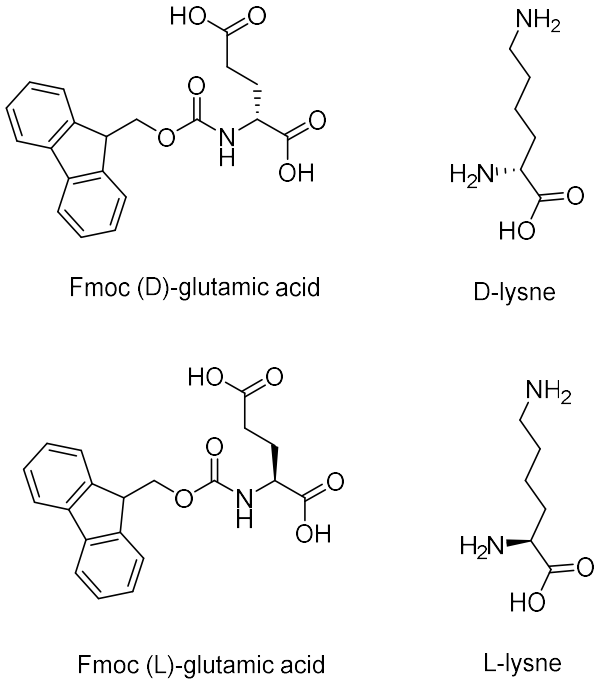

Scheme 1.9 Chemical structures of Fmoc-(L/D)Glu and (L/D)Lys (Glu: Glutamic acid, Lys: lysine).[187]

1.4 Characterization of individual and multi-component gels

To define a gel, it is essential to determine the principal interactions at different length scales. Characterizing supramolecular gels across various length scales is challenging due to the dynamic nature of the non-covalent interactions that construct the gelator molecules. A wide range of methodologies is employed to extract information regarding self-assembly, and combining multiple methods yields an enhanced understanding of the self-assembly process. Each characterization method possesses distinct advantages and limitations. Here, we discuss some standard techniques used to characterize the self-assembly modes in gelation. As we observed in Scheme 1.5, the primary level assembly is associated with molecular aggregation via various non-covalent interactions. Various spectroscopic technologies such as NMR, UV-visible, fluorescence, FT-IR, and circular dichroism are used to investigate the molecular level assembly.[115, 199]

Changes in chemical shift can be noticed, accompanied by the formation of supramolecular gels triggered by non-covalent interactions. However, ^{1}H-NMR exhibits significant constraints in examining the interactions among gelators in the gel state owing to limited mobility. Escuder and co-workers employed HRMAS ^{1}H-NMR to characterize the conformational behavior of supramolecular gels produced from valine to elucidate the structures and properties of the molecular aggregates inside the fibrillar network.[200] The supramolecular gel has pH- and thermoresponsive properties, demonstrating effective reversibility in gel-sol phase transitions triggered by thermal changes or the addition of base and acid. Consequently, pH-responsive assembly and disassembly processes were validated by ^{1}H-NMR spectra. Solid-state NMR serves as an effective technique for examining the molecular structure of hydrogels in a gel-like solid phase, utilizing methods such as magic-angle spinning (MAS) NMR.[201, 202] Rutgeerts *et al*. employed variable-temperature NMR to examine the gel-sol transition of supramolecular hydrogels derived from a bis-urea compound. They conducted NMR on the material at temperatures ranging from 30.0 to 90.0 °C in increments of 10.0 °C (*Figure 1.28*). As the temperature was raised, the hydrogel transitioned from a gel to a solution, and the NMR peaks narrowed and shifted slightly upfield, indicating enhanced proton mobility.[203, 204]

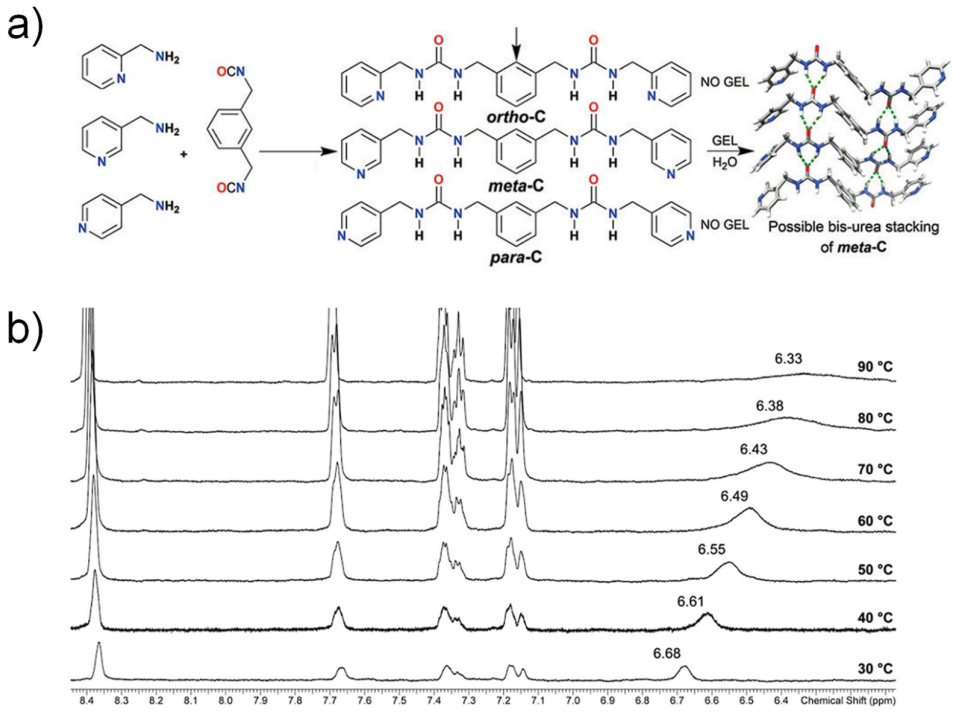

Figure 1.28 a) Synthesis of the novel low molecular weight hydrogelator, meta-C, and other derivatives, para-C and ortho-C and b) Variable temperature ^{1}H NMR spectra of meta-C.[203]

Damodaran's group has studied solid-state NMR to analyze the self-assembly in enantiomeric multi-component gels. The solid-state ^{13}C NMR of enantiomeric 1R and 1S xerogels were identical due to the similar three-dimensional packing in these structures.[69] However, they observed that the self-assembly in the racemate (1-rac) is different from its enantiomers, but the mixed gel 1R+1S network is a mixture of fibers from both enantiomers

and the racemate, as the NMR spectra matched with both enantiomers and racemate, indicating the presence of both self-sorted and co-assembled fibers in 1R+1S (*Figure 1.29*).

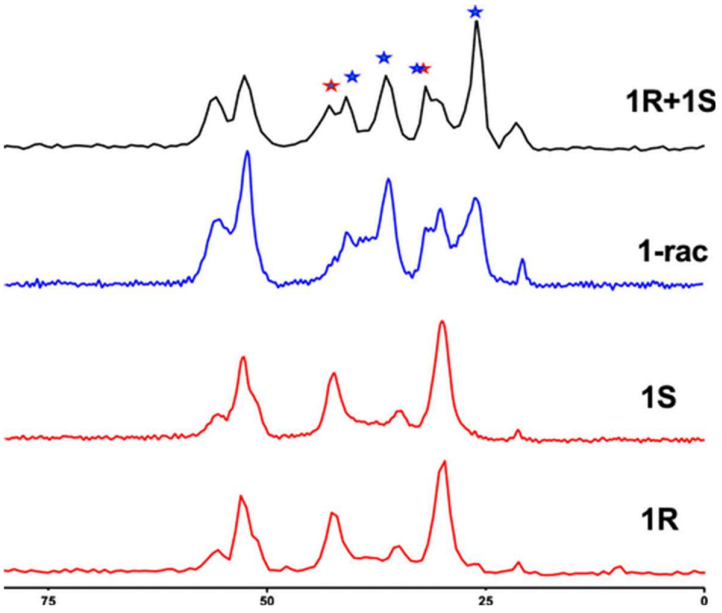

*Figure 1.29 Comparison of the solid-state ^{13}C NMR of 1R, 1S, 1-rac, and 1R+1S (*indicates the corresponding peaks in enantiomers and racemate).*[69]

UV-Vis spectroscopy is extensively employed in the characterization of supramolecular gels since it can recognize changes in the hydrophobicity of the environment around a specific group within the gelator and reveal the non-covalent interactions.[205-210] Gunnlaugsson and coworkers studied the complexation of their terpyridine-based tripodal ligand with $EuCl_3$ using UV-visible spectroscopy, which resulted in luminescent hydrogels (*Figure 1.30*).

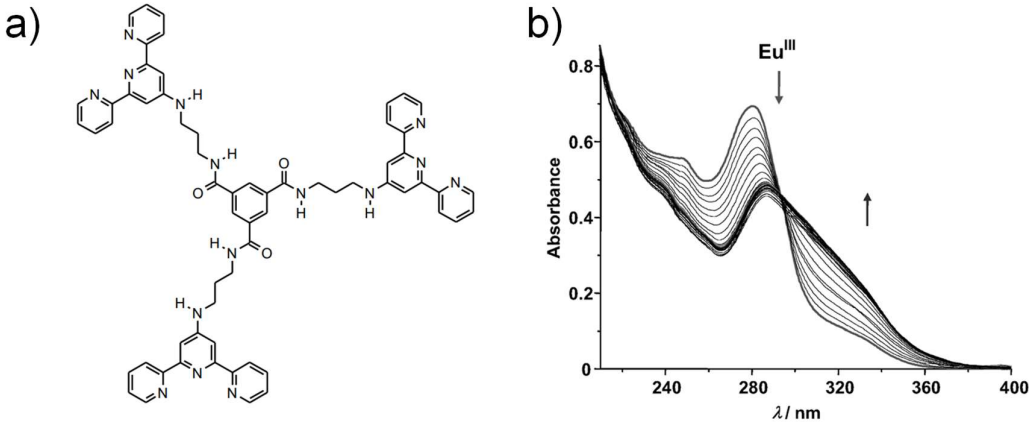

Figure 1.30 a) Chemical structure of the ligand and b) Changes in absorption of ligand ($1x10^{-5}$ M) upon titrating with $EuCl_3$ (0-9 equivalents) in methanol at 298 K.[210]

The absorption spectrum of ligand L ($1x10^{-5}$ M) in methanol solution showed an absorption maxima at approximately 280 nm, assigned to the tpy π—π transition. Upon the addition of

$EuCl_3$, a bathochromic shift arising from Eu(III) ions was observed, with the appearance of a shoulder peak at approximately 320 nm, thereby indicating the formation of a (Eu/L) complex (*Figure 1.30*).[210]

Supramolecular hydrogel characterization can be achieved by comparing the differences in the FT-IR spectra of solution and gel forms. This evaluates the bonds that have appeared or disappeared, allowing the identification of the driving force for gelation.[211, 212] Xingyi Li's group has studied the hydrogelation of the compound succinate paclitaxel (PTX-SA) using FTIR. The stretching vibrations at 1650 and 1738 cm^{-1} corresponded to carbonyl groups of -COOH and -COO- groups, respectively.[211] The reduction in the strength of the stretching vibration at 1738 cm^{-1} was attributed to the self-hydrolysis of ester bonds in PTX-SA during hydrogelation. Furthermore, the new stretching vibration at 1578 cm^{-1} was associated with the hydrogel's ionization of the carboxylate group (*Figure 1.31*).

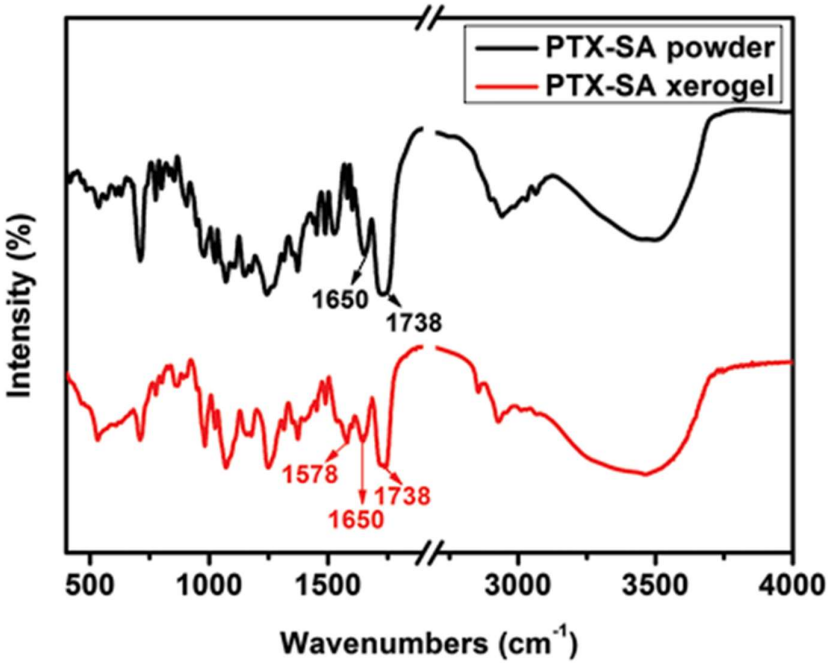

Figure 1.31 FTIR spectra of PTX-SA powder and PTX-SA xerogel.[211]

The molecules aggregation leads to the formation of 1-D fibers, and the fiber level assembly can be studied using various microscopic techniques such as scanning electron microscopy (SEM), transmission electron microscopy (TEM), atomic force microscopy (AFM), and circular dichroism (CD).[213] Also, it includes specific modern techniques such as small-angle X-ray scattering (SAXS) and small-angle neutron scattering (SANS).[214] Scanning electron microscopy (SEM) is a powerful imaging technique used to analyze the surface topology of the dried gel utilizing an electron beam, which produces secondary electrons upon interaction with the sample.[115, 199]

Damodaran and coworkers studied the self-assembly of enantiomeric amino acid-based low-molecular-weight gelators (MVBTA) using SEM analysis. The chirality of the molecules was observed to be transcribed into their hierarchical gel fibers (*Figure 1.32*). Twisted fibers were observed with the enantiomeric xerogels, while the mixed gel displayed tape-like or needle-shaped morphologies (*Figure 1.32*).[215]

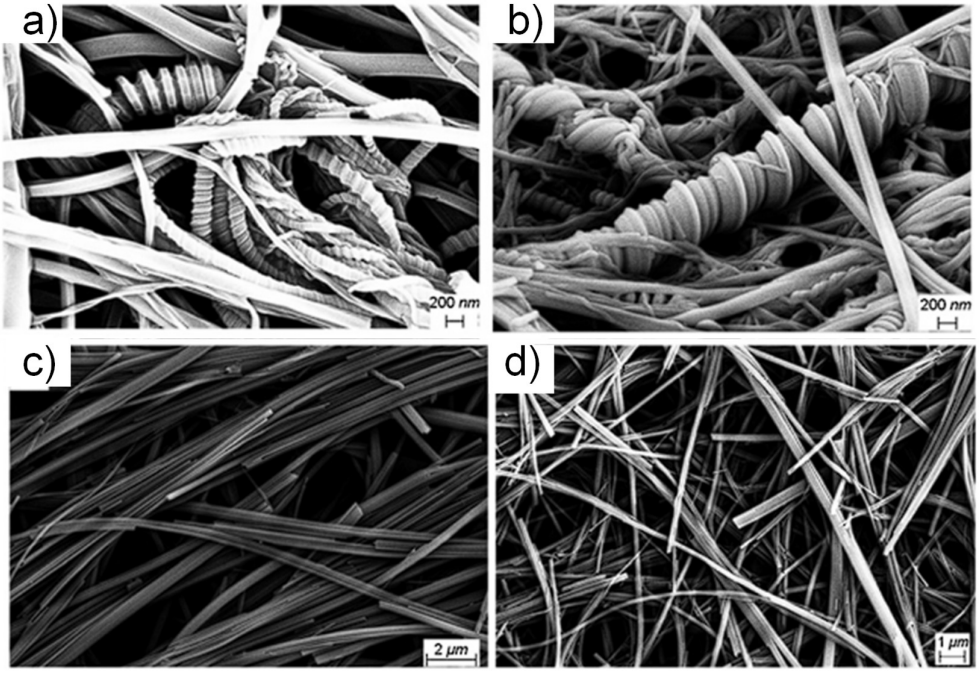

Figure 1.32 SEM images of the enantiomeric xerogels of MVBTA (at 2.0 wt/ v%), a) R and b) S enantiomers in mesitylene, and mixed enantiomeric xerogels (at 2.0 wt/ v%) c) mesitylene and d) o-xylene.[215]

On the other hand, TEM requires samples to be very thin to allow the electrons to pass through. TEM has a higher resolution compared to SEM, which helps to fetch information about internal structure, crystal structure, and defects.[216, 217] AFM utilizes a sharp tip attached to a flexible cantilever, which interacts with the sample's surface to be measured. A laser beam is used to measure the deflection of the cantilever and finally constructs the sample's surface, which gives valuable information about the surface roughness, texture, and other physical properties.[218, 219] Circular dichroism is often used to monitor the self-assembly process of fibers, as helpful information about the secondary structure and chiral properties can be analyzed.[220] Small-angle X-ray scattering (SAXS) is a powerful analytical technique used to study the structure of materials at the nanoscale. It involves measuring the intensity of the scattered X-rays at small angles.[221] SAXS usually provides valuable information about the size, shape, and distribution of particles.[222] SANS utilizes neutrons instead of X-rays to analyze the structure of materials at the nanoscale.[223] Since it utilizes neutrons, it interacts with atomic nuclei, making SANS effective for studying lighter elements.[214, 224]

Our group has performed SANS to compare the packing between enantiomers and mixed gels. SANS experiments in toluene-d_8 with enantiomeric and mixed gels, showed a

completely different pattern with the mixed gel (1R+S) compared with the enantiomeric gels (1R or 1S) which strongly implies the presence of co-assembled network (*Figure 1.33*).[215]

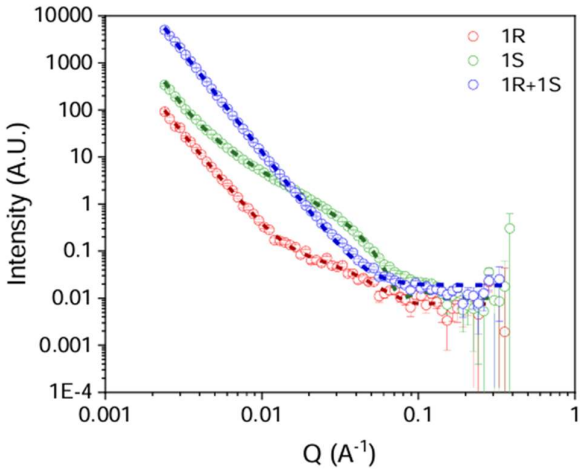

Figure 1.33 SANS for 1R, 1S, and 1R+1S in aromatic solvent, toluene-d_8.[215]

The predominant tool for elucidating information on network-level assembly is rheology. The network-level assembly of the gelators results from the entanglement or cross-linking of the fibers. Rheology quantifies the solid-like properties of the semi-solid soft material when subjected to external stress or strain.[225, 226] An amplitude sweep experiment will provide you with details about the maximum strain that can be applied to a particular gel, while frequency sweep experiments can be used to compare the mechanical strength of the gels. Adam's group has worked with a known gelator 1ThNapFF which gelled in DMSO/water (1:4, v/v) at 0.2 wt/v% (*Figure 1.34*).[227]

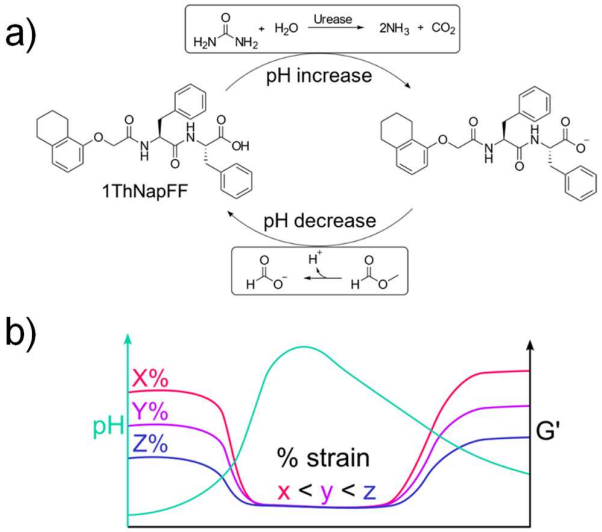

Figure 1.34 a) The compound 1ThNapFF undergoes deprotonation in the presence of urea and urease, and then the base-catalysed hydrolysis of methyl formate reduces the pH and regenerates the structure of 1ThNapFF and b) G' profile of a dynamic system undergoing gel-to-sol-to-gel transition.[227]

A gel-to-sol-to-gel process is constructed using urease, urea, and methyl formate. The pH increases within 20 minutes upon adding urea and urease, leading to a sol phase transition (*Figure 1.34*). A pH-triggered gel forms when the pH falls below the gelator's apparent pKa (~6.3) in the presence of hydrolysis of methyl formate.

Damodaran and coworkers showed that mixing enantiomeric gels based on bis(urea) compounds leads to mixed gel with enhanced mechanical strength.[69] The mechanical strength of all gels was assessed by measuring the force necessary to penetrate a certain distance into a gel, resulting in a force versus distance graph. The results showed that a larger force was observed with the mixed gel 1R+1S compared with enantiomeric 1R, 1S, and 1-rac gels. Furthermore, an increased area under the curve signifies a more robust structure, as showed by the 1R+1S, suggesting that this gel exhibited superior strength relative to the other systems (*Figure 1.35*).

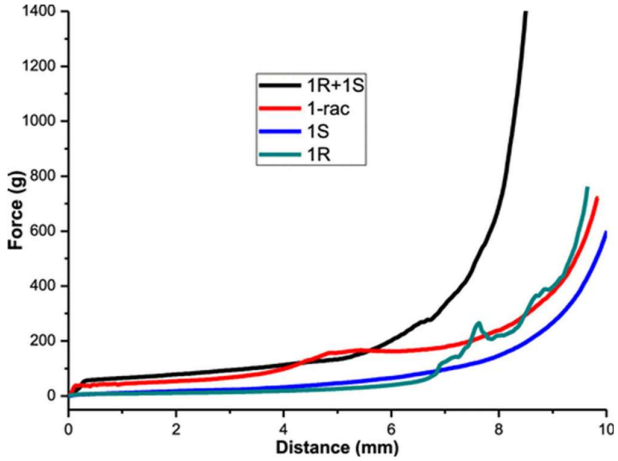

Figure 1.35 Comparison of mechanical strength for gels 1R, 1S, 1-rac, and 1R+1S in toluene at 5.0 wt %.[69]

Single crystal X-ray diffraction (SCXRD) analysis of the gelator molecules can give us valuable information about the solid-state interactions.[121-124, 129, 228-230] Pfeffer's group has studied the gelation behavior in enantiomeric phenylalanine functionalized norbornene using SCXRD, while the racemic form turned to be a non-gelator.[231] Adam and coworkers studied the self-sorting behavior in a multi-component dipeptide based gel by analyzing the crystals formed within the gel.[232] Their analysis revealed that the gel grown crystals matched the cell parameters and afforded an isostructural single crystal phase with the crystals of the individual gelator. SCXRD analysis on the fibrous crystals formed in the gel revealed that the helical assembly responsible for the gel formation was controlled by the chirality of the phenylalanine functionality. When the single crystal structure of the gelator is accessible, one may examine the nature of various solid-state interactions and can generate a simulated powder X-ray diffraction (PXRD). This powder pattern is compared with the PXRD pattern acquired from either the native gel or xerogels or bulk materials to understand the purity of the bulk material and identify key interactions that hold the gel network. Nevertheless, the crystal structure of a gelator does not consistently reflect the molecular arrangement inside gelator fibers, and in certain instances, the extraction of solvent from the gel network may lead to artifacts.[233-235] This remains one of the most effective methods for analyzing the involvement of non-covalent interactions in the self-assembly of a gelator. Damodaran and

coworkers have showed the crystallographic evidence of the self-assembly process in multi-component gels derived from amino acid derivatives, demonstrating that the structural similarity of the enantiomers can facilitate specific co-assembly (*Figure 1.36*).[175]

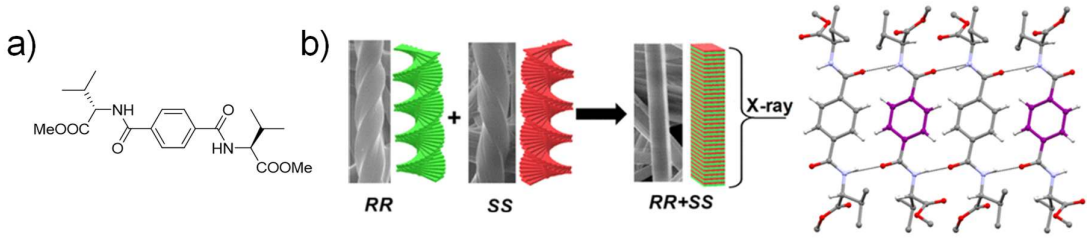

Figure 1.36 a) Chemical structure of the gelator and b) mixing enantiomers (1:1) to obtain specific co-assembly.[175]

At the same time, combining experimental approaches with computational modelling and simulations will also assist current-day research in obtaining more details and provide an outlook for their expanded use in future studies.

1.5 Application of Supramolecular gels

Supramolecular gels possess a wide range of potential applications owing to stimuli-responsiveness, self-healing, and biocompatible properties. In biomedical applications, supramolecular gels can be used for drug delivery, as the gels encapsulate and release drugs in a controlled manner by targeting specific organs in the body.[236] Gels can act as scaffolds for cell growth and tissue regeneration in tissue engineering. [237, 238] The porous nature of the gels allows for nutrient and oxygen transport, supporting cell growth. [239] Supramolecular gels can be loaded with antimicrobial agents for wound healing purposes.[240-242] Supramolecular gels act as sensors as they can detect heavy metal ions, toxic gases, or other pollutants.[243, 244] These are analyzed by studying the optoelectronic properties of gels. These gels have also been found to be useful in the cosmetics and food industry as thickening, stabilizing, and emulsifying agents.[245-247] The self-assembled fibers can also act as catalytic sites.[248] Chiral gels can be used for asymmetric synthesis and chiral recognition purposes.[249, 250] Supramolecular gels are also used as a medium for crystal growth.[79] Gel fibers serve as nucleation-templating surfaces that facilitate epitaxial growth and affect crystallization outcomes through molecular recognition.[251] The doctoral thesis is mainly focused on using LMWGs as antibacterial agents and sensors and as a media for the crystal growth of polymorphic drugs.

1.5.1 Antibacterial activity

Pathogenic bacteria in vulnerable interfaces or wounds can result in infection, leading to a substantial rise in toxins that may considerably prolong or disrupt the healing process. This issue is further intensified by the escalating global antimicrobial resistance dilemma, wherein antimicrobial agents conventionally employed to restrict, avert, or eradicate pathogenic microbial proliferation have become ineffective.[252] Supramolecular hydrogels have shown great potential towards antimicrobial therapy. Generally, these supramolecular

structures exhibit biocompatibility and ease of degradation. Hydrogel systems accelerate wound healing due to their resemblance to the extracellular matrix and their capacity to retain substantial amounts of water, hence maintaining moisture in the wound region.[253] Supramolecular gels can facilitate antibacterial activity via two methods: (a) gels can be used to encapsulate antimicrobial agents and provide controlled release over time, and (b) proper design of the gelator molecule can result in gels with inherent antimicrobial properties.[87, 253-262] Encapsulating and releasing the drug/antibacterial agent can be attributed to the stimuli-responsive character of the hydrogels which can trigger the target-oriented release of the drug agents. Supramolecular gels formed via non-covalent interactions allow the drug to get encapsulated in the gel matrix, protecting it from degradation. The gel can be predesigned to optimize encapsulation and release of the drug of interest. The gel matrix facilitates the slow diffusion of the antibacterial compound, ensuring a continuous release over time. This is essential for sustaining optimal concentrations of the agent at the infection site, and finally the gel breaks in response to surrounding factors such as temperature or pH. Supramolecular gels can encapsulate several antibacterial drugs or integrate them with additional therapeutic agents, potentially resulting in synergistic effects that improve overall antibacterial efficacy.

Supramolecular gelators which have peptides or drug-like moiety in their gelator structure have numerous advantages.[253] Antimicrobial peptides (AMPs) constitute a unique category of supramolecular peptides that can self-assemble in water to form hydrogels exhibiting antibacterial capabilities.[263] The improved antibacterial properties of AMPs allow them to demonstrate bactericidal activity against various multidrug-resistant pathogens.[264] The antibacterial action comprises three primary steps: a) The initial stage involves the formation of electrostatic interactions between the cationic groups of peptides and the bacterial outer membrane, b) subsequent accumulation of these peptides on the bacterial surface, and c) the insertion of these accumulated peptides into the bacterial cell wall, thereby disrupting the structural integrity of bacterial cells.[265, 266] Picchio and coworkers developed pyrogallol-based supramolecular hydrogels (*Figure 1.37a*) for the controlled topical delivery of hydrophobic drugs such as silver sulfadiazine (SSD).[267]

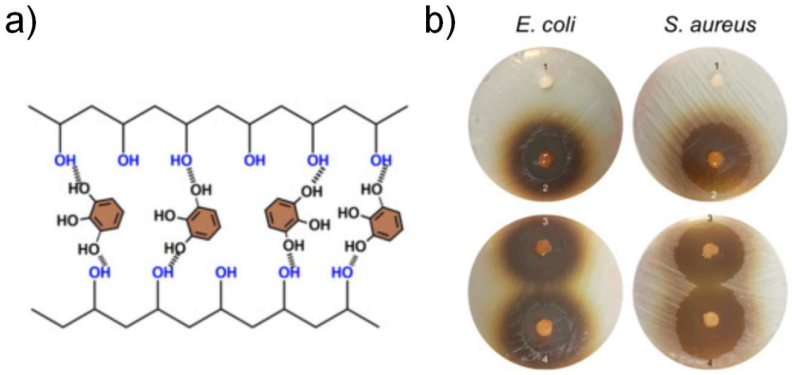

Figure 1.37 a) Schematic representation of hydrogel's structure and b) Antimicrobial activity of (top to bottom) PVA, $HG_{0\%}$, $HG_{5\%}$, and $HG_{5\%}$ loaded with SSD against E. coli and S. aureus.[267]

Their study focused on the capacity of hydrogels (HG) to release SSD in reaction to proteases, which are overexpressed in non-healing wounds. This technique facilitates target-

specific drug release, thus improving therapeutic effectiveness. Antibacterial studies revealed the activity of the hydrogel against *S. aureus* and *E. coli*, which can be attributed to the presence of polyphenols (*Figure 1.37b*). The hydrogels exhibited a sustained release profile of SSD over 24 hours in vitro. Biocompatibility assays utilizing mouse fibroblast cells demonstrated no substantial reduction in cell viability.

Xu's group has developed a hydrogelator based on Vancomycin by introducing a pyrene group to the C-terminal of the backbone of Vancomycin. Vancomycin–pyrene had significantly greater potency, about three orders of magnitude higher, than its precursor, vancomycin, against vancomycin-resistant enterococci. This was attributed to the occurrence of self-assembly and aggregation locally on the bacterial cell surface.[268] Pyridine *N*-oxide-based compounds were previously reported to show antimicrobial activity.[268, 269] Our group has demonstrated that the pyridyl *N*-oxide based hydrogelators exhibit antibacterial activity against Gram-positive and Gram-negative bacteria (*Figure 1.38*).[116]

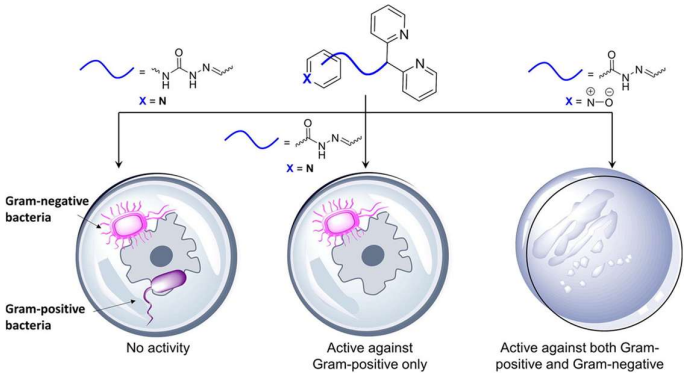

Figure 1.38 Schematic representation of the antibacterial properties of various compounds.[116]

1.5.2 As a crystal growth media

Before analyzing gel as a crystallizing media, it is crucial to understand the process of gelation vs crystallization. Gelation resembles crystallization as both have similar nucleation points in the solution (*Scheme 1.10*).[270-272]

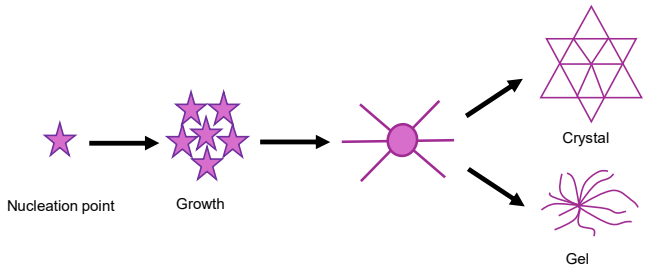

Scheme 1.10 Competition of crystalline network and gel fiber formation from similar nucleation point.

Crystals are formed through the highly ordered arrangement of molecules in three dimensions, while gels arise from the self-assembly of gelators in one dimension to create fibrils that eventually entangle into a three-dimensional network. [74, 273] The processes of crystallization and gelation are significantly influenced by molecular structure, solvent choice, and external stimuli, and the formation of gels and crystals is often unpredictable. [27, 233, 271]

Gel phase crystallization represents an example of orthogonal self-assembly of the crystals and gel network.[27] The gel medium prevents sedimentation and limits convection by providing continuous and diffusion-limited growth.[274, 275] The gel surface is an additional component in the crystallization media, and its chemical composition may influence crystal nucleation, growth, or both processes. LMWGs have been used to crystallize inorganic substances, proteins, and active pharmaceutical ingredients, and the gel environment can influence factors such as crystal habit and polymorphism.[35, 37, 232, 276-278]

The method of crystal growth in gels originated from the research of German chemist Raphael Eduard Liesegang, who noted the notable periodic precipitation in gels referred to as 'Liesegang rings' (*Figure 1.39a &b*). These exquisite patterns emerge from the periodic deposition of a sparingly soluble salt, such as silver(I) chromate, when a soluble precursor, such as silver(I) nitrate, diffuses through a hydrogel containing potassium chromate.[279]

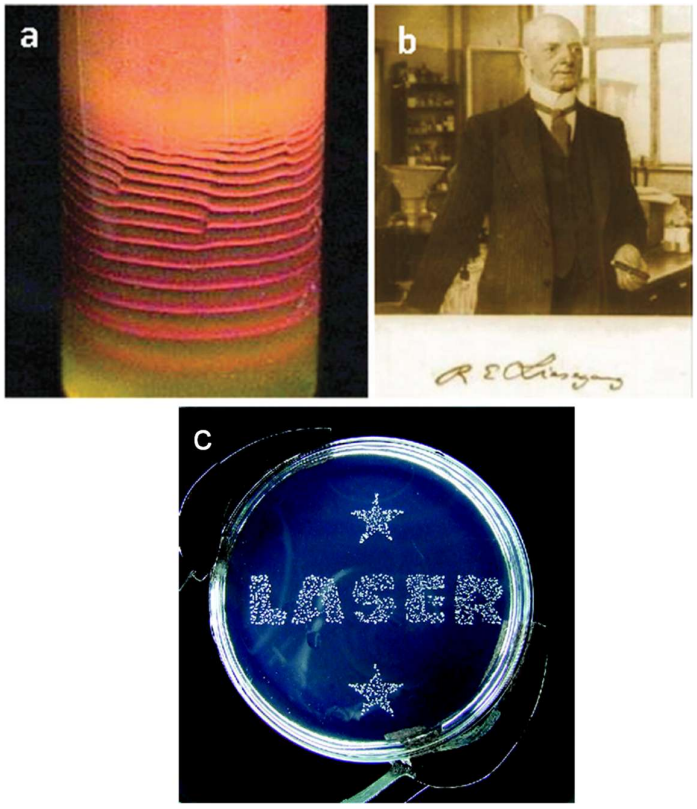

Figure 1.39 a) Liesegang rings,[279] b) Raphael Eduard Liesegang and c) photograph showing spatial control of laser-induced nucleation of KCl in an agarose gel.[280]

Alexander and co-workers reported the laser-induced nucleation of an aqueous gel that was saturated with potassium chloride. An optical mask was used to control the exposure of the gel to the laser. Only the area exposed to near-infrared laser power showed nucleation (*Figure 1.39c*).[280]

Gunnlaugsson and co-workers reported the novel technique for growing nanowires from a drop cast supramolecular gel containing common halide salts like NaCl, KCl, and KI, as the supramolecular gel stabilized the wire growth mechanism (*Figure 1.40*).[281]

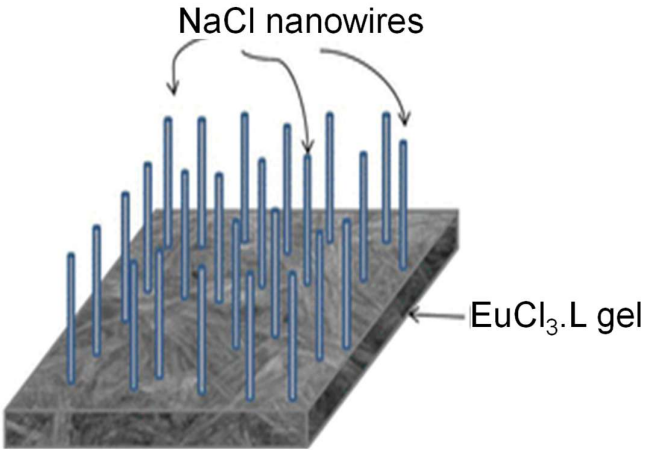

Figure 1.40 Schematic representation of formation of NaCl nanowires.[281]

The crystallization of highly polymorphic drug precursor ROY in bis(urea) based LMWGs tagged with drug mimicking functional groups led to the preferential formation of the metastable R polymorph, in contrast to the Y form produced in solution or random gels (*Figure 1.41*).[274]

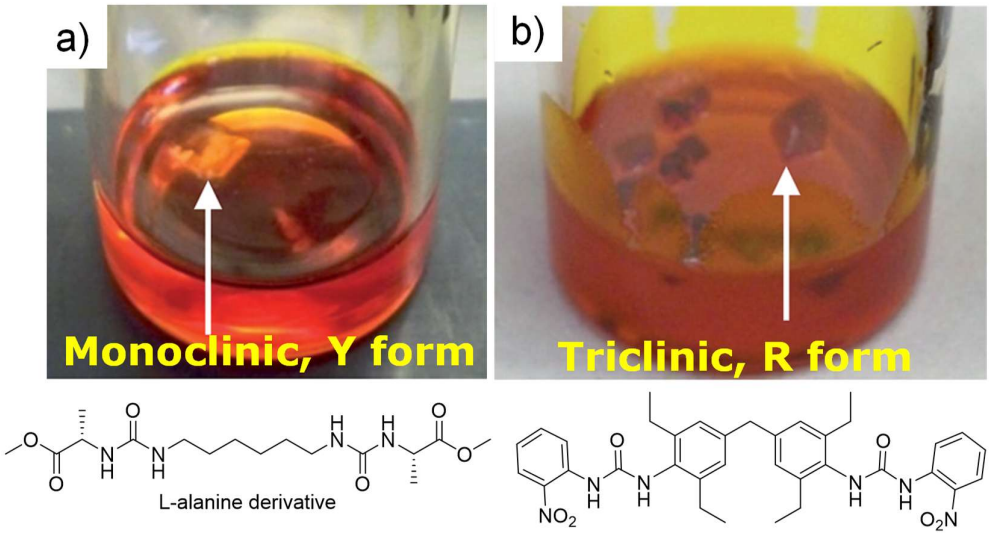

Figure 1.41 Crystallization of ROY in a) random gel and b) drug-mimicking gels.[274]

Our group reported gel phase crystallization of copper(II) isonicotinate–*N*-oxide complex, which existed in three forms. Crystallization in aqueous ethanol resulted in the formation of blue and green crystals, while the use of a L-3Nox LMWG, resulted in the selective crystallization of the blue crystals under identical conditions (*Figure 1.42*). By analyzing the solution and gel phase crystallization results, they observed that the blue form is thermodynamically stable under ambient conditions.[135]

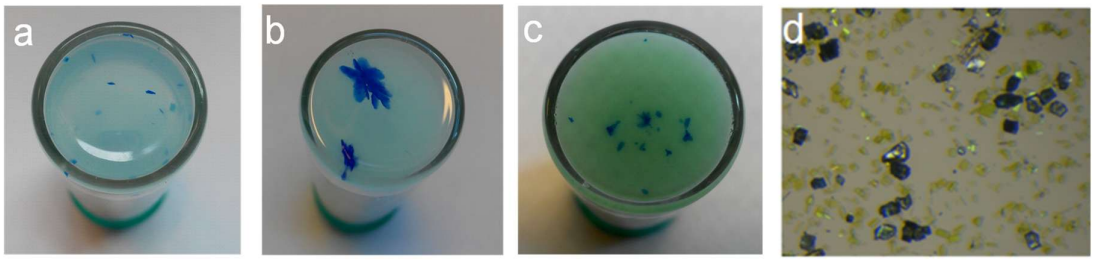

Figure 1.42 Gel phase crystallization of Cu(II) complex, a) agarose gel, b) Val-TMA, c)L-3Nox, and d) solution state.[135]

In the pharmaceutical sector, crystallization serves as an effective method to alter the characteristics of active pharmaceutical ingredients (APIs). The crystal habit and polymorphism of active pharmaceutical ingredients (APIs) significantly influence critical pharmaceutical properties, including stability, dissolution rate, solubility, bioavailability, processing characteristics, compressibility, flowability, and surface characteristics. Therefore, controlling solid-state properties is a crucial economic and formulation challenge. Possessing methods that enhance the scope of API polymorph screening would significantly benefit the pharmaceutical sector.[282, 283]

1.5.3 Sensors

The stimuli-responsive property of the supramolecular gels extends its scope of applications in the fields of sensing, actuators, drug delivery, and optoelectronics materials. Gels are highly adsorbent materials which possess very large surface areas and are suited for the adsorption of unwanted compounds. McNeil's group employed Hg(II) to initiate the gelation of a low molecular weight gelator by interacting with a quinoaxalinone, resulting in a complex comprising two ligands and one mercury ion.[284] The same group also reported a Pb(II) sensor, as their system formed gel in the presence of lead due to the Pb-S interactions.[285] They have also triggered gelation using old paints contaminated with lead. D'Anna *et al*. utilized sugar-derived gelators to remediate Cr(VI) anions from wastewater at a neutral pH. The sugar units bonded to the chromium-based oxoanions via hydrogen bond interactions and reduced Cr(VI) into Cr(III).[286] Bhattacharya and coworkers developed a biocompatible fluorescent LMWG that experienced oxidative degradation in the presence of hypochlorite, resulting in a gel-to-sol transition and altering the fluorescence intensity (*Figure 1.43*).[287]

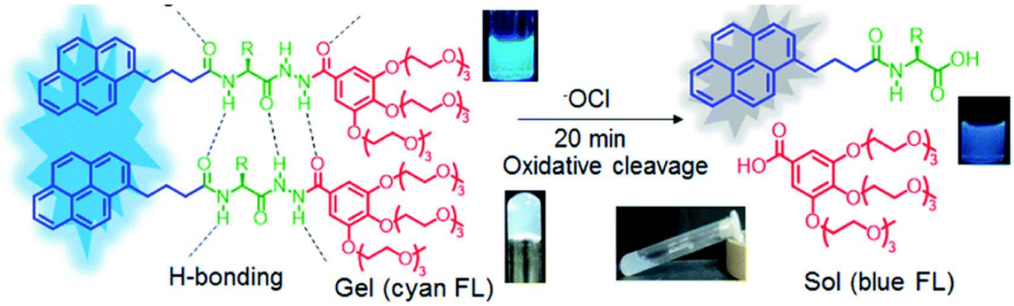

Figure 1.43 Schematic representation of the interaction of gelator with ClO-.[287]

Damodaran and coworkers also designed stimuli-responsive supramolecular gels by tuning the non-covalent interactions of functional groups. The study focused on the impact of functional groups, specifically the hydroxyl group, on the stimuli-responsive properties of the gels (*Figure 1.44*). They used a C_3-symmetric benzene-1,3,5-tricarboxamide (BTA) platform attached to the methyl ester of phenylalanine (MPBTA) and tyrosine (MTBTA) to investigate gelation behaviour.[288]

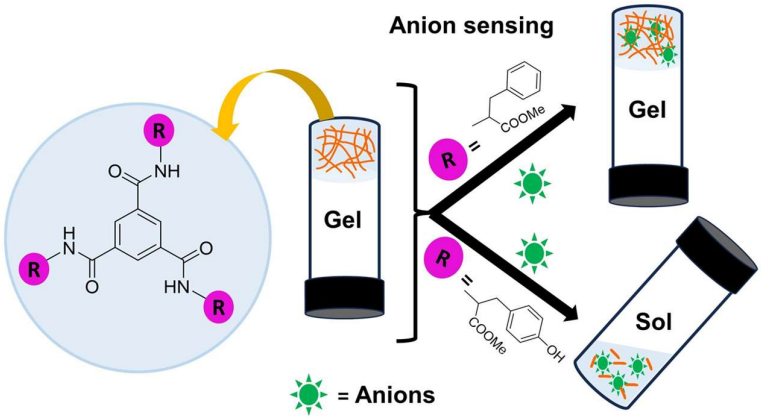

Figure 1.44 Stimuli-responsive properties of the MPBTA gels (1.4 wt/v%) and MTBTA gels (4.5 wt/v%) in DMF/water mixture (1:1, v/v) towards various sodium salts.[288]

Lloyd *et al*. studied anion-induced gelation in 1-(3-Methyl-1H-pyrazol-5-yl)-3-(3-nitrophenyl)urea, which forms hydrogels in acidic conditions (pH 1-2) (*Figure 1.45*).[130] The physical characteristics of these hydrogels, such as morphology and strength, can be altered by modifying the anion linked to the gelator.

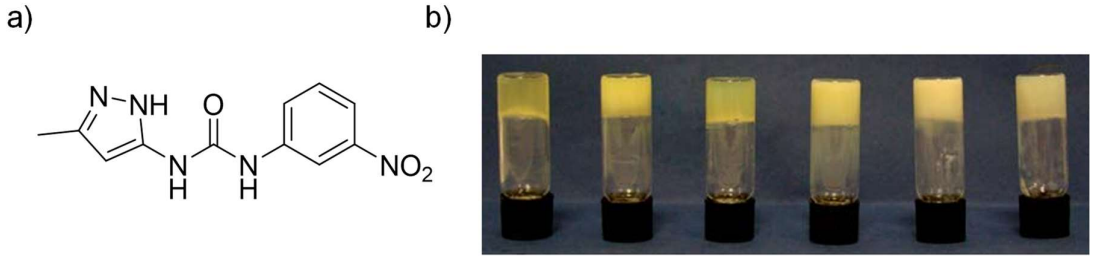

Figure 1.45 a)1-(3-Methyl-1H-pyrazol-5-yl)-3-(3-nitrophenyl)urea and b) 1.0% protonated gels in water acidified with, from left to right, $EtPO_3H_2$; $MePO_3H_2$; H_3PO_4; H_2SO_4; HPF_6 and HBF_4.[130]

Chloride salts do not produce gels, while nitrate-based gels are susceptible to crystallization. The work emphasizes the distinctive characteristics of pyrazole-based gelators in comparison with bis(urea) gelators, notably their capacity to produce stable gels under specific conditions. The same group also worked on a series of chiral bis(urea) compounds with oligomethylene spacers and S-phenylethyl end groups as low molecular weight gelators.[131] They have studied how anion complexation affected the gel properties, including the weakening of gels due to competitive anion interactions. The incorporation of tetrabutylammonium salts of various anions markedly influenced the rheological characteristics of the gels. Strongly binding anions, including acetate and halides, resulted in significant decreases in gel strength and gel dissolution at low concentrations.

1.6 Objective of the thesis

Analyzing the gel structure or controlling the gel state properties is difficult due to the dynamic nature of the non-covalent interactions, which influences the gel state properties. This dynamic nature makes them highly sensitive to external stimuli like pH, temperature, mechanical stress, and salts/ions. Consequently, comprehending the molecular self-assembly of supramolecular gels presents a formidable challenge. However, modifying the functional groups of LMWGs that play an important role in gel network formation will help to tune the gelation and is an excellent strategy for evaluating the role of specific interactions in gel formation. In this aspect, the main objective of this thesis is to study the nature, position, and spatial orientation of functional groups in dictating gel state properties in individual gels and multi-component gels.

The overall doctoral dissertation is divided into four parts. In the first part, we examined self-assembly in gels composed of a single component by evaluating the influence of specific functionalities. We have modified the functionality to tune the gelation properties. The parent pyridyl functionality was modified to the corresponding pyridyl *N*-oxides to observe hydrogelation. X-ray diffraction studies showed significant insights into the solid-state and non-covalent interactions of the *N*-oxide based gelators. Similarly, we have also studied the role of hydrogen bond functionalities in LMWGs by modifying the hydrogen bonding moieties (urea to thiourea) and analyzed the coordination-driven self-assembly. These obtained molecules were chosen to sense various metal salts, including transition metal salts, which revealed salt-induced gelation or metallogelation. Thus, we were able to study the specific role of functionalities in tuning the gelation properties.

In the second part, we analyzed the spatial orientation of functional groups in dictating gel state properties. We have studied and compared the gelation properties of isomeric molecules. Gelation properties were compared using rheology and SEM. X-ray diffraction studies were performed to confirm the spatial orientation of the functional groups. The effect of spatial orientation of functional groups was utilized for crystallizing small molecule drug-metronidazole in both the drug-mimicking and non-mimicking gelators. The results indicate that crystal habit modification arises selectively from gels based on the mimetic gelators, which confirms the specific interaction of growing crystals onto the surface of the gel fibers. Similarly, we studied the gelation properties of multi-functional carbamate based molecules and analyzed how the spatial orientation of functional groups resulted in hydrogelation. We later performed coordination-driven self-assembly by treating the molecules with certain

transition metal salts to study the antibacterial properties of all these compounds. Thus, we have studied the role of spatial orientation of functional groups in gel state properties and how it influences crystal growth.

In the third part, we have analyzed the self-assembly modes in chiral multi-component systems based on individual components with structurally similar (enantiomers) and non-similar (donor or acceptor moieties) functionalities to evaluate the role of different functional groups on the self-assembly modes in multi-component gels. We have examined the gelation of all individual chiral compounds, enantiomeric mixtures, and mixed chiral compounds based on donor and acceptor moieties and analyzed self-assembly using rheology, SEM and XRD. Computation studies were performed to study the nature of the functionalities by analyzing the electronic distribution. These results showed self-assembly process depends on the functional groups leading to self-assembled system based on hydrogen bond or donor-acceptor interaction.

In the last part, we have extensively studied the role of functionalities in multi-component gels based on enantiomers. We have incorporated various flexible and rigid functionalities of the central core of the molecule to study the effect of rigidity on the nature of self-assembly modes in mixed gels. We have studied the effect of specific functionality (phenyl moiety) in enantiomeric multi-component gels and analyzed the effect of mixed gels in the presence of salts/ions. We have also analyzed the role of the flexibility of the linker in the multi-component gels based on enantiomers. We investigated the transformation of self-assembly modes from kinetically favored orthogonal self-assembly to thermodynamically favored co-assembly, influenced by the nature of the solvent and temperature. Thus, we have shown the significant contribution of specific functionality in tuning the self-assembly modes in individual and multi-component gels. The findings of this thesis work will enlighten the chemist in designing smart materials with precisely tailored features.

2.0 Role of functional groups on the self-assembly process in individual gels

The self-assembly process of supramolecular gels depends on various parameters and various analytical techniques (spectroscopic, microscopic, and X-ray diffraction) have been used to understand the role of these parameters to evaluate the mechanism of gelation process. X-ray diffraction methods have been proven to be one of the promising tools in understanding the gelator structure and its self-assembly behavior. However, predicting the gel structure is a difficult task because of the dynamic nature of the non-covalent interactions, leading to low molecular order in the overall gel state. In this chapter, we demonstrate that modifying existing supramolecular architecture is an efficient strategy to design and synthesize supramolecular gels with tunable and predictable properties. The structural modification of the functional groups will lead to the alteration of specific interactions arising from the particular functional group, which can be considered an excellent strategy for evaluating the role of specific interactions in gel formation. The presence of multifunctional groups such as pyridyl, *N*-oxides, urea or amide makes these moieties highly responsive towards an external stimulus such as salts/ions. We have studied the effect of these salts/ions on tuning the gelation properties so as to find the sensing ability of these compounds towards certain salts/ions. We have also studied the role of hydrogen bond functionalities in LMWGs by modifying the hydrogen bonding moieties of the non-gelators (urea to thiourea). The application of these materials in sensing various metal salts including transition metal salts were evaluated, which revealed salts-induced gelation. This enabled us to analyze the role of specific functional groups in tuning the gelation properties.This chapter is divided into two sections.

2.1. Modification of the functional groups to evaluate the role of specific interactions on the self-assembly process and evaluate their application as sensors.

Article-I

The structural modification of existing supramolecular architecture is an efficient strategy to design and synthesize supramolecular gels with tunable and predictable properties. In this study, we have altered bis(pyridyl urea) molecules using various linkers, specifically hexylene and butylene, to produce their respective bis(pyridyl-*N*-oxide urea) derivatives. The gelation characteristics of both the parent and modified compounds were examined, revealing that the alteration of the 3-pyridyl moieties to their respective 3-pyridyl-*N*-oxides facilitated hydrogelation. The stability of the parent and modified compounds was assessed by sol-gel transition temperature (T_{gel}) and rheological studies, while single-crystal X-ray diffraction was employed to investigate the solid-state interactions of the gelators. The dried gels' morphologies were examined using scanning electron microscopy (SEM), which indicated that the structural alteration did not significantly affect the gel morphology. The stimuli-responsive behavior of these gels in the presence of salts in DMSO/water was assessed using rheological studies, which demonstrated that the *N*-oxides exhibited increased gel strength in the majority of cases. Nonetheless, the gel network disintegrated in the presence of chloride salts of aluminum(III), zinc(II), copper(II), and cadmium(II). The mechanical strength of the parent gels diminished in the presence of salts, suggesting that the structural alteration led to more robust gels in most instances. The altered compounds produced gels at concentrations below

the minimum gel concentration in the presence of various salts, signifying salt-induced gelation. These results demonstrate the formation and disruption capabilities of the gel network in response to external stimuli (salts), which elucidates the potential of using LMWGs based on *N*-oxide moieties as smart materials.

Article-II

The relative position and spatial arrangement of functional groups significantly influence the gelation properties of stimuli-responsive supramolecular gels. In this study, we synthesized and studied mono- and bis-pyridyl-*N*-oxide derivatives of *N*-(4-pyridyl)nicotinamide (L_1–L_3). The gelation characteristics of these *N*-oxide compounds were compared with the isomeric mono-/bis-pyridyl-*N*-oxide compounds of *N*-(4-pyridyl)isonicotinamide. Hydrogels derived from L_1 and L_3 exhibited superior thermal and mechanical stability compared to their isomeric counterparts. The surface morphology of the xerogels of di-*N*-oxides (L_3 and diNO) produced from water was examined using scanning electron microscopy (SEM), which indicated that the relative positioning of *N*-oxide moieties did not significantly influence gel morphology. Single-crystal X-ray diffraction was employed for solid-state structural research to elucidate the fundamental mechanism of gel formation. We have examined the stimuli-responsive behavior of the *N*-oxide moieties in water and aqueous mixtures in the presence of various salts. We investigated the influence of different salts on the gelation properties of hydrogels, and the findings demonstrated that the salts might facilitate gelation in L_1 and L_3 at concentrations lower than the minimum required for the gelators. The mechanical properties were assessed by rheological studies, demonstrating that the modified compounds exhibited improved gel strength in the majority of instances. Cadmium chloride exhibited supergelator properties at a minimal concentration (0.7 wt% of L_3), resulting in the formation of robust hydrogels at higher concentrations of L_3. The findings indicate that the spatial arrangement of N-oxide moieties is essential for the effective interaction between the gelator and salts/ions, leading to low molecular weight gelators with tunable characteristics.

2.2. Analyzing the role of hydrogen bonding functionalities in inducing coordination-driven self-assembly.

Article-III

We then analyzed the role of the hydrogen bond functionalities in the self-assembly process of bis(pyridyl)urea compounds by replacing the hydrogen bonding moieties of non-gelators. We have chosen *N*,*N*'–bis(2/3-pyridyl)urea (2-BPU and 3–BPU), non-gelators, which may be due to the absence of complementary urea tape hydrogen bonding because the nitrogen atom and the carbonyl groups displayed intramolecular interaction with the pyridyl nitrogen atom and C-H moieties. We have replaced the urea with a thiourea group to alter these interactions, which resulted in *N*,*N*'–bis(2/3–pyridyl)thiourea (2-PTU and 3-PTU). We analyzed the gelation properties of thiourea based compounds and found it to be non-gelators, which prompted us to check whether metal salts could induce the gelation. The results indicated selective gelation of 2-PTU and 3-PTU with various copper salts (1:2 metal-to-ligand ratio) in DMF/water (1:1, v/v). The mechanical strength of these metallogels was studied using rheology, and the fibrous morphology of the dried gels was examined using scanning electron microscopy (SEM). We have analyzed the role of coordination-driven self-assembly in these metallogels using various techniques such as UV-visible spectroscopy and X-ray diffraction.

These results revealed that the modification of hydrogen bonding moieties of the molecules could induce coordination-driven self-assembly.

.

Article-I

This project is published in a peer-reviewed journal and included as published. Minor variations may arise from the original article owing to formatting issues.

Publication details:

"**Making and Breaking of Gels: Stimuli-Responsive Properties of Bis(Pyridyl-N-oxide Urea) Gelators**"

Sreejith Sudhakaran Jayabhavan, Dipankar Ghosh, and Krishna K. Damodaran*

Molecules, **2021**, *26*(21), 6420.

Author contributions:

S.S.J. and K.K.D. planned and designed the research; **S.S.J** and D.G. synthesized the gelators, performed characterizations, solved single crystal structures and evaluated gelation properties. **S.S.J.** and K.K.D. wrote the initial manuscript draft and all authors reviewed the main manuscript.

molecules

MDPI

Article

Making and Breaking of Gels: Stimuli-Responsive Properties of Bis(Pyridyl-*N*-oxide Urea) Gelators

Sreejith Sudhakaran Jayabhavan, Dipankar Ghosh and Krishna K. Damodaran *

Department of Chemistry, Science Institute, University of Iceland, Dunhagi 3, 107 Reykjavík, Iceland; ssj37@hi.is (S.S.J.); dipankar@hi.is (D.G.)
* Correspondence: krishna@hi.is; Tel.: +354-525-4846; Fax: +354-552-8911

Abstract: The structural modification of existing supramolecular architecture is an efficient strategy to design and synthesize supramolecular gels with tunable and predictable properties. In this work, we have modified bis(pyridyl urea) compounds with different linkers, namely hexylene and butylene, to their corresponding bis(pyridyl-*N*-oxide urea). The gelation properties of both the parent and the modified compounds were studied, and the results indicated that modification of the 3-pyridyl moieties to the corresponding 3-pyridyl-*N*-oxides induced hydrogelation. The stability of the parent and modified compounds were evaluated by sol-gel transition temperature (T_{gel}) and rheological measurements, and single-crystal X-ray diffraction was used to analyze the solid-state interactions of the gelators. The morphologies of the dried gels were analyzed by scanning electron microscopy (SEM), which revealed that the structural modification did not induce any prominent effect on the gel morphology. The stimuli-responsive behavior of these gels in the presence of salts in DMSO/water was evaluated by rheological experiments, which indicated that the modified compounds displayed enhanced gel strength in most cases. However, the gel network collapsed in the presence of the chloride salts of aluminum(III), zinc(II), copper(II), and cadmium(II). The mechanical strength of the parent gels decreased in the presence of salts, indicating that the structural modification resulted in robust gels in most cases. The modified compounds formed gels below minimum gel concentration in the presence of various salts, indicating salt-induced gelation. These results show the making and breaking ability of the gel network in the presence of external stimuli (salts), which explains the potential of using LMWGs based on *N*-oxide moieties as stimuli-responsive materials.

Keywords: LMWGs; stimuli-responsive; structural modification; pyridyl urea; pyridyl-*N*-oxide

Citation: Sudhakaran Jayabhavan, S.; Ghosh, D.; Damodaran, K.K. Making and Breaking of Gels: Stimuli-Responsive Properties of Bis(Pyridyl-*N*-oxide Urea) Gelators. *Molecules* **2021**, *26*, 6420. https://doi.org/10.3390/molecules26216420

Academic Editors: Francesca D'Anna, Salvatore Marullo and Carla Rizzo

Received: 30 September 2021
Accepted: 21 October 2021
Published: 24 October 2021

1. Introduction

Stimuli-responsive low molecular weight gelators (LMWGs) [1–5] are an excellent class of soft materials because the gelation properties can be switched on/off by an external stimulus, such as heat, light, sound, redox, pH, and salts/ions. These semi-solid materials with unique physical properties display various applications [6–13] in catalysis, cell culture, crystal growth media, drug delivery, tissue engineering, and sensing and dynamic gels. The supramolecular architecture of LMWGs (3-D network) is fabricated by the molecular self-assembly of the gelator with entrapped solvent molecules, which is stabilized by various non-bonding interactions [12,14–18], such as hydrogen bonding, van der Waals interactions, π-π stacking, etc. Various analytical techniques (spectroscopic, microscopic, and X-ray diffraction) [19–23] have been used to study the mechanism of gelation, and X-ray diffraction methods have been proven to be one of the promising tools in understanding the gelator structure and its aggregation behavior [24–28]. However, predicting the gel structure or controlling the gel state properties is difficult because of the dynamic nature of the non-bonding interactions, leading to low molecular order in the overall gel state [12,14–18,29]. Thus, understanding the molecular self-assembly of supramolecular gels is a challenging task, enabling us to design LMWGs with predictable properties. The

role of specific interactions in gel formation can be analyzed by modifying the functional groups of LMWGs that play an important role in gel network formation.

The modification of these functional groups will lead to the alteration of specific interactions arising from the particular functional group, which can be considered as an excellent strategy to evaluate the role of specific interactions in gel formation [30,31]. For example, Zinchuan et al. have synthesized a cholesterol-based dendrimer gelator from the parent terminal alkyne-based gelator and have shown that the modified compounds formed gel in polar solvents compared to the parent compound, which only formed gel in nonpolar solvents [32]. McNeil's group has developed nitrite sensor-based LMWGs from a known azosulfonate gelator scaffold [33]. We have shown that the tris(pyridyl-*N*-oxide) gelator obtained by modifying trimesic amide-based LMWG can be used as a crystallizing medium for copper(II) isonicotinate–*N*-oxide complex [34]. The gelation properties of the parent and the modified gelators were compared to analyze the importance of specific interactions and the nature of the functional groups in tuning gelation properties by modifying pyridyl groups of *N*–(4–pyridyl)isonicotinamide to *N*–oxide groups [31]. The compounds with *N*–oxide groups have several advantages over the parent pyridyl-*N* atom due to the presence of additional lone pairs in the *N*-oxide moiety, which could lead to enhanced interactions with solvent/guest molecules. For example, Xu et al. showed that modified metal-organic frameworks with *N*-oxide moieties displayed enhanced C_2H_2 and CO_2 adsorptions [35]. Compounds with pyridine-*N*-oxide moieties are an excellent organocatalyst in various racemic and enantioselective reactions and act as oxidant in various oxidation reactions [36]. We have also modified pyridyl mono(urea)-based compounds [25] to pyridyl-*N*-oxide mono(urea) compounds and showed that the modified compounds formed highly resistant gels towards inorganic salts/ions [30]. We have successfully correlated the solid-state interactions with the gelation properties in mono(urea) LMWGs [30], which prompted us to evaluate the effect of structural modification in bis(pyridyl urea)-based compounds.

The gelation properties of bis(pyridyl urea) compounds have extensively been studied due to their ease of synthesis, cost-effectiveness, flexibility towards structural modification, and stimuli-responsive properties [29,37–39]. The presence of pyridyl groups could enhance the stimuli-responsive properties of bis(pyridyl urea) LMWGs in the presence of salts/ions [38]. The addition of salts could alter the non-bonding interactions, which might disrupt the self-assembly of the gelator constructively, by triggering gelation [40–42], or destructively, leading to gel dissolution [4,5]. The electrostatic interaction associated with the ions and the acidic/basic properties of the cations/anions plays a significant role in the interaction between the gelator and the salt [5,43]. Furthermore, the functional groups in a gelator also play a vital role, which acts as a binding or reaction site towards salts/ions [43,44]. Yang et al. reported the fluoride ion-induced gel-sol transition in a naphthalene-based bis(urea) gelator and have shown that the process can be reversed by adding trifluoroacetic acid [45]. The detection of iodide ions by bis(pyridyl urea) gels in the presence of various other anions was reported by Ghosh et al. [46]. Piepenbrock et al. reported the silver salt-induced gelation of bis(pyridyl urea) in tetrahydrofuran–water mixtures [47]. Thus, LMWGs based on bis(pyridyl urea) are excellent stimuli-responsive soft materials. In this work, we will evaluate the stimuli-responsive properties of bis(pyridyl urea) and the modified compounds in the presence of various cations and anions.

2. Results and Discussion

2.1. Design and Synthesis

The modification of the pyridyl functionality in pyridyl urea-based compounds could alter the N—H···N interactions to N—H···O interactions. Recently, we have shown that modifying pyridyl groups to the corresponding pyridyl-*N*-oxides [30] can restore the N—H···O interactions, leading to enhanced gelation ability. In this work, we have selected bis(pyridyl urea)-based compounds (**3-HBU** [29], **3-BBU** [48], **4-HBU**, and **4-BBU**; see Scheme 1) as the parent compounds. The structural modification of these compounds will enable us to study the effect of functional group modification on the gelation properties

of bis(pyridyl urea) systems and the specific role of N—H···O/N—H···N synthons in gel formation. The linker in bis(urea) compounds also plays an important role in gel formation by influencing the spatial arrangements of the functional groups and tuning the hydrophilic/hydrophobic interactions [8,49]. Thus, we have selected hexylene and butylene-based linkers connected to the 3-pyridyl/4-pyridyl urea moieties (Scheme 1). The hexylene linked bis-ureas (**3-HBU** and **4-HBU**) were synthesized by reacting 3–aminopyridine/4–aminopyridine with hexamethylene diisocyanate (Scheme S1) [29]. The butylene analogs (**3-BBU** and **4-BBU**) were obtained from the reaction of 1,4-diaminobutane and 3-pyridyl isocyanate/4-pyridyl isocyanate (Scheme S2). The oxidation of the pyridyl groups to pyridyl-*N*-oxide by 3–chloroperoxybenzoic acid (Scheme S3) resulted in compounds **1**–**4** (Scheme 1).

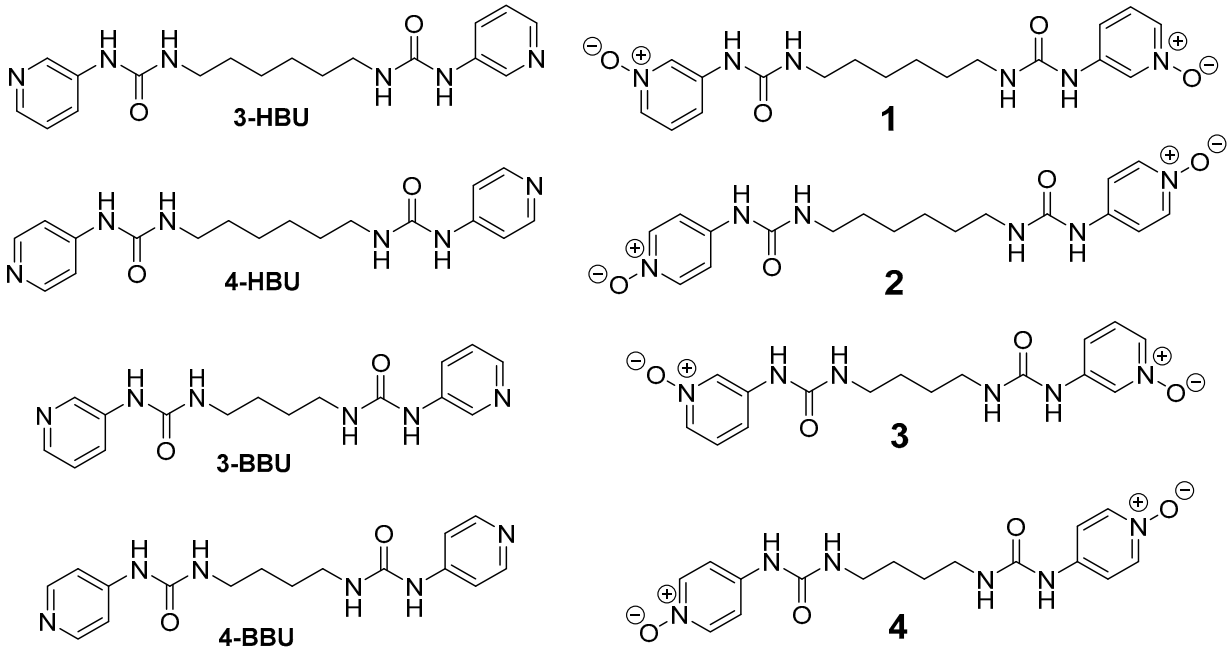

Scheme 1. Parent bis(pyridyl urea) and the corresponding *N*–oxide compounds obtained by modifying the pyridyl moieties.

2.2. Gelation Experiments

The gelation studies of the parent bis(pyridyl urea) compounds and the modified *N*-oxides were performed in various solvents/solvent mixtures. A standard procedure was followed for gelation experiments, 1.0 mL of the corresponding solvent was added to 10.0 mg of the compound in a standard 7.0 mL sealed vial, and the mixture was heated to obtain a clear solution, which was cooled to room temperature and left undisturbed for 24.0 h. Gelation was not observed for all the compounds at this concentration, which prompted us to perform the gelation test at a higher concentration (up to 5.0 *wt*/*v*%; Table S1). A vial inversion test was performed to confirm the gelation, and the gelation test indicated that both the parent and modified compounds were insoluble in hydrocarbons, such as toluene, xylenes, and mesitylene, and polar aliphatic solvents (THF, 1,2-dibromoethane, and acetonitrile). The modified *N*-oxide compounds were found to be less soluble in organic solvents but more soluble in water, which can be attributed to the strong hydrophilic interactions of the *N*-oxide moiety.

The parent bis(pyridyl urea) compounds were insoluble in water, but the modified compounds **1**, **3**, and **4** formed hydrogels at 2.0, 3.0, and 7.0 wt%, respectively, indicating that the structural modification has induced hydrogelation (Figure 1). We have also analyzed the gelation properties in mixed aqueous solvents (Table S1), and compounds **3-HBU**, **3-BBU**, and **3** formed gels in DMF/water (1:1, *v*/*v*). Gelation was also observed in a DMSO/water (1:1, *v*/*v*) and ethylene glycol (EG)/water 3:7 (*v*/*v*) mixture for **3-**

HBU, **3-BBU**, **1**, and **3**. However, gelation was not observed for the 4-pyridyl derivatives (**4-HBU** and **4-BBU**) and **2** in the above solvents/solvent mixtures (Table S1), indicating the importance of relative positions of the functionalities in gel formation [24,37].

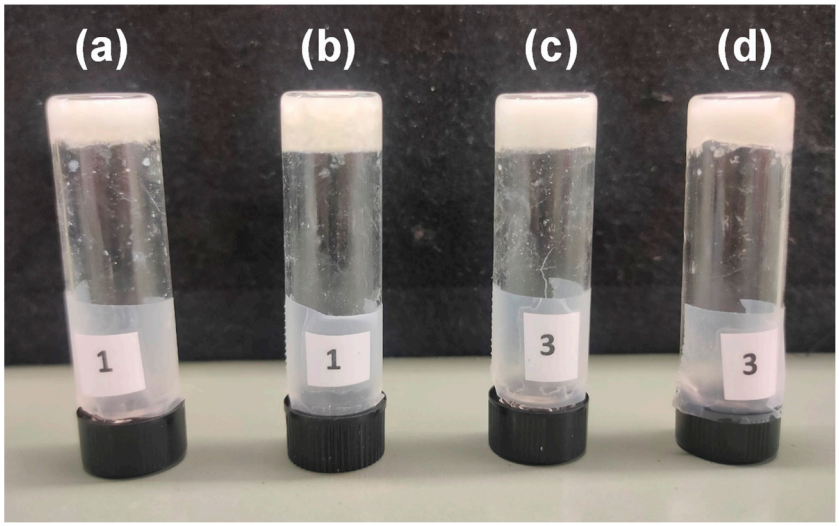

Figure 1. Gels obtained with compound **1** in water (**a**) and DMSO/water (1:1 v/v) (**b**), and compound **3** in water (**c**) and DMSO/water (1:1 v/v) (**d**).

The relative gelling ability and thermal stability of the parent and modified gels were analyzed by comparing the minimum gel concentration (MGC) and sol-gel transition temperature (T_{gel}) experiments, respectively. MGC is the minimum concentration of the compound, which is required to form a stable gel under ambient conditions. We have chosen DMSO/water (1:1, v/v) and EG/water (3:7, v/v) as the solvent systems since both parent (**3-HBU** and **3-BBU**) and modified compounds (**1** and **3**) formed gels in these solvent mixtures. The MGC of compound **1** was found to be 3.8 wt/v% in DMSO/water (1:1, v/v), which is slightly less than the MGC of **3-HBU** (4.0 wt/v%) (Table S2). Compound **3** formed gel at a lower concentration compared to **3-BBU** in all cases. Thus, the functional group modification led to a decrease in MGC of the pyridyl-*N*-oxide compounds. We have also analyzed the effect of the hexylene and butylene linkers, which indicated that increasing the alkyl chain length resulted in lower MGC (Table S2).

2.3. Thermal Stability

The gel-to-sol transition temperature (T_{gel}) was recorded to compare the thermal stability of the modified gelators with the parent compounds. The thermal stability of **3-HBU** was found to be very high in comparison with gelator **1** in both DMSO/water (1:1, v/v) and EG/water (3:7, v/v). A similar trend was observed for **3-BBU** in comparison with compound **3**, where the T_{gel} value of **3-BBU** was found to be considerably higher (Table 1). Thus, the modification of functional groups could alter the thermal stability, which indicated that the nature of the functional groups played an important role in determining the thermal stability of the gel network. The thermal stability of LMWGs also depends on the linkers, and we have compared the T_{gel} of hexylene and butylene-based compounds. These results indicated that the hexylene-based **3-HBU** gel was more thermally stable than the butylene-based **3-BBU** in 1:1 (v/v) DMSO/water. A similar trend was observed for the modified compounds (**1** and **3**) in DMSO/water (1:1, v/v), but a reverse trend was observed in EG/water (3:7, v/v) (Table 1), indicating that both linkers and solvents played a vital role in dictating the thermal stability of LMWGs.

Table 1. Determination of sol-gel transition temperature (T_{gel}).

Solvent	Tgel (°C)			
	3-HBU	**3-BBU**	**1**	**3**
Water	—	—	85.8 *	67.8 *
Ethylene glycol	69.9 *	—	—	—
DMSO: water (1:1, *v*/*v*)	94.4 #	—	62.8 #	—
	99.3 ##	96.6 ##	65.9 ##	61.9 ##
DMF: water (1:1, *v*/*v*)	84.8 ##	93.3 ##	—	55.6 ##
EG: water (3:7, *v*/*v*)	93.9 #	—	59.1 #	—
	98.4 ##	104.8 ##	64.2 ##	68.7 ##

* = 3.0 *wt*/*v*%, # = 4.0 *wt*/*v*%, ## = 5.0 *wt*/*v*%.

2.4. Rheology

The mechanical and solid-like properties of the bis(pyridyl-*N*-oxide urea) gels and the corresponding parent gelators were evaluated using rheology [50,51]. The mechanical strengths of **3-HBU** and gelator **1** were measured at 5.0 *wt*/*v*% in DMSO/water (1:1, *v*/*v*) and EG/water (3:7, *v*/*v*). Initially, an oscillatory strain-sweep experiment to determine the linear viscoelastic region (LVR) was performed to check whether the characteristic of the gel is retained or not because the gel networks undergo reversible deformation within the LVR. The results indicated that both the modified gelator **1** and its parent **3-HBU** had narrow LVR as the storage modulus G′ decreased after 0.05% of the shear strain (Figure S1). The point at which the elastic gel converts to a viscous fluid, accompanied by a sudden decrease in the G′, is known as the crossover point [50,51].

The crossover points for **3-HBU** and **1** in both the solvent mixtures were found to be within 3.0–10.0% of shear strain. Similar experiments were also performed to compare the gel strength of **3-BBU** and **3** in DMSO/water (1:1, *v*/*v*) and EG/water (3:7, *v*/*v*) at 5.0 *wt*/*v*%, respectively. Analyzing the LVR indicated that for **3-BBU,** the G′ decreased on increasing the shear strain above 0.02% but decreased after 0.05% of the shear strain for gelator **3**. The crossover point for **3-BBU** gelator was found to be around 0.5–2.0% of strain, but this was slightly higher (3.0–10.0)% of strain for gelator **3** (Figure S2). These results demonstrated that the mechanical strength of the parent and modified compounds in DMSO/water (1:1, *v*/*v*) and EG/water (3:7, *v*/*v*) displayed a narrow LVR in all cases, which proved that the gelators formed soft gels. Furthermore, above 10.0% of strain, all the gels were found to behave as a viscous fluid, indicated by the steep decrease in the G′.

Frequency sweep experiments were performed at a constant strain of 0.02% (within LVR) in a range of 0.1–10.0 Hz, which displayed a constant elastic (*G*′) and viscous (*G*″) moduli under varying frequency. The relative gel strength of **3–HBU** and **1** was compared by performing frequency sweep experiments on the gels prepared at 5.0 *wt*/*v*% in EG/water (3:7, *v*/*v*). The modified gelator **1** displayed a higher elastic modulus (G′) than the parent gelator **3-HBU** (~25 times). In DMSO/water (1:1, *v*/*v*), the G′ for **1** at 5.0 *wt*/*v*% was around ten times higher than the gelator **3-HBU** (Figure S3). The experiments performed with **3-BBU** and gelator **3** at 5.0 *wt*/*v*% also displayed similar results. Similarly, the G′ for gelator **3** was found to be approximately 25 times higher than **3-BBU** in EG/water (3:7, *v*/*v*) and around ten times higher in DMSO/water (1:1, *v*/*v*) (Figure 2). These results showed that the functional group modification enhanced mechanical strength, presumably due to the alteration of non-bonding interactions in the modified compounds.

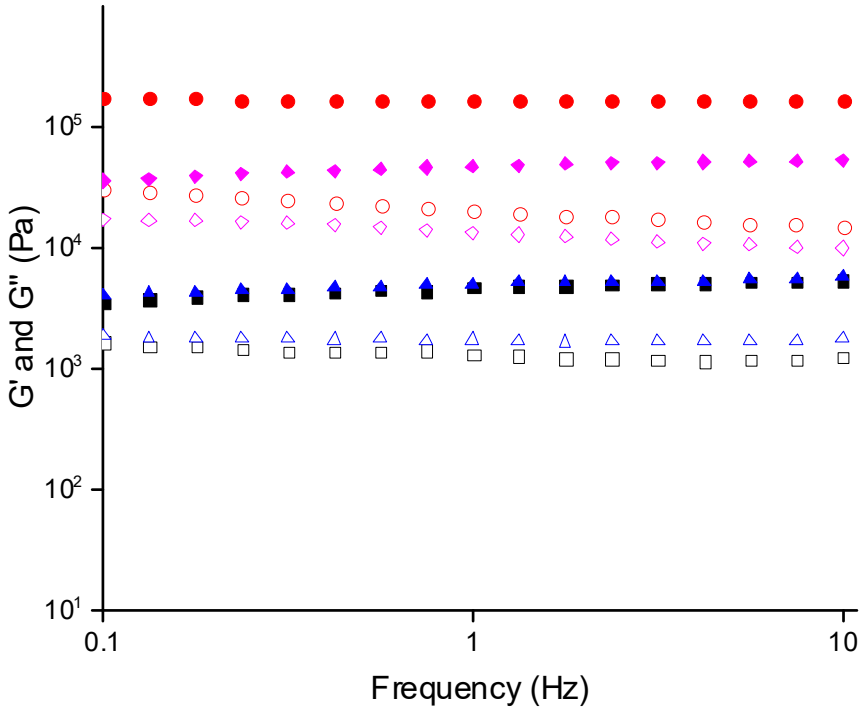

Figure 2. Frequency sweep experiments of gels of **3-BBU** and **3**, 5.0 *wt*/*v*% at 25.0 °C with a constant strain of 0.02%. Color codes: In EG/water (3:7, *v*/*v*) **3-BBU** G′ (■) and G″ (□), compound **3** G′ (●) and G″ (○), and in DMSO/water (1:1, *v*/*v*) **3-BBU** G′ (▲) and G″ (Δ), and compound **3** G′ (⧫) and G″ (◊).

2.5. Gel Morphology

The surface morphology of the xerogels was analyzed by scanning electron microscopy (SEM). We have performed SEM of the xerogels from DMSO/water (1:1, *v*/*v*) to compare the morphology of the xerogels of gelator **1** and **3-HBU**. Xerogel of **3-HBU** prepared at 4.0 *wt*/*v*% in DMSO/water (1:1, *v*/*v*) displayed plate-like morphology with dimensions ranging from 5.0–40.0 μm (Figure 3a), and the structurally modified gelator **1** also displayed fibers (10.0–60.0 μm) with similar plate-like morphology (Figure 3b). Similarly, the xerogels of the parent gelator **3-BBU** (dimension 20.0–100.0 μm) and **3** (dimension 2.0–10.0 μm) in DMSO/water (1:1, *v*/*v*) at 5.0 *wt*/*v*% displayed plate-shaped morphology (Figure S4a,b).

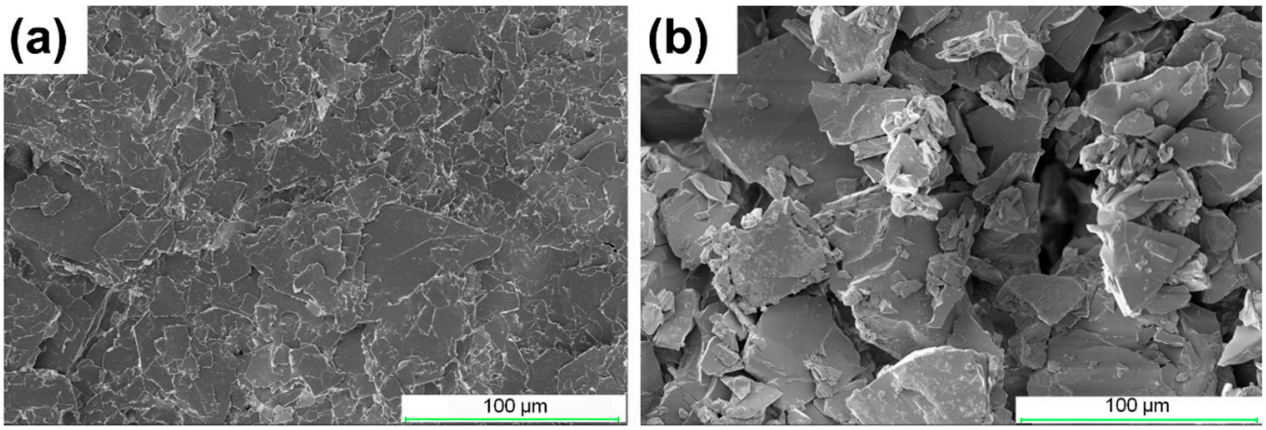

Figure 3. SEM images of xerogels of (**a**) **3-HBU,** and (**b**) **1** in DMSO/water (1:1, *v*/*v*) at 4.0 *wt*/*v*%, respectively.

We have also performed the SEM of the xerogels of **1** and **3** in water at 3.0 wt%, and the hydrogelator **1** displayed fibrous morphology with thin and long fibers of thickness ranging

from 0.1–0.5 µm (Figure 4a), but a plate-shaped morphology with a dimension of 2.0–16.0 µm was observed for gelator **3** (Figure 4b). Thus, the functional group modification of the bis(pyridyl urea)-based compounds to the corresponding bis(pyridyl-*N*-oxide urea) did not affect the morphologies of the gelators in DMSO/water (1:1, *v*/*v*), but solvent-induced morphological change was observed in hydrogels of **1,** indicating the role of solvents in the morphology of the gel fibers.

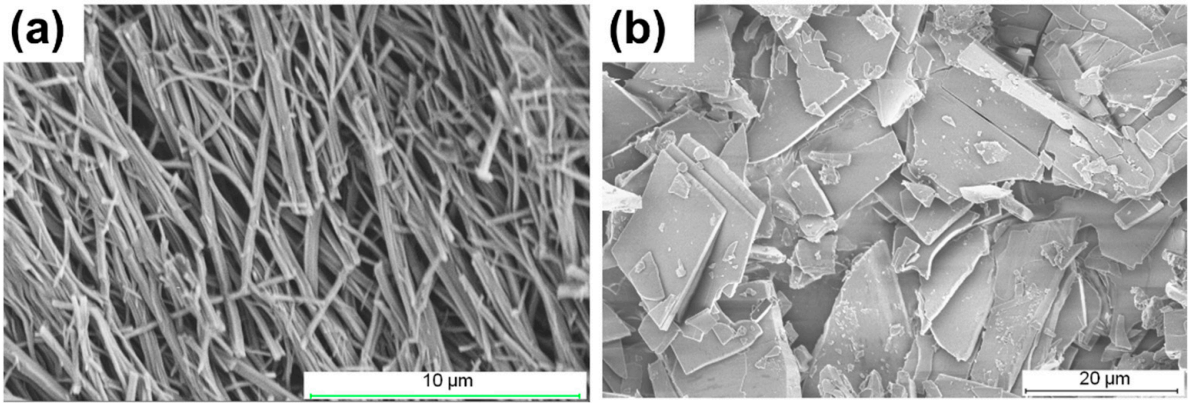

Figure 4. SEM images of xerogels in water at 3.0 wt%: (**a**) **1** and (**b**) **3**.

2.6. Single Crystal X-ray Diffraction

Single crystal X-ray diffraction analysis will enable us to analyze the non-bonding interactions of the *N*-oxide gelators in solid-state, which could be correlated to the gelation properties. Needle-shaped crystals of gelator **1** were obtained from DMSO/water, and single-crystal X-ray analysis revealed that compound **1** crystallized in monoclinic space group C2/c with one water molecule (**1**·H_2O) (Table S3).

Compound **1** has an inversion center resulting in the anti-conformation of the urea and the *N*-oxide moieties. The urea moieties displayed bifurcated hydrogen bonding with the *N*-oxide moieties via N—H···O interactions (2.8749(16) and 2.9531(17) Å; Table S4), resulting in a one-dimensional urea α-tape-like architecture (Figure 5) similar to complementary urea N—H···O=C aggregation. The one-dimensional chains are interconnected by O—H···O interactions between the pyridyl-*N*-oxide moiety and the solvent water molecule (Figure S5a).

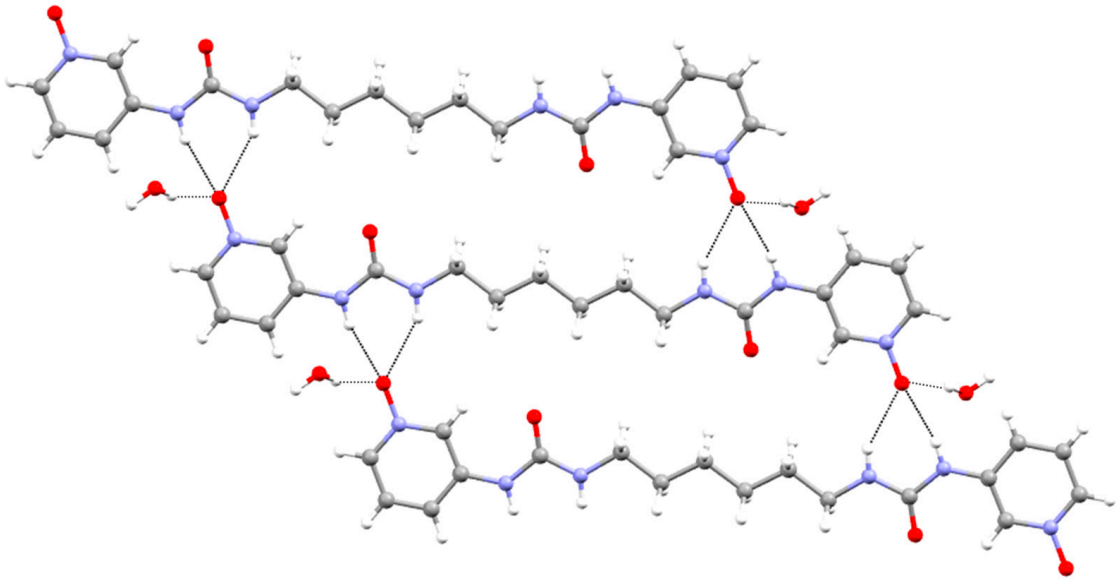

Figure 5. One-dimensional chain of **1**·H_2O displaying bifurcated hydrogen bonding.

Gelator **3** was crystallized with two water molecules (**3**·2H_2O) in a monoclinic space group $P2_1/n$ (Table S3). The overall conformation of the molecule was non-planar, and the urea and the *N*-oxide moieties adopted an anti-confirmation due to the inversion center (Figure 6a). One of the nitrogen atoms of the urea moieties was hydrogen-bonded to the pyridyl-*N*-oxide via N—H· · · O interactions (3.0246(16) Å) to form a two-dimensional hydrogen bonded network. The solvent water molecule was entrapped in this network (Figure 6b), which was stabilized by hydrogen bonding interactions with the other nitrogen atom of the urea motif (N—H· · · O = 2.8011(17) Å) and the oxygen atom of the pyridyl-*N*-oxide moieties of adjacent network (O· · · H—O = 2.8329(18) and 2.9013(18) Å) to form a porous architecture (Figure S5b), which was further stabilized by various non-bonding interactions (Table S4).

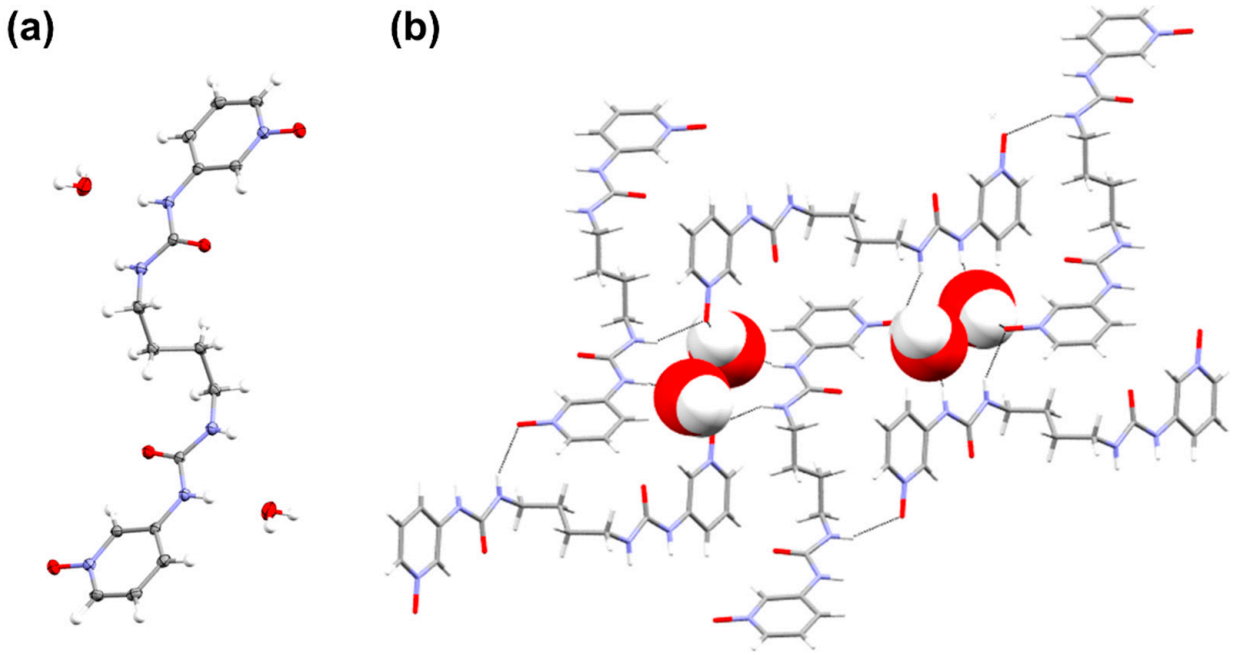

Figure 6. (**a**) Molecular structure of **3**·2H_2O and (**b**) two-dimensional network with entrapped water molecule (space fill model).

The compound **4-BBU** was crystallized in the monoclinic space group $P2_1/n$ with an inversion center. The urea moieties displayed anti-confirmation and the molecular structure was non-planar similar to **3** (Figure S6a). One of the nitrogen atoms of the urea moieties of **4-BBU** displayed N—H· · · O interactions (2.9871(15) Å) with the oxygen atom of the carbonyl moieties to form a one-dimensional hydrogen-bonded chain (Figure S6b). The second nitrogen atom of the urea moieties interacted with the pyridyl nitrogen from the adjacent molecule via N· · · H—N interactions (2.986(2) Å), which connected the two orthogonal one-dimensional chains to form a two-dimensional hydrogen-bonded network. The corresponding *N*-oxide compound **4** also crystallized in monoclinic space group $P2_1/n$ with an inversion center, and the urea moieties adopted an anti-confirmation (Figure S7a). The nitrogen atoms of the urea moieties displayed bifurcated hydrogen bonding with the oxygen atom of the pyridyl-*N*-oxide moieties (2.7887(18) and 2.9988(18) Å) to form a two-dimensional hydrogen-bonded sheet architecture (Figure S7b) with cavities. The solvent water molecules located in these cavities (Figure S7c) were hydrogen-bonded to the oxygen atoms of the carbonyl (2.889(2) Å) and pyridyl-*N*-oxide (2.788(2) Å) moieties, respectively.

The crystal structures of the parent compounds were compared to the modified compounds to analyze how structural modification affected the non-bonding interactions in the solid-state. The comparison of the solid-state structures of **3-BBU** [48] and the corresponding *N*-oxide **3** indicated that the structural modification changed the hydrogen bonding

pattern of the urea moieties of **3-BBU** from N···H—N/N—H···O interactions [48] to N—H···O interactions in **3**. The comparison of structures of **4-BBU** and the corresponding *N*-oxide **4** also revealed the alteration of non-bonding interactions; for example, the N···H—N interactions were also replaced by N—H···O interactions in **4**. We were not able to compare the solid-state structure of **1** with the parent compound because crystallization **3-HBU** was unsuccessful, despite several trials. We have compared the solid-state interactions of gelator **1** and **3**, and gelator **1** displayed a urea α-tape-like architecture via N—H···O interactions involving the urea and pyridyl-*N*-oxide moieties similar to complementary urea hydrogen bonding. However, the N—H···O interactions in **3** resulted in a two-dimensional hydrogen-bonded network, indicating that linkers play an important role in dictating the one-dimensional chain, which is crucial for better gelation properties [48].

2.7. X-ray Powder Diffraction (XRPD)

X-ray Powder Diffraction is an important technique to identify the phase purity of bulk solids, which is performed by comparing the XRPD pattern of the bulk crystals with the simulated pattern obtained from the crystal structure. Moreover, the comparison of the powder X-ray patterns of the dried gels with the simulated pattern obtained from the crystal structure may provide useful information about the interactions involved in the gel network formation [14,19,28,31,52–54]. Although the drying process of the gels can lead to artifacts, this method can be considered as an elegant approach to correlate the self-assembly process in LMWGs [55].

We have compared the XRPD pattern of the xerogel of **1** obtained from DMSO/water (1:1, *v*/*v*) at 4.0 *wt*/*v*%, which did match with the simulated pattern. The XRPD pattern of the bulk crystals of gelator **1**·H_2O was also found to be similar to the simulated pattern, except an extra peak at 2θ ≈ 11.0°, presumably due to the solvent water molecules (Figure S8). Similarly, for gelator **3**, the XRPD pattern of the bulk crystals and the xerogel obtained from DMSO/water (1:1, *v*/*v*) at 5.0 *wt*/*v*% matched with the simulated pattern of the single crystal of **3**·2H_2O (Figure 7)**.** However, a slight shift was observed with bulk crystals and xerogels at higher 2θ (> 25.0°) compared to the simulated pattern of the single crystal of **3**·2H_2O. The XRPD pattern of the xerogel of **1** and **3** at 3.0 wt% in water was different from that of the simulated patterns, indicating that the gelator might adopt different structures depending on the gelling solvent (Figures S8 and S9).

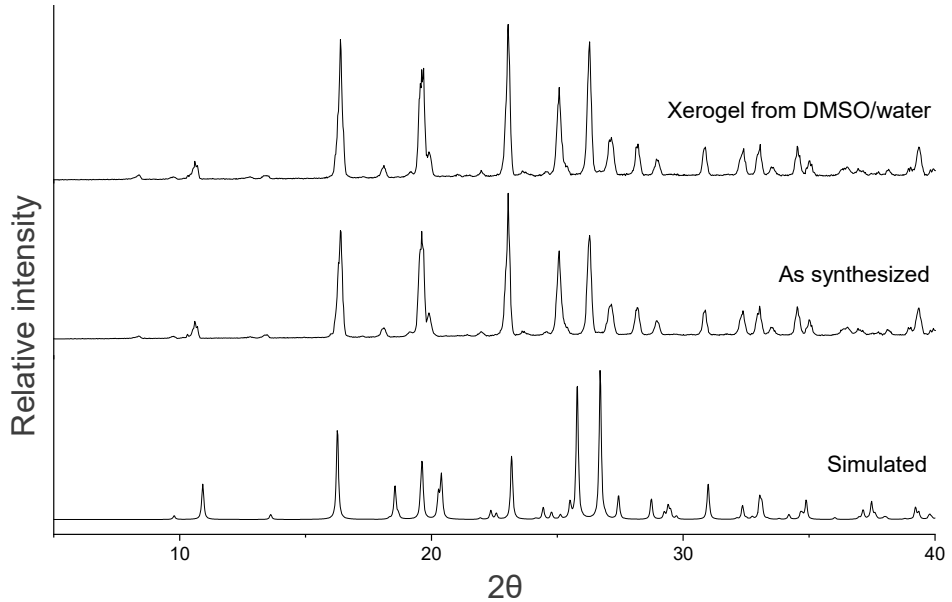

Figure 7. Comparison of the simulated pattern from single-crystal data, bulk-crystals synthesized from DMSO/water, and xerogel from DMSO/water (1:1, *v*/*v*) of compound **3**.

We have also recorded the XRPD pattern of the **3-BBU** bulk crystals and xerogel. The XRPD patterns of the bulk crystals and the xerogels obtained from DMSO/water (1:1, *v*/*v*) at 5.0 *wt*/*v*% were superimposable, but it was found to be different from the simulated pattern (Figure S10). The XRPD pattern of **4-BBU** (as-synthesized) was identical to the simulated pattern (Figure S11), but the pattern of **4** (as-synthesized) did not match with the simulated pattern, presumably due to a different crystal packing in the presence of the solvent water molecule (Figure S12).

2.8. Physical Properties in the Presence of Salts

The stimuli-responsive properties of LMWGs [1–5,56] were studied in the presence salts/ions, for example, making or breaking of the gel network. Xu et al. have synthesized an organogel with pyrene fluorophore and urea-sulfonamide anion binding sites to show the effect of ion's size in gelation [57]. Pang et al. reported the gel-sol transition in the presence of selective anion [58]. Adam's group has demonstrated a Ca^{2+} induced hydrogelation at alkaline pH in LMWGs based on dipeptide derivatives [59]. The presence of pyridyl/pyridyl-*N*-oxide moieties in our compounds makes them ideal candidates as stimuli-responsive soft materials because these groups are known to interact with the salts/ions. We have previously reported the anion sensing studies of pyridyl-*N*-oxide compounds [30] and have shown that gel-sol transition can be used to detect cyanide ions [60]. This prompted us to explore the effect of salts in the gelation properties of bis(pyridyl urea) and its corresponding bis(pyridyl-*N*-oxide urea) compounds.

The effect of salts on the thermal stability and mechanical strength of the gel network was analyzed by T_{gel} experiments and rheology, respectively. The stimuli-responsive properties were analyzed by treating the gels with various potassium salts, such as KF, KCl, KBr, KI, and KCN, in DMSO/water mixture, and the gelation properties of the modified *N*-oxide compounds were compared to the corresponding parent gelators. The gels of compounds **1** and **3-HBU** were prepared in DMSO/water (1:1, *v*/*v*) at 4.0 *wt*/*v*%, and the parent and modified gelators were stable in the presence of all the salts (1.0 and 3.0 equivalents). The thermal stability of the parent and modified compounds in the presence of these salts indicated a slightly increase in T_{gel} values for gelator **1** in the presence of the salts (1.0 equivalents), but the values were comparable with the pure gelator for **1** at 3.0 equivalents of salts. However, the T_{gel} values for **3** in the presence of 1.0 and 3.0 equivalents of salts were similar to the pure gelators (Table S5). The thermal stability of **3-HBU** and **3-BBU** decreased in the presence of the salts, and these results indicated that salts could interfere with gelator-solvent molecule interactions, thereby affecting the thermal stability of these gels [61].

We have analyzed the mechanical strength of the gels in the presence of salts, and the frequency sweep experiments revealed that the relative gel strength of the parent gelator **3-HBU** decreased in the presence of 1.0 and 3.0 equivalents of KF, KCl, KBr, KI, and KCN (Figure 8a). This is presumably due to the interaction of the pyridyl group with the salts affecting the non-bonding interactions responsible for the mechanical strength of the gelator. There was a considerable decrease in the mechanical strength of parent gelator **3-HBU** in the presence of 3.0 equivalents of KCl, KI, and KCN. However, a reverse trend was observed for the modified compound **1** in the presence of (1.0 and 3.0 equivalents) potassium salts (halides and cyanide). The mechanical strength was slightly reduced when the concentration of the salts was increased (3.0 equivalents) compared to the 1.0 equivalent of the salts, but the mechanical strength was higher than the pure gel in all cases (Figure 8b).

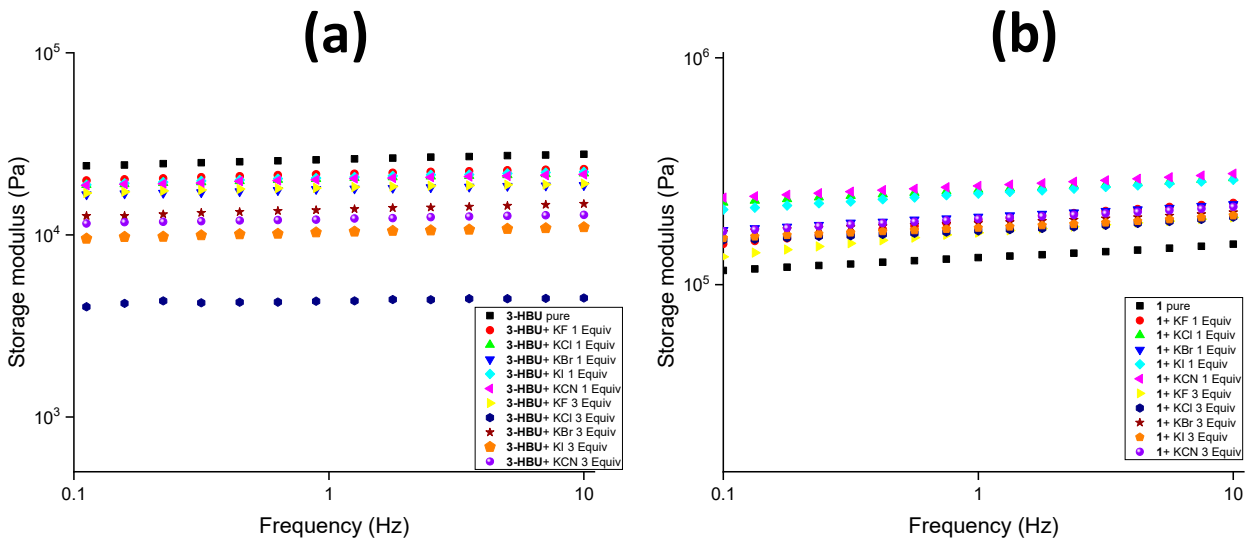

Figure 8. Frequency sweep experiments at 4.0 wt/v% in DMSO/water (1:1, v/v) in the presence of various salts of potassium at 25.0 °C with a constant strain of 0.02%, (**a**) **3-HBU** and (**b**) Gelator **1**.

The treatment of various anions of the potassium salts (halides and cyanides) gave similar enhancement in the mechanical strength of the modified compound **1**, which indicates that the enhanced mechanical strength does not depend on the size and nature of the anions. This prompted us to check the stimuli-responsive properties of gelators in the presence of various cations, and we have selected the chloride salts of cations of group IA (sodium), group IIA (calcium and magnesium), group III (aluminum), and transition metals (copper, zinc, and cadmium; Table S6). The results indicated that enhanced mechanical properties were observed in the presence of 1.0 and 3.0 equivalents of chlorides salts of sodium, magnesium, and calcium (Figure S13a). However, weak gels were obtained at 1.0 equivalent of $CuCl_2$ and $CdCl_2$ (1.0 and 3.0 equivalents), but the gelation was ceased in the presence of 3.0 equivalents of $CuCl_2$, 1.0 and 3.0 equivalents of $ZnCl_2$ and $AlCl_3$, respectively (Figure S14). Similar experiments performed with parent **3-HBU** revealed that the presence of chlorides salts (1.0 and 3.0 equivalents) of sodium, magnesium, and calcium decreased the mechanical strength compared to the pure gelator, but a reverse trend was observed for $CuCl_2$ (1.0 and 3.0 equivalents) and $ZnCl_2$ (1.0 equivalents), presumably due to the formation of metallogels (Figure S13b). However, the gel network collapsed in the presence of $CdCl_2$ and $AlCl_3$ salts (1.0 and 3.0 equivalents) and 3.0 equivalents of $ZnCl_2$.

Similarly, we have compared the mechanical strength of **3-BBU** and **3** at 5.0 wt/v% in DMSO/water (1:1, v/v) in the presence of salts mentioned above (Table S6). The mechanical strength of the parent gelator **3-BBU** was reduced in the presence of potassium halides and cyanide (Figure 9a), similar to **3-HBU,** and the maximum difference was observed for KF and KI. The presence of these ions enhanced the mechanical strength of gelator **3,** similar to gelator **1** (Figure 9b), and the maximum enhancement was observed for KCl (3.0 equivalents). The experiments were performed with various chloride salts of cations of group IA, group IIA, group III, and transition metals (copper, zinc, and cadmium) revealed that the mechanical strength of **3** increased in the presence of 1.0 and 3.0 equivalents of chlorides salts of sodium, magnesium, calcium, and cadmium (Figure S15a). The gel network collapsed in the presence of $ZnCl_2$ (3.0 equivalents), $CuCl_2$ (1.0 and 3.0 equivalents), and $AlCl_3$ (1.0 and 3.0 equivalents). The experiments performed with parent **3-BBU** in the presence of NaCl, $MgCl_2$, and $CaCl_2$ (1.0 and 3.0 equivalents) displayed a decrease in mechanical strength (Figure S15b). The gel network of **3-BBU** collapsed in the presence of 1.0 and 3.0 equivalents of $ZnCl_2$, $CdCl_2$, and $AlCl_3$; however, thermo-irreversible metallogels were obtained with $CuCl_2$ (1.0 and 3.0 equivalents), with more enhanced mechanical strength than the pure gelator [29].

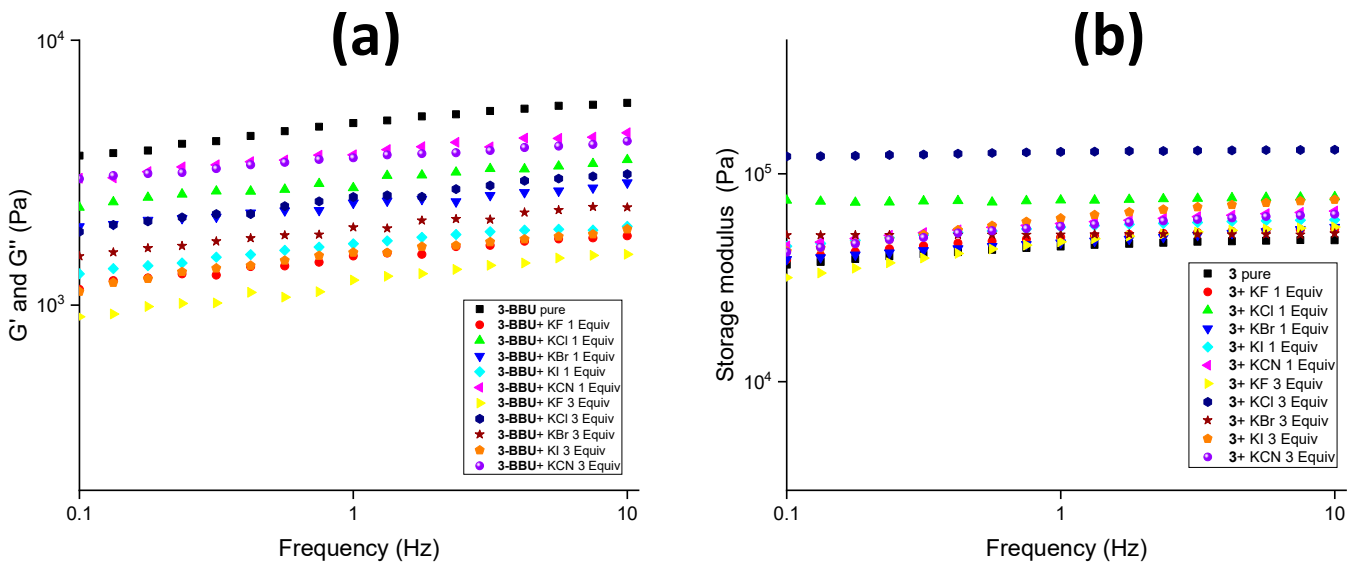

Figure 9. Frequency sweep experiments at 5.0 *wt*/*v*% in DMSO/water (1:1, *v*/*v*) in the presence of various salts of potassium at 25.0 °C with a constant strain of 0.02%, (**a**) **3-BBU**, (**b**) Gelator **3**.

The ability of the modified compounds (**1** and **3**) to form hydrogels prompted us to evaluate the stimuli-responsive properties in water in the presence of salts (Table S7), which will enable us to detect anions/cations in water [9,60–62]. The rheological experiments on the hydrogels of modified compound **1** (2.5 wt%) and compound **3** (3.5 wt%) in the presence of various salts (Table S7) indicated that potassium halides and cyanide enhanced the mechanical strength of both the hydrogels. A 2-fold increase in mechanical strength was observed for **1** with KCN (1.0 equivalents) (Figure 10a), with KCl for **3** (1.0 equivalents), and with KBr (1.0 equivalents) for both **1** and **3** (Figure 10a,b). Increasing the concentration of the salts (3.0 equivalents) gave similar results but the gel strength was increased compared to the corresponding gelator without additives. We have also performed experiments with sodium halides, nitrates of calcium and magnesium, magnesium sulfate, and chloride salts of calcium, magnesium, strontium, barium, cesium, aluminum, copper, zinc, and cadmium. These results indicated that the presence of these salts enhanced the mechanical strength of compounds **1** and **3**, except for chlorides of aluminum, zinc, cadmium, and copper. Compound **1** (2.5 wt%) formed gel in the presence of 1.0 equivalent of transition metal chlorides and aluminum chloride, but gelation was not observed with 3.0 equivalents of these salts. However, 1.0 equivalent of aluminum chloride did not have a prominent effect on the mechanical strength of gelator **3** (3.5 wt%), but a colloidal solution was observed at 3.0 equivalents. Gels were not obtained for **3** in the presence of 1.0 and 3.0 equivalents of the chloride salts of zinc, cadmium, and copper. These results indicated that the gel network collapsed in the presence of aluminum chloride, cadmium chloride, zinc chloride, and copper chloride in water, but the other salts enhanced the gelation properties (Table S7).

To confirm the role of the salts in gelation properties, we have repeated the experiments at different concentrations, such as minimum gel concentration (MGC) and below MGC. The gelation experiments were performed at MGC with compounds **1** (1.5 wt%) and **3** (2.5 wt%) in the presence of all these salts (Table S7) for rheological studies. The addition of salts (1.0 and 3.0 equivalents), such as potassium halides, potassium cyanide, and chlorides of sodium, magnesium, and calcium, enhanced the mechanical strength of the hydrogels. The mechanical strength was increased (~4-fold) in the presence of the majority of salts for gelator **3** (2.5 wt%), and, for gelator **1** (1.5 wt%), the enhancement of mechanical strength was ~5-fold for the chloride salts of potassium, magnesium, calcium, and potassium fluoride (Figure S16). The experiments repeated with various other salts revealed similar results (enhanced mechanical strength), except for aluminum chloride (1.0 and 3.0 equivalents), and 3.0 equivalents of the transition metal chlorides of cadmium,

zinc, and copper ceased gelation. The experiments were performed below MGC to test the ability of these salts to induce gelation in compounds **1** (1.0 wt%) and **3** (2.0 wt%). The results indicated that the salts, such as potassium halides, potassium cyanide, and chlorides of sodium, magnesium, and calcium (1.0 and 3.0 equivalents), induced gelation in **1** and **3** at a concentration below MGC, which was confirmed by vial inversion test, and the gelation properties were analyzed by frequency sweep experiments (Figure S17a,b). However, these gel networks collapsed after adding 3.0 equivalents of chlorides salts of either aluminum, cadmium, zinc, or copper (Figure 11). Furthermore, the presence of $AlCl_3$ (1.0 or 3.0 equivalents) and 3.0 equivalents of $CdCl_2$, $ZnCl_2$, and $CuCl_2$ did not induce gelation at concentration below MGC in **1** and **3**.

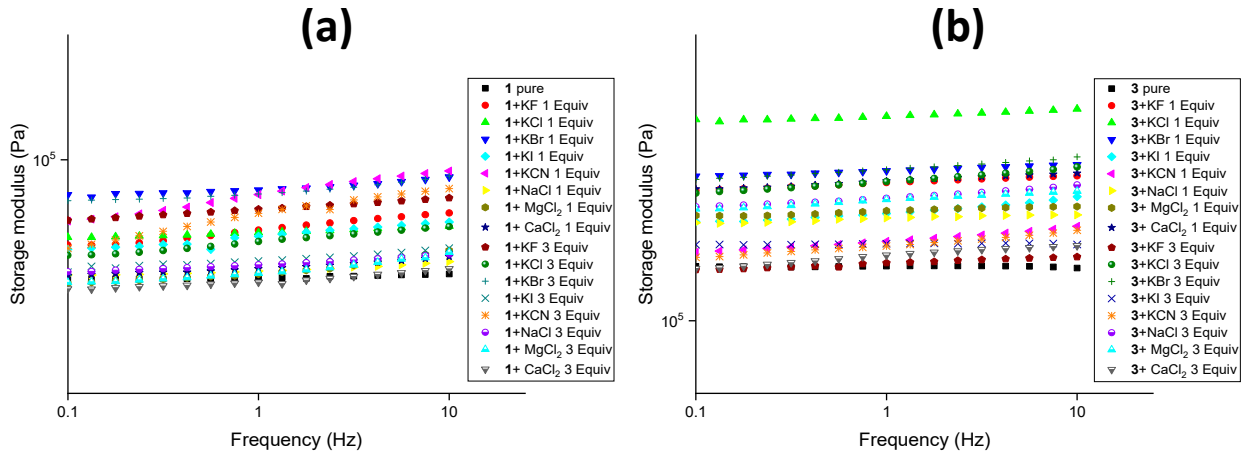

Figure 10. Frequency sweep experiments above MGC in water in the presence of salts at 25.0 °C with a constant strain of 0.02%, (**a**) compound **1** at 2.5 wt%, and (**b**) compound **3** at 3.5 wt%.

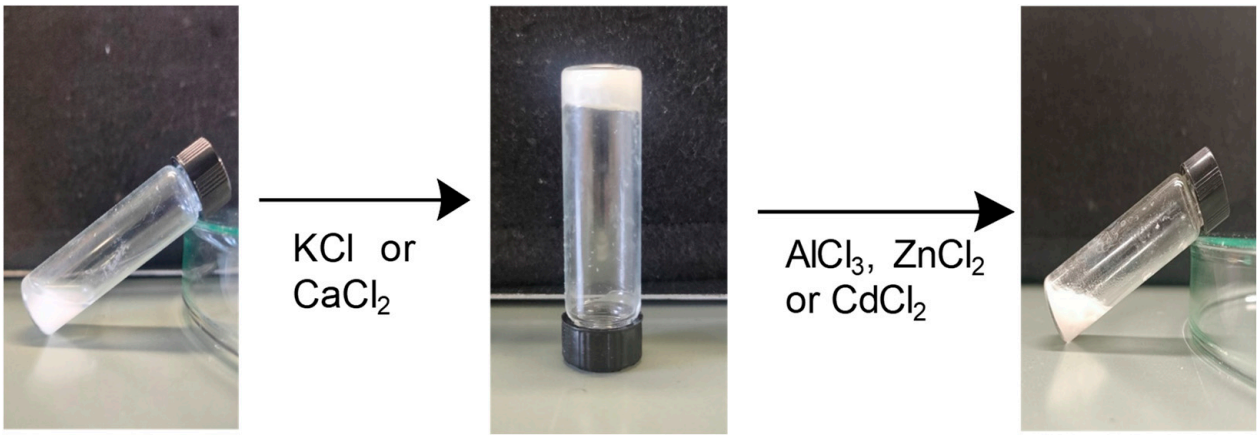

Figure 11. Making and breaking of gels in the presence of salts for compound **1** at 1.0 wt%.

The enhanced gelation of the *N*-oxide gelators in the presence of salts prompted us to analyze the effect of these salts on compounds **2** and **4**. Compound **2** formed precipitate in water, and the interaction of **4** with the salts were similar to gelators **1** and **3** (Figure S18). We have also performed the experiments with the parent bis(pyridyl urea) compounds in the presence of 1.0 and 3.0 equivalents of these salts, but gelation was not observed due to the poor solubility of the compounds in water. Thus, the structural modification increased the hydrophilic nature in the modified compounds (*N*-oxides), resulting in higher solubility and better interaction of the compounds with ions in water. The interaction of the gelators with the salts favored gelation, which was evident from higher G' values in the frequency sweep experiment and the gel formation below MGC. Thus, LMWGs acted

as stimuli-responsive gelators where gelation was turned ON or OFF in the presence of respective salts/ions.

We further analyzed the morphology of the xerogels of the *N*-oxide gels in water in the presence of potassium fluoride, calcium, and magnesium chlorides using SEM. The xerogel of **1** below MGC (1.0 wt%, partial gel) displayed fibrous morphology with fiber diameter 0.5–2.0 μm (Figure S19a). SEM performed on the xerogels of gelator **1** at 1.0 wt% in the presence of 3.0 equivalents of these salts displayed thin and long dense fibrous bundles (Figure S19b–d). Similarly, we have analyzed the morphology of the xerogels of **3** at 2.0 wt% (below MGC, partial gel) in the presence of the salts (3.0 equivalents). The SEM images displayed plate-shaped morphology in all cases, and no distinct morphological change was identified (Figure S20a–d).

3. Materials and Methods

The starting materials and solvents were purchased commercially from Sigma-Aldrich (MEDOR ehf, Reykjavik, Iceland) and TCI-Europe ((Boereveldseweg, Belgium) and were utilized as supplied. Gelation experiments were conducted using deionized water. A Bruker Avance 400 spectrometer (Rheinstetten, Germany) was used to record ^{1}H and ^{13}C NMR spectra (Figure S21–S32), and the scanning electron microscopy (SEM) (Carl Zeiss, Oberkochen, Germany) was recorded on a Leo Supra 25 microscope. The rheological experiments were performed on Anton Paar modular compact rheometer MCR 302 (Graz, Austria). A Bruker D8 venture (Karlsruhe, Germany) and PANalytical instrument (Almelo, Netherlands) were used to carry out single-crystal X-ray diffraction (SCXRD) and powder X-ray diffraction (XRPD) experiments. Isonicotinoyl azide [63], **3-HBU** [**29**], and **3-BBU** [**48**] were synthesized following the reported procedure, and the analytical data matched with the reported compounds.

3.1. Synthesis of Ligands

3.1.1. 1,1′-(Hexane-1,6-diyl)bis(3-(pyridin-4-yl)urea) (**4-HBU**)

A solution of diisocyanatohexane (3.6 g, 21.2 mmol) was dissolved in 30.0 mL of dry acetonitrile and was added dropwise to a stirring solution of 4-aminopyridine (4.0 g, 42.5 mmol) in 50.0 mL of dry acetonitrile. The mixture was heated to reflux for about 48 h, until a thick precipitate was formed. The precipitate was filtered, washed with acetonitrile, and air-dried to obtain the product. Yield: 77.0%. ^{1}H NMR (400 MHz, DMSO-d_6) δ (ppm): 11.02 (s, 2H), 8.48 (d, J = 6.90 Hz, 4H), 7.80 (d, J = 6.64 Hz, 4H), 7.26 (t, J = 5.66 Hz, 2H), 3.19–3.09 (m, 4H), 1.50–1.41 (m, 4H), 1.38–1.28 (m, 4H). ^{13}C {^{1}H} NMR (100 MHz, DMSO-d_6) δ (ppm): 153.77, 153.67, 142.01, 112.10, 39.04, 29.15, 25.93. HRMS (APCI): calcd for $C_{18}H_{25}N_6O_2$ [M + H]$^+$, 357.2034; found, 357.2034.

3.1.2. 1,1′-(Butane-1,4-diyl)bis(3-(pyridin-4-yl)urea) (**4-BBU**)

A solution of isonicotinoyl azide (1.5 g, 10.0 mmol) in toluene (50 mL) was refluxed at 110.0 °C for 2 h under a nitrogen atmosphere and cooled to room temperature. A solution of 1,4-diaminobutane (500 μL, 5.0 mmol) and triethylamine (1.4 mL, 10.0 mmol) in 40 mL toluene was added dropwise to the reaction mixture at room temperature. The resulting pale-yellow solution was further refluxed overnight, and the white precipitate formed was filtered. The residue was washed with methanol and dried in air to obtain the product as a white solid. The compound was recrystallized from methanol/water (3:1, v/v). Yield: 1.25 g, 76.2%. ^{1}H NMR (400 MHz, DMSO-d_6) δ (ppm): 8.87 (s, 2H), 8.27 (dd, J = 4.72, 1.64 Hz, 4H), 7.35 (d, J = 6.44 Hz, 4H), 6.39 (t, J = 5.72 Hz, 2H), 3.11 (m, 4H), 1.45 (m, 4H). ^{13}C {^{1}H} NMR (100 MHz, DMSO-d_6) δ (ppm): 154.56, 149.65, 147.36, 111.76, 38.78, 27.05. HRMS (APCI): calcd for $C_{16}H_{21}N_6O_2$ [M + H]$^+$, 329.1726; found, 329.1721.

3.1.3. 3,3′-(((Hexane-1,6-diylbis(azanediyl))bis(carbonyl))bis(azanediyl))bis(pyridine 1-oxide)) (**1**)

3–chloroperoxybenzic acid (0.42 g, 2.44 mmol) was added in portions to a solution of **3-HBU** (0.3 g, 0.84 mmol) in 5.0 mL DMF, and the solution was stirred overnight at room temperature [30]. The precipitate formed was filtered and washed with cold water and diethyl ether, and the crude product was recrystallized from hot water. Yield: 72.0%. ^{1}H NMR (400 MHz, DMSO-d_6) δ (ppm): 8.82 (s, 2H), 8.56 (s, 2H), 7.79 (d, *J* = 6.2 Hz, 2H), 7.24 (dd, J = 8.53, 6.12 Hz, 2H), 7.20–7.14 (m, 2H), 6.39 (t, *J* = 5.63 Hz, 2H), 3.07 (q, *J* = 6.53 Hz, 4H), 1.49–1.38 (m, 4H), 1.35–1.23 (m, 4H). ^{13}C {^{1}H} NMR (100 MHz, DMSO-d_6) δ (ppm): 154.52, 139.80, 131.56, 128.55, 125.86, 114.47, 39.11, 29.52, 26.05. HRMS (APCI): calcd for $C_{18}H_{24}N_6NaO_4$ [M + Na]$^+$, 411.1751; found, 411.1748.

3.1.4. 4,4′-(((Hexane-1,6-diylbis(azanediyl))bis(carbonyl))bis(azanediyl))bis(pyridine 1-oxide) (**2**)

Compound **2** was synthesized following a similar procedure to compound **1**. The precipitate obtained from the solution of **4-HBU** (0.6 g, 1.68 mmol) and 3–chloroperoxybenzic acid (0.84 g, 4.88 mmol) in 15.0 mL DMF was filtered. The residue was stirred overnight in 0.05 M HCl to remove unreacted starting materials. The mixture was filtered, washed with water, and dried. The product was recrystallized from hot water. Yield: 62.0%. ^{1}H NMR (400 MHz, DMSO-d_6) δ (ppm): 10.08 (s, 2H), 8.33 (d, *J* = 7.47 Hz, 4H), 7.62 (d, *J* = 7.47 Hz, 4H), 6.85 (t, *J* = 5.65 Hz, 2H), 3.10 (q, *J* = 6.50 Hz, 2H), 1.48–1.38 (m, 2H), 1.36–1.26 (m, 2H). ^{13}C {^{1}H} NMR (100 MHz, DMSO-d_6) δ (ppm): 153.99, 144.87, 139.57, 113.58, 39.08, 29.28, 25.93. HRMS (APCI): calcd for $C_{18}H_{24}N_6NaO_4$ [M + Na]$^+$, 411.1751; found, 411.1752.

3.1.5. 3,3′-(((Butane-1,4-diylbis(azanediyl))bis(carbonyl))bis(azanediyl))bis(pyridine 1-oxide) (**3**)

The reaction procedure was similar to compound **1**. 3–chloroperoxybenzic acid (0.94 g, 5.48 mmol) and **3-BBU** (0.6 g, 1.82 mmol) were added to DMF (10.0 mL). The precipitate was filtered and washed with cold water and ether and was recrystallized from THF/water (1:1, *v*/*v*). Yield: 68.0%. ^{1}H NMR (400 MHz, DMSO-d_6) δ (ppm): 8.82 (s, 2H), 8.55 (t, *J* = 1.89 Hz, 2H), 7.79 (dt, *J* = 6.17, 1.40 Hz, 2H), 7.26–7.20 (m, 2H), 7.19–7.15 (m, 2H), 6.41 (t, *J* = 5.70 Hz, 2H), 3.10 (q, *J* = 5.7 Hz, 4H), 1.49–1.40 (m, 4H). ^{13}C {^{1}H} NMR (100 MHz, DMSO-d_6) δ (ppm): 154.53, 139.76, 131.57, 128.55, 125.84, 114.40, 38.90, 27.05. HRMS (APCI): calcd for $C_{16}H_{20}N_6NaO_4$ [M + Na]$^+$, 383.1444; found, 383.1438.

3.1.6. 4,4′-(((Butane-1,4-diylbis(azanediyl))bis(carbonyl))bis(azanediyl))bis(pyridine 1-oxide) (**4**)

Compound **4** was synthesized following a similar procedure to compound **2**. The compound was recrystallized from water (40.0 mg/mL). Yield: 55.0%. ^{1}H NMR (400 MHz, DMSO-d_6) δ (ppm): 9.00 (s, 2H), 7.99 (d, *J* = 7.48 Hz, 4H), 7.40 (d, *J* = 7.52 Hz, 4H), 6.40 (t, *J* = 5.88 Hz, 2H), 3.09 (m, 4H), 1.44 (m, 4H). ^{13}C {^{1}H} NMR (100 MHz, DMSO-d_6) δ (ppm): 154.92, 150.37, 139.04, 114.61, 39.36, 27.53. HRMS (APCI): calcd for $C_{16}H_{20}N_6O_4Na$ [M + Na]$^+$, 383.1444; found, 383.1438.

3.2. Gelation Studies

Gelation properties were evaluated with all the compounds in various solvents by weighing 10.0 mg of the compound in a standard 7.0 mL vial (ID = 15.0 mm), into which 1.0 mL of the solvent was added, and the vial was sealed. The mixture was then sonicated and slowly heated to obtain a clear solution and was left undisturbed. An inversion test was conducted to confirm the gelation. Gelation tests were also conducted in the mixed aqueous system, and 10.0 mg of the compound was dissolved in 0.5 mL of the appropriate solvent in a standard 7.0 mL vial, followed by the addition of 0.5 mL distilled water. The mixture was sonicated and heated to obtain a transparent solution. The solution was cooled to room temperature, left undisturbed, and a vial inversion test confirmed gel formation. The

experiments were repeated with higher concentrations of the compounds (up to 50.0 mg) to test gelation.

3.2.1. Minimum Gel Concentration (MGC)

The MGC was performed in suitable solvents by weighing various concentration of the compounds in a standard 7.0 mL vial and adding 1.0 mL of solvent/solvent mixture. The mixture was sonicated and heated gradually to dissolve the compounds completely and the solution was kept at room temperature for gel formation. The minimum amount of the compound required to form a stable gel after 24 h was recorded as the MGC.

3.2.2. T_{gel} Experiments

In a 7.0 mL standard vial, the required amount of gelator and 1.0 mL of solvent was added. The mixture was sonicated and heated to dissolve and left undisturbed for gelation. After 24 h, a ball-drop method was performed to observe the gel to sol transition temperature (T_{gel}). A spherical glass ball was carefully placed on the top of the gel and immersed in an oil bath. A magnetic stirrer and a thermometer were equipped to monitor the temperature as the oil bath was gradually heated at 10.0 °C per minute. As temperature increases, the glass ball slowly gets immersed into the gels, and the temperature at which the ball touched the bottom of the vial was recorded as T_{gel}.

3.3. Rheology

An Anton Paar Modular Compact Rheometer MCR 302 was used to conduct rheological measurements. A 2.5 cm stainless steel parallel plate geometry configuration was used to measure the mechanical strength. Oscillatory measurements were conducted at a constant temperature of 25.0 °C in all cases. A Peltier temperature control hood was used as a solvent trap, which maintained a temperature of 25.0 °C for frequency and amplitude sweeps. Gels were prepared by dissolving an appropriate amount of the corresponding gelator in 1.0 mL of solvent. The experiments were performed after 24 h by scooping ~1.0 mL portion of gel onto the plate. A constant frequency of 1.0 Hz was maintained during amplitude sweep with log ramp strain (ϒ) ranges 0.01–100%. The frequency sweep was then carried out between 0.1 and 10.0 Hz within the linear viscoelasticity domain (0.02% strain). The experiments were also conducted in the presence of different salts in water and DMSO/water (1:1, *v*/*v*), with a similar procedure as mentioned above.

3.4. Scanning Electron Microscopy (SEM)

SEM was performed on a Leo Supra 25 microscope which analyzed the surface morphologies of the xerogels. Gels of **3-HBU** (4.0 *wt*/*v*%), **3-BBU** (5.0 *wt*/*v*%), **1** (4.0 *wt*/*v*%), and **3** (5.0 *wt*/*v*%) were prepared in DMSO/water (1:1, *v*/*v*). We have also prepared the hydrogels of **1** at 1.5 wt% (also at a higher concentration, 3.0 wt%) and at 2.5 wt% for compound **3**. The gels were filtered after 24 h and dried under a fume hood to obtain the xerogel. A small portion of the xerogel was placed on a pin mount with the carbon tab on top, coated with gold for 5–6 min to prevent charging of the surface, and was loaded, and the images were recorded at an operating voltage of 3.0 kV with a working distance 3–4 mm. An in-lens detector was used to record the SEM images. SEM of the xerogel of gelator **1** and **3** in the presence of certain salts of potassium, magnesium, and calcium in water was also recorded.

3.5. Single Crystal X-ray Diffraction

Single crystal of compound **1** was obtained by the slow evaporation of 10.0 mg of the compound in 2.0 mL of DMSO/water (1:1 *v*/*v*) to obtain needle-shaped crystals. Similarly, for compound **3**, a solvent composition of 2.0 mL of DMSO/water (1:2 *v*/*v*) of 10.0 mg of the compound was utilized to obtain the single crystals with needle-shaped morphology within a span of 24 h. X-ray quality crystals of **4-BBU** were obtained from a methanol/water (3:1, *v*/*v*) solution (10.0 mg/mL), and the slow evaporation of 40.0 mg of the compound **4** in

1.0 mL of water yielded needle-shaped single crystals. A Bruker D8 Venture (Photon100 CMOS detector) diffractometer equipped with Cryostream (Oxford Cryosystems) open-flow nitrogen cryostats was used for the X-ray analysis. The data was collected using MoKα radiation (λ = 0.71073 Å) for the crystals **1** at 293(2) K, **4-BBU** and **4** at 296(2) K, and compound **3** at 150(2) K. The unit cell determination, data collection, data reduction, structure solution/refinement, and empirical absorption correction (SADABS) were carried out using Apex III software (Bruker AXS: Madison, WI, USA, 2015). The structure was solved by direct method and refined by the full-matrix least-squares on F^2 for all data using SHELXTL version 2017/1 (University of Göttingen, Göttingen, Germany) [64]. All non-disordered nonhydrogen atoms were refined anisotropically, and the hydrogen atoms were placed in the calculated positions and refined using a riding model, except for the solvent water molecules in structures **1**, **3**, and **4**, where the hydrogen atoms were located on the Fourier map and refined. The crystallographic data and hydrogen bonding parameters are given in Tables S3 and S4 (see Supplementary Materials). The crystallographic data was deposited at the Cambridge Crystallographic Data Center, which can be obtained free of charge, and the CCDC numbers are 2113251–2113254.

3.6. X-ray Powder Diffraction

The bulk crystals of compounds **1** and **3** were obtained by the slow evaporation of the solution of **1** and **3** (20.0 mg in 5.0 mL DMSO/water 1:1, *v*/*v*). The crystals were filtered, dried in the air, and ground to a fine powder. The xerogels compound **1** were prepared from corresponding gels made in water at 2.0 wt% and DMSO/water (1:1, *v*/*v*) at 4.5 *wt*/*v*%. Gels were further filtered and dried in a fume hood to obtain the xerogel. A similar strategy was employed to prepare xerogels of compound **3** in water at 2.5 wt% and DMSO/water (1:1, *v*/*v*) at 5.0 *wt*/*v* %. XRPD studies with **3-BBU** were performed with bulk crystals obtained from THF/water (1:1, *v*/*v*) and xerogels at 5.0 *wt*/*v*% in EG/water (3:7, *v*/*v*) and DMSO/water (1:1, *v*/*v*) to compare with the reported crystal structure. XRPD was also performed with as-synthesized compound **4** and **4-BBU** and was matched with the simulated data. All experiments were carried out in a PANalytical instrument with Cu anode (Almelo, Netherlands), between 2θ from 4.0 to 50.0, and a step size of 0.02.

4. Conclusions

The functional group modification of bis(pyridyl urea) compounds to corresponding bis(pyridyl-*N*-oxide urea) was performed to tune the gelation properties of LMWGs by altering the specific non-bonding interaction. The analysis of the gelation properties revealed that the modification of the functional groups induced hydrogelation in 3-pyridyl-based bis(urea *N*-oxides) compounds (**1** and **3**). The structural modification enhanced the mechanical stabilities of the modified compounds (**1** and **3**), but the thermal stability of the gels in DMSO/water (1:1, *v*/*v*) and EG/water (3:7, *v*/*v*) were lower than the parent gelators. The morphologies of the gels were analyzed by SEM, which indicated that plate-shaped morphologies were observed in most cases, except for the hydrogel **1** with fibrous morphology. Single crystal X-ray diffraction revealed that the structural modification resulted in the alteration of non-bonding interactions and the modified compounds displayed N—H$\cdots$O interactions involving the urea and pyridyl-*N*-oxide moieties, similar to complementary urea hydrogen bonding. The stimuli-responsive properties of the parent and modified gelators were studied in the presence of various salts. The addition of salts resulted in enhanced mechanical strength of the modified *N*-oxide gels, but a reverse behavior was observed for the parent gelators. The anion/cation sensing properties of the gelators in water were evaluated at different gelator concentrations, and the results indicated that the majority of the salts enhanced the gelation properties, but the gel network collapsed in the presence of aluminum chloride, cadmium chloride, zinc chloride, and copper chloride. Gelation was induced by various salts/ions in the modified compounds at concentration below MGC, with enhanced mechanical strength. Thus, these stimuli responsive LMWGs

can act as sensors, and the gelation can be turned ON/OFF in the presence of respective salts/ions.

Supplementary Materials: The following are available online. Scheme S1: Synthetic route for the parent gelators **3-HBU** and **4-HBU**; Scheme S2: Synthetic route for the parent gelators **3-BBU** and **4-BBU**; Scheme S3: Synthetic route for the *N*-oxides; Table S1: Gelation details; Table S2: Determination of Minimum Gel Concentration (MGC); Table S3: Crystal data; Table S4: Hydrogen bonding parameters; Table S5: T_{gel} experiments in the presence of salts in DMSO/water (1:1, v/v); Table S6: Stimuli-responsive properties of the parent and modified compounds: comparing the G′ values in DMSO/water (1:1, v/v)*; Table S7: Stimuli-responsive properties of the modified compounds **1**, **3**, and **4**: comparing the G′ values in water*; Figure S1: Amplitude sweep experiments with gels of **3-HBU** and **1** (5.0 wt/v%) at 25.0 °C with a constant frequency of 1.0 Hz; Figure S2: Amplitude sweep experiments with gels of **3-BBU** and **3** (5.0 wt/v%) at 25.0 °C with a constant frequency of 1.0 Hz; Figure S3: Frequency sweep experiments with gels of **3-HBU** and **1** (5.0 wt/v%) at 25.0 °C with a constant strain of 0.02%; Figure S4: SEM images of xerogels in DMSO/water (1:1, v/v) at 5.0 wt/v% (a) **3-BBU**, and (b) **3**; Figure S5: (a) One-dimensional chains interconnected by O—H···O interactions between the pyridyl-N-oxide moiety and the solvent water molecule in gelator **1** and (b) two-dimensional porous architecture of gelator **3** with entrapped water molecules; Figure S6: (a) Molecular structure of **4-BBU** and (b) one-dimensional chain of **4-BBU** formed by N···H—O interactions; Figure S7: (a) Molecular structure of **4**·2H_2O, (b) bifurcated hydrogen bonding of the urea and pyridyl-*N*-oxide moieties resulting in two-dimensional hydrogen-bonded sheet, and (c) solvent water molecules entrapped in the cavities of the two-dimensional sheets; Figure S8: Comparison of the simulated pattern from single-crystal X-ray structure of compound **1** with the XRPD pattern of the bulk crystals obtained from DMSO/water, xerogel from DMSO/water (1:1, v/v, 4.0 wt/v%), and xerogel from water at 3.0 wt%; Figure S9: Comparison of the simulated pattern from single-crystal X-ray structure of compound **3** with the XRPD pattern of the xerogel from water at 3.0 wt%; Figure S10: Comparison of the simulated pattern from single-crystal X-ray structure of compound **3-BBU** with the XRPD pattern of as-synthesized bulk crystals obtained from THF/water, xerogel from DMSO/water (1:1, v/v); Figure S11: Comparison of the simulated pattern from single-crystal X-ray structure of **4-BBU** with the XRPD pattern of the bulk crystals obtained from MeOH/water; Figure S12: Comparison of the simulated pattern from single-crystal X-ray structure of **4**: with the XRPD pattern of bulk crystals obtained from water; Figure S13: Frequency sweep experiments at 4.0 wt/v% in DMSO/water (1:1, v/v) in the presence of various salts of chlorides at 25.0 °C with a constant strain of 0.02%, (a) gelator **1**, and (b) **3-HBU**; Figure S14: Gel network of **1** collapsing in the presence of 3.0 equivalents of $ZnCl_2$ or $AlCl_3$; Figure S15: Frequency sweep experiments at 5.0 wt/v% in DMSO/water (1:1, v/v) in the presence of various salts of chlorides at 25.0 °C with a constant strain of 0.02%, (a) gelator **3**, and (b) **3-BBU**; Figure S16: Frequency sweep experiments at MGC in water in presence of salts at 25.0 °C with a constant strain of 0.02%, (a) compound **1** at 1.5 wt%, and (b) compound **3** at 2.5 wt%; Figure S17: Frequency sweep experiments below MGC in water in presence of salts at 25.0 °C with a constant strain of 0.02%, (a) compound **1** at 1.0 wt%, and (b) compound **3** at 2.0 wt%; Figure S18: Frequency sweep experiments with compound **4** in the presence of 3.0 equivalents of the salts in water at 25.0 °C with a constant strain of 0.02%, (a) 7.0 wt%, and (b) 5.0 wt%; Figure S19: SEM images of xerogels of **1** obtained from pure water at 1.0 wt% (below MGC), (a) partial gel, and in the presence of 3.0 equivalents of (b) potassium fluoride, (c) magnesium chloride, and (d) calcium chloride; Figure S20: SEM images of xerogels of **3** obtained from pure water at 2.0 wt% (below MGC), (a) partial gel, and in the presence of 3.0 equivalents of (b) potassium fluoride, (c) magnesium chloride, and (d) calcium chloride; Figure S21: ^{1}H NMR spectrum of compound **4-HBU**; Figure S22: ^{13}C NMR spectrum of compound **4-HBU**; Figure S23: ^{1}H NMR spectrum of compound **4-BBU**; Figure S24: ^{13}C NMR spectrum of compound **4-BBU**; Figure S25: ^{1}H NMR spectrum of compound **1;** Figure S26: ^{13}C NMR spectrum of compound **1**; Figure S27: ^{1}H NMR spectrum of compound **2**; Figure S28: ^{13}C NMR spectrum of compound **2**; Figure S29: ^{1}H NMR spectrum of compound **3**; Figure S30: ^{13}C NMR spectrum of compound **3**; Figure S31: ^{1}H NMR spectrum of compound **4**; Figure S32: ^{13}C NMR spectrum of compound **4**.

Author Contributions: Conceptualization, S.S.J. and K.K.D. methodology, K.K.D., S.S.J. and D.G.; software, S.S.J. and D.G.; validation, S.S.J.; formal analysis, S.S.J., D.G. and K.K.D.; investigation, S.S.J. and D.G.; resources, K.K.D.; data curation, K.K.D.; writing—original draft preparation, K.K.D.;

writing—review and editing, S.S.J., D.G. and K.K.D.; visualization, K.K.D., S.S.J. and D.G.; supervision, K.K.D.; project administration, K.K.D.; funding acquisition, K.K.D. All authors have read and agreed to the published version of the manuscript.

Funding: This research received no external funding.

Institutional Review Board Statement: Not applicable.

Informed Consent Statement: Not applicable.

Data Availability Statement: Not applicable.

Acknowledgments: We thank University of Iceland Research Fund and Science Institute for funding. We acknowledge Sigríður Jónsdóttir, University of Iceland, for NMR and mass spectrometry, and Friðrik Magnus, University of Iceland, for powder X-ray diffraction analysis. S.S.J. thanks the University of Iceland for the doctoral research grant. We thank Rannís Iceland for infrastructure grants (150998-0031 and 191763-0031) for a single crystal X-ray diffractometer and rheometer.

Conflicts of Interest: The authors declare no conflict of interest.

Sample Availability: Samples of the compounds are available in limited quantity from the authors.

References

1. Chu, C.-W.; Schalley, C.A. Recent Advances on Supramolecular Gels: From Stimuli-Responsive Gels to Co-Assembled and Self-Sorted Systems. *Org. Mater.* **2021**, *3*, 25–40.
2. Panja, S.; Adams, D.J. Stimuli responsive dynamic transformations in supramolecular gels. *Chem. Soc. Rev.* **2021**, *50*, 5165–5200.
3. Jones, C.D.; Steed, J.W. Gels with sense: Supramolecular materials that respond to heat, light and sound. *Chem. Soc. Rev.* **2016**, *45*, 6546–6596.
4. Yang, X.; Zhang, G.; Zhang, D. Stimuli responsive gels based on low molecular weight gelators. *J. Mater. Chem.* **2012**, *22*, 38–50.
5. Piepenbrock, M.-O.M.; Lloyd, G.O.; Clarke, N.; Steed, J.W. Metal- and Anion-Binding Supramolecular Gels. *Chem. Rev.* **2010**, *110*, 1960–2004.
6. Kumar, D.K.; Steed, J.W. Supramolecular gel phase crystallization: Orthogonal self-assembly under non-equilibrium conditions. *Chem. Soc. Rev.* **2014**, *43*, 2080–2088.
7. Fang, W.; Zhang, Y.; Wu, J.; Liu, C.; Zhu, H.; Tu, T. Recent Advances in Supramolecular Gels and Catalysis. *Chem. Asian J.* **2018**, *13*, 712–729.
8. Foster, J.A.; Damodaran, K.K.; Maurin, A.; Day, G.M.; Thompson, H.P.G.; Cameron, G.J.; Bernal, J.C.; Steed, J.W. Pharmaceutical polymorph control in a drug-mimetic supramolecular gel. *Chem. Sci.* **2017**, *8*, 78–84. [PubMed]
9. Du, X.; Zhou, J.; Shi, J.; Xu, B. Supramolecular Hydrogelators and Hydrogels: From Soft Matter to Molecular Biomaterials. *Chem. Rev.* **2015**, *115*, 13165–13307.
10. Babu, S.S.; Praveen, V.K.; Ajayaghosh, A. Functional π-Gelators and Their Applications. *Chem. Rev.* **2014**, *114*, 1973–2129.
11. Truong, W.T.; Su, Y.; Meijer, J.T.; Thordarson, P.; Braet, F. Self-Assembled Gels for Biomedical Applications. *Chem. Asian J.* **2011**, *6*, 30–42. [PubMed]
12. Banerjee, S.; Das, R.K.; Maitra, U. Supramolecular gels 'in action'. *J. Mater. Chem.* **2009**, *19*, 6649–6687.
13. Van Bommel, K.J.C.; Stuart, M.C.A.; Feringa, B.L.; van Esch, J. Two-stage enzyme mediated drug release from LMWG hydrogels. *Org. Biomol. Chem.* **2005**, *3*, 2917–2920.
14. Dastidar, P. Supramolecular gelling agents: Can they be designed? *Chem. Soc. Rev.* **2008**, *37*, 2699–2715. [PubMed]
15. Estroff, L.A.; Hamilton, A.D. Water Gelation by Small Organic Molecules. *Chem. Rev.* **2004**, *104*, 1201–1218. [CrossRef]
16. De Loos, M.; Feringa, B.L.; van Esch, J.H. Design and Application of Self-Assembled Low Molecular Weight Hydrogels. *Eur. J. Org. Chem.* **2005**, *2005*, 3615–3631. [CrossRef]
17. George, M.; Weiss, R.G. Molecular Organogels. Soft Matter Comprised of Low-Molecular-Mass Organic Gelators and Organic Liquids. *Acc. Chem. Res.* **2006**, *39*, 489–497. [CrossRef] [PubMed]
18. Hirst, A.R.; Escuder, B.; Miravet, J.F.; Smith, D.K. High-Tech Applications of Self-Assembling Supramolecular Nanostructured Gel-Phase Materials: From Regenerative Medicine to Electronic Devices. *Angew. Chem. Int. Ed.* **2008**, *47*, 8002–8018.
19. Yu, G.; Yan, X.; Han, C.; Huang, F. Characterization of supramolecular gels. *Chem. Soc. Rev.* **2013**, *42*, 6697–6722.
20. Cao, X.; Meng, L.; Li, Z.; Mao, Y.; Lan, H.; Chen, L.; Fan, Y.; Yi, T. Large Red-Shifted Fluorescent Emission via Intermolecular π–π Stacking in 4-Ethynyl-1,8-naphthalimide-Based Supramolecular Assemblies. *Langmuir* **2014**, *30*, 11753–11760.
21. Das, U.K.; Banerjee, S.; Dastidar, P. Remarkable Shape-Sustaining, Load-Bearing, and Self-Healing Properties Displayed by a Supramolecular Gel Derived from a Bis-pyridyl-bis-amide of L-Phenyl Alanine. *Chem. Asian J.* **2014**, *9*, 2475–2482.
22. Li, P.; Dou, X.-Q.; Tang, Y.-T.; Zhu, S.; Gu, J.; Feng, C.-L.; Zhang, D. Gelator-polysaccharide hybrid hydrogel for selective and controllable dye release. *J. Colloid Interface Sci.* **2012**, *387*, 115–122. [CrossRef]
23. Tang, Y.-T.; Dou, X.-Q.; Ji, Z.-A.; Li, P.; Zhu, S.-M.; Gu, J.-J.; Feng, C.-L.; Zhang, D. C2-symmetric cyclohexane-based hydrogels: A rational designed LMWG and its application in dye scavenging. *J. Mol. Liq.* **2013**, *177*, 167–171.

24. Kumar, D.K.; Jose, D.A.; Dastidar, P.; Das, A. Nonpolymeric Hydrogelator Derived from N-(4-Pyridyl)isonicotinamide. *Langmuir* **2004**, *20*, 10413–10418. [CrossRef] [PubMed]
25. Kumar, D.K.; Jose, D.A.; Das, A.; Dastidar, P. First snapshot of a nonpolymeric hydrogelator interacting with its gelling solvents. *Chem. Commun.* **2005**, 4059–4061.
26. Wang, Y.; Tang, L.; Yu, J. Investigation of Spontaneous Transition from Low-Molecular-Weight Hydrogel into Macroscopic Crystals. *Cryst. Growth Des.* **2008**, *8*, 884–889. [CrossRef]
27. Braga, D.; d'Agostino, S.; D'Amen, E.; Grepioni, F. Polymorphs from supramolecular gels: Four crystal forms of the same silver(i) supergelator crystallized directly from its gels. *Chem. Commun.* **2011**, *47*, 5154–5156.
28. Ghosh, D.; Lebedytė, I.; Yufit, D.S.; Damodaran, K.K.; Steed, J.W. Selective gelation of N-(4-pyridyl)nicotinamide by copper(ii) salts. *CrystEngComm* **2015**, *17*, 8130–8138. [CrossRef]
29. Byrne, P.; Lloyd, G.O.; Applegarth, L.; Anderson, K.M.; Clarke, N.; Steed, J.W. Metal-induced gelation in dipyridyl ureas. *New J. Chem.* **2010**, *34*, 2261–2274. [CrossRef]
30. Ghosh, D.; Bjornsson, R.; Damodaran, K.K. Role of N–Oxide Moieties in Tuning Supramolecular Gel-State Properties. *Gels* **2020**, *6*, 41.
31. Ghosh, D.; Mulvee, M.T.; Damodaran, K.K. Tuning Gel State Properties of Supramolecular Gels by Functional Group Modification. *Molecules* **2019**, *24*, 3472.
32. Ge, J.; Guo, J.; Yu, X.; Li, Y.; Ma, Z. Structural Tunability on Naphthalimide-Based Dendrimer Gelators via Glaser Coupling Interaction with Tailored Gelation Solvent Polarity and Stimuli-Responsive Properties. *Langmuir* **2021**, *37*, 2677–2682. [PubMed]
33. Zurcher, D.M.; Adhia, Y.J.; Romero, J.D.; McNeil, A.J. Modifying a known gelator scaffold for nitrite detection. *Chem. Commun.* **2014**, *50*, 7813–7816.
34. Ghosh, D.; Ferfolja, K.; Drabavičius, Ž.; Steed, J.W.; Damodaran, K.K. Crystal habit modification of Cu(ii) isonicotinate–N-oxide complexes using gel phase crystallisation. *New J. Chem.* **2018**, *42*, 19963–19970.
35. Xu, T.; Fan, L.; Jiang, Z.; Zhou, P.; Li, Z.; Lu, H.; He, Y. Immobilization of N-oxide functionality into NbO-type MOFs for significantly enhanced C_2H_2/CH_4 and CO_2/CH_4 separations. *Dalton Trans.* **2020**, *49*, 7174–7181. [PubMed]
36. Koukal, P.; Ulč, J.; Nečas, D.; Kotora, M. Pyridine N-Oxides and Derivatives Thereof in Organocatalysis. In *Heterocyclic N-Oxides*; Larionov, O.V., Ed.; Springer International Publishing: Cham, Switzerland, 2017; pp. 29–58.
37. Rutgeerts, L.A.J.; Soultan, A.H.; Subramani, R.; Toprakhisar, B.; Ramon, H.; Paderes, M.C.; De Borggraeve, W.M.; Patterson, J. Robust scalable synthesis of a bis-urea derivative forming thixotropic and cytocompatible supramolecular hydrogels. *Chem. Commun.* **2019**, *55*, 7323–7326.
38. Steed, J.W. Anion-tuned supramolecular gels: A natural evolution from urea supramolecular chemistry. *Chem. Soc. Rev.* **2010**, *39*, 3686–3699.
39. Salpage, S.R.; Xu, Y.; Som, B.; Sindt, A.J.; Smith, M.D.; Shimizu, L.S. Pyridyl-phenylethynylene bis-urea macrocycles: Self-assembly and utility as a nanoreactor for the selective photoreaction of isoprene. *RSC Adv.* **2016**, *6*, 98350–98355.
40. Naota, T.; Koori, H. Molecules that assemble by sound: An application to the instant gelation of stable organic fluids. *J. Am. Chem. Soc.* **2005**, *127*, 9324–9325. [PubMed]
41. Fages, F. Metal coordination to assist molecular gelation. *Angew. Chem. Int. Ed.* **2006**, *45*, 1680–1682.
42. Offiler, C.A.; Jones, C.D.; Steed, J.W. Metal 'turn-off', anion 'turn-on' gelation cascade in pyridinylmethyl ureas. *Chem. Commun.* **2017**, *53*, 2024–2027.
43. Li, L.; Sun, R.; Zheng, R.; Huang, Y. Anions-responsive supramolecular gels: A review. *Mater. Des.* **2021**, *205*, 109759. [CrossRef]
44. Maeda, H. Anion-Responsive Supramolecular Gels. *Chem. Eur. J.* **2008**, *14*, 11274–11282. [PubMed]
45. Yang, H.; Yi, T.; Zhou, Z.; Zhou, Y.; Wu, J.; Xu, M.; Li, F.; Huang, C. Switchable fluorescent organogels and mesomorphic superstructure based on naphthalene derivatives. *Langmuir* **2007**, *23*, 8224–8230.
46. Ghosh, K.; Panja, S.; Bhattacharya, S. Naphthalene linked pyridyl urea as a supramolecular gelator: A new insight into naked eye detection of I^- in the gel state with semiconducting behaviour. *RSC Adv.* **2015**, *5*, 72772–72779.
47. Piepenbrock, M.-O.M.; Clarke, N.; Steed, J.W. Rheology and silver nanoparticle templating in a bis (urea) silver metallogel. *Soft Matter* **2011**, *7*, 2412–2418. [CrossRef]
48. Byrne, P.; Turner, D.R.; Lloyd, G.O.; Clarke, N.; Steed, J.W. Gradual transition from NH$\cdots$ pyridyl hydrogen bonding to the N—H$\cdots$O Tape synthon in pyridyl ureas. *Cryst. Growth Des.* **2008**, *8*, 3335–3344. [CrossRef]
49. Piepenbrock, M.-O.M.; Lloyd, G.O.; Clarke, N.; Steed, J.W. Gelation is crucially dependent on functional group orientation and may be tuned by anion binding. *Chem. Commun.* **2008**, 2644–2646.
50. Goodwin, J.W.; Hughes, R.W. *Rheology for Chemists: An Introduction*; Royal Society of Chemistry: London, UK, 2008.
51. Guenet, J.-M. *Organogels: Thermodynamics, Structure, Solvent Role, and Properties*; Springer International Publishing: Cham, Switzerland, 2016.
52. Jayabhavan, S.S.; Steed, J.W.; Damodaran, K.K. Crystal Habit Modification of Metronidazole by Supramolecular Gels with Complementary Functionality. *Cryst. Growth Des.* **2021**, *21*, 5383–5393. [CrossRef]
53. Tómasson, D.A.; Ghosh, D.; Kurup, M.R.P.; Mulvee, M.T.; Damodaran, K.K. Evaluating the role of a urea-like motif in enhancing the thermal and mechanical strength of supramolecular gels. *CrystEngComm* **2021**, *23*, 617–628.
54. Ghosh, D.; Farahani, A.D.; Martin, A.D.; Thordarson, P.; Damodaran, K.K. Unraveling the Self-Assembly Modes in Multicomponent Supramolecular Gels Using Single-Crystal X-ray Diffraction. *Chem. Mater.* **2020**, *32*, 3517–3527.

55. Adams, D.J. Does drying affect gel networks? *Gels* **2018**, *4*, 32.
56. Echeverria, C.; Fernandes, S.N.; Godinho, M.H.; Borges, J.P.; Soares, P.I.P. Functional Stimuli-Responsive Gels: Hydrogels and Microgels. *Gels* **2018**, *4*, 54.
57. Xu, Y.-L.; Li, C.-T.; Cao, Q.-Y.; Wang, B.-Y.; Xie, Y. A pyrenyl-appended organogel for fluorescence sensing of anions. *Dyes Pigm.* **2017**, *139*, 681–687.
58. Pang, X.; Ge, J.; Yu, X.; Li, Y.; Shen, F.; Wang, Y.; Ren, J. An "off–on" fluorescent naphthalimide-based sensor for anions: Its application in visual F− and AcO− discrimination in a self-assembled gel state. *New J. Chem.* **2019**, *43*, 10554–10559.
59. Panja, S.; Adams, D.J. Gel to gel transitions by dynamic self-assembly. *Chem. Commun.* **2019**, *55*, 10154–10157.
60. Ghosh, D.; Deepa; Damodaran, K.K. Metal complexation induced supramolecular gels for the detection of cyanide in water. *Supramol. Chem.* **2020**, *32*, 276–286.
61. Xu, Y.; Wang, C.; Tam, K.C.; Li, L. Salt-Assisted and Salt-Suppressed Sol−Gel Transitions of Methylcellulose in Water. *Langmuir* **2004**, *20*, 646–652. [PubMed]
62. Park, J.S.; Jeong, S.; Ahn, B.; Kim, M.; Oh, W.; Kim, J. Selective response of cyclodextrin-dye hydrogel to metal ions. *J. Incl. Phenom. Macrocycl. Chem.* **2011**, *71*, 79–86.
63. Hao, Y.; Tian, T.; Kang, Y.; Chang, T.; Fu, X.; Zhu, Z.; Meng, X.; Panchal, B.; Qin, S. Potassium iodide and bis (pyridylcarbamate) electrostatic synergy in the fixation reaction of CO 2 and epoxides. *New J. Chem.* **2020**, *44*, 15811–15815.
64. Sheldrick, G. Crystal structure refinement with SHELXL. *Acta Cryst. C* **2015**, *71*, 3–8.

Supporting Information

Making and Breaking of Gels: Stimuli-responsive Properties of Bis(Pyridyl-*N*-oxide Urea) Gelators

Sreejith Sudhakaran Jayabhavan, Dipankar Ghosh and Krishna K. Damodaran*

1. Synthetic scheme

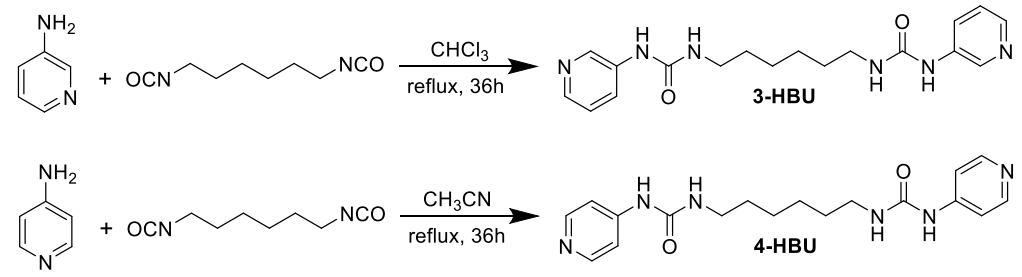

Scheme S1. Synthetic route for the parent gelators **3-HBU** and **4-HBU**.

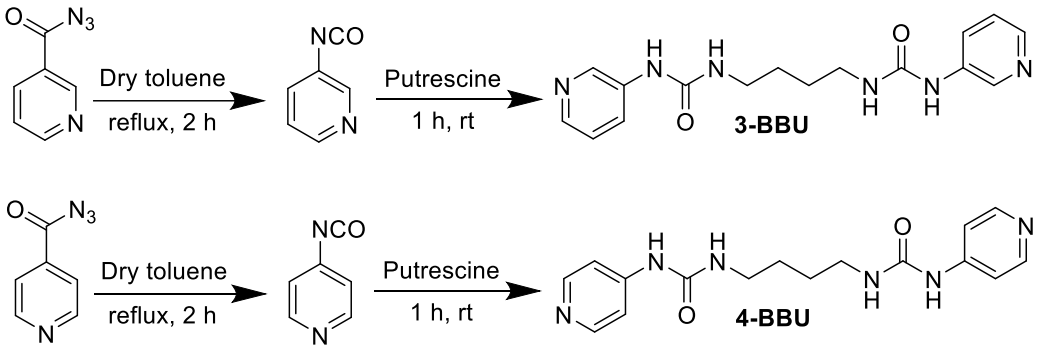

Scheme S2. Synthetic route for the parent gelators **3-BBU** and **4-BBU**.

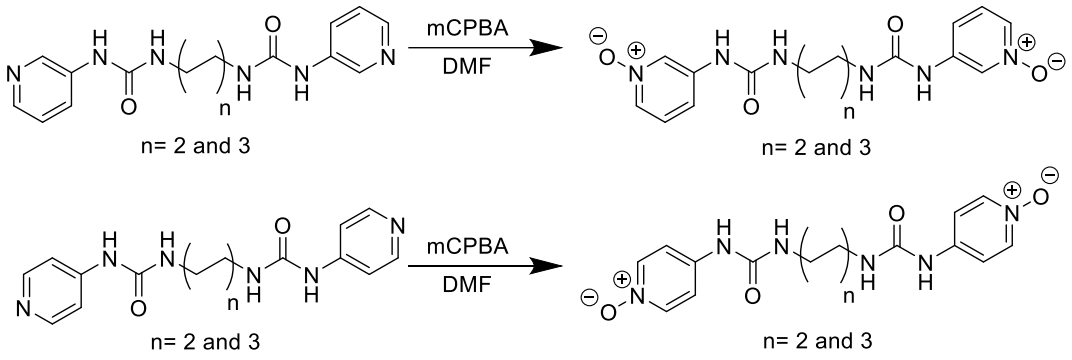

Scheme S3. Synthetic route for the *N*-oxides.

2. Gelation studies

The gelation studies were performed by taking a 10.0 mg of the compounds in 1.0 mL of the solvent/solvent mixture. The mixture was heated and sonicated and cooled to room temperature. When a clear solution was observed, another 10.0 mg of the compounds was added and the procedure was repeated until a gel was obtained, or up to 50.0 mg/mL concentration. The observations were recorded 24 h after the experiments.

Table S1: Gelation details

Solvents	**3-HBU**	**4-HBU**	**3-BBU**	**4-BBU**	**1**	**2**	**3**	**4**
water	I	I	I	I	G*	Ppt	G**	PG$^{\#\#}$
DMSO	S	S	S	S	S	Ppt	S	I
DMF	S	S	S	S	S	Ppt	S	I
Nitrobenzene	S	S	S	S	I	I	Ppt	I
1,2-dibromoethane	I	I	I	I	I	I	I	I
THF	I	I	I	I	I	I	I	I
Acetonitrile	I	I	I	I	I	I	I	I
o-xylene	I	I	I	I	I	I	I	I
m-xylene	I	I	I	I	I	I	I	I
p-xylene	I	I	I	I	I	I	I	I
Mesitylene	I	I	I	I	I	I	I	I
Ethanol	Ppt	Ppt	Ppt	Ppt	I	I	I	I
1-propanol	Ppt	Ppt	Ppt	Ppt	I	I	I	I
1-butanol	Ppt	Ppt	Ppt	Ppt	I	I	I	I
1-pentanol	Ppt	Ppt	Ppt	Ppt	I	I	I	I
Benzyl alcohol	S	S	S	S	S	S	S	I
Ethylene glycol	G**	S	Cry	S	Ppt	S	Ppt	Ppt
DMSO:water (1:1, v/v)	G$^{\#}$	C	G$^{\#\#}$	C	G$^{\#}$	Ppt	G$^{\#\#}$	Ppt
DMF:water (1:1, v/v)	G$^{\#\#}$	C	G$^{\#\#}$	C	Ppt	Ppt	G$^{\#\#}$	Ppt
EG:water (3:7, v/v)	G$^{\#}$	C	G$^{\#\#}$	C	G$^{\#}$	Ppt	G$^{\#\#}$	S

G= gel, I= insoluble, S= solution, C= colloid, Ppt= precipitate, PG= partial gel, Cry= crystals, *=2.0 wt/v%, **= 3.0 wt/v%, $^{\#}$= 4.0 wt/v%, $^{\#\#}$= 5.0 wt/v%.

Table S2: Determination of Minimum Gel Concentration (MGC)

Solvent	**MGC (wt/v%)**			
	3-HBU	**3-BBU**	**1**	**3**
water	---	---	1.6	2.5
Ethylene glycol	2.8	---	---	---
DMSO:water (1:1, v/v)	4.0	4.8	3.8	4.5
DMF:water (1:1, v/v)	4.5	4.8	---	4.5
EG:water (3:7, v/v)	3.8	4.5	3.8	4.0

3. Rheology

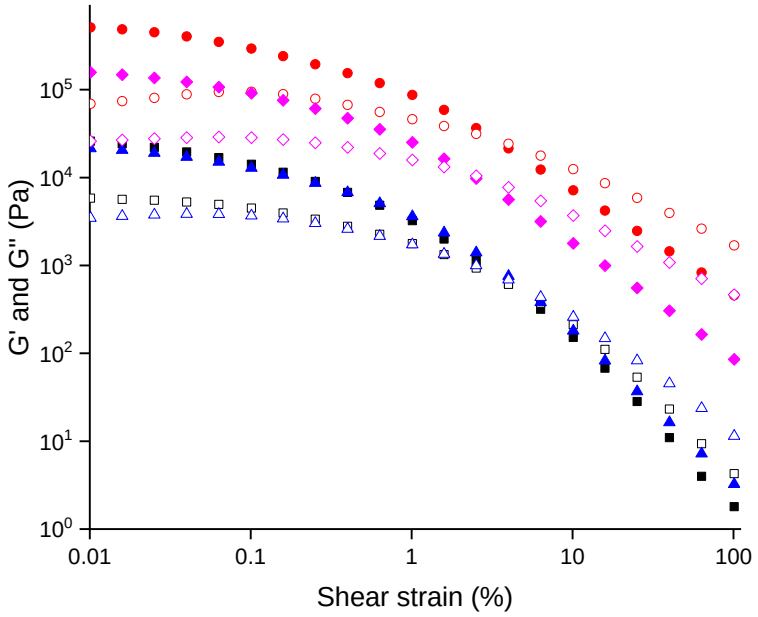

Figure S1. Amplitude sweep experiments with gels of **3-HBU** and **1** (5.0 wt/v%) at 25.0 °C with a constant frequency of 1.0 Hz. Color codes: In EG/water (3:7, v/v) **3-HBU** G′ (■) and G′′ (□), compound **1** G′ (●) and G′′ (○), and in DMSO/water (1:1, v/v) **3-HBU** G′ (▲) and G′′ (Δ), and compound **1** G′ (♦) and G′′ (◊).

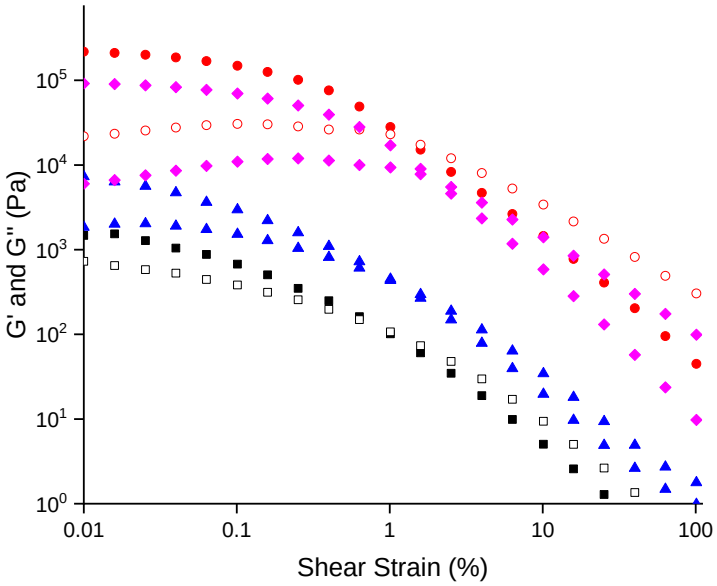

Figure S2. Amplitude sweep experiments with gels of **3-BBU** and **3** (5.0 wt/v%) at 25.0 °C with a constant frequency of 1.0 Hz. Color codes: In EG/water (3:7, v/v) **3-BBU** G′ (■) and G′′ (□), compound **3** G′ (●) and G′′ (○), and in DMSO/water (1:1, v/v) **3-BBU** G′ (▲) and G′′ (Δ), and compound **3** G′ (♦) and G′′ (◊).

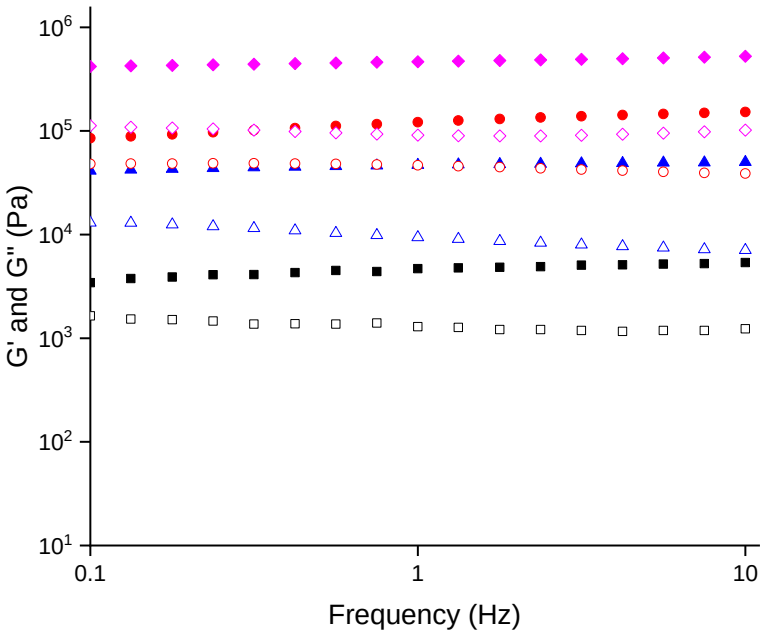

Figure S3. Frequency sweep experiments with gels of **3-HBU** and **1** (5.0 wt/v%) at 25.0 °C with a constant strain of 0.02%. Color codes: In EG/water (3:7, v/v) **3-HBU** G′ (■) and G′′ (□), compound **1** G′ (●) and G′′ (○), and in DMSO/water (1:1, v/v) **3-HBU** G′ (▲) and G′′ (Δ), and compound **1** G′ (♦) and G′′ (◊).

4. Scanning electron microscopy

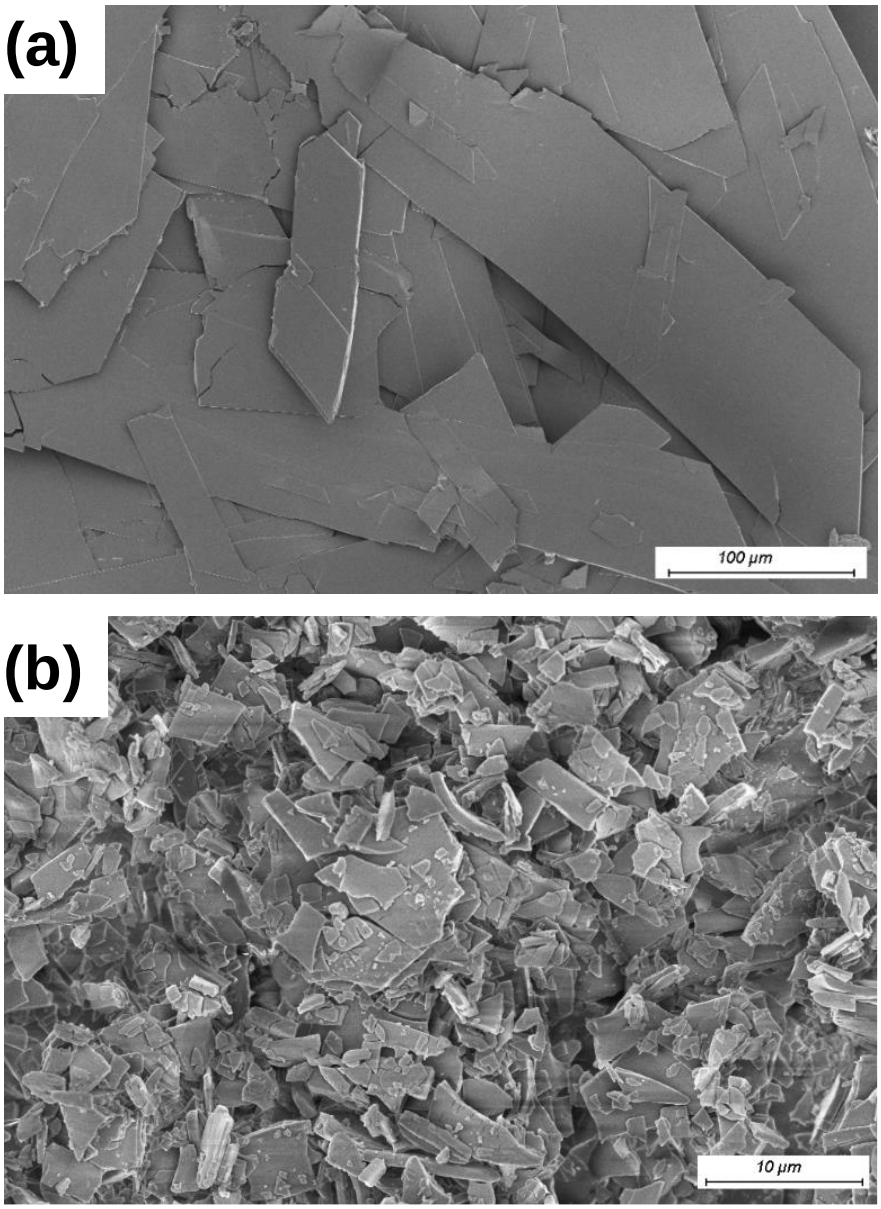

Figure S4. SEM images of xerogels in DMSO/water (1:1, v/v) at 5.0 wt/v%, (a) **3-BBU**, and (b) **3**.

5. X-ray crystallography

Table S3: Crystal data

Crystal data	**1.H_2O**	**3.2H_2O**	**4-BBU**	**4.2H_2O**
Empirical formula	$C_{18}H_{26}N_6O_5$	$C_{16}H_{24}N_6O_6$	$C_{16}H_{20}N_6O_2$	$C_{16}H_{24}N_6O_6$
Color	Colorless	Colorless	Colorless	Colorless
Formula weight	406.45	396.41	328.38	396.41
Crystal size (mm)	0.40 x 0.16 x 0.12	0.16 x 0.09 x 0.06	0.50 x 0.01 x 0.08	0.44 x 0.072 x 0.065
Crystal system	Monoclinic	Monoclinic	Monoclinic	Monoclinic
Space group	C2/c	$P2_1/n$	$P2_1/n$	$P2_1/n$
a (Å)	13.860(3)	4.9830(4)	4.9644(3)	4.7570(3)
b (Å)	5.281(2)	10.8892(9)	15.5022(13)	11.5219(7)
c (Å)	25.954(5)	16.1948(14)	10.5214(9)	16.9900(10)
α (°)	90	90	90	90
β (°)	94.00(3)	90.699(3)	96.893(3)	93.104(2)
γ (°)	90	90	90	90
Volume ($Å^3$)	1895.1(9)	878.68(13)	803.87(11)	929.85(10)
Z	4	2	2	2
$D_{calc.}$(g/cm^3)	1.425	1.498	1.357	1.416
F(000)	864	420	348	420
μ (mm^{-1}) MoK_α	0.106	0.116	0.094	0.110
Temperature (K)	293(2)	150(2)	296(2)	296(2)
Reflections collected/ unique/observed [I>2σ(I)]	22066/2564/ 2207	16106/2010/ 1574	18333/1713/ 1324	33014/1845/ 1357
Data/restraints/parameters	2564/0/136	2010/0/135	1713/0/109	1845/0/135
Goodness of fit on F^2	1.036	1.049	1.096	1.071
Final R indices [I>2σ(I)]	R_1 = 0.0395 wR_2 = 0.0985	R_1 = 0.0406 wR_2 = 0.0891	R_1 = 0.0434 wR_2 = 0.0993	R_1 = 0.0410 wR_2 = 0.0858
R indices (all data)	R_1 = 0.0525 wR_2 = 0.1033	R_1 = 0.0602 wR_2 = 0.0970	R_1 = 0.0636 wR_2 = 0.1094	R_1 = 0.0677 wR_2 = 0.0951

Table S4: Hydrogen bonding parameters

Compound 1.H_2O						
No.	Donor—H···Acceptor	D–H(Å)	H···A(Å)	D···A(Å)	∠D—H···A(°)	Symmetry operation
1	O(15)—H(1)···O(1)	0.858(18)	1.983(18)	2.8224(14)	165.8(16)	-1/2+x,1/2+y,z
2	N(8)—H(8)···O(1)	0.86	2.16	2.8749(16)	140	-1/2+x,1/2+y,z
3	N(11)—H(11)···O(1)	0.86	2.25	2.9531(17)	139	-1/2+x,1/2+y,z
4	C(3)—H(3)···O(15)	0.93	2.42	3.0953(17)	130	1/2+x,1/2+y,z
Compound 3.2H_2O						
No.	Donor—H···Acceptor	D–H (Å)	H···A (Å)	D···A (Å)	∠D—H···A (°)	Symmetry operation
1	N(8)—H(8)···O(14)	0.88	1.95	2.8011(17)	163	x,y,z
2	N(11)—H(11)···O(1)	0.88	2.21	3.0246(16)	153	-1/2+x,1/2-y,1/2+z
3	O(14)—H(14A)···O(1)	0.88(2)	2.05(2)	2.9013(18)	162(2)	3/2-x,1/2+y,1/2-z
4	O(14)—H(14B)···O(1)	0.94(3)	1.90(3)	2.8329(18)	171(2)	1/2-x,1/2+y,1/2-z
5	C(4)—H(4)···O(10)	0.95	2.41	3.3514(18)	174	3/2-x,1/2+y,1/2-z
Compound 4-BBU						
No.	Donor—H···Acceptor	D–H (Å)	H···A (Å)	D···A (Å)	∠D—H···A (°)	Symmetry operation
1	N(7)—H(7)···N(1)	0.86	2.27	2.986(2)	141	-1/2+x,3/2-y,1/2+z
2	N(10)—H(10)···O(9)	0.86	2.17	2.9871(15)	157	-1+x,y,z
Compound 4.2H_2O						
No.	Donor—H···Acceptor	D–H (Å)	H···A (Å)	D···A (Å)	∠D—H···A (°)	Symmetry operation
1	N(8)—H(8)···O(1)	0.86	1.96	2.7887(18)	163	3/2-x,-1/2+y,1/2-z
2	N(11)—H(11)···O(1)	0.86	2.24	2.9988(18)	147	3/2-x,-1/2+y,1/2-z
3	O(14)—H(14A)···O(1)	1.10(3)	1.69(3)	2.788(2)	176.4(19)	2-x,1-y,1-z
4	O(14)—H(14B)···O(10)	0.89(3)	2.01(3)	2.889(2)	169(3)	x,y,z
5	C(6)—H(6)···O(14)	0.93	2.58	3.201(2)	125	1/2+x,1/2-y,-1/2+z

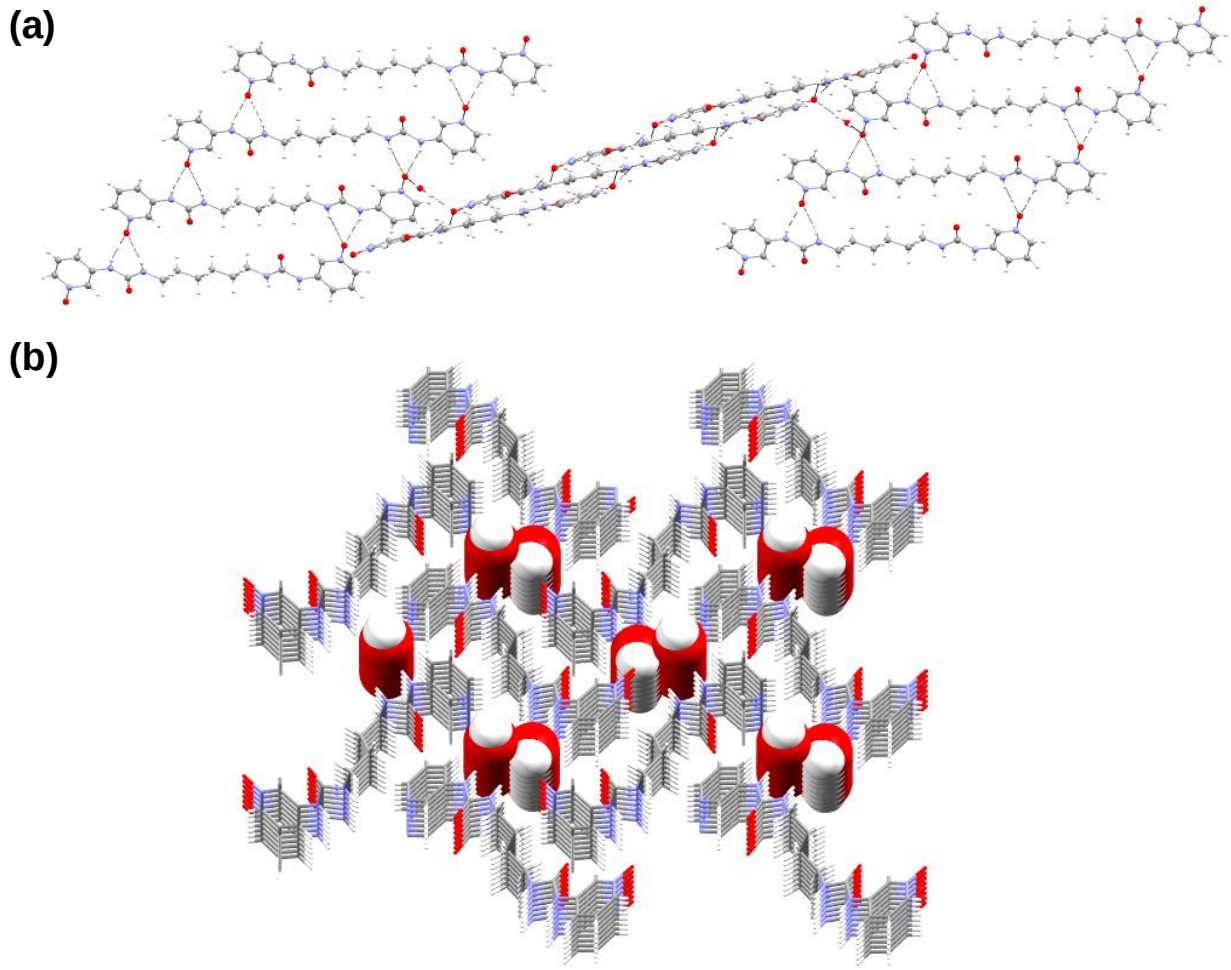

Figure S5. (a) One-dimensional chains interconnected by O—H···O interactions between the pyridyl-N-oxide moiety and the solvent water molecule in gelator **1** and (b) two-dimensional porous architecture in gelator **3** with entrapped water molecules.

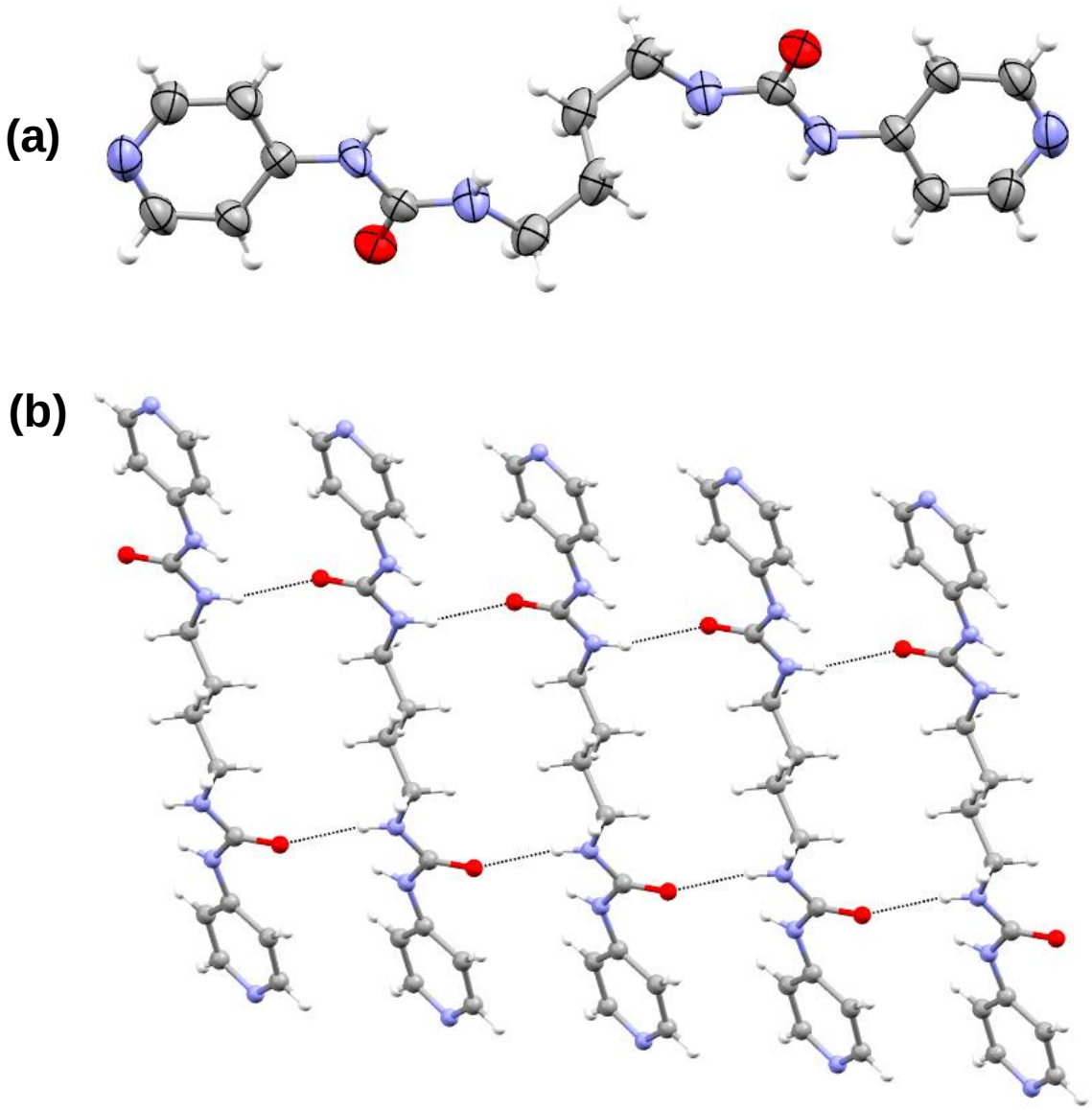

Figure S6. (a) Molecular structure of **4-BBU** and (b) one-dimensional chain of **4-BBU** formed by N···H—O interactions.

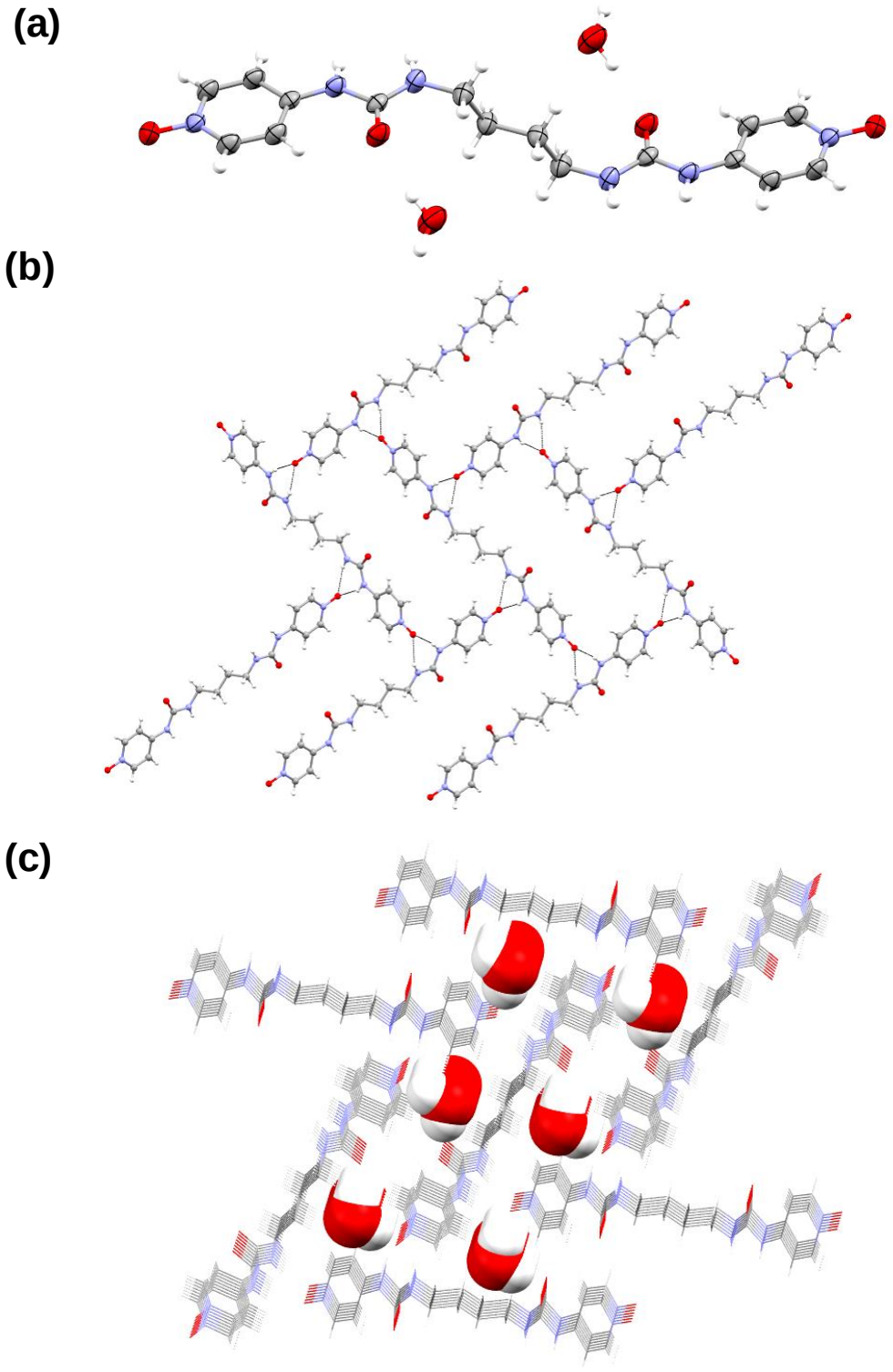

Figure S7. (a) Molecular structure of **4**•2H_2O, (b) bifurcated hydrogen bonding of the urea and pyridyl-*N*-oxide moieties resulting in two-dimensional hydrogen-bonded sheet and (c) solvent water molecules entrapped in the cavities of the two-dimensional sheets.

6. X-ray powder diffraction

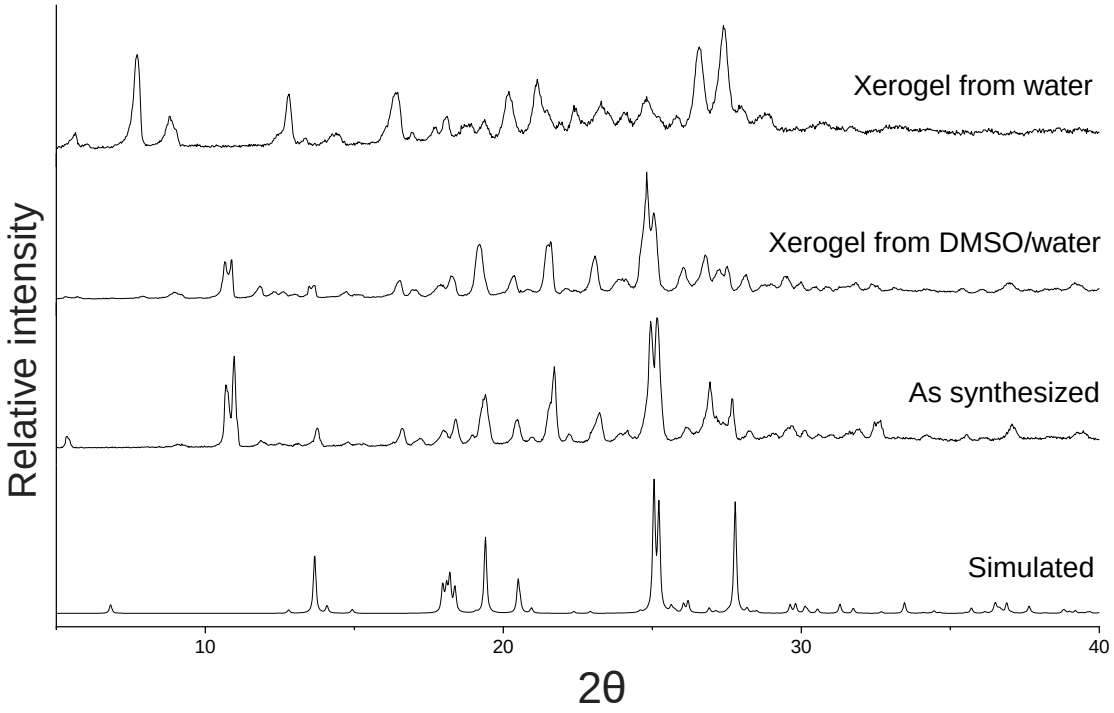

Figure S8. Comparison of the simulated pattern from single-crystal X-ray structure of compound **1** with the XRPD pattern of the bulk crystals obtained from DMSO/water, xerogel from DMSO/water (1:1, v/v, 4.0 wt/v%), and xerogel from water at 3.0 wt%.

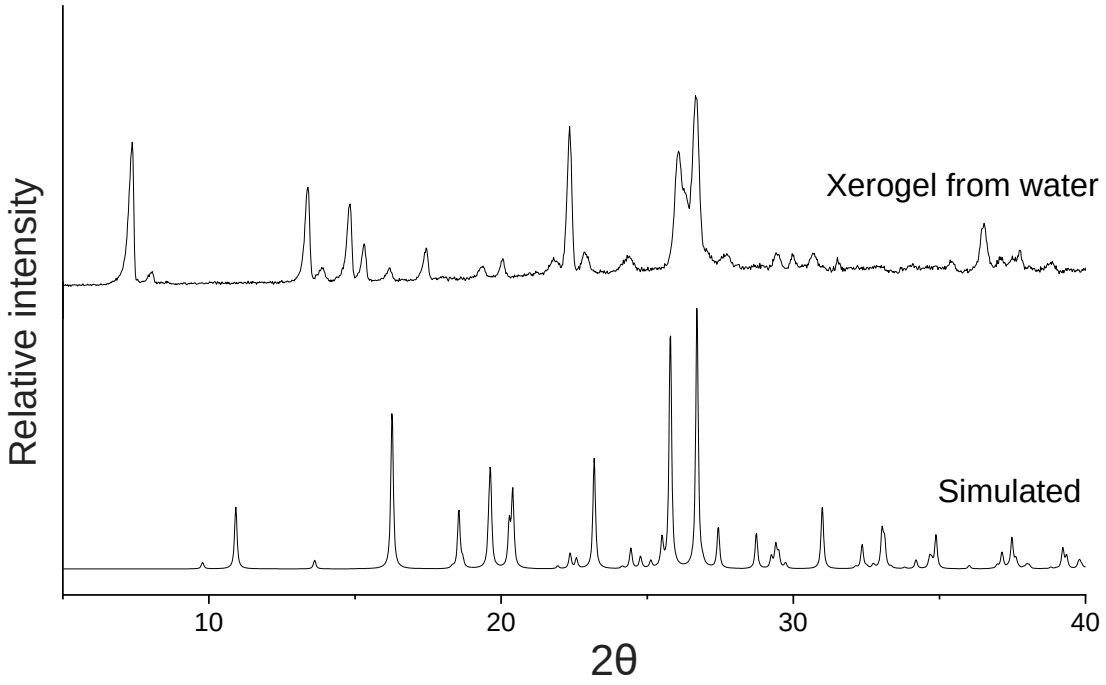

Figure S9. Comparison of the simulated pattern from single-crystal X-ray structure of compound **3** with the XRPD pattern of the xerogel from water at 3.0 wt%.

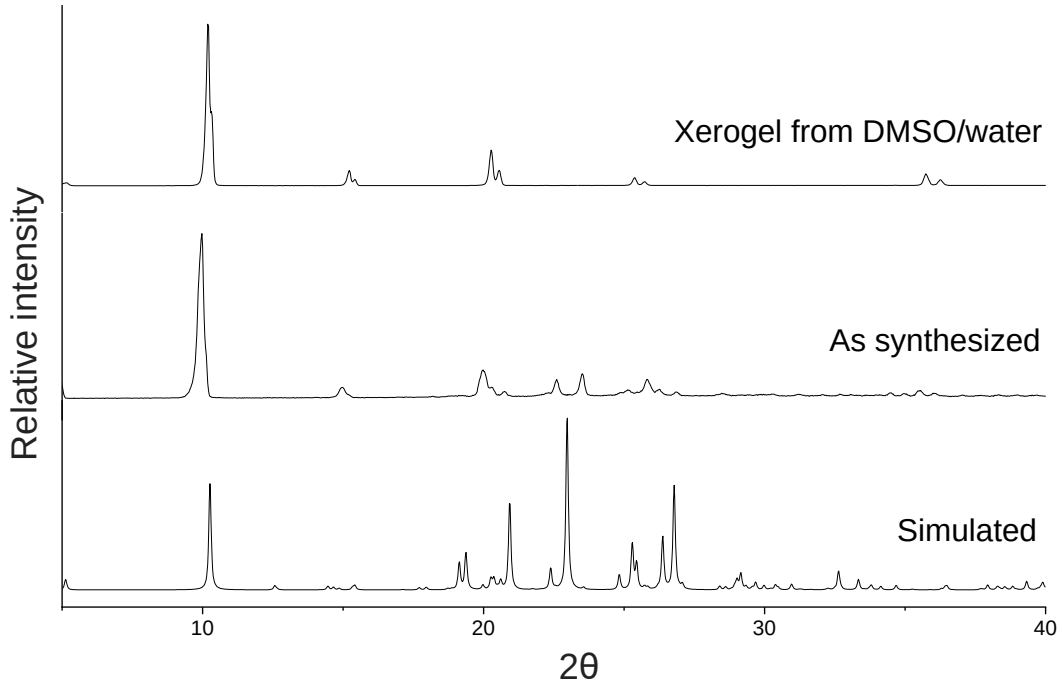

Figure S10. Comparison of the simulated pattern from single-crystal X-ray structure of compound **3-BBU** with the XRPD pattern of as-synthesized bulk crystals obtained from THF/water, xerogel from DMSO/water (1:1, v/v).

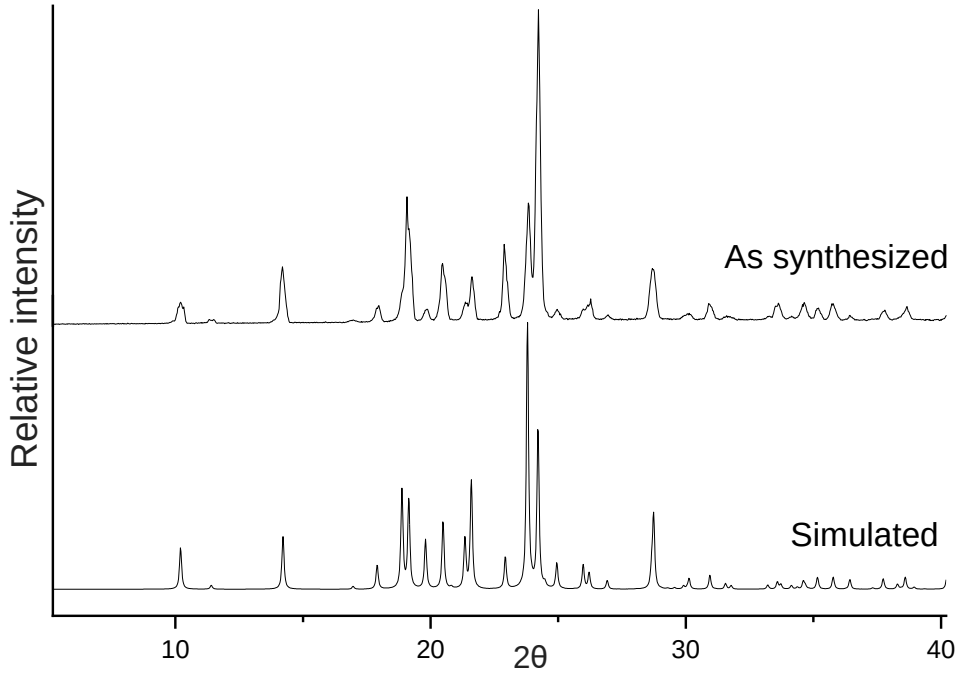

Figure S11. Comparison of the simulated pattern from single-crystal X-ray structure of **4-BBU** with the XRPD pattern of the bulk crystals obtained from MeOH/water.

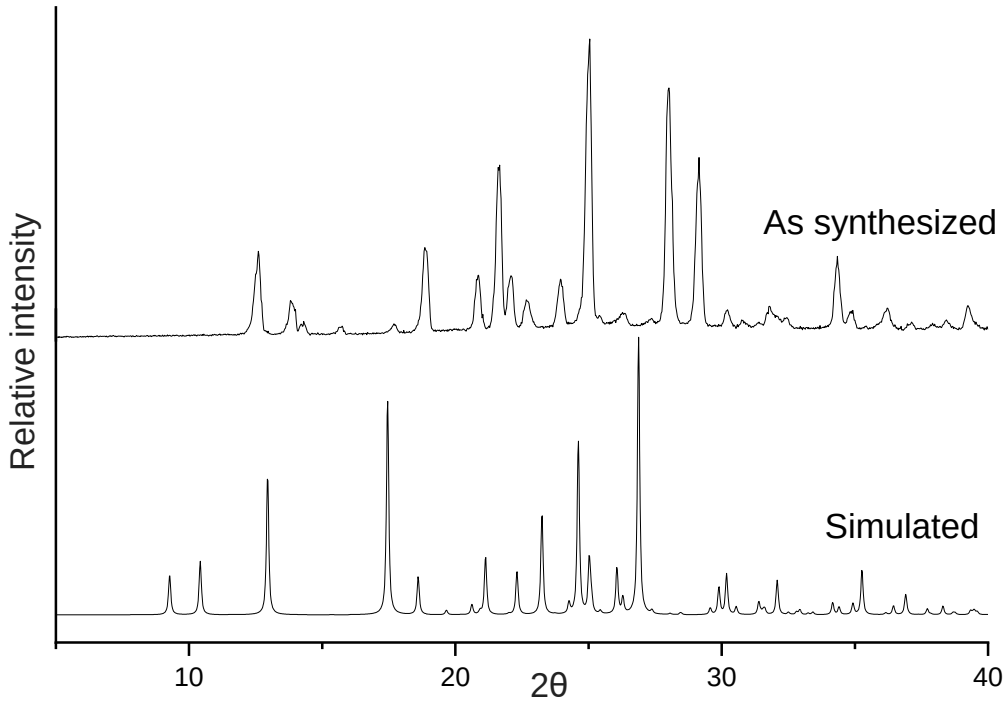

Figure S12. Comparison of the simulated pattern from single-crystal X-ray structure of **4**: with the XRPD pattern of bulk crystals obtained from water.

7. Physical properties in the presence of salts

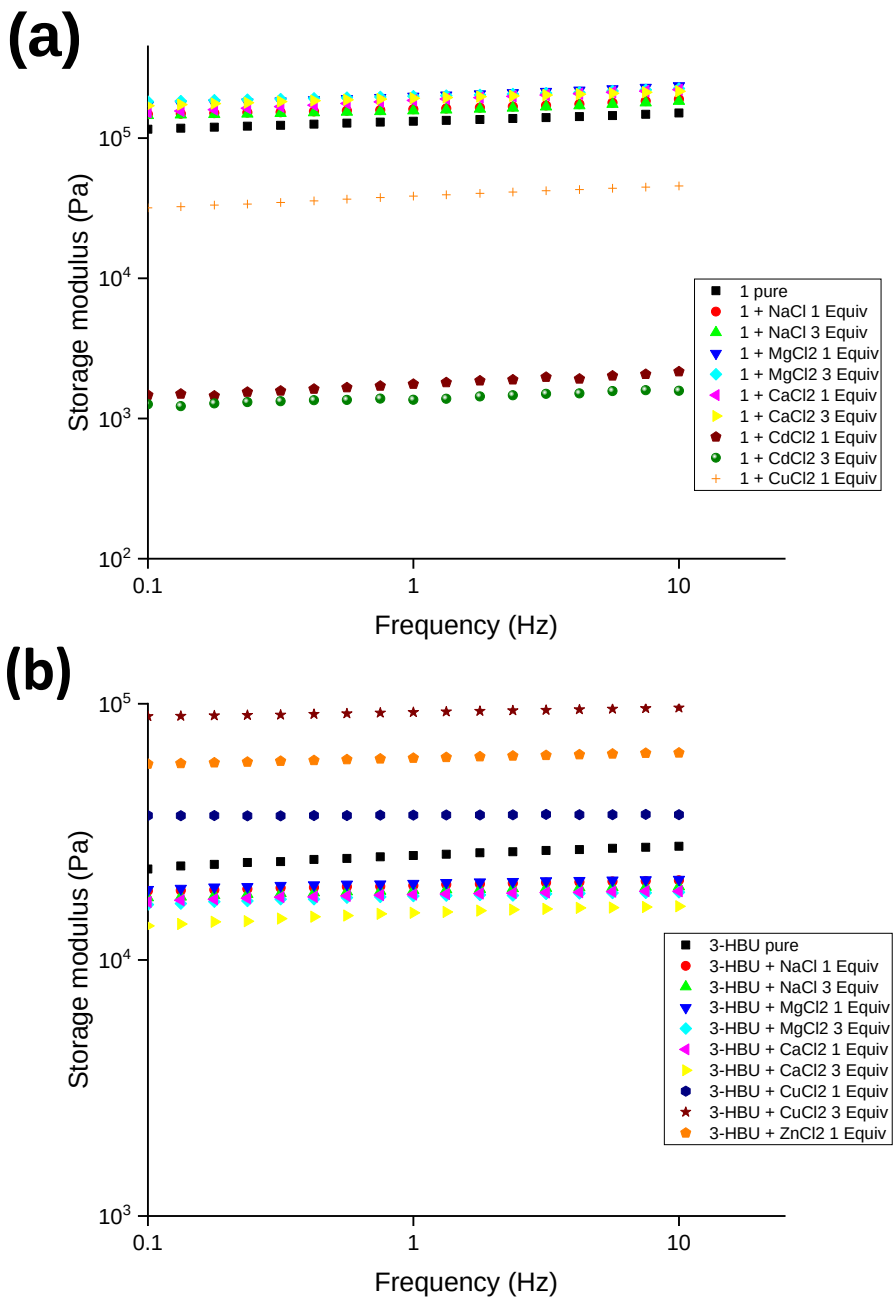

Figure S13. Frequency sweep experiments at 4.0 wt/v% in DMSO/water (1:1, v/v) in the presence of various salts of chlorides at 25.0 °C with a constant strain of 0.02%, (a) gelator **1**, and (b) **3-HBU**.

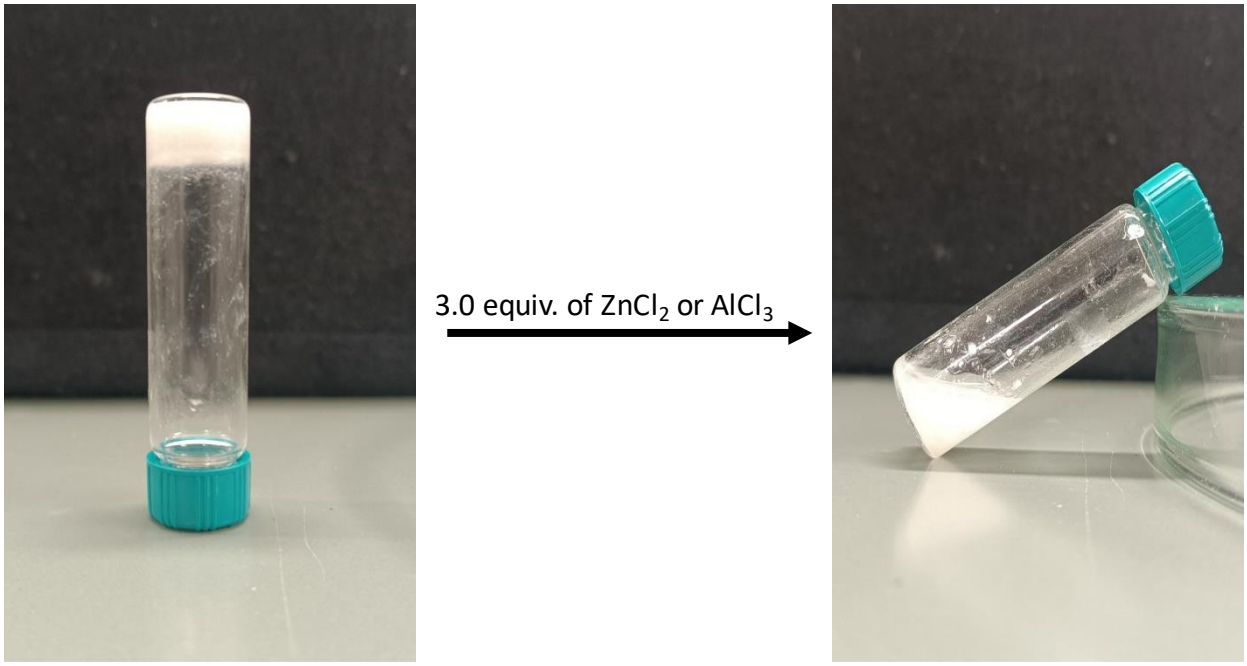

Figure S14. Gel network of **1** collapsing in the presence of 3.0 equiv. of $ZnCl_2$ or $AlCl_3$.

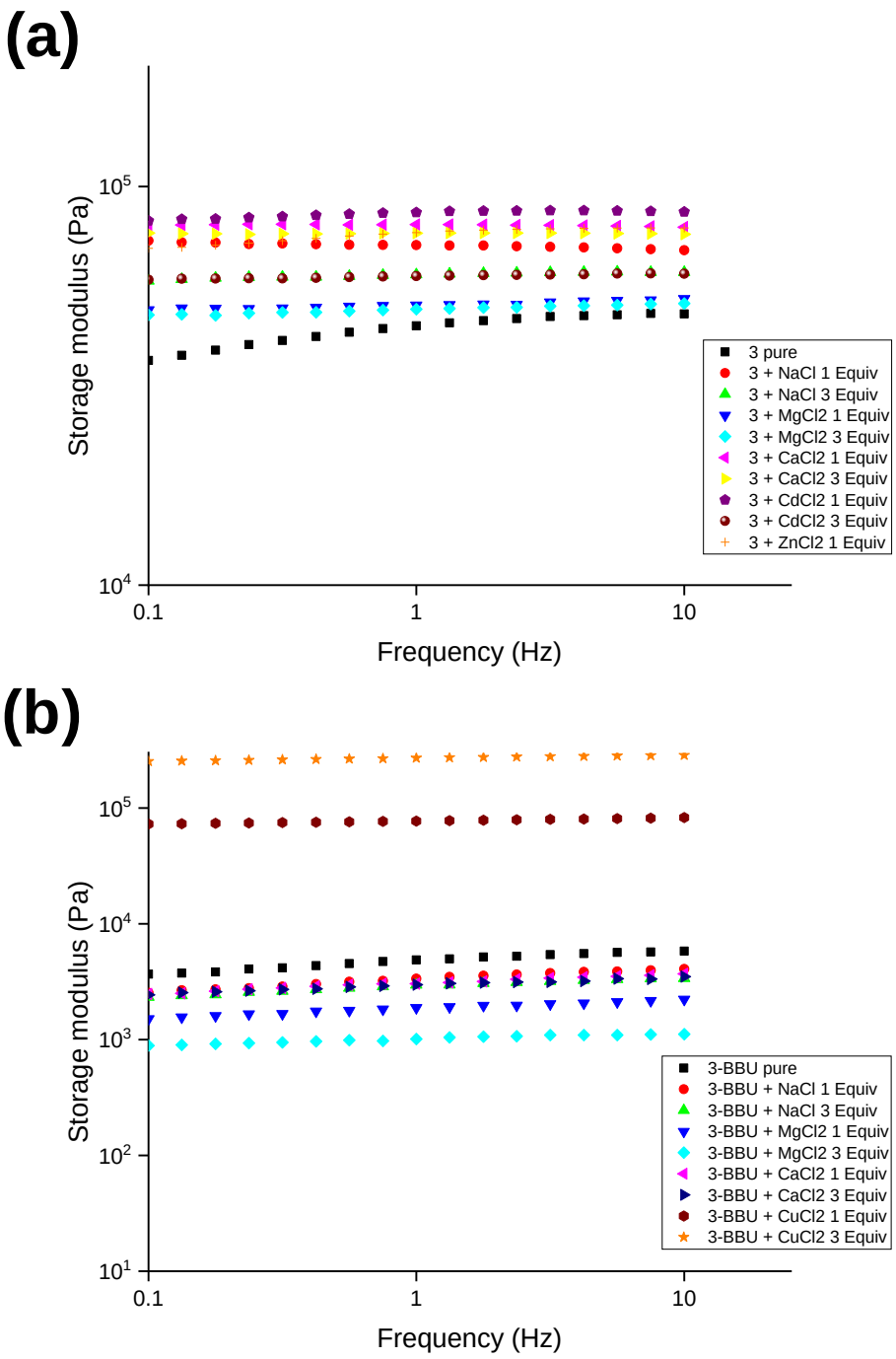

Figure S15. Frequency sweep experiments at 5.0 wt/v% in DMSO/water (1:1, v/v) in the presence of various salts of chlorides at 25.0 °C with a constant strain of 0.02%, (a) gelator **3**, and (b) **3-BBU**.

Table S5: T_{gel} experiments in the presence of salts in DMSO/water (1:1, v/v)

Salts	Equivalence	T_{gel} (°C)			
		4.0 wt/v%		5.0 wt/v%	
		3-HBU	1	3-BBU	3
Ligand pure		93.2	62.9	94.9	61.3
KF	1	91.8	67.8	93.9	62.8
	3	90.3	62.9	88.9	61.1
KCl	1	92.5	67.3	95.0	63.1
	3	90.1	63.1	91.0	59.9
KBr	1	92.1	66.1	91.3	60.3
	3	89.2	63.0	88.3	58.2
KI	1	90.3	66.5	90.4	60.1
	3	89.3	62.0	89.4	59.4
KCN	1	91.1	66.8	88.9	59.4
	3	89.0	62.6	86.4	58.0

Table S6: Stimuli-responsive properties of the parent and modified compounds: comparing the G' values in DMSO/water (1:1, v/v)*

Salt added	**Equivalents (equiv.)**	**3-HBU** (4.0 wt/v%)	**1** (4.0 wt/v%)	**3-BBU** (5.0 wt/v%)	**3** (5.0 wt/v%)
KF	1.0	0.8-fold	1.5-fold	0.3-fold	1.1-fold
	3.0	0.7-fold	1.3-fold	0.2-fold	1.1-fold
KCl	1.0	0.8-fold	1.9-fold	0.6-fold	1.6-fold
	3.0	0.2-fold	1.3-fold	0.5-fold	2.5-fold
KBr	1.0	0.7-fold	1.5-fold	0.5-fold	1.1-fold
	3.0	0.5-fold	1.4-fold	0.4-fold	1.1-fold
KI	1.0	0.8-fold	1.9-fold	0.3-fold	1.3-fold
	3.0	0.4-fold	1.3-fold	0.3-fold	1.6-fold
KCN	1.0	0.8-fold	2.0-fold	0.8-fold	1.4-fold
	3.0	0.4-fold	1.4-fold	0.7-fold	1.3-fold
NaCl	1.0	0.8-fold	1.2-fold	0.7-fold	1.4-fold
	3.0	0.7-fold	1.2-fold	0.6-fold	1.3-fold
$MgCl_2$	1.0	0.7-fold	1.6-fold	0.4-fold	1.1-fold
	3.0	0.7-fold	1.5-fold	0.2-fold	1.1-fold
$CaCl_2$	1.0	0.7-fold	1.5-fold	0.6-fold	1.6-fold
	3.0	0.6-fold	1.4-fold	0.6-fold	1.6-fold
$CuCl_2$	1.0	1.3-fold	0.3-fold	14.1-fold	---
	3.0	3.5-fold	---	44.5-fold	---
$ZnCl_2$	1.0	2.4-fold	---	---	1.6-fold
	3.0	---	---	---	---
$CdCl_2$	1.0	---	0.01-fold	---	1.6-fold
	3.0	---	0.01-fold	---	1.2-fold
$AlCl_3$	1.0	---	---	---	---
	3.0	---	---	---	---

*The mechanical strength is compared with the corresponding wt/v% of the pure gelator in the absence of salts.

Table S7: Stimuli-responsive properties of the modified compounds **1**, **3** and **4**: comparing the G' values in water*

Salt added	Equivalents (equiv.)	Gelator 1		Gelator 3		Gelator 4	
		2.5 wt%	1.5 wt%	3.5 wt%	2.5 wt%	7.0 wt%	5.0 wt%
KF	1.0	1.6-fold	4.5-fold	1.9-fold	4.6-fold	---	---
	3.0	1.7-fold	5.3-fold	1.1-fold	5.2-fold	---	---
KCl	1.0	1.4-fold	6.1-fold	2.9-fold	2.9-fold	---	---
	3.0	1.4-fold	6.5-fold	1.9-fold	3.9-fold	1.1-fold	1.1-fold
KBr	1.0	2.0-fold	1.5-fold	2.0-fold	2.7-fold	---	---
	3.0	2.0-fold	1.3-fold	2.1-fold	4.6-fold	---	---
KI	1.0	1.5-fold	1.2-fold	1.1-fold	4.6-fold	---	---
	3.0	1.2-fold	1.4-fold	1.6-fold	1.2-fold	---	---
KCN	1.0	2.1-fold	1.8-fold	1.3-fold	1.1-fold	---	---
	3.0	1.9-fold	1.9-fold	1.3-fold	1.3-fold	---	---
NaCl	1.0	1.1-fold	3.4-fold	1.4-fold	1.9-fold	---	---
	3.0	1.2-fold	3.1-fold	1.8-fold	3.3-fold	1.4-fold	1.0-fold
$MgCl_2$	1.0	1.2-fold	7.6-fold	1.5-fold	2.4-fold	---	---
	3.0	1.2-fold	5.8-fold	1.7-fold	3.6-fold	1.9-fold	1.7-fold
$CaCl_2$	1.0	1.1-fold	3.6-fold	1.9-fold	2.6-fold	---	---
	3.0	1.1-fold	5.0-fold	1.2-fold	3.6-fold	2.9-fold	2.7-fold
$CuCl_2$	1.0	1.1-fold	1.1-fold	---	2.1-fold	---	---
	3.0	---	---	---	---	---	---
$ZnCl_2$	1.0	1.8-fold	1.1-fold	---	1.5-fold	---	---
	3.0	---	---	---	---	---	---
$CdCl_2$	1.0	1.3-fold	1.1-fold	---	2.3-fold	---	---
	3.0	---	---	---	---	---	---
$AlCl_3$	1.0	1.1-fold	---	1.0-fold	---	---	---
	3.0	---	---	---	---	---	---
$Mg(NO_3)_2$	1.0	1.2-fold	1.3-fold	1.6-fold	1.2-fold	---	---
	3.0	1.2-fold	1.2-fold	1.4-fold	1.8-fold	---	---
$Ca(NO_3)_2$	1.0	1.5-fold	1.4-fold	1.5-fold	2.1-fold	---	---
	3.0	1.5-fold	1.2-fold	1.7-fold	2.5-fold	---	---
$MgSO_4$	1.0	1.6-fold	1.6-fold	1.8-fold	2.2-fold	---	---
	3.0	1.6-fold	1.3-fold	2.0-fold	1.9-fold	---	---
$CsCl_2$	1.0	1.5-fold	1.8-fold	1.9-fold	1.1-fold	---	---
	3.0	1.6-fold	1.3-fold	1.3-fold	1.7-fold	---	---
$SrCl_2$	1.0	1.1-fold	1.6-fold	1.4-fold	2.2-fold	---	---
	3.0	1.3-fold	1.5-fold	1.6-fold	2.3-fold	---	---
$BaCl_2$	1.0	1.6-fold	1.4-fold	1.6-fold	3.8-fold	---	---
	3.0	1.5-fold	1.6-fold	1.9-fold	1.8-fold	---	---

*The mechanical strength is compared with the corresponding wt% of the pure gelator in the absence of salts.

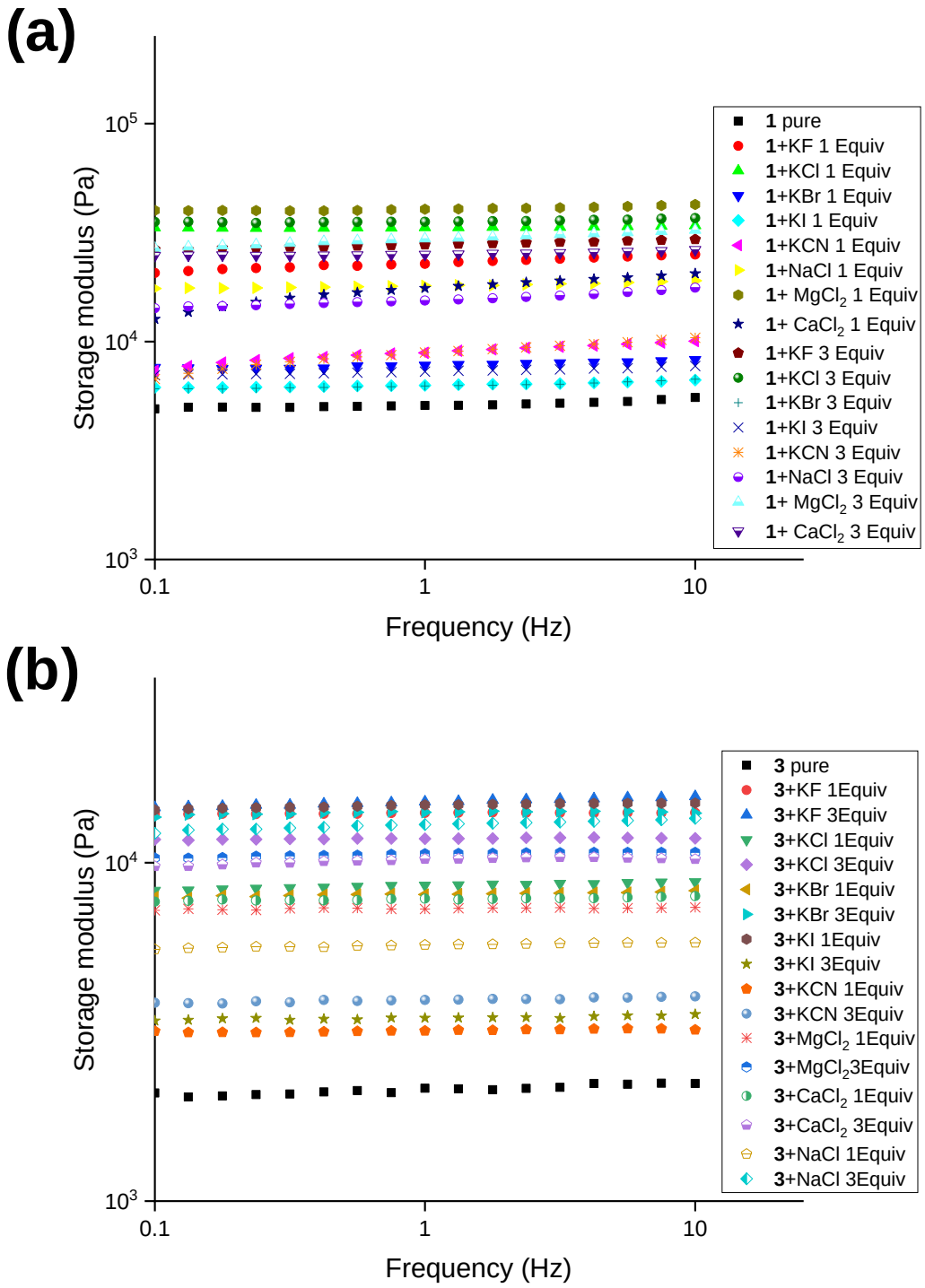

Figure S16. Frequency sweep experiments at MGC in water in presence of salts at 25.0 °C with a constant strain of 0.02%, (a) compound **1** at 1.5 wt%, and (b) compound **3** at 2.5 wt%.

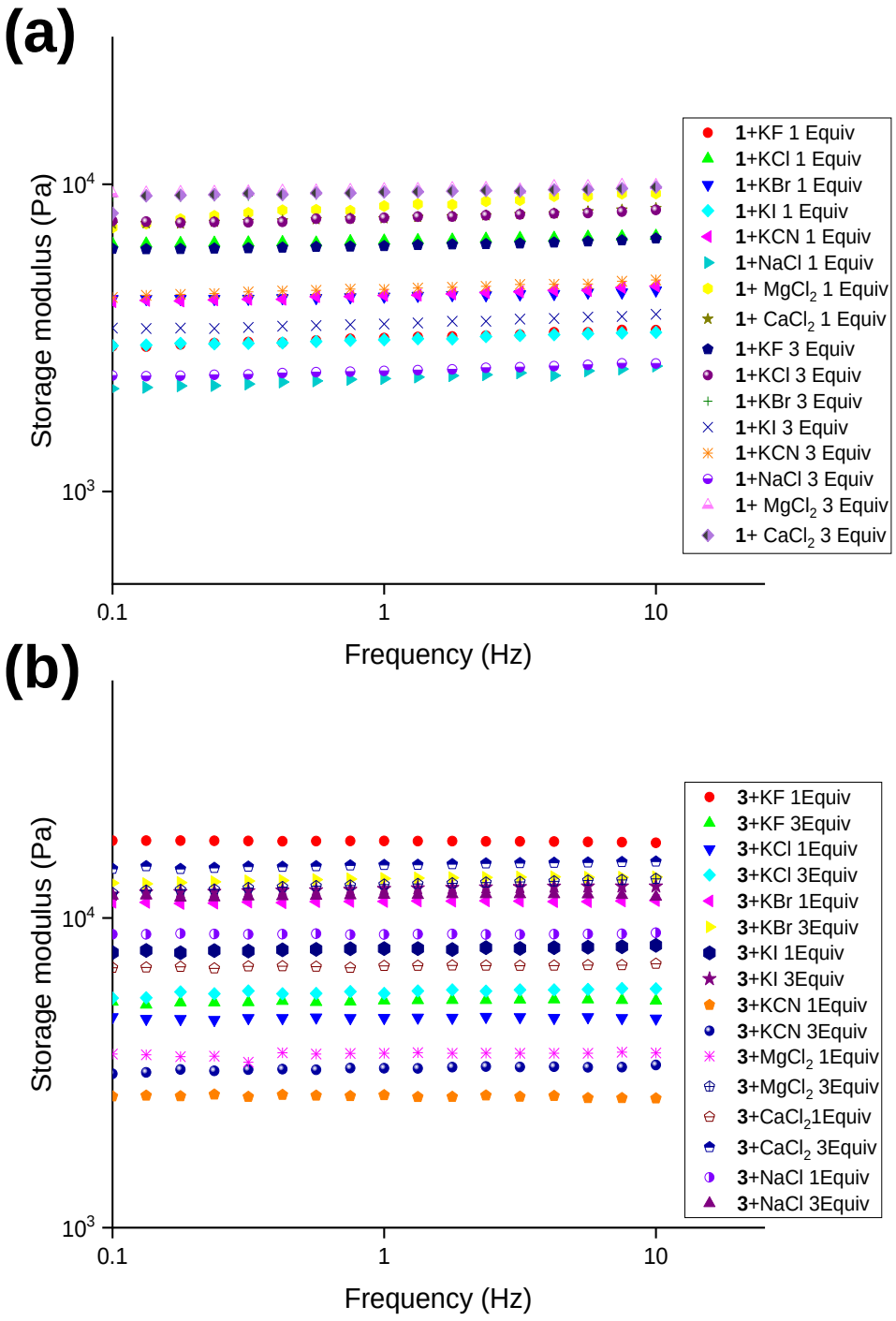

Figure S17. Frequency sweep experiments below MGC in water in presence of salts at 25.0 °C with a constant strain of 0.02%, (a) compound **1** at 1.0 wt%, and (b) compound **3** at 2.0 wt%.

*Physical properties of compound **4** in the presence of salts*: The experiments were first performed at 7.0 wt% of **4** in the presence of chloride salts of potassium, sodium, magnesium and calcium, and the analysis of mechanical strength revealed a 2-3-fold increase of G' in the presence of magnesium chloride and calcium chloride (Figure S18a).The experiments were then performed at 5.0 wt/v% of **4** in water in the presence of various salts such as potassium chloride, sodium chloride, magnesium chloride and calcium chloride. At 1.0 equivalent of the salts, no gel was obtained, but on increasing the salt concentration to 3.0 equivalents, gelation was observed for **4** with all these salts. The mechanical strength of these gels was evaluated by frequency sweep experiments and was compared with the partial gel obtained with the pure compound **4** at 5.0 wt/v%. The comparison of the rheological data revealed that the mechanical strength of **4** was similar to the KCl mixture, but 2-3-fold increase in G' was recorded for the gels with magnesium chloride and calcium chloride (Figure S18b).

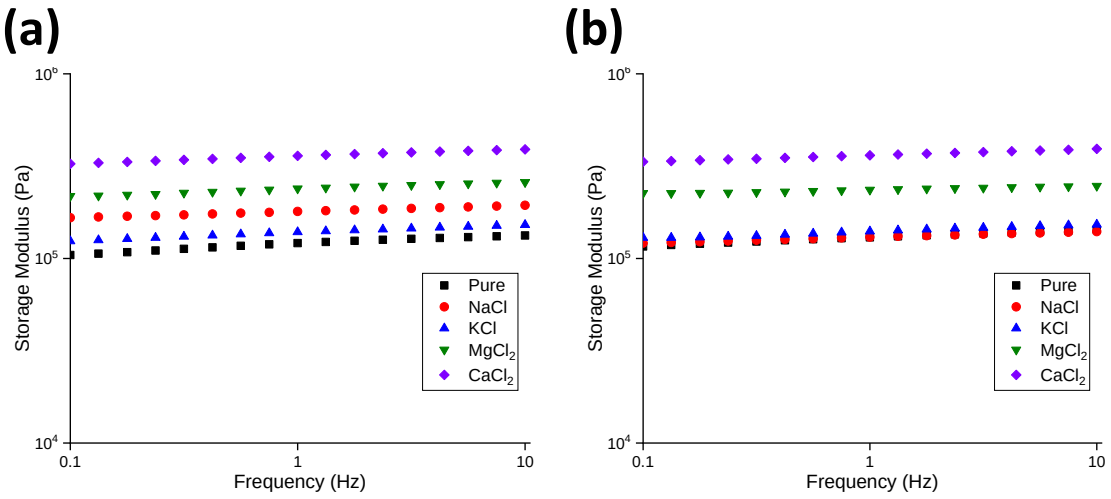

Figure S18. Frequency sweep experiments with compound **4** in the presence of 3.0 equivalents of the salts in water at 25.0 °C with a constant strain of 0.02%, (a) 7.0 wt%, and (b) 5.0 wt%.

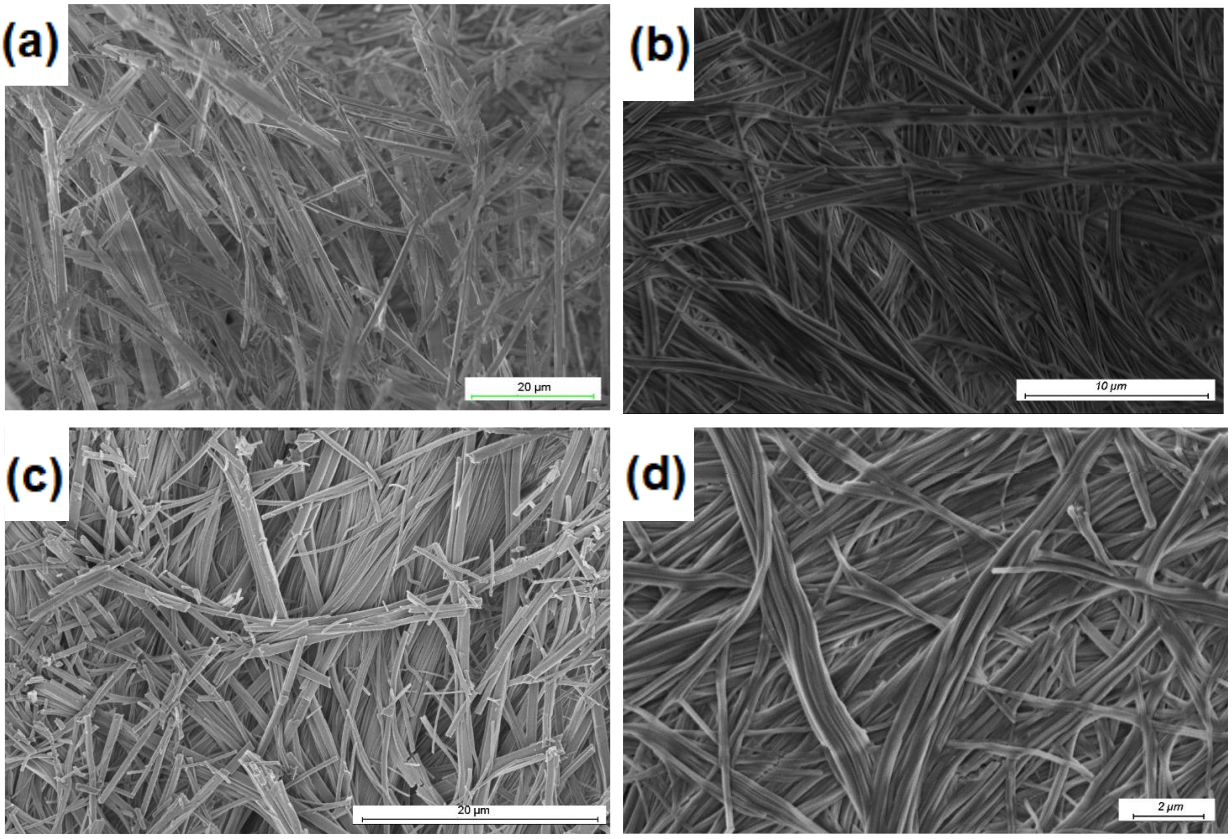

Figure S19. SEM images of xerogels of **1** obtained from pure water at 1.0 wt% (below MGC), (a) partial gel, and in the presence of 3.0 equiv. of (b) potassium fluoride, (c) magnesium chloride, and (d) calcium chloride.

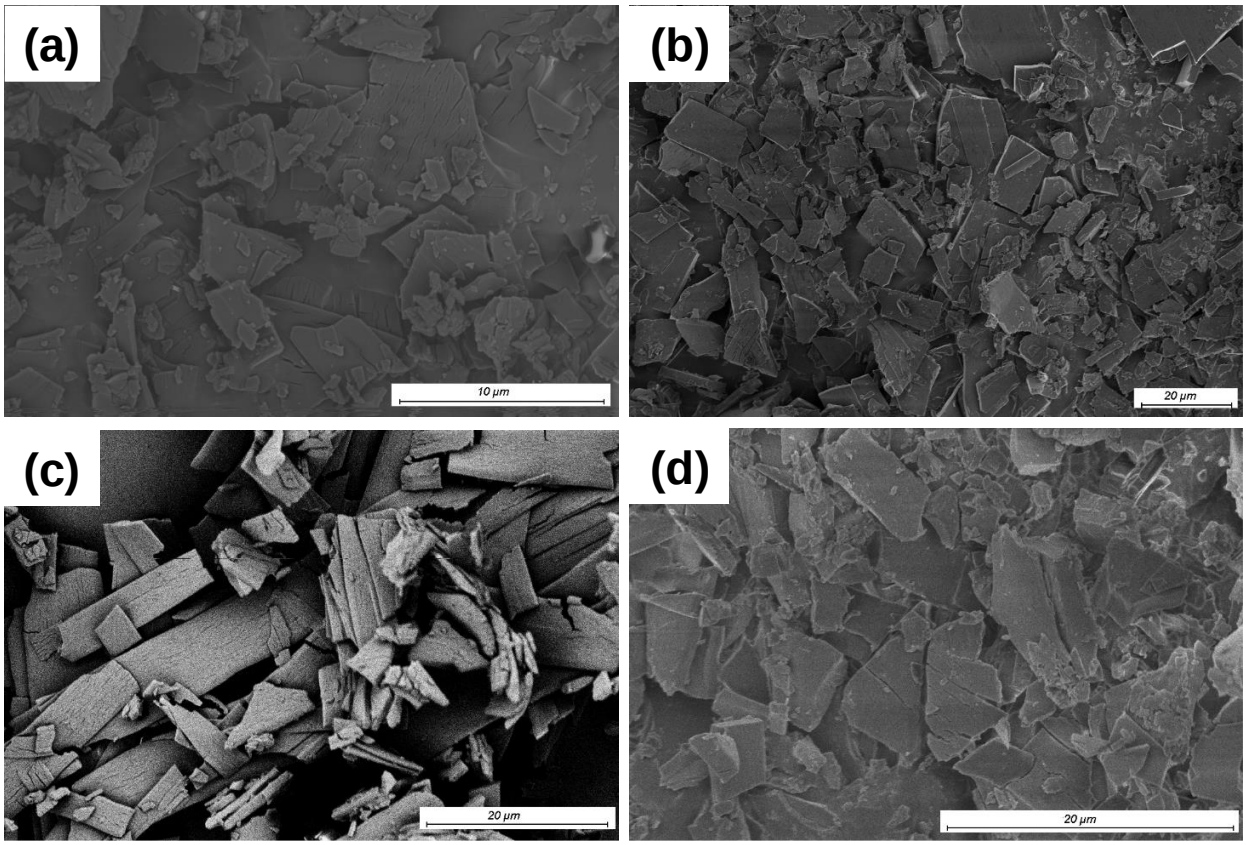

Figure S20. SEM images of xerogels of **3** obtained from pure water at 2.0 wt% (below MGC), (a) partial gel, and in the presence of 3.0 equiv. of (b) potassium fluoride, (c) magnesium chloride, and (d) calcium chloride.

8. NMR spectra

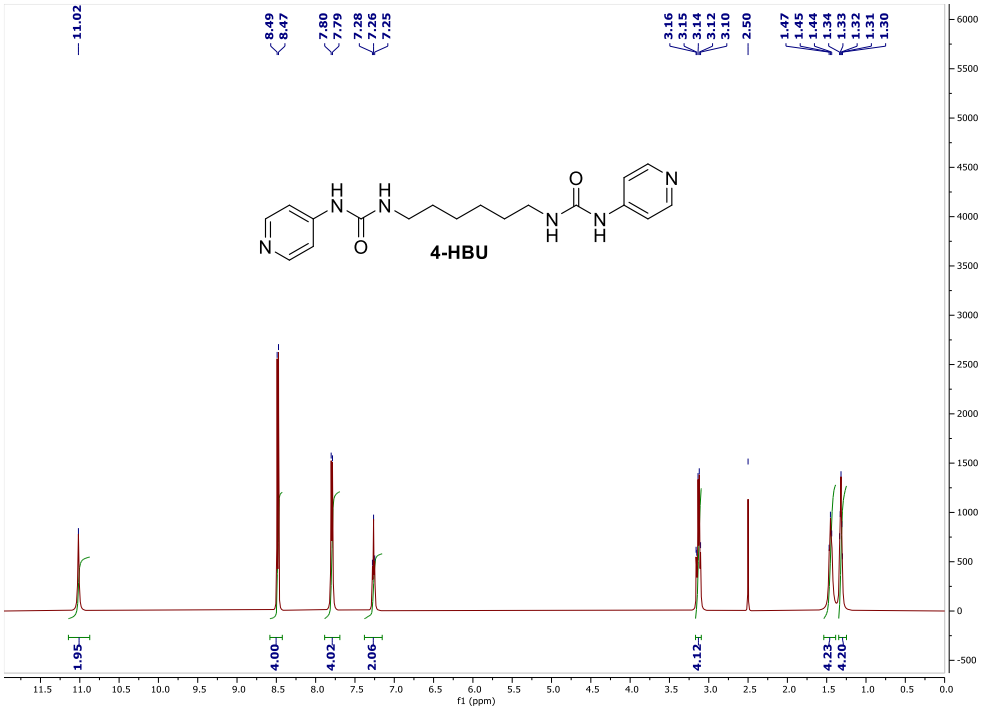

Figure S21. ^{1}H NMR spectrum of compound **4-HBU**.

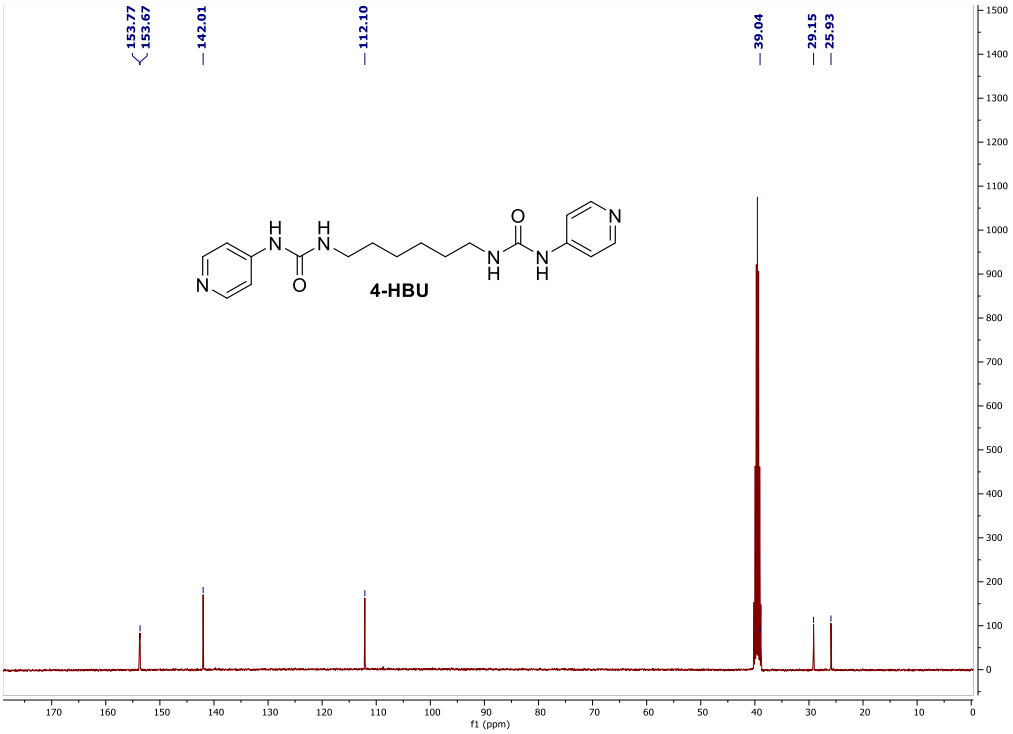

Figure S22. ^{13}C NMR spectrum of compound **4-HBU**.

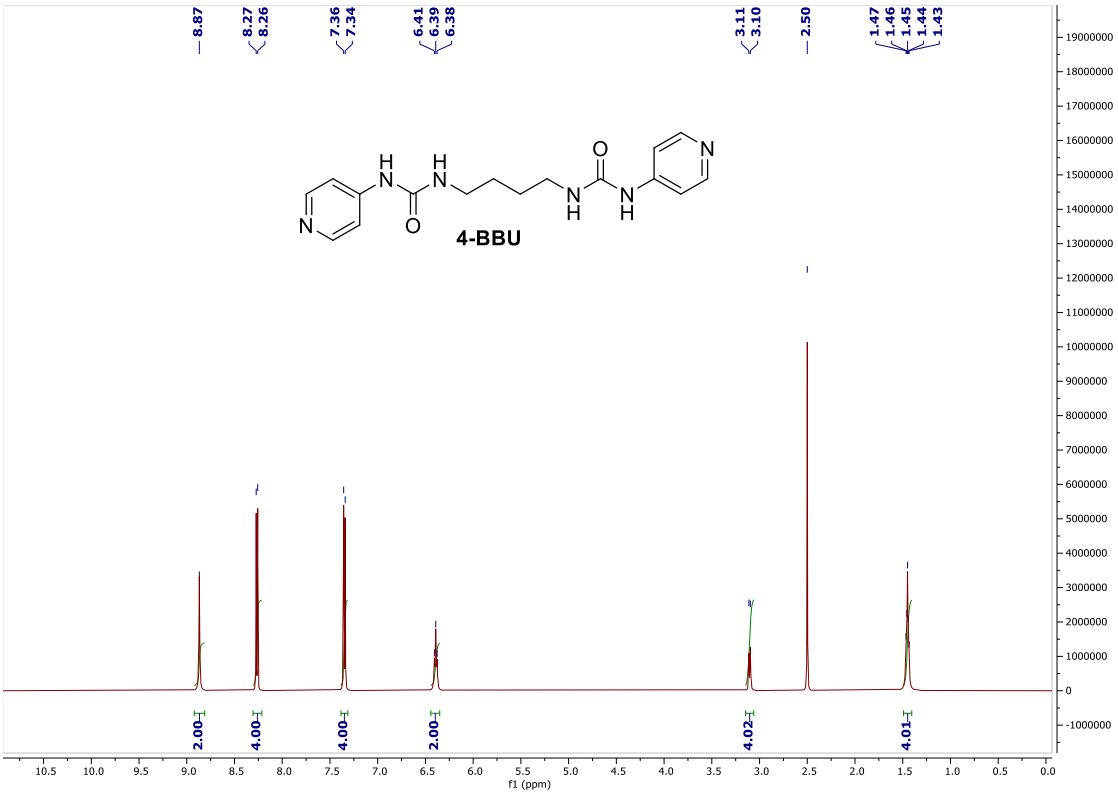

Figure S23. ^{1}H NMR spectrum of compound **4-BBU**.

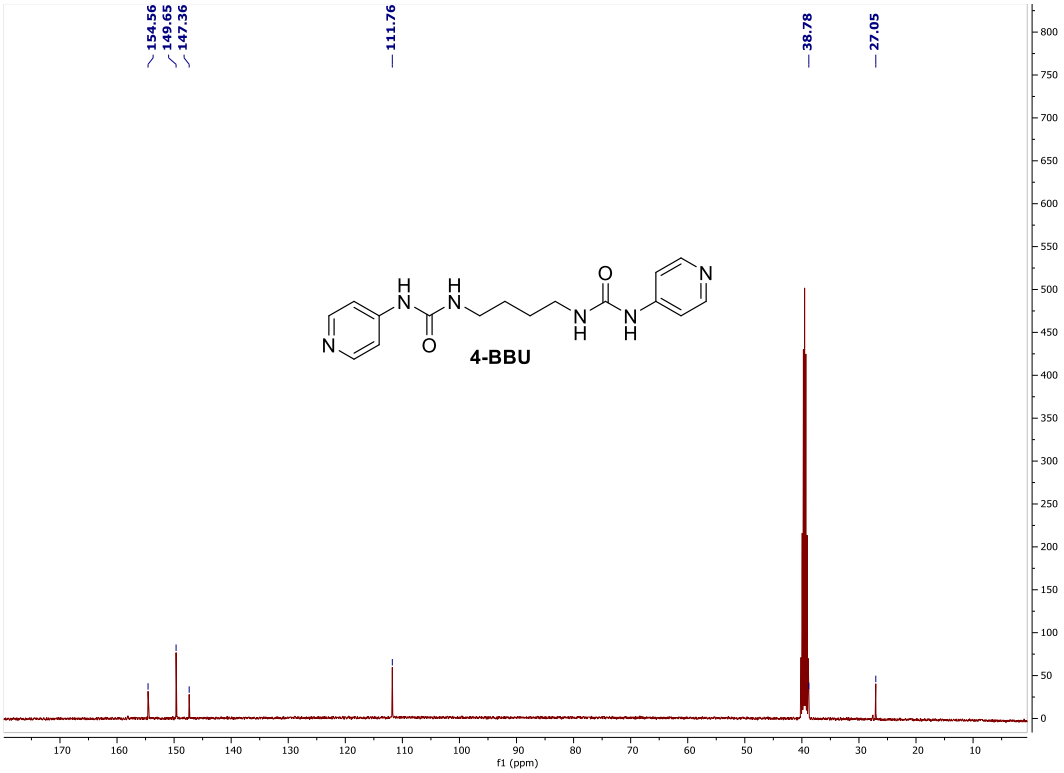

Figure S24. ^{13}C NMR spectrum of compound **4-BBU**.

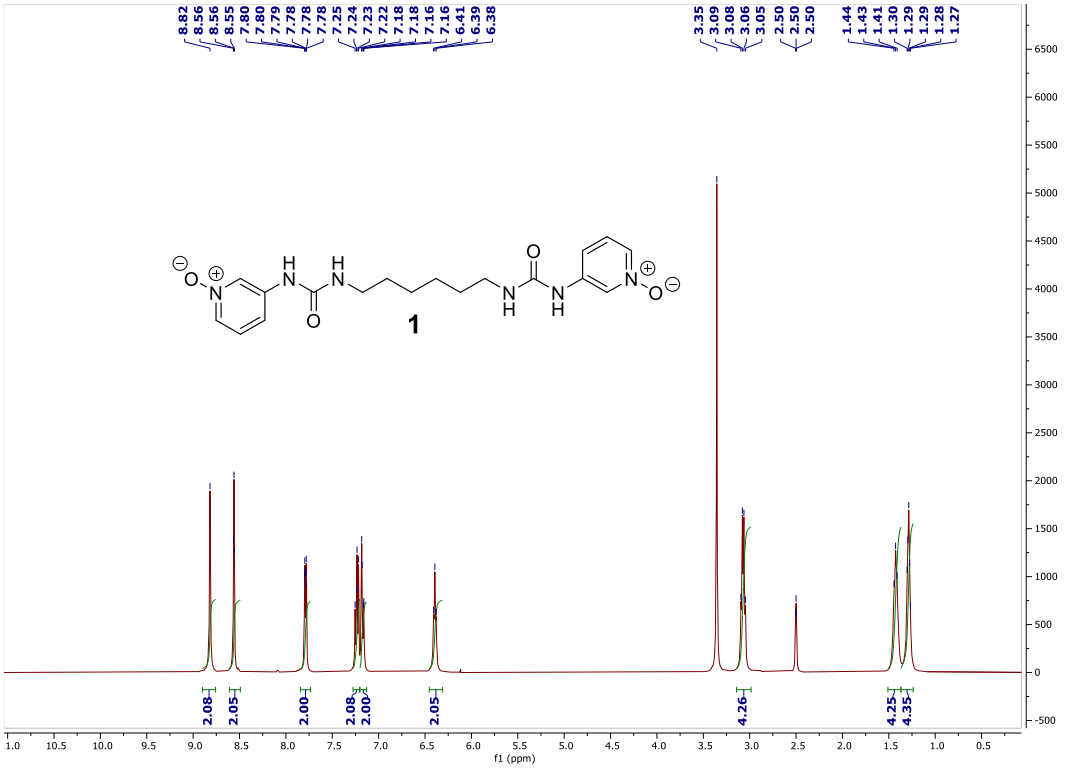

Figure S25. ^{1}H NMR spectrum of compound **1**.

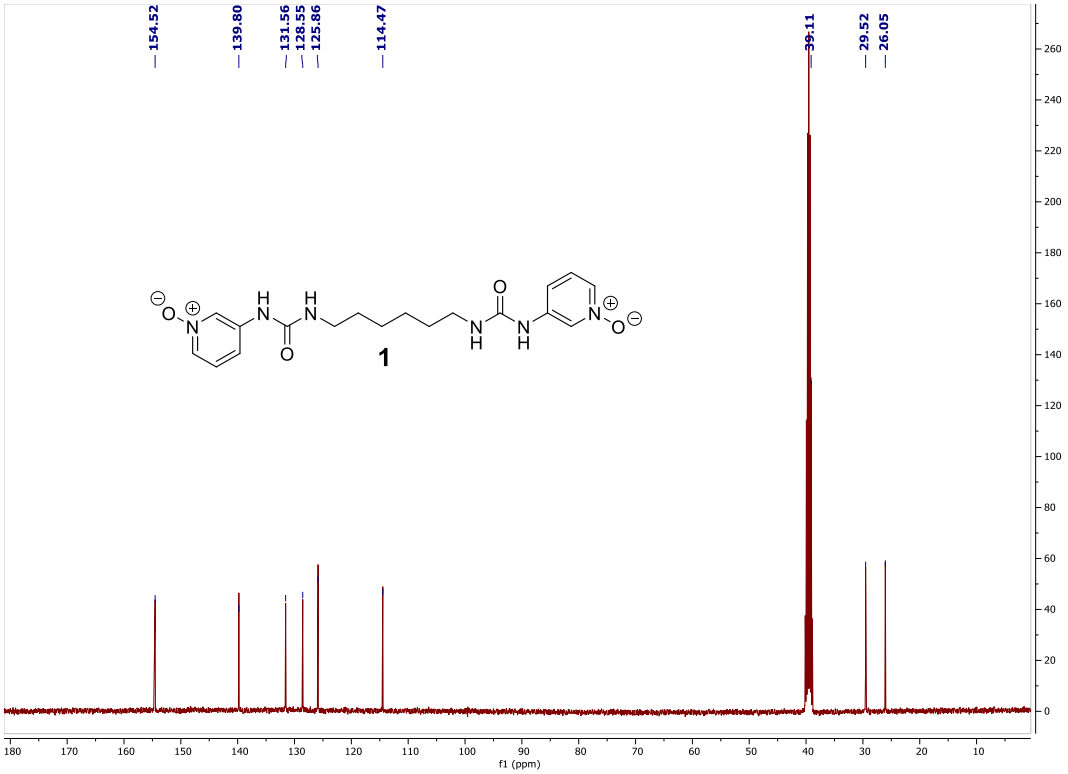

Figure S26. ^{13}C NMR spectrum of compound **1**.

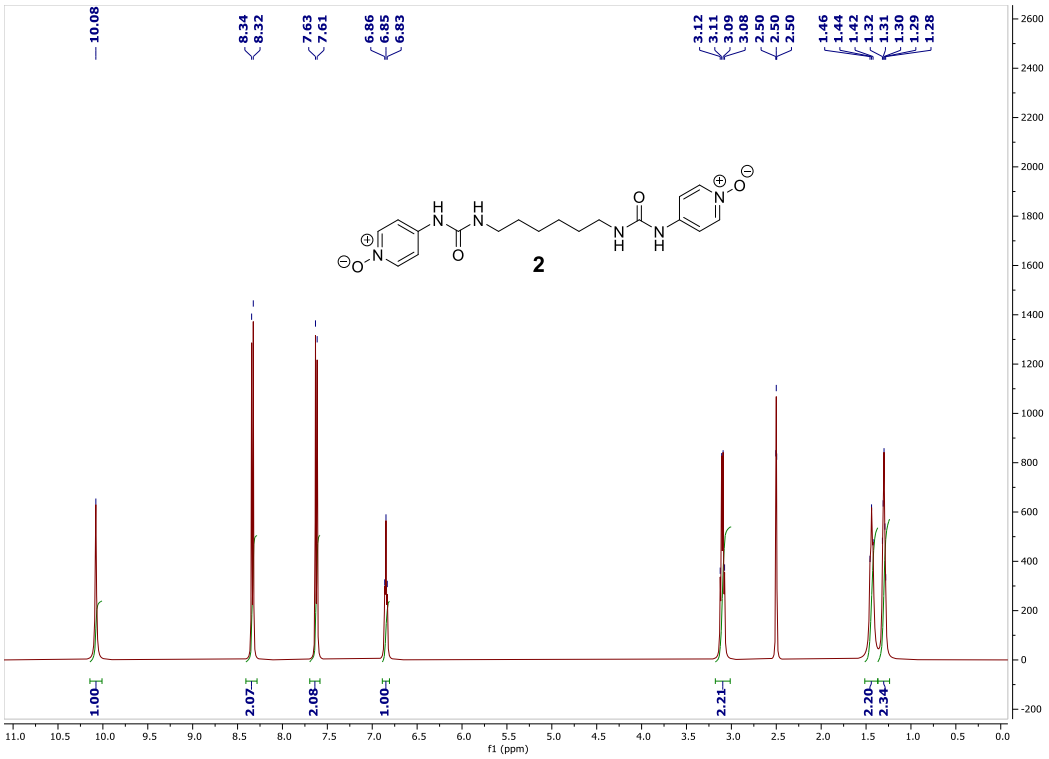

Figure S27. ^{1}H NMR spectrum of compound **2**.

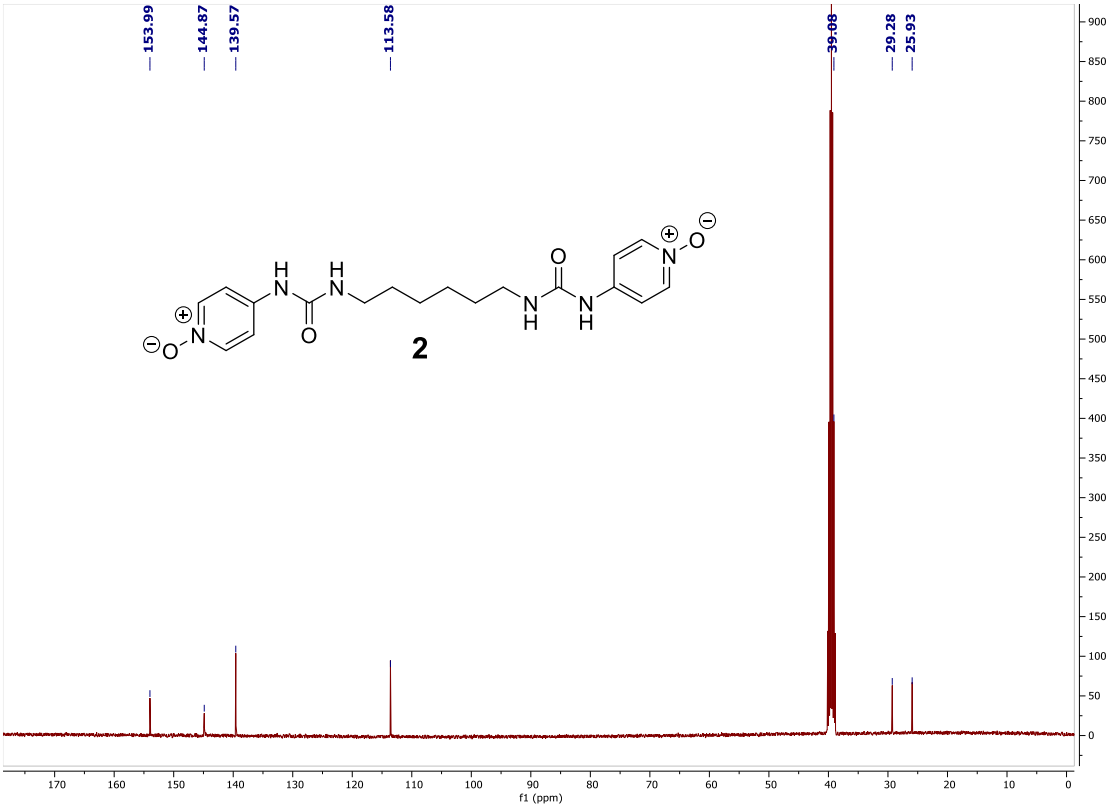

Figure S28. ^{13}C NMR spectrum of compound **2**.

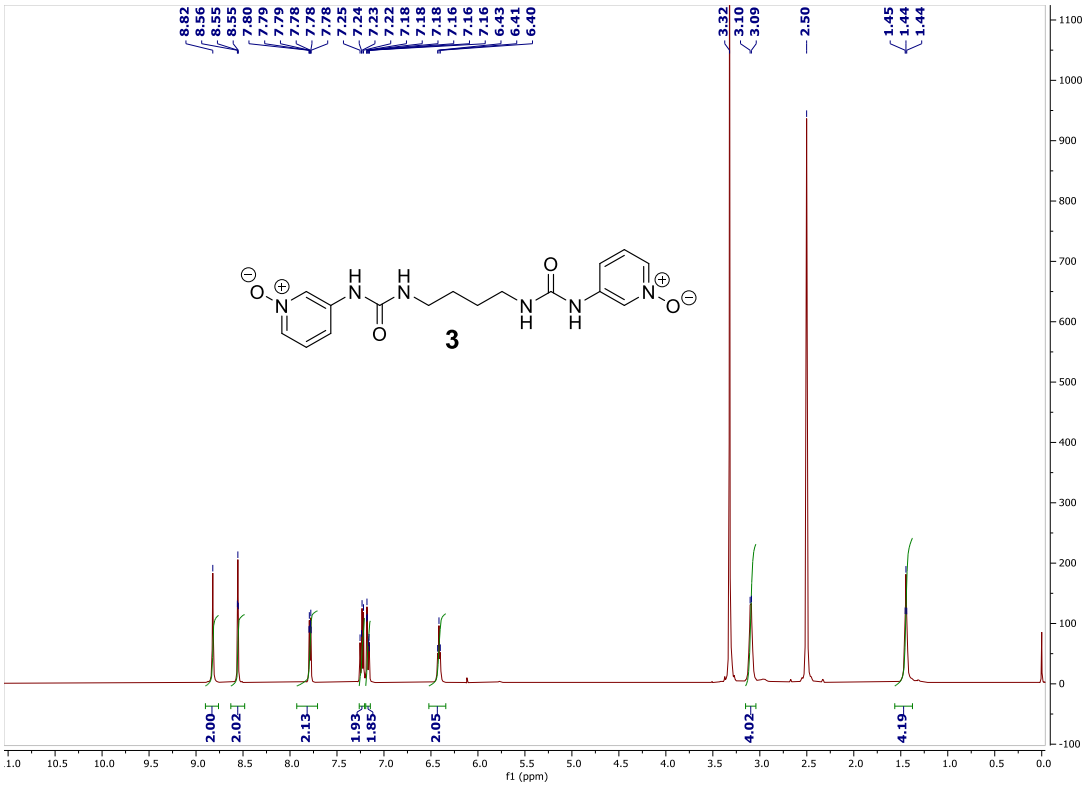

Figure S29. ^{1}H NMR spectrum of compound **3**.

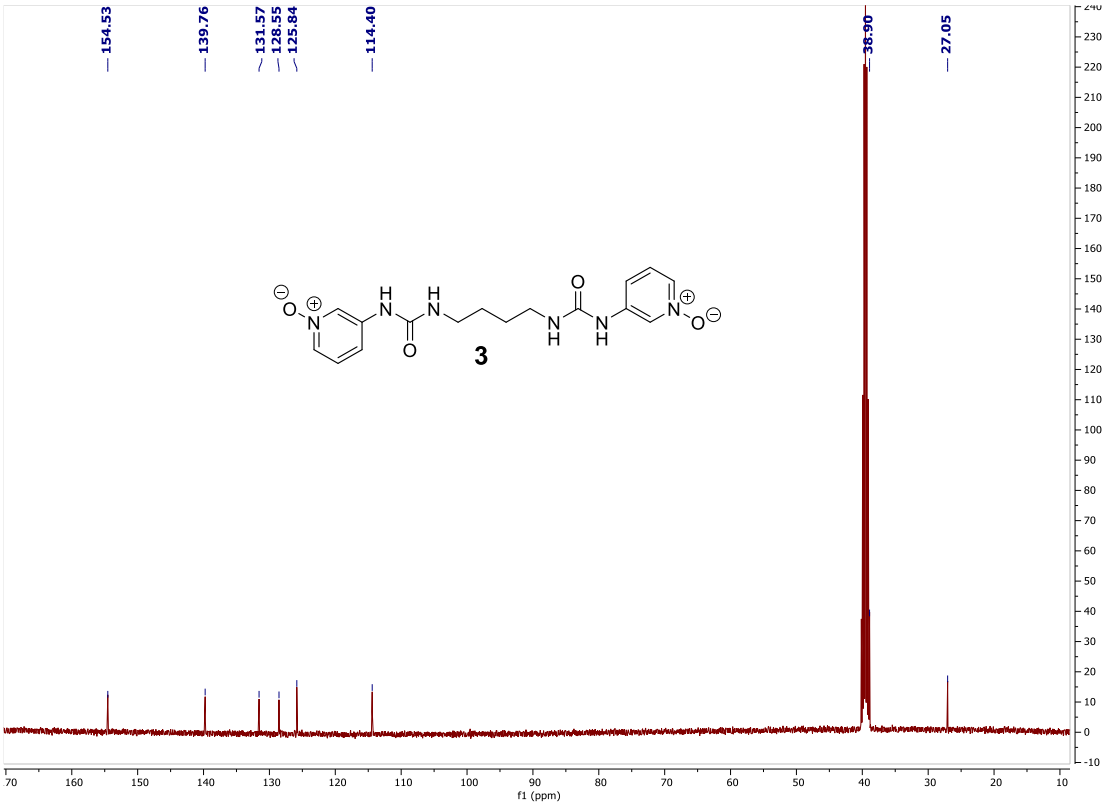

Figure S30. ^{13}C NMR spectrum of compound **3**.

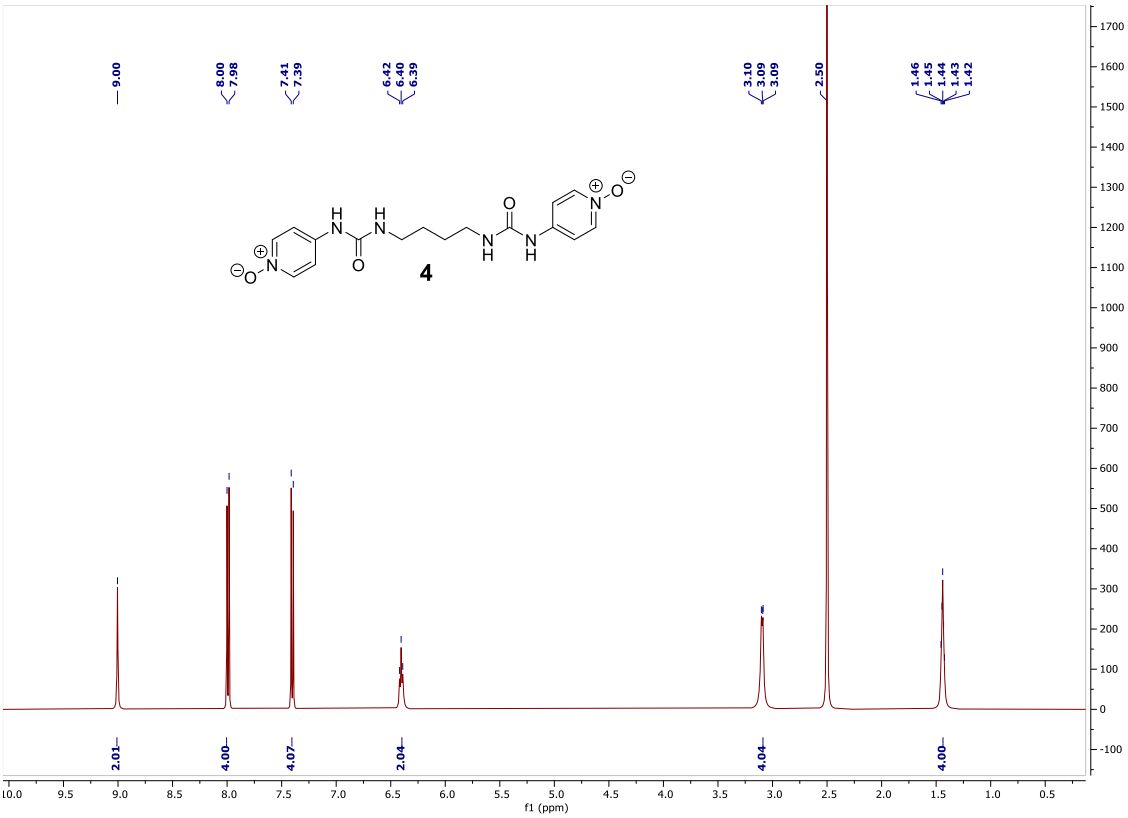

Figure S31. ^{1}H NMR spectrum of compound **4**.

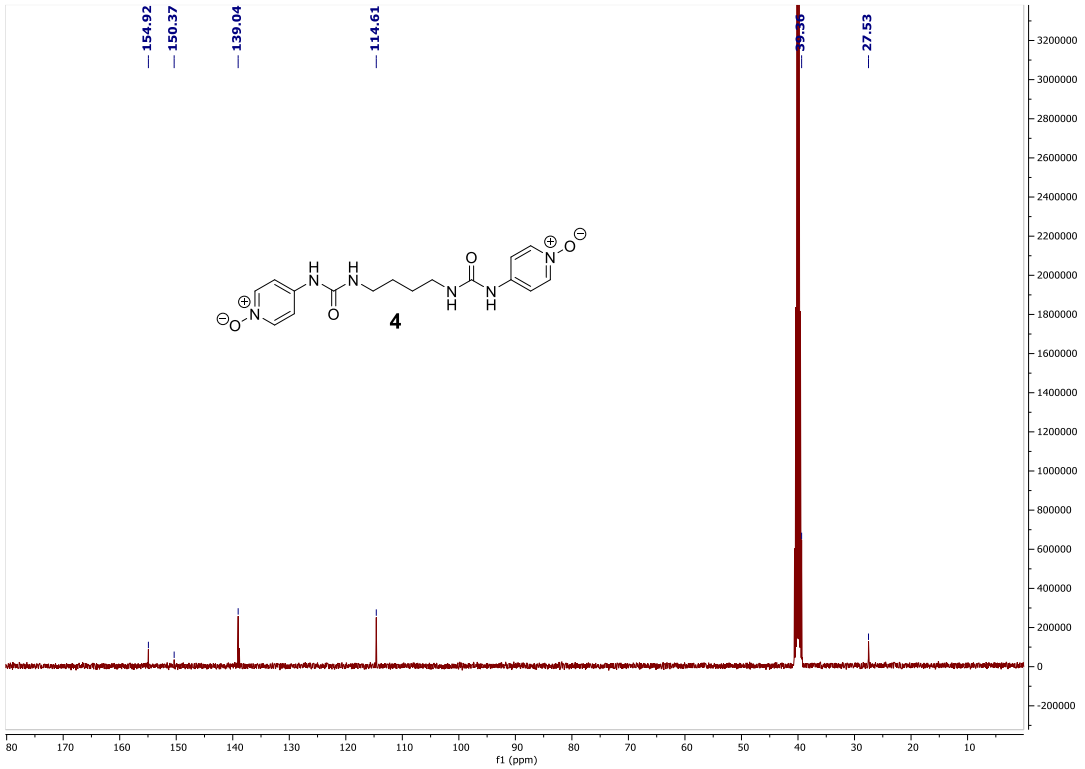

Figure S30. ^{13}C NMR spectrum of compound **4**.

Article-II

This project is published in a peer-reviewed journal and included as published. Minor variations may arise from the original article owing to formatting issues.

Publication details:

"**Stimuli-responsive Properties of Supramolecular Gels based on Pyridyl-N-oxide Amides**"

Sreejith. S. Jayabhavan, B. Kristinsson, Dipankar Ghosh, C. Breton, and Krishna K. Damodaran*

Gels, **2023**, *9*(2), 89.

Part of this research was the BS project of B. Kristinsson

Author contributions:

D.G., B.K., and K.K.D. planned and designed the research; B.K., D.G**.** synthesized the gelators **S.S.J.** repeated the procedure to obtain sufficient gelators for the studies, **S.S.J**. performed characterizations such as rheology, SEM, and PXRD. D.G. solved single crystal structures and. **S.S.J.** and B.K. carried out the rheology measurements associated with anion sensing. **S.S.J.,** B.K., and K.K.D. wrote the initial manuscript draft and all authors reviewed the main manuscript.

gels

MDPI

Article

Stimuli-Responsive Properties of Supramolecular Gels Based on Pyridyl-*N*-oxide Amides

Sreejith Sudhakaran Jayabhavan, Baldur Kristinsson, Dipankar Ghosh, Charlène Breton and Krishna K. Damodaran *

Department of Chemistry, Science Institute, University of Iceland, Dunhagi 3, 107 Reykjavík, Iceland
* Correspondence: krishna@hi.is; Tel.: +354-525-4846; Fax: +354-552-8911

Abstract: The nature of functional groups and their relative position and orientation play an important role in tuning the gelation properties of stimuli-responsive supramolecular gels. In this work, we synthesized and characterized mono-/bis-pyridyl-*N*-oxide compounds of *N*-(4-pyridyl)nicotinamide (**L$_1$**–**L$_3$**). The gelation properties of these *N*-oxide compounds were compared with the reported isomeric counterpart mono-/bis-pyridyl-*N*-oxide compounds of *N*-(4-pyridyl)isonicotinamide. Hydrogels obtained with **L$_1$** and **L$_3$** were thermally and mechanically more stable than the corresponding isomeric counterparts. The surface morphology of the xerogels of di-*N*-oxides (**L$_3$** and **diNO**) obtained from the water was studied using scanning electron microscopy (SEM), which revealed that the relative position of *N*-oxide moieties did not have a prominent effect on the gel morphology. The solid-state structural analysis was performed using single-crystal X-ray diffraction to understand the key mechanism in gel formation. The versatile nature of *N*-oxide moieties makes these gels highly responsive toward an external stimulus, and the stimuli-responsive behavior of the gels in water and aqueous mixtures was studied in the presence of various salts. We studied the effect of various salts on the gelation behavior of the hydrogels, and the results indicated that the salts could induce gelation in **L$_1$** and **L$_3$** below the minimum gelator concentration of the gelators. The mechanical properties were evaluated by rheological experiments, indicating that the modified compounds displayed enhanced gel strength in most cases. Interestingly, cadmium chloride formed supergelator at a very low concentration (0.7 wt% of **L$_3$**), and robust hydrogels were obtained at higher concentrations of **L$_3$**. These results show that the relative position of *N*-oxide moieties is crucial for the effective interaction of the gelator with salts/ions resulting in LMWGs with tunable properties.

Keywords: supramolecular gels; isomeric LMWGs; pyridyl *N*-oxide; stimuli-responsive systems; anion/cation-responsive gels; metallogels; cadmium sensor

Citation: Jayabhavan, S.S.; Kristinsson, B.; Ghosh, D.; Breton, C.; Damodaran, K.K. Stimuli-Responsive Properties of Supramolecular Gels Based on Pyridyl-*N*-oxide Amides. *Gels* **2023**, *9*, 89. https://doi.org/10.3390/gels9020089

Academic Editors: Francesco Caridi, Giuseppe Paladini and Andrea Fiorati

Received: 26 December 2022
Revised: 15 January 2023
Accepted: 17 January 2023
Published: 20 January 2023

1. Introduction

Soft materials based on stimuli-responsive systems [1–4] have gained widespread interest because of their tunable properties with respect to external stimuli such as electricity, light, heat, voltage, magnetic field, mechanical stress, pH, and salts/ions. Supramolecular gels based on low-molecular-weight gelators (LMWGs) [5–14] are an excellent class of stimuli-responsive materials with intriguing potential applications, such as sensors, dynamic gels, tissue engineering, and as media for crystal growth and catalysis [14–26]. The self-assembly of gelator molecules in a solvent medium leads to the formation of LMWGs with a three-dimensional fibrous network stabilized by various non-covalent interactions. The self-assembly process depends on various parameters [27–33], such as temperature, pressure, sound, solvent, functional groups, and gelator structure, which can significantly affect the gel network. The nature of the non-bonding interaction and the molecular structure of the gelator play a crucial role in gel network formation. However, predicting the mechanism of the self-assembly process and the gel structure is challenging, because the non-covalent interactions are dynamic in nature. The self-assembly process

also depends on the spatial orientation of the functional groups. Understanding the role of building blocks/functional groups and the nature of the non-bonding interactions will help researchers to design smart materials based on LMWGs with intriguing properties. The formation of a one-dimensional (1D) hydrogen-bonded chain can be considered as one of the key primary interactions for the gel network formation in LMWGs [6,8,34]. The incorporation of supramolecular synthons [35] or functional groups with hydrogen-bond functionalities such as urea and amide that can assemble into a 1D array have extensively been used to generate LMWGs, which indicates the importance of the 1D hydrogen-bonded chain [6,8].

LMWGs based on amide groups as supramolecular synthons are an important class of supramolecular gels with tunable properties [36–39]. Amide-based LMWGs display complementary N–H ··O=C interactions arising from the N−H donor and C=O acceptor of the amide moieties to form a one-dimensional chain, which self-assembles to a three-dimensional network (3D) via cooperative and unidirectional hydrogen bonding [40]. These 3D networks can immobilize solvent molecules to form organo/hydrogels [41–47]. The adjacent functional groups strongly influence the hydrogen-bonding synthons, and the gelation properties can be altered by introducing moieties that interact with the amide/urea groups. For example, attaching the pyridyl group to the amide moiety can change the intermolecular interaction involving urea/amide groups, which leads to a N···H–N hydrogen-bonding synthon due to the interaction between urea/amide groups and the pyridyl moiety [45,48]. The addition of pyridyl functionality has resulted in highly robust pyridyl amide LMWGs [45,48–50], at typical low gelator concentrations, which can be utilized as stimuli-responsive supramolecular systems [11,51–54]. Incorporating pyridyl amide moieties offers the possibility of synthesizing several isomers, depending on the relative position of the pyridyl nitrogen atom. Furthermore, they provide several advantages, such as ease of obtaining crystalline materials and modification of the pyridyl groups by simple organic reactions. For example, the gelation properties of bis-pyridyl LMWGs can be tuned by replacing the pyridyl group with the corresponding pyridyl-*N*-oxide [55], resulting in pyridyl-*N*-oxide LMWGs.

Compounds based on pyridyl-*N*-oxide moieties have gained widespread interest in synthetic chemistry, biochemistry, and pharmacology due to their intriguing potential applications in medicinal science [56–59]. This is presumably due to the characteristic of the N–O bond [60], which can be considered as a NO donating bond with an important contribution from the oxygen atom (ON back-donation). The substituents play an important role in the stability of the N–O bond; for example, additional stability can be achieved by adding electron-withdrawing substituents, but a reverse trend is observed for electron-donating groups [60]. Incorporating pyridyl-*N*-oxide moieties will lead to enhanced hydrogen bonding and increased solubility in water [55,61] because of the hydrogen-bonding capabilities of the pyridyl-*N*-oxide moiety. Thus, pyridyl-*N*-oxides have a great prospect as hydrogelators, but, surprisingly, the utilization of this functionality in LMWGs is unexplored [55,62,63]. The relative position of the functional groups plays a crucial role in gel network formation in pyridyl-amide/urea gelators, and compounds derived from the *N*-(4-pyridyl) moiety were proved to be superior gelators over the other positional isomers [45,49]. The *N*-oxide moieties could also play an important role in the self-assembly process and the gelation properties of LMWGs [64], and, to the best of our knowledge, the role of the relative position in the gelation properties has not been reported for pyridyl amide *N*-oxides. We have reported the gelation ability of mono-/bis-pyridyl-*N*-oxide compounds of N-(4-pyridyl)isonicotinamide (4PINA) [55] and have shown that bis-pyridyl-*N*-oxide (**diNO**, Scheme 1) displayed better gelation properties compared to mono-pyridyl-*N*-oxides. In this work, we are analyzing the role of the relative position of *N*-oxide moieties in gel network formation by comparing the gelation ability of isomeric pyridyl-*N*-oxide amides in water. The application of the isomeric mono-/bis-pyridyl-*N*-oxide amide LMWGs as sensors will be evaluated by analyzing the stimuli-responsive properties of these LMWGs towards various cations and anions.

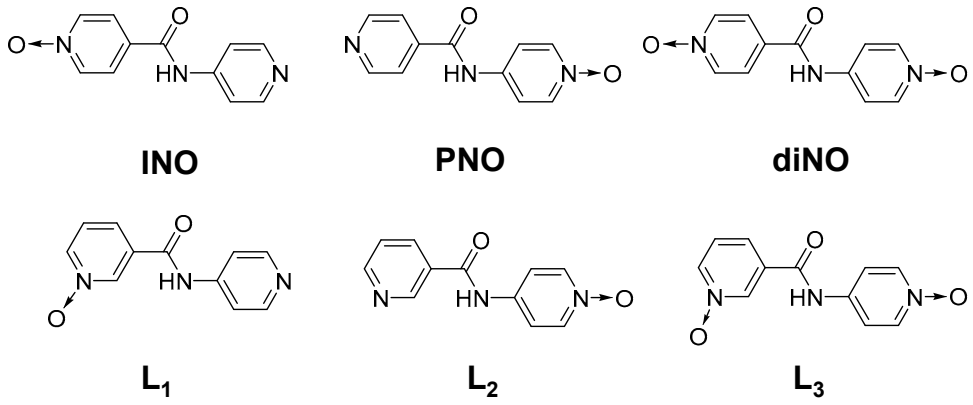

Scheme 1. Isomeric mono/di-*N*-oxides of bis-pyridyl amides.

2. Results and Discussion

We analyzed the role of positional isomers of *N*-oxide moieties in gelation properties by replacing the isonicotinic acid *N*-oxide with nicotinic acid *N*-oxide to form *N*-(4-pyridyl)nicotinamide *N*-oxide compounds (4PNANO, Scheme 1). The mono-pyridyl-*N*-oxide compounds of 4PNANO (**L1** and **L2**) were synthesized by reacting the corresponding *N*-oxide amine/acid (Schemes S1 and S2), but the bis-pyridyl-*N*-oxide compound was synthesized by oxidizing *N*-(4-pyridyl) nicotinamide with 3-chloroperoxybenzic acid (Scheme S3).

2.1. Gelation Experiments

The ability of **L1**–**L3** to form hydrogels was evaluated in water (1.0 wt%) or aqueous mixtures (1.0 wt/v%). In a typical experiment, 10.0 mg of the compound in 1.0 mL water/aqueous mixtures was heated in a sealed vial to obtain a clear solution, and the mixture was cooled to room temperature. The solution was left undisturbed until gelation was observed, which was confirmed by the vial inversion test. The results indicated that **L1**–**L3** did not form a gel in water at 1.0 wt%, and the experiments were performed at higher concentrations of the gelators. **L1** and **L3** formed gels in water at 2.0 wt%, but **L2** did not form a gel. The minimum gelator concentration (MGC) required to form the gel network was evaluated by adding different amounts of the gelator (10.0–30.0 mg) to 1.0 mL water. The gelation experiments at various concentrations indicated that the MGC of **L1** and **L3** was 1.8 wt% in water. We also tested the gelation properties of **L1**-**L3** in aqueous mixtures (1:1, *v*/*v*) of high polar solvents such as MeOH, EtOH, DMF, and DMSO, and the results were similar to the experiments performed in water (Table 1). Gels were obtained in all cases for **L1** and **L3** at 2.0 wt/v%, indicating that the presence of cosolvents did not affect the *N*-oxide gel's self-assembly process.

Table 1. Minimum gelator concentration and T_{gel} values of **L1** and **L3** (2.0 wt/v%) in water and aqueous mixtures.

	L1		**L3**	
Solvents	**MGC (wt/v%)**	T_{gel} (°C)	**MGC (wt/v%)**	T_{gel} (°C)
Water	1.8	128.0	1.8	76.9
MeOH/water	2.0	77.1	2.0	69.7
EtOH/water	2.0	73.2	2.0	63.3
DMF/water	2.0	76.5	2.0	74.3
DMSO/water	2.0	87.9	2.0	94.2

2.2. Thermal Stability

The thermal stabilities of the gels were evaluated by measuring the temperature at which the gel network collapsed, and gels underwent phase transformation to a solution, which is known as gel-to-solution transition temperature (T_{gel}). A small spherical glass ball

was placed on top of the preformed gels at various concentrations of the gelators in the standard vials, and the temperature was increased at a constant rate. As the temperature increased, the ball touched the bottom of the vial, and this temperature was recorded as the T_{gel}. We performed the T_{gel} experiments at the MGC of the gelators in water, and the T_{gel} values for **L1** and **L3** were 128.0 °C and 76.9 °C, respectively. The experiments performed at higher concentrations of **L3** showed an increase in T_{gel} value (92.9 °C), and the results indicated that increasing the concentration of the gelators enhanced the thermal stability of the gel network. The thermal stabilities of **L1** and **L3** were analyzed in various aqueous solvents (Table 1), and the T_{gel} values were lower compared to the corresponding hydrogels. This was presumably due to the favorable interaction between the gelator molecules and the polar solvents, leading to enhanced solubility of the gelators in these mixed solvents, except for **L3** in DMSO/water (1:1, *v*/*v*). We compared the MGC value and the thermal stability of **L3** with the isomeric *N*-oxides (**diNO**) [55] to see whether the relative position of the *N*-oxide moieties affected the self-assembly process and the gel state properties. The MGC for **L3** in water was 1.8 wt%, whereas a higher MGC was observed for isomeric **diNO** (4.0 wt%). The thermal stability of the **L3** network in water was also higher than the isomeric **diNO**, and these results indicate that changing the isonicotinic *N*-oxide to nicotinic *N*-oxide leads to better gel network formation.

2.3. Rheology

Rheology is an important tool in studying the deformation and flow characteristics of supramolecular gels [65,66]. The mechanical strength of the gelators was analyzed by performing the amplitude- and frequency-sweep experiments on the hydrogels of **L1** and **L3** at 2.0 wt%. Initially, an oscillatory strain-sweep experiment was performed to evaluate the linear viscoelastic region (LVR), because the gel network undergoes reversible deformation inside LVR. The results demonstrated that **L1** and **L3** hydrogels had a narrow LVR, as the storage modulus G′ declined after 0.02% of the shear strain (Figure S1). An abrupt decrease in the G′ is observed at the crossover point [65,66], where the gel breaks into a viscous fluid. The crossover points for **L1** and **L3** hydrogels were within the range of 1.0–5.0% of the shear strain. The frequency-sweep experiments showed constant elastic (G′) and viscous (G″) moduli with a frequency range of 0.1–10.0 Hz at a constant strain of 0.02% (within LVR).

Frequency-sweep experiments were performed with **L1** and **L3** hydrogels (2.0 wt%) at a constant strain of 0.02% (within LVR) in a range of 0.1–10.0 Hz, which displayed constant elastic (G′) and viscous (G″) moduli under varying frequency. The hydrogel of **L1** displayed a higher elastic modulus (~10 times, Figure 1a) compared to the **L3** hydrogel. The enhanced mechanical stability can be correlated to the molecular structure of **L1**, which indicates that the 4-pyridyl functionality in **L1** plays a crucial role in the thermal and mechanical strength of the gel. The role of the relative position of the *N*-oxide moieties in the mechanical strength was analyzed by performing the frequency-sweep experiments on **L3** and isomeric **diNO** hydrogels at 4.0 wt%. The comparison of the elastic (G′) and viscous (G″) moduli of **L3** and isomeric **diNO** gels revealed that **L3** hydrogels displayed enhanced mechanical strength (~1.8-fold stronger) than the **diNO** hydrogels, which indicated that the mechanical strength of the gel network depended on the position of the pyridyl *N*-oxide moiety (Figure 1b).

We also performed the frequency-sweep experiments with **L1** and **L3** gels in DMSO/water and DMF/water (1:1, *v*/*v*) at 2.0 wt/v%, and the aqueous mixture gels of **L1** were stronger (2–3-fold) than the hydrogel of **L1** at 2.0 wt%. A similar trend was found for the aqueous mixture gels of **L3** in the DMSO/water gel (~2-fold stronger than **L3** hydrogels), but the DMF/water gel displayed similar mechanical strength as that of the hydrogel of **L3** at 2.0 wt% (Figure S2).

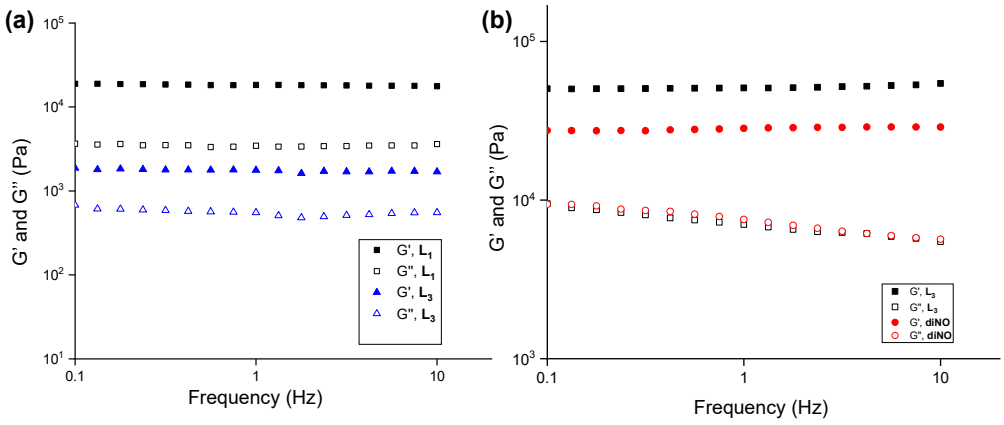

Figure 1. Frequency-sweep experiments performed on (**a**) $\mathbf{L_1}$ and $\mathbf{L_3}$ gels at 2.0 wt% and (**b**) $\mathbf{L_3}$ and **diNO** gels at 4.0 wt% in water at a constant strain of 0.02% at 20.0 °C, respectively.

2.4. Scanning Electron Microscopy (SEM)

SEM is an important technique to visualize the morphology of gel fibers [12,67] and can be used to distinguish the self-assembly modes in supramolecular gels by analyzing the morphology of the gel fibers [68,69]. The morphologies of the fibrous network of $\mathbf{L_1}$ and $\mathbf{L_3}$ xerogels were analyzed by performing SEM on the dried gels in water at the minimum gelator concentration (1.8 wt%). $\mathbf{L_1}$ displayed rod-like morphology with thickness ranging from 0.3–3.0 µm, but twisted rod-like morphologies were observed from $\mathbf{L_3}$ xerogels, and the thickness of the fibers was within the range of 1.0–3.0 µm (Figure S3). SEM performed at 2.0 wt% (above MGC) on $\mathbf{L_1}$ xerogels showed rod-like morphologies with thickness ranging from 0.5–4.0 µm (Figure 2a), but flake-like morphologies were observed for $\mathbf{L_3}$, with dimensions ranging from 4.0–16.0 µm (Figure 2b). The comparison of the SEM images of $\mathbf{L_3}$ and isomeric **diNO** xerogels [55] from water at 4.0 wt% revealed that the morphologies of the gels did not depend on the relative position of the pyridyl *N*-oxide moiety (Figure S4).

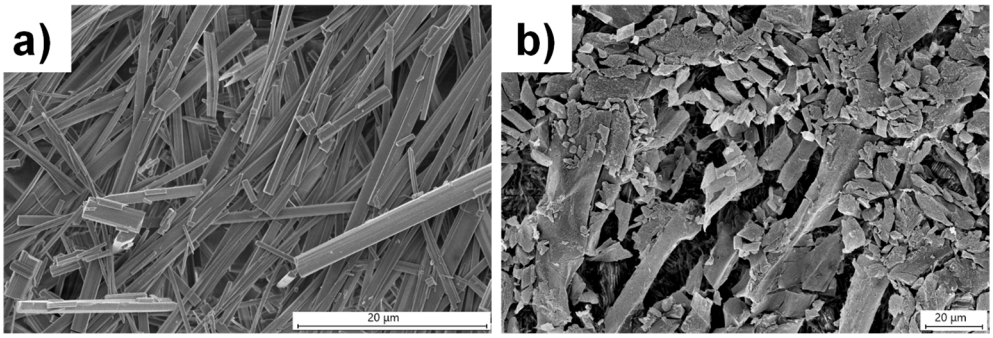

Figure 2. SEM images of xerogels in water with (**a**) $\mathbf{L_1}$ and (**b**) $\mathbf{L_3}$ at 2.0 wt%.

We also analyzed the morphologies of $\mathbf{L_1}$ and $\mathbf{L_3}$ in the aqueous mixtures of DMSO and methanol (1:1, *v*/*v*) to evaluate the effect of solvents on the morphologies of gel fibers. The xerogel of $\mathbf{L_1}$ prepared from DMSO/water and methanol/water (1:1, *v*/*v*, respectively) at 2.0 wt/v% displayed needle-shaped morphology with dimensions ranging from 0.5–6.0 µm (Figure S5). However, long rod-shaped morphology with fiber width ranging from 2.0 to 20.0 µm (Figure S6) was observed for $\mathbf{L_3}$ xerogels in DMSO/water and methanol/water (1:1, *v*/*v*, respectively) at 2.0 wt/v%. These results indicate that morphologies of the fibrous network depend on the solvent system.

2.5. Structural Analysis

2.5.1. Single Crystal X-ray Diffraction

The slow evaporation of a dilute solution of **L_3** resulted in X-ray-quality single crystals of **L_3**. The analysis of the crystals using a polarized light microscope indicated that needle-shaped crystals with trace amounts of plate-shaped crystals were formed. The solid-state structural data were analyzed by single-crystal diffraction analysis, which helped us to correlate the key non-bonding interactions in the solid state and the gelation properties. The structural analysis of the needle-shaped crystals revealed that **L_3** crystallized in a monoclinic space group ($P2_1/c$) with a solvent water molecule (**L_3**•H_2O) (Figure 3a and Table S1). The N-H moiety of the amide group displayed hydrogen-bonding interaction with the *N*-oxide moiety of the nicotinamide moieties via N–H···O interactions (Table S2), resulting in a R_2^2 (14) hydrogen-bonded dimer [70] of **L_3**. The oxygen atom of the aminopyridine *N*-oxide displayed a bifurcated hydrogen bonding with the solvent water molecule via O—H···O interactions, resulting in a 1D hydrogen-bonded chain of the dimers (Figure 3b). This 1D hydrogen-bonded chain can be considered as one of the crucial factors for supramolecular gelation [6,8] in LMWGs. The comparison of the crystal structure of **L_3**•H_2O with the isomeric **diNO** revealed the absence of such 1D hydrogen-bonded chains, which could be one of the factors in the better gelation ability and mechanical strength of **L_3**•H_2O compared to isomeric **diNO**.

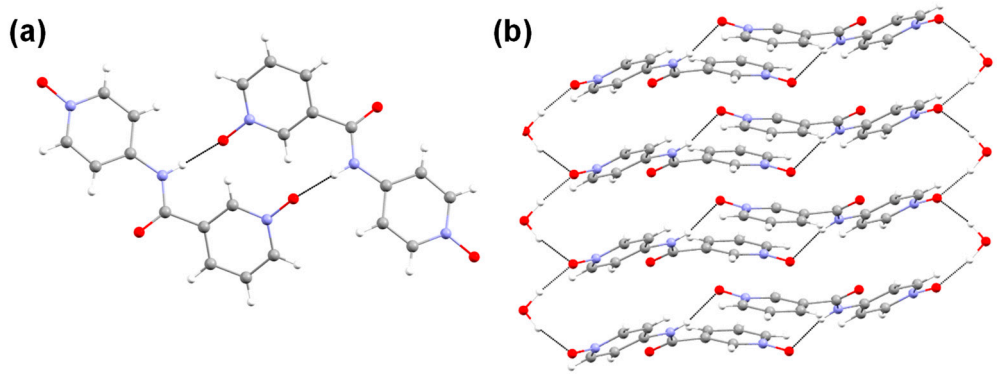

Figure 3. (**a**) Hydrogen-bonded dimer of **L_3** stabilized by N–H···O interactions and (**b**) the aminopyridine *N*-oxide moiety interacting with the water molecule to form a 1D hydrogen-bonded chain of the dimers.

We also analyzed the solid-state structure of the plate-shaped crystals (minor product), which indicated that **L_3** crystallized in the monoclinic space group ($P2/c$) with two water molecules (**L_3**•$2H_2O$) (Figure S7 and Table S1). The molecule was planar compared to **L_3**•H_2O, but a similar interaction was observed between the amide and *N*-oxide moieties, resulting in a (R_2^2) (14) hydrogen-bonded dimer [70]. However, the aminopyridine *N*-oxide moiety displayed a bifurcated hydrogen bond with two water molecules, resulting in two-dimensional porous architecture (Figure S7b), which was further stabilized by various non-bonding interactions (Table S2).

2.5.2. Powder X-ray Diffraction (PXRD)

Powder X-ray diffraction is a rapid and powerful tool to obtain an insight into the packing modes of solids. Comparing the PXRD pattern of the bulk material with the simulated pattern acquired from the single-crystal structure enabled us to evaluate the phase purity of the material [63,71]. We have shown that comparing the PXRD pattern of the xerogels with the simulated pattern of the gelator structure could provide information about the key interactions in the gel network architecture [6,12,32,55,72]. This method can be considered as an excellent strategy to correlate the self-assembly process in LMWGs despite the artefacts affecting the drying process [73]. We recorded the PXRD pattern of the **L_3** crystals obtained via recrystallization from hot water (10.0 mg in 2.0 mL) and **L_3** xerogel

from pure water at 2.0 wt%. The PXRD pattern of the bulk crystals and the xerogel matched with the simulated pattern of the needle-shaped crystals $\mathbf{L_3}\bullet H_2O$ (Figure 4), indicating that the hierarchical assembly of the xerogel network matched with the solid-state structure of $\mathbf{L_3}\bullet H_2O$. The simulated pattern of $\mathbf{L_3}\bullet 2H_2O$ did not match with the PXRD pattern of the bulk crystals and the xerogel, which indicated that the second form did not correspond to the structure of the xerogels (Figure S8).

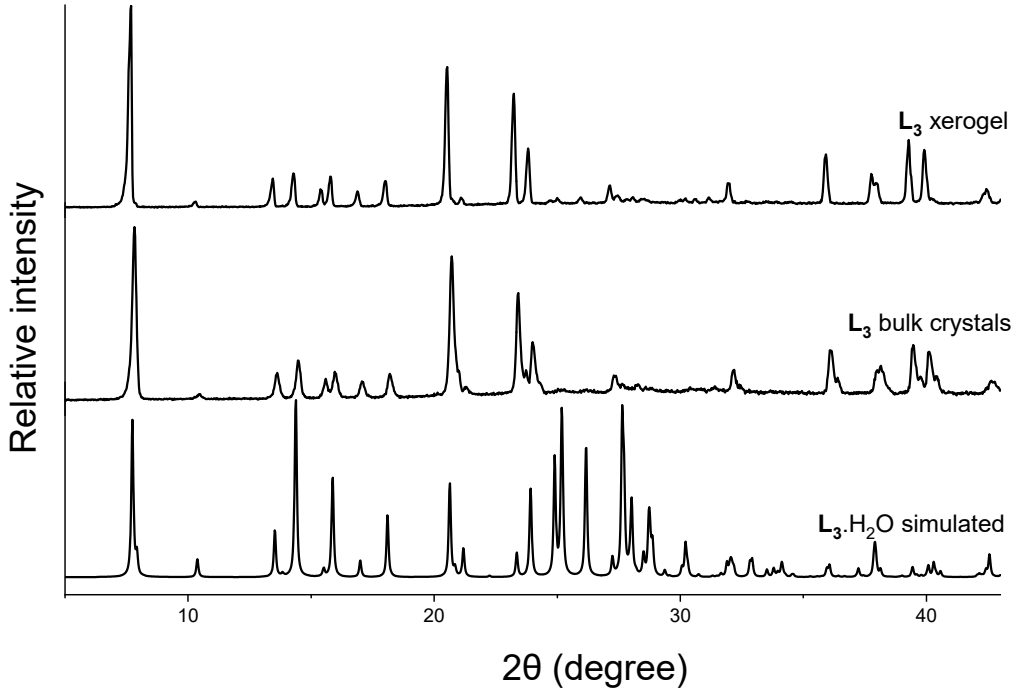

Figure 4. Comparison of the simulated pattern from single-crystal X-ray structure of $\mathbf{L_3}\bullet H_2O$ with the PXRD pattern of the bulk crystals obtained from water and xerogel from water at 2.0 wt%.

2.6. Stimuli-Responsive Properties

LMWGs based on pyridyl-*N*-oxides display smart responses towards external stimuli because the molecular interactions of *N*-oxide moieties are based on partial charges, and the gelation can be turned ON/OFF in the presence of respective salts/ions. The cation/anions interact with gelator molecules constructively or destructively, depending on the electrostatic interaction and acidic/basic properties of the cations/anions [52,74]. The constructive interaction could trigger/enhance the gelation process [30,75,76], but a destructive interaction may lead to the dissolution/collapse of the gel network [27,39].

2.6.1. Anion Sensing

We have previously reported the pyridyl-*N*-oxide-based compound's sensing ability towards salts/ions [64,77] and have shown that cyanide ions can be detected using the gel-sol transition [62]. This prompted us to study the effect of salts/ions on the gelation properties of the *N*-oxide compounds of *N*-(4-pyridyl)nicotinamide. The stimuli-responsive properties of $\mathbf{L_1}$ and $\mathbf{L_3}$ in water were analyzed by treating the compounds at concentrations below MGC (at 1.5 wt%) with various halides of sodium and potassium ions (1.0 equiv.). Gel formation was observed for $\mathbf{L_1}$ at 1.5 wt% in the presence of 1.0 equivalence of NaF, NaCl, NaBr, KF, KCl, KBr, and KI (Table S3). The experiments performed at a lower concentration of $\mathbf{L_1}$ (1.2 wt%) resulted in selective gelation in the presence of 1.0 equivalence of KCl. The stimuli-responsive properties of $\mathbf{L_3}$ in the presence of sodium and potassium halide salts (1.0 equiv.) displayed gel formation at 1.5 wt%. These results indicate the stimuli-responsive properties of $\mathbf{L_1}$ and $\mathbf{L_3}$ in water, where the salts/ions induce gel network formation (Table S3). The anion-sensing ability of $\mathbf{L_1}$ and $\mathbf{L_3}$ (1.5 wt%) was further analyzed

in the presence of other anions, such as KNO_3, KBF_4, KPF_6, and $K_2C_2O_4$ (Table S3). Gels were obtained for all ions with **L_3**, but a colloidal solution was observed with **L_1** at 1.5 wt%. We compared the stimuli-responsive properties of **L_1** and **L_3** with isomeric *N*-oxides **INO** and **diNO**, respectively. The non-gelator **INO** (isomeric *N*-oxide of **L_1**) did not form any gels in the presence of 1.0 equivalence of sodium and potassium salts in pure water at 1.5 wt%. The isomeric *N*-oxide of **L_3 (diNO)** also failed to form gels at 1.5 wt%, which indicated that the effective interaction between the compound and the salts/ions was affected by the position of the *N*-oxide functionality. However, the **diNO** (MGC, 4.0 wt%) formed gels at a concentration below MGC (3.0 wt%) with these salts (1.0 equiv.).

The comparison of the mechanical strength of the gels (1.5 wt%) in the presence of halide salts of sodium and potassium with the hydrogels of **L_1** and **L_3** at MGC (1.8 wt%) revealed that enhanced mechanical strength was observed in both cases (Figure 5 and Table S4). A ~5.7-fold increase in the mechanical strength of **L_3** (1.5 wt%) was observed in the presence of KCl and a ~4.3-fold increase with NaCl (Figure 5b). We further studied the effect of other anions (KNO_3, KBF_4, KPF_6, and $K_2C_2O_4$) with **L_1** and **L_3** (1.5 wt%) below MGC, and **L_1** failed to form stable gels in the presence of these salts. However, the mixed gel of **L_3** and the anions displayed enhanced mechanical strength compared to the **L_3** hydrogels (Figure 5b and Table S4).

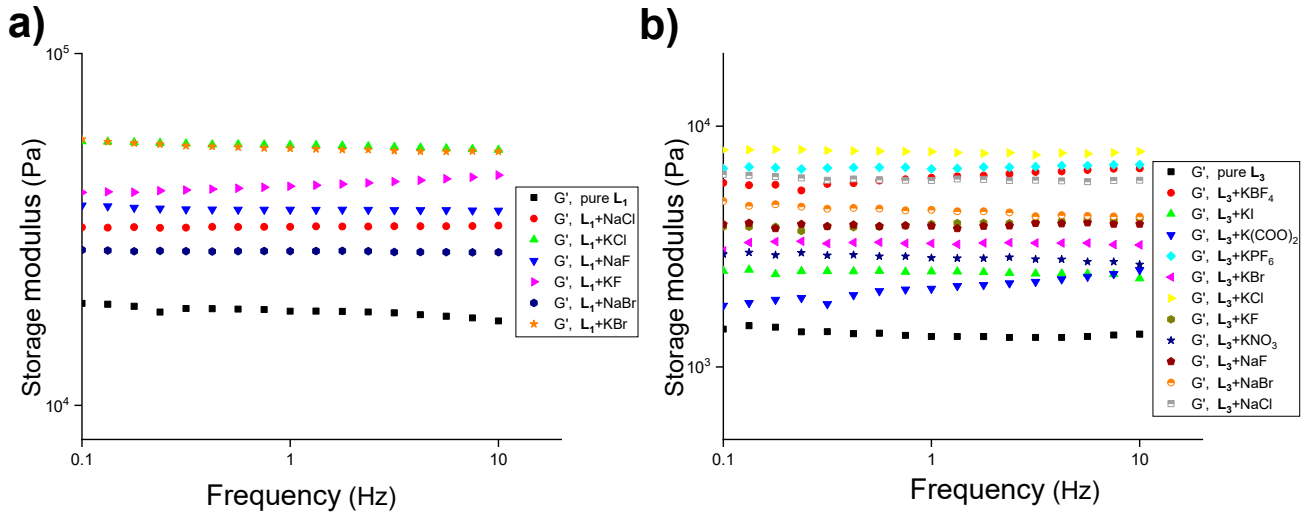

Figure 5. Frequency-sweep experiments of **L_1** and **L_3** at 1.5 wt% in water at 20.0 °C in the presence of various salts of sodium and potassium (1.0 equiv.) with a constant strain of 0.02%, (**a**) **L_1** (pure ligand at 1.8 wt%), and (**b**) **L_3** (pure ligand at 1.8 wt%).

The effect of anions on the morphology of the gel network was studied by analyzing the SEM images of the xerogels with anions. The xerogel of **L_1** and **L_3** in the presence of NaCl displayed fibrous morphologies with diameters ranging from 100 to 800 nm and 1.0 to 5.0 μm, respectively (Figure 6). The PXRD analysis of the xerogel of **L_3** hydrogels at 1.5 wt% in the presence of 1.0 equivalence of NaCl and KCl showed a similar pattern with the pure xerogel of **L_3** at 1.8 wt%, which suggested that the anions interacted with **L_3** to form a stable gel below MGC without affecting the original network (Figure S9).

2.6.2. Cation Sensing

The gelation property was observed to be independent of the size and nature of the anions, which prompted us to study the stimuli-responsive properties of **L_1** and **L_3** with chloride salts having various countercations (1.0 equiv.) at a concentration below MGC (1.5 wt%). **L_1** formed a stable gel in the presence of 1.0 equivalence CsCl, $MgCl_2$, $CaCl_2$, $SrCl_2$, and $BaCl_2$, but no gels were observed in the presence of 1.0 equivalence of NH_4Cl. On the other hand, **L_3** formed a gel in the presence of all of the above-mentioned chloride salts (Table S5). The mechanical strength of **L_1** and **L_3** with these salts was evaluated to

observe the effect of cations in gel network formation. Analysis of the results indicated that the addition of chloride salts of magnesium, calcium, strontium, and barium enhanced the mechanical strength (1.5–3.0-fold) of $\mathbf{L_1}$ compared to $\mathbf{L_1}$ (1.8 wt%) hydrogel (Figure 7a and Table S6). A similar trend was observed for $\mathbf{L_3}$ gels in the presence of the chloride salts of magnesium, calcium, strontium, barium, cesium, and ammonium (Figure 7b and Table S6).

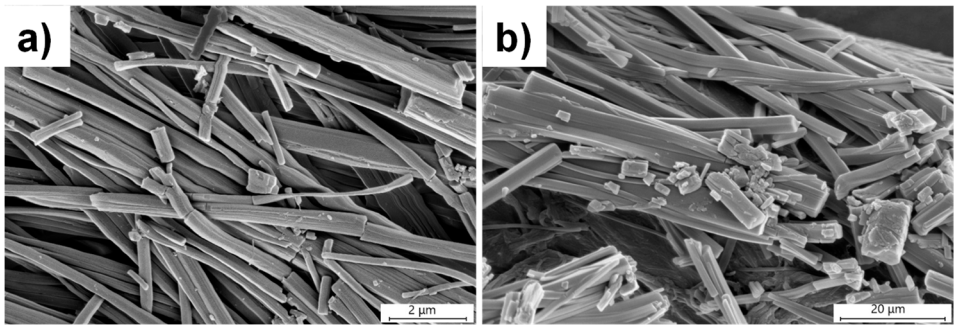

Figure 6. SEM images of xerogels obtained from pure water at 2.0 wt% in the presence of 1.0 equivalence of NaCl, (**a**) $\mathbf{L_1}$, and (**b**) $\mathbf{L_3}$.

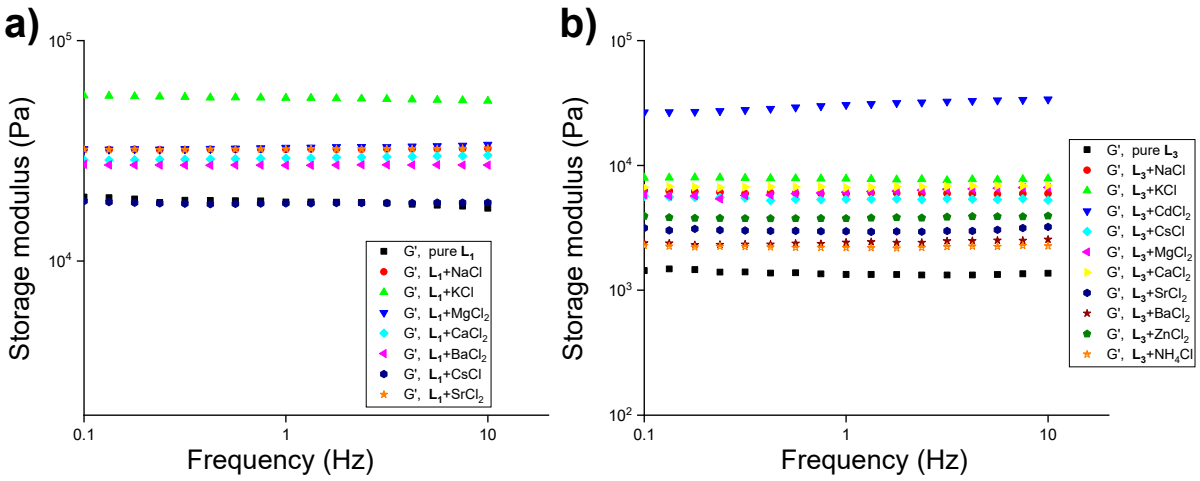

Figure 7. Frequency-sweep experiments with 1.5 wt% of the compound in the presence of various salts of chlorides (1.0 equiv.) in water at 20.0 °C with a constant strain of 0.02%, (**a**) $\mathbf{L_1}$ (pure ligand at 1.8 wt%), and (**b**) $\mathbf{L_3}$ (pure ligand at 1.8 wt%).

The cation-sensing ability of the isomeric *N*-oxide compounds (**INO** and **diNO**) were compared with $\mathbf{L_1}$ and $\mathbf{L_3}$ gels in the presence of various cations. Gelation was not observed for both **INO** and **diNO** at 1.5 wt% in the presence of $MgCl_2$ and $CaCl_2$ (1.0 equiv.) However, **diNO** formed stable hydrogel at 3.0 wt% (below MGC) with 1.0 equivalence $MgCl_2$ and $CaCl_2$. The comparison of the sensing ability of the isomeric *N*-oxides confirms that the relative position of *N*-oxide plays a crucial role in cation sensing. SEM performed on the dried gels of $\mathbf{L_1}$ and $\mathbf{L_3}$ at 2.0 wt% in the presence of $MgCl_2$ (1.0 equiv.) revealed that the morphology of the xerogels was identical to the xerogels of $\mathbf{L_1}$ and $\mathbf{L_3}$ hydrogels (2.0 wt%, Figure S10). PXRD studies with the chloride salts of magnesium and calcium (1.0 equiv) at 1.5 wt% of $\mathbf{L_3}$ showed no change compared to the powder pattern of the xerogel of $\mathbf{L_3}$ at 1.8 wt%, suggesting similar molecular packing (Figure S11). The molecular interactions of *N*-oxide moieties are based on partial charges, and the enhanced gelation property in the presence of anions/cations may be attributed to the favorable interactions between the *N*-oxide moieties and anions/cations, which is presumably due to the combination of the non-bonding and ionic interactions. The enhanced mechanical properties of $\mathbf{L_1}$ and $\mathbf{L_3}$ in the presence of various cations prompted us to study the stimuli-responsive properties of $\mathbf{L_1}$ and $\mathbf{L_3}$ with transition metal salts, which could form metallogels.

Metallogels based on transition metals are multi-responsive soft materials with intriguing potential applications in cosmetics, food processing, drug delivery, and catalysis [78,79]. Metal-based supramolecular gels are formed by the addition of metal ions to a gelator/non-gelator, and the interaction of the metal salt with the gelator could induce/enhance gelation properties to form metallogels [52,79]. However, the addition of metal salts could disrupt the key interactions in the gel network, leading to the dissolution of the gel network [52,79]. The metal-coordination-driven self-assembly plays a key role in the formation of a gel network, which is supported by various non-covalent interactions [80,81]. The presence of the coordinating functionality (pyridyl *N*-oxide moiety) and a hydrogen-bonding group (amide moiety) in **L_1** and **L_3** will make these gelators ideal candidates for metal-based supramolecular gels [52].

The effect of transition metal salts on the stimuli-responsive property of the hydrogel was studied by adding one equivalent of the metal salt ($CuCl_2$, $ZnCl_2$, or $CdCl_2$) to **L_1** or **L_3** at 1.5 wt%. Gels were not obtained for **L_1** in the presence of these transition metal chlorides. However, **L_3** gelled at 1.5 wt% in the presence of $ZnCl_2$ and $CdCl_2$ (1.0 equiv.), but no gel was observed with $CuCl_2$. We repeated the experiments by lowering the concentration of **L_3** (0.7 wt%), and selective gel formation was observed with a 1.0 equivalence of $CdCl_2$, highlighting the specific sensing of cadmium chloride at this concentration (Figure 8). The **L_3**-$CdCl_2$ gelator obtained at 0.7 wt% of **L_3** and $CdCl_2$ (1.0 equiv.) was stable for several weeks, and the experiments performed at lower concentrations of $CdCl_2$ (0.5 equiv.) resulted in precipitation (Figure 8). We further analyzed the gelation behavior of **L_3** in the aqueous mixtures (1:1, *v*/*v*) of methanol, ethanol, DMF, and DMSO at 2.0 wt/v% in the presence of 1.0 equivalence of $ZnCl_2$ and $CdCl_2$. We observed gelation with $ZnCl_2$ and $CdCl_2$ in the aqueous mixtures of DMF/DMSO, but gels were formed with $CdCl_2$ in MeOH/water and EtOH/water. The gelation ability of **INO** with $ZnCl_2$ and $CdCl_2$ was previously reported by our group [62]. The isomeric **diNO** formed a precipitate below 2.5 wt% with 1.0 equivalence of $CuCl_2$ or $CdCl_2$, which highlighted the effective gelation ability of **L_3** over the isomeric gelator **diNO** in the presence of transition metals. However, hydrogels were formed at 2.5 wt% (below MGC) with 1.0 equivalence of $CuCl_2$ or $CdCl_2$, and a precipitate was formed in the presence of $ZnCl_2$.

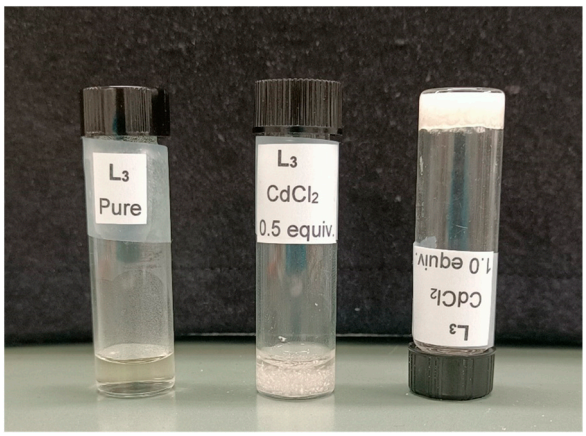

Figure 8. Stimuli-responsive behavior of **L_3** at 0.7 wt% in the presence of $CdCl_2$.

The mechanical strength of the gels with transition metals was analyzed by performing frequency-sweep experiments, and an abrupt increase in the mechanical strength (~24.7 fold) was observed for **L_3** (1.5 wt%) with $CdCl_2$ (1.0 equiv.). We studied the mechanical strength of the gels at 2.0 wt/v% of **L_3** with $CdCl_2$ in water and a 1:1 (*v*/*v*) aqueous mixture of methanol, ethanol, DMSO, and DMF. A steep increase in the mechanical strength was observed for **L_3**-$CdCl_2$ gels in water (~35.6-fold), methanol/water (~175-fold), ethanol/water (~91.7-fold), and DMF/water (~34.3-fold) with **L_3** (2.0 wt/v%) (Figure 9).

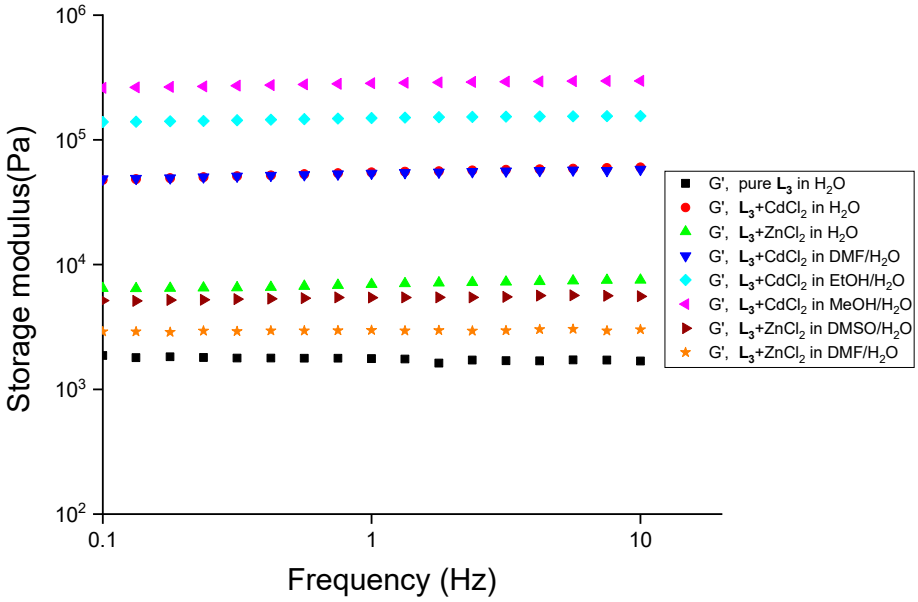

Figure 9. Frequency-sweep experiments with **L3** at 2.0 wt% and in the presence of chloride salts of zinc and cadmium (1.0 equiv.) in various solvent mixtures at 20.0 °C with a constant strain of 0.02%.

Similarly, we observed an enhanced mechanical strength for **L3** gels at 2.0 wt% with 1.0 equivalence of $ZnCl_2$ in water (~4.4-fold), DMF/water (~1.8-fold), and DMSO/water (~3.3-fold) (Figure 9).

The morphological analysis of the dried gels at 2.0 wt% of **L3** with 1.0 equivalence of $CdCl_2$ from water revealed rod-shaped morphology with fiber width ranging from 0.4 to 4.0 µm (Figure S12). Long needle-shaped fibers were observed for dried gels at 0.7 wt% of **L3** with 1.0 equivalence of $CdCl_2$, and the diameter of the fibers ranged from 1.0 to 6.0 µm (Figure 10a). The xerogels obtained from DMSO/water (1:1, *v*/*v*) at 2.0 wt% of **L3** and $CdCl_2$ (1.0 equiv.) displayed similar fibrous morphology, with a fiber width range of 0.1–1.0 µm (Figure 10b).

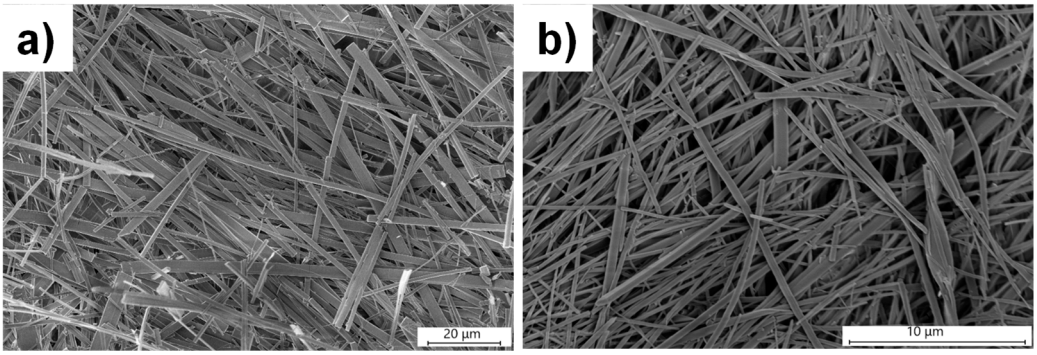

Figure 10. SEM images of xerogels obtained with **L3** in the presence of 1.0 equivalence of $CdCl_2$ in (**a**) 0.7 wt% in pure water and (**b**) 2.0 wt/v% in DMSO/water (1:1, *v*/*v*).

We analyzed the powder X-ray patterns of the dried gels at 2.0 wt% and 0.7 wt% of **L3** hydrogels in the presence of 1.0 equivalence of $CdCl_2$, respectively. Analysis of the PXRD pattern revealed a different PXRD pattern for mixed **L3**-$CdCl_2$ xerogels compared to the **L3** xerogel at 2.0 wt% (Figure S13) in both cases. This may be attributed to the complexation of **L3** with $CdCl_2$, resulting in the formation of a stable hydrogel at a lower ligand concentration (0.7 wt%) induced by metal-ligand-driven supramolecular self-assembly. PXRD pattern of the mixed **L3**-$CdCl_2$ xerogels at 2.0 wt/v% of **L3** obtained from an aqueous mixture (1:1, *v*/*v*) of methanol, ethanol, DMF, and DMSO did not match with the xerogel

of $\mathbf{L_3}$, which confirmed that interaction of $\mathbf{L_3}$ with $CdCl_2$ was independent of solvent composition. However, the PXRD patterns of mixed $\mathbf{L_3}$-$CdCl_2$ in different solvent mixtures were not similar, because the crystal packing was affected by the nature of the solvent (Figure S13). The morphology, PXRD pattern, and gel-state properties of $\mathbf{L_3}$-$CdCl_2$ gels suggest that $\mathbf{L_3}$ interacts with $CdCl_2$, which may be considered as metallogels. PXRD studies with $ZnCl_2$ (1.0 equiv) at 1.5 wt% of $\mathbf{L_3}$ in water and in aqueous mixtures (1:1, *v*/*v*) of DMF and DMSO matched with the xerogel of $\mathbf{L_3}$ at 1.8 wt%, indicating similar solid-state structure (Figure S14). This suggests that $ZnCl_2$ exists as non-coordinated metal salts in the gel network, and the gelation properties can be explained based on the fact that metal nanoparticles and non-coordinated metal complexes are known to enhance the gelation properties of LMWGs [82–85].

3. Conclusions

The role of the relative position of functional groups in the gelation properties of LMWGs was studied by analyzing the gelation properties of isomeric mono-/bis-pyridyl-*N*-oxide compounds. We synthesized mono-/bis-pyridyl-*N*-oxide compounds of *N*-(4-pyridyl)nicotinamide ($\mathbf{L_1}$-$\mathbf{L_3}$), and the gelation properties of $\mathbf{L_1}$ and $\mathbf{L_3}$ were compared with isomeric *N*-oxide compounds (**INO** and **diNO**, respectively). Gelation tests revealed that $\mathbf{L_1}$ and $\mathbf{L_3}$ formed hydrogels, whereas $\mathbf{L_2}$ was a non-gelator, which underlines the importance of the nicotinamide *N*-oxide moiety in gel network formation. Comparing the gelation behavior of $\mathbf{L_1}$ and $\mathbf{L_3}$ with corresponding isomeric *N*-oxide compounds (**INO** and **diNO**) revealed that the relative position of the *N*-oxide moieties played a crucial role in the self-assembly process of LMWGs. SEM analysis revealed that the morphology was independent of the relative position of the pyridyl *N*-oxide moiety. Single-crystal X-ray diffraction of $\mathbf{L_3}$ revealed the existence of a 1D hydrogen-bonded chain, which was crucial for gel network formation. The solid-state structure was correlated to the xerogels to obtain an insight into the key interactions responsible for gel network formation. The stimuli-responsive properties of $\mathbf{L_1}$–$\mathbf{L_3}$ were studied with various salts/ions, and anion-induced gelation was observed for $\mathbf{L_1}$ and $\mathbf{L_3}$ in the water below MGC with $\mathbf{L_1}$ and $\mathbf{L_3}$ in water. $\mathbf{L_3}$ was very versatile in nature, as it formed a gel below MGC with most of the salts or transition metal salts, which showed the cooperative interaction between the *N*-oxide and salts/ions. An abrupt increase in the mechanical property of $\mathbf{L_3}$ was observed in the presence of 1.0 equivalence of cadmium chloride, and a stable gel was formed at a very low concentration of the gelator (0.7 wt%). The effective sensing of cadmium chloride may be due to the metal-ligand coordination-driven supramolecular assembly. We showed that the salt-induced gelation depended on the nature and the position of the functional group, which will open the door for designing LMWGs based on *N*-oxide moieties with intriguing features.

4. Materials and Methods

The starting materials and solvents were obtained from Sigma-Aldrich (MEDOR ehf, Reykjavik, Iceland) and TCI-Europe (Boereveldseweg, Belgium) and utilized as provided. Deionized water was used to perform the gelation studies. The NMR spectra (^{1}H and ^{13}C, Figures S15–S20) were recorded with a Bruker Avance 400 spectrometer (Rheinstetten, Germany), and the scanning electron microscopy (SEM) images were captured with a Leo Supra 25 microscope (Carl Zeiss, Oberkochen, Germany). The mechanical strength evaluation was performed in an Anton Paar's MCR 302 (Graz, Austria) modular compact rheometer. Single-crystal X-ray diffraction (SCXRD) and powder X-ray diffraction (PXRD) experiments were carried out using a Bruker D8 venture (Karlsruhe, Germany) and PANalytical instrument (Almelo, Netherlands), respectively. We synthesized the *N*-oxide compounds by replacing the pyridyl group of *N*-(pyridin-4-yl)nicotinamide (**4PNA**) with pyridyl *N*-oxides [45]. Synthesis of 3-carboxypyridine 1-oxide [86] and 4-aminopyridine 1-oxide [87] was performed following literature and confirmed by matching the analytical

data with the reported compounds. The INO and **diNO** compounds were synthesized by following the reported procedure from our previous work [55].

4.1. Synthesis of Ligands

4.1.1. Synthesis of 3-(pyridin-4-ylcarbamoyl) pyridine 1-oxide (L_1)

To a 100.0 mL two-neck round bottom flask we added 3-carboxypyridine 1-oxide (4.0 g, 30.0 mmol) with 20.0 mL of thionyl chloride, and the solution was refluxed overnight. The solvents were evaporated to dryness, and the corresponding acid chloride formed was used for the next step without further purification. Anhydrous DMF (around 25.0 mL) was added into the flask, followed by 4-aminopyridine (2.7 g, 28.7 mmol), and the mixture was cooled in an ice bath to 0 °C with constant stirring. A solution of triethylamine (4.5 mL) in 10.0 mL DMF was added dropwise to the reaction mixture at 0 °C over an hour, and the resulting yellow colloidal solution was stirred at room temperature overnight. To this mixture, water was added, resulting in a thick precipitate, which was filtered. The precipitate was then stirred in a 5.0% $NaHCO_3$ solution for 4.0 h and was filtered. The residue was washed with an excess of cold water, air-dried, and recrystallized from hot water to obtain the product. Yield 70.0%. ^{1}H NMR (400 MHz, DMSO-d_6) δ (ppm): δ 10.80 (s, 1H), 8.74 (s, 1H), 8.51 (d, J = 5.8 Hz, 2H), 8.43 (d, J = 6.6 Hz, 1H), 7.81 (d, J = 8.0 Hz, 1H), 7.74 (d, J = 6.0 Hz, 2H), 7.59 (t, J = 7.3 Hz, 1H). ^{13}C {^{1}H} NMR (101 MHz, DMSO-d_6) δ 162.65, 150.46, 145.27, 141.29, 138.02, 133.63, 126.58, 124.49, 114.11. HRMS (APCI): $C_{11}H_{10}N_3O_2$ $[M + H]^+$, 216.0768; found, 216.0765.

4.1.2. Synthesis of 4-(nicotinamido) pyridine 1-oxide (L_2)

Compound **L_2** was synthesized by following a similar procedure used for compound **L_1**. Nicotonic acid (1.0 g, 8.12 mmol), thionyl chloride (20.0 mL), 4-aminopyridine 1-oxide (0.89 g, 8.12 mmol), and triethylamine (2.26 mL) in 30.0 mL DMF. Yield 68.0%. ^{1}H NMR (400 MHz, DMSO-d_6) δ 10.96 (s, 1H), 9.11 (s, 1H), 8.78 (dd, *J* = 4.8, 1.6 Hz, 1H), 8.32–8.28 (m, 1H), 8.19 (d, *J* = 7.5 Hz, 2H), 7.83 (d, *J* = 7.5 Hz, 2H), 7.60–7.56 (m, 1H). ^{13}C {^{1}H} NMR (101 MHz, DMSO-d_6) δ 164.48, 152.59, 148.79, 138.92, 136.31, 135.64, 129.84, 123.61, 116.86. HRMS (APCI): $C_{11}H_9N_3NaO_2$ $[M + Na]^+$, 238.0587; found, 238.0594.

4.1.3. Synthesis of 3-((1-oxidopyridin-4-yl) carbamoyl) pyridine 1-oxide (L_3)

To a 100.0 mL round-bottomed flask, *N*-(pyridin-4-yl) nicotinamide (2.0 g, 10.0 mmol) and MeOH (40.0 mL) were added to dissolve and stirred. 3-Chloroperoxybenzic acid (6.8 g, 40.0 mmol) was added in portions over 15.0 min to the solution and was refluxed overnight. The solution was filtered, and the precipitate was washed with 5.0% sodium bicarbonate and thrice with cold water. The precipitate was further recrystallized from hot water. Yield 55.0%. ^{1}H NMR (400 MHz, DMSO-d_6) δ 10.90 (s, 1H), 8.73 (s, 1H), 8.42 (m, 1H), 8.19 (d, *J* = 7.6 Hz, 2H), 7.81 (m, 1H), 7.79 (d, *J* = 7.6 Hz, 2H), 7.61–7.57 (m, 1H). ^{13}C {^{1}H} NMR (101 MHz, DMSO-d_6) δ 162.01, 141.31, 138.94, 137.92, 135.69, 133.50, 126.63, 124.45, 116.97. HRMS (APCI): $C_{11}H_9N_3O_2$ $[M + Na]^+$, 254.0536; found, 254.0540.

4.2. Gelation Studies

Hydrogelation ability was evaluated with all of the compounds by weighing different amounts (ranging from 10.0 to 40.0 mg) of the compound in a standard 7.0 mL vial; 1.0 mL of water was added, and the vial was sealed. The vial containing the mixture was then sonicated and slowly heated to obtain a clear solution, which was then left undisturbed for 24.0 h. Gelation was confirmed via a vial inversion test. Gelation tests were also performed in aqueous mixtures by dissolving the compound in 0.5 mL of distilled water and 0.5 mL of an appropriate solvent, and the vial was sealed. The mixture was sonicated, heated to obtain a clear solution, and checked for gelation ability. Gelation tests were performed in the presence of various salts with 15.0 mg of the compounds (**L_1** and **L_3**) in 1.0 mL of water followed by the addition of 1:1 molar equivalent of an appropriate salt. The mixture was sonicated and heated after sealing the vial to obtain a transparent solution. The solution

was left undisturbed, and a vial inversion test confirmed gel formation. The experiments were repeated three times to confirm the results.

4.2.1. Minimum Gelator Concentration (MGC)

MGC was performed in deionized water/aqueous mixtures by weighing various concentrations of the compounds in a standard 7.0 mL vial and adding 1.0 mL of deionized water/aqueous mixtures. The corresponding mixture was sonicated and gradually heated to dissolve the compounds, and the solution was kept at room temperature for gel formation. The minimum amount of the compound required to form a stable gel after 24.0 h was recorded as the MGC.

4.2.2. T_{gel} Experiments

The necessary amount of gelator and 1.0 mL of solvent were added to a 7.0 mL standard vial. After sonication, the mixture was heated to obtain a clear solution, and the mixture was left undisturbed to gel. A ball-drop method was used to observe the gel-to-solution transition temperature after 24.0 h (T_{gel}). A spherical glass ball was carefully positioned on top of the gel and the vial was immersed in an oil bath; a thermometer and a magnetic stirrer were equipped to check the temperature. The oil bath was gradually heated at 10.0 °C per minute. The glass ball slowly became immersed into the gel as the temperature increased, and the temperature at which the ball touched the bottom of the vial was recorded as T_{gel}.

4.3. Rheology

A 2.5 cm stainless steel parallel plate geometry configuration was used to perform the rheological measurements. In all cases, oscillatory measurements were conducted at a constant temperature of 20.0 °C. To maintain a constant temperature of 20.0 °C and to prevent solvent loss for amplitude and frequency sweeps, a Peltier temperature control hood was employed. Gels were prepared by dissolving an appropriate amount of gelator in 1.0 mL of solvent/solvent mixtures. After 24 h, amplitude-sweep experiments were carried out by adding approximately ~1.0 mL of gel to the plate. The frequency was maintained at 1.0 Hz during the amplitude sweep with log ramp strain (Y) ranges of 0.01–100%. The frequency-sweep experiments were carried out between 0.1 and 10.0 Hz within the linear viscoelasticity domain (0.02% strain). The experiments were also performed in the presence of various salts at 1:1 molar equivalent in water with a similar procedure as mentioned above.

4.4. Scanning Electron Microscopy (SEM)

The surface morphologies of the xerogels were analyzed on a Leo Supra 25 microscope. Gels of **L_1** and **L_3** were prepared in water at 2.0 wt%. We also prepared the aqueous mixture gels of **L_3** at 2.0 wt%. The gels were filtered after 24.0 h and dried under a fume hood to obtain the xerogel. A small part of xerogel was placed on a pin mount with the carbon tab on top, coated with gold for 5.0–6.0 min (~15.0 nm thickness) to avoid surface charging, and pictures were acquired at 3.0 kV with a working distance of 3–4 mm. An in-lens detector captured the SEM images. SEM of the xerogel of gelator **L_1** in the presence of sodium, magnesium, and calcium salts and **L_3** in the presence of sodium, magnesium, zinc (II), and cadmium (II) salts were also recorded.

4.5. Single-Crystal X-ray Diffraction

Crystals of compound **L_3** were obtained by the slow evaporation of 10.0 mg of the compound in 3.0 mL of water to obtain needle- and block-shaped crystals. X-ray analysis was performed on a Bruker D8 Venture (Photon100 CMOS detector) diffractometer provided with Cryostream (Oxford Cryosystems) open-flow nitrogen cryostats. The data were collected using MoKα radiation (λ = 0.71073 Å) for the plate-shaped crystals at 296(2) K and CuK_α radiation (λ = 1.542 Å) for the needle-shaped crystal at 302(2) K. Apex III

software (Bruker AXS: Madison, WI, USA, 2015) was utilized for the unit cell determination, data collection, data reduction, structure solution/refinement, and empirical absorption correction (SADABS). A direct method was used for solving the structure and was refined by the full-matrix least-squares on F^2 for all data using SHELXTL version 2017/1 [88]. All non-disordered non-hydrogen atoms were refined anisotropically, and all of the hydrogen atoms were placed in the calculated positions and refined using a riding model, except for solvent water molecules. The hydrogen atoms of water molecules were located on the Fourier map and refined. The crystallographic data and hydrogen-bonding parameters are given in Tables S1 and S2 (see Supplementary Materials). The crystallographic data were deposited at the Cambridge Crystallographic Data Centre and can be obtained free of charge, and the CCDC numbers are 2226289–2226290.

4.6. Powder X-ray Diffraction (PXRD)

The bulk crystals of compound **L₃** were obtained by the slow evaporation of the solution of **L₃** (20.0 mg in 3.0 mL water). The crystals were filtered, dried in the air, and ground to a fine powder. The xerogels of **L₃** were prepared from water and the aqueous mixtures, following a similar procedure as mentioned above. We also performed PXRD of the dried gels at 2.0 wt/v% in various solvents/solvent mixtures obtained by adding different salts at 1:1 molar equivalent. All experiments were performed on a PANalytical device with a Cu anode, 2θ from 5.0 to 60.0°, and a 0.02 step size.

Supplementary Materials: The following supporting information can be downloaded at: https://www.mdpi.com/article/10.3390/gels9020089/s1, Scheme S1. Synthesis of **L₁**, Scheme S2. Synthesis of **L₂**, Scheme S3. Synthesis of **L₃**. Figure S1. Amplitude-sweep experiments with gels of **L₁** and **L₂** (2.0 wt%) in water at 20.0 °C with a constant frequency of 1.0 Hz, Figure S2. Frequency-sweep experiments with gels of **L₁** and **L₃** (2.0 wt%) in aqueous mixtures at 20.0 °C with a constant strain of 0.02%, Figure S3. SEM images of (a) **L₁** and (b) **L₃** xerogels in water at 1.8 wt%, Figure S4. SEM images of the xerogels of (a) **L₃** and (b) **diNO** gels obtained from water at 4.0 wt%, Figure S5. SEM images of **L₁** xerogels in (a) DMSO/water (1:1, *v*/*v*) and (b) methanol/water (1:1, *v*/*v*) at 2.0 wt/v%, Figure S6. SEM images of **L₃** xerogels from (a) DMSO/water (1:1, *v*/*v*), and (b) methanol/water (1:1, *v*/*v*) at 2.0 wt/v%, Figure S7. (a) Molecular structure of **L₃**•2H_2O and (b) two-dimensional hydrogen-bonded network with water molecules (space fill model) located in the cavity, Figure S8. Comparison of the simulated pattern of the single-crystal X-ray structure of **L₃**•2H_2O with the PXRD pattern of the bulk crystals obtained from water, and xerogel from water at 2.0 wt%, Figure S9. PXRD pattern of xerogels obtained from the hydrogel of **L₃** at 2.0 wt% and in the presence of 1.0 equivalence of NaCl and KCl, Figure S10. SEM images of xerogels of (a) **L₁** and (b) **L₃** at 2.0 wt% obtained from water in the presence of 1.0 equivalence of $MgCl_2$, Figure S11. Comparison of the PXRD pattern of xerogels (2.0 wt%) of **L₃** hydrogels and the gels in the presence of 1.0 equivalence of $MgCl_2$ and $CaCl_2$, Figure S12. SEM images of the xerogels of **L₃** in the presence of 1.0 equivalence of $CdCl_2$ in water at 2.0 wt%, Figure S13. Comparison of the PXRD pattern of **L₃** xerogel with the PXRD pattern of the xerogels of **L₃**-$CdCl_2$ mixture in various solvents, Figure S14. Comparison of the PXRD pattern of **L₃** xerogel from water with the PXRD pattern of the xerogels of the mixture (**L₃** + $ZnCl_2$) in various solvents, Figure S15. ^{1}H NMR spectrum of compound **L₁**, Figure S16. ^{13}C NMR spectrum of compound **L₁**, Figure S17. ^{1}H NMR spectrum of compound **L₂**, Figure S18. ^{13}C NMR spectrum of compound **L₂**, Figure S19. ^{1}H NMR spectrum of compound **L₃**, Figure S20. ^{13}C NMR spectrum of compound **L₃**. Table S1: Crystal data, Table S2: Hydrogen-bonding parameters, Table S3: Stimuli-responsive properties of the gelators **L₁** and **L₃**: Anion sensing in water at 1.5 wt%, Table S4: Increase in G′ values of the gelators at 1.5 wt% in the presence of various sodium and potassium salts in comparison with the hydrogels (1.8 wt%), Table S5: Stimuli-responsive properties of the gelators **L₁** and **L₃**: Cation sensing in water at 1.5 wt%, Table S6: Increase in G′ values of the gelators at 1.5 wt% in the presence of chloride salts of various cations in comparison with the hydrogels (1.8 wt%).

Author Contributions: Conceptualization, S.S.J., B.K., D.G. and K.K.D.; methodology, S.S.J., B.K., C.B., D.G. and K.K.D.; software, S.S.J. and D.G.; validation, S.S.J. and K.K.D.; formal analysis, S.S.J., D.G., B.K., C.B. and K.K.D.; investigation, S.S.J., D.G. and B.K.; resources, K.K.D.; data curation, K.K.D.; writing—original draft preparation, K.K.D.; writing—review and editing, S.S.J., B.K., D.G. and

K.K.D.; visualization, S.S.J. and K.K.D.; supervision, K.K.D.; project administration, K.K.D.; funding acquisition, K.K.D. All authors have read and agreed to the published version of the manuscript.

Funding: This research received no external funding.

Institutional Review Board Statement: Not applicable.

Informed Consent Statement: Not applicable.

Data Availability Statement: Not applicable.

Acknowledgments: We thank the University of Iceland Research Fund and Science Institute for funding. S.S.J. thanks the University of Iceland for the doctoral research grant. We acknowledge Sigríður Jónsdóttir, University of Iceland, for NMR and mass spectrometry and Friðrik Magnus, University of Iceland, for powder X-ray diffraction analysis. The single-crystal X-ray diffractometer and rheometer used for this research were purchased under the Rannís Iceland infrastructure grants (150998-0031 and 191763-0031).

Conflicts of Interest: The authors declare no conflict of interest.

References

1. McConnell, A.J.; Wood, C.S.; Neelakandan, P.P.; Nitschke, J.R. Stimuli-Responsive Metal–Ligand Assemblies. *Chem. Rev.* **2015**, *115*, 7729–7793. [CrossRef] [PubMed]
2. Theato, P.; Sumerlin, B.S.; O'Reilly, R.K.; Epps, I.I.I.T.H. Stimuli responsive materials. *Chem. Soc. Rev.* **2013**, *42*, 7055–7056. [CrossRef]
3. Shigemitsu, H.; Hamachi, I. Supramolecular Assemblies Responsive to Biomolecules toward Biological Applications. *Chem. Asian J.* **2015**, *10*, 2026–2038. [CrossRef] [PubMed]
4. Segarra-Maset, M.D.; Nebot, V.J.; Miravet, J.F.; Escuder, B. Control of molecular gelation by chemical stimuli. *Chem. Soc. Rev.* **2013**, *42*, 7086–7098. [CrossRef]
5. Banerjee, S.; Das, R.K.; Maitra, U. Supramolecular gels 'in action'. *J. Mater. Chem.* **2009**, *19*, 6649–6687. [CrossRef]
6. Dastidar, P. Supramolecular gelling agents: Can they be designed? *Chem. Soc. Rev.* **2008**, *37*, 2699–2715. [CrossRef] [PubMed]
7. de Loos, M.; Feringa, B.L.; van Esch, J.H. Design and Application of Self-Assembled Low Molecular Weight Hydrogels. *Eur. J. Org. Chem.* **2005**, *2005*, 3615–3631. [CrossRef]
8. Estroff, L.A.; Hamilton, A.D. Water gelation by small organic molecules. *Chem. Rev.* **2004**, *104*, 1201–1218. [CrossRef]
9. George, M.; Weiss, R.G. Molecular Organogels. Soft Matter Comprised of Low-Molecular-Mass Organic Gelators and Organic Liquids†. *Acc. Chem. Res.* **2006**, *39*, 489–497. [CrossRef]
10. Hirst, A.R.; Escuder, B.; Miravet, J.F.; Smith, D.K. High-Tech Applications of Self-Assembling Supramolecular Nanostructured Gel-Phase Materials: From Regenerative Medicine to Electronic Devices. *Angew. Chem. Int. Ed.* **2008**, *47*, 8002–8018. [CrossRef]
11. Steed, J.W. Anion-tuned supramolecular gels: A natural evolution from urea supramolecular chemistry. *Chem. Soc. Rev.* **2010**, *39*, 3686–3699. [CrossRef] [PubMed]
12. Yu, G.; Yan, X.; Han, C.; Huang, F. Characterization of supramolecular gels. *Chem. Soc. Rev.* **2013**, *42*, 6697–6722. [CrossRef] [PubMed]
13. Chivers, P.R.A.; Smith, D.K. Shaping and structuring supramolecular gels. *Nat. Rev. Mater.* **2019**, *4*, 463–478. [CrossRef]
14. Kumar, D.K.; Steed, J.W. Supramolecular gel phase crystallization: Orthogonal self-assembly under non-equilibrium conditions. *Chem. Soc. Rev.* **2014**, *43*, 2080–2088. [CrossRef]
15. Truong, W.T.; Su, Y.; Meijer, J.T.; Thordarson, P.; Braet, F. Self-assembled gels for biomedical applications. *Chem. Asian J.* **2011**, *6*, 30–42. [CrossRef]
16. Foster, J.A.; Damodaran, K.K.; Maurin, A.; Day, G.M.; Thompson, H.P.; Cameron, G.J.; Bernal, J.C.; Steed, J.W. Pharmaceutical polymorph control in a drug-mimetic supramolecular gel. *Chem. Sci.* **2017**, *8*, 78. [CrossRef]
17. Zhu, J.; Wang, R.; Geng, R.; Zhang, X.; Wang, F.; Jiao, T.; Yang, J.; Bai, Z.; Peng, Q. A facile preparation method for new two-component supramolecular hydrogels and their performances in adsorption, catalysis, and stimuli-response. *RSC Adv.* **2019**, *9*, 22551–22558. [CrossRef]
18. Qu, R.; Shen, L.; Qu, A.; Wang, R.; An, Y.; Shi, L. Artificial Peroxidase/Oxidase Multiple Enzyme System Based on Supramolecular Hydrogel and Its Application as a Biocatalyst for Cascade Reactions. *ACS Appl. Mater. Interfaces* **2015**, *7*, 16694–16705. [CrossRef]
19. Zhang, J.; Bai, Y.; Yu, Q.; Ma, Z.; Liu, Q.; Zhou, F.; Liu, W.; Cai, M. Physicochemical and Tribological Performance of Bi-Component Supramolecular Gel Lubricants. *Adv. Mater. Interfaces* **2019**, *6*, 1801391. [CrossRef]
20. Yan, L.; Li, G.; Ye, Z.; Tian, F.; Zhang, S. Dual-responsive two-component supramolecular gels for self-healing materials and oil spill recovery. *Chem. Commun.* **2014**, *50*, 14839–14842. [CrossRef]
21. Patterson, A.K.; Smith, D.K. Two-component supramolecular hydrogel for controlled drug release. *Chem. Commun.* **2020**, *56*, 11046–11049. [CrossRef] [PubMed]
22. Buerkle, L.E.; Rowan, S.J. Supramolecular gels formed from multi-component low molecular weight species. *Chem. Soc. Rev.* **2012**, *41*, 6089–6102. [CrossRef] [PubMed]

23. Du, X.; Zhou, J.; Shi, J.; Xu, B. Supramolecular Hydrogelators and Hydrogels: From Soft Matter to Molecular Biomaterials. *Chem. Rev.* **2015**, *115*, 13165–13307. [CrossRef] [PubMed]
24. Cao, X.; Gao, A.; Hou, J.-t.; Yi, T. Fluorescent supramolecular self-assembly gels and their application as sensors: A review. *Coord. Chem. Rev.* **2021**, *434*, 213792. [CrossRef]
25. Picci, G.; Mulvee, M.T.; Caltagirone, C.; Lippolis, V.; Frontera, A.; Gomila, R.M.; Steed, J.W. Anion-Responsive Fluorescent Supramolecular Gels. *Molecules* **2022**, *27*, 1257. [CrossRef]
26. Oliveira, C.B.P.; Gomes, V.; Ferreira, P.M.T.; Martins, J.A.; Jervis, P.J. Peptide-Based Supramolecular Hydrogels as Drug Delivery Agents: Recent Advances. *Gels* **2022**, *8*, 706. [CrossRef]
27. Cui, J.; Liu, A.; Guan, Y.; Zheng, J.; Shen, Z.; Wan, X. Tuning the Helicity of Self-Assembled Structure of a Sugar-Based Organogelator by the Proper Choice of Cooling Rate. *Langmuir* **2010**, *26*, 3615–3622. [CrossRef]
28. Huang, X.; Terech, P.; Raghavan, S.R.; Weiss, R.G. Kinetics of 5α-Cholestan-3β-yl N-(2-Naphthyl)carbamate/n-Alkane Organogel Formation and Its Influence on the Fibrillar Networks. *J. Am. Chem. Soc.* **2005**, *127*, 4336–4344. [CrossRef]
29. Huang, H.; Zhu, X.; Su, L.; Wang, H.; Yang, Y. Effect of temperature on self-assembly/disassembly transition of dialkylurea supramolecular gels at high pressure. *RSC Adv.* **2013**, *3*, 11854–11859. [CrossRef]
30. Naota, T.; Koori, H. Molecules That Assemble by Sound: An Application to the Instant Gelation of Stable Organic Fluids. *J. Am. Chem. Soc.* **2005**, *127*, 9324–9325. [CrossRef]
31. Chen, S.; Fan, Y.; Song, J.; Xue, B. The remarkable role of hydrogen bond, halogen, and solvent effect on self-healing supramolecular gel. *Mater. Today Chem.* **2022**, *23*, 100719. [CrossRef]
32. Jayabhavan, S.S.; Steed, J.W.; Damodaran, K.K. Crystal Habit Modification of Metronidazole by Supramolecular Gels with Complementary Functionality. *Cryst. Growth Des.* **2021**, *21*, 5383–5393. [CrossRef]
33. Bera, S.; Basu, S.; Jana, B.; Dastidar, P. Real-time Observation of Macroscopic Helical Morphologies under Optical Microscope: A Curious Case of π–π Stacking Driven Molecular Self-assembly of an Organic Gelator Devoid of Hydrogen Bonding. *Angew. Chem. Int. Ed.* **2022**, e202216447. [CrossRef]
34. van Esch, J.H.; Feringa, B.L. New Functional Materials Based on Self-Assembling Organogels: From Serendipity towards Design. *Angew. Chem. Int. Ed.* **2000**, *39*, 2263–2266. [CrossRef]
35. Desiraju, G.R. Supramolecular Synthons in Crystal Engineering—A New Organic Synthesis. *Angew. Chem. Int. Ed.* **1995**, *34*, 2311–2327. [CrossRef]
36. Weiss, R.G.; Terech, P. (Eds.) *Molecular Gels: Materials with Self-Assembled Fibrillar Networks*; Springer: Berlin/Heidelberg, Germany, 2006; p. 978.
37. Fages, F.; Voegtle, F.; Zinic, M. Systematic design of amide- and urea-type gelators with tailored properties. *Top. Curr. Chem.* **2005**, *256*, 77–131.
38. Isare, B.; Pensec, S.; Raynal, M.; Bouteiller, L. Bisurea-based supramolecular polymers: From structure to properties1. *C. R. Chim.* **2016**, *19*, 148–156. [CrossRef]
39. Moulin, E.; Armao, J.J.; Giuseppone, N. Triarylamine-Based Supramolecular Polymers: Structures, Dynamics, and Functions. *Acc. Chem. Res.* **2019**, *52*, 975–983. [CrossRef]
40. Gale, P.A.; Busschaert, N.; Haynes, C.J.E.; Karagiannidis, L.E.; Kirby, I.L. Anion receptor chemistry: Highlights from 2011 and 2012. *Chem. Soc. Rev.* **2014**, *43*, 205–241. [CrossRef]
41. Dzolic, Z.; Cametti, M.; Dalla Cort, A.; Mandolini, L.; Zinic, M. Fluoride-responsive organogelator based on oxalamide-derived anthraquinone. *Chem. Commun.* **2007**, 3535–3537. [CrossRef]
42. Kotova, O.; Daly, R.; dos Santos, C.M.G.; Boese, M.; Kruger, P.E.; Boland, J.J.; Gunnlaugsson, T. Europium-Directed Self-Assembly of a Luminescent Supramolecular Gel from a Tripodal Terpyridine-Based Ligand. *Angew. Chem. Int. Ed.* **2012**, *51*, 7208–7212. [CrossRef] [PubMed]
43. Feng, L.; Cavicchi, K.A. Investigation of the relationships between the thermodynamic phase behavior and gelation behavior of a series of tripodal trisamide compounds. *Soft Matter* **2012**, *8*, 6483–6492. [CrossRef]
44. Mukhopadhyay, S.; Ira; Krishnamoorthy, G.; Maitra, U. Dynamics of Bound Dyes in a Nonpolymeric Aqueous Gel Derived from a Tripodal Bile Salt. *J. Phys. Chem. B* **2003**, *107*, 2189–2192. [CrossRef]
45. Kumar, D.K.; Jose, D.A.; Dastidar, P.; Das, A. Nonpolymeric Hydrogelator Derived from N-(4-Pyridyl)isonicotinamide. *Langmuir* **2004**, *20*, 10413–10418. [CrossRef]
46. Li, Z.; Cao, J.; Li, H.; Liu, H.; Han, F.; Liu, Z.; Tong, C.; Li, S. Self-assembled drug delivery system based on low-molecular-weight bis-amide organogelator: Synthesis, properties and in vivo evaluation. *Drug Delivery* **2016**, *23*, 3168–3178. [CrossRef]
47. Bradberry, S.J.; Dee, G.; Kotova, O.; McCoy, C.P.; Gunnlaugsson, T. Luminescent lanthanide (Eu(iii)) cross-linked supramolecular metallo co-polymeric hydrogels: The effect of ligand symmetry. *Chem. Commun.* **2019**, *55*, 1754–1757. [CrossRef]
48. Chandran, S.K.; Nath, N.K.; Cherukuvada, S.; Nangia, A. N–H ... N(pyridyl) and N–H ... O(urea) hydrogen bonding and molecular conformation of N-aryl-N′-pyridylureas. *J. Mol. Struct.* **2010**, *968*, 99–107. [CrossRef]
49. Kumar, D.K.; Jose, D.A.; Das, A.; Dastidar, P. First snapshot of a nonpolymeric hydrogelator interacting with its gelling solvents. *Chem. Commun.* **2005**, 4059–4061. [CrossRef]
50. Kumar, D.K.; Jose, D.A.; Dastidar, P.; Das, A. Nonpolymeric Hydrogelators Derived from Trimesic Amides. *Chem. Mater.* **2004**, *16*, 2332–2335. [CrossRef]

51. Lloyd, G.O.; Piepenbrock, M.-O.M.; Foster, J.A.; Clarke, N.; Steed, J.W. Anion tuning of chiral bis(urea) low molecular weight gels. *Soft Matter* **2012**, *8*, 204–216. [CrossRef]
52. Piepenbrock, M.-O.M.; Lloyd, G.O.; Clarke, N.; Steed, J.W. Metal- and Anion-Binding Supramolecular Gels. *Chem. Rev.* **2010**, *110*, 1960–2004. [CrossRef] [PubMed]
53. Lloyd, G.O.; Steed, J.W. Anion-tuning of supramolecular gel properties. *Nat. Chem.* **2009**, *1*, 437–442. [CrossRef] [PubMed]
54. Piepenbrock, M.-O.M.; Lloyd, G.O.; Clarke, N.; Steed, J.W. Gelation is crucially dependent on functional group orientation and may be tuned by anion binding. *Chem. Commun.* **2008**, 2644–2646. [CrossRef] [PubMed]
55. Ghosh, D.; Mulvee, M.T.; Damodaran, K.K. Tuning Gel State Properties of Supramolecular Gels by Functional Group Modification. *Molecules* **2019**, *24*, 3472. [CrossRef]
56. Reddy, L.S.; Babu, N.J.; Nangia, A. Carboxamide–pyridine N-oxide heterosynthon for crystal engineering and pharmaceutical cocrystals. *Chem. Commun.* **2006**, 1369–1371. [CrossRef]
57. Mfuh, A.M.; Larionov, O.V. Heterocyclic N-oxides-an emerging class of therapeutic agents. *Curr. Med. Chem.* **2015**, *22*, 2819–2857. [CrossRef]
58. Saikia, B.; Khatioda, R.; Bora, P.; Sarma, B. Pyridine N-oxides as coformers in the development of drug cocrystals. *CrystEngComm* **2016**, *18*, 8454–8464. [CrossRef]
59. Puttreddy, R.; Beyeh, N.K.; Ras, R.H.A.; Trant, J.F.; Rissanen, K. Endo-/exo- and halogen-bonded complexes of conformationally rigid C-ethyl-2-bromoresorcinarene and aromatic N-oxides. *CrystEngComm* **2017**, *19*, 4312–4320. [CrossRef]
60. Łukomska, M.; Rybarczyk-Pirek, A.J.; Jabłoński, M.; Palusiak, M. The nature of NO-bonding in N-oxide group. *PCCP* **2015**, *17*, 16375–16387. [CrossRef]
61. Sauvée, C.; Ström, A.; Haukka, M.; Sundén, H. A Multi-Component Reaction towards the Development of Highly Modular Hydrogelators. *Chem. Eur. J.* **2018**, *24*, 8071–8075. [CrossRef]
62. Ghosh, D.; Deepa; Damodaran, K.K. Metal complexation induced supramolecular gels for the detection of cyanide in water. *Supramol. Chem.* **2020**, *32*, 276–286. [CrossRef]
63. Ghosh, D.; Ferfolja, K.; Drabavičius, Ž.; Steed, J.W.; Damodaran, K.K. Crystal habit modification of Cu(ii) isonicotinate–N-oxide complexes using gel phase crystallisation. *New J. Chem.* **2018**, *42*, 19963–19970. [CrossRef]
64. Ghosh, D.; Bjornsson, R.; Damodaran, K.K. Role of N–Oxide Moieties in Tuning Supramolecular Gel-State Properties. *Gels* **2020**, *6*, 41. [CrossRef]
65. Goodwin, J.W.; Hughes, R.W. *Rheology for Chemists: An Introduction*; Royal Society of Chemistry: London, UK, 2008.
66. Guenet, J.-M. *Organogels: Thermodynamics, Structure, Solvent Role, and Properties*; Springer: Berlin/Heidelberg, Germany, 2016.
67. Denzer, B.R.; Kulchar, R.J.; Huang, R.B.; Patterson, J. Advanced Methods for the Characterization of Supramolecular Hydrogels. *Gels* **2021**, *7*, 158. [CrossRef]
68. Tomasson, D.A.; Ghosh, D.; Kržišnik, Z.; Fasolin, L.H.; Vicente, A.n.A.; Martin, A.D.; Thordarson, P.; Damodaran, K.K. Enhanced mechanical and thermal strength in mixed-enantiomers-based supramolecular gel. *Langmuir* **2018**, *34*, 12957–12967. [CrossRef] [PubMed]
69. Ghosh, D.; Farahani, A.D.; Martin, A.D.; Thordarson, P.; Damodaran, K.K. Unraveling the Self-Assembly Modes in Multicomponent Supramolecular Gels Using Single-Crystal X-ray Diffraction. *Chem. Mater.* **2020**, *32*, 3517–3527. [CrossRef]
70. Bernstein, J.; Davis, R.E.; Shimoni, L.; Chang, N.-L. Patterns in Hydrogen Bonding: Functionality and Graph Set Analysis in Crystals. *Angew. Chem. Int. Ed.* **1995**, *34*, 1555–1573. [CrossRef]
71. Ghosh, D.; Lebedytė, I.; Yufit, D.S.; Damodaran, K.K.; Steed, J.W. Selective gelation of N-(4-pyridyl) nicotinamide by copper (ii) salts. *CrystEngComm* **2015**, *17*, 8130–8138. [CrossRef]
72. Tómasson, D.A.; Ghosh, D.; Kurup, M.P.; Mulvee, M.T.; Damodaran, K.K. Evaluating the role of a urea-like motif in enhancing the thermal and mechanical strength of supramolecular gels. *CrystEngComm* **2021**, *23*, 617–628. [CrossRef]
73. Mears, L.L.E.; Draper, E.R.; Castilla, A.M.; Su, H.; Zhuola; Dietrich, B.; Nolan, M.C.; Smith, G.N.; Doutch, J.; Rogers, S.; et al. Drying Affects the Fiber Network in Low Molecular Weight Hydrogels. *Biomacromolecules* **2017**, *18*, 3531–3540. [CrossRef]
74. Li, L.; Sun, R.; Zheng, R.; Huang, Y. Anions-responsive supramolecular gels: A review. *Mater. Des.* **2021**, *205*, 109759. [CrossRef]
75. Fages, F. Metal coordination to assist molecular gelation. *Angew. Chem. Int. Ed.* **2006**, *45*, 1680–1682. [CrossRef] [PubMed]
76. Offiler, C.A.; Jones, C.D.; Steed, J.W. Metal 'turn-off', anion 'turn-on' gelation cascade in pyridinylmethyl ureas. *Chem. Commun.* **2017**, *53*, 2024–2027. [CrossRef] [PubMed]
77. Sudhakaran Jayabhavan, S.; Ghosh, D.; Damodaran, K.K. Making and Breaking of Gels: Stimuli-Responsive Properties of Bis (Pyridyl-N-oxide Urea) Gelators. *Molecules* **2021**, *26*, 6420. [CrossRef] [PubMed]
78. Lima, J.C.; Rodríguez, L. Supramolecular gold metallogelators: The key role of metallophilic interactions. *Inorganics* **2014**, *3*, 1–18. [CrossRef]
79. Tam, A.Y.-Y.; Yam, V.W.-W. Recent advances in metallogels. *Chem. Soc. Rev.* **2013**, *42*, 1540–1567. [CrossRef]
80. Adarsh, N.; Sahoo, P.; Dastidar, P. Is a crystal engineering approach useful in designing metallogels? A case study. *Cryst. Growth Des.* **2010**, *10*, 4976–4986. [CrossRef]
81. Häring, M.; Díaz, D.D. Supramolecular metallogels with bulk self-healing properties prepared by in situ metal complexation. *Chem. Commun.* **2016**, *52*, 13068–13081. [CrossRef]
82. Bhattacharjee, S.; Bhattacharya, S. Pyridylenevinylene based Cu2+-specific, injectable metallo(hydro)gel: Thixotropy and nanoscale metal-organic particles. *Chem. Commun.* **2014**, *50*, 11690–11693. [CrossRef]

83. Bhattacharjee, S.; Samanta, S.K.; Moitra, P.; Pramoda, K.; Kumar, R.; Bhattacharya, S.; Rao, C.N.R. Nanocomposite Made of an Oligo(p-phenylenevinylene)-Based Trihybrid Thixotropic Metallo(organo)gel Comprising Nanoscale Metal-Organic Particles, Carbon Nanohorns, and Silver Nanoparticles. *Chem. Eur. J.* **2015**, *21*, 5467–5476. [CrossRef]
84. Kumar Vemula, P.; Aslam, U.; Ajay Mallia, V.; John, G. In Situ Synthesis of Gold Nanoparticles Using Molecular Gels and Liquid Crystals from Vitamin-C Amphiphiles. *Chem. Mater.* **2007**, *19*, 138–140. [CrossRef]
85. Paul, M.; Sarkar, K.; Dastidar, P. Metallogels Derived from Silver Coordination Polymers of C3-Symmetric Tris(pyridylamide) Tripodal Ligands: Synthesis of Ag Nanoparticles and Catalysis. *Chem. Eur. J.* **2015**, *21*, 255–268. [CrossRef]
86. Schobert, R.; Biersack, B. cis-Dichloroplatinum (II) complexes with aminomethylnicotinate and -isonicotinate ligands. *Inorg. Chim. Acta* **2005**, *358*, 3369–3376. [CrossRef]
87. Gardner, J.N.; Katritzky, A.R. N-oxides and related compounds. Part V. The tautomerism of 2- and 4-amino- and -hydroxy-pyridine 1-oxide. *J. Chem. Soc.* **1957**, *875*, 4375–4385. [CrossRef]
88. Sheldrick, G. Crystal structure refinement with SHELXL. *Acta Crystallogr. Sect. C* **2015**, *71*, 3–8. [CrossRef]

Supporting Information

Stimuli-responsive Properties of Supramolecular Gels based on Pyridyl-*N*-oxide Amides

Sreejith Sudhakaran Jayabhavan [1], Baldur Kristinsson [1], Dipankar Ghosh [1], Charlène Breton [1], and Krishna K. Damodaran [1,*]

Table of contents

1. Synthetic scheme

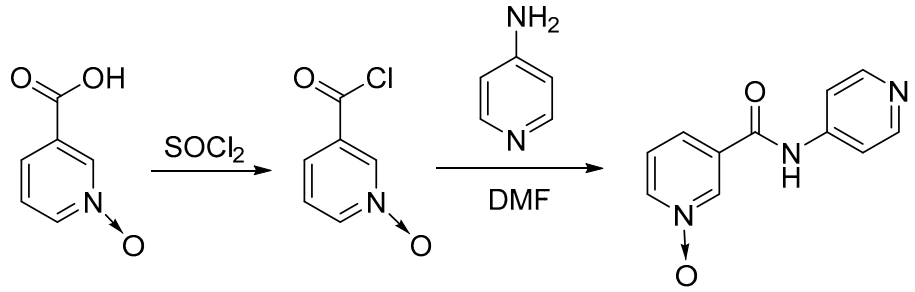

Scheme S1. Synthesis of L_1

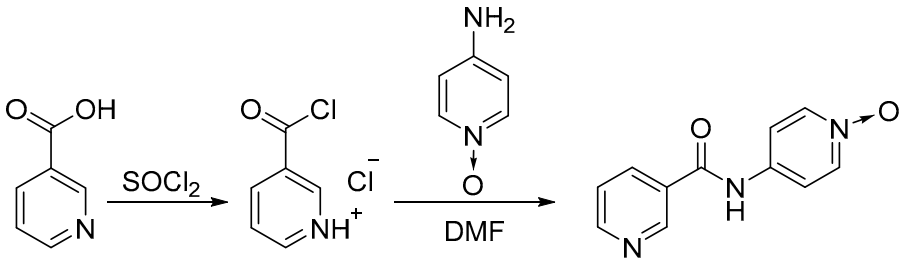

Scheme S2. Synthesis of L_2

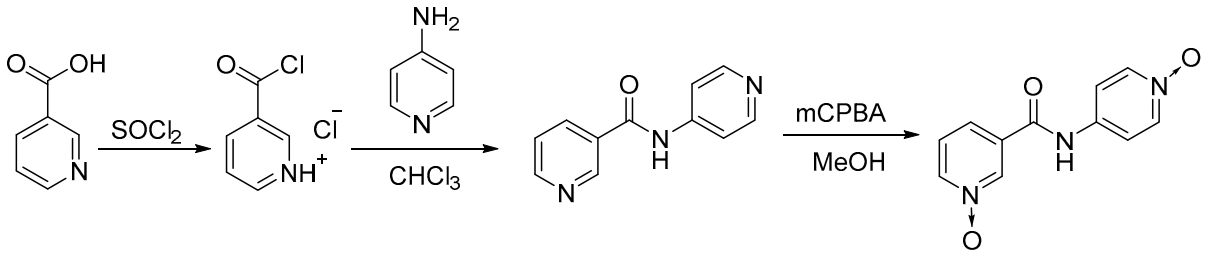

Scheme S3. Synthesis of L_3

2. Rheology

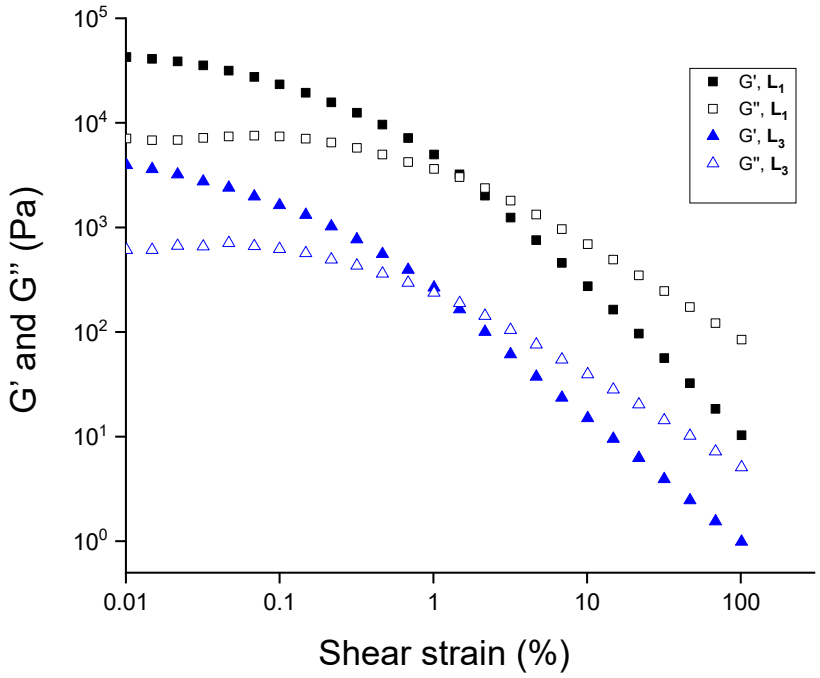

Figure S1. Amplitude-sweep experiments with gels of $\mathbf{L_1}$ and $\mathbf{L_2}$ (2.0 wt%) in water at 20.0 °C with a constant frequency of 1.0 Hz.

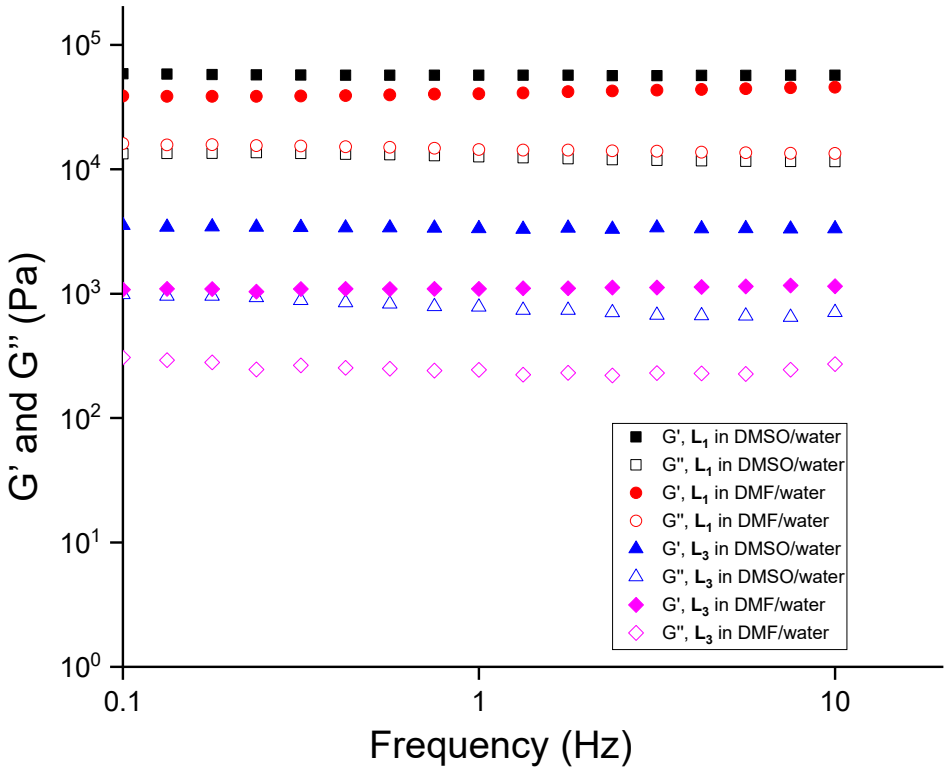

Figure S2. Frequency-sweep experiments with gels of $\mathbf{L_1}$ and $\mathbf{L_3}$ (2.0 wt%) in aqueous mixtures at 20.0 °C with a constant strain of 0.02%.

3. Scanning electron microscopy (SEM)

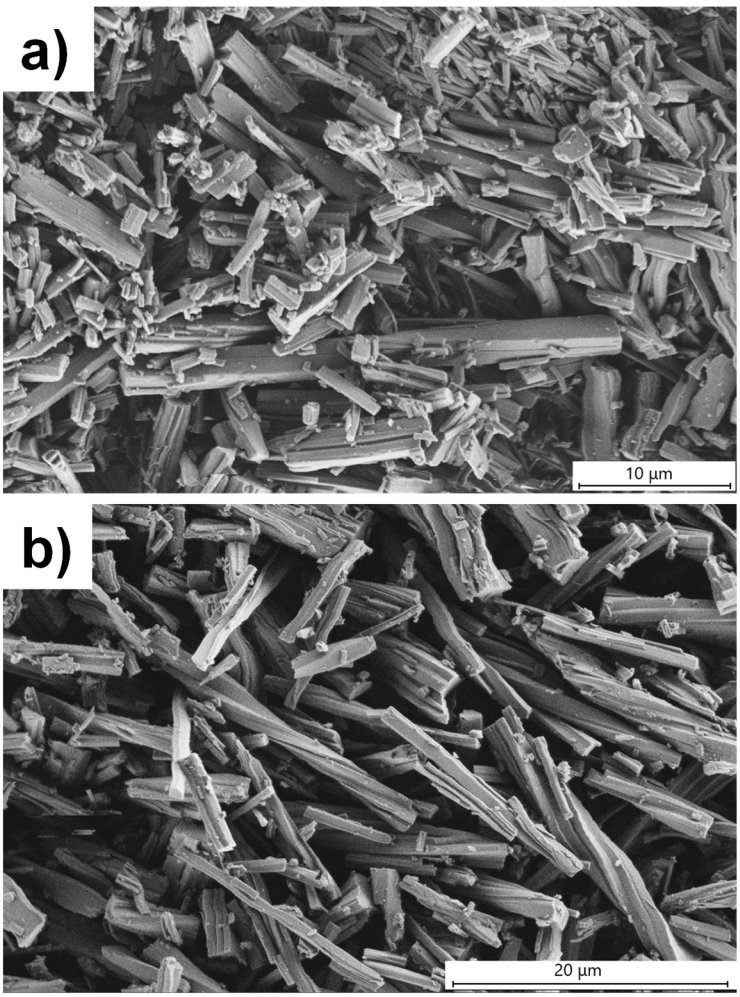

Figure S3. SEM images of (a) $\mathbf{L_1}$ and (b) $\mathbf{L_3}$ xerogels in water at 1.8 wt%.

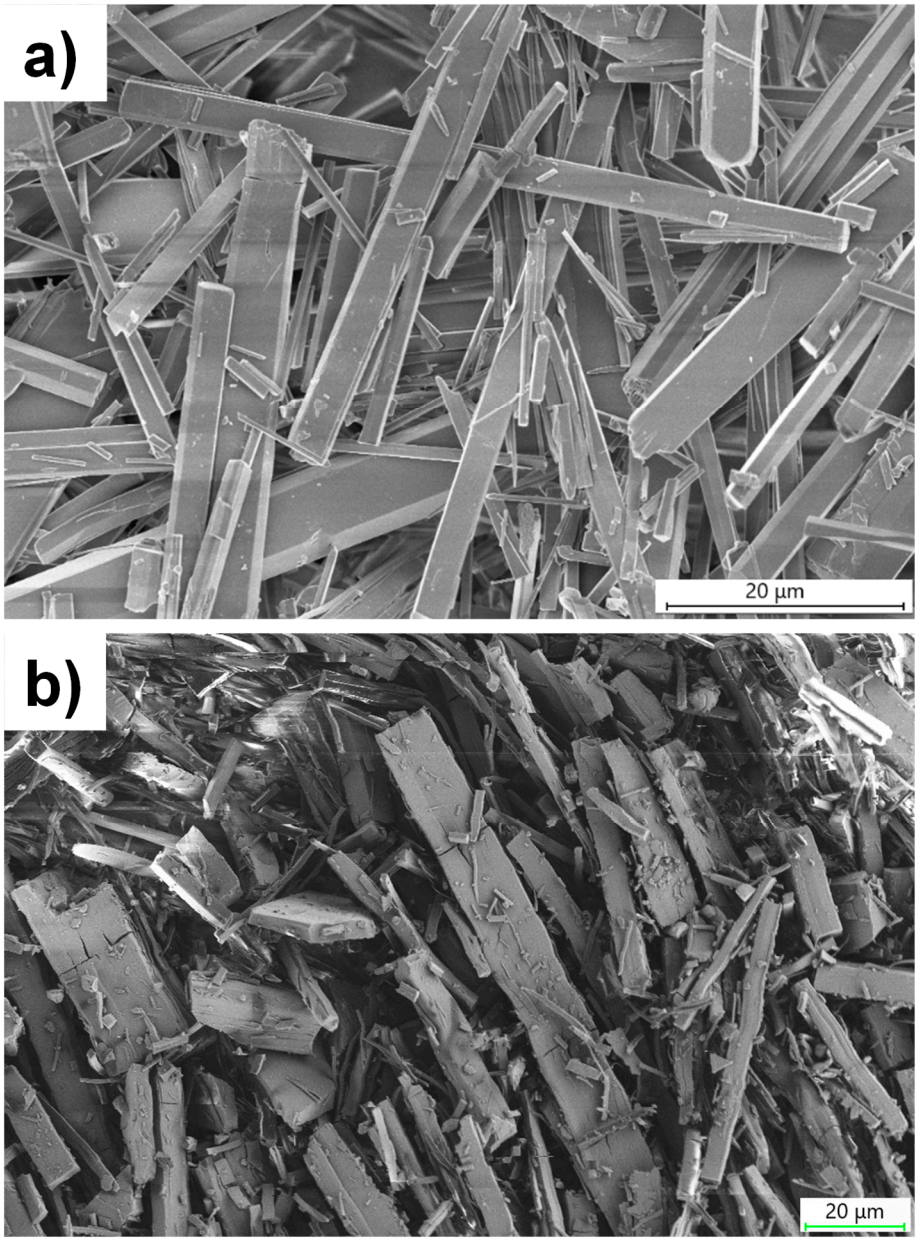

Figure S4. SEM images of the xerogels of (a) $\mathbf{L_3}$ and (b) **diNO** gels obtained from water at 4.0 wt%.

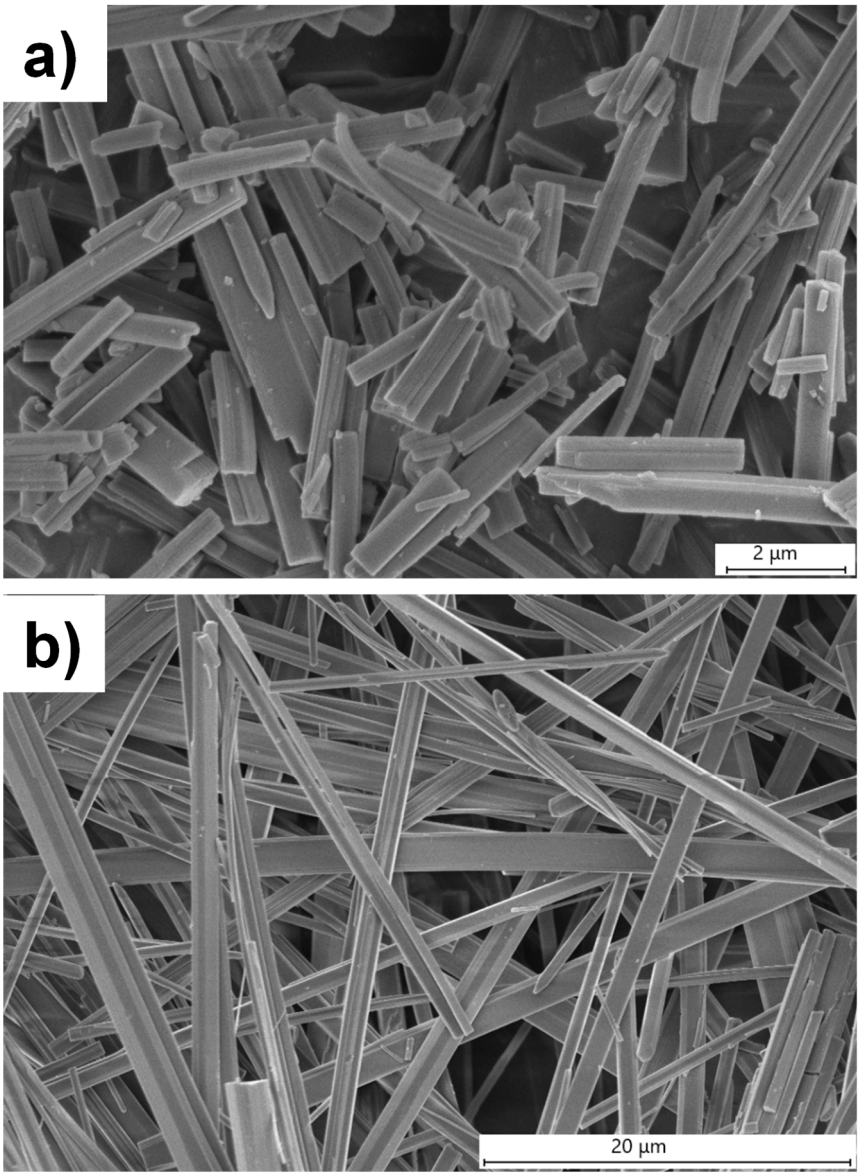

Figure S5. SEM images of $\mathbf{L_1}$ xerogels in (a) DMSO/water (1:1, v/v) and (b) methanol/water (1:1, *v*/*v*) at 2.0 wt/v%.

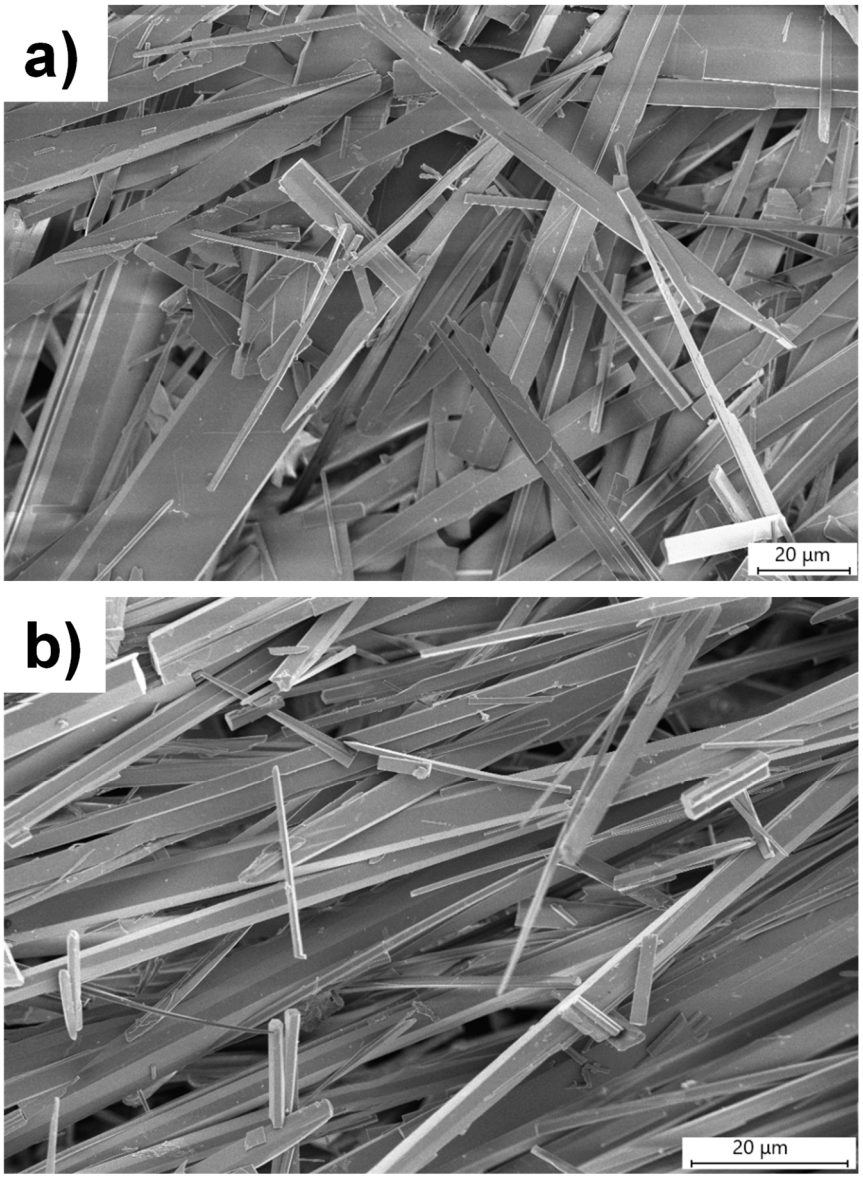

Figure S6. SEM images of $\mathbf{L_3}$ xerogels from (a) DMSO/water (1:1, *v*/*v*), and (b) methanol/water (1:1, *v*/*v*) at 2.0 wt/v%.

4. X-ray crystallography

Table S1: Crystal data

Crystal data	**L₃**•H_2O	**L₃**•$2H_2O$
Empirical formula	$C_{11}H_{11}N_3O_4$	$C_{11}H_{11}N_3O_4$
Color	Colorless	Colorless
Formula weight	249.23	249.23
Crystal size (mm)	0.19 x 0.05 x 0.03	0.22 x 0.16 x 0.10
Crystal system	Monoclinic	Monoclinic
Space group	$P2_1/c$	$P2/c$
a (Å)	3.73500(10)	8.1758(8)
b (Å)	12.7975(4)	5.6771(5)
c (Å)	22.9071(8)	23.529(2)
α (°)	90	90
β (°)	90.0100(14)	97.127(2)
γ (°)	90	90
Volume (Å^3)	1094.93(6)	1083.66(18)
Z	4	4
$D_{calc.}$(g/cm^3)	1.512	1.528
F(000)	520	520
μ (mm^{-1})	0.998 (CuK_α)	0.119 (MoK_α)
Temperature (K)	302(2)	296(2)
Reflections collected/ unique/observed [I>2σ(I)]	15306/ 1730/ 1369	17613/ 2500/ 2071
Data/restraints/parameters	1730/0/171	2500/0/172
Goodness of fit on F^2	1.045	1.062
Final R indices [I>2σ(I)]	R_1 = 0.0457 wR_2 = 0.1126	R_1 = 0.0409 wR_2 = 0.1062
R indices (all data)	R_1 = 0.0624 wR_2 = 0.1227	R_1 = 0.0524 wR_2 = 0.1144

Table S2: Hydrogen bonding parameters

Compound L_3•H_2O						
No.	Donor—H···Acceptor	D–H(Å)	H···A(Å)	D···A(Å)	∠D—H···A(°)	Symmetry operation
1	O(18)—H(1)···O(15)	1.00(3)	1.79(3)	2.782(3)	170(3)	1+x,y,z
2	O(18)—H(2)···O(15)	0.97(5)	1.85(5)	2.796(3)	165(4)	x,y,z
3	O(18)—H(2)···N(14)	0.97(5)	2.48(4)	3.318(3)	145(4)'	x,y,z
4	N(10)—H(10)···O(1)	0.86	2.01	2.852(2)	166	1-x,2-y,-z
5	C(4)—H(4)···O(15)	0.93	2.58	3.266(3)	131	1+x,3/2-y,-1/2+z
6	C(7)—H(7)···O(1)	0.93	2.47	3.354(3)	158	-x,2-y,-z
7	C(13)—H(13)···O(9)	0.93	2.52	3.166(3)	127	-x,1-y,-z
8	C(16)—H(16)···O(18)	0.93	2.55	3.235(3)	131	1-x,1/2+y,1/2-z
Compound L_3•$2H_2O$						
No.	Donor—H···Acceptor	D–H(Å)	H···A(Å)	D···A(Å)	∠D—H···A(°)	Symmetry operation
1	N(10)—H(10)···O(1)	0.86	2.07	2.8956(16)	161	1-x,-y,1-z
2	O(18)—H(18)···O(17)	0.87(2)	1.88(2)	2.7447(18)	175(2)	1-x,2-y,1-z
3	O(19)—H(19)···O(17)	0.91(2)	1.91(2)	2.8185(19)	173(2)	x,2-y,-1/2+z
4	C(7)—H(7)···O(1)	0.93	2.35	3.2486(18)	163	1-x,-y,1-z
5	C(13)—H(13)···O(9)	0.93	2.37	3.1134(17)	137	-x,2-y,1-z
6	C(15)—H(15)···O(18)	0.93	2.39	3.129(2)	136	1-x,1-y,1-z
7	C(16)—H(16)···O(1)	0.93	2.39	3.155(2)	139	1-x,-y,1-z

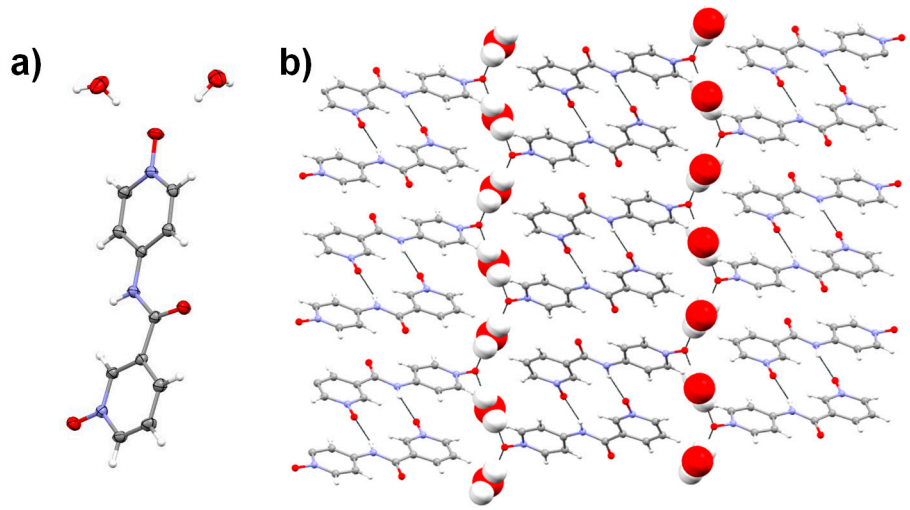

Figure S7. (a) Molecular structure of **L₃**•2H_2O and (b) two-dimensional hydrogen-bonded network with water molecules (space fill model) located in the cavity.

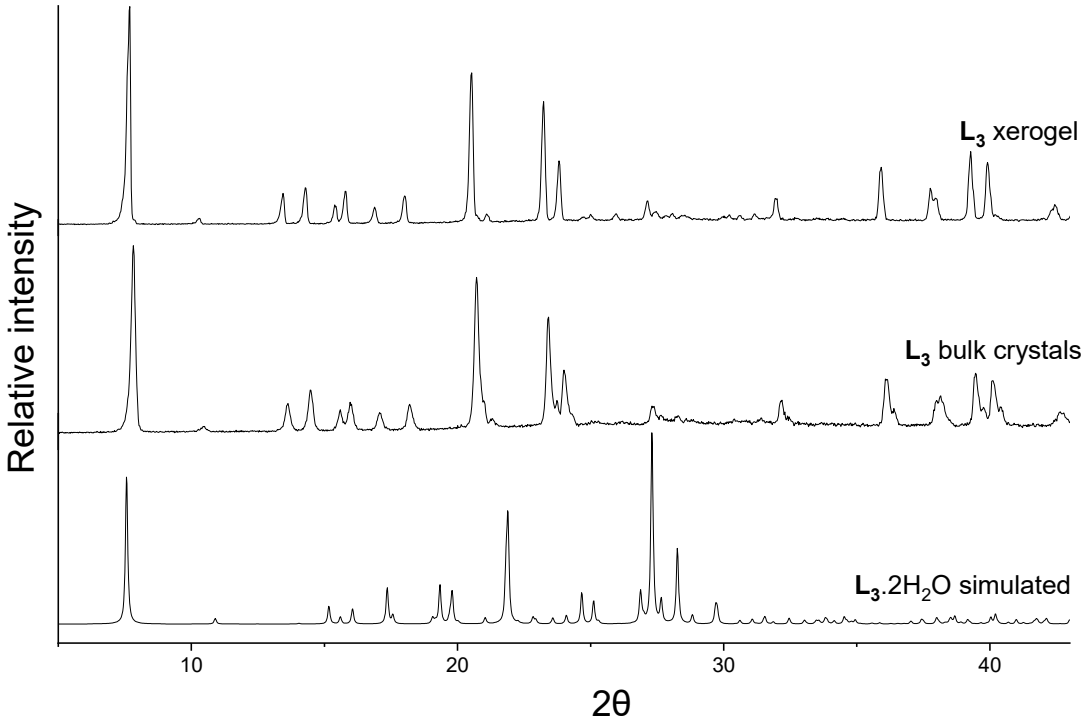

Figure S8. Comparison of the simulated pattern of the single-crystal X-ray structure of **L₃**.2H_2O with the PXRD pattern of the bulk crystals obtained from water, and xerogel from water at 2.0 wt%.

5. Physical properties of the gels in the presence of salts

Table S3: Stimuli-responsive properties of the gelators **L_1** and **L_3**: Anion sensing in water at 1.5 wt%

Salts (1.0 equiv.)	**L_1**	**L_3**
NaF	G	G
NaCl	G	G
NaBr	G	G
NaI	Ppt	PG
KF	G	G
KCl	G	G
KBr	G	G
KI	G	G
$NaNO_3$	C	G
$NaSO_4$	C	Ppt
NaN_3	C	G
KCN	C	S
$KClO_4$	Ppt	PG
KPF_6	C	G
KBF_4	C	G
KSCN	C	PG
$K_2C_2O_4$	C	G
KNO_3	C	G

C-colloid, G-gel, PG-partial gel, Ppt-Precipitate

Table S4: Increase in G' values of the gelators at 1.5 wt% in the presence of various sodium and potassium salts in comparison with the hydrogels (1.8 wt%)

Salt added	**Equivalence (equiv.)**	**L_1 1.5%**	**L_3 1.5%**
NaF	1.0	2.0-fold	2.8-fold
KF	1.0	2.6-fold	3.0-fold
NaCl	1.0	1.8-fold	4.3-fold
KCl	1.0	3.0-fold	5.7-fold
NaBr	1.0	1.5-fold	3.0-fold
KBr	1.0	3.0-fold	2.3-fold
KI	1.0	---	1.7-fold
KNO_3	1.0	---	1.9-fold
KBF_4	1.0	---	4.8-fold
KPF_6	1.0	---	5.0-fold
$K_2C_2O_4$	1.0	---	1.8-fold

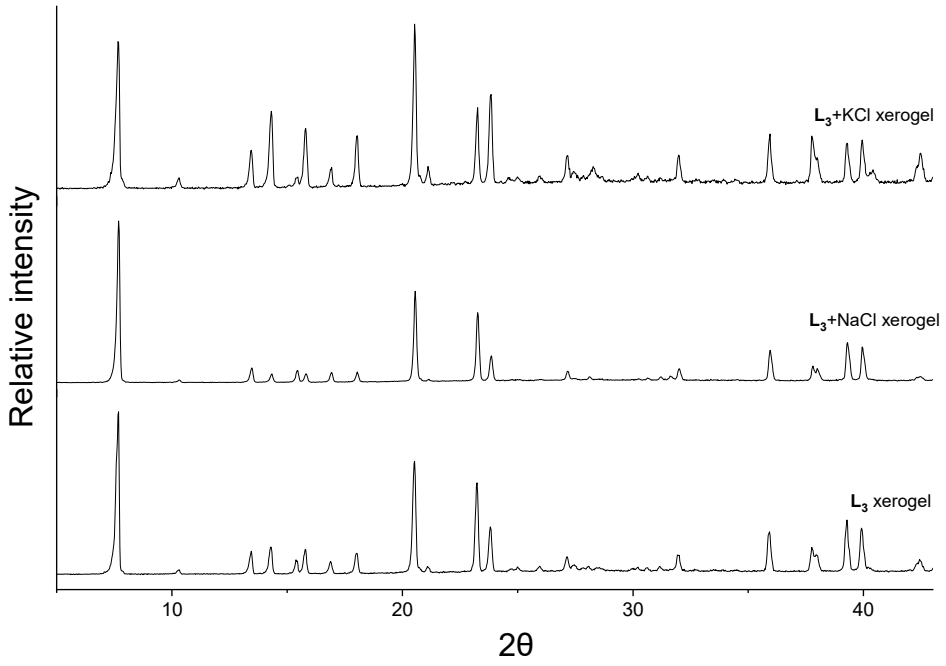

Figure S9. PXRD pattern of xerogels obtained from the hydrogel of $\mathbf{L_3}$ at 2.0 wt% and in the presence of 1.0 equivalence of NaCl and KCl.

Table S5: Stimuli-responsive properties of the gelators $\mathbf{L_1}$ and $\mathbf{L_3}$: Cation sensing in water at 1.5 wt%

Salts (1.0 equiv.)	**L_1**	**L_3**
CsCl	G	G
$MgCl_2$	G	G
$CaCl_2$	G	G
$SrCl_2$	G	G
$BaCl_2$	G	G
$AlCl_3$	S	PG
NH_4Cl	PG	G
$CuCl_2$	Ppt	PG
$ZnCl_2$	Ppt	G
$CdCl_2$	Ppt	G

Table S6: Increase in G' values of the gelators at 1.5 wt% in the presence of chloride salts of various cations in comparison with the hydrogels (1.8 wt%)

Salt added	**Equivalence**	**L_1**	**L_3**
CsCl	1.0	1.1-fold	3.8-fold
$MgCl_2$	1.0	1.9-fold	4.8-fold
$CaCl_2$	1.0	1.7-fold	5.0-fold
$SrCl_2$	1.0	1.8-fold	2.3-fold
$BaCl_2$	1.0	1.5-fold	1.8-fold
NH_4Cl	1.0	---	1.6-fold
$CuCl_2$	1.0	---	-----
$ZnCl_2$	1.0	---	2.8-fold
$CdCl_2$	1.0	---	24.7-fold

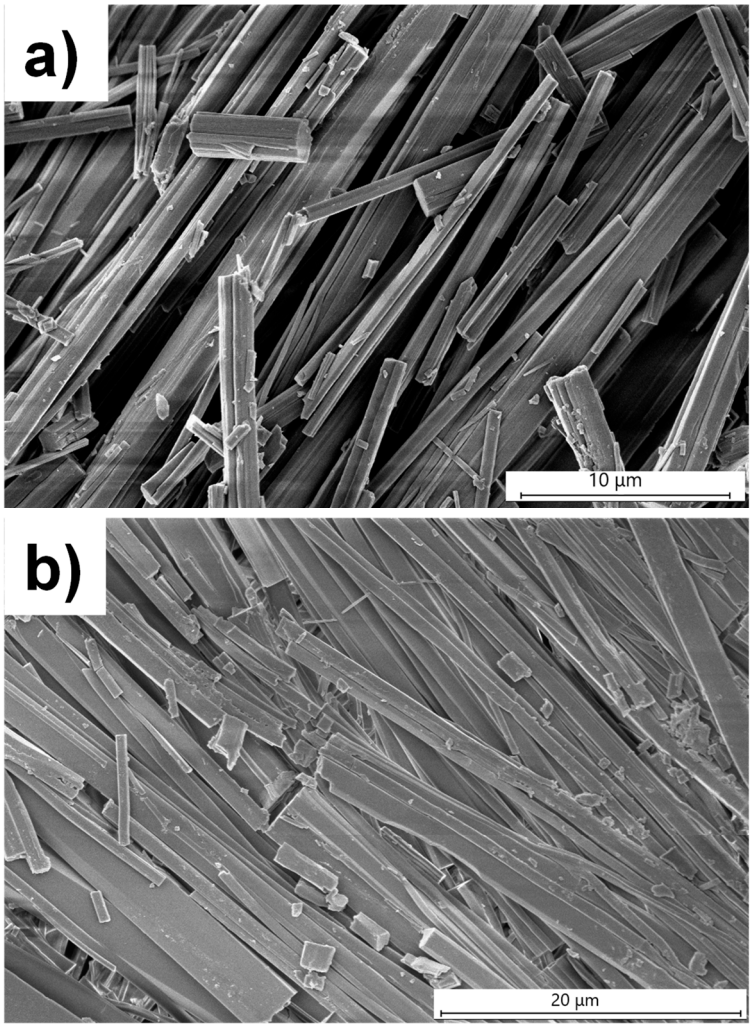

Figure S10. SEM images of xerogels of (a) $\mathbf{L_1}$ and (b) $\mathbf{L_3}$ at 2.0 wt% obtained from water in the presence of 1.0 equivalence of $MgCl_2$.

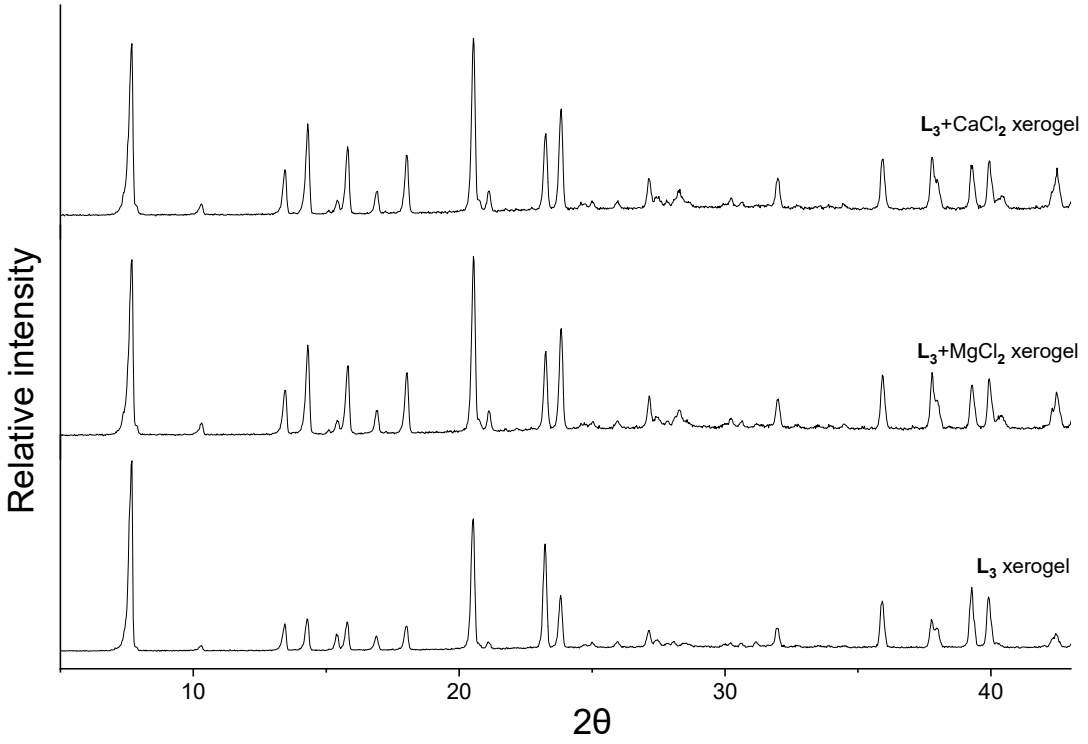

Figure S11. Comparison of the PXRD pattern of xerogels (2.0 wt%) of **L_3** hydrogels, and the gels in the presence of 1.0 equivalence of $MgCl_2$ and $CaCl_2$.

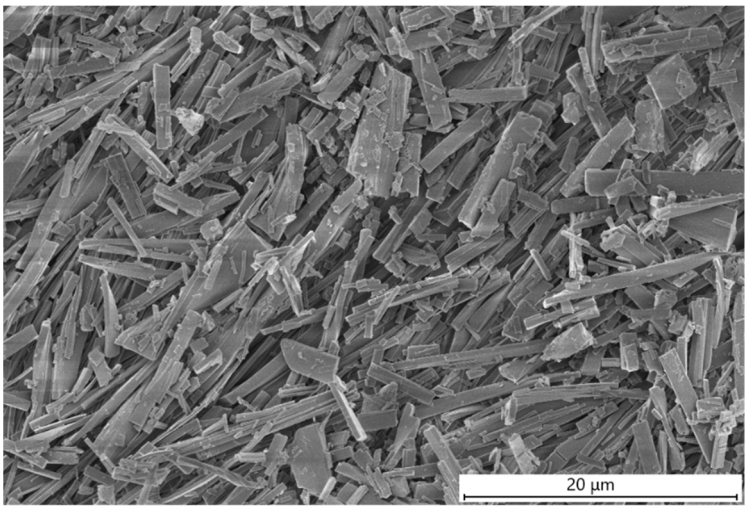

Figure S12. SEM images of the xerogels of **L_3** in the presence of 1.0 equivalence of $CdCl_2$ in water at 2.0 wt%.

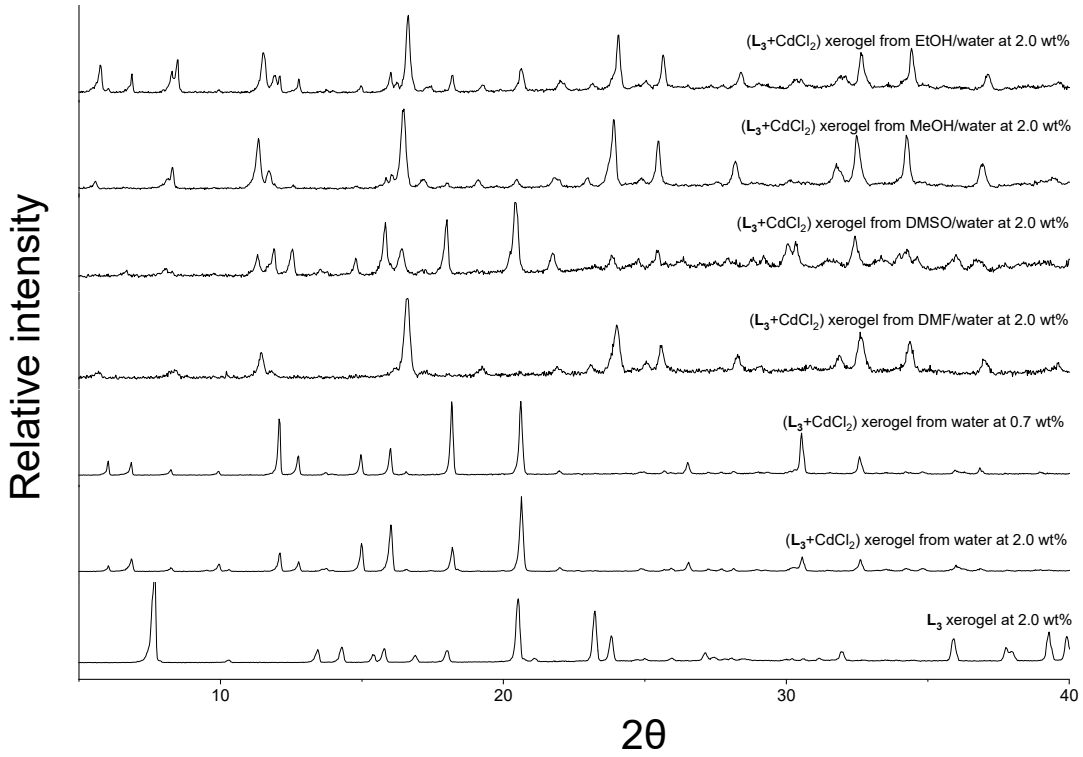

Figure S13. Comparison of the PXRD pattern of **L_3** xerogel with the PXRD pattern of the xerogels of **L_3**-$CdCl_2$ mixture in various solvents.

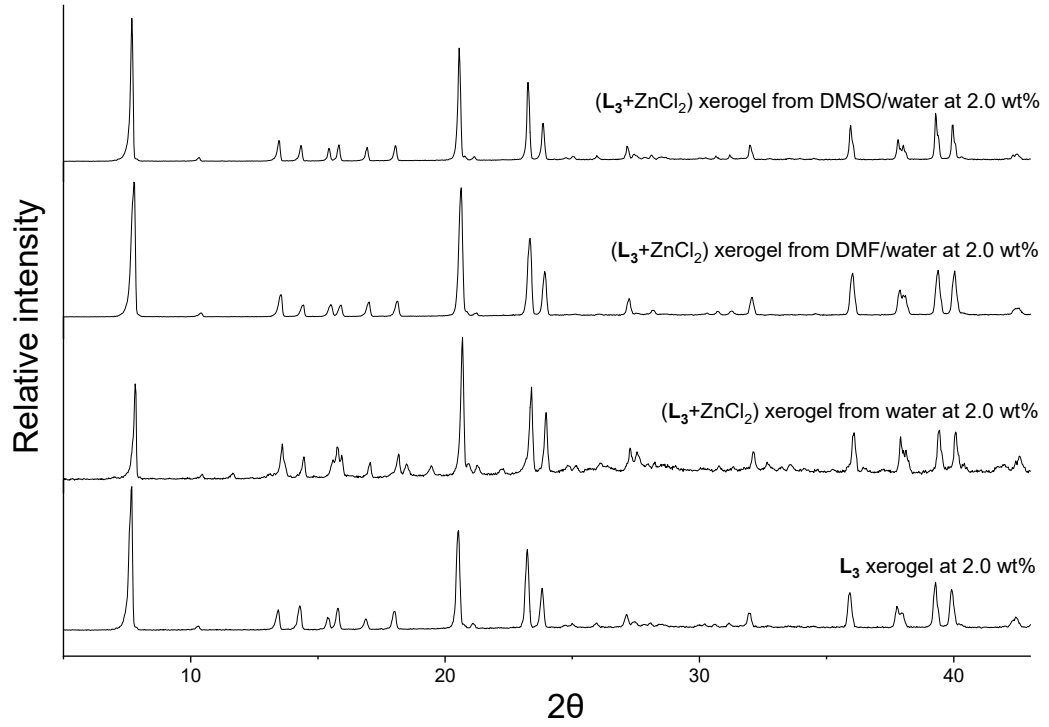

Figure S14. Comparison of the PXRD pattern of **L_3** xerogel from water with the PXRD pattern of the xerogels of the mixture (**L_3** + $ZnCl_2$) in various solvents.

6. NMR spectra

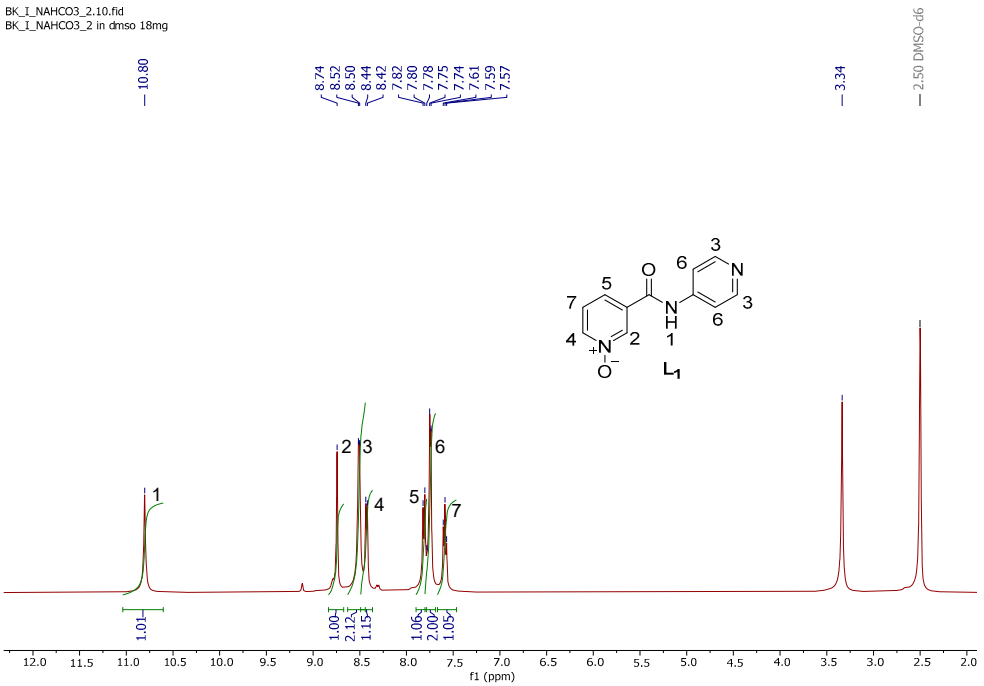

Figure S15. ^{1}H NMR spectrum of compound **L_1**.

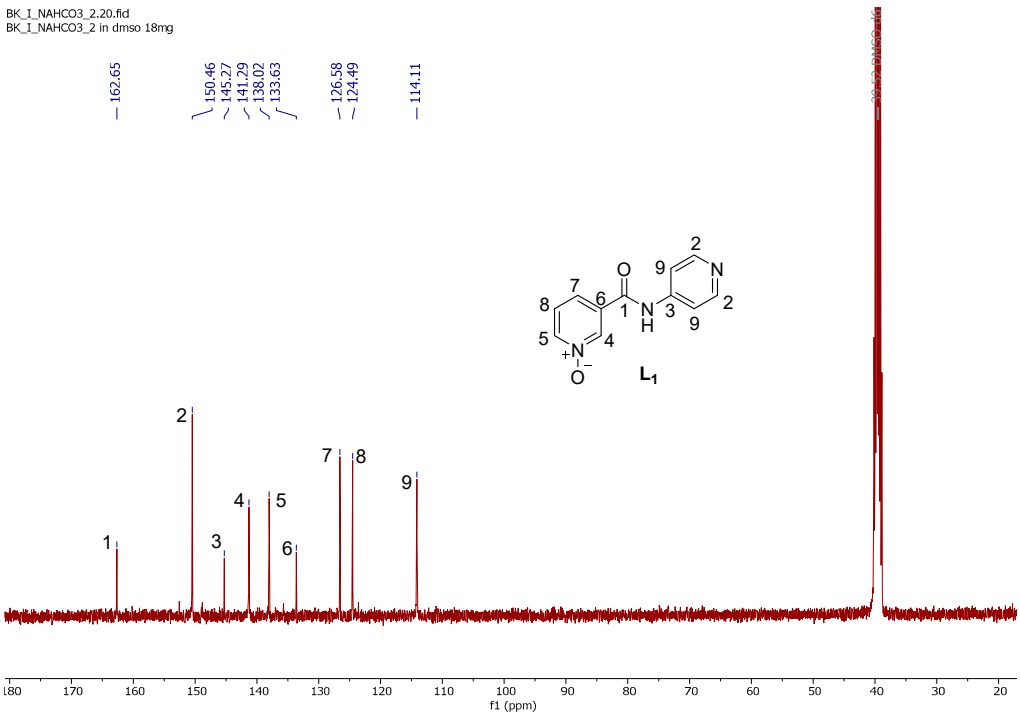

Figure S16. ^{13}C NMR spectrum of compound **L_1**.

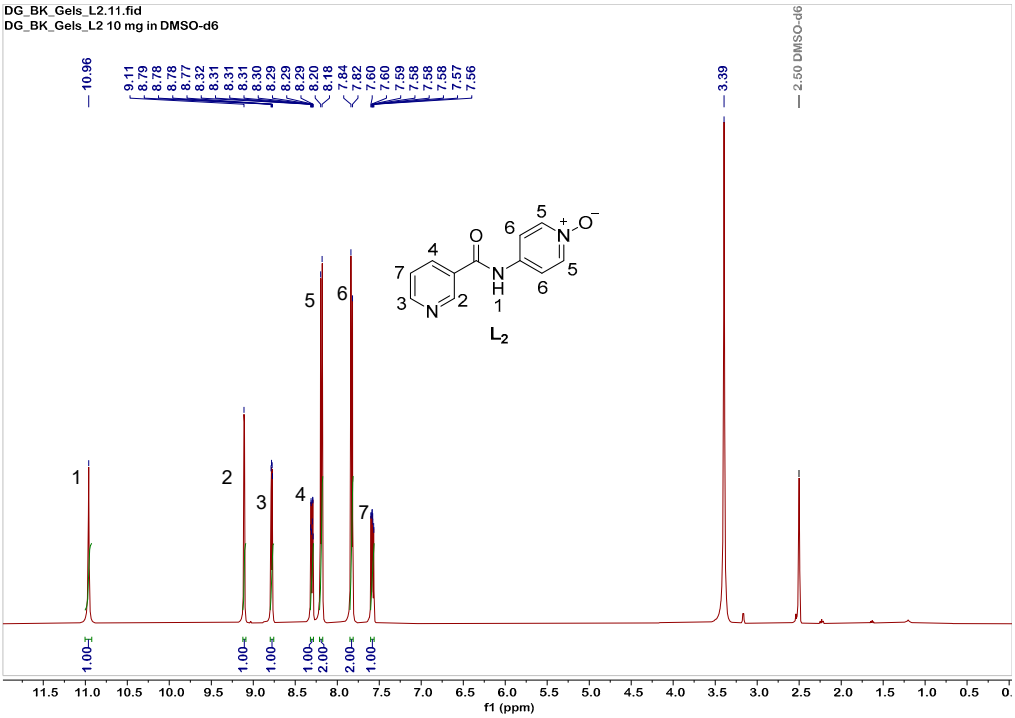

Figure S17. ^{1}H NMR spectrum of compound **L_2**.

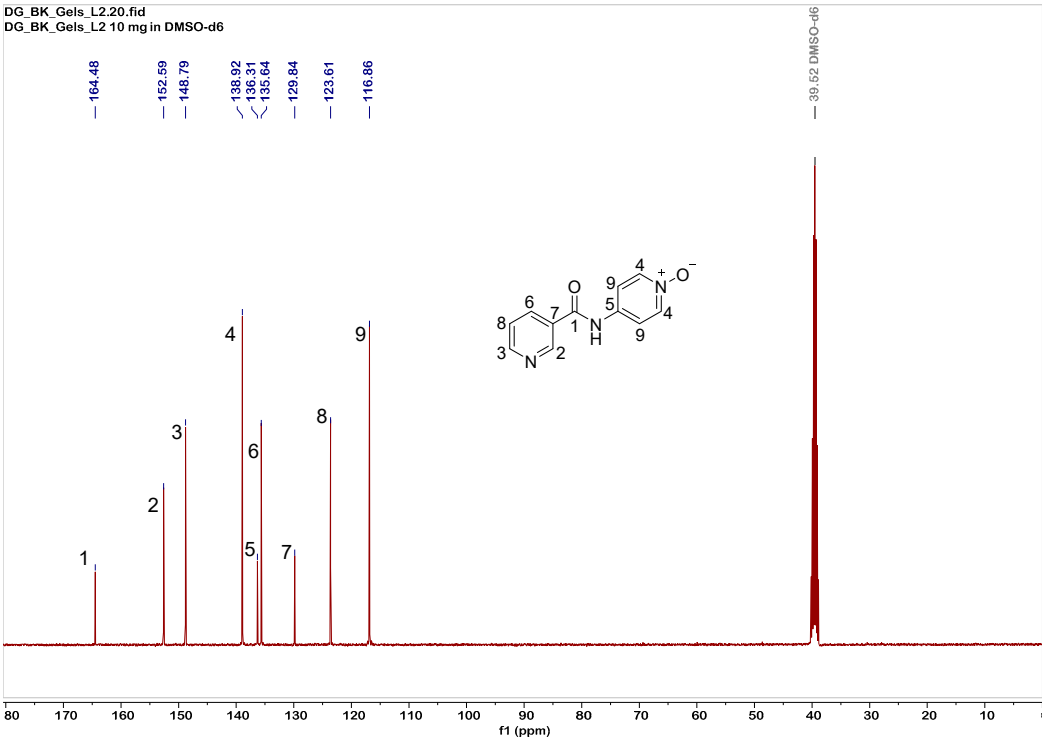

Figure S18. ^{13}C NMR spectrum of compound **L_2**.

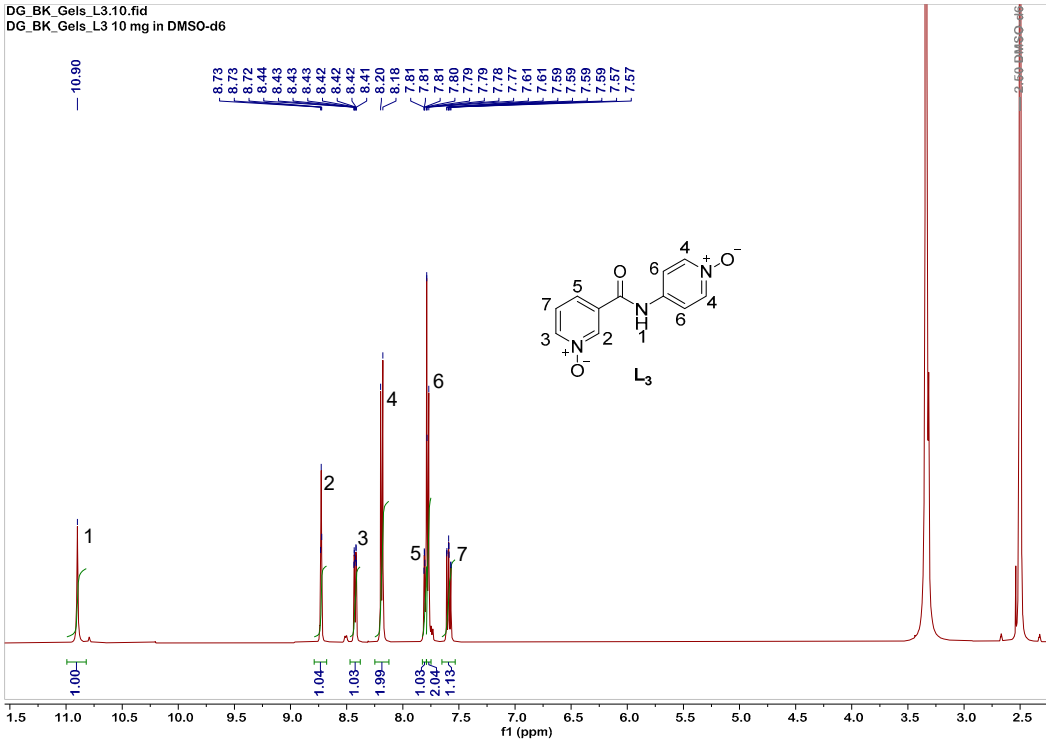

Figure S19. ^{1}H NMR spectrum of compound **L_3**.

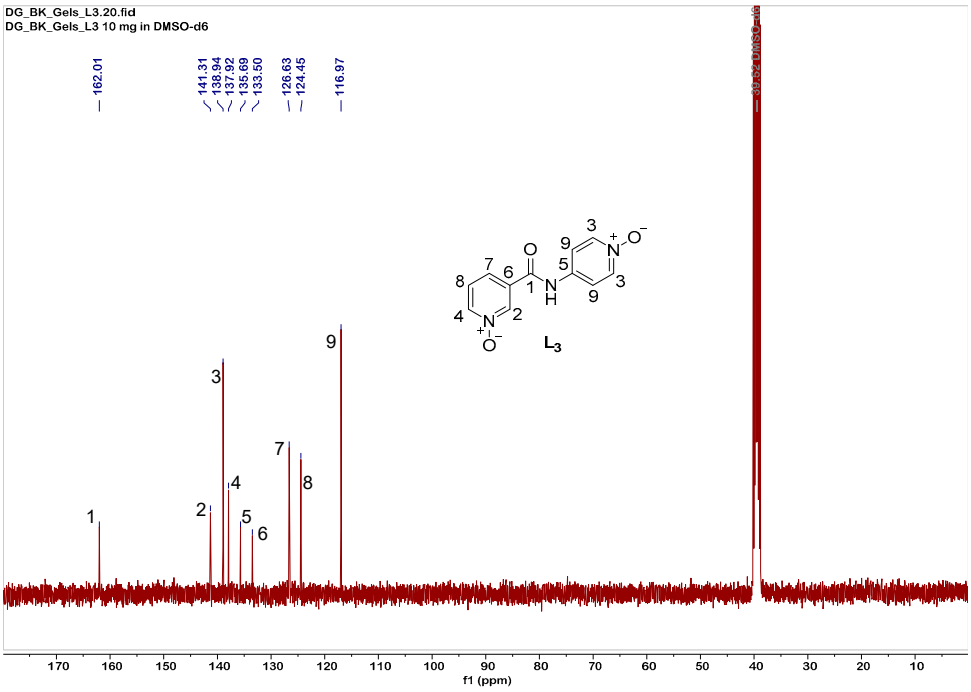

Figure S20. ^{13}C NMR spectrum of compound **L_3**.

Article-III

This manuscript is in its final form and prepared for submission to a peer-reviewed journal, and is presented as in the current version.

Publication details:

"**Selective gelation of bis(pyridyl)thiourea by copper (II) salts"**

Sreejith. S. Jayabhavan, and Krishna K. Damodaran*

Author contributions:

S.S.J. and K.K.D. planned and designed the research; **S.S.J.** synthesized the gelators, performed characterizations, solved single crystal structures and evaluated gelation properties. **S.S.J.** and K.K.D. wrote the initial manuscript draft and all authors reviewed the main manuscript.

Selective Gelation of Bis(Pyridyl)Thiourea by Copper(II) Salts

Sreejith Sudhakaran Jayabhavan, and Krishna K. Damodaran*

Department of Chemistry, Science Institute, University of Iceland, Dunhagi 3, 107 Reykjavík, Iceland.

Correspondence: krishna@hi.is; Tel: +354-525-4846; Fax: +354-552-8911

Abstract: The role of specific hydrogen bonding functionalities in the self-assembly process of bis(pyridyl)urea compounds was studied by altering the hydrogen bonding moieties. We have chosen *N,N'*–bis(2/3-pyridyl)urea (2-BPU and 3–BPU), that are non-gelators presumably due to the absence of complementary urea α-tape hydrogen bonding and the nitrogen atom and the carbonyl groups of the urea moiety displayed intramolecular interaction with the pyridyl nitrogen atom and C-H moieties. We replaced the urea with a thiourea group to alter these interactions, which resulted in *N,N'*–bis(2/3–pyridyl)thiourea (2-PTU and 3-PTU). The modification of the hydrogen bonding functionality did not yield a gel, which prompted us to check whether metal salts could induce the gelation. Metallogelation experiments revealed a selective gelation of 2-PTU and 3-PTU with various copper salts (1:2 metal-to-ligand ratio) in DMF/water (1:1, v/v) but the metal complexes of 2-BPU and 3–BPU did not form a gel. Interestingly, we observed a color change from yellow to green with 2-PTU+$Cu(OAc)_2$ metallogel over time. The mechanical strength of these metallogels was studied using rheology, and the fibrous morphology of the dried gels was examined using scanning electron microscopy (SEM). We have analyzed the role of coordination-driven self-assembly in these metallogels using various techniques such as UV-visible spectroscopy and X-ray diffraction. The selective gelation of all the copper(II) salts compared to the other metal salts may be attributed to the effective interaction between the thiourea ligands and copper(II) salts, which resulted in the formation of a prominent gel network via coordination-driven self-assembly.

Keywords: Low molecular weight gelators (LMWGs), Metallogels, Thiourea, X-ray diffraction.

1.0 Introduction

Supramolecular gels composed of low molecular weight gelators (LMWGs) possess remarkable potential applications, including cell culture, tissue engineering, drug

delivery, catalysis, and as a medium for controlled crystal growth.[1] LMWGs provide numerous benefits compared to traditional polymer gels, including ease of synthesis, tunable gel state properties, dynamicity, and adaptive responsiveness to external stimuli.[2-4] Analyzing the structural features in LMWGs will enhance the understanding of self-assembly during the gelation process.[1, 2, 5, 6] However, the formidable task involved in the understanding of self-assembly relies on studying the role of non-covalent interaction, which is highly dynamic in nature. The gel network in LMWGs relies on multiple non-covalent interactions, including hydrogen bonding, π-π stacking, ion-dipole interactions, and van der Waals forces.[2, 3, 6, 7, 8] Modifying the functional groups of the gelator/non-gelator is an effective approach to elucidate the significance of particular non-covalent interactions in the gelation process.[9] Our group has previously studied the functional group modification induced changes in the gel state properties. The oxidation of pyridyl functionality to their corresponding *N*-oxides resulted in the formation of hydrogels.[10]

We envisioned studying the role of hydrogen bond functionalities in the self-assembly process of bis(pyridyl)urea compounds by modifying the hydrogen bonding moieties of the gelators (urea to thiourea). Ureas and thioureas are well-known for their ability to form hydrogen bonds.[13] The use of these functionalities has shown growing application in various self-assembled network materials.[14] On the other hand, thiourea functionality is important because of its reactivity and its various applications in material science.[15] Thiourea-derived compounds demonstrate many biological properties such as antibacterial, anti-inflammatory, and anticancer properties.[16] Thiourea functions as a ligand in coordination chemistry, creating compounds with diverse metal ions and find an important role in catalysis.[17] Moreover, thiourea-based derivatives exhibit enhanced anion binding due to the higher acidity of thiocarbonyl groups compared to their urea counter functionality.[18] Thiourea functionalized gelators are very rarely reported, which

can be attributed to its poor hydrogen bonding ability. Weiss and coworkers reported a series of organogels consisting of thiourea derivative with various *n*-alkyl substituents at the nitrogen atoms.[19] They observed that the derivative with longer alkyl chain length gelled in various solvents with very high thermal strength compared to its shorter chain length analogues. Song and coworkers have outlined thiourea-based gels with anion-responsive behavior, for example, in the presence of certain anions such as fluoride, the gel exhibited visible bending and color changes.[20] The thiourea based compounds are well known for the metal binding properties leading to metal complexation induced gelation resulting in metal-based supramolecular gels or metallogels. Metallogels based on LMWGs exhibit robust coordination interactions between the organic component and the metal center, serving as a principal driving force in the establishment of the gel fiber network. Metal coordination is integral to the gelator shape, but interaction between the discrete complexes via non-covalent interactions also plays a major role that leads to the formation of 3-D fibrillar gel networks rather than metal−ligand bonding.[11] Thus gel fibers might originate from the self-assembly of distinct complexes, coordination polymers, or cross-linked coordination polymers.[12] Kwit's group has studied the metallogelation ability of thiourea derivative of trianglimine and reported the formation of stable chiral metallogels with silver (Ag(I)), copper (Cu(I)), and copper (Cu(II)) salts in *N,N*'-dimethylformamide (DMF) solvent.[21] Extensive studies have been conducted on the structures of *N,N*′-(substituted-2-pyridyl)thioureas and their intra−/intermolecular hydrogen bonding interactions.[22] Reports have been made on *N,N*′-bis(substituted-2-pyridyl) thioureas in conjunction with Cu(I) and Zn(II) ions.[23]

The incorporation of heterocyclic rings into thiourea molecules is anticipated to yield a broader spectrum of potential H-bonding interactions.[24] For example, introducing pyridyl groups can facilitate potential hydrogen bonding interactions as well as binding site for

during metal complexation. However, if the structures include a 2-pyridyl or similar ortho-substituted nitrogen heterocycle effective intermolecular hydrogen bonding is not observed, as the conventional urea tape is interrupted by the rotation on one side of the molecule around the bond connecting the urea nitrogen and the carbonyl group.[13] The resulting conformation is then stabilized by the formation of an intramolecular NH···N pyridyl hydrogen bond between the rotating pyridyl and the opposing N–H moiety. Pike and coworkers reported an oxidative cyclization with *N,N'*–bis(2–pyridyl)thiourea ligand upon reacting it with copper(I) salts over a week-long crystallization experiment.[25] The advantage of having pyridyl thiourea moiety is their binding ability to metal complexes leading to metal-containing LMWGs. Adams group reported that oxovanadium (IV) complexes formed with *N,N'*-bis(2-pyridyl)thiourea ligand had various catalytic, antimicrobial, and antioxidant properties.[26]

In this work, we have analyzed the role of the hydrogen bond functionalities by replacing the hydrogen bonding moieties of a non-gelator: namely *N,N'*–bis(2/3–pyridyl)urea (2-BPU or 3–BPU). The urea moiety was replaced with a thiourea group to alter the non-covalent interactions resulting in *N,N'*–bis(2/3–pyridyl)thiourea (2-PTU or 3-PTU). The presence of both the thiourea and pyridyl groups tags for the multi-functional nature of these ligands. This opens the door to analyze the coordination-driven self-assembly with 3-PTU and 2-PTU, due to the presence of both thiourea and pyridyl based coordination moieties in the ligand. To the best of our knowledge metallogels formed via coordination-driven self-assembly in pyridyl thiourea derivatives are not reported.

2.0 Experimental Section

2.1 Materials and Methods

The starting materials and solvents were purchased from Sigma-Aldrich (MEDOR ehf, Reykjavik, Iceland), TCI-Europe (Boereveldseweg, Belgium), and Fluorochem (Glossop, UK), and were used as supplied. Deionized water was used for all the experiments. Characterization of the molecules was carried out using ^{1}H NMR spectroscopy, which were recorded on a Bruker Avance 400 spectrometer (Rheinstetten, Germany), and the SEM images (Carl Zeiss, Oberkochen, Germany) were captured on a Leo Supra 25 microscope. The rheological studies were conducted using an Anton Paar modular compact rheometer MCR 302 (Graz, Austria). X-ray diffraction studies were performed on Bruker D8 (Karlsruhe, Germany) and PANalytical (Almelo, Netherlands) (XRD) instruments for single-crystal (SCXRD) and powder (PXRD) diffraction experiments, respectively.

2.2 Synthesis

The synthesis and characterization of 2-PTU[26] and 3-PTU[13] have been reported previously, and the analytical and spectroscopic data matched those reported in the literature.

2.3. Gelation Studies

Approximately 10.0 mg of the chemical compounds and 1.0 mL of the respective solvent were added into a standard 7.0 mL vial with an inner diameter of 15.0 mm. The vial was capped, and the mixture was subsequently sonicated and gradually heated to achieve a clear solution. The solution was allowed to remain undisturbed for gelation, and a vial-inversion test was conducted to verify gelation. The studies were conducted again at

higher quantities, ranging up to 50.0 mg of the compound, to evaluate the gelation property.

2.4 Metallogelation

The solution was prepared by dissolving the appropriate amount of ligand (0.1-0.3 mmol) in 0.5 mL of DMF and combining it with 0.5 mL of a transition metal salt in water (0.05-0.15 mmol), maintaining a 1:2 metal to ligand ratio. The nature of the mixture was initially noticed and allowed to stand undisturbed for approximately 24.0 hours to verify gelation.

2.3 Rheology

The gel's mechanical strength was assessed utilizing an MCR 302 Anton Paar modular compact rheometer, consisting of a 2.5 cm stainless steel parallel plate geometry with a measurement gap of 1.00 mm. The experiments were performed by applying roughly 1.0 mL of gel onto the plate. A Peltier temperature control hood was utilized to avoid solvent evaporation and maintain a stable temperature of 20.0 °C during frequency and amplitude sweeps. Amplitude sweeps were performed at a constant frequency of 1.0 Hz and a logarithmic ramp strain (γ) varying from 0.01% to 100%. Frequency sweeps were conducted between 0.1 and 10.0 Hz within the linear viscoelasticity range at a strain of 0.05%. Metallogels were prepared with 2-PTU/3-PTU with metal salts in DMF/water (1:1, v/v) at 1:2 metal/ligand ratio, 4.6 wt/v% of ligand with $Cu(NO_3)_2$, $Cu(OAc)_2$, $Cu(OBz)_2$ and 6.9 wt/v% of ligand with $CuSO_4$, $CuCl_2$, and $Cu(ClO_4)_2$.

2.4 Scanning Electron Microscopy (SEM)

A similar procedure as mentioned above with rheology was employed to obtain gels for SEM studies. The gels were filtered and air-dried to obtain the xerogels. A small amount of the xerogel was positioned on a pin mount, with the carbon tab placed above it. The

mount underwent a gold coating process lasting 5-6 minutes, resulting in a thickness of approximately 9.0-12.0 nm of gold layer, which prevents charging of the surface upon exposure to X-rays. Following this, the specimen was placed onto a Leo Supra 25 microscope, which was set to operate at a voltage of 3.0 kilovolts and a working distance ranging from 3.0 to 4.0 millimeters. The SEM images were captured utilizing an in-lens detector.

2.5 X-ray crystallography

Single-crystal X-ray Diffraction (SCXRD): Single crystals of 2-PTU+$Cu(OBz)_2$ were obtained by dissolving 7.6 mg of copper(II) benzoate in DMF (2.0 mL) and layered with 11.5 mg of 2-PTU dissolved in 2.0 mL of ethanol. Green-colored crystals were formed over a period of 5- 7 days. To obtain the single crystals of $CdCl_2$+2-PTU, the ligand 2-PTU (11.5 mg) and cadmium chloride (4.6 mg) were dissolved in 4 mL DMF via slow heating and allowed for slow evaporation, and the colorless single crystals were obtained in 4 -6 days. Single crystal X-ray analysis was performed on a Bruker D8 Venture (Photon100 CMOS detector) diffractometer with Cryostream (Oxford Cryosystems) open-flow nitrogen cryostats. The unit cell dimensions were measured, and the data collection was performed at 305(2) K Cu(OBz)-2-PTU and 298(2) K for $CdCl_2$-2-PTU using MoKα radiation (λ = 0.71073 Å). The unit cell determination, data collection, data reduction, structure solution, refinement, and empirical absorption correction were performed in apex-III software (Bruker AXS: Madison, WI, 2015). All structures were solved using the direct method and refined using the full-matrix least-squares on F2 for all data using SHELXTL. All non-disordered non-hydrogen atoms were refined anisotropically. All the hydrogen atoms were placed in calculated positions and a riding model was utilized to refine the hydrogen atoms. The crystal structures were plotted using the program Mercury. Crystallographic data for the complexes are deposited to

Cambridge Crystallographic Data Centre as supplementary publication (CCDC no: 2414627-2414628).

2.6 UV-visible spectroscopy

Agilent Cary UV-vis Multicell Peltier spectrometer was utilized to study UV-visible absorption studies. The data was collected at a bandwidth of 2.0 nm. A 3.0 mL cuvette with a path length of 1.0 cm was employed for the experiments. The complex 2-PTU+$Cu(OBz)_2$ was prepared at a concentration of 4.17 x 10^{-5} M of ligand in DMF/water (1:1, v/v) and at a 1:2 metal-to-ligand ratio.

3.0 Results and Discussion

3.1 Design and Synthesis

We have synthesized 1,3-di(pyridin-3-yl)thiourea (3-PTU) and 1,3-di(pyridin-2-yl)thiourea (2-PTU) and matched the analytical data with the reported data (Figure 1). The 2-PTU was synthesized by refluxing the 2-amino pyridine and carbon disulphide with triethylamine as a base.[27] While 3-PTU was synthesized using a different protocol, the 3-amino pyridine and carbon disulphide were refluxed in pyridine (Scheme S1 and S2).[13] The ligands 3-BPU and 2-BPU were synthesized by following protocols reported by our group.[28]

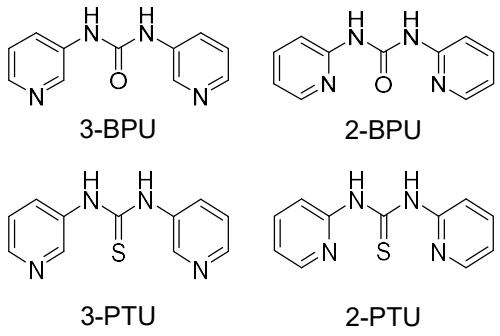

Figure 1. Chemical structures of the urea and thiourea compounds.

3.2 Gelation Experiments

Initially, we performed a typical gelation test with all the urea and thiourea ligands in various solvents/solvent mixtures. Gelation experiments with 2-PTU and 3-PTU revealed that they are non-gelators (Table S1). Both the 2-PTU and 3-PTU were insoluble in xylenes, mesitylene, and THF. 3-PTU dissolved in water at 1.0 wt%; however, higher concentrations did not dissolve in water. Ligands crystallized in 1:1, v/v aqueous mixtures of methanol and DMSO. The non-gelling property of 2-BPU and 3-BPU was confirmed by testing the gelation in various solvents/solvent mixtures.

The non-gelling behavior of these compounds prompted us to analyze the coordination-induced self-assembly. For this purpose, we used various transition metal salts, and reacted with ligands, at 1:2 metal-to-ligand ratio, in DMF/water (1:1, v/v). The metallogelation studies with 2-BPU and 3-BPU resulted in precipitate in most of the cases, and no gels were obtained (Table S3 and S4).

Metal complexation experiments with 2-PTU revealed selective gel formation with copper(II) salts (Table 1). Similarly, metal complexation experiments with 3-PTU also showed selective gel formation with copper(II) salts, resulting in green gels in all cases (Table S2). Copper(II) chlorate, copper(II) acetate and copper(II) nitrate formed gels with 3-PTU at a lower concentration of the ligand (2.3 wt/v%), while copper(II) chloride, copper(II) bromide and copper(II) sulfate required 6.9 wt/v% of the ligand to form the metallogel. The copper(II) benzoate ($Cu(OBz)_2$) did not form a gel with 3-PTU, in fact, due to poor solubility, we dissolved both the ligand and copper(II) benzoate in DMF (0.5 mL), and 0.5 mL water was added.

Table 1. Metallogelation experiments with 2-PTU at 1:2 metal to ligand ratio and 0.05-0.15 mmol of metal salts in 1.0 mL of DMF/water (1:1, v/v).

Metal salts	Ligand wt/v%	Initial Observation	Final Observation
$Cu(NO_3)_2.3H_2O$	2.3-4.6	Green solution	Gel
$CuSO_4.5H_2O$	2.3-4.6	Red solution	Gel
$Cu(OAc)_2.2H_2O$	2.3-4.6	Yellow solution	Gel
$CuCl_2$	2.3-4.6	Green solution	Gel
$CuBr_2$	2.3-4.6	Green solution	Gel
$Cu(ClO_4)_2.6H_2O$	6.9	Green solution	Gel
$Cu(OBz)_2$	2.3	Yellow solution	Gel
$ZnCl_2$	6.9	solution	Precipitate
$ZnNO_3.6H_2O$	6.9	solution	Precipitate
$Cd(NO_3)_2.4H_2O$	6.9	solution	Precipitate
$CdCl_2$	6.9	solution	Precipitate
$CoCl_2.6H_2O$	6.9	Pink solution	Precipitate
$NiCl_2.6H_2O$	6.9	Green Solution	Precipitate
$FeCl_3$	6.9	Yellow solution	Precipitate
$MnCl_2.4H_2O$	6.9	solution	Precipitate
$CrCl_3$	6.9	Green solution	Precipitate

The gelation experiments with other transition metal salts resulted in precipitation, and experiments were also performed at a higher concentration of the ligand (6.9 wt/v%, 0.3 mmol) (Table 1). The copper(II) chlorate-2-PTU gelled at a higher concentration (6.9 wt/v%) than the other copper(II) salts. Interestingly, the 2-PTU gelled with copper(II) acetate and copper(II) benzoate with a color change. The gel changed its color from yellow to green over a certain period of time, which can be attributed to the structural changes. The same gels also exhibited thixotropic behavior, with self-healing properties.

3.3 Rheology

The analysis of gel strength was performed using rheological studies. Rheology is an excellent tool for comparing the mechanical strength and even studying self-healing properties of semi-solid materials.[29] The amplitude experiments were first performed with the 2-PTU-based metallogels, the copper(II) chlorate-2-PTU-based gel showed a linear viscoelastic region around 0.05% of strain, while all the other copper-2-PTU based gels revealed a LVR region about 0.5% of strain, and a cross over point around 3.0-10.0% of strain (Figure S1). The amplitude sweep experiments with 3-PTU based gels revealed an LVR of about 0.5% of strain and cross-over point around 5.0-15.0% of shear strain (Figure S2). Frequency sweep experiments with all the gels at a constant strain of 0.05% showed that the 2-PTU based copper(II) metallogels showed better mechanical strength compared to the copper-3-PTU based metallogels (Figure 2 and S3).

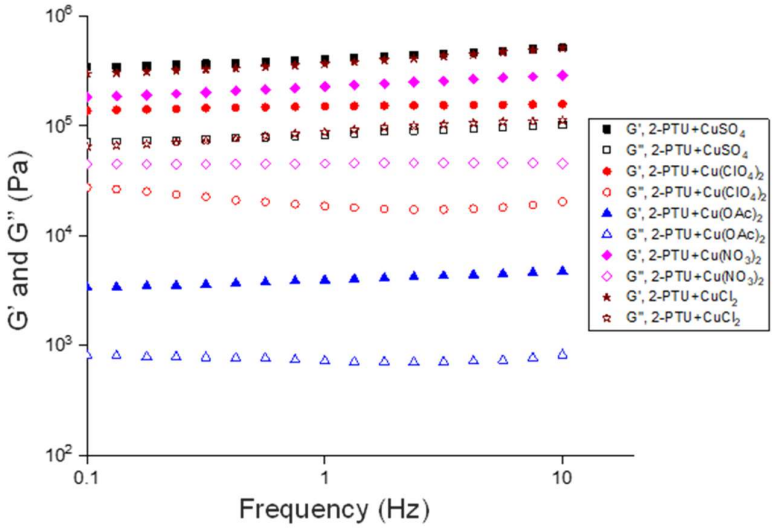

Figure 2. Frequency sweep experiments with 2-PTU with metal salts in DMF/water (1:1, v/v) at 1:2 metal/ligand ratio, 4.6 wt/v% of ligand with $Cu(NO_3)_2$, $Cu(OAc)_2$ and 6.9 wt/v% of ligand with $CuSO_4$, $CuCl_2$, and $Cu(ClO_4)_2$, at 20.0 °C measured at a constant strain of 0.05%.

The copper(II) chloride and copper(II) sulfate based 2-PTU gels showed the maximum mechanical strength, while the copper(II) nitrate based-3-PTU gel showed the minimum mechanical strength. We performed the amplitude sweeps experiments with the gels obtained from 2-PTU+$Cu(OBz)_2$ at 2.3 wt/v% and observed the LVR region at about 1.0% of strain (Figure S4). Frequency sweep within the LVR region at 0.05% showed that the gel-to-gel transition was accompanied by a slight increase in mechanical strength (Figure S5). This indicated that the green gel exhibited better mechanical strength than the yellow gel. Finally, we have analyzed the self-healing property of the 2-PTU+$Cu(OBz)_2$ gel at 4.6 wt/v% of the ligand (Figure S6). We have recorded the frequency sweep experiments to check the thixotropic nature of these gels by lifting the piston after the measurement, positioning it back to the sample every 3 minutes, and repeating the experiments. The results showed that mechanical strength was not affected, rather a slight increment in mechanical strength was observed after each trial, which revealed the self-healing nature of the metallogel.

3.4 Gel Morphology

Scanning electron microscopy (SEM) is an important tool for analyzing the surface morphology of dried gels.[8, 30] The metallogels were filtered and dried by keeping them in the hood overnight. SEM images of 2-PTU based metallogels based on copper(II) chloride, copper(II) bromide, copper(II) nitrate, copper(II) chlorate and copper(II) benzoate, showed highly dense and thin fibers with fiber width dimensions 0.1-1.0 μm (Figure 3 and S7a), while the 2-PTU metallogel based on copper(II) sulfate revealed flake-shaped morphology (Figure S7b).

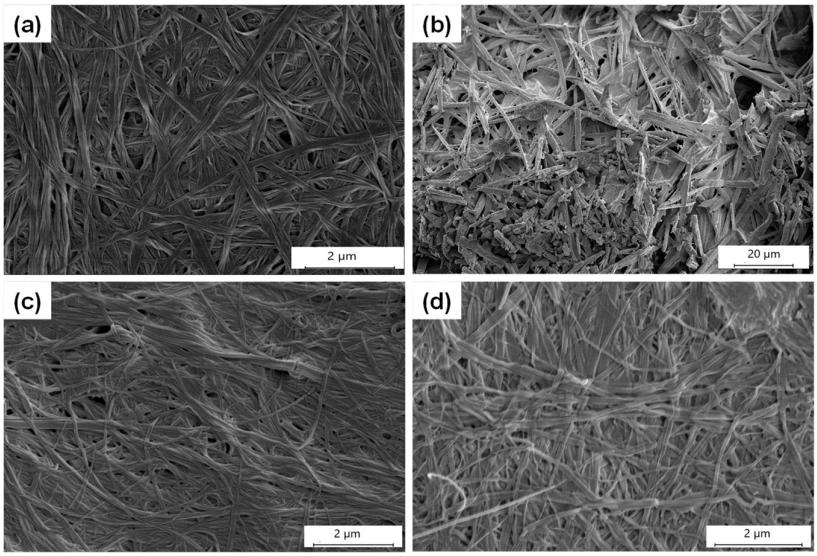

Figure 3. SEM images of the xerogels obtained from 2-PTU with metal salts in DMF/water (1:1, v/v) at 1:2 metal/ligand ratio, with ligand 6.9 wt/v% and (a) $CuCl_2$, (b) $CuBr_2$, and ligand 4.6 wt/v% with (c) $Cu(NO_3)_2$, and (d) $Cu(OBz)_2$.

SEM images of 3-PTU-based metallogels based on copper(II) chloride, copper(II) bromide, copper(II) nitrate, copper(II) sulfate and copper(II) chlorate showed flake-shaped or plate-shaped morphology (Figure S8-S9), while the copper(II) acetate-based 3-PTU metallogel showed rod-shaped fibers with width ranging 0.1-0.5 µm (Figure S8d).

3.5 Single-crystal X-ray diffraction (SCXRD)

Single-crystal X-ray diffraction (SCXRD) is an excellent tool to analyze the key interactions in the solid-state structure of the ligand or complexes and correlate these interactions with the bulk material or dried gel state, which will help to identify the role of these interactions in the self-assembly modes. The introduction of heterocyclic rings like pyridyl functionality into thiourea compounds is expected to produce a wider range of possible hydrogen bonding interactions. Furthermore, they can function as ligands in coordination complexes for building various self-assembled network materials. Selective gelation of 3-PTU and 2-PTU with various copper(II) salts was studied by analyzing the

solid-state interactions in these complexes. We have tried various crystallization methods for the metalation of 2-PTU and 3-PTU with various transition metal salts. The ligand 3-PTU did not yield any crystals with any transition metal salts; however, to our success, we obtained crystals with cadmium chloride and copper(II) benzoate with 2-PTU at a 1:2 metal to ligand ratio (Table S5&S6). Analyzing both the structures revealed that the ligand underwent reconstruction via oxidative cyclization (Figure 4).

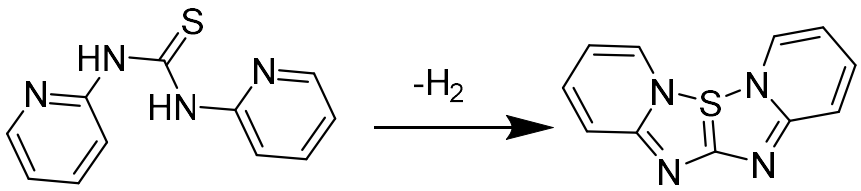

Figure 4. Oxidative cyclization of 2-PTU ligand.

The 2-PTU and copper(II) benzoate complex crystallized in *P*-1 space group. The single crystals were obtained by slow evaporation of DMF-ethanol mixture of copper(II) benzoate and 2-PTU to give a 1 : 2 complex of formula $[Cu(2\text{-}PTU)_2(OBz)_2(H_2O)_2]$. The copper(II) metal center was located on an inversion center with a distorted octahedral geometry. The axial positions were occupied by one of the nitrogen atoms of the thiourea functionality and the equatorial positions were occupied by carboxylate oxygen atoms of benzoate moieties and two water molecules. Analysis of the hydrogen bonding interaction revealed an intramolecular hydrogen bonding via coordinated water molecule and the non-coordinated nitrogen atom of the thiourea functionality (Figure 5a). The presence of intramolecular hydrogen bonding within the complex could be attributed to the gelation ability of the metallogel. The powder X-ray diffraction pattern of the 2-PTU+$Cu(OBz)_2$ gel showed an amorphous nature in gel and dried gel states, making it hard to confirm the nature of interactions in the gel or dried gel state. On the other hand, the single crystals of cadmium(II) chloride and 2-PTU were obtained from the slow evaporation of 1:2 metal to ligand ratio in DMF solvent resulting in a binuclear one-dimensional coordination

polymer of the formula $[Cd(2\text{-}PTU)(Cl)_4]_n$ (Figure 5b). The complex crystallized in a monoclinic space group $P2_1/c$, with the cadmium metal center displaying a distorted square pyramidal geometry.

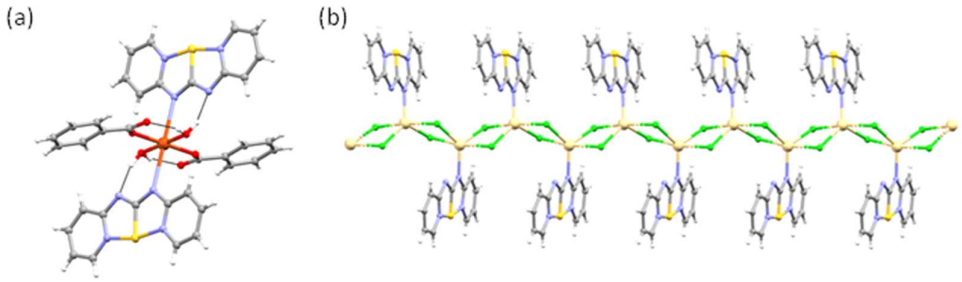

Figure 5. (a) Intramolecular hydrogen bonding (black dotted lines) in $[Cu(2\text{-}PTU)_2(OBz)_2(H_2O)_2]$, (b) 1-D coordination polymer of $[Cd(2\text{-}PTU)(Cl)_4]_n$.

3.6 UV-visible spectroscopy

The transformation of yellow gel to green gel in 2-PTU+$Cu(OBz)_2$ over a period of time prompted us to evaluate the structural changes in the gel structure using UV-Visible spectroscopy. We prepared a solution of 2-PTU+$Cu(OBz)_2$ at a concentration 4.17 x 10^{-5} M of ligand, and 1:2, metal-to-ligand ratio in 1:1 (v/v) DMF/water (Figure 6).

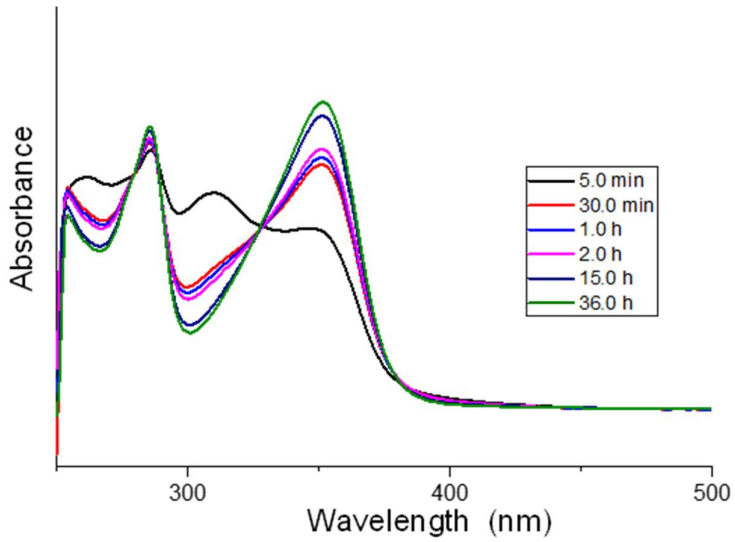

Figure 6. UV studies with the complex 2-PTU+$Cu(OBz)_2$ at a conc. 4.17 x 10^{-5} M of ligand in DMF/water (1:1, v/v) at various time intervals.

At the beginning up on mixing metal and ligand, a yellow solution was observed, which changed color to green over 12.0 hours (Figure S10). A similar observation was also obtained in the gel state (Figure S11). UV studies showed that the yellow solution showed absorption peaks at 275 nm, 310 nm, and 350 nm in 5.0 minutes. UV-Vis absorption was analyzed at different time intervals such as 30 min, 1.0 h, 2.0 h, 15.0 h, and 36.0 h. Around 2.0 h the absorption peak at 310 nm almost vanished, and the intensity of the peak at 350 nm was enhanced. This can be attributed to the structural changes in the ligands (oxidative cyclization) as confirmed using single crystal X-ray diffraction. Similar results in UV-Vis absorption were obtained at a prolonged period of upto 36.0 h, which shows the stability of the cyclized form. The color change in the 2-PTU+$Cu(OBz)_2$ gel may be due to this oxidative cyclization of the ligand associated with the coordination-driven self-assembly with copper benzoate salts.

4.0 Conclusions

We have synthesized *N,N'*–bis(2/3-pyridyl)urea (2-BPU and 3–BPU) and *N,N'*–bis(2/3-pyridyl)thiourea (2-PTU and 3–PTU) and studied the gelation properties in various solvents, which revealed that both are non-gelators. This envisaged us to test metal-induced gelation with these molecules due to the multifunctionality of these ligands. The ligands 2-BPU and 3-BPU did not yield any metallogels, which can be attributed to the poor coordination ability of the urea functionality. On the other hand, metallogelation studies with thiourea ligands revealed selective gelation of 3-PTU/2-PTU with copper(II) salts. The selective gelation of copper(II) salts, in contrast to other metal salts, can be ascribed to the efficient interaction between thiourea ligands and copper(II) salts, leading to the establishment of a significant gel network by coordination-driven self-assembly. The mechanical strength of these metallogels was studied using rheology, which revealed the 2-PTU-based metallogel showed better mechanical strength than the 3-PTU-based

metallogels. The fibrous morphology of the dried gels was examined using scanning electron microscopy (SEM), which revealed dense thin fibers with 2-PTU-based metallogels, while flake or plate-shaped morphology was observed with 3-PTU-based metallogels in most cases. These results revealed that the modification of hydrogen bonding moieties of the molecules could induce coordination-driven self-assembly.

Acknowledgments

We thank University of Iceland Research Fund and Science Institute for funding. S.S.J. thanks the University of Iceland for the Doctoral research grant. We also acknowledge Dr. Sigríður Jónsdóttir and Dr. Fridrick Magnus, University of Iceland for NMR/Mass spectroscopy and powder X-ray diffraction analysis, respectively. We thank Rannís Iceland for infrastructure grants (150998–0031 & 191763–0031) for a single crystal X-ray diffractometer and Rheometer.

Disclosure statement

The authors report there are no competing interests to declare.

Author Contributions

S.S.J. and K.K.D. planned and designed the research; S.S.J. synthesized the gelators, performed characterizations, solved single crystal structures, and evaluated gelation properties. S.S.J. and K.K.D. wrote the initial manuscript draft, and all authors reviewed the main manuscript.

References

(1) Truong, W. T.; Su, Y.; Meijer, J. T.; Thordarson, P.; Braet, F. Self-assembled gels for biomedical applications. *Chem. Asian J.* **2011**, *6* (1), 30-42. Kumar, D. K.; Steed, J. W. Supramolecular gel phase crystallization: orthogonal self-assembly under non-equilibrium conditions. *Chem. Soc. Rev.* **2014**, *43* (7), 2080-2088. Foster, J. A.; Damodaran, K. K.; Maurin, A.; Day, G. M.; Thompson, H. P.; Cameron, G. J.; Bernal, J. C.; Steed, J. W. Pharmaceutical polymorph control in a drug-mimetic supramolecular gel. *Chem. Sci.* **2017**, *8* (1), 78. Dawn, A. Supramolecular gel as the template for catalysis,

inorganic superstructure, and pharmaceutical crystallization. *Int. J. Mol. Sci.* **2019**, *20* (3), 781.
(2) Dastidar, P. Supramolecular gelling agents: can they be designed? *Chem. Soc. Rev.* **2008**, *37* (12), 2699-2715.
(3) Jones, C. D.; Steed, J. W. Gels with sense: supramolecular materials that respond to heat, light and sound. *Chem. Soc. Rev.* **2016**, *45* (23), 6546-6596, 10.1039/C6CS00435K.
(4) Steed, J. W. Anion-tuned supramolecular gels: a natural evolution from urea supramolecular chemistry. *Chem. Soc. Rev.* **2010**, *39* (10), 3686-3699.
(5) Banerjee, S.; Das, R. K.; Maitra, U. Supramolecular gels 'in action'. *J. Mater. Chem.* **2009**, *19* (37), 6649-6687, 10.1039/B819218A. de Loos, M.; Feringa, B. L.; van Esch, J. H. Design and Application of Self-Assembled Low Molecular Weight Hydrogels. *Eur. J. Org. Chem.* **2005**, *2005* (17), 3615-3631. George, M.; Weiss, R. G. Molecular Organogels. Soft Matter Comprised of Low-Molecular-Mass Organic Gelators and Organic Liquids†. *Acc. Chem. Res.* **2006**, *39* (8), 489-497.
(6) Estroff, L. A.; Hamilton, A. D. Water Gelation by Small Organic Molecules. *Chem. Rev.* **2004**, *104* (3), 1201-1218. Kumar, D. K.; Steed, J. W. Supramolecular gel phase crystallization: orthogonal self-assembly under non-equilibrium conditions. *Chemical Society Reviews* **2014**, *43* (7), 2080-2088, 10.1039/C3CS60224A.
(7) Zhao, X.; Zhang, S. Molecular designer self-assembling peptides. *Chem. Soc. Rev.* **2006**, *35* (11), 1105-1110. Meazza, L.; Foster, J. A.; Fucke, K.; Metrangolo, P.; Resnati, G.; Steed, J. W. Halogen-bonding-triggered supramolecular gel formation. *Nat. Chem.* **2013**, *5* (1), 42-47.
(8) Yu, G.; Yan, X.; Han, C.; Huang, F. Characterization of supramolecular gels. *Chem. Soc. Rev.* **2013**, *42* (16), 6697-6722, 10.1039/C3CS60080G.
(9) Ghosh, D.; Bjornsson, R.; Damodaran, K. K. Role of N–Oxide Moieties in Tuning Supramolecular Gel-State Properties. *Gels* **2020**, *6* (4), 41. Ghosh, D.; Mulvee, M. T.; Damodaran, K. K. Tuning Gel State Properties of Supramolecular Gels by Functional Group Modification. *Molecules* **2019**, *24* (19), 3472.
(10) Jayabhavan, S. S.; Kristinsson, B.; Ghosh, D.; Breton, C.; Damodaran, K. K. Stimuli-Responsive Properties of Supramolecular Gels Based on Pyridyl-N-oxide Amides. *Gels* **2023**, *9* (2), 89. Sudhakaran Jayabhavan, S.; Ghosh, D.; Damodaran, K. K. Making and Breaking of Gels: Stimuli-Responsive Properties of Bis(Pyridyl-N-oxide Urea) Gelators. *Molecules* **2021**, *26* (21), 6420.
(11) Piepenbrock, M.-O. M.; Lloyd, G. O.; Clarke, N.; Steed, J. W. Metal- and Anion-Binding Supramolecular Gels. *Chem. Rev.* **2010**, *110* (4), 1960-2004.
(12) Gavara, R.; Llorca, J.; Lima, J. C.; Rodríguez, L. A luminescent hydrogel based on a new Au(i) complex. *Chem. Commun.* **2013**, *49* (1), 72-74, 10.1039/C2CC37262B. Ishi-i, T.; Iguchi, R.; Snip, E.; Ikeda, M.; Shinkai, S. [60]Fullerene Can Reinforce the Organogel Structure of Porphyrin-Appended Cholesterol Derivatives: Novel Odd−Even Effect of the (CH2)n Spacer on the Organogel Stability. *Langmuir* **2001**, *17* (19), 5825-5833. Isozaki, K.; Ogata, K.; Haga, Y.; Sasano, D.; Ogawa, T.; Kurata, H.; Nakamura, M.; Naota, T.; Takaya, H. Metal array fabrication through self-assembly of Pt-complex-bound amino acids. *Chem. Commun.* **2012**, *48* (33), 3936-3938, 10.1039/C2CC17530D. Adarsh, N. N.; Dastidar, P. A New Series of ZnII Coordination Polymer Based Metallogels Derived from Bis-pyridyl-bis-amide Ligands: A Crystal Engineering Approach. *Cryst. Growth Des.* **2011**, *11* (1), 328-336. Piepenbrock, M.-O. M.; Clarke, N.; Steed, J. W. Rheology and silver nanoparticle templating in a bis(urea) silver metallogel. *Soft Matter* **2011**, *7* (6), 2412-2418, 10.1039/C0SM00647E. Hanabusa, K.; Maesaka, Y.; Suzuki, M.; Kimura, M.; Shirai, H. Low Molecular Weight Gelator

Containing β-Diketonato Ligands: Stabilization of Gels by Metal Coordination. *Chem. Lett.* **2005**, *29* (10), 1168-1169.
(13) Saxena, A.; Pike, R. D. Hydrogen-Bonding Networks in Heterocyclic Thioureas. *J. Chem. Crystallogr.* **2007**, *37* (11), 755-764.
(14) Tobe, Y.; Sasaki, S.-i.; Mizuno, M.; Hirose, K.; Naemura, K. Novel self-assembly of m-xylylene type dithioureas by head-to-tail hydrogen bonding. *J. Org. Chem.* **1998**, *63* (21), 7481-7489. Succaw, G. L.; Weakley, T. J.; Han, F.; Doxsee, K. M. Crystal engineering with bis (thiourea) derivatives. *Cryst. Growth Des.* **2005**, *5* (6), 2288-2298.
(15) Sahu, S.; Rani Sahoo, P.; Patel, S.; Mishra, B. Oxidation of thiourea and substituted thioureas: a review. *J. Sulphur Chem.* **2011**, *32* (2), 171-197.
(16) Strzyga-Łach, P.; Kurpios-Piec, D.; Chrzanowska, A.; Szczepaniak, J.; Bielenica, A. 1, 3-Disubstituted thiourea derivatives: Promising candidates for medicinal applications with enhanced cytotoxic effects on cancer cells. *Eur. J. Pharmacol.* **2024**, *982*, 176885.
(17) Swaminathan, S.; Jerome, P.; Deepak, R. J.; Karvembu, R.; Oh, T. H. Platinum group metal (PGM) complexes having acylthiourea ligand system as catalysts or anticancer agents. *Coord. Chem. Rev.* **2024**, *503*, 215620.
(18) Kundu, S.; Egboluche, T. K.; Hossain, M. A. Urea- and Thiourea-Based Receptors for Anion Binding. *Acc. Chem. Res.* **2023**, *56* (11), 1320-1329. Zhang, Z.; Schreiner, P. R. (Thio)urea organocatalysis—What can be learnt from anion recognition? *Chem. Soc. Rev.* **2009**, *38* (4), 1187-1198, 10.1039/B801793J.
(19) George, M.; Tan, G.; John, V. T.; Weiss, R. G. Urea and Thiourea Derivatives as Low Molecular-Mass Organogelators. *Chem. Eur. J.* **2005**, *11* (11), 3243-3254.
(20) Ha, S.; Lee, J.; Kim, K.-s.; Choi, E. J.; Nhem, P.; Song, C. Anion-Responsive Thiourea-Based Gel Actuator. *Chem. Mat.* **2019**, *31* (15), 5735-5741.
(21) Prusinowska, N.; Szymkowiak, J.; Kwit, M. Enantiopure Tertiary Urea and Thiourea Derivatives of Trianglamine Macrocycle: Structural Studies and Metallogeling Properties. *J. Org. Chem.* **2018**, *83* (3), 1167-1175.
(22) West, D.; Hermetet, A.; Ackerman, L.; Valdés-Martínez, J.; Hernández-Ortega, S. 3-Phenyl-1-(2-pyridyl) thiourea. *Acta Crystallogr., Sect. C: Cryst. Struct. Commun.* **1999**, *55* (5), 811-813. Hermetet, A. K.; Ackerman, L. J.; Swearingen, J. K.; Presto, C. A.; Kelman, D. R.; Giesen, J. M.; Goldberg, K. I.; Kaminsky, W.; West, D. X. Structural studies of N-2-(6-picolyl)-N′-tolylthioureas. *J. Chem. Crystallogr.* **2002**, *32*, 17-25. West, D. X.; Swearingen, J. K.; Hermetet, A. K.; Ackerman, L. J. Structural and spectral studies of N-2-(pyridyl)-, N-2-(4-, 5-, and 6-picolyl)-and N-2-(4, 6-lutidyl)-N′-2-methoxyphenylthioureas. *J. Mol. Struct.* **2001**, *562* (1-3), 95-105.
(23) Fan, Y.; Lu, H.; Hou, H.; Zhou, Z.; Zhao, Q.; Zhang, L.; Cheng, F. STRUCTURES OF COPPER(I) AND ZINC(II) COMPLEXES WITH N,N′-BIS(2-PYRIDINYL)THIOUREA (BPT). *J. Coord. Chem.* **2000**, *50* (1), 65-72.
(24) Venkatachalam, T.; Sudbeck, E.; Uckun, F. Structural influence on the anisotropic intermolecular hydrogen bonding in solid state of substituted thioureas: evidence by X-ray crystal structure. *J. Mol. Struct.* **2004**, *687* (1-3), 45-56.
(25) Saxena, A.; Dugan, E. C.; Liaw, J.; Dembo, M. D.; Pike, R. D. Copper (I) complexes of heterocyclic thiourea ligands. *Polyhedron* **2009**, *28* (18), 4017-4031.
(26) Adam, M. S. S.; Youssef, M. M.; Aboelghar, M. F.; Hafez, A. M.; El-Ayaan, U. Synthesis and characterization of binary and ternary oxovanadium complexes of N, N′-(2-pyridyl) thiourea and curcumin: Catalytic oxidation potential, antibacterial, antimicrobial, antioxidant and DNA interaction studies. *Appl. Organomet. Chem.* **2017**, *31* (7), e3650.
(27) Adam, M. S. S.; Youssef, M. M.; Aboelghar, M. F.; Hafez, A. M.; El-Ayaan, U. Synthesis and characterization of binary and ternary oxovanadium complexes of N,N′-(2-

pyridyl)thiourea and curcumin: Catalytic oxidation potential, antibacterial, antimicrobial, antioxidant and DNA interaction studies. *Appl. Organomet. Chem.* **2017**, *31* (7), e3650.
(28) Kumar, D. K.; Jose, D. A.; Das, A.; Dastidar, P. First snapshot of a nonpolymeric hydrogelator interacting with its gelling solvents. *Chem. Commun.* **2005**, (32), 4059-4061.
(29) Goodwin, J. W.; Hughes, R. W. *Rheology for chemists: an introduction*; Royal Society of Chemistry, 2008. Guenet, J.-M. *Organogels: Thermodynamics, structure, solvent role, and properties*; Springer, 2016. Jayabhavan, S. S.; Myneni, H.; Riedel, M.; Damodaran, K. K. Analysing the self-assembly modes in chiral multi-component gels based on donor and acceptor moieties. *Supramol. Chem.* **2023**, *34* (9-10), 414-426.
(30) Tomasson, D. A.; Ghosh, D.; Kržišnik, Z.; Fasolin, L. H.; Vicente, A. n. A.; Martin, A. D.; Thordarson, P.; Damodaran, K. K. Enhanced mechanical and thermal strength in mixed-enantiomers-based supramolecular gel. *Langmuir* **2018**, *34* (43), 12957-12967. Kuppadakkath, G.; Jayabhavan, S. S.; Damodaran, K. K. Supramolecular Gels Based on C3-Symmetric Amides: Application in Anion-Sensing and Removal of Dyes from Water. *Molecules* **2024**, *29* (9), 2149.

SUPPORTING INFORMATION

Selective Gelation of Bis(Pyridyl)Thiourea by Copper (II) Salts

Sreejith Sudhakaran Jayabhavan and Krishna K. Damodaran*

Contents

1. Synthetic scheme

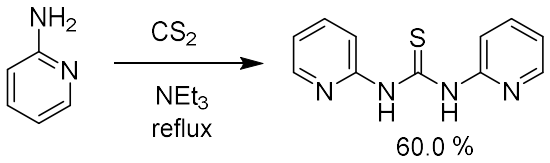

Scheme S1. Synthetic route for 2-PTU.

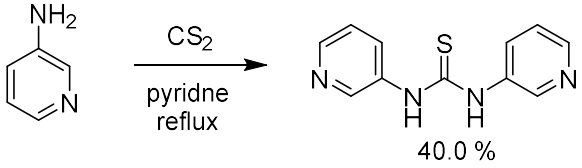

Scheme S2. Synthetic route for 3-PTU.

2. Gelation studies

Table S1. Gelation Experiments

Solvent	Gelation test at 1.0-5.0 wt/v%	
	2-PTU	**3-PTU**
water	I	Cry
THF	I	I
MeOH	Ppt	Ppt
p-xylene	I	I
nitrobenzene	S	S
mesitylene	I	I
DMF	S	S
DMSO	S	S
MeOH/water	Cry	Cry
DMSO/water	Cry	Cry+ppt

Ppt= precipitate, Cry= Crystals, I= Insoluble, and aqueous mixtures were taken at 1:1, v/v.

Table S2. Metallogelation experiments with 3-PTU at 1:2 metal to ligand ratio and 0.05-0.15 mmol of metal salts

Metal salts	Ligand wt/v%	Initial Observation	Final Observation
$Cu(NO_3)_2.3H_2O$	2.3-4.6	Green solution	**Gel**
$CuSO_4.5H_2O$	6.9	Green solution	**Gel**
$Cu(OAc)_2.2H_2O$	2.3-4.6	Green solution	**Gel**
$CuCl_2$	6.9	Green solution	**Gel**
$CuBr_2$	6.9	Green solution	**Gel**
$Cu(ClO_4)_2.6H_2O$	2.3-4.6	Green solution	**Gel**
$Cu(OBz)_2$ **	2.3	Green solution	colloid
$ZnCl_2$	6.9	solution	Precipitate
$ZnNO_3$	6.9	solution	Precipitate
$Cd(NO_3)_2.4H_2O$	6.9	solution	Precipitate
$CdCl_2$	6.9	solution	Precipitate
$CoCl_2$	6.9	Pink solution	Precipitate
$NiCl_2$	6.9	Green Solution	Precipitate
$FeCl_3$	6.9	Red solution	Precipitate
$MnCl_2$	6.9	solution	Ligand crystals
$CrCl_3$	6.9	Green solution	Ligand crystals

**- Dissolved both metal salt and ligand in DMF by sonication and added water

3. Rheology

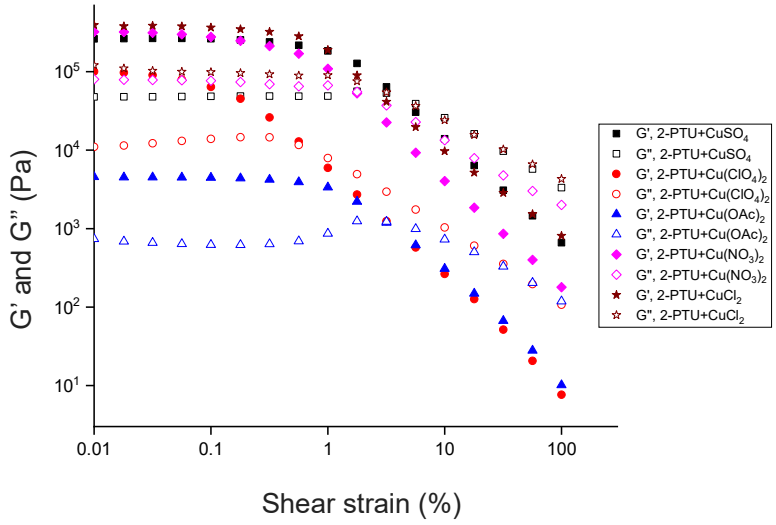

Figure S1. Amplitude sweep experiments with 2-PTU with metal salts in DMF/water (1:1, v/v) at 1:2 metal/ligand ratio, 4.6 wt/v% of ligand with $Cu(NO_3)_2$, $Cu(OAc)_2$ and 6.9 wt/v% of ligand with $CuSO_4$, $CuCl_2$, and $Cu(ClO_4)_2$, at 20.0 °C measured at a constant frequency of 1.0 Hz.

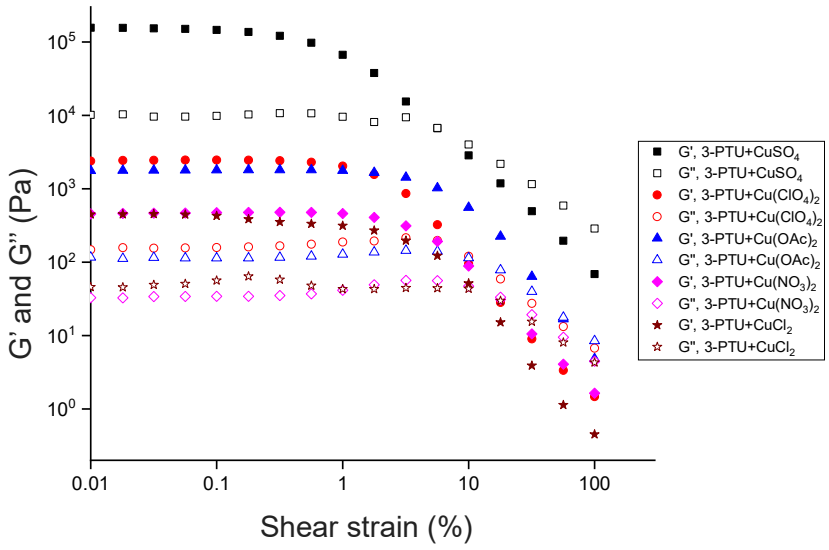

Figure S2. Amplitude sweep experiments with 3-PTU with metal salts in DMF/water (1:1, v/v) at 1:2 metal/ligand ratio, 4.6 wt/v% of ligand with $Cu(NO_3)_2$, $Cu(OAc)_2$ and 6.9 wt/v% of ligand with $CuSO_4$, $CuCl_2$, and $Cu(ClO_4)_2$, at 20.0 °C measured at a constant frequency of 1.0 Hz.

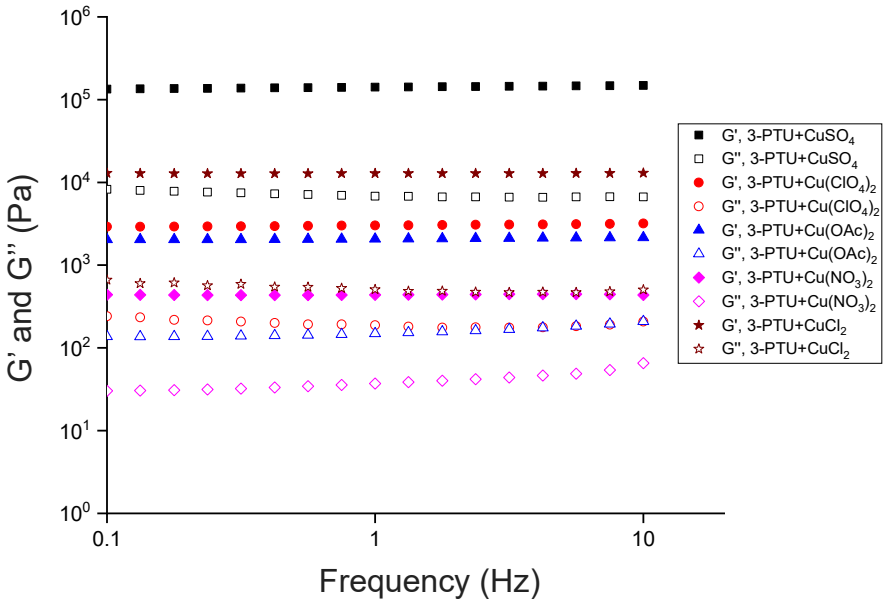

Figure S3. Frequency sweep experiments with 3-PTU with metal salts in DMF/water (1:1, v/v) at 1:2 metal/ligand ratio, 4.6 wt/v% of ligand with $Cu(NO_3)_2$, $Cu(OAc)_2$ and 6.9 wt/v% of ligand with $CuSO_4$, $CuCl_2$, and $Cu(ClO_4)_2$, at 20.0 °C measured at a constant strain of 0.05%.

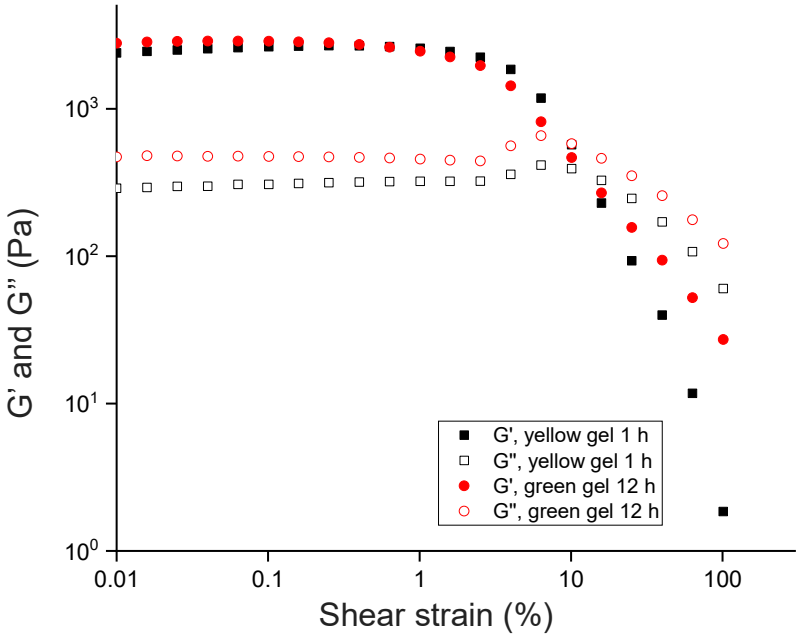

Figure S4. Amplitude sweep experiments with gels of 2-PTU+$Cu(OBz)_2$ at 2.3 wt/v% of the 2-PTU, in DMF/water 1:1, v/v, at 1:2 metal to ligand ratio and at 20.0 °C measured at a constant frequency of 1.0 Hz

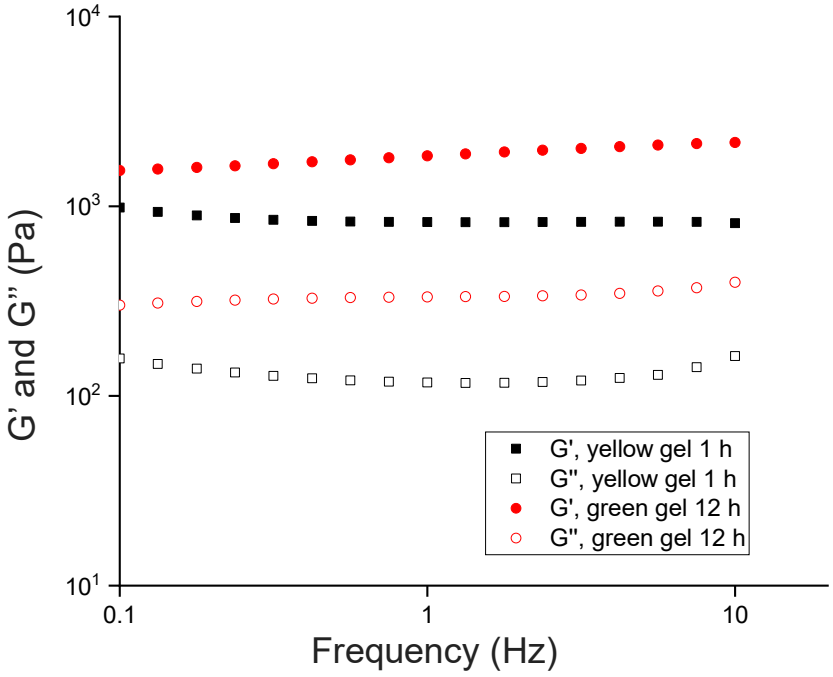

Figure S5. Frequency sweep experiments with gels of 2-PTU+$Cu(OBz)_2$ at 2.3 wt/v% of the 2-PTU, in DMF/water 1:1, v/v, at 1:2 metal to ligand ratio and at 20.0 °C measured at a constant strain of 0.05%.

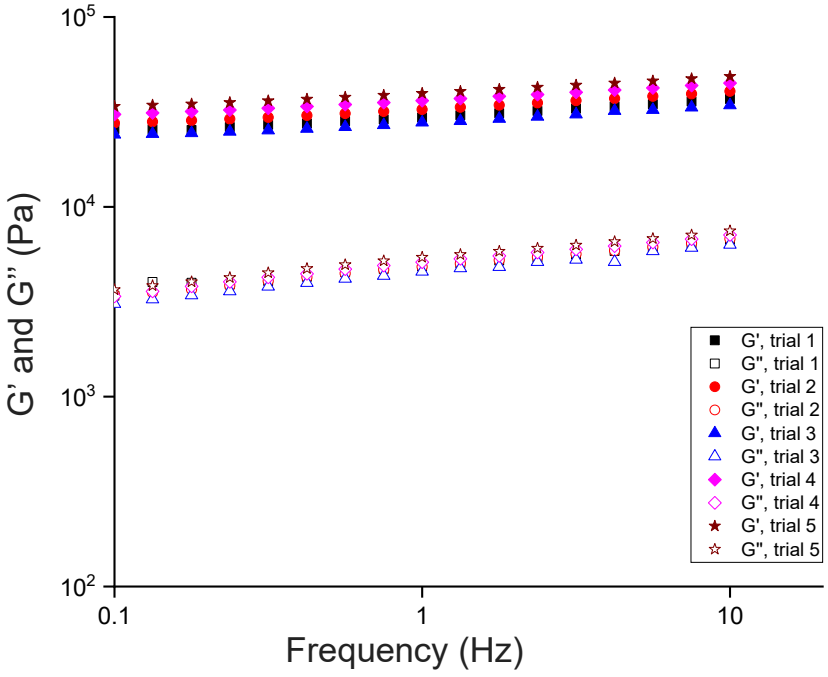

Figure S6. Frequency sweep experiments with gels of 2-PTU+$Cu(OBz)_2$ at 4.6 wt/v% of the 2-PTU, in DMF/water 1:1, v/v, at 1:2 metal to ligand ratio and at 20.0 °C measured at a constant strain of 0.05% over 5 trials.

4. Scanning electron microscopy

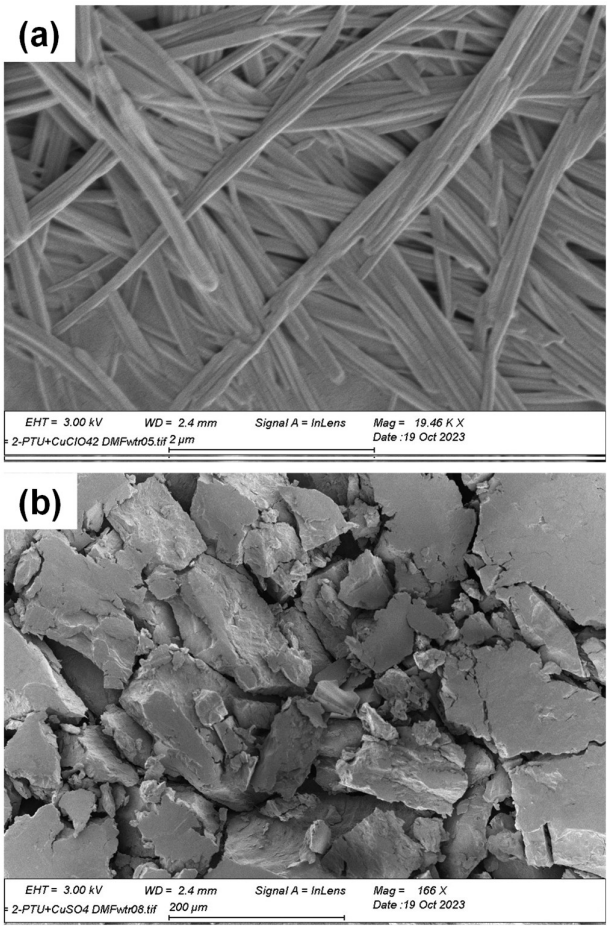

Figure S7. SEM images of the xerogels obtained from 2-PTU with metal salts in DMF/water (1:1, v/v) at 1:2 metal/ligand ratio, with ligand 6.9 wt/v% and (a) $Cu(ClO_4)_2$, (b) $CuSO_4$.

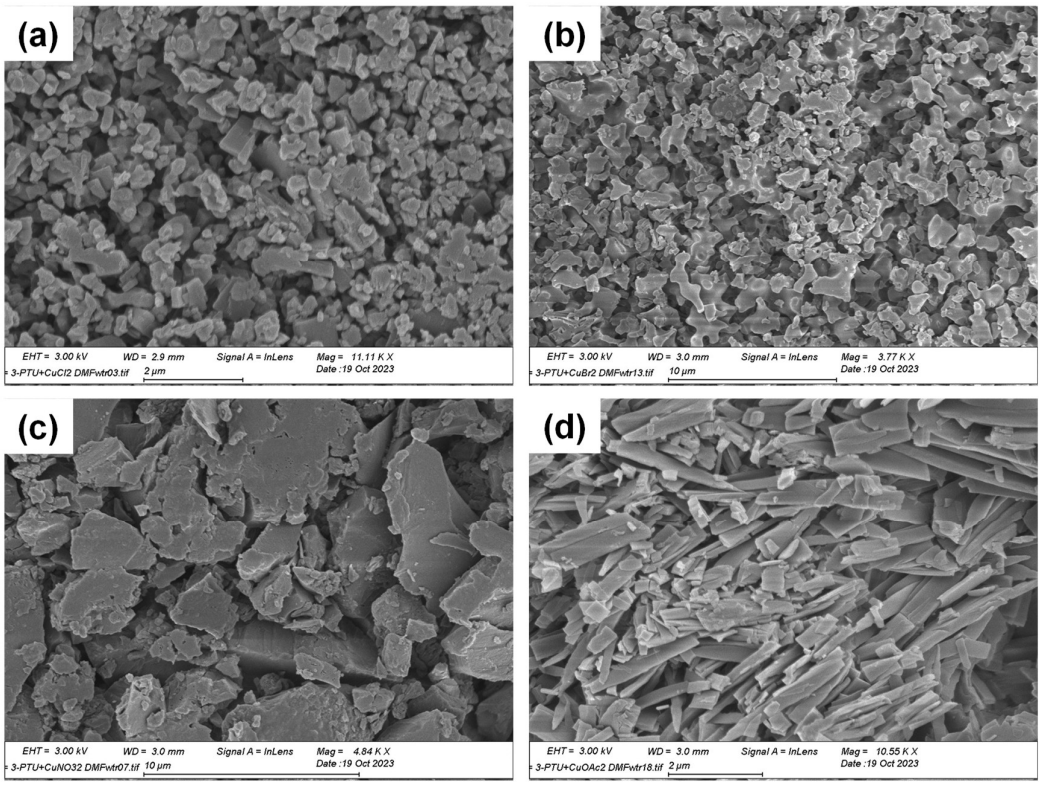

Figure S8. SEM images of the xerogels obtained from 3-PTU with metal salts in DMF/water (1:1, v/v) at 1:2 metal/ligand ratio, with ligand 6.9 wt/v% and (a) $CuCl_2$, (b) $CuBr_2$, and ligand 4.6 wt/v% with (c) $Cu(NO_3)_2$ and (d) $Cu(OAc)_2$.

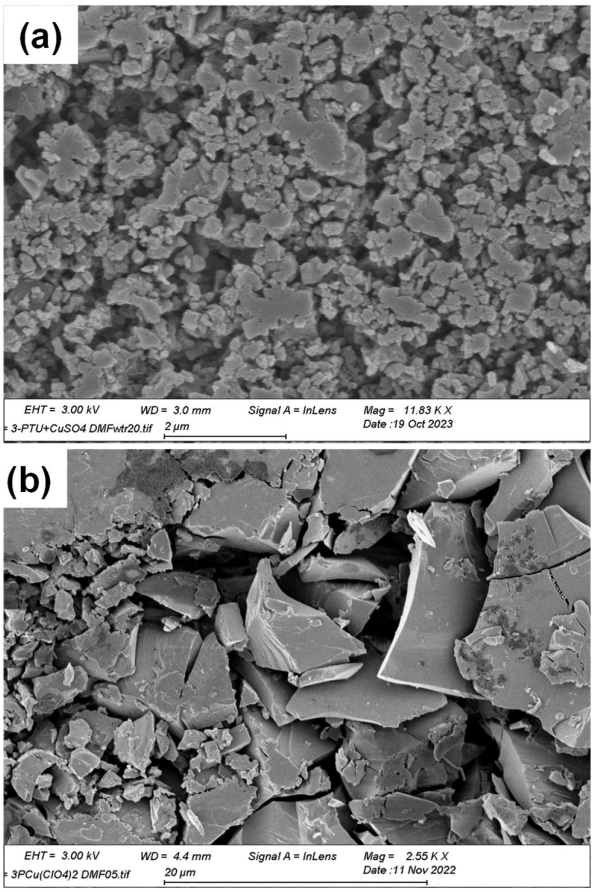

Figure S9. SEM images of the xerogels obtained from 3-PTU with metal salts in DMF/water (1:1, v/v) at 1:2 metal/ligand ratio, with ligand 6.9 wt/v% and (a) $CuSO_4$, (b) $Cu(ClO_4)_2$.

5. X-ray crystallography

Table S4. Crystal data for thiourea complexes

Crystal data	**2-PTU+Cu(OBz)$_2$**	**2-PTU+CdCl$_2$**
File name	**SSJ_III_154_4**	**SSJ_III_189**
Empirical formula	$C_{36}H_{30}CuN_8O_6S_2$	$C_{11}H_{18}CdN_4Cl_2S$
Color	Green	Colorless
Formula weight	798.34	444.51
Crystal size (mm)	0.500 x 0.400 x 0.200	0.290 x 0.030 x 0.020
Crystal system	Triclinic	Monoclinic
Space group	*P*-1	$P2_1/c$
a (Å)	9.9593(4)	18.2754(11)
b (Å)	9.9807(5)	19.9150(11)
c (Å)	10.6694(5)	7.2545(4)
α (°)	67.553(2)	90
β (°)	65.7050(10)	96.628(2)
γ (°)	68.489(2)	90
Volume (Å^3)	865.29(7)	2622.7(3)
Z	1	8
$D_{calc.}$(g/cm^3)	1.532	2.085
F(000)	411	1600
μ (mm^{-1}) MoK_α	0.812	2.220
Temperature (K)	305(2)	298(2)
Reflections collected/ unique/observed [I>2σ(I)]	199354/ 21287/14169	47679/ 5558/4103
Data/restraints/parameters	21287/0/247	5558/0/343
Goodness of fit on F^2	1.043	1.024
Final R indices [I>2σ(I)]	R_1 = 0.0407 wR_2 = 0.1162	R_1 = 0.0335 wR_2 = 0.0547
R indices (all data)	R_1 = 0.0700 wR_2 = 0.1396	R1 = 0.0620 wR2 = 0.0614

Table S5. Hydrogen bonding parameters for thiourea complexes

Compound 2-PTU+Cu(OBz)$_2$						
No.	Donor–H···Acceptor	D–H**/Å**	H···A**/Å**	D···A**/Å**	∠D–H···A**/°**	Symmetry operation
1	O(2)–H(2)···O(5)	0.756(13)	1.884(12)	2.5823(11)	153.4(13)	1-x,1-y,1-z
2	O(2)–H(2A)···N(18)	0.84(2)	1.939(19)	2.7270(9)	157(2)	1-x,1-y,1-z
3	C(14)–H(14)···O(5)	0.93	2.51	3.4199(14)	165	-x,1-y,2-z
4	C(27)–H(27)···O(2)	0.93	2.44	3.2720(11)	149	x,y,z
Compound 2-PTU+CdCl$_2$						
No.	Donor–H···Acceptor	D–H**/Å**	H···A**/Å**	D···A**/Å**	∠D–H···A**/°**	Symmetry operation
1	C(13I)–H(13I)···Cl(33)	0.93	2.68	3.456(4)	141	1-x,1/2+y,3/2-z
2	C(19I)–H(19I)···Cl(36)	0.93	2.80	3.698(4)	163	2-x,-1/2+y,1/2-z
3	C(31I)–H(31I)···Cl(35)	0.93	2.68	3.563(4)	158	2-x,-1/2+y,1/2-z

6. Color transformation

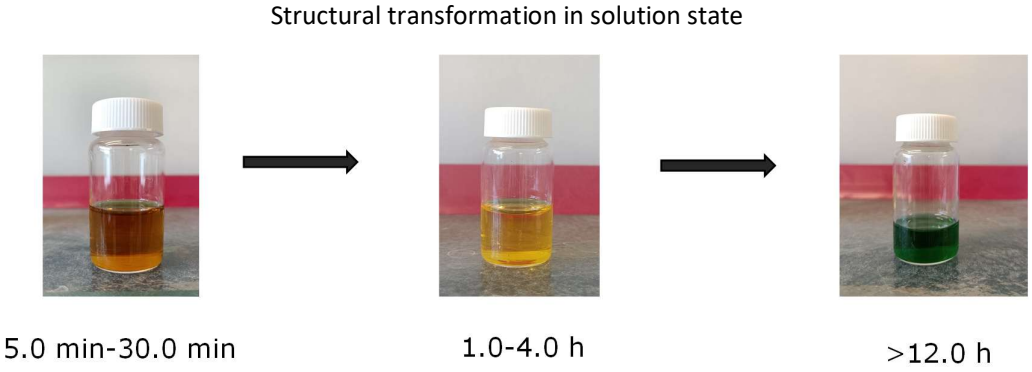

Figure S10. Sol-to-Sol transformation with 2-PTU+$Cu(OBz)_2$ in 10 mL of DMF/water (1:1, v/v) and 23.0 mg of 2-PTU and 1:2 metal-to-ligand ratio.

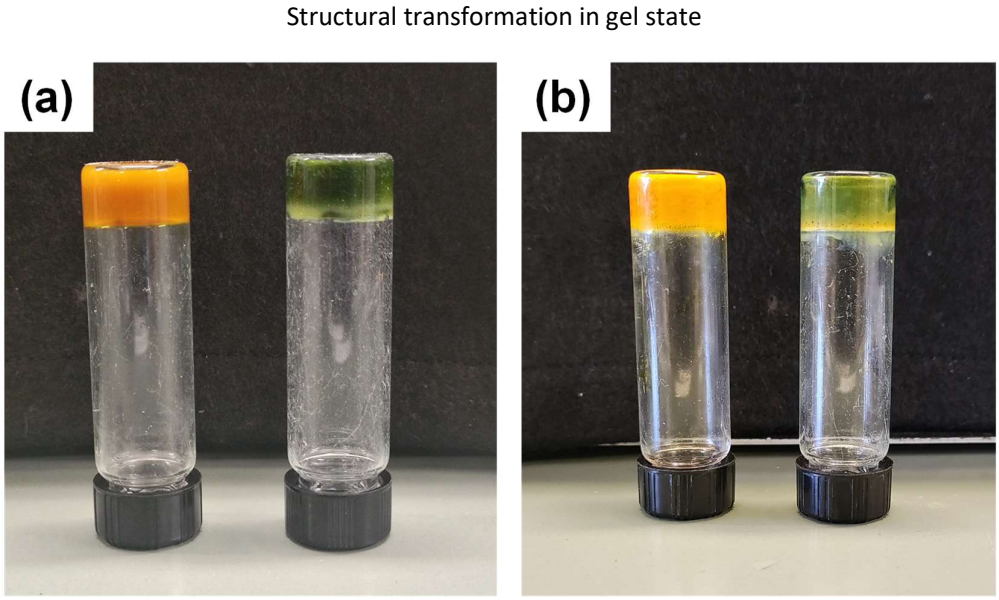

Figure S11. Gel-to-gel transformation with 2-PTU-based metallogels based on (a) $Cu(OAc)_2$ and (b) $Cu(OBz)_2$, in DMF/water (1:1, v/v) and 46.0 mg of 2-PTU and 1:2 metal-to-ligand ratio.

3.0 Role of the arrangement/position of the functional groups

In this chapter, we are analyzing the effect and nature of the functional group of LMWGs towards the applications such as gel phase crystallization and antibacterial activities. Understanding the importance of functional groups and the characteristics of non-covalent interactions can aid researchers to create novel materials derived from LMWGs with tunable properties. Gel phase crystallization is a prime example of orthogonal self-assembly of the crystals and gel network. LMWGs have been used to crystallize inorganic substances, proteins, and active pharmaceutical ingredients, and the gel environment can influence factors such as crystal habit and polymorphism. The structural similarity between the crystallization substrate and the gelator is a significant factor in gel phase crystallization, such that the gelator molecules can interact with the substrate, which could influence the epitaxial crystal growth to favor crystallization of metastable or hard-to-nucleate solid forms. Similarly, the presence of certain functionalities can induce biological activity, including anti-inflammatory and analgesic properties. Thus, we incorporated carbamate-based *N*-oxides with metronidazole functionality to test their antibacterial properties. We also analyzed the coordination-driven self-assembly with these multifunctional carbamate-based *N*-oxides ligands.

This chapter is divided into two sections.

3.1. Evaluating the role of isomeric active pharmaceutical ingredient (API) functionalities on the self-assembly process to develop API mimicking LMWGs as a crystallizing media for APIs.

Article-IV

A series of bis(urea) compounds featuring complementary functional groups analogous to the therapeutic drug metronidazole and its structural isomer isometronidazole have been designed and synthesized. The gelation characteristics of these compounds were examined in several solvent/solvent combinations. The mechanical strength of the isomeric gelators was assessed by rheology, and the morphologies of the xerogels were examined via scanning electron microscopy to observe fibrous morphology. These gels served as a medium for the crystallization of metronidazole, leading to a significant change in the habit of the metronidazole crystals within the drug-mimicking gels. Nonetheless, crystallization in the nonmimetic isomeric gel produced a habit similar to that of those in the solution state. The results demonstrate that the drug-mimetic gels interact with the drug crystal's surface, resulting in novel morphologies.

3.2. Incorporating functional groups with antibacterial properties in LMWGs to generate isomeric metal-based LMWGs as antibacterial agents and evaluate the role of these functional groups in the self-assembly process.

Article-V

We have synthesized and studied carbamates derived from metronidazole (a nitroimidazole antibiotic) by incorporating 3/4-pyridyl functionality in tandem with their corresponding *N*-oxides. We observed that the modification of functional groups by the introduction of an *N*-oxide functionality in 3-pyridyl-based carbamate could induce hydrogelation. We have conducted metallogelation experiments using the pyridyl substituted compounds and their corresponding *N*-oxides with several transition metal salts. The results indicated that the 3-pyridyl-based carbamate formed gel with cadmium(II) chloride in a DMF/water (1:1, v/v) mixture, while the corresponding *N*-oxide produced a gel with silver(I) nitrate in a DMF/water (1:9, v/v) solution. The 4-pyridyl-based carbamate was unable to form metallogels, but the corresponding *N*-oxide successfully generated a gel with copper(II) sulfate in a DMF/water (1:1, v/v) mixture. Antibacterial investigations involving cadmium(II) and silver(I) complexes have demonstrated efficacy against gram-negative and gram-positive bacteria.

Article-IV

This project is published in a peer-reviewed journal and included as published. Minor variations may arise from the original article owing to formatting issues.

Publication details:

"**Crystal Habit Modification of Metronidazole by Supramolecular Gels with Complementary Functionality**"

Sreejith S. Jayabhavan, J. W. Steed, and Krishna K. Damodaran*

Cryst. Growth Des. **2021**, *21*, 9, 5383–5393.

Author contributions:

SSJ and KKD planned and designed the research; **SSJ** synthesized the gelators and performed characterizations, KKD solved single crystal structures, and **SSJ** evaluated gelation properties. **SSJ,** JWS and KKD wrote the initial manuscript draft, and all authors reviewed the main manuscript.

CRYSTAL GROWTH & DESIGN

pubs.acs.org/crystal

Article

Crystal Habit Modification of Metronidazole by Supramolecular Gels with Complementary Functionality

Published as part of a Crystal Growth and Design virtual special issue on Nonclassical Crystallization in Synthetic and Natural Systems

Sreejith Sudhakaran Jayabhavan, Jonathan W. Steed,* and Krishna K. Damodaran*

Cite This: *Cryst. Growth Des.* 2021, 21, 5383−5393

Read Online

ACCESS | Metrics & More | Article Recommendations | Supporting Information

ABSTRACT: A series of bis(urea) compounds with complementary functional groups similar to the pharmaceutical drug metronidazole and a structural isomer isometronidazole have been synthesized. The gelation properties of these compounds were studied in various solvent/solvent mixtures. The mechanical strength of the isomeric gelators was compared using rheology, and the morphologies of the xerogels were analyzed by scanning electron microscopy. These gels were used as media for metronidazole crystallization resulting in a marked habit modification of the metronidazole crystals in the drug-mimicking gels. However, crystallization in the nonmimetic isomeric gel resulted in morphologies similar to the solution state. These results indicate that the drug-mimetic gels interact with the surface of the drug crystal giving rise to new morphologies.

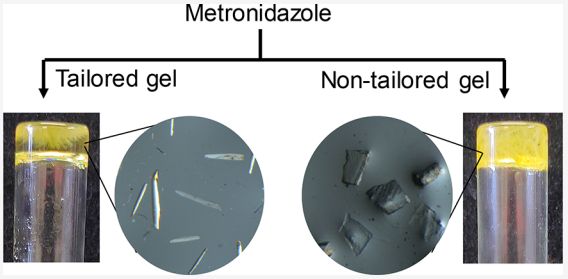

INTRODUCTION

Supramolecular gels based on low molecular weight gelators (LMWGs)[1−7] have become highly topical in the last two decades owing to their intriguing potential applications in drug delivery, separation techniques, as templates for inorganic and polymer materials, and as media for crystallization. Crystallization in gel media dates back at least as far as the discovery of the well-known "Liesegang rings", which represent periodic precipitation in gels.[8] Gel phase crystallization represents an example of orthogonal self-assembly of the crystals and gel network.[9] The gel medium limits convection and prevents sedimentation by providing continuous, diffusion-limited growth,[10,11] as well as influencing the nucleation behavior of the crystals.[12] LMWGs have been used to crystallize inorganic substances, proteins, and active pharmaceutical ingredients,[13−18] and the gel environment can influence factors such as crystal habit and polymorphism.[9] LMWGs can provide various advantages as media for crystal growth, such as facile synthesis, long shelf life, and easy modification of functional groups. There have been a few recent reports of crystallization within LMWG,[9] for example, calcite crystallization in a bis(urea) gel[19] and crystallization of aspirin, caffeine, indomethacin and carbamazepine in toluene-based tetraamide organogels.[20] We have shown that LMWGs can be used as a medium for crystallizing inorganic complexes and reported the selective crystallization of one particular form (form I) of a copper(II) isonicotinate-*N*-oxide complex.[21] We have shown that designing gelators that mimic the crystallization substrate can enable the gelator molecules to interact with the substrate, offering the possibility of epitaxial crystal growth and hence favoring metastable or hard-to-nucleate solid forms of molecular crystals including pharmaceutically relevant compounds.[9−11,19−27]

Previous work on gel phase crystallization using crystallization substrate-mimicking gelators has resulted in the crystal habit modification of isoniazid[28] and cisplatin.[29] Crystallization in bis(urea) LMWGs tagged with functional groups (Scheme 1) similar to a highly polymorphic drug precursor, ROY, resulted in the selective crystallization of the metastable R polymorph in contrast to the Y form obtained in solution.[10] Recently, drug-mimicking LMWGs have been used to prevent concomitant crystallization.[30] Thus, structural similarity between the crystallization substrate and the gelator is potentially significant in gel phase crystallization. In the present work, we have designed bis(urea) compounds that mimic the antibiotic metronidazole as well as isomeric control gelators in order to study the outcome of the drug-mimetic gel phase crystallization of this drug substance.

Received: June 8, 2021
Revised: July 8, 2021
Published: July 30, 2021

https://doi.org/10.1021/acs.cgd.1c00659
Cryst. Growth Des. 2021, 21, 5383−5393

Scheme 1. Gel Phase Crystallization in Drug-Mimetic and Nonmimetic Gels[a]

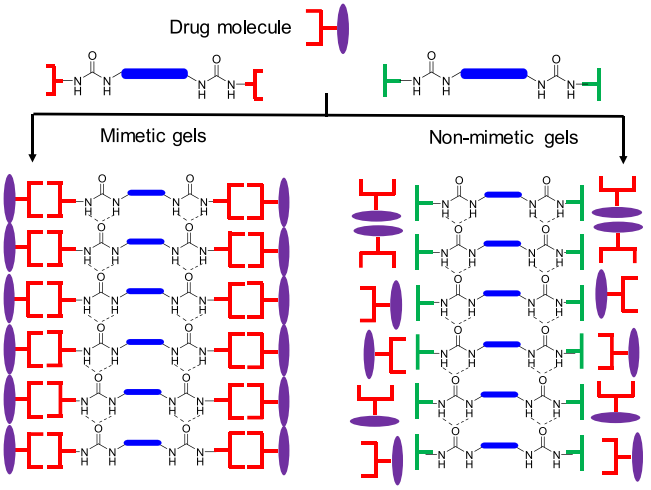

[a]Red lines represent drug-mimicking functional groups, and the green lines indicate random functional groups. Specific interactions between the gel fiber and the drug in the mimetic case can give rise to changes in morphology and polymorphic form.

Metronidazole, a nitroimidazole antibiotic, is used to treat periodontal disease and shows activity against anaerobic protozoa and bacteria.[31−34] There are two polymorphs reported for this drug in the Cambridge Structural Database[35] (form I, CSD refcode MNIMET)[36] and (form II, CSD refcode MNIMET01). The solid forms of metronidazole are an area of interest as a result of its poor tableting properties. Di Martino et al. have demonstrated that the crystal habit of metronidazole is influenced by both the solvent polarity index and the crystallization method.[37] This prompted us to study gel phase crystallization of metronidazole using drug-mimicking compounds as gelators. However, designing LMWGs with specified properties and structure is challenging, and LMWGs are often discovered by serendipity. This is because the structure and properties of the supramolecular gels rely primarily on the geometry and spatial arrangement of the building blocks and also the nature of intermolecular interactions.[38,39] The gel−solute interactions can potentially affect both nucleation and crystal growth rates in a supramolecular gel phase crystallization.[40] Thus, the spatial arrangement of the functional groups and gelator aggregation mode are both of interest in supramolecular gel phase crystallization. We have designed gelators based on the bis(urea) backbone with a complementary functional group similar to metronidazole and isometronidazole. The urea motif chosen is well-known to form α-tapes resulting in fibrils that could align the drug-derived functional groups as a locally ordered array on the surface of the gel fibers (Scheme 1).[3,41,42] The resulting LMWGs are anticipated to have a fibrous surface that chemically matches the crystallization substrate,[10] which offers the possibility of epitaxial crystal growth.[9] We have selected structural isomers as the complementary functional groups to analyze the effect of positional isomers on gelation in LMWGs. In this work, we report the gelation and gel phase crystallization in LMWGs based on derivatives of both metronidazole and its structural isomer isometronidazole. Comparison of the gelation abilities of metronidazole and isometronidazole bis(urea) compounds will enable us to study the role of the position of functional groups on gelation and gel phase crystallization in LMWGs.

EXPERIMENTAL SECTION

Materials and Methods. All the starting materials and reagents were commercially available (Sigma-Aldrich and TCI Europe) and used as supplied except for metronidazole, which was purchased from Accel Pharmtech, USA. ^{1}H and ^{13}C NMR spectra (Figures S1−S12, see Supporting Information) were recorded on a Bruker AVANCE 400 spectrometer, and scanning electron microscopy (SEM) was performed on a Leo Supra 25 microscope. Single-crystal X-ray diffraction (SCXRD) and powder X-ray diffraction (PXRD) were carried out using a Bruker D8 venture and PANalytical instrument.

Synthesis. The bis(urea) compounds of metronidazole (**1**−**3**) and isometronidazole (**4**−**6**) were synthesized following a general procedure by reacting the amine precursors with the corresponding diisocyanates. The amine precursors of metronidazole and isometronidazole were synthesized as described below.

*Synthesis of 1-(2-Bromoethyl)-2-methyl-5-nitro-1H-imidazole (**7**).* Compound **7** was synthesized by slightly modifying the reported procedure.[43] Bromine solution (1.6 mL, 32.2 mmol) was added to a stirred solution of triphenylphosphine (8.4 g, 32.1 mmol) in DCM (100 mL) at 0 °C, followed by the dropwise addition of triethylamine (4.5 mL, 32.0 mmol). Metronidazole (5.0 g, 29.2 mmol) was added in portion to the above solution and was equilibrated to room temperature after 10 min. The mixture was stirred for 30 min, and the excess bromine was quenched with a saturated solution of aqueous sodium thiosulfate (10.0 mL). Water (50.0 mL) was added to the mixture, and the organic phase was separated and treated with 40.0 mL of 1.0 M HCl. The organic phase was discarded, and the aqueous layer was extracted with DCM (3 × 30 mL) to remove the excess triphenylphosphine oxide impurities. The solution was treated with 2.0 M sodium hydroxide solution to precipitate the product, which was extracted with DCM (3 × 40 mL), dried over sodium sulfate, and evaporated in a rotary vapor to yield the product as a yellow solid. Yield: 78.0%. ^{1}H NMR (400 MHz, chloroform-*d*) δ 7.97 (s, 1H), 4.67 (t, J = 6.2 Hz, 2H), 3.69 (t, J = 6.2 Hz, 2H), 2.57 (s, 3H). ^{13}C{^{1}H} NMR (100 MHz, chloroform-*d*) δ 151.12, 138.24, 133.51, 47.40, 29.53, 14.81. HRMS (APCI): calcd for $C_6H_9N_3O_2BrN$ $[M + H]^+$, 233.9873; found, 233.9862.

Synthesis of 1-(2-Azidoethyl)-2-methyl-5-nitro-1H-imidazole[43] *(**8**).* Sodium azide (1.25 g, 19.8 mmol) was added in portions to a solution of compound **7** (3.0 g, 12.8 mmol) in 40.0 mL of DMF, and the mixture was stirred at 60 °C for 22 h. The solvent DMF was evaporated, and 40 mL of water was added. The mixture was extracted with DCM (3 × 40 mL), and the organic parts were combined, dried over sodium sulfate, and evaporated to obtain the product as a yellowish powder. Yield: 99.0%. ^{1}H NMR (400 MHz, chloroform-*d*) δ 7.98 (s, 1H), 4.44 (dd, J = 6.0, 5.0 Hz, 2H), 3.78 (t, J = 6.1 Hz, 2H), 2.54 (s, 3H). ^{13}C{^{1}H} NMR (100 MHz, chloroform-*d*) δ 151.33, 138.29, 133.42, 50.98, 45.57, 14.57. HRMS (APCI): calcd. for $C_6H_9N_6O_2$ $[M + H]^+$, 197.0781; found, 197.0776.

Synthesis of 2-(2-Methyl-5-nitro-1H-imidazol-1-yl)ethan-1-amine[44] *(**9**).* Compound **8** (5.8 g, 29.6 mmol) was dissolved in a mixture of 60.0 mL of THF and 7.5 mL of water and was treated with triphenylphosphine (16.3 g, 62.2 mmol). The mixture was stirred at room temperature for 15 h and was concentrated (∼10.0 mL). The mixture was treated with 2.0 M HCl (20.0 mL) and was washed with DCM (3 × 30 mL) to remove the impurities. The aqueous layer was evaporated to obtain a white powder, which was washed with a methanol/DCM mixture (1:9, v/v) to yield amine dihydrochloride (**9**·2HCl). The crude product was recrystallized from acidic DMF solution. Yield: 73.0%. ^{1}H NMR (400 MHz, DMSO-d_6) δ 8.57 (s, 3H), 8.37 (s, 1H), 4.62 (t, J = 6.6 Hz, 2H), 3.30−3.17 (m, 2H), 2.61 (s, 3H). ^{13}C{^{1}H} NMR (100 MHz, DMSO-d_6) δ 150.43, 137.79, 129.16, 42.98, 37.28, 12.93. HRMS (APCI): calcd for $C_6H_{10}N_4O_2Na$ $[M + H]^+$, 171.0877; found, 171.0876.

Synthesis of 1-(2-Bromoethyl)-2-methyl-4-nitro-1H-imidazole[45] *(**10**).* A solution of 2-methyl-4-nitro-1*H*-imidazole (5.0 g, 39.3 mmol), potassium carbonate (13.5 g, 97.6 mmol), and 1,2-dibromoethane

https://doi.org/10.1021/acs.cgd.1c00659
Cryst. Growth Des. 2021, 21, 5383−5393

(17.0 mL, 196.5 mmol) was prepared in 50.0 mL of DMF, and the mixture was stirred overnight at room temperature. The solution was evaporated, and 40.0 mL of water was added and extracted with DCM (3 × 30 mL). The organic layers were combined and evaporated to dryness. The crude product was obtained as a yellow-white solid, which was purified by column chromatography (eluent: DCM with methanol gradient, 0−0.5%). Yield: 65.0%. ^{1}H NMR (chloroform-*d*, 400 MHz) δ 7.77 (s, 1H), 4.36 (t, J = 6.1 Hz, 2H, 3.64 (t, J = 6.1 Hz, 2H), 2.47 (s, 3H). ^{13}C{^{1}H} NMR (100 MHz, chloroform-*d*) δ 146.83, 144.97, 119.62, 48.32, 29.21, 13.33. HRMS (APCI): calcd for $C_6H_8N_3O_2BrNa$ [M + Na]$^+$, 255.9692; found, 255.9693.

*Synthesis of 1-(2-Azidoethyl)-2-methyl-4-nitro-1H-imidazole (**11**).* The reaction procedure was similar to compound **8**. Compound **10** (3.2 g, 13.7 mmol), sodium azide (1.3 g, 20.5 mmol), and 40.0 mL of DMF. Yield: 98.0%. ^{1}H NMR (400 MHz, chloroform-*d*) δ 7.76 (s, 1H), 4.08 (t, J = 6.1 Hz, 2H), 3.73 (t, J = 6.1 Hz, 2H), 2.45 (s, 3H). ^{13}C{^{1}H} NMR (100 MHz, chloroform-*d*) δ 146.75, 145.04, 119.80, 50.86, 46.12, 13.16. HRMS (APCI): calcd for $C_6H_8N_6O_2Na$ [M + Na]$^+$, 219.0601; found, 219.0598.

*Synthesis of 2-(2-Methyl-4-nitro-1H-imidazol-1-yl)ethan-1-amine[44] (**12**).* The reaction procedure was similar to compound **9**. Compound **11** (2.25 g, 11.5 mmol), triphenylphosphine (6.17 g, 23.6 mmol), and THF/water (20/2.5 mL). The amine was recrystallized as a hydrochloride salt in acidic ethanol solution (**12**·HCl). Yield: 73.0%. ^{1}H NMR (400 MHz, DMSO-d_6) δ 8.43 (s, 1H), 8.37 (s, 3H), 4.32 (t, J = 6.1 Hz, 2H), 3.25 (t, J = 6.1 Hz, 2H), 2.40 (s, 3H). ^{13}C{^{1}H} NMR (100 MHz, DMSO-d_6) δ 145.59, 145.50, 122.36, 43.69, 38.28, 12.76. HRMS (APCI): calcd for $C_6H_{10}N_4O_2Na$ [M + Na]$^+$, 193.0696; found, 193.0692.

*Synthesis of Bis(3,5-diethyl-4-isocyanatophenyl)methane (**13**).* The bis(isocyanate) was synthesized according to a reported procedure.[46] Yield: 95.0%. ^{1}H NMR (400 MHz, chloroform-*d*) δ 6.87 (s, 4H), 3.85 (s, 2H), 2.65 (q, J = 7.6 Hz, 8H), 1.22 (t, J = 7.6 Hz, 12H). ^{13}C{^{1}H} NMR (100 MHz, chloroform-*d*) δ 138.91, 138.49, 127.96, 126.94, 41.12, 25.70, 14.24.

General Procedure for the Synthesis of Bis(urea) Compounds. The amine hydrochloride (2.1 equiv) was dissolved in chloroform by adding triethylamine (4.0 equiv) at room temperature. A solution of the corresponding diisocyanate (1.0 equiv) was added dropwise to the above mixture and was refluxed overnight under a nitrogen atmosphere. The precipitate formed was filtered and stirred with saturated sodium bicarbonate solution for 24 h. The mixture was filtered, and the residue was washed with a copious amount of water and dried to isolate the product.

*Synthesis of 1,1′-(Hexane-1,6-diyl)bis(3-(2-(2-methyl-5-nitro-1H-imidazol-1-yl)ethyl)urea) (**1**).* The crude compound was recrystallized from ethanol. Yield: 75.0%. ^{1}H NMR (400 MHz, DMSO-d_6) δ 8.00 (s, 2H), 6.01−5.90 (m, 4H), 4.29 (t, J = 5.7 Hz, 4H), 3.37−3.28 (m, 4H), 2.90 (q, J = 6.4 Hz, 4H), 2.38 (s, 6H), 1.29 (m, 4H), 1.24−1.15 (m, 4H). ^{13}C{^{1}H} NMR (100 MHz, DMSO-d_6) δ 157.23, 150.88, 137.82, 132.50, 45.73, 38.55, 38.21, 29.31, 25.46, 13.12. HRMS (APCI): calcd for $C_{20}H_{32}N_{10}O_6Na$ [M + Na]$^+$, 531.2398; found, 531.2403.

*Synthesis of 1,1′-(1,3-Phenylenebis(propane-2,2-diyl))bis(3-(2-(2-methyl-5-nitro-1H-imidazol-1-yl)ethyl)urea) (**2**).* The crude material was recrystallized from isopropanol. Yield: 72.0%. ^{1}H NMR (400 MHz, DMSO-d_6) δ 8.00 (s, 2H), 7.27 (s, 1H), 7.24−7.14 (m, 1H), 7.08 (d, J = 7.7 Hz, 2H), 6.28 (s, 2H), 5.91 (t, J = 6.0 Hz, 2H), 4.27 (t, J = 5.4 Hz, 4H), 3.37−3.28 (m, 4H), 2.41 (s, 6H), 1.47 (s, 12H). ^{13}C{^{1}H} NMR (100 MHz, DMSO-d_6) δ 156.22, 150.91, 147.51, 137.84, 132.52, 126.69, 121.80, 120.63, 53.65, 45.84, 37.84, 29.26, 13.25. HRMS (APCI): calcd for $C_{26}H_{36}N_{10}O_6Na$ [M + Na]$^+$, 607.2711; found, 607.2712.

*Synthesis of 1,1′-(Methylenebis(2,6-diethyl-4,1-phenylene))bis(3-(2-(2-methyl-5-nitro-1H-imidazol-1-yl)ethyl)urea) (**3**).* The crude compound was recrystallized in ethanol. Yield: 75.0%. ^{1}H NMR (400 MHz, DMSO-d_6) δ 7.98 (s, 2H), 7.39 (s, 2H), 6.91 (s, 4H), 6.26 (s, 2H), 4.32 (t, J = 5.7 Hz, 4H), 3.78 (s, 2H), 3.45 (s, 4H), 2.44 (s, 6H), 2.39−2.32 (m, 8H), 1.03 (t, J = 7.5 Hz, 12H). ^{13}C{^{1}H} NMR (100 MHz, DMSO-d_6) δ 156.62, 151.47, 141.99, 139.28, 138.55, 133.06, 132.24, 126.11, 46.52, 40.81, 38.72, 24.29, 14.65, 14.00. HRMS (APCI): calcd for $C_{35}H_{46}N_{10}O_6Na$ [M + Na]$^+$, 725.3494; found, 725.3473.

*Synthesis of 1,1′-(Hexane-1,6-diyl)bis(3-(2-(2-methyl-4-nitro-1H-imidazol-1-yl)ethyl)urea) (**4**).* The precipitate was then washed with ethyl acetate to obtain the pure product as a white powder. Yield: 79.0%. ^{1}H NMR (400 MHz, DMSO-d_6) δ 8.21 (s, 2H), 5.94 (t, J = 5.8 Hz, 4H), 4.01 (t, J = 5.7 Hz, 4H), 3.37−3.29 (m, 4H), 2.92 (q, J = 6.5 Hz, 4H), 2.31 (s, 6H), 1.30 (m, 4H), 1.18 (m, 4H). ^{13}C{^{1}H} NMR (100 MHz, DMSO-d_6) δ 157.85, 145.34, 145.30, 122.27, 46.78, 39.50, 39.08, 29.88, 26.03, 12.45. HRMS (APCI): calcd for $C_{20}H_{32}N_{10}O_6Na$ [M + Na]$^+$, 531.2398; found, 531.2400.

*Synthesis of 1,1′-(1,3-Phenylenebis(propane-2,2-diyl))bis(3-(2-(2-methyl-4-nitro-1H-imidazol-1-yl)ethyl)urea) (**5**).* The crude compound was purified by washing with diethyl ether and ethyl acetate. Yield: 79.0%. ^{1}H NMR (400 MHz, DMSO-d_6) δ 8.20 (s, 2H), 7.27 (s, 1H), 7.22−7.09 (m, 1H), 7.11−6.89 (m, 2H), 6.28 (s, 2H), 5.91 (t, J = 6.0 Hz, 2H), 3.98 (t, J = 5.8 Hz, 4H), 3.34−3.27 (m, 4H), 2.32 (s, 6H), 1.47 (s, 12H). ^{13}C{^{1}H} NMR (100 MHz, DMSO-d_6) δ 156.84, 148.16, 145.33, 145.30, 127.22, 122.30, 122.23, 121.19, 54.23, 46.81, 39.08, 29.85, 12.52. HRMS (APCI): calcd for $C_{26}H_{36}N_{10}O_6Na$ [M + Na]$^+$, 607.2711; found, 607.2711.

*Synthesis of 1,1′-(Methylenebis(2,6-diethyl-4,1-phenylene))bis(3-(2-(2-methyl-4-nitro-1H-imidazol-1-yl)ethyl)-urea) (**6**).* Purification was performed by washing the crude compound with dichloromethane to yield a white powder. Yield: 80.0%. ^{1}H NMR (400 MHz, DMSO-d_6) δ 8.18 (s, 2H), 7.39 (s, 2H), 6.92 (s, 4H), 6.26 (m, 2H), 4.04 (t, J = 5.8 Hz, 4H), 3.78 (s, 2H), 3.48−3.37 (m, 4H), 2.44−2.36 (m, 8H), 2.35 (s, 6H), 1.02 (t, J = 7.5 Hz, 12H). ^{13}C{^{1}H} NMR (100 MHz, DMSO-d_6) δ 157.07, 145.75, 145.68, 142.46, 139.50, 132.91, 126.63, 122.98, 47.35, 41.28, 24.76, 24.30, 15.05, 13.10. HRMS (APCI): calcd for $C_{35}H_{46}N_{10}O_6Na$ [M + Na]$^+$, 725.3494; found, 725.3459.

*Synthesis of Isometronidazole (2-(2-Methyl-4-nitro-1H-imidazol-1-yl)ethan-1-ol) (**14**).* A solution of 2-methyl-4-nitro-1*H*-imidazole (0.30 g, 2.4 mmol), potassium carbonate (0.97 g, 7.9 mmol), bromoethanol (830 μL, 11.8 mmol), and potassium iodide (0.39 g, 2.4 mmol) was added to DMF (20.0 mL) in a round bottomed flask, and the mixture was stirred overnight at room temperature. The solvent was evaporated and dried, the mixture was purified by column chromatography in DCM using a methanol gradient (0.0−0.5%), and the product was recrystallized from ethanol/diethyl ether. Yield: 81.0%. ^{1}H NMR (400 MHz, methanol-d_4) δ 8.08 (s, 1H), 4.15−4.08 (m, 2H), 3.87−3.80 (m, 2H), 2.45 (s, 3H). ^{13}C{^{1}H} NMR (100 MHz, methanol-d_4) δ 145.96, 145.48, 121.00, 60.32, 49.17, 11.48. HRMS (APCI): calcd for $C_6H_9N_3O_3Na$ [M + H]$^+$, 194.0536; found, 194.0537.

Gelation Details. *Gelation Test.* In a standard 7.0 mL vial (ID = 15.0 mm), an appropriate amount of the gelator and 1.0 mL of suitable solvent were added, and the vial was sealed. The mixture was then sonicated and heated until a clear solution was obtained. The solution was left undisturbed for gelation, and a vial-inversion test was performed to confirm gelation.

Minimum Gel Concentration (MGC). The gel was prepared following the above procedure by dissolving the compounds in 1.0 mL of solvent. An additional amount of the solvent was added in portions, and the gelation process was repeated until a trace amount of the solvent was observed on the top of the gel. The excess solvent was removed, and MGC of the gelator was determined by calculating the weight percent of the compound.

T_{gel} Experiment. The appropriate amount of the gelator was taken in a standard 7.0 mL vial, and 1.0 mL of solvent was added. The mixture was sonicated and heated to dissolve and left undisturbed. A tiny spherical glass ball was carefully put on the top of the gel after 24 h and was heated in an oil bath fitted with a thermosensor and magnetic stirrer. The temperature of the oil bath was steadily raised by 10.0 °C per minute. The temperature at which the glass ball touched the bottom of the vial was recorded as T_{gel}.

Rheology. Rheological experiments were performed in nitrobenzene. The mechanical strength of the gelators was measured using

https://doi.org/10.1021/acs.cgd.1c00659
Cryst. Growth Des. 2021, 21, 5383−5393

an MCR 102 Anton Paar modular compact rheometer with a 2.5 cm stainless steel parallel plate geometry. Gels were prepared by dissolving 30.0 mg of the corresponding gelator in 1.0 mL of nitrobenzene. Experiments were carried out carefully by scooping a ~1.0 mL portion of gel on the plate. A Peltier temperature control hood was used to avoid the solvent evaporation and to maintain a temperature of 25.0 °C for frequency and amplitude sweeps. Amplitude sweeps were performed with a constant frequency of 1.0 Hz and log ramp strain (γ) = 0.01−100%, while the frequency sweeps were carried out between 0.1 and 10.0 Hz within the linear viscoelasticity domain (0.02% strain).

Scanning Electron Microscopy (SEM). The surface morphologies of the xerogels were examined using SEM. Gels of compounds (**1**−**6**) were prepared in nitrobenzene at 3.0 wt/v %, and the gel was filtered after 24 h and dried in air to obtain the xerogel. A small portion of the xerogel was placed on a pin mount with the carbon tab on top, which was coated with gold for 5−6 min and was loaded on a Leo Supra 25 microscope at an operating voltage of 3.0 kV and a working distance 3−4 mm. An in-lens detector was used to record the SEM images. We have also performed the SEM of dried gel of gelator **3** from DMSO/water (7:3, v/v, 3.0 wt/v %), ethanol (0.3 wt/v %), and 1,4-dioxane (0.5 wt/v %). The SEM of gelators **2** and **4** was performed on the xerogels from DMSO/water (1:1, v/v) at 5.0 wt/v %.

Crystallography. *Single-Crystal X-ray Diffraction.* Single crystals of metronidazole and isometronidazole amine hydrochlorides were obtained by the slow evaporation of the acidic solution of the compounds in DMF/water (1:1 v/v) and ethanol/water (1:1 v/v), respectively. X-ray quality crystals of compound **2** were obtained by the slow evaporation of a nitromethane solution of the compound. X-ray analysis was performed on a Bruker D8 Venture (Photon100 CMOS detector) diffractometer equipped with Cryostream (Oxford Cryosystems) open-flow nitrogen cryostats. The data for the crystals of metronidazole (**9**·2HCl) and isometronidazole (**12**·HCl)-based amines were collected using CuK_α radiation (λ = 1.542 Å) at 295(2) K, and MoK_α radiation (λ = 0.71073 Å) at 150(2) K was used for gelator **2**. Apex-III software (Bruker AXS: Madison, WI, 2015) was used for the unit cell determination, data collection, data reduction, structure solution/refinement, and empirical absorption correction. All structures were solved by direct method and refined by the full-matrix least-squares on F^2 for all data using SHELXTL.[47] The disordered imidazole moieties and the solvent molecule of gelator **2** were modeled using free variable (FVAR) instructions and were refined isotropically. All other nondisordered non-hydrogen atoms were refined anisotropically. All the hydrogen atoms were placed in the calculated positions and refined using a riding model. Crystallographic data for the structures have been deposited to Cambridge Crystallographic Data Centre as supplementary publication (CCDC nos. 2088742−2088744).

Powder X-ray Diffraction (PXRD). The PXRD of the isolated metronidazole crystals from gel phase crystallization and the solution phase were recorded on a PANalytical instrument with 2θ ranging from 4.0−60.0°. The crystals were isolated from the crystallizing medium, washed with hexane, dried, and ground to fine powder, and PXRD was recorded. We have also performed the PXRD of the synthesized metronidazole and isometronidazole-based amine hydrochlorides to ensure the purity of bulk products. Xerogels of **2** were prepared by filtering the gels from the corresponding solvents, and the PXRD was performed after drying the xerogels in the fume hood for 16 h.

Gel Phase Crystallization. The gel phase crystallization was performed in nitrobenzene and aqueous solution (1:1, v/v) of DMSO and DMF. The experiments were performed in a standard 7.0 mL vial with the gelator and the drug molecule in 1.0 mL of the solvent. Experiments were performed at various concentrations of the gelator and the drug moiety to study the effect on the gel phase crystallization. The gels were removed after 24 h and analyzed under a Leica MC190 HD digital microscope. We have repeated several batches of gel phase crystallization experiments, and the gels were analyzed at different time intervals (up to 3 weeks).

RESULTS AND DISCUSSION

Metronidazole and isometronidazole-mimicking bis(urea) compounds (Scheme 2) were synthesized by reacting the corresponding amine precursors of these compounds with different diisocyanates (Scheme 3).

Scheme 2. Metronidazole and Isometronidazole-Mimicking Bis(urea) Compounds

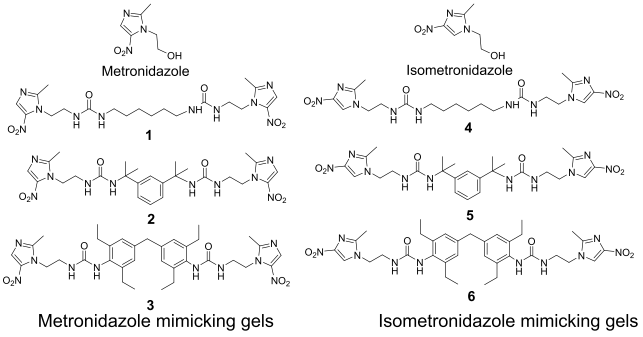

Scheme 3. Synthesis of Metronidazole and Isometronidazole Bis(urea) Compounds

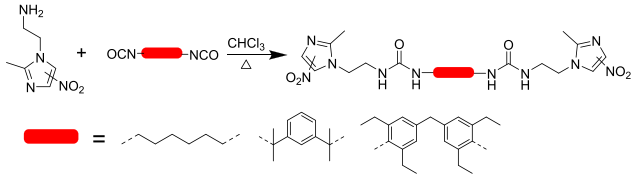

We selected diisocyanates with different linkers, namely, hexylene, sterically hindered *m*-dipropylenephenylene and tetraethyl diphenylmethane derivatives, which have been previously used as effective linkers for LMWGs.[10] The preparation of the amine precursors of metronidazole and isometronidazole is outlined in Scheme 4.

Scheme 4. Synthesis of Metronidazole and Isometronidazole-Based Amine Precursors

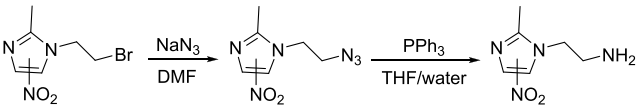

The hydroxyl group of metronidazole was converted to the bromo derivative *via* bromination, while the bromo derivative of isometronidazole was synthesized from 2-methyl-4(5)-nitroimidazole *via* substitution reaction with 1,2-diethyl bromide (Scheme S2, see Supporting Information).[10,48] The bromo derivatives were converted to azide and then reduced to the corresponding amines in the presence of triphenylphosphine (Scheme 4). The products were then converted to the hydrochloride salts by treatment with dilute HCl.

The molecular structure of these two isomeric amine hydrochloride salts was confirmed by single-crystal X-ray diffraction (Tables S1 and S2 and Figure S13, see Supporting Information). The reaction of the metronidazole amine derivative in the presence of Et_3N with the diisocyanates outlined in Scheme 3 in chloroform yielded compounds **1**, **2**,

https://doi.org/10.1021/acs.cgd.1c00659
Cryst. Growth Des. 2021, 21, 5383−5393

and **3**, respectively. Similarly, the reaction of the isometronidazole amine derivative with these diisocyanates yielded **4**, **5**, and **6**.

Gelation Studies. The gelation properties of the bis(urea) compounds were tested in a wide range of solvents (Table S3, see Supporting Information). The gelation tests were carried out by heating the gelator (10 mg) in a suitable solvent (1.0 mL) in a sealed vial (1.0 wt/v %) to give a transparent solution. The vial was left undisturbed, and the gel formation was confirmed by a vial inversion test.

Metronidazole-mimicking compounds (**1**−**3**) formed gels in nitrobenzene at 1.0 wt/v % (Figure 1), and gel formation was confirmed by a simple inversion test in all cases. Compound **2** formed gel in 1,2-dibromoethane, chlorobenzene, and 1,4-dioxane at 2.0 wt/v %. The metronidazole-mimicking diphenylmethane derivative (**3**) formed gel in cyclopentanone and cyclohexanone at 1.0 wt/v % and in ethylene glycol at 2.0 wt/v %. The insolubility of compound **3** at 1.0 wt/v % in alcohols and nonpolar solvents prompted us to check the gelation properties at a lower concentration (≤0.5 wt/v %), and gelation was observed in ethanol, *n*-propanol, *n*-butanol, *n*-pentanol, 1,4-dioxane, and nitromethane. The gelation studies of isometronidazole-mimicking compounds (**4**−**6**) revealed that gelation was observed at a higher concentration (3.0 wt/v %) in nitrobenzene compared to metronidazole derivatives **1**−**3**. In the case of compound **5**, sonication was required to induce gelation in nitrobenzene prior to cooling. The diphenylmethane-derived isometronidazole analogue (**6**) gelled ethylene glycol at 3.0 wt/v % and DMF at 4.0 wt/v %. We have also studied the gelation properties of these compounds in aqueous solution (1:1, v/v) of DMF and DMSO. Compound **6** formed gel in DMF/water at 3.0 wt/v %, and compound **4** formed gels in DMSO/water and DMF/water at 4.0 and 5.0 wt/v %, respectively. Compound **3** formed gels in DMF/water and DMSO/water mixture at 3.0 wt/v % when the solvent combination was changed to 7:3 (v/v).

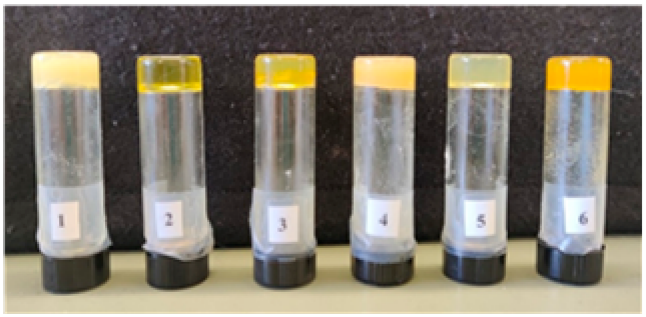

Figure 1. Gels of bis(urea) compounds (**1**−**6**) obtained from nitrobenzene.

The minimum gel concentration (MGC) is the minimum amount of the compound required to form a self-supporting gel. The MGC of the gelators was evaluated in various solvents (Table S4, see Supporting Information). The MGC measurements of metronidazole-based gelators **1**−**3** in nitrobenzene (Table 1) establish that compound **3** has lower MGC values. Comparing the MGCs of mimetic and nonmimetic gels in nitrobenzene indicated that the MGCs of the nonmimetic compounds **4**−**6** are higher. Compound **3** can be considered as a supergelator in 1-propanol, ethanol, 1-butanol, nitromethane, 1,4-dioxane, and 1-pentanol because the MGC is less than 0.5 wt/v % (Table S4, see Supporting Information). The MGC in DMSO/water for gelator **2** (1:1, v/v) and **3** (7:3, v/v) is 2.5 wt/v % and 3.0 wt/v %, respectively.

Table 1. Minimum Gel Concentration and T_{gel} at 3.0 wt/v % of the Gelators in Nitrobenzene

compound	MGC (wt/v %)	T_{gel} (°C)
1	0.8	103.7
2	0.9	84.3
3	0.5	151.4
4	2.8	145.4
5	2.5	118.8
6	2.8	153.8

Thermal Stability. The thermal stability of the gels was evaluated by recording the transition temperature (T_{gel}) at which the gel converts to the solution phase. T_{gel} experiments were performed for all gels at 3.0 wt/v % in nitrobenzene, and the results indicate that gelator **2** has the lowest T_{gel} value (Table 1). The T_{gel} experiments performed at a lower concentration (1.0 wt/v %) for compounds **1**−**3** in nitrobenzene revealed the highest thermal stability for gels of **3** (Table S5, see Supporting Information), and the thermal stability increases with concentration. The thermal stability of the diphenylmethane-derived gelator is higher than the other gelators in most cases (Table S5, see Supporting Information). The T_{gel} of the mimetic and the nonmimetic gelators in nitrobenzene were compared to see the effect of the spatial arrangement of the functional groups, which indicates that the thermal stability of the mimetic gels (**1**−**3**) is lower than nonmimetic gelators (**4**−**6**).

Mechanical Strength. Rheology has been used to evaluate the solid-like properties and the stiffness of the gels.[49,50] Rheology is used to quantify the deformation and flow characteristics of supramolecular gels, and rheological experiments provide information about the gel structural characteristics.[51−53] The mechanical properties of the bis(urea) gelators were measured at 3.0 wt/v % in nitrobenzene. A strain sweep was performed to determine the linear viscoelastic region (LVR), at a constant frequency of 1.0 Hz, and the elastic modulus (G') was independent of the applied strain. Most of the gelators displayed a constant G' up to 0.1% strain, except for compound **1**, where the G' value decreased after 0.02% (Figure 2). The cross-over point for gelators **2** and **5** was found to be around 0.5−3.0% strain, while the cross-over point for gelators **1**, **3**, **4**, and **6** is around 5.0−15.0% strain.

Frequency sweep experiments were performed within a range of 0.1−10 Hz at a constant strain of 0.02%. A constant elastic (G') and viscous (G'') moduli under varying frequency establish that these materials are true gels (Figure S14). Interestingly, the mimetic gelator **2** displays higher G' and G'' compared to all the other gelators, indicating a comparatively stronger network in nitrobenzene. Gels of compounds **2** and **5** are stiffer (>200 kPa) compared to other bis(urea) gelators in nitrobenzene and the elastic modulus (G') is around 2-fold higher than the other bis(urea) gels. Comparison of the mimetic gelators (**1**−**3**) revealed that gelator **2** displayed higher G' and G'' values indicating a strong gel network. The mechanical strength of the gel network in **3** was more robust than gelator **1**. For the nonmimetic gelators (**4**−**6**), the gel of **5** was found to be a stiffer gel, and the G' and G'' values of gels of **4** and **6** were comparable and low, suggesting a weaker gel network in these gels. The difference in mechanical strength

https://doi.org/10.1021/acs.cgd.1c00659
Cryst. Growth Des. 2021, 21, 5383−5393

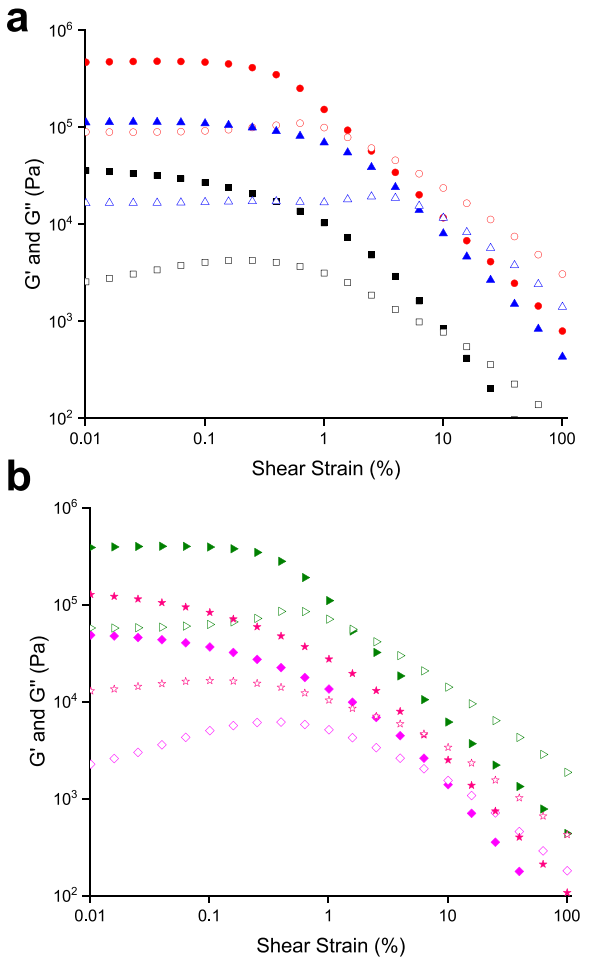

Figure 2. Amplitude sweep experiments of bis(urea) gels (3.0 wt/v %) in nitrobenzene at 25.0 °C with a constant frequency of 1.0 Hz. Color codes: (a) gelator-**1** G' (black solid square) and G'' (black open square), gelator-**2** G' (red solid circle) and G'' (red open circle), gelator-**3** G' (blue solid triangle) and G'' (blue open triangle up), and (b) gelator-**4** G' (pink solid diamond) and G'' (pink open diamond), gelator-**5** G' (green solid triangle right-facing) and G'' (green open triangle right-facing), gelator-**6** G' (orange solid star) and G'' (orange open star).

for **2** and **5** may be attributed to the favorable network formation in nitrobenzene compared to others.

Gel Morphology. The morphology of the dried gel fibrils was analyzed by SEM. SEM performed on the dried gels of all the gelators from nitrobenzene (3.0 wt/v %) revealed a fibrous network in most cases. Gelator **1** displayed needle-shaped morphology (Figure 3a) with a thickness ranging from 1.0 to 3.0 μm. Gelator **2**, **3**, and **5** displayed an entangled fibrous network (Figure 3b and Figures S15–S16, see Supporting Information), and the diameter of the fibers ranged from 200 to 400 nm. The gelator **4** displayed a plate-shaped morphology with a diameter of around 1.0–4.0 μm (Figure 3c). The dibenzyl linker-based gelator **6** displayed long needle-shaped morphology (Figure 3d).

SEM images recorded for gelator **3** at 3.0 wt/v % in DMSO/water (7:3, v/v) displayed needle-shaped morphology (Figure 4a).[54−56] Similarly, the SEM images of gelator **4** from DMSO/water (1:1, v/v) at 4.0 wt/v % displayed thicker needles (Figure S17, see Supporting Information). We also performed the SEM of gelator **3** xerogel obtained from 1,4-dioxane (0.5

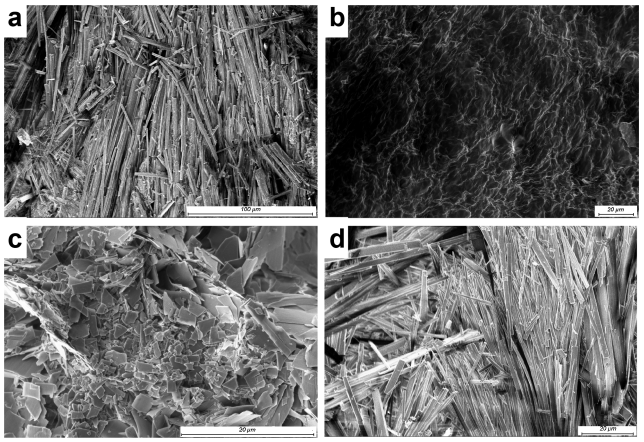

Figure 3. SEM images of the xerogel of (a) **1**, (b) **2**, (c) **4**, and (d) **6** from nitrobenzene at 3.0 wt/v %.

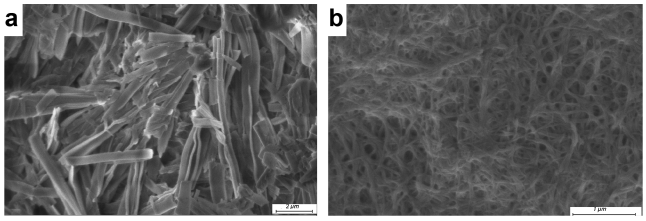

Figure 4. SEM images of gelator **3**: from (a) DMSO/water (7:3, v/v) at 3.0 wt/v % and (b) 1,4-dioxane (0.5 wt/v %).

wt/v %, Figure 4b) and ethanol (0.33 wt/v %, Figure S18, see Supporting Information), and the images displayed helical fibrous aggregates with fiber thickness ranging from 20 to 40 nm.

Single-Crystal X-ray Diffraction. X-ray quality single crystals of **2** were obtained *via* slow cooling of the nitromethane solution and characterized by X-ray crystallography (Figure S19 and Tables S1 and S2, see Supporting Information). The compound displays the characteristic one-dimensional (1-D) hydrogen-bonded urea α-tape motif resulting from the complementary crisscross urea hydrogen bonding from one of the urea moieties (Figure 5a). These 1-D zigzag tapes interact with adjacent tapes via N−H···O hydrogen-bonding interaction arising from the second urea

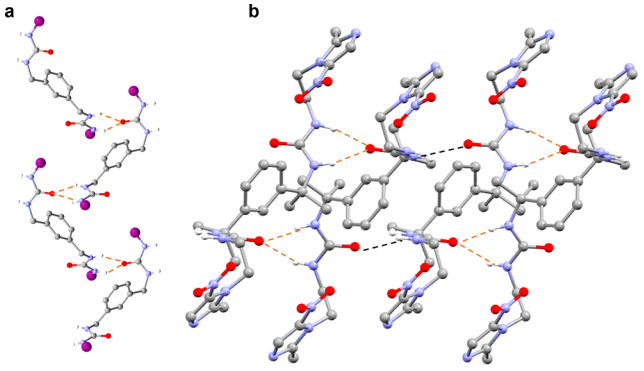

Figure 5. Illustration of crystal structure in **2** (a) 1-D hydrogen-bonded zigzag chains via complementary urea hydrogen bonding (the purple sphere represents the metronidazole mimetic fragment) and (b) adjacent 1-D chains interact with each other (broken black lines) to form a 2-D hydrogen-bonded network.

https://doi.org/10.1021/acs.cgd.1c00659
Cryst. Growth Des. 2021, 21, 5383−5393

motif to form a 2-D hydrogen-bonded sheet architecture Figure 5b). The nitrogen and oxygen atoms of the imidazole moiety of adjacent 2-D networks interact with each other to form voids with entrapped nitromethane (Figure S19, see Supporting Information). The comparison of the powder X-ray diffraction pattern (PXRD) of the bulk crystal with the simulated pattern obtained from the crystal structure[21,56−58] confirmed the phase purity of the crystals (Figure S20, see Supporting Information). The comparison of the powder diffraction pattern of either the native gel or the dried gel with the calculated pattern from the crystal structure can provide information about the structure of xerogels.[21,56−59] Although the drying process can result in artifacts,[60] this approach may provide useful information about the self-assembly process in LMWGs.[1,7,21,56−59] The comparison of the PXRD pattern of the dried gel from nitrobenzene with the crystal structure indicated that the two materials are different solid forms. However, the PXRD pattern of the xerogel of **2** from nitrobenzene and chlorobenzene matched with the pattern of bulk crystals of a second solid form of **2** obtained from isopropanol. The PXRD pattern of the DMSO/water (1:1, v/v) xerogels proved to be more similar to the pattern calculated from the single-crystal structure (Figure S21, see Supporting Information). These results indicate that there are at least two types of gelator structure obtained depending on the crystallizing or gelling solvent.

Gel Phase Crystallization. The ability of the gelators to gel nitrobenzene prompted us to select nitrobenzene as a solvent for gel phase crystallization of the target drug material. The metronidazole was purified by recrystallization from DMSO/water (1:1, v/v) prior to crystallization studies. Initially, we performed the solution phase crystallization of metronidazole from nitrobenzene to optimize the crystallization conditions. Plate-shaped crystals of metronidazole in a herringbone fashion (Figure 6a) were observed in nitrobenzene (30 mg/mL) after a day (Table S6, see Supporting Information). Experiments performed at higher concentrations also resulted in crystals with a similar morphology after 2−3 h.

Gel phase crystallization was performed by dissolving metronidazole and the gelators in 1.0 mL of nitrobenzene, and the mixture was sonicated and heated to yield a transparent solution. The solution was left undisturbed at ambient temperature, and gelation was observed in 5−10 min. The gels were analyzed by polarized light microscopy after 24 h, which indicated the formation of crystals within the gels in most cases (Table S7, see Supporting Information). The optimized concentration of metronidazole was found to be 50 mg/mL, and the experiments performed with 30 mg/mL did not result in any crystals after 2−3 weeks. The experiments were performed at 2.0 wt/v % for gelator **1** because the gels were not stable at lower concentrations in the presence of crystallization substrate. Analysis of the crystals obtained from gelator **1** indicated that needle-shaped crystals were formed (Figure 6b). The experiments performed in gelators **2** at 1.0 wt/v % yielded transparent gels, and crystal growth was observed after 24 h (Figure S22, see Supporting Information). The morphology of the crystals was found to be similar to the crystals from gelator **1** (Figure 6c).

Gel phase crystallization in gelator **3** at 1.0 wt/v % resulted in a herringbone pattern of needle-shaped crystals clumped together (Figure 6d). Gel phase crystallization experiments were performed in several batches, and the crystals were analyzed at different time intervals over 2−3 weeks, which

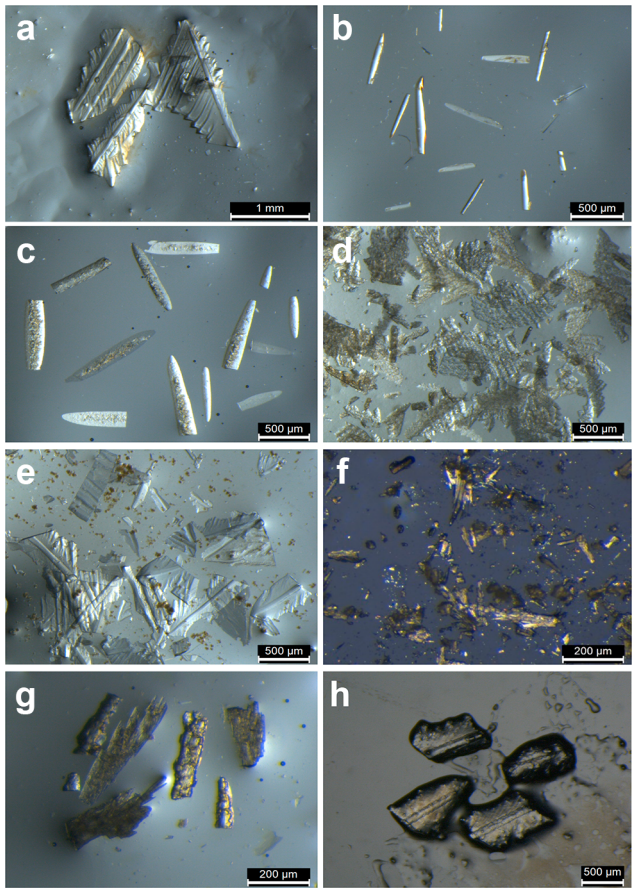

Figure 6. Comparison of crystals of metronidazole from solution and gel phase crystallization (GPC) in nitrobenzene. (a) Solution phase and (b) gel phase crystallization in **1**, (c) **2**, (d) **3**, (e) **4**, (f) **5**, (g) **6**, and (h) alanine gelator, respectively.

indicated that the morphologies of the crystals were consistent batch-to-batch and over time. The crystallization experiments were repeated with increasing concentrations of metronidazole (75 and 100 mg/mL), and the morphologies were similar to the 50 mg/mL experiments. The experiments performed at 3.0 wt/v % of the gelators **1**−**3** also resulted in morphologies similar to 1.0 wt/v % of the corresponding gelators.

For comparison, gel phase crystallization was also carried out with the isometronidazole-mimetic gelators **4**−**6**. A gelator concentration of 6.0 wt/v % (Table S8, see Supporting Information) was used to avoid dissolution of gels in the presence of crystallization substrate. The experimental procedure was similar to the mimetic gels, and partial gels were observed for gelator **5** in the presence of metronidazole. Plate-shaped crystals in a herringbone morphology were observed for gels of gelator **4**, and similar results were observed at higher concentrations of metronidazole (Figure 6e). Gel phase crystallization experiments in gelator **5** were achieved by sonicating the mixture prior to cooling, but crystals were not formed even at a higher concentration of metronidazole after a month. Analysis of the partial gels of gelator **5** obtained by a normal gel phase crystallization procedure indicated the formation of microneedle crystals of metronidazole (Figure 6f). The experiments performed with gelator **6** resulted in clusters of crystals arranged in a herringbone fashion (Figure 6g). Crystallization of metronidazole was also undertaken in an unrelated (non-metronida-

https://doi.org/10.1021/acs.cgd.1c00659
Cryst. Growth Des. 2021, 21, 5383−5393

zole-mimetic) bis(urea) gelator based on L-phenyl alanine methyl ester at 2.0 wt/v % (Figure S23, see Supporting Information), which resulted in plate-shaped crystals clumped in a herringbone pattern (Figure 6h). The needle-shape morphology obtained in the case of the mimetic gels may be attributed to the epitaxial growth of metronidazole crystals on gel fibers due to their favorable interactions with structurally similar functional groups of the LMWGs.

Face indexing of representative crystals grown from solution and from gels of compounds **1**−**6** revealed a complex and varied influence of all the gels on morphology. The solution-grown crystals have a relatively simple morphology and express faces with mainly low indices, namely, $(\bar{1}00)$, $(0\bar{1}0)$, and $(00\bar{1})$, as well as a large $(1\bar{1}5)$ face. The morphology of gel-grown crystals proved much more complex and unique to each gel with multiple high-index faces being expressed. For example, crystals obtained from nitrobenzene gels of **3** exhibit a wedge shape expressing a large $(0\bar{9}7)$ face, Figure 7. Other

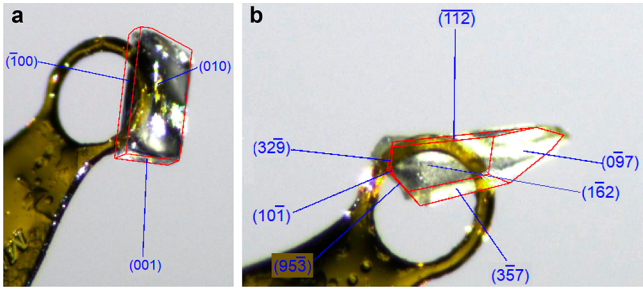

Figure 7. Face-indexed morphology of metronidazole crystals (a) grown from nitrobenzene solution, (b) wedge-shaped crystal from a nitrobenzene gel of metronidazole-mimetic gelator **3** expressing higher-order faces.

gel-grown samples all expressed a wide variety of faces and asymmetric morphology (Supporting Information Figures S27−S33, see Supporting Information). This implies a variety of specific adsorption modes of the gel fibers to the growing crystals.

We performed the rheology experiments of the gels in the presence of metronidazole (50 mg/mL) in nitrobenzene at 3.0 wt/v %, and isometronidazole-mimicking gels formed partial gels. The mechanical strength of the mimetic gels (**1**−**3**) was increased in the presence of the drug additive (Figure S34, see Supporting Information). At higher gelator concentration (6.0 wt/v %), gels were observed in all cases with increased mechanical strength compared to the corresponding gels without drug additives, expect for **4** and **5** (Figures S35−S36, see Supporting Information). This prompted us to check whether the discrepancy in the stabilities is related to the kinetic trapping of the self-assembled structures by annealing the gels.[61,62] This was achieved by performing a gel-to-sol transition by heating the gels after 12 h, and the solution thus obtained was left undisturbed for gelation. The mechanical strength of mimetic and nonmimetic gels did not show any drastic change compared to the corresponding nonannealed gels (Figures S37−S40, see Supporting Information). The mechanical strength of the mimetic gels (**1**−**5**) in the presence of the metronidazole displayed similar results compared to the corresponding nonannealed gels, but the mechanical strength of **6** decreased after annealing (Figures S38 and S40, see Supporting Information). However, the thermal stabilities of the gels were found to be lower in the presence of the additives (Tables S9−S11). The enhanced mechanical properties of the mimicking gelators (**1**−**3**) in the presence of crystallization substrate indicate a favorable interaction of the gelator molecules with the substrates presumably due to the similarity in the functional group. However, a reverse phenomenon was observed for the nonmimetic gelators (**4**−**6**), which clearly indicates the importance of structural similar functional groups in LMWGs and the crystallization substrates.

In contrast to nitrobenzene, solution phase crystallization of metronidazole in aqueous DMF and DMSO (1:1 and 7:3, v/v) resulted in long, needle-shaped crystals (Figure S24, see Supporting Information). The gel phase crystallization with gelator **2** in DMSO/water (1:1, v/v) resulted in needle-shaped crystals, while microneedle-shaped crystals were obtained with gelator **3** in DMSO/water (7:3, v/v) and gelator **4** in DMSO/water (1:1, v/v), (Figure S25, see Supporting Information). The gel phase crystallization in DMF/water (1:1, v/v) with gelator **4** and **6** resulted in microneedle crystals, respectively. Thus, unlike nitrobenzene, gel phase crystallization in aqueous DMF and DMSO does not show crystal habit modification with any gelator, presumably due to the interaction of LMWGs with hydrogen-bonding solvents, which prevents the drug from interacting with the complementary sites in the gelators.

The role of LMWGs in tuning crystallization was analyzed by performing solution phase crystallization in the presence of dissolved gelators **3**, **4**, **5**, and **6**, which resulted in plate-shaped crystals clumped in a herringbone pattern similar to the solution phase crystal morphology (Figure S26, see Supporting Information). However, the experiments with **1** and **2** displayed a mixture of plate-shaped crystals with herringbone patterns and needle-shaped crystals. These results suggest that the gel medium plays a vital role in inducing crystal habit modification rather than just the gelator molecule itself in solution. The solution/gel phase crystallization of isometronidazole did not yield any crystals.

X-ray analysis performed on all the crystals revealed no difference in polymorphic form with the known form I[36] produced in all cases. The phase purity of the bulk crystal was analyzed by comparing the PXRD of the bulk crystal with the simulated pattern obtained from the crystal structure reported.[21,56−58] These data were obtained using bulk crystals isolated from the gel phase and solution phase crystallization experiments. The comparison of the PXRD pattern of the metronidazole crystals from the solution and gel phase crystallization with the simulated pattern of the crystal structure revealed superimposable patterns (Figure 8 and Figure S41, see Supporting Information), indicating phase purity of the bulk solid.

CONCLUSIONS

We have synthesized six bis(urea) compounds with functional groups mimicking either metronidazole (**1**−**3**) or its isomer isometronidazole (**4**−**6**). The gelation studies revealed that metronidazole-mimetic compound **3** gels various solvents compared to the isomeric gelator **6**. The T_{gel} experiments suggested that gels based on the isometronidazole gelators **4**−**6** have a higher thermal stability than the mimetic gels **1**−**3**. The comparison of the mechanical strength of the gelators in nitrobenzene revealed that the metronidazole-mimetic gelators **2** and **3** are more mechanically robust compared to the isomeric analogues **5** and **6**, but the hexylene-linker based gelator **4** forms a stronger gel compared with that of gelator **1**. The morphologies of the dried gels were analyzed by SEM,

https://doi.org/10.1021/acs.cgd.1c00659
Cryst. Growth Des. 2021, 21, 5383−5393

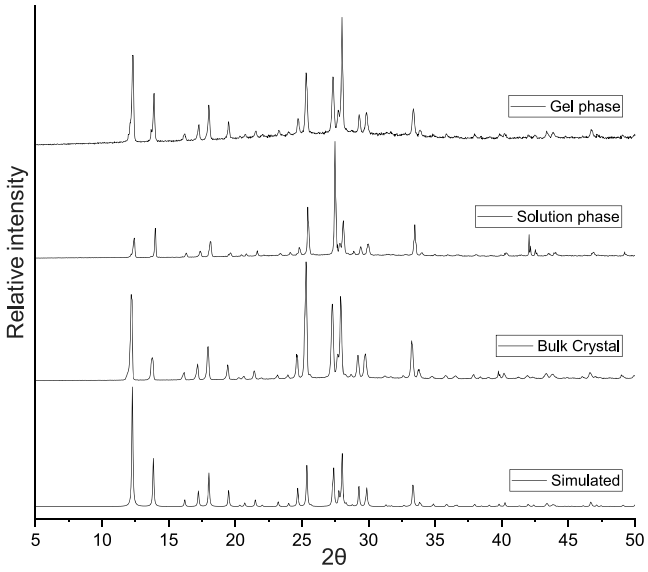

Figure 8. Comparison of PXRD pattern of metronidazole: simulated from single-crystal data, bulk crystals obtained from DMSO/water, crystals from solution phase and gel phase crystallization from gelator **1** in nitrobenzene.

which showed the presence of the entangled networks in most cases. Gel phase crystallization was performed in nitrobenzene since all the compounds formed gels in this solvent. The morphology of metronidazole crystals obtained from solution phase and gel phase crystallization was analyzed by polarized light microscopy. Plate-shaped crystals aggregated in a herringbone fashion were observed from solution phase crystallization. Crystallization from the isometronidazole-based gels displayed different morphologies such as plate-shaped (**4**), microcrystals (**5**), and thicker needles (**6**). The morphologies of the crystals obtained from the mimetic metronidazole gel (**1**−**3**) were consistent, displaying needle-shaped crystals, and the needle-shaped crystals in **3** were clumped together in a herringbone fashion. The results indicate that crystal habit modification (plate to needle morphology) arises selectively from gels based on the mimetic gelators. This crystal habit modification can be attributed to adsorption of the growing crystals onto the surface of the gel fibers and potentially epitaxial crystal growth in the case of the mimetic gels.

■ ASSOCIATED CONTENT

Supporting Information

The Supporting Information is available free of charge at https://pubs.acs.org/doi/10.1021/acs.cgd.1c00659.

^{1}H NMR spectra, further gelation studies, rheology, SEM images, single-crystal X-ray diffraction, and PXRD of metronidazole/isometronidazole mimetic amines and gelator **2**, face indexing and comparison of PXRD metronidazole from different gelators (PDF)

Accession Codes

CCDC 2088742−2088744 contain the supplementary crystallographic data for this paper. These data can be obtained free of charge via www.ccdc.cam.ac.uk/data_request/cif, or by emailing data_request@ccdc.cam.ac.uk, or by contacting The Cambridge Crystallographic Data Centre, 12 Union Road, Cambridge CB2 1EZ, UK; fax: +44 1223 336033.

■ AUTHOR INFORMATION

Corresponding Authors

Krishna K. Damodaran − *Department of Chemistry, Science Institute, University of Iceland, Dunhagi 3 107 Reykjavík, Iceland;* orcid.org/0000-0002-9741-2997; Phone: +354 525 4846; Email: krishna@hi.is; Fax: +354 552 8911

Jonathan W. Steed − *Department of Chemistry, Durham University, Durham DH1 3LE, U.K.;* orcid.org/0000-0002-7466-7794; Email: jon.steed@durham.ac.uk

Author

Sreejith Sudhakaran Jayabhavan − *Department of Chemistry, Science Institute, University of Iceland, Dunhagi 3 107 Reykjavík, Iceland*

Complete contact information is available at: https://pubs.acs.org/10.1021/acs.cgd.1c00659

Notes

The authors declare no competing financial interest.

■ ACKNOWLEDGMENTS

We thank University of Iceland Research Fund and Science Institute for funding. S.S.J. thanks the University of Iceland for the doctoral research grant. We thankfully acknowledge Dr. Dmitry S. Yufit, Department of Chemistry, Durham University, U.K., for face indexing the crystals from different gelators. We also acknowledge Dr. Sigríður Jónsdóttir and Dr. Friðrik Magnus, University of Iceland, for NMR/mass spectroscopy and powder X-ray diffraction analysis, respectively. We thank Rannís Iceland for infrastructure grants (150998-0031 and 191763-0031) for a single-crystal X-ray diffractometer and rheometer.

■ REFERENCES

(1) Dastidar, P. Supramolecular gelling agents: can they be designed? *Chem. Soc. Rev.* **2008**, *37* (12), 2699−2715.

(2) de Loos, M.; Feringa, B. L.; van Esch, J. H. Design and Application of Self-Assembled Low Molecular Weight Hydrogels. *Eur. J. Org. Chem.* **2005**, *2005* (17), 3615−3631.

(3) Estroff, L. A.; Hamilton, A. D. Water Gelation by Small Organic Molecules. *Chem. Rev.* **2004**, *104* (3), 1201−1218.

(4) George, M.; Weiss, R. G. Molecular Organogels. Soft Matter Comprised of Low-Molecular-Mass Organic Gelators and Organic Liquids†. *Acc. Chem. Res.* **2006**, *39* (8), 489−497.

(5) Hirst, A. R.; Escuder, B.; Miravet, J. F.; Smith, D. K. High-Tech Applications of Self-Assembling Supramolecular Nanostructured Gel-Phase Materials: From Regenerative Medicine to Electronic Devices. *Angew. Chem., Int. Ed.* **2008**, *47* (42), 8002−8018.

(6) Steed, J. W. Anion-tuned supramolecular gels: a natural evolution from urea supramolecular chemistry. *Chem. Soc. Rev.* **2010**, *39* (10), 3686−3699.

(7) Yu, G.; Yan, X.; Han, C.; Huang, F. Characterization of supramolecular gels. *Chem. Soc. Rev.* **2013**, *42* (16), 6697−6722.

(8) Liesegang, R. E. Chemische Reaktionen in Gallerten. *Naturwiss. Wochenschr.* **1896**, *11*, 353.

(9) Kumar, D. K.; Steed, J. W. Supramolecular gel phase crystallization: orthogonal self-assembly under non-equilibrium conditions. *Chem. Soc. Rev.* **2014**, *43* (7), 2080−2088.

(10) Foster, J. A.; Damodaran, K. K.; Maurin, A.; Day, G. M.; Thompson, H. P. G.; Cameron, G. J.; Bernal, J. C.; Steed, J. W. Pharmaceutical polymorph control in a drug-mimetic supramolecular gel. *Chem. Sci.* **2017**, *8* (1), 78−84.

(11) Hektisch, H. K.; Dennis, J.; Hanoka, J. I. Crystal growth in gels. *J. Phys. Chem. Solids* **1965**, *26* (3), 493−496.

(12) Duffus, C.; Camp, P. J.; Alexander, A. J. Spatial Control of Crystal Nucleation in Agarose Gel. *J. Am. Chem. Soc.* **2009**, *131* (33), 11676−11677.
(13) Buerkle, L. E.; Rowan, S. J. Supramolecular gels formed from multi-component low molecular weight species. *Chem. Soc. Rev.* **2012**, *41* (18), 6089−6102.
(14) Edwards, W.; Smith, D. K. Enantioselective Component Selection in Multicomponent Supramolecular Gels. *J. Am. Chem. Soc.* **2014**, *136* (3), 1116−1124.
(15) Cross, E. R.; Sproules, S.; Schweins, R.; Draper, E. R.; Adams, D. J. Controlled Tuning of the Properties in Optoelectronic Self-Sorted Gels. *J. Am. Chem. Soc.* **2018**, *140* (28), 8667−8670.
(16) Draper, E. R.; Eden, E. G. B.; McDonald, T. O.; Adams, D. J. Spatially resolved multicomponent gels. *Nat. Chem.* **2015**, *7*, 848.
(17) Colquhoun, C.; Draper, E. R.; Eden, E. G. B.; Cattoz, B. N.; Morris, K. L.; Chen, L.; McDonald, T. O.; Terry, A. E.; Griffiths, P. C.; Serpell, L. C.; Adams, D. J. The effect of self-sorting and co-assembly on the mechanical properties of low molecular weight hydrogels. *Nanoscale* **2014**, *6* (22), 13719−13725.
(18) Raeburn, J.; Adams, D. J. Multicomponent low molecular weight gelators. *Chem. Commun.* **2015**, *51* (25), 5170−5180.
(19) Estroff, L. A.; Addadi, L.; Weiner, S.; Hamilton, A. D. An organic hydrogel as a matrix for the growth of calcite crystals. *Org. Biomol. Chem.* **2004**, *2* (1), 137−141.
(20) Aparicio, F.; Matesanz, E.; Sanchez, L. Cooperative self-assembly of linear organogelators. Amplification of chirality and crystal growth of pharmaceutical ingredients. *Chem. Commun.* **2012**, *48* (46), 5757−5759.
(21) Ghosh, D.; Ferfolja, K.; Drabavičius, Ž.; Steed, J. W.; Damodaran, K. K. Crystal habit modification of Cu(ii) isonicotinate-N-oxide complexes using gel phase crystallisation. *New J. Chem.* **2018**, *42* (24), 19963−19970.
(22) Kennedy, S. R.; Jones, C. D.; Yufit, D. S.; Nicholson, C. E.; Cooper, S. J.; Steed, J. W. Tailored supramolecular gel and microemulsion crystallization strategies - is isoniazid really monomorphic? *CrystEngComm* **2018**, *20* (10), 1390−1398.
(23) Foster, J. A.; Piepenbrock, M.-O. M.; Lloyd, G. O.; Clarke, N.; Howard, J. A. K.; Steed, J. W. Anion-switchable supramolecular gels for controlling pharmaceutical crystal growth. *Nat. Chem.* **2010**, *2*, 1037.
(24) Diao, Y.; Whaley, K. E.; Helgeson, M. E.; Woldeyes, M. A.; Doyle, P. S.; Myerson, A. S.; Hatton, T. A.; Trout, B. L. Gel-Induced Selective Crystallization of Polymorphs. *J. Am. Chem. Soc.* **2012**, *134* (1), 673−684.
(25) Pauchet, M.; Morelli, T.; Coste, S.; Malandain, J.-J.; Coquerel, G. Crystallization of (±)-Modafinil in Gel: Access to Form I, Form III, and Twins. *Cryst. Growth Des.* **2006**, *6* (8), 1881−1889.
(26) Kaufmann, L.; Kennedy, S. R.; Jones, C. D.; Steed, J. W. Cavity-containing supramolecular gels as a crystallization tool for hydrophobic pharmaceuticals. *Chem. Commun.* **2016**, *52* (66), 10113−10116.
(27) Daly, R.; Kotova, O.; Boese, M.; Gunnlaugsson, T.; Boland, J. J. Chemical Nano-Gardens: Growth of Salt Nanowires from Supramolecular Self-Assembly Gels. *ACS Nano* **2013**, *7* (6), 4838−4845.
(28) Kennedy, S. R.; Jones, C. D.; Yufit, D. S.; Nicholson, C. E.; Cooper, S. J.; Steed, J. W. Tailored supramolecular gel and microemulsion crystallization strategies - is isoniazid really monomorphic? *CrystEngComm* **2018**, *20* (10), 1390−1398.
(29) Dawn, A.; Andrew, K. S.; Yufit, D. S.; Hong, Y.; Reddy, J. P.; Jones, C. D.; Aguilar, J. A.; Steed, J. W. Supramolecular Gel Control of Cisplatin Crystallization: Identification of a New Solvate Form Using a Cisplatin-Mimetic Gelator. *Cryst. Growth Des.* **2015**, *15* (9), 4591−4599.
(30) Saikia, B.; Mulvee, M. T.; Torres-Moya, I.; Sarma, B.; Steed, J. W. Drug Mimetic Organogelators for the Control of Concomitant Crystallization of Barbital and Thalidomide. *Cryst. Growth Des.* **2020**, *20* (12), 7989−7996.
(31) Shinn, D. Metronidazole in acute ulcerative gingivitis. *Lancet* **1962**, *279* (7240), 1191.
(32) Tally, F. P.; Sutter, V. L.; Finegold, S. M. Metronidazole versus anaerobes. In vitro data and initial clinical observations. *Calif. Med.* **1972**, *117* (6), 22−26.
(33) Tally, F. P.; Sutter, V. L.; Finegold, S. M. Treatment of anaerobic infections with metronidazole. *Antimicrob. Agents Chemother.* **1975**, *7* (5), 672−5.
(34) Löfmark, S.; Edlund, C.; Nord, C. Metronidazole Is Still the Drug of Choice for Treatment of Anaerobic Infections. *Clin. Infect. Dis.* **2010**, *50* (Suppl 1), S16−S23.
(35) Groom, C. R.; Bruno, I. J.; Lightfoot, M. P.; Ward, S. C. The Cambridge Structural Database. *Acta Crystallogr., Sect. B: Struct. Sci., Cryst. Eng. Mater.* **2016**, *72* (2), 171−179.
(36) Blaton, N. M.; Peeters, O. M.; De Ranter, C. J. 2-(2-Methyl-5-nitro-1-imidazolyl)ethanol (metronidazole). *Acta Crystallogr., Sect. B: Struct. Crystallogr. Cryst. Chem.* **1979**, *35* (10), 2465−2467.
(37) Di Martino, P.; Censi, R.; Malaj, L.; Capsoni, D.; Massarotti, V.; Martelli, S. Influence of solvent and crystallization method on the crystal habit of metronidazole. *Cryst. Res. Technol.* **2007**, *42* (8), 800−806.
(38) Bhattacharjee, S.; Bhattacharya, S. Role of synergistic [small pi]-[small pi] stacking and X-H[three dots, centered]Cl (X = C, N, O) H-bonding interactions in gelation and gel phase crystallization. *Chem. Commun.* **2015**, *51* (32), 7019−7022.
(39) Jones, C. D.; Steed, J. W. Gels with sense: supramolecular materials that respond to heat, light and sound. *Chem. Soc. Rev.* **2016**, *45* (23), 6546−6596.
(40) Dawn, A.; Mirzamani, M.; Jones, C. D.; Yufit, D. S.; Qian, S.; Steed, J. W.; Kumari, H. Investigating the effect of supramolecular gel phase crystallization on gel nucleation. *Soft Matter* **2018**, *14* (46), 9489−9497.
(41) van Esch, J.; Kellogg, R. M.; Feringa, B. L. Di-urea compounds as gelators for organic solvents. *Tetrahedron Lett.* **1997**, *38* (2), 281−284.
(42) Schoonbeek, F. S.; van Esch, J. H.; Hulst, R.; Kellogg, R. M.; Feringa, B. L. Geminal Bis-ureas as Gelators for Organic Solvents: Gelation Properties and Structural Studies in Solution and in the Gel State. *Chem. - Eur. J.* **2000**, *6* (14), 2633−2643.
(43) Romero, M. A. Synthesis of New Energetic Materials and Ionic Liquids Derived from Metronidazole. *Org. Chem. Int.* **2016**, *2016*, 1−8.
(44) Wu, M.; El-Kattan, Y.; Lin, T.-H.; Ghosh, A.; Vadlakonda, S.; Kotian, P. L.; Babu, Y. S.; Chand, P. Synthesis of 9-[1-(Substituted)-3-(phosphonomethoxy)propyl]adenine Derivatives as Possible Antiviral Agents. *Nucleosides, Nucleotides Nucleic Acids* **2005**, *24* (10−12), 1543−1568.
(45) Xu, Z.; Zhang, S.; Feng, L.-S.; Li, X.-N.; Huang, G.-C.; Chai, Y.; Lv, Z.-S.; Guo, H.-Y.; Liu, M.-L. Synthesis and In Vitro Antimycobacterial and Antibacterial Activity of 8-OMe Ciprofloxacin-Hydrozone/Azole Hybrids. *Molecules* **2017**, *22* (7), 1171.
(46) Akae, Y.; Iijima, K.; Tanaka, M.; Tarao, T.; Takata, T. Main Chain-Type Polyrotaxanes Derived from Cyclodextrin-Based Pseudo[3]rotaxane Diamine and Macromolecular Diisocyanate: Synthesis, Modification, and Characterization. *Macromolecules* **2020**, *53* (6), 2169−2176.
(47) Sheldrick, G. M. Crystal structure refinement with SHELXL. *Acta Crystallogr., Sect. C: Struct. Chem.* **2015**, *71* (1), 3−8.
(48) Kajfez, F.; Sunjic, V.; Kolbah, D.; Fajdiga, T.; Oklobdzija, M. 1-Substitution in 2-methyl-4(5)-nitroimidazole. I. Synthesis of compounds with potential antitrichomonal activity. *J. Med. Chem.* **1968**, *11* (1), 169−171.
(49) Goodwin, J. W.; Hughes, R. W. Introduction. In *Rheology for Chemists: An Introduction (2)*; The Royal Society of Chemistry, 2008; Chapter 1, pp 1−13.
(50) Guenet, J.-M. *Organogels: Thermodynamics, Structure, Solvent Role, and Properties*; Springer, 2016.
(51) Dawn, A.; Kumari, H. Low Molecular Weight Supramolecular Gels Under Shear: Rheology as the Tool for Elucidating Structure-Function Correlation. *Chem. - Eur. J.* **2018**, *24* (4), 762−776.

https://doi.org/10.1021/acs.cgd.1c00659
Cryst. Growth Des. 2021, 21, 5383−5393

(52) Sathaye, S.; Mbi, A.; Sonmez, C.; Chen, Y.; Blair, D. L.; Schneider, J. P.; Pochan, D. J. Rheology of peptide- and protein-based physical hydrogels: Are everyday measurements just scratching the surface? *Wiley Interdiscip. Rev. Nanomed. Nanobiotechnol.* **2015**, *7* (1), 34−68.
(53) Draper, E. R.; Adams, D. J. Low-Molecular-Weight Gels: The State of the Art. *Chem.* **2017**, *3* (3), 390−410.
(54) Jin, Q.; Zhang, L.; Liu, M. Solvent-Polarity-Tuned Morphology and Inversion of Supramolecular Chirality in a Self-Assembled Pyridylpyrazole-Linked Glutamide Derivative: Nanofibers, Nanotwists, Nanotubes, and Microtubes. *Chem. - Eur. J.* **2013**, *19* (28), 9234−9241.
(55) Tómasson, D. A.; Ghosh, D.; Kržišnik, Z.; Fasolin, L. H.; Vicente, A. A.; Martin, A. D.; Thordarson, P.; Damodaran, K. K. Enhanced Mechanical and Thermal Strength in Mixed-Enantiomers-Based Supramolecular Gel. *Langmuir* **2018**, *34* (43), 12957−12967.
(56) Ghosh, D.; Farahani, A. D.; Martin, A. D.; Thordarson, P.; Damodaran, K. K. Unraveling the Self-Assembly Modes in Multicomponent Supramolecular Gels Using Single-Crystal X-ray Diffraction. *Chem. Mater.* **2020**, *32* (8), 3517−3527.
(57) Ghosh, D.; Lebedytė, I.; Yufit, D. S.; Damodaran, K. K.; Steed, J. W. Selective gelation of N-(4-pyridyl)nicotinamide by copper(ii) salts. *CrystEngComm* **2015**, *17* (42), 8130−8138.
(58) Ghosh, D.; Bjornsson, R.; Damodaran, K. K. Role of N-Oxide Moieties in Tuning Supramolecular Gel-State Properties. *Gels* **2020**, *6* (4), 41.
(59) Tómasson, D. A.; Ghosh, D.; Kurup, M. R. P.; Mulvee, M. T.; Damodaran, K. K. Evaluating the role of a urea-like motif in enhancing the thermal and mechanical strength of supramolecular gels. *CrystEngComm* **2021**, *23* (3), 617−628.
(60) Adams, D. J. Does Drying Affect Gel Networks? *Gels* **2018**, *4* (2), 32.
(61) Fuentes-Caparrós, A. M.; de Paula Gómez-Franco, F.; Dietrich, B.; Wilson, C.; Brasnett, C.; Seddon, A.; Adams, D. J. Annealing multicomponent supramolecular gels. *Nanoscale* **2019**, *11* (7), 3275−3280.
(62) Panja, S.; Fuentes-Caparrós, A. M.; Cross, E. R.; Cavalcanti, L.; Adams, D. J. Annealing Supramolecular Gels by a Reaction Relay. *Chem. Mater.* **2020**, *32* (12), 5264−5271.

https://doi.org/10.1021/acs.cgd.1c00659
Cryst. Growth Des. 2021, 21, 5383−5393

Supporting Information

Crystal Habit Modification of Metronidazole by Supramolecular Gels with Complementary Functionality

Sreejith Sudhakaran Jayabhavan,† Jonathan W. Steed,‡* and Krishna K. Damodaran†*

†Department of Chemistry, Science Institute, University of Iceland, Dunhagi 3, 107 Reykjavík, Iceland. Tel: +354 525 4846, Fax: +354 552 8911.

‡Department of Chemistry, Durham University, South Road, Durham DH1 3LE, UK.

E-mail: jon.steed@durham.ac.uk (JWS) and krishna@hi.is (KKD)

1. Scheme and NMR spectra

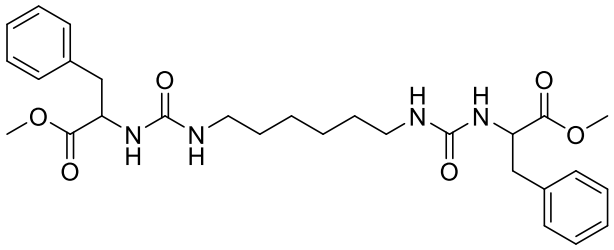

Scheme S1. Non-tailored gel.

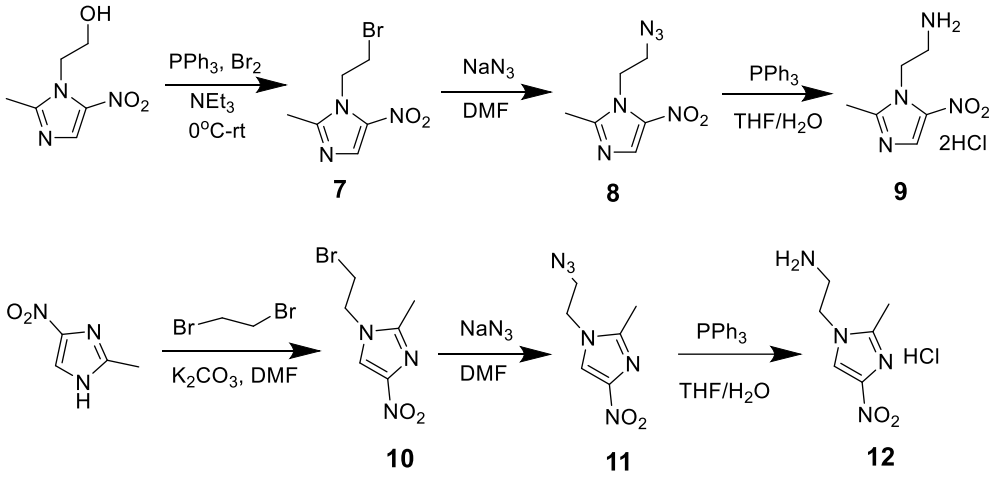

Scheme S2. Synthesis of amine precursors.

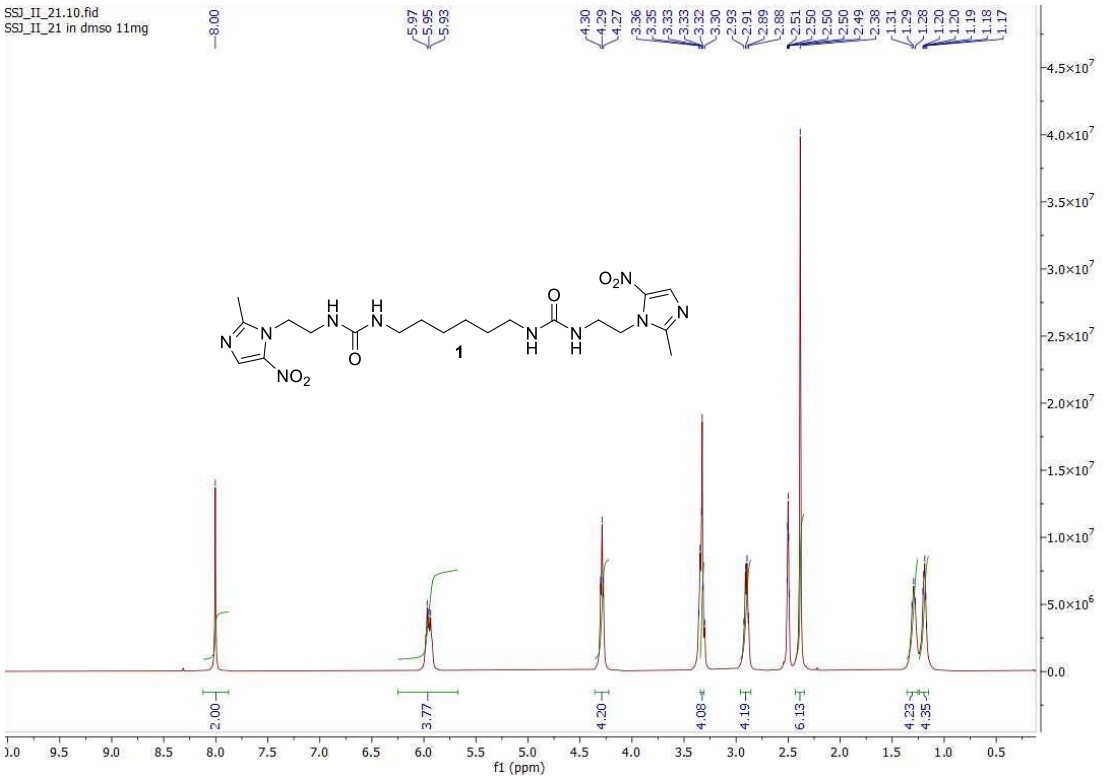

Figure S1. ^{1}H NMR spectrum of compound **1**.

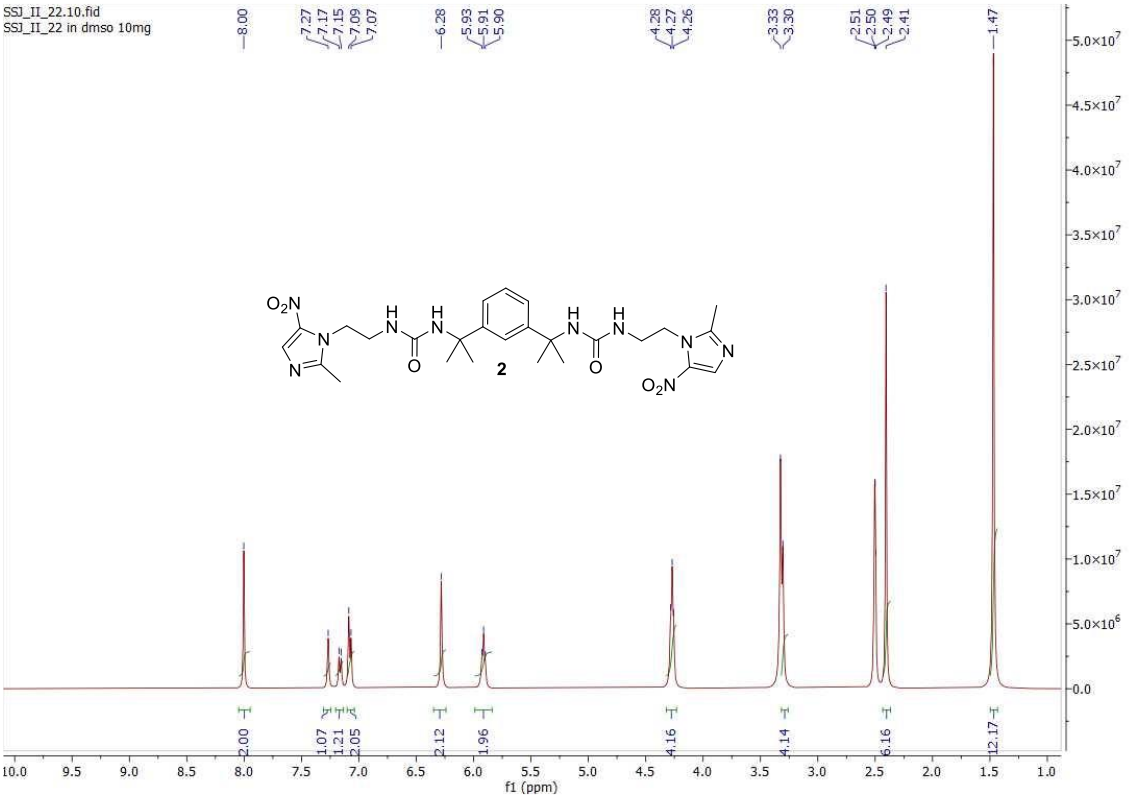

Figure S2. ^{1}H NMR spectrum of compound **2**.

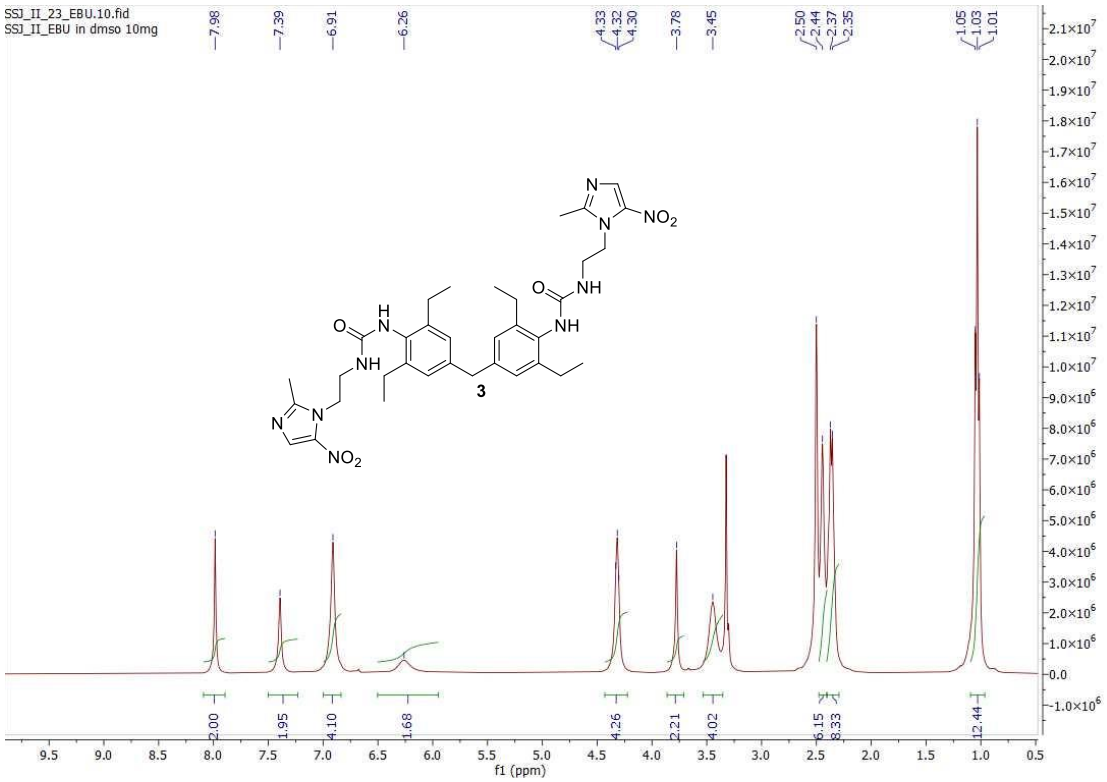

Figure S3. ^{1}H NMR spectrum of compound **3**.

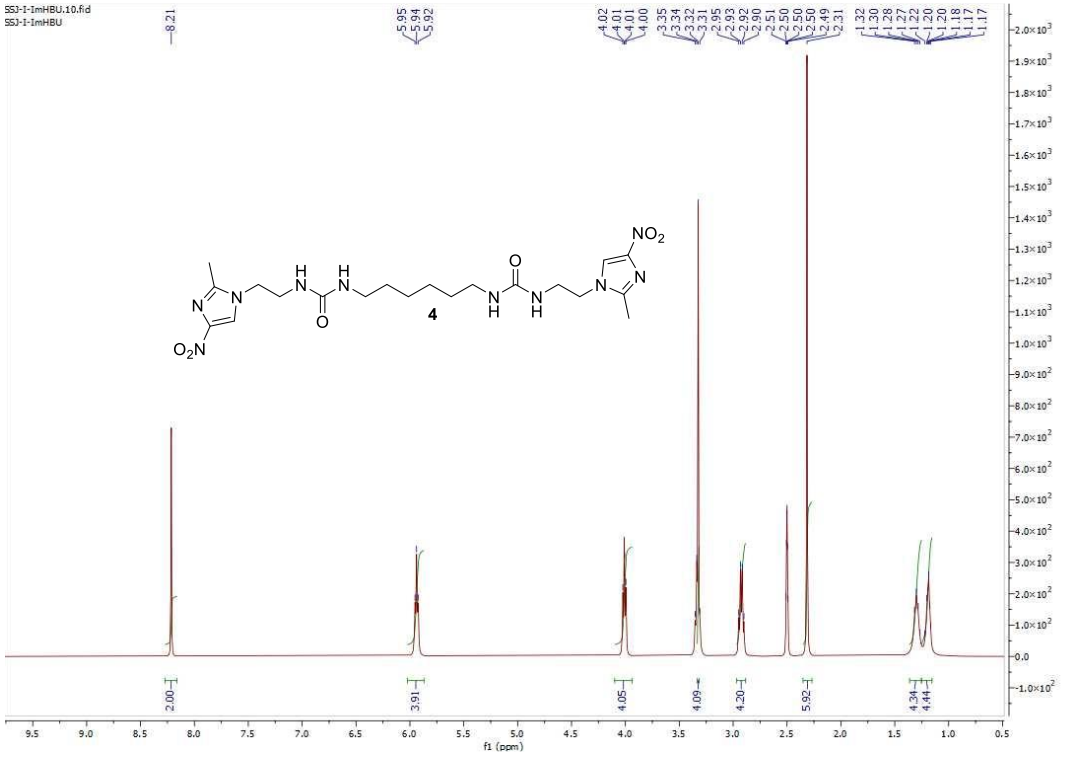

Figure S4. ^{1}H NMR spectrum of compound **4**.

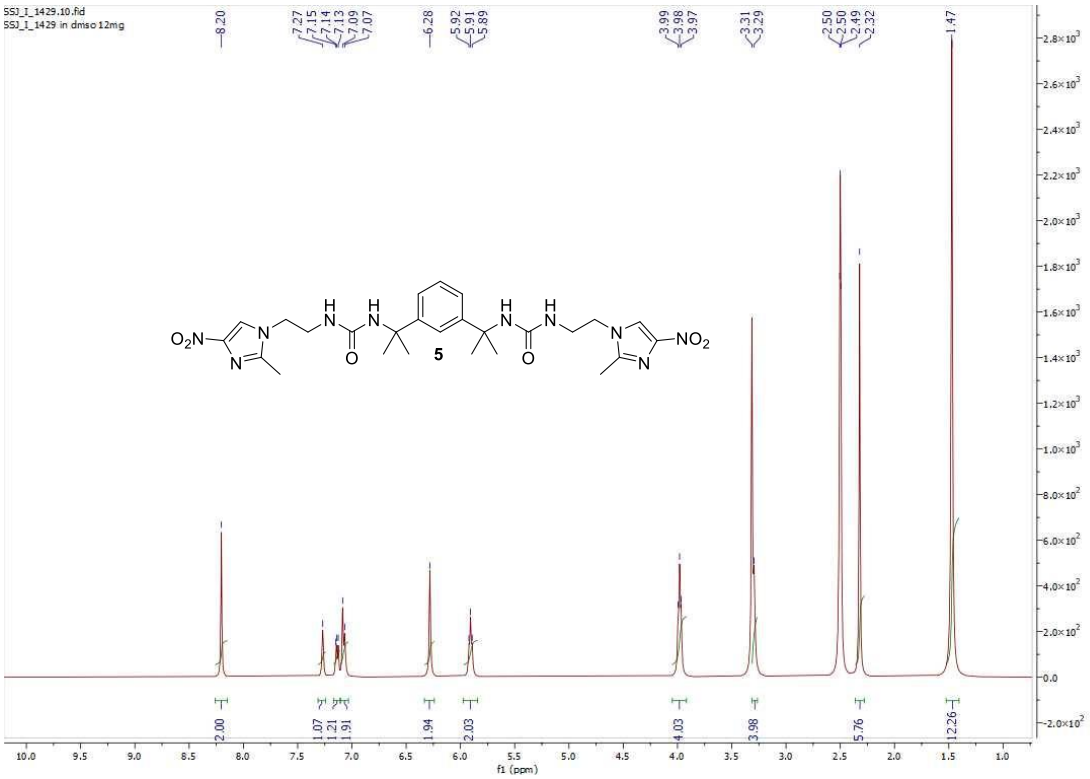

Figure S5. ^{1}H NMR spectrum of compound **5**.

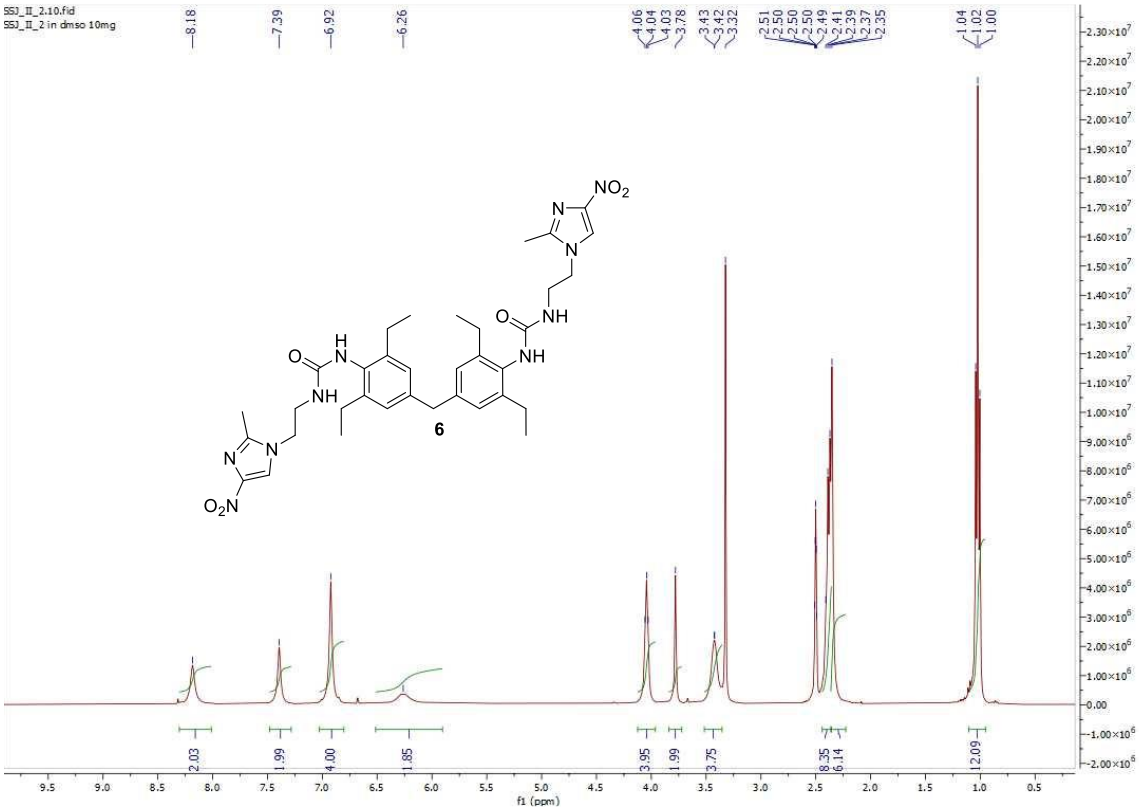

Figure S6. ^{1}H NMR spectrum of compound **6**.

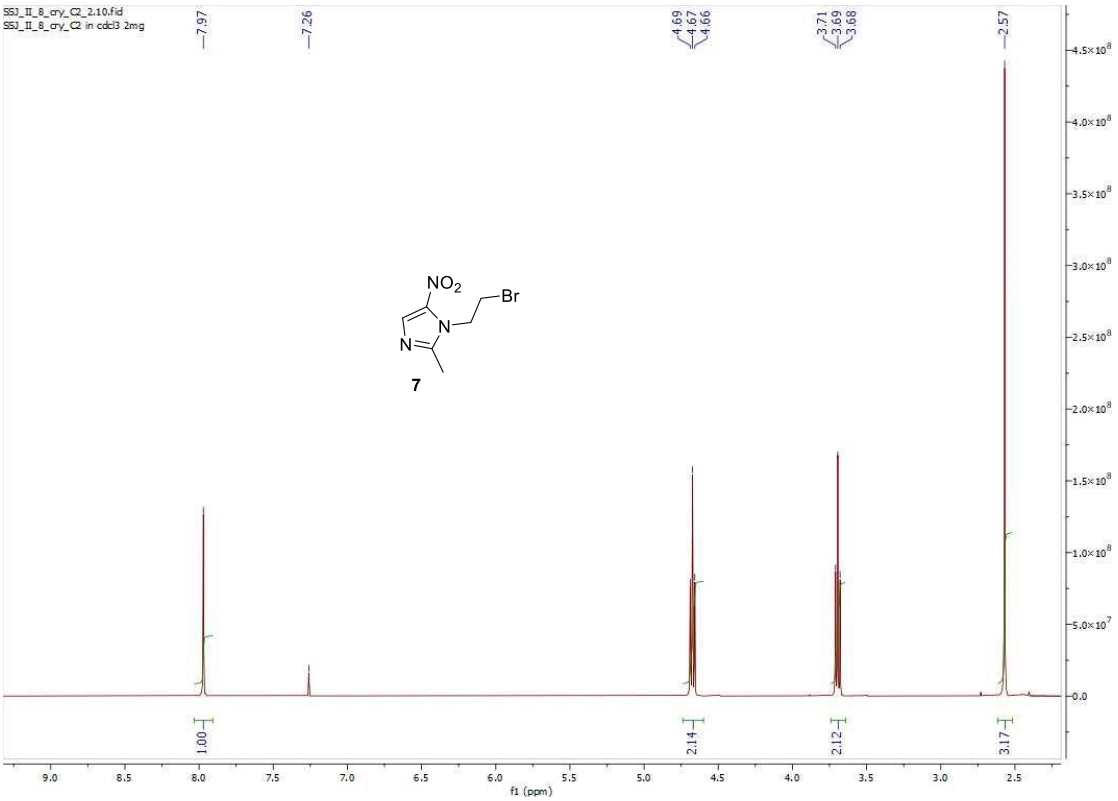

Figure S7. ^{1}H NMR spectrum of compound **7.**

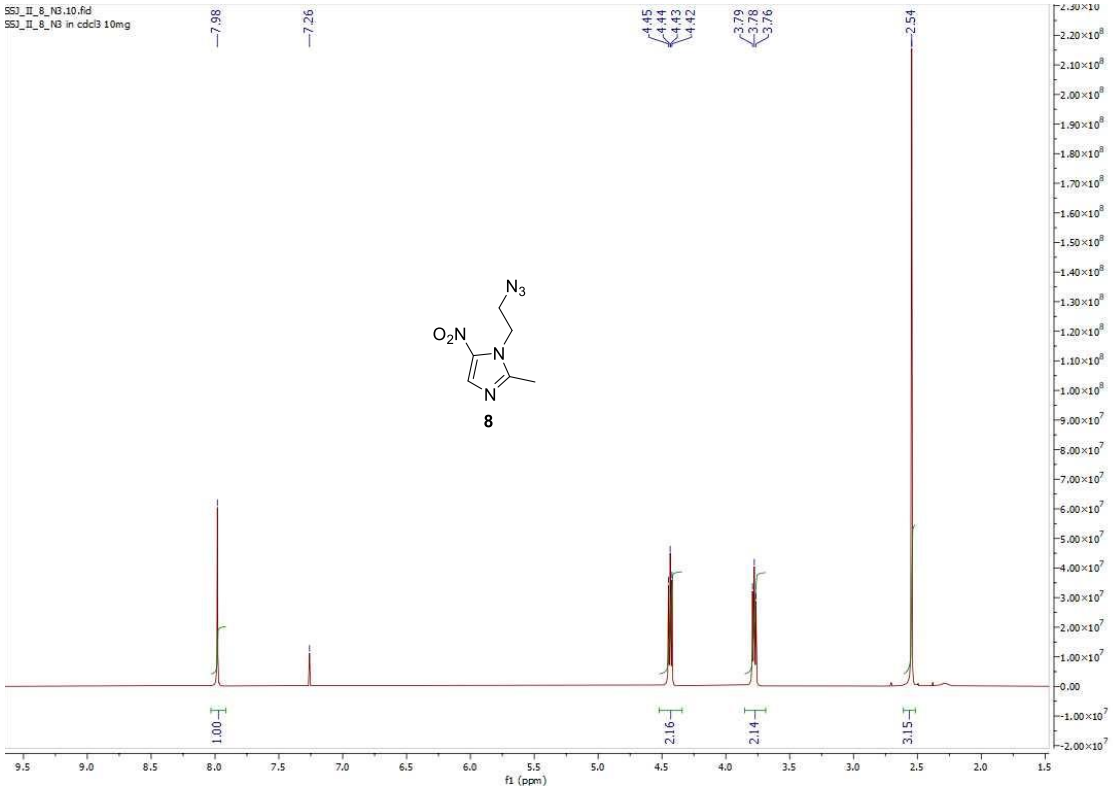

Figure S8. ^{1}H NMR spectrum of compound **8**.

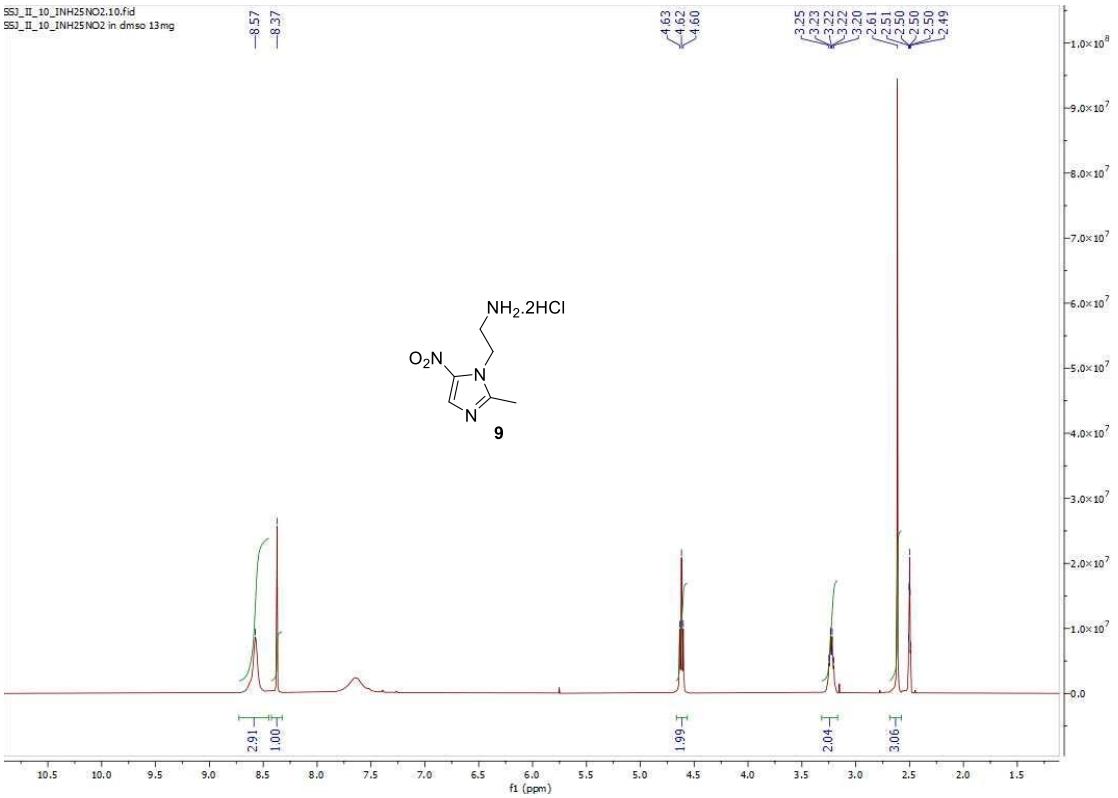

Figure S9. ^{1}H NMR spectrum of compound **9**.

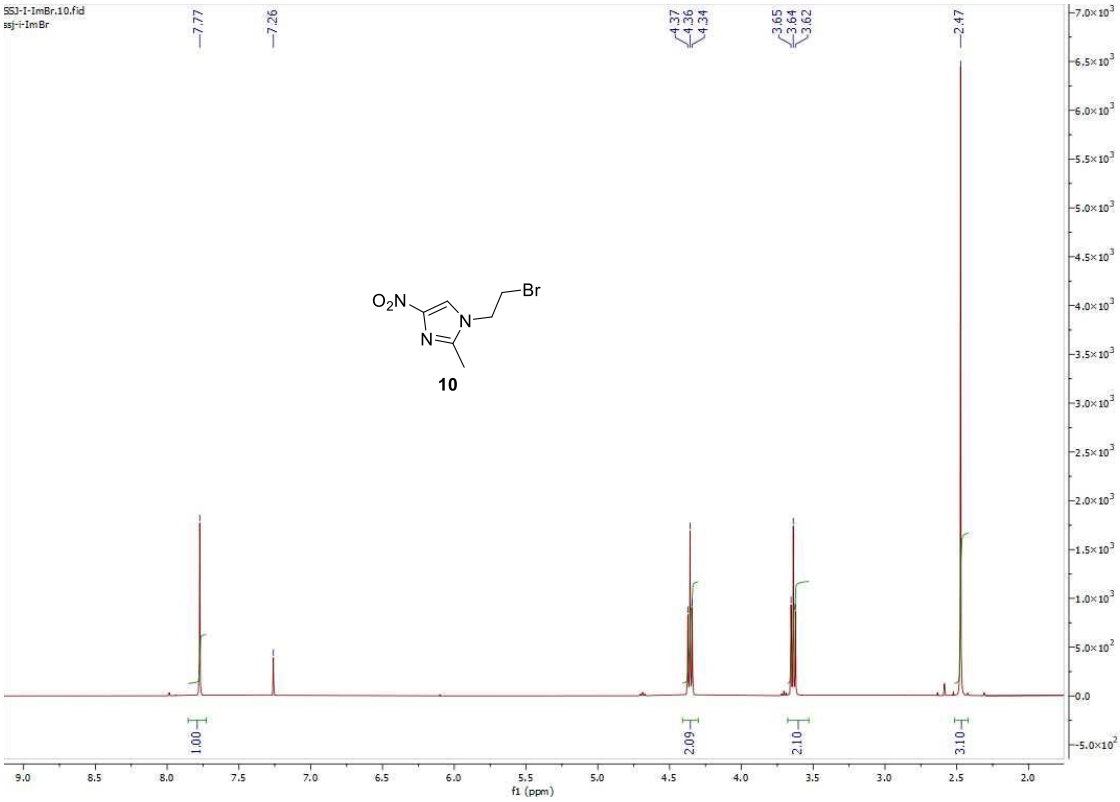

Figure S10. ^{1}H NMR spectrum of compound **10**.

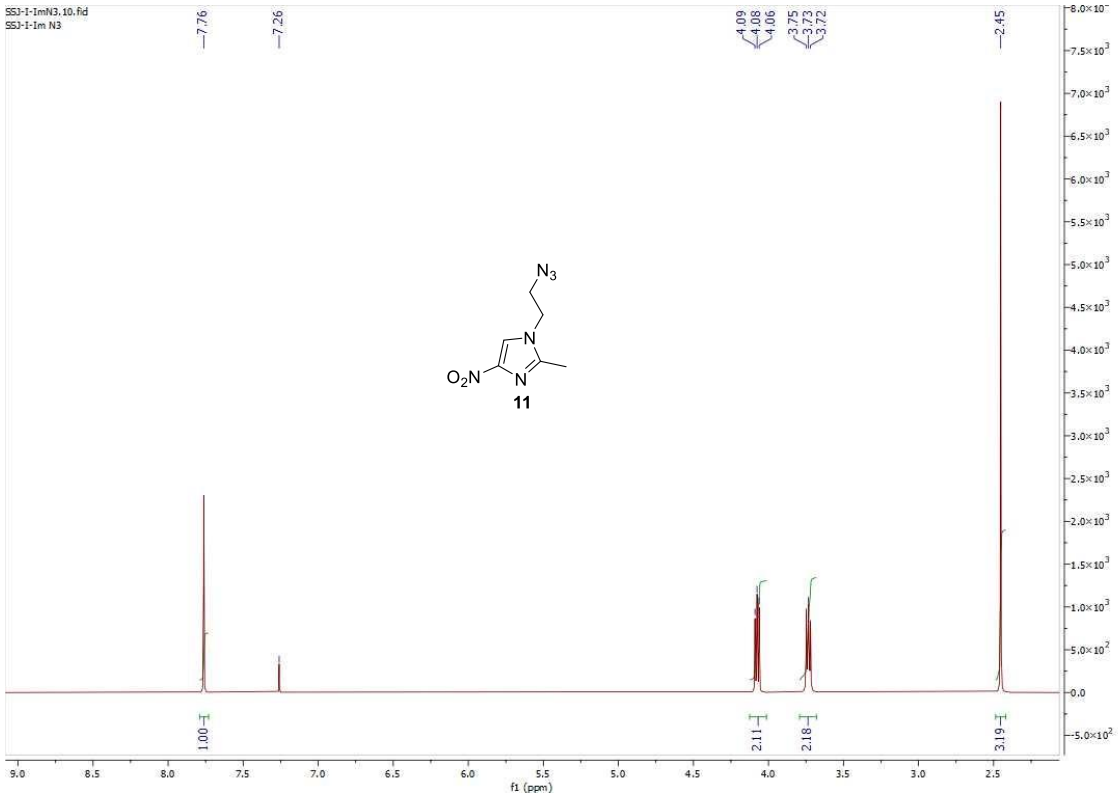

Figure S11. ^{1}H NMR spectrum of compound **11**.

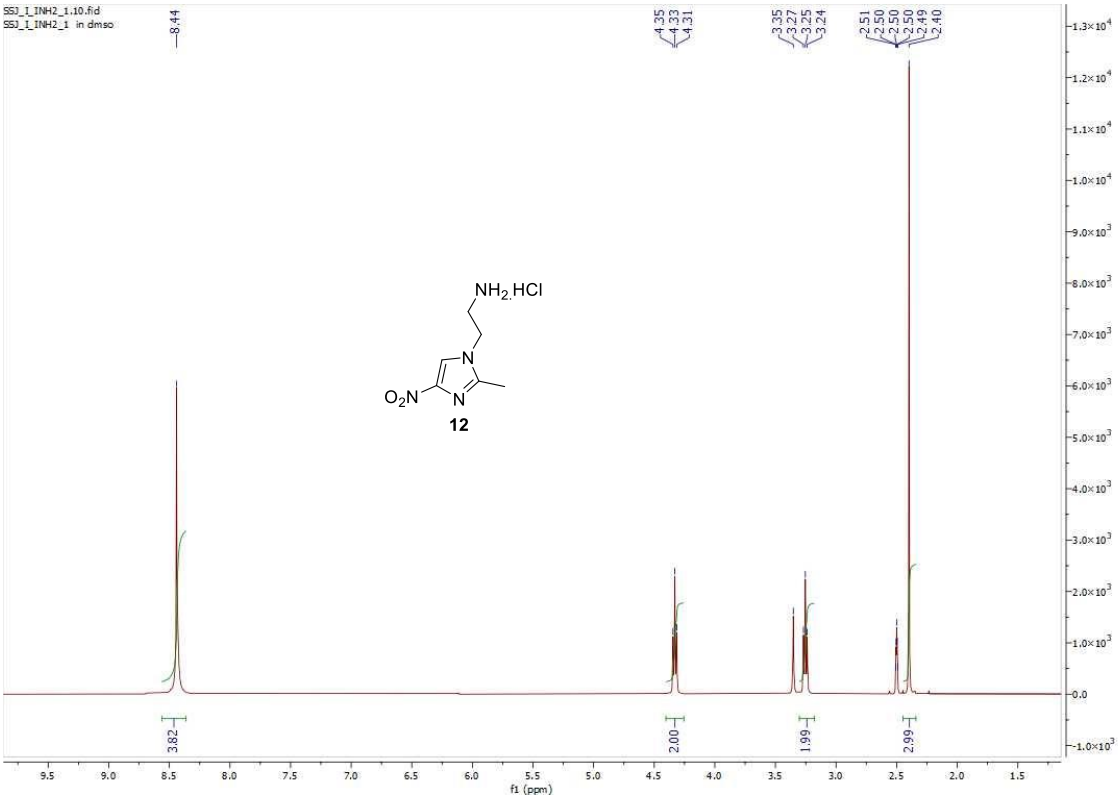

Figure S12. ^{1}H NMR spectrum of compound **12**.

2. X-ray crystallography

Table S1: Crystal data

Crystal data	**9.2HCl**	**12.HCl**	**Gelator 2.MeNO$_2$**
Empirical formula	$C_6H_{12}Cl_2N_4O_2$	$C_6H_{11}ClN_4O_2$	$C_{54}H_{72}N_{22}O_{16}$
Color	Colorless	Colorless	Yellow
Formula weight	243.10	206.64	1285.33
Crystal size (mm)	0.50 x 0.07 x 0.06	0.11 x 0.07 x 0.04	0.40 x 0.29 x 0.06
Crystal system	Tetragonal	Orthorhombic	Monoclinic
Space group	$I4_1/a$	$Pna2_1$	$P2_1/n$
a (Å)	26.6626(16)	7.0050(2)	9.3621(8)
b (Å)	26.6626(16)	17.2263(4)	11.7552(9)
c (Å)	6.5375(4)	7.7293(2)	29.148(3)
α (°)	90	90	90
β (°)	90	90	90.299(3)
γ (°)	90	90	90
Volume (Å^3)	4647.5(6)	932.70(4)	3207.7(5)
Z	16	4	2
$D_{calc.}$(g/cm^3)	1.390	1.472	1.331
F(000)	2016	432	1356
μ (mm^{-1})	CuK_α = 4.932	CuK_α = 3.468	MoK_α= 0.101
Temperature (K)	295(2)	295(2)	150(2)
Reflections collected/ unique/observed [I>2σ(I)]	24057/2294/2106	6424/1644/1597	87572/6574/4788
Data/restraints/parameters	2294/0/129	1644/1/121	6574/0/478
Goodness of fit on F^2	1.066	1.082	1.022
Final R indices [I>2σ(I)]	R_1 = 0.0339 wR_2 = 0.0976	R_1 = 0.0217 wR_2 = 0.0576	R_1 = 0.0866 wR_2 = 0.2318
R indices (all data)	R_1 = 0.0369 wR_2 = 0.1003	R_1 = 0.0227 wR_2 = 0.0581	R_1 = 0.1150 wR_2 = 0.2587

Table S2: Hydrogen bonding parameters

9.2HCl						
No.	Donor---H···Acceptor	D–H**/Å**	H···A**/Å**	D···A**/Å**	∠D---H···A**/°**	Symmetry operation
1	N(7)---H(8)···Cl(14)	0.86	2.15	3.0015(15)	169	x,y,z
2	N(12)---H(12A)···Cl(13)	0.89	2.74	3.3966(17)	131	1-x,3/2-y,z
3	N(12)---H(12B)···Cl(13)	0.89	2.22	3.0928(15)	166	x,y,z
4	N(12)---H(12C)···Cl(13)	0.89	2.35	3.211(2)	161	5/4-y,1/4+x,1/4-z
5	C(6)---H(6)···Cl(14)	0.93	2.70	3.6248(19)	175	1-x,1-y,2-z
6	C(11)---H(11B)···O(4)	0.97	2.56	3.304(2)	133	-1/4+y,5/4-x,1/4-z
7	C(11)---H(11A) ···Cl(13)	0.97	2.77	3.433(2)	126	5/4-y,1/4+x,5/4-z
12.HCl						
No.	Donor---H···Acceptor	D–H**/Å**	H···A**/Å**	D···A**/Å**	∠D---H···A**/°**	Symmetry operation
1	N(12)---H(12A)···N(4)	0.89	2.06	2.951(2)	175	1/2+x,1/2-y,z
2	N(12)---H(12B)···Cl(13)	0.89	2.30	3.1802(17)	170	1-x,1-y,1/2+z
3	N(12)---H(12C)···Cl(13)	0.89	2.28	3.1582(15)	171	x,y,z
4	C(3)---H(3B)···Cl(13)	0.96	2.78	3.709(2)	163	1-x,1-y,1/2+z
5	C(9)---H(9)···Cl(13)	0.93	2.65	3.562(2)	169	1-x,1-y,-1/2+z
6	C(10)---H(10B)···Cl(13)	0.97	2.78	3.548(2)	136	-1+x,y,z
2.Nitromethane						
No.	Donor---H···Acceptor	D–H**/Å**	H···A**/Å**	D···A**/Å**	∠D---H···A**/°**	Symmetry operation
1	N(15)---H(15)···O(30)	0.88	2.02	2.829(3)	152	1/2-x,-1/2+y,1/2-z
2	N(28)---H(28)···O(14)	0.88	2.07	2.861(3)	149	3/2-x,1/2+y,1/2-z
3	N(31)---H(31)···O(14)	0.88	2.17	2.939(4)	146	3/2-x,1/2+y,1/2-z
4	C(6)---H(6)···N(7)	0.95	2.62	3.343(6)	133	-x,-y,-z
5	C(9)---H(9A)···N(40A)	0.98	2.57	3.367(12)	139	3/2-x,-1/2+y,1/2-z
6	C(32A)---H(32C)···O(51)	0.99	2.34	3.21(4)	146	x,1+y,z

Crystal Structures

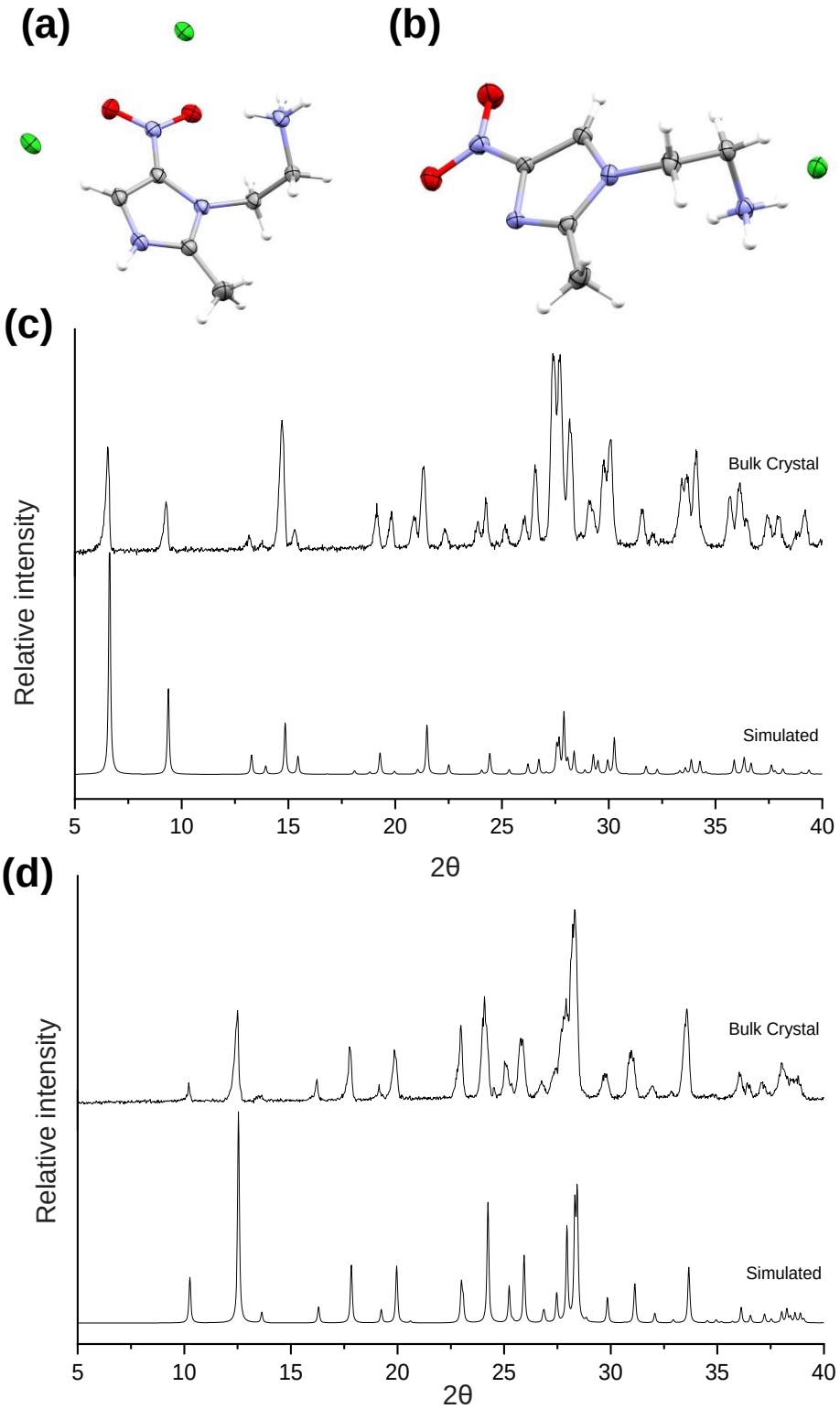

Figure S13. Asymmetric unit of (a) Compound **9.2HCl** and (b) Compound **12.HCl,** Comparison of PXRD pattern, simulated and the bulk crystals of (c) compound **9.2HCl** and (d) compound **12.HCl**, respectively.

3. Gelation studies

Table S3: Gelation experiments

Solvents	Gelation test at 1.0 wt/v%					
	1	**2**	**3**	**4**	**5**	**6**
Nitrobenzene	G	G	G	G**	G**	G**
1,2-dibromoethane	C	G*	I	I	Ppt	I
Chlorobenzene	I	G*	I	I	I	I
o-xylene	C	C	C	I	I	I
m-xylene	C	C	C	I	I	I
p-xylene	C	C	C	I	I	I
Mesitylene	C	C	C	I	I	I
Ethanol	Ppt	Ppt	$G^{\$\$}$	I	Ppt	I
1-propanol	Ppt	Cry	$G^{\$\$}$	I	C	I
2-propanol	Ppt	Cry	C	I	C	I
1-butanol	Ppt	S	$G^{\$\$}$	I	C	I
1-pentanol	S	S	$G^{\$}$	I	C	I
Benzyl alcohol	S	S	S	S	S	S
Ethylene glycol	S	S	G*	I	S	G**
Cyclopentanone	S	S	G	I	S	I
Cyclohexanone	S	S	G	I	S	I
1,4-dioxane	I	G*	$G^{\$}$	Ppt	C	I
Nitromethane	Ppt	Cry	$G^{\$\$}$	C	Ppt	I
DMF	Ppt	S	Ppt	S	S	G***
DMSO:water(1:1, v/v)	Ppt	G**	G**‡	G***	Ppt	C
DMF:water(1:1, v/v)	Ppt	Ppt	G**‡	G***	Ppt	G**

G= gel, I= insoluble, S= solution, C= colloid, Ppt= precipitate, Cry= crystals, G*=2.0 wt/v%, G**= 3.0 wt/v%, G***= 4.0 wt/v%, G****= 5.0 wt/v%, ‡= (7:3, v/v) solvent composition, compound **3** was insoluble in ethanol, 1-propanol, 1-butanol, 1-pentanol, 1-4 dioxane and nitromethane at 1.0 wt/v%, but formed gel at 0.5 wt/v% ($G^{\$}$) and $G^{\$\$}$= 0.4 wt/v%.

Table S4: Determination of Minimum Gel Concentration (MGC)

Solvents	**MGC (wt/v%)**					
	1	**2**	**3**	**4**	**5**	**6**
Nitrobenzene	0.8	0.9	0.5	2.8	2.5	2.8
1,2-dibromoethane	---	1.2	---	---	---	---
Chlorobenzene	---	1.5	---	---	---	---
Ethylene glycol	---	---	1.2	---	---	2.7
Cyclopentanone	---	---	0.8	---	---	---
Cyclohexanone	---	---	1.0	---	---	---
1,4-dioxane	---	1.7	0.5	---	---	---
Ethanol	---	---	0.33	---	---	---
1-propanol	---	---	0.25	---	---	---
1-butanol	---	---	0.33	---	---	---
1-pentanol	---	---	0.5	---	---	---
Nitromethane	---	---	0.33	---	---	---
DMF				---	---	3.8
DMSO:water(1:1, v/v)	---	2.5	---	4.0	---	---
DMSO:water(7:3, v/v)	---	---	3.0	---	---	---
DMF:water(1:1, v/v)	---	---	---	4.5	---	3.0
DMF:water(7:3, v/v)	---	---	3.0	---	---	---

Table S5: Determination of Sol-gel Transition Temperature (T_{gel})

Solvents	T_{gel} **(°C)**					
	1	**2**	**3**	**4**	**5**	**6**
Nitrobenzene	95.3*	69.2*	140.1*	145.4***	118.8***	153.8***
Nitrobenzene	103.7***	84.3***	151.4***	---	---	---
Cyclopentanone	---	---	99.5*	---	---	---
Cyclohexanone	---	---	101.4*	---	---	---
Ethanol	---	---	89.6##	---	---	---
1-propanol	---	---	93.4#	---	---	---
1-butanol	---	---	94.6##	---	---	---
1-pentanol	---	---	95.1###	---	---	---
Nitromethane	---	---	89.8##	---	---	---
1,4-dioxane	---	64.8**	98.7###	---	---	---
Chlorobenzene	---	109.6**	---	---	---	---
Ethylene glycol	---	---	121.1**	---	---	149.6***
DMF	---	---	---	---	---	91.0$
DMSO:water (1:1, v/v)	---	84.8***	---	104.5$	---	---
DMF:water (1:1), v/v)	---	---	---	100.2$$	---	105.2***
DMSO:water (7:3, v/v)	---	---	111.3***	---	---	---
DMF:water (7:3, v/v)	---	---	110.6***	---	---	---

*= 1.0 wt/v%, **= 2.0 wt/v%, ***= 3.0 wt/v%, #= 0.25 wt/v%, ##= 0.33 wt/v%, ###= 0.5 wt/v%, $= 4.0 wt/v%, $$= 4.5 wt/v%.

4. Rheology

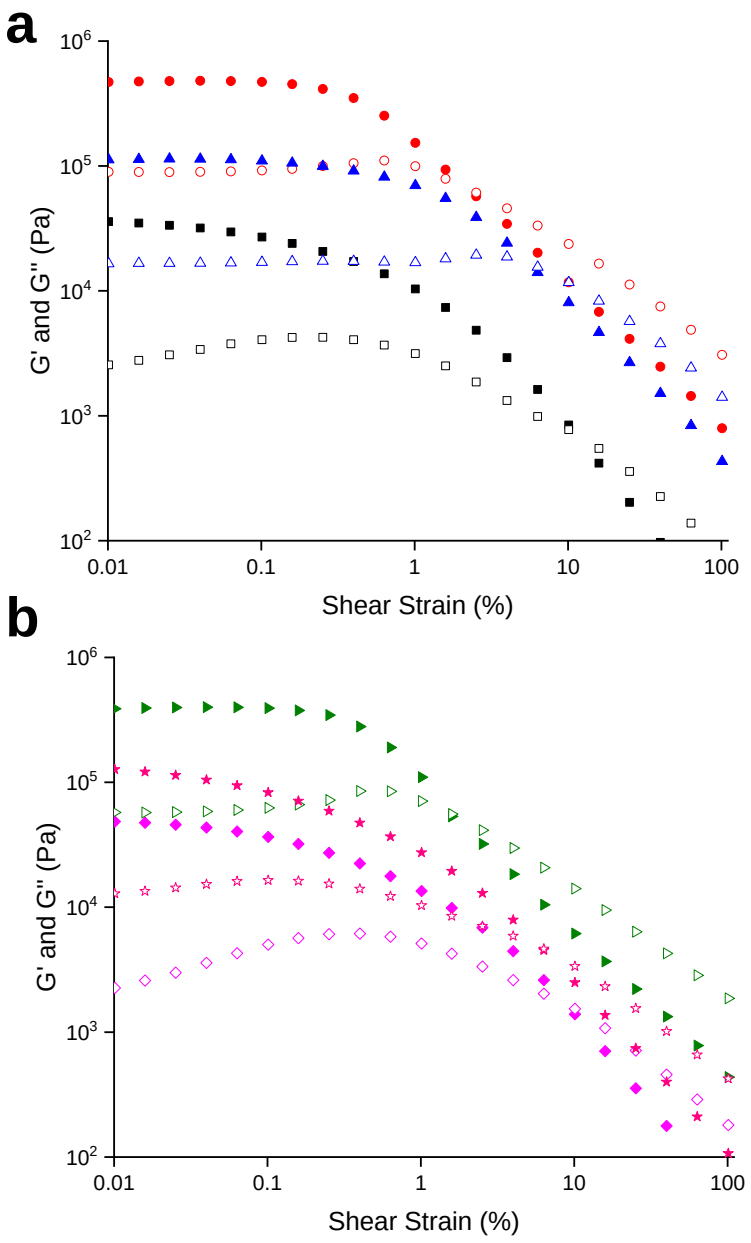

Figure S14. Freequency sweep experiments of bis-(urea) gels (3.0 wt/v%) in nitrobenzene at 25.0 °C with a constant frequency of 1.0 Hz. Color codes: (a) gelator-**1** G' (■) and G'' (□), gelator-**2** G' (●) and G'' (○), gelator-**3** G' (▲) and G'' (Δ), and (b) gelator-**4** G' (◆) and G'' (◊), gelator-**5** G' (►) and G'' (▷), gelator-**6** G' (★) and G'' (☆).

5. Scanning electron microscopy

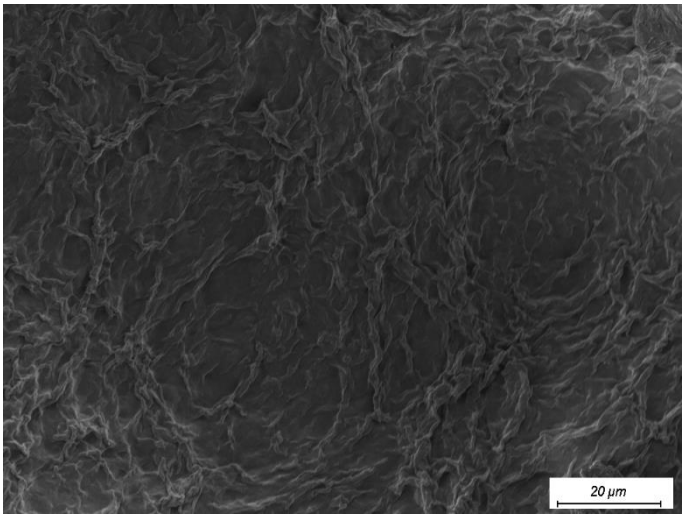

Figure S15. SEM images of xerogels of gelator **3** in nitrobenzene at 3.0 wt/v%.

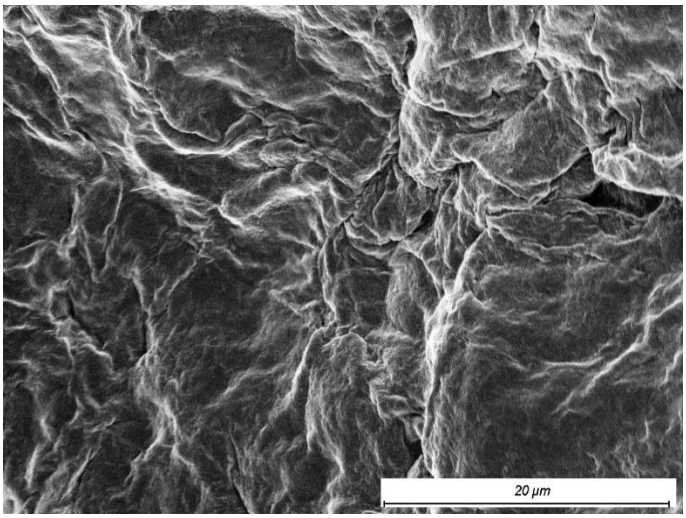

Figure S16. SEM images of xerogels of gelator **5** in nitrobenzene at 3.0 wt/v%.

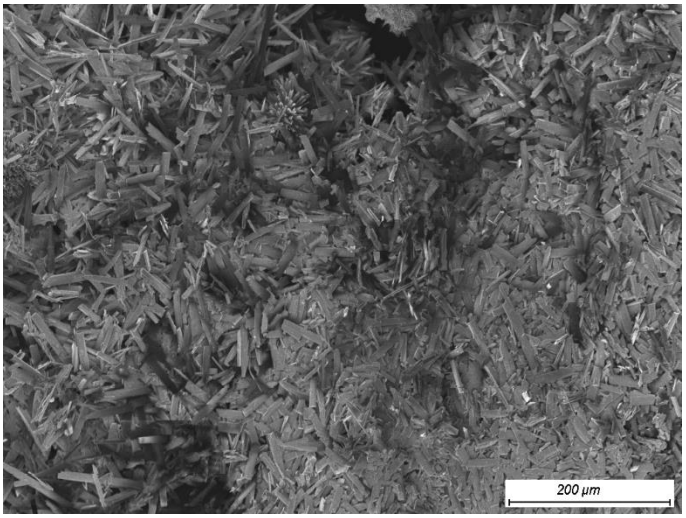

Figure S17. SEM images of xerogels of gelator **4** in DMSO/water (1:1, v/v) at 4.0 wt/v%.

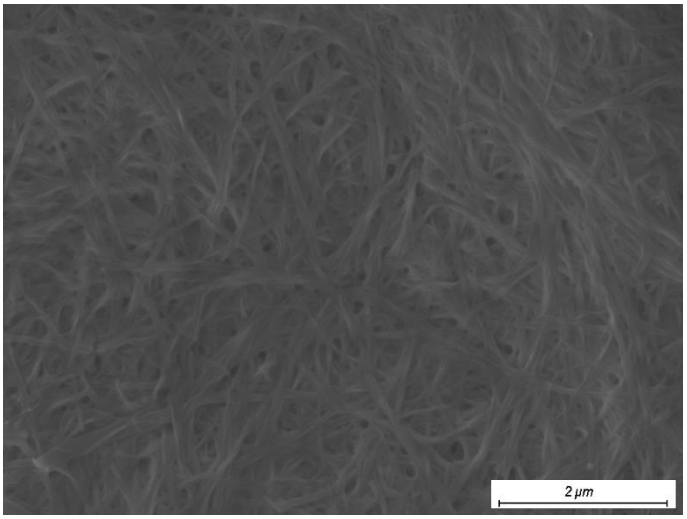

Figure S18. SEM images of xerogels of gelator **3** in ethanol at 0.33 wt/v%.

6. Crystal Structure of gelator 2

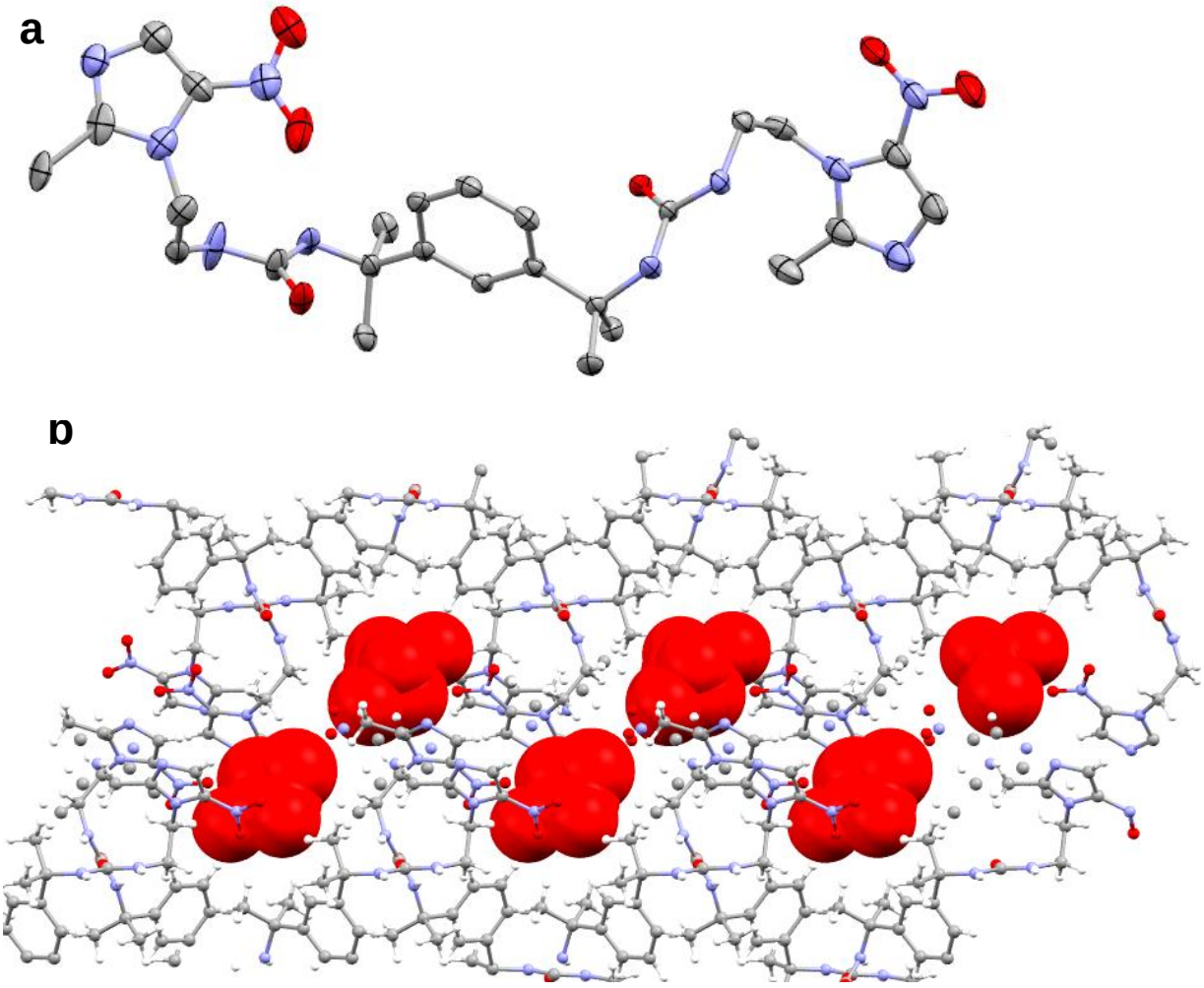

Figure S19. (a) Molecular structure of **2** and (b) packing diagram showing the porous 3-D hydrogen bonded network in **2**.

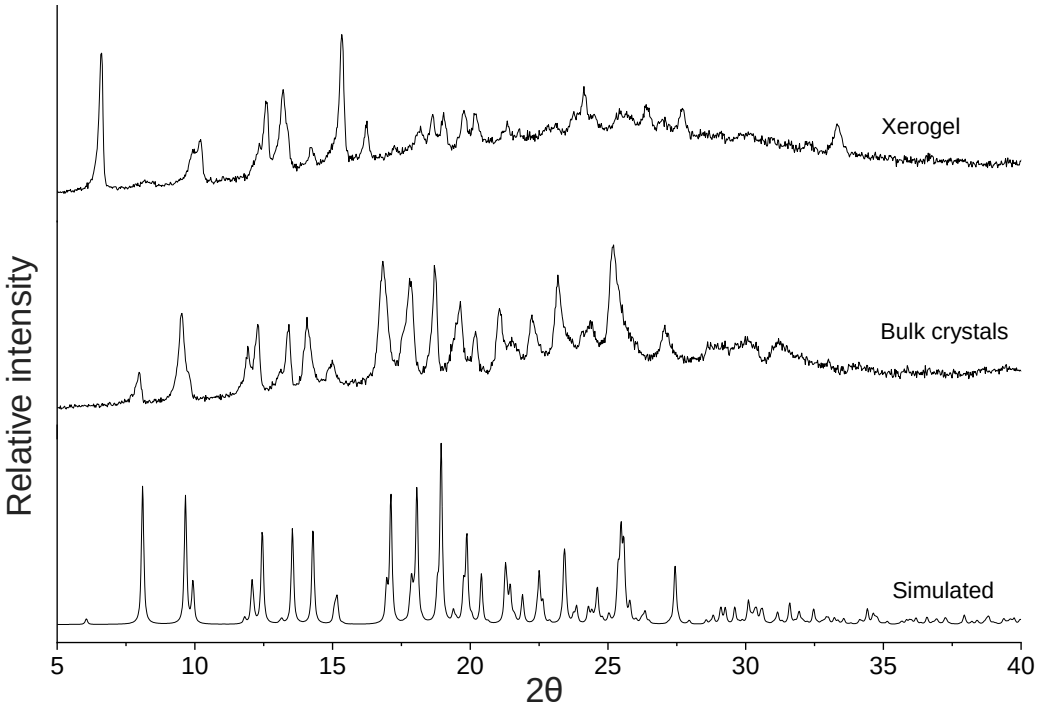

Figure S20. Comparison of simulated pattern and PXRD pattern of the bulk crystals from nitromethane and xerogels from nitrobenzene.

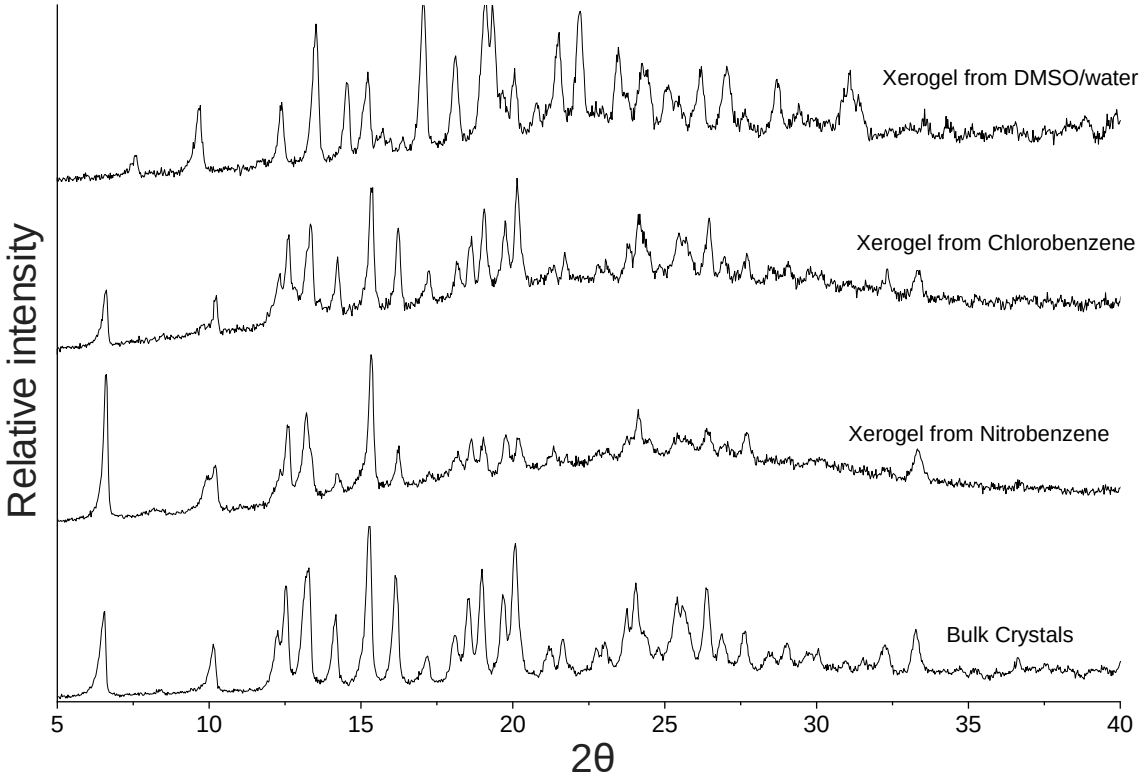

Figure S21. Comparison of PXRD pattern of the bulk crystals from isopropanol and xerogels from chlorobenzene, nitrobenzene and DMSO/water (1:1, v/v) gels (3.0 wt/v%), respectively.

7. Gel phase crystallization studies

Table S6: Solution-phase crystallization of metronidazole in 1.0 mL of solvent

Solvent	Drug (mg)	Crystal morphology
Nitrobenzene	30	Thick Plate shaped (HB fashion) in 1-2 day
	40	Thick Plate shaped (HB fashion) in 12-24 h
	50	Thick Plate shaped (HB fashion) in 4-6 h
	75	Thick Plate shaped (HB fashion) in 2h
	100	’’
DMSO:water (1:1, v/v)	70	Long-needles
	100	’’
DMSO:water (7:3, v/v)	80	’’
	100	’’
DMF:water (1:1, v/v)	140	’’
	150	’’
DMF:water (7:3, v/v)	150	’’
	180	’’

*HB= Herringbone pattern.

Table S7: Gel-phase crystallization of metronidazole in mimetic gelators (**1**-**3**)

Wt/v%	Drug (mg)	Observation					
		Gelator 1		Gelator 2		Gelator 3	
		After 1 h	After 24 h	After 1 h	After 24 h	After 1 h	After 24 h
0.3	50	S	Needles and plates (HB)	S	Plates (HB)	S	Plates (HB)
0.3	75	S	’’	S	’’	S	’’
0.3	100	S	’’	S	’’	S	’’
0.5	50	S	’’	S	Needles and plates (HB)	G	Needle-shaped (HB)
0.5	75	S	’’	S	’’	G	’’
0.5	100	S	’’	S	’’	G	’’
1.0	50	PG	Needle-shaped crystals	G	Needle-shaped crystals	G	’’
1.0	75	PG	’’	G	’’	G	’’
1.0	100	PG	’’	G	’’	G	’’
2.0	50	G	’’	G	’’	G	’’
2.0	75	G	’’	G	’’	G	’’
2.0	100	G	’’	G	’’	G	’’
3.0	50	G	’’	G	’’	G	’’
3.0	75	G	’’	G	’’	G	’’
3.0	100	G	’’	G	’’	G	’’

S = Solution, G = Gel, PG = Partial gel, HB= Herringbone pattern.

Table S8: Gel-phase crystallization of metronidazole in non-mimetic gelators (**4**-**6**)

Wt/v%	Drug (mg)	Observation					
		Gelator 4		Gelator 5		Gelator 6	
		After 1 h	After 24 h	After 1 h	After 24 h	After 1 h	After 24 h
0.5	50	S	Plates (HB)	S	Plates (HB)	S	Plates (HB)
0.5	75	S	’’	S	’’	S	’’
0.5	100	S	’’	S	’’	S	’’
1.0	50	S	’’	S	’’	PG	No crystals
1.0	75	S	’’	S	’’	PG	Plates (HB)
1.0	100	S	’’	S	’’	PG	’’
2.0	50	S	’’	S	’’	PG	No crystals
2.0	75	S	’’	S	’’	PG	Thick needles (HB)
2.0	100	S	’’	S	’’	PG	’’
3.0	50	S	’’	S	’’	G	’’
3.0	75	S	’’	S	’’	G	’’
3.0	100	S	’’	S	’’	G	’’
6.0	50	PG	Plates (HB)	G*	No crystals	G	’’
6.0	75	G	’’	G*	’’	G	’’
6.0	100	G	’’	G*	’’	G	’’
7.0	50	G	’’	PG	Micro-needles (HB)	--	--
7.0	75	G	’’	PG	’’	--	--
7.0	100	G	’’	PG	’’	--	--

S = Solution, G = Gel, PG = Partial gel, HB= Herringbone pattern.

Note: G*= Gels were obtained by sonication prior to cooling (no crystals were obtained), similar results were obtained even at higher concentration of **5** (10.0 wt/v%) and crystallization substrate (150 mg/mL).

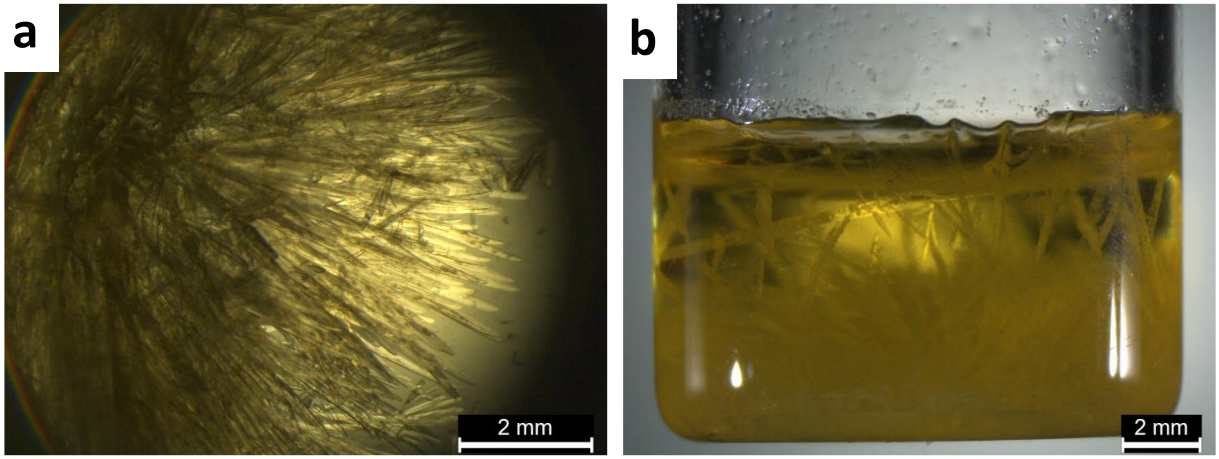

Figure S22. Needle-shaped crystals of metronidazole grown in gel of compound **2**, (a) top view and (b) side view.

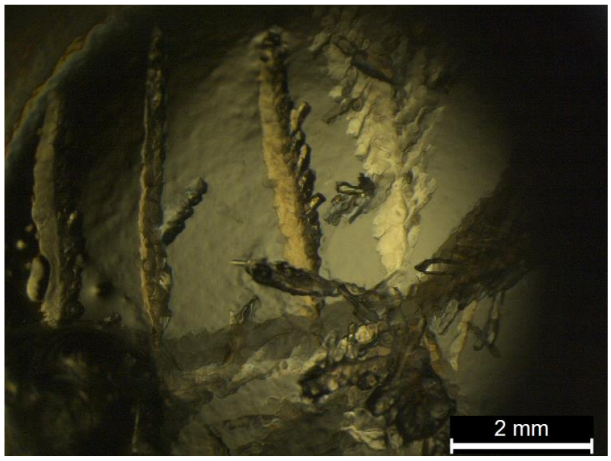

Figure S23. Plate-shaped crystals (with a herringbone pattern) of metronidazole (50 mg/mL) formed in L-phenyl alanine methyl ester based bis-(urea) gel in nitrobenzene at 2.0 wt/v%.

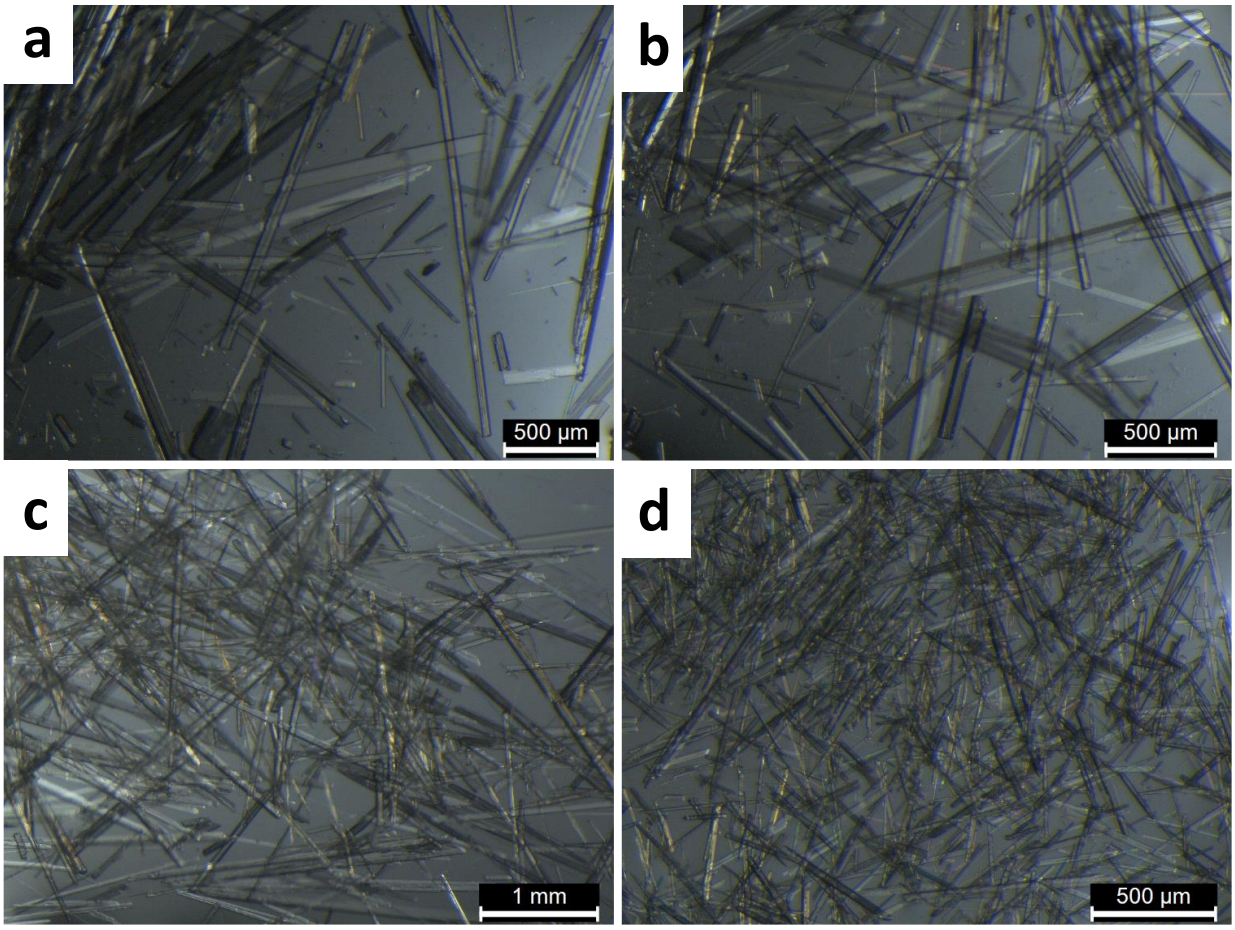

Figure S24. Solution phase crystallization of metronidazole in (a) DMSO/water (1:1, v/v) at 70 mg/mL, (b) DMSO/water (7:3, v/v) at 80 mg/mL, (c) DMF/water (1:1, v/v) at 140 mg/mL, and (d) DMF/water (7:3, v/v) at 150 mg/mL.

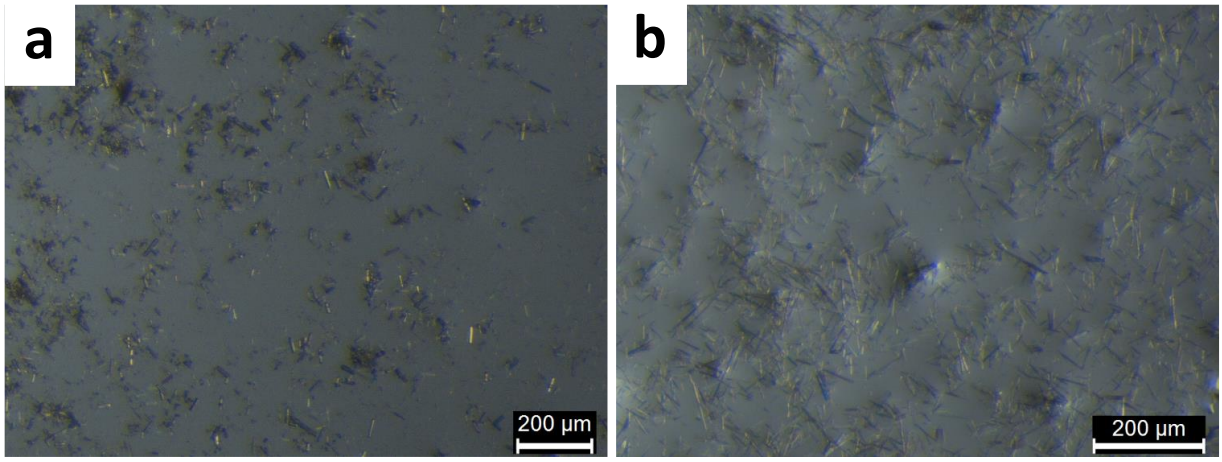

Figure S25. Gel phase crystallization of metronidazole in (a) gelator **3** in DMSO/water (7:3, v/v) at 100 mg/mL, (b) gelator 4 in DMSO/water (1:1, v/v) at 80 mg/mL.

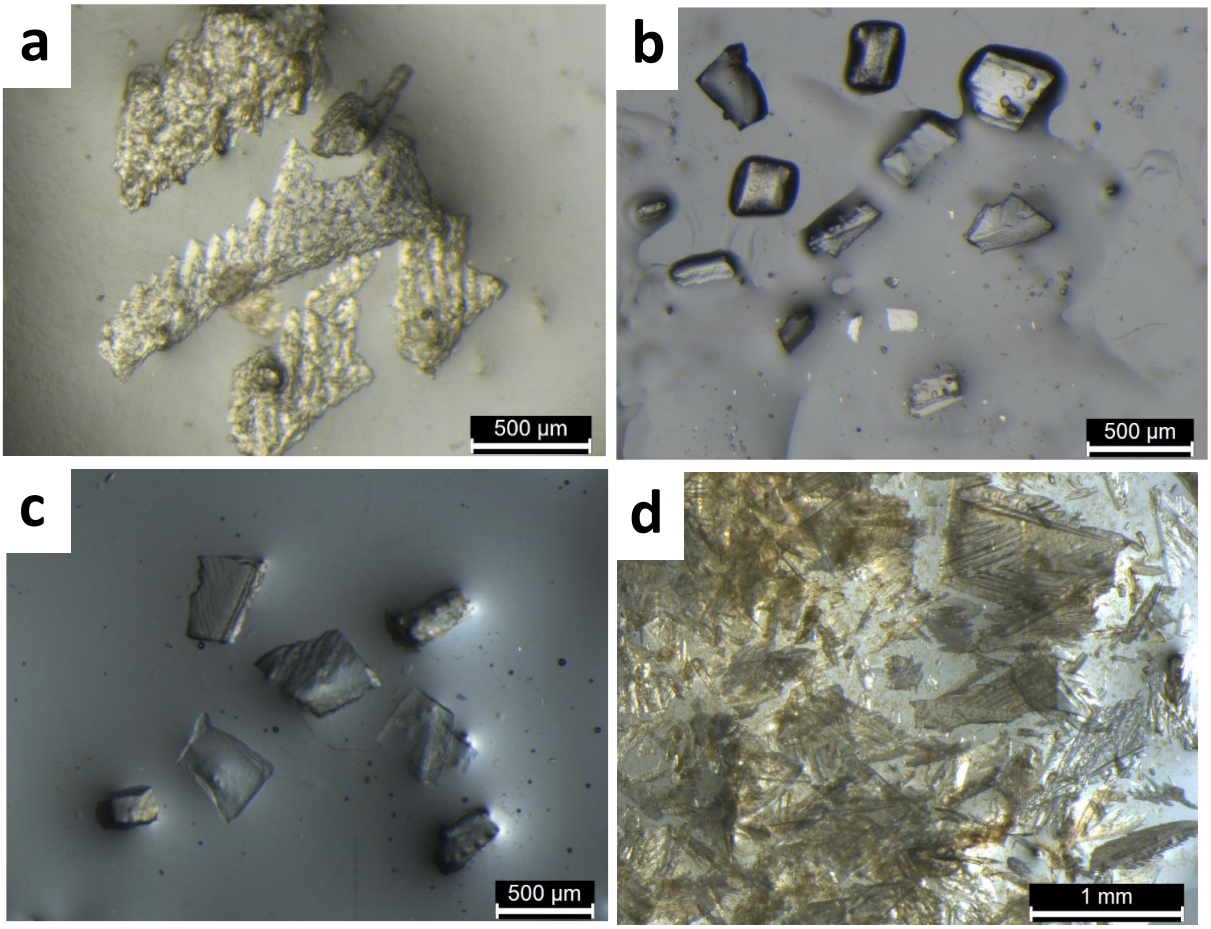

Figure S26. Crystals from solution phase crystallization of metronidazole at 50 mg/mL in nitrobenzene with gelators (a) **3** at 0.3 wt/v%, (b) **4** at 0.5 wt/v%, (c) **5** at 0.5 wt/v%, and (d) **6** at 0.5 wt/v%.

8. Single Crystal Face Indexing

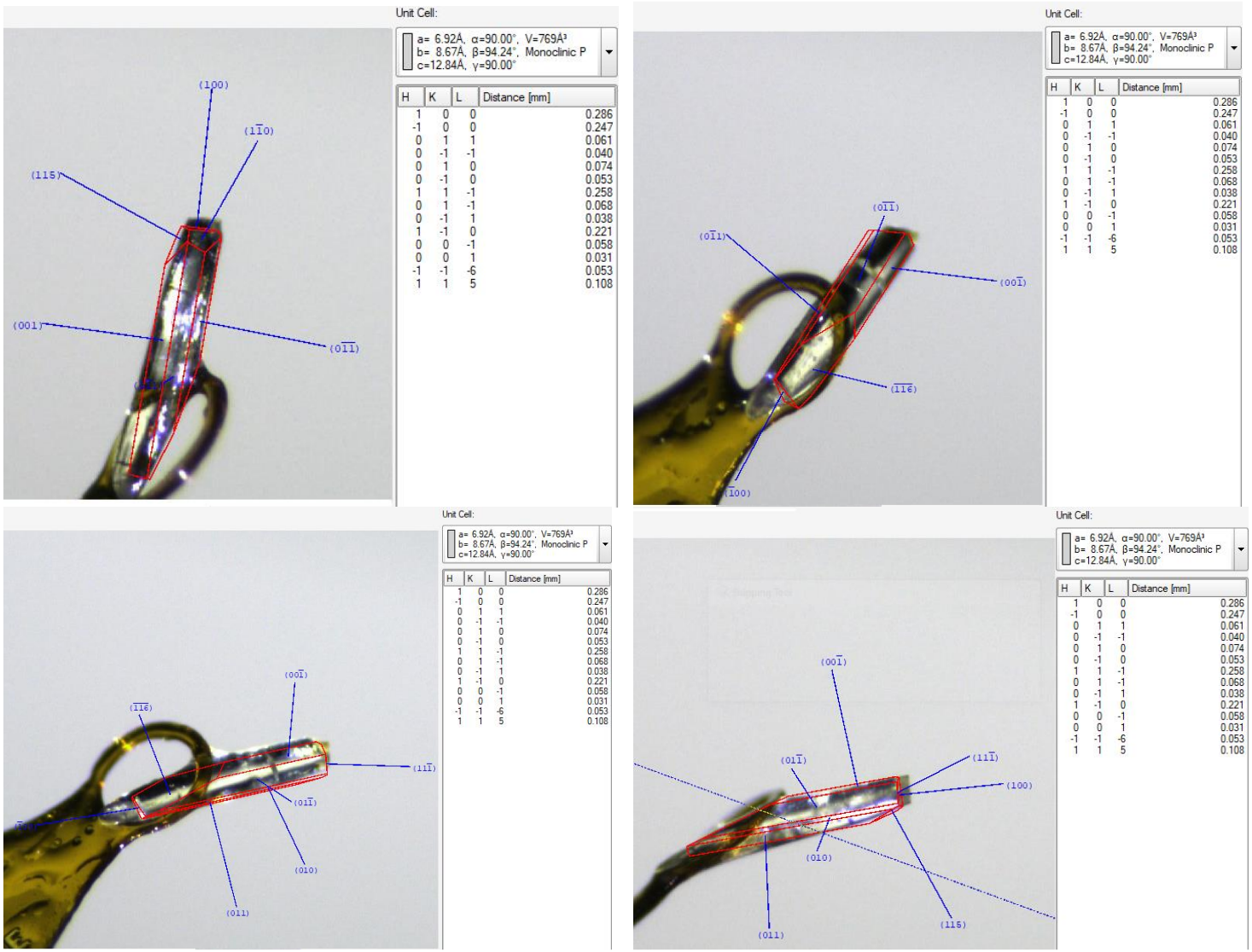

Figure S27. Indexed faces of needle-shaped crystals of metronidazole from gelator **1**.

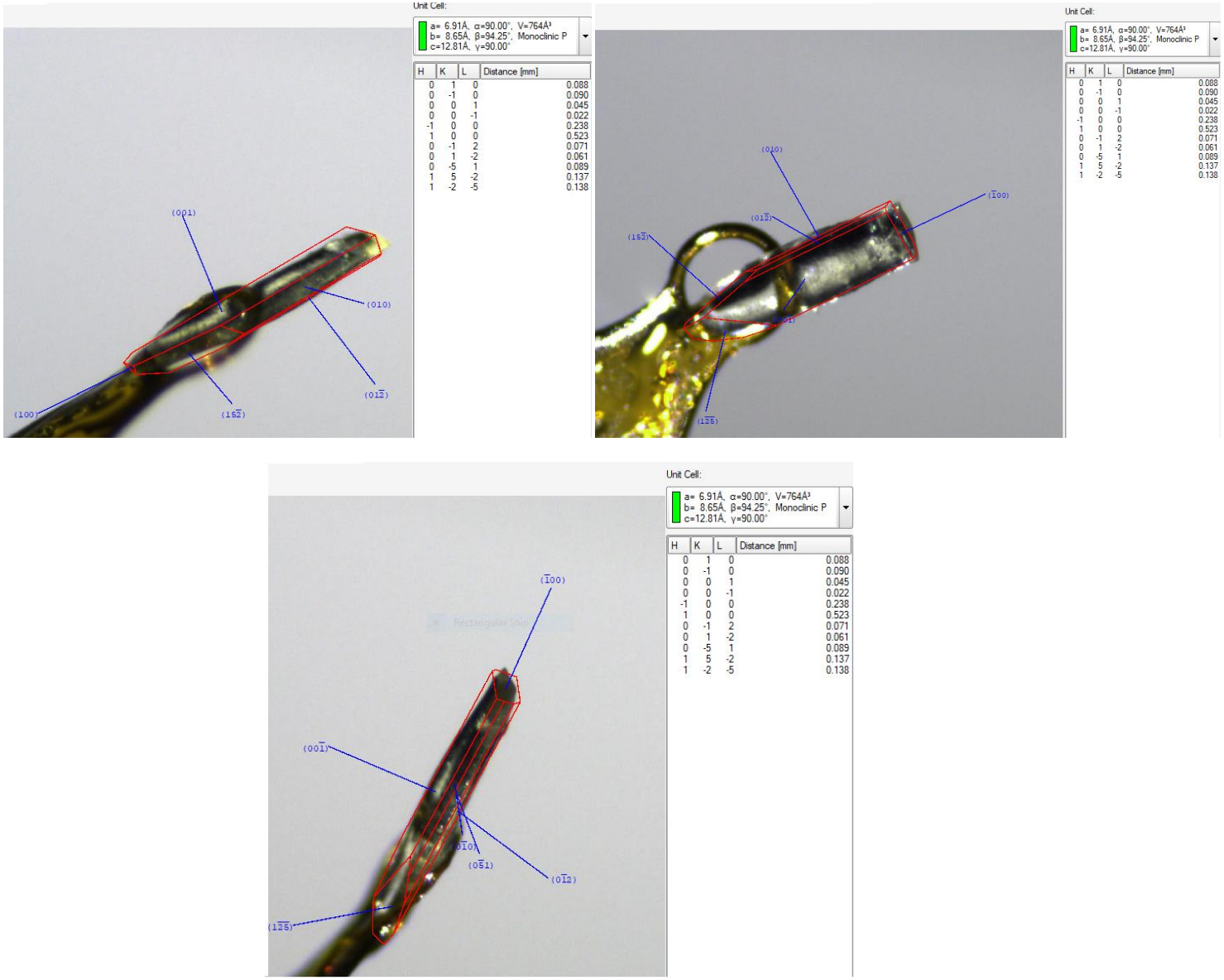

Figure S28. Indexed faces of needle-shaped crystals of metronidazole from gelator **2**.

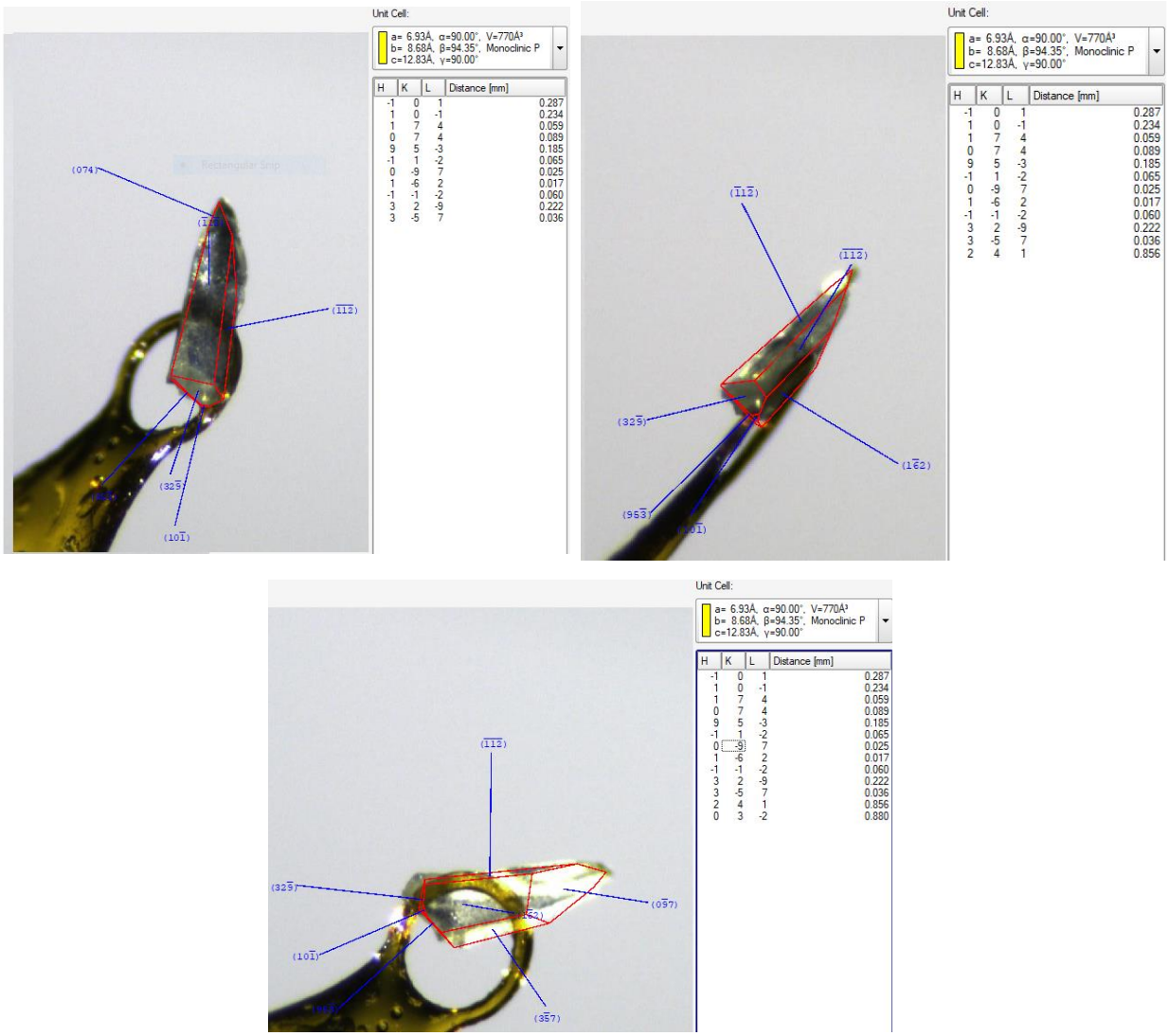

Figure S29. Indexed faces of needle-shaped crystals of metronidazole from gelator **3**.

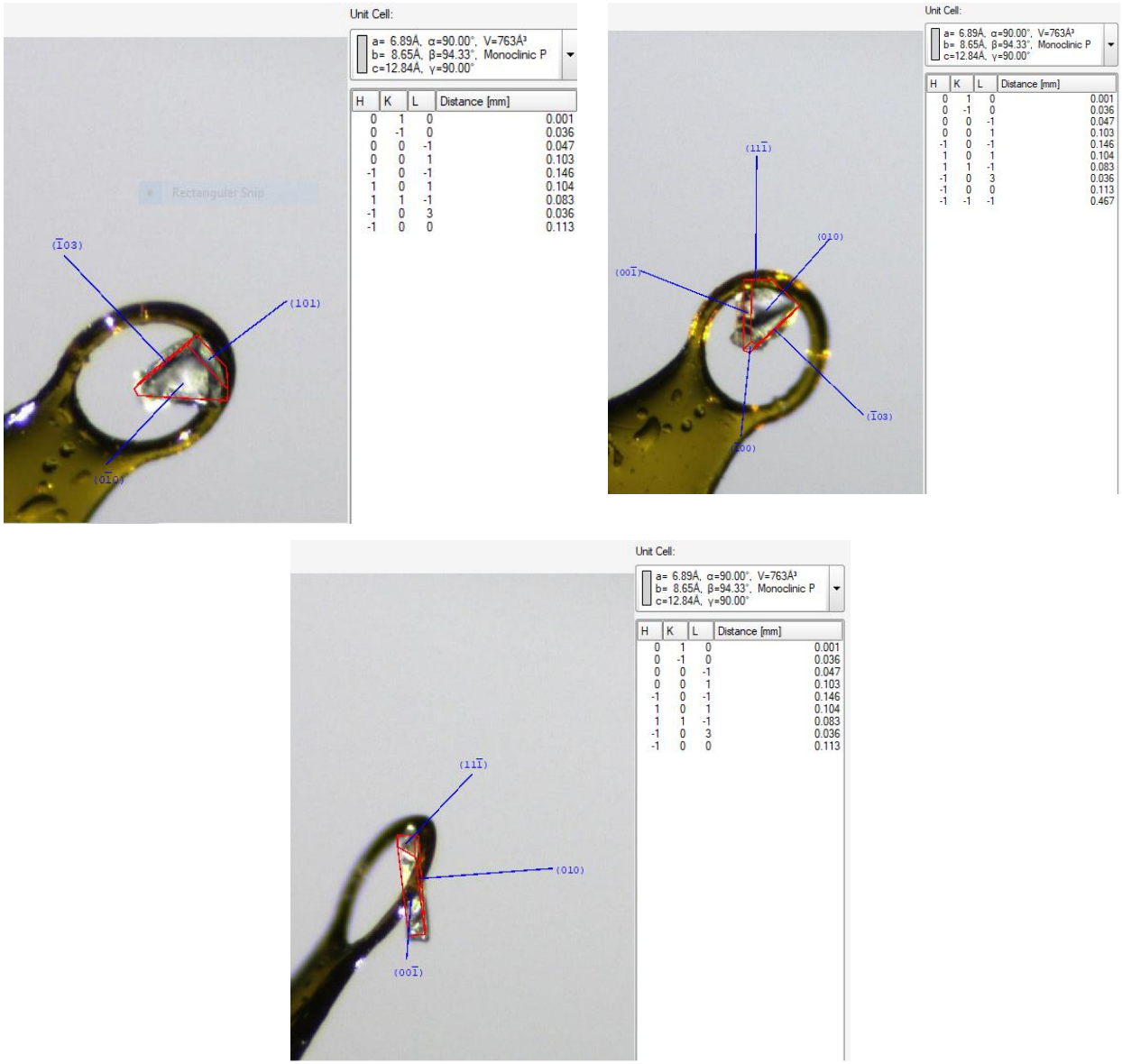

Figure S30. Indexed faces of block-shaped crystals of metronidazole from gelator **4**.

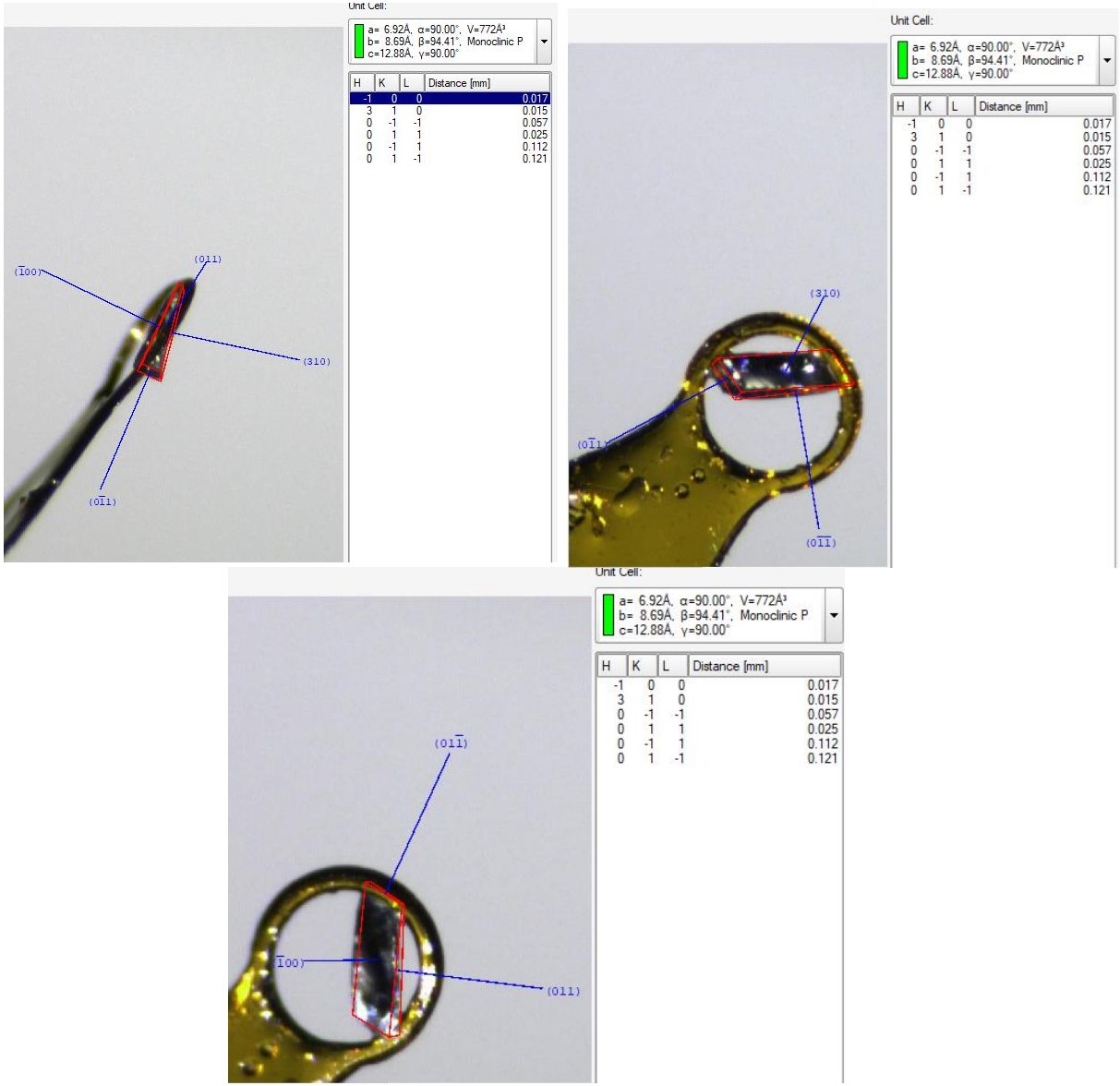

Figure S31. Indexed faces of block-shaped crystals of metronidazole from gelator **5**.

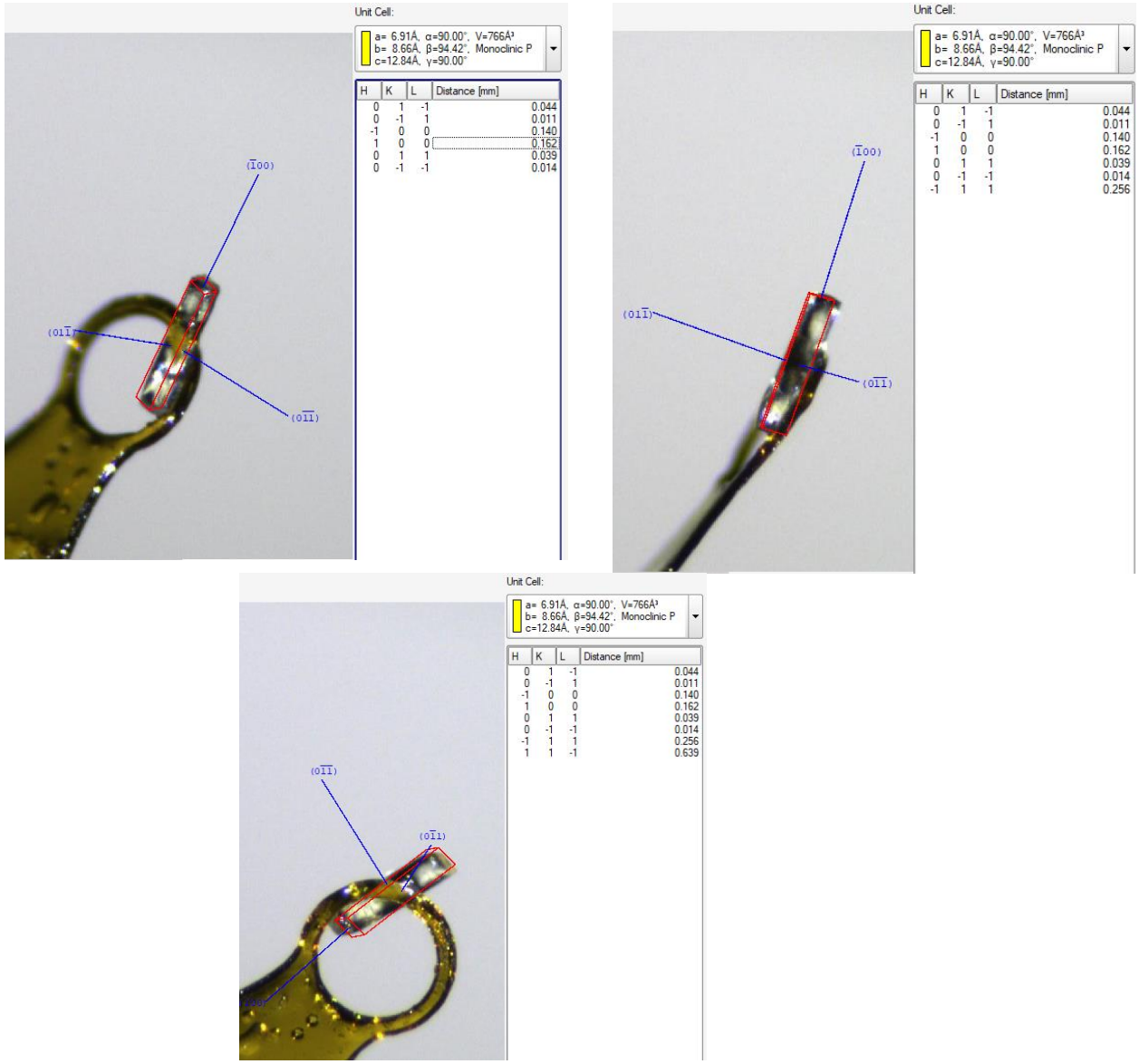

Figure S32. Indexed faces of block-shaped crystals of metronidazole from gelator **6**.

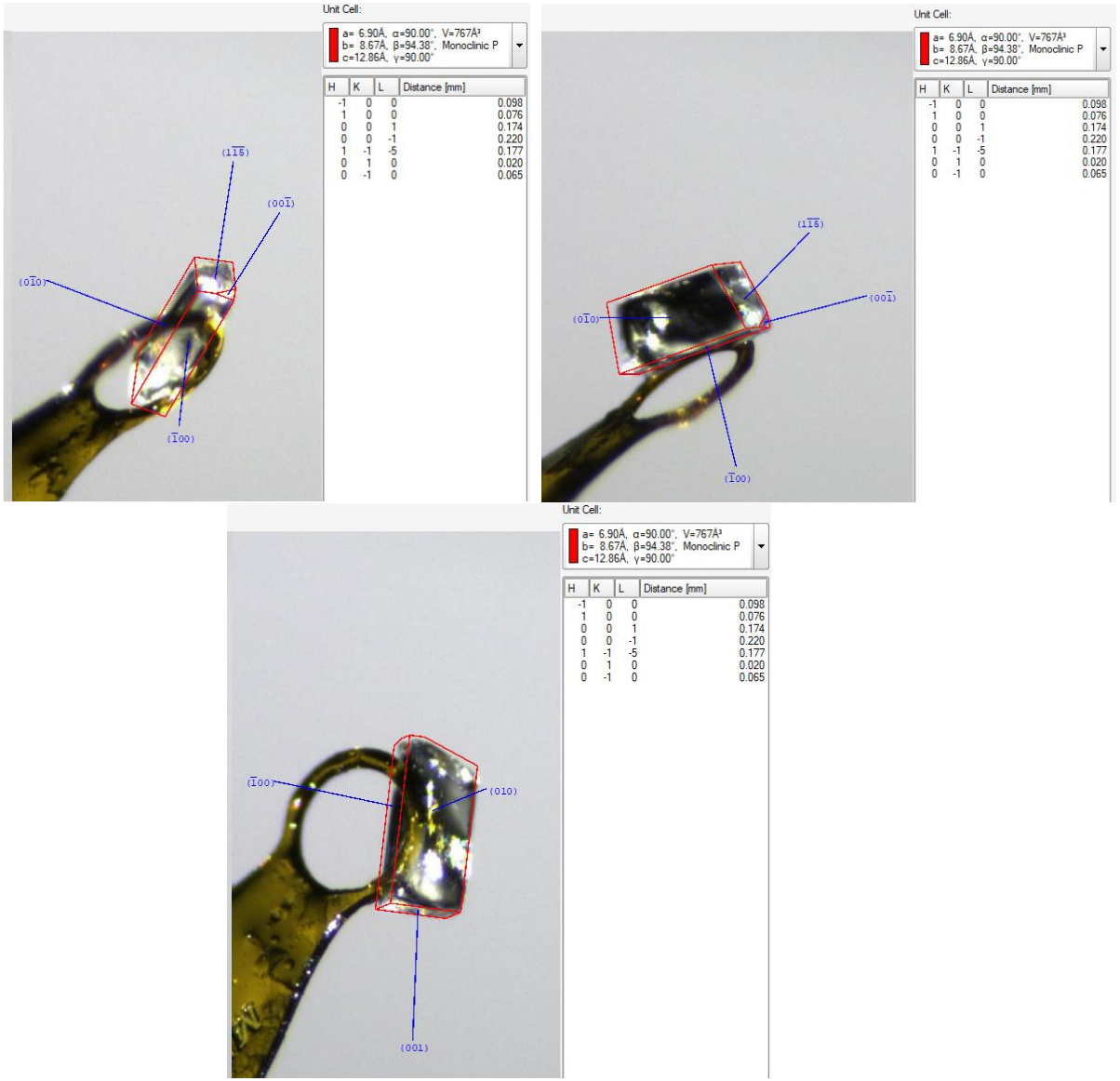

Figure S33. Indexed faces of block-shaped crystals from solution phase crystallization of metronidazole in the absence of gel.

9. Physical properties in the presence of additives

The mechanical strength was found to increase with gelators (**1**-**3**) in the presence of metronidazole. For gelator **1** the elastic modulus (*G*') increased 7-fold, while for **2** & **3** a 2-fold increase was observed (Figure S34).

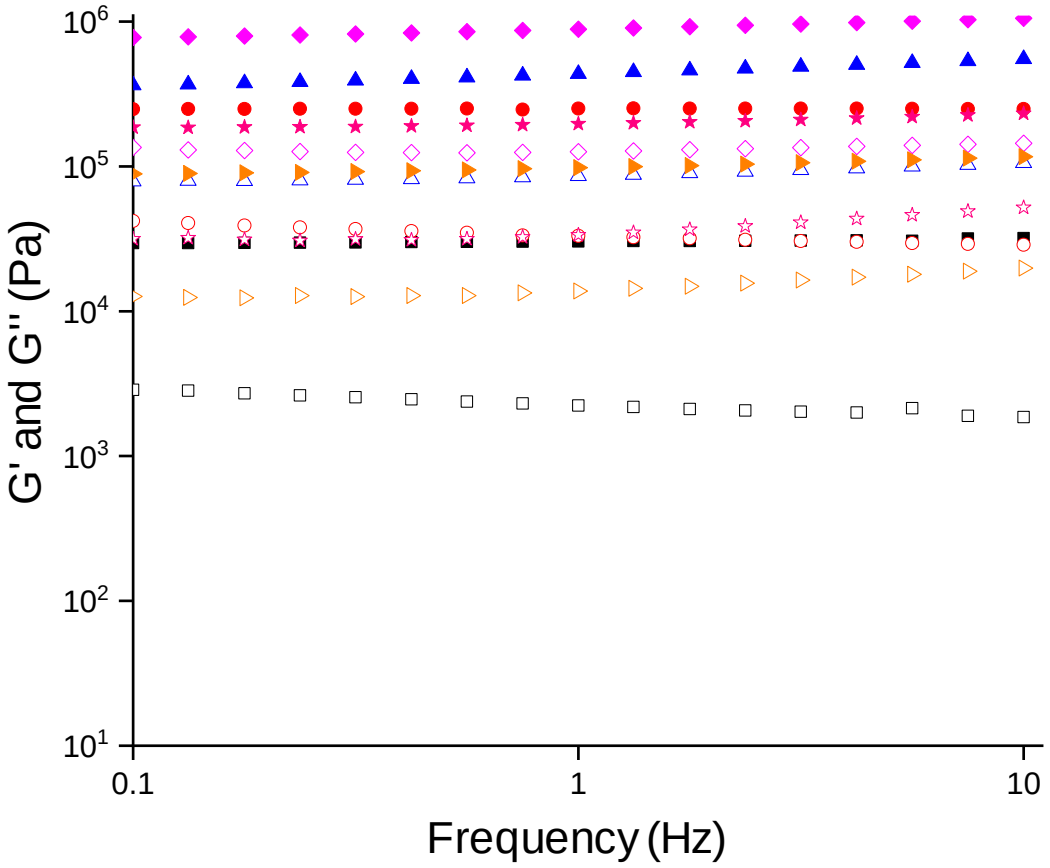

Figure S34. Frequency sweep of mimicking bis-(urea) gels (3.0 wt/v%) in nitrobenzene. Color codes: gelator- **1** G' (■) and G'' (□), gelator- **2** G' (▲) and G'' (Δ), gelator- **3** G' (▶) and G'' (▷), and experiments performed in the presence of 50.0 mg of metronidazole; gelator- **1** G' (●) and G'' (○), gelator- **2** G' (◆) and G'' (◊), gelator- **3** G' (★) and G'' (☆).

We have performed the experiments at 6.0 wt/v% of the gelator. The mechanical strength was found to increase with gelators (**1**-**3**) in the presence metronidazole. For gelator **1** and **3**, the elastic modulus (*G*') was increased 7-fold and 1.5-fold, respectively and a slight increase was observed for gelator **2**.

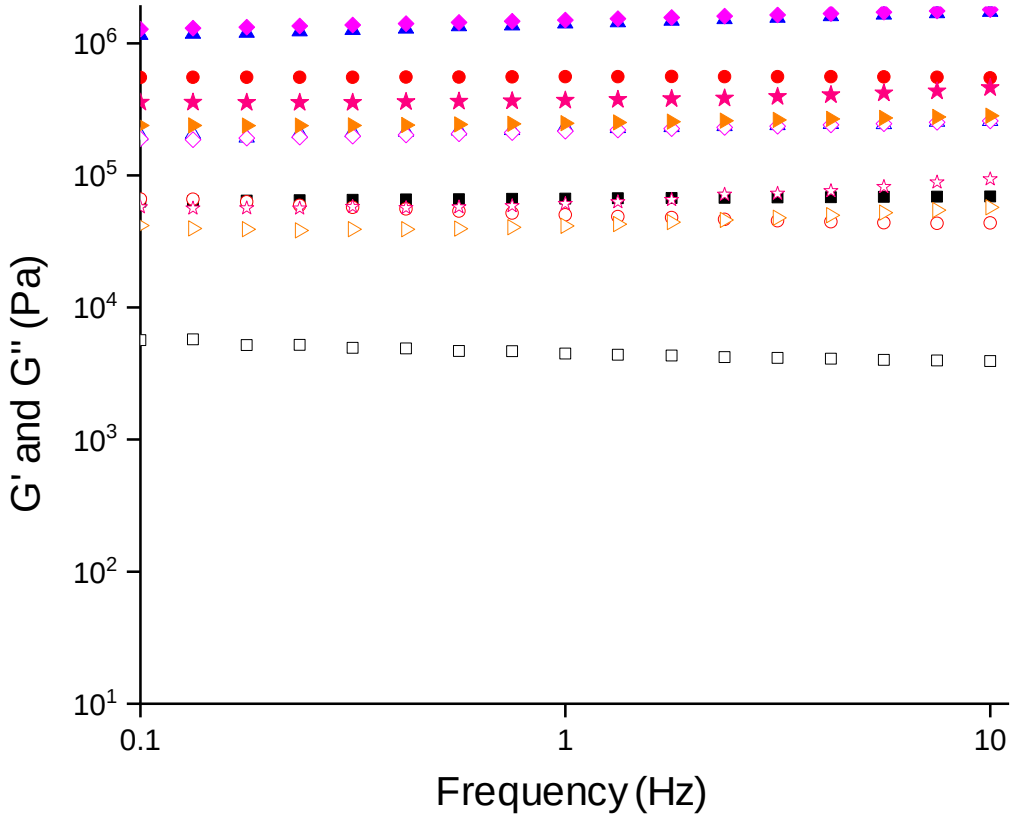

Figure S35. Frequency sweep of mimicking bis-(urea) gels (6.0 wt/v%) in nitrobenzene. Color codes: gelator- **1** G' (■) and G'' (□), gelator- **2** G' (▲) and G'' (Δ), gelator- **3** G' (▶) and G'' (▷), and experiments performed in the presence of 50.0 mg of metronidazole; gelator- **1** G' (●) and G'' (○), gelator- **2** G' (◆) and G'' (◊), gelator- **3** G' (★) and G'' (☆).

The experiments were performed with non-mimetic gelators. The mechanical strength was found to increase with gelator **6** around 1.6-fold in the presence metronidazole compared to pure gel, but it decreased with gelators **4** & **5** around 2-fold in the presence metronidazole.

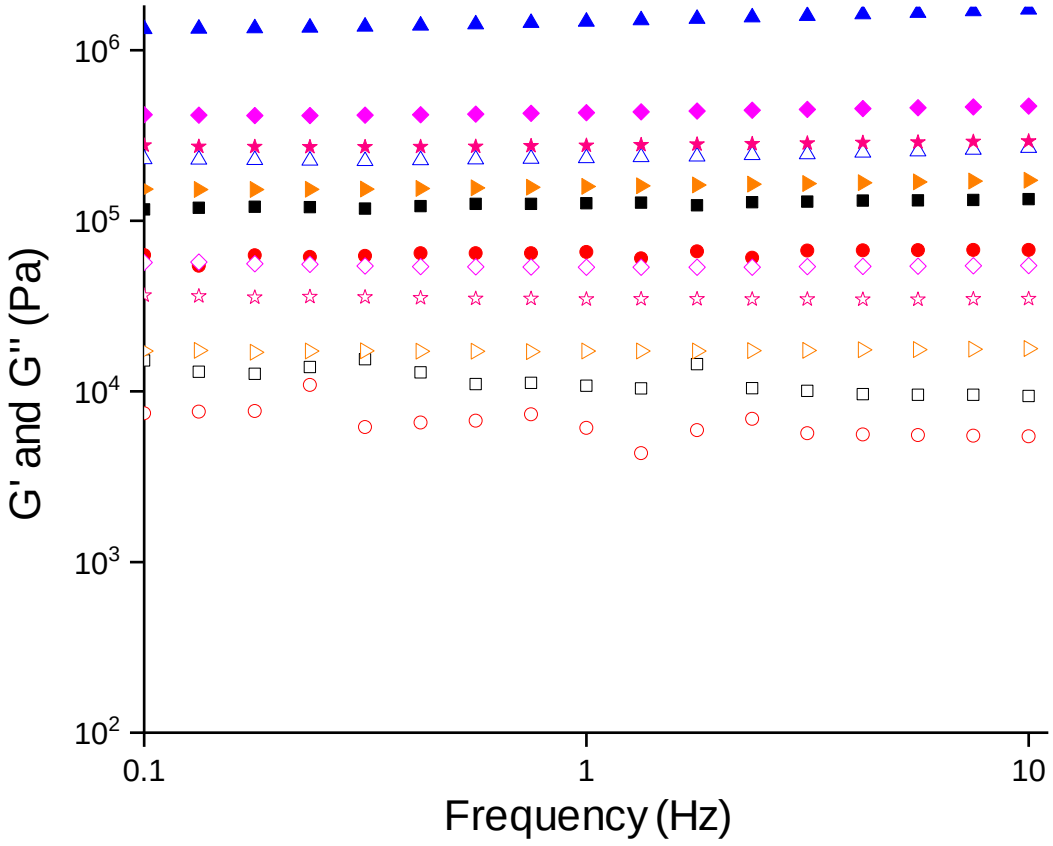

Figure S36. Frequency sweep of non-mimicking bis-(urea) gels (6.0 wt/v%) in nitrobenzene. Color codes: gelator- **4** G' (■) and G'' (□), gelator- **5** G' (▲) and G'' (Δ), gelator- **6** G' (▶) and G'' (▷), and experiments were performed in presence of 50.0 mg of metronidazole; gelator- **4** G' (●) and G'' (○), gelator- **5** G' (◆) and G'' (◊), gelator- **6** G' (★) and G'' (☆).

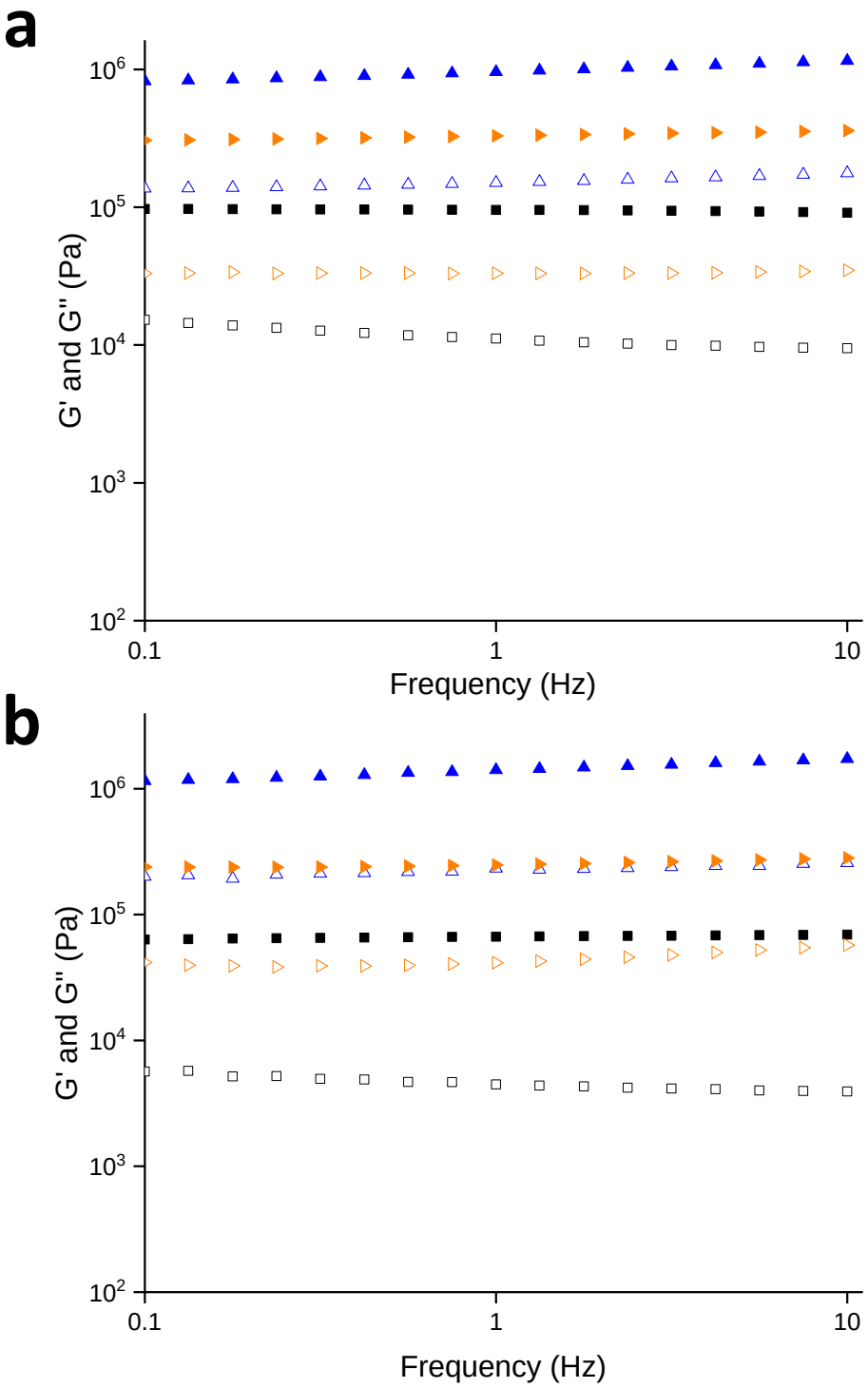

Figure S37. Comparison of frequency sweep experiments of mimicking bis-(urea) gels (a) before and (b) after annealing at (6.0 wt/v%) in nitrobenzene. Color codes: gelator- **1** G′ (■) and G′′ (□), gelator- **2** G′ (▲) and G′′ (Δ), gelator- **3** G′ (►) and G′′ (▷).

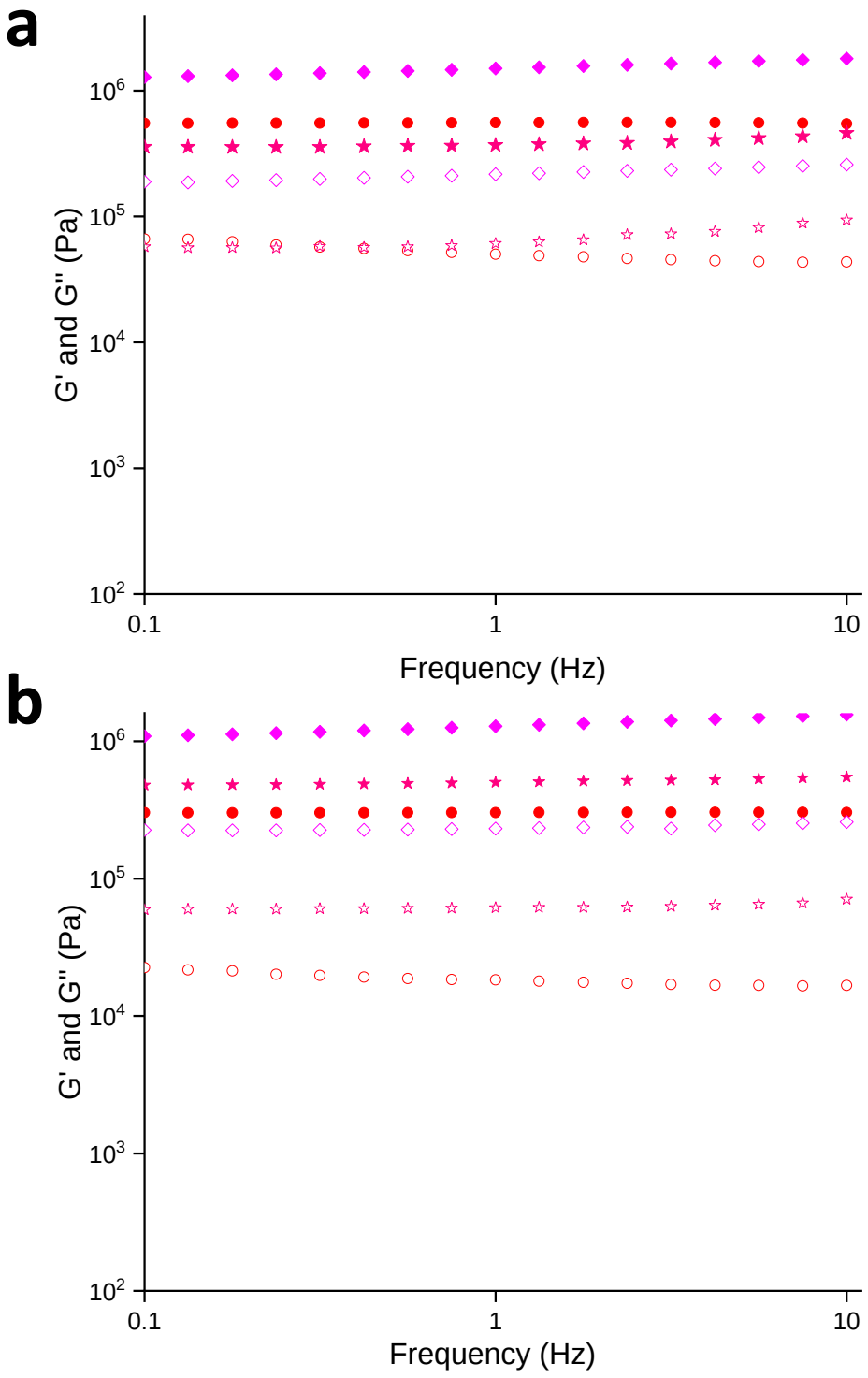

Figure S38. Comparison of frequency sweep of mimicking bis-(urea) gels (a) before and (b) after annealing at (6.0 wt/v%) in nitrobenzene in the presence of metronidazole (50.0 mg/mL). Color codes: gelator- **1** G' (●) and G'' (○), gelator- **2** G' (◆) and G'' (◊), gelator- **3** G' (★) and G'' (☆).

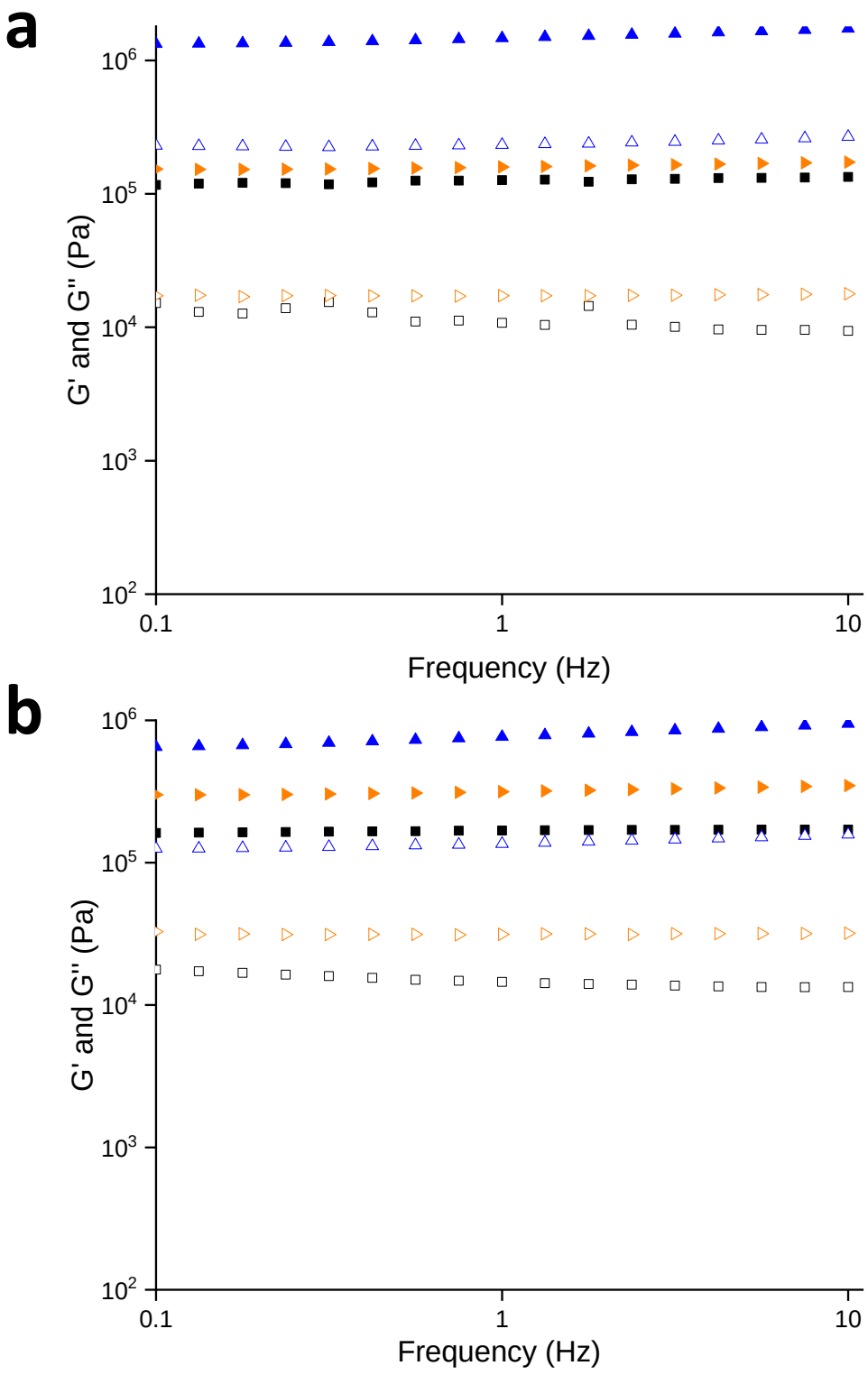

Figure S39. Comparison of frequency sweep experiments of non-mimicking bis-(urea) gels (a) before and (b) after annealing at (6.0 wt/v%) in nitrobenzene. Color codes: gelator- **4** G' (■) and G'' (□), gelator- **5** G' (▲) and G'' (Δ), gelator- **6** G' (►) and G'' (▷).

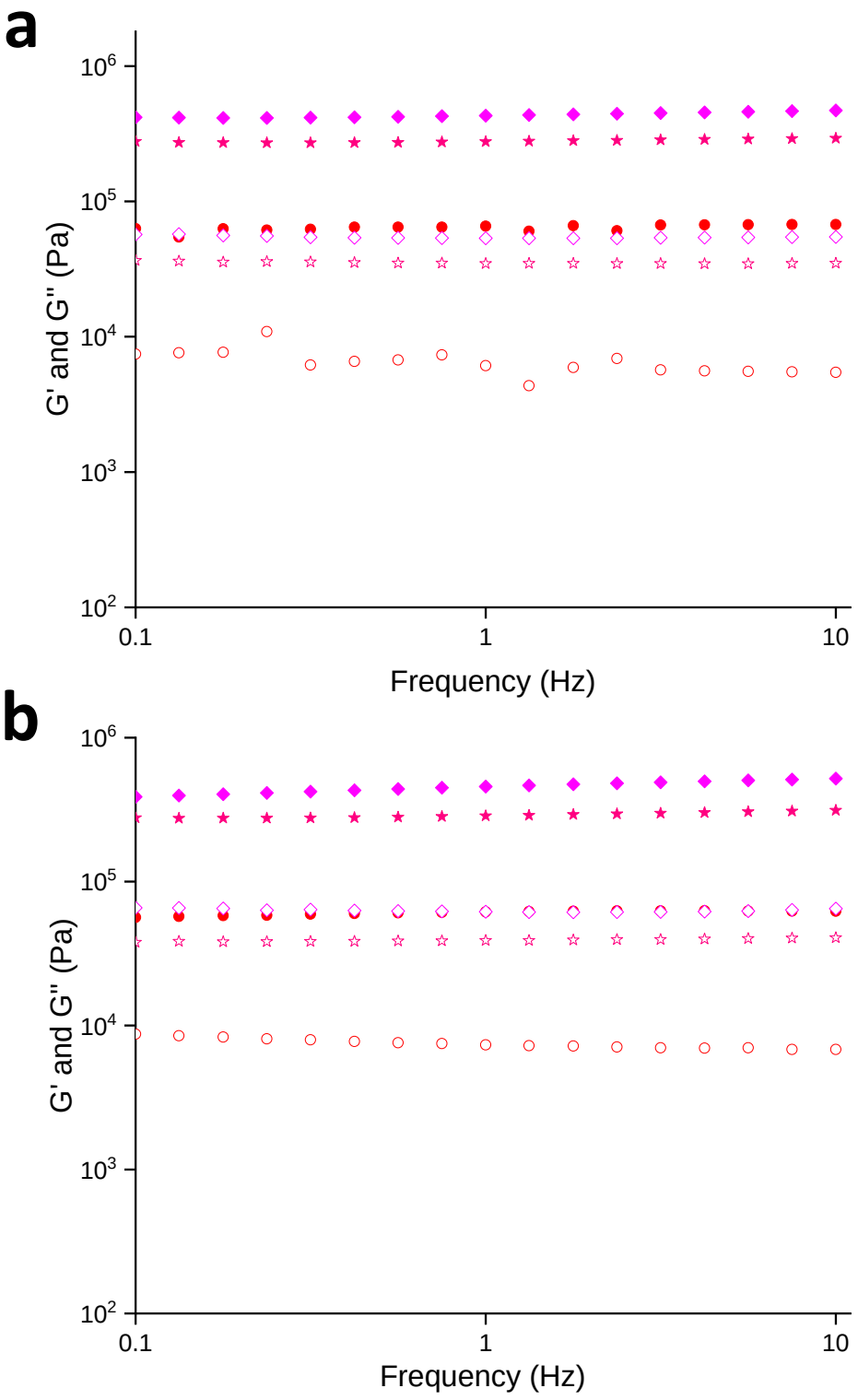

Figure S40. Comparison of frequency sweep of non-mimicking bis-(urea) gels (a) before and (b) after annealing at (6.0 wt/v%) in nitrobenzene in the presence of metronidazole (50.0 mg/mL). Color codes: gelator- **4** G' (●) and G'' (○), gelator- **5** G' (◆) and G'' (◊), gelator- **6** G' (★) and G'' (☆).

Table S9: Thermal Stabilities of gels at 3.0 wt/v% in the presence of metronidazole.

Gelators	Amount of drug (mg)	T_{gel} (°C) without additives	T_{gel} (°C) in the presence of metronidazole	T_{gel} (°C) in the presence of Isometronidazole
1	50	103.7	96.5	99.8
2	50	84.3	73.3	77.5
3	50	151.4	149.4	148.6

Table S10: Thermal Stabilities of gels at 6.0 wt/v% in the presence of metronidazole.

Gelators	Amount of drug (mg)	T_{gel} (°C) without additives	T_{gel} (°C) in the presence of metronidazole
1	50	123.2	117.6
2	50	93.5	79.8
3	50	163.1	153.1
4	50	148.1	137.9
5	50	125.1	113.6
6	50	167.8	158.6
1	100	123.2	113.3
2	100	93.5	77.4
3	100	163.1	150.4
4	100	148.1	131.6
5	100	125.1	111.4
6	100	167.8	155.2

Table S11: Thermal Stabilities of gels at 6.0 wt/v% after annealing.

Gelators	Amount of drug (mg)	T_{gel} (°C) without additives	T_{gel} (°C) in the presence of metronidazole
1	50	121.5	118.6
2	50	90.4	77.7
3	50	157.3	149.4
4	50	144.7	132.9
5	50	120.2	116.6
6	50	166.1	160.4

10. Powder X-ray diffraction

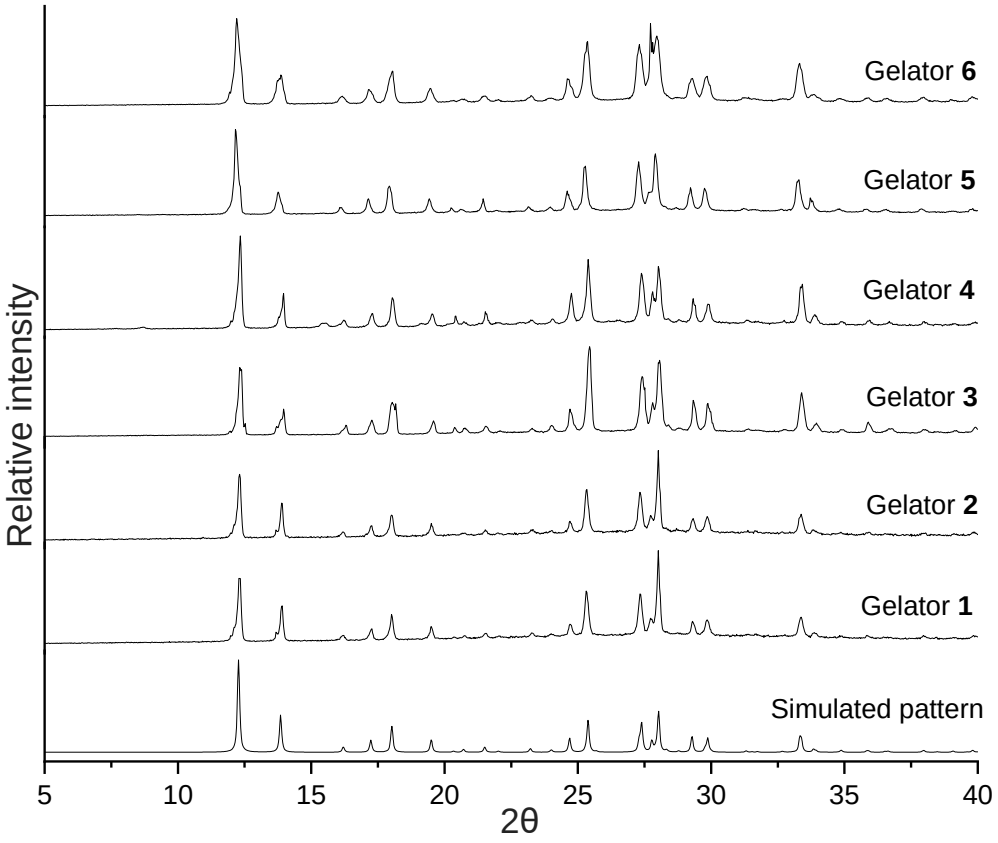

Figure S41. Comparison of simulated pattern of the crystal structure of metronidazole with the PXRD pattern of crystals isolated from gels (**1**-**6**).

Article-V

This manuscript is in its final form and preparing for submission to a peer-reviewed journal. It is presented as the current version.

Publication details:

"**Evaluating the Self-Assembly and Antibacterial Activity of Tailored Supramolecular Gels**"

Sreejith S. Jayabhavan, Arthi Chandramouli, Jayakumar Rangasamy, and Krishna K. Damodaran*

Author contributions:

SSJ and KKD planned and designed the research; **SSJ** synthesized the gelators, performed characterizations, solved single crystal structures and evaluated gelation properties. AC and **SSJ** performed antibacterial studies and JR evaluated the antibacterial results. **SSJ** and KKD wrote the initial manuscript draft and all authors reviewed the main manuscript.

Evaluating the Self-Assembly and Antibacterial Activity of Tailored Supramolecular Gels

Sreejith Sudhakaran Jayabhavan,[a] Arthi Chandramouli,[b] Jayakumar Rangasamy,[b] and Krishna K. Damodaran[a]*

[a]Department of Chemistry, Science Institute, University of Iceland, Dunhagi 3, 107 Reykjavík, Iceland.

[b]Polymeric Biomaterials Lab, School of Nanosciences and Molecular Medicine, Amrita Vishwa Vidyapeetham, Kochi 682041, India.

*Corresponding author.

E-mail addresses: ssj37@hi.is (Sreejith Sudhakaran Jayabhavan), arthic@acnsmm.aims.amrita.edu (Arthi Chandramouli), rjayakumar@aims.amrita.edu (Jayakumar Rangasamy) and krishna@hi.is (Krishna K. Damodaran).

Keywords: Low molecular weight gelator (LMWGs), Pyridyl *N*-oxide, antibacterial activity, Coordination polymer, X-ray Crystallography

Abstract: We have synthesized and characterized metronidazole (a nitroimidazole antibiotic) based carbamates with 3/4-pyridyl functionality and their corresponding *N*-oxides. The functional group modification was achieved by introducing an *N*-oxide functionality in 3-pyridyl carbamate induced hydrogelation. We have also performed metallogelation studies with the parent compound and their corresponding *N*-oxides with various transition metal salts. The studies revealed that the 3-pyridyl based carbamate formed gel with cadmium(II) chloride in DMF/water (1:1, v/v) and the corresponding *N*-oxide formed gel with silver(I) nitrate in DMF/water (1:9, v/v). However, the 4-pyridyl based carbamate did not result in metallogels, but the corresponding *N*-oxide formed a gel with copper sulphate in DMF/water (1:1, v/v). Antibacterial studies with the cadmium(II) and silver(I) complexes of ligands have shown activity against gram-positive and gram-negative bacteria.

1. Introduction

The development of new antibacterial agents for bacterial infections caused by drug-resistant bacteria is an area of current interest because of the increase in nonhealing wounds, sepsis, or death related to drug-resistant bacteria. Efforts have been made to develop antibacterial agents based on various organic/inorganic materials and antibacterial agents incorporated in gels to overcome the resistance offered by drug-resistant bacteria. Gel-based antibacterial agents display excellent antibacterial activities due to their matching biocompatibility with living tissue, soft texture, and superior water-holding capacity for moist wound-healing environments [1, 2]. Polymeric gels derived from natural and synthetic polymeric materials have extensively been used as antibacterial agents, but the bulk-scale production and biological application of the materials are limited due to the difficulty in designing specific monomers and the complexity of synthetic steps involving toxic cross-linking agents. Supramolecular gels based on low molecular weight gelators (LMWGs) are an excellent class of soft materials with tunable properties that can be readily synthesized from cheap starting materials [3-6]. Due to their reversible nature, LMWGs fall under the category of stimuli-responsive materials and display various applications in the medicinal field, such as tissue engineering, drug delivery, and antibacterial and anticancer agents [7-9]. LMWGs are formed by the self-assembly of small organic

molecules into a network of fibers via non-bonding interactions that can trap solvent, creating the gel network [4, 10-15]. The nature of supramolecular self-assembly is influenced by various factors such as pH, temperature, concentration, gelator structure, or the presence of an external entity [16-20]. Furthermore, understanding the significance of functional groups, along with the nature of non-bonding interactions, could help researchers to develop advanced materials based on LMWGs with tunable properties [21-26].

The incorporation of additional functional groups along with hydrogen bonding capabilities, like urea, amide, carbamate, thiourea, and pyridyl, could enhance the self-assembly process, leading to gel network formation. The pyridyl groups have been well explored in LMWGs due to the simplicity of acquiring crystalline materials and their modification of pyridyl groups via facile chemical processes. Moreover, several isomers can be synthesized by altering the relative position of the pyridyl nitrogen atom. We have shown that the gelation properties of bis-pyridyl LMWGs can be tuned by substituting the pyridyl group with pyridyl-*N*-oxide, yielding pyridyl-*N*-oxide LMWGs [27]. Because of its fascinating applications in medical research, compounds based on pyridyl-*N*-oxide moieties have attracted a lot of attention in the fields of synthetic chemistry, biochemistry, and pharmacology. The intriguing properties of *N*-oxide moieties arises from the π-type back-donation of the O-N bond to the N-O donating bond in the *N*-oxide moieties [25-28]. The stability of the N–O bond can be enhanced by the presence of electron withdrawing groups. Moreover, pyridyl-*N*-oxides moieties have shown enhanced hydrogen bonding, which makes them soluble in water [29-32]. We studied the antibacterial activity of supramolecular *N*-oxide gels obtained by the structural modification of the existing pyridyl gelators, which showed excellent antibacterial activity towards [28]. This prompted us to incorporate additional functional groups with well-known antibacterial properties to enhance the activity. We have selected metronidazole as the antibacterial agent, which is an antibiotic and antiprotozoal agent frequently employed for dealing with diverse infections [29].

Metronidazole is a nitroimidazole-based compound and is highly productive against anaerobic bacteria and certain protozoa [30-33], making it a significant pharmaceutical agent in clinical and surgical environments. Metronidazole is available in a variety of formulations, including oral pills, topical gels, and intravenous formulations. This allows a flexible application of the medication, which can be tailored to the specific type and severity of the infection [34, 35]. Pal's group investigated the osteogenic effects of the anti-microbial drug metronidazole (MTZ) on bone healing and regeneration and designed an injectable sustained-release in situ gel formulation of the drug that improved fracture healing efficacy by 3.5-fold compared to oral administration [36]. Zhou and coworkers synthesized naphthalimide-derived metronidazoles as potential antibacterial agents and observed that one of the derivatives could inhibit DNA replication by forming a steady supramolecular complex with DNA and interact with human serum albumin (HSA) via hydrogen bonds and hydrophobic effects [37]. Rawat and coworkers have shown the enhanced antibacterial activity of metronidazole–triazole conjugates compared to the reference drug tetracycline [38]. Efforts have been made to combine the advantages of LMWGs and metronidazole by encapsulating the drug in the gel network. Gupta and coworkers have reported the pH-responsive drug release of metronidazole from the drug-loaded gel to the buffer solution and the drug release was studied using UV-visible spectroscopy [39]. The same group reported the effective encapsulation and release of metronidazole within the gel matrix at physiological pH conditions at 37 °C [40]. Pal *et al*. demonstrated that a soy lecithin-based organogel, in a sunflower oil-water mixture and the antibiotic metronidazole, operated as an ointment with controlled release in vitro [41]. However, metronidazole-based LMWGs as antibacterial agents are rare [22, 27], which prompted us to incorporate metronidazole drug into pyridyl/*N*-oxide compounds. In this work, the metronidazole functionalities were appended to carbamate-based pyridyl/*N*-oxide compounds and their antibacterial activities were evaluated. The coordination-driven self-assembly

in these molecules were also studied due to the multi-functional character of these ligands. The combination of these functional groups with an active metal center could enhance the antibacterial activity of metronidazole [45], leading to LMWGs with intriguing antibacterial properties.

2. Results and Discussions

Metronidazole moieties can be incorporated in LMWGs and we have reported their application in gel phase crystallization, such as crystal habit modification of metronidazole drug in metronidazole-based LMWGs[22]. This was achieved by incorporating bis(urea) functionalities to generate multi-functional ligands based on metronidazole as LMWGs [22]. We have also shown that *N*-oxide gels are excellent stimuli-responsive materials towards anions [27]. Herein, we have designed a multi-functional ligand by incorporating metronidazole into a carbamate-based pyridyl/*N*-oxide compound (PCM and PCMNox) and have synthesized two carbamate-based molecules (Figure 1). The carbamate functional group was selected because certain carbamates exhibit significant biological activity, including anti-inflammatory and analgesic properties [42, 43], and the self-assembly in carbamates is similar to the biological self-assembly involving hydrogen bonding [44]. We also synthesized a compound without the pyridyl moiety (CM) to study the role of pyridyl/*N*-oxide functionality in the gelation process.

2.1. Synthesis

The compound CM was synthesized following a standard protocol by reacting phenyl isocyanate with metronidazole in the presence of triethylamine (Scheme S1). The compounds 3-PCM and 4-PCM were synthesized by reacting the corresponding pyridyl isocyanates with metronidazole and were further oxidized to obtain the *N*-oxides (Scheme S2 and S3). All the synthesized compounds were characterized via NMR (Figure S1-S10) and mass spectrometry.

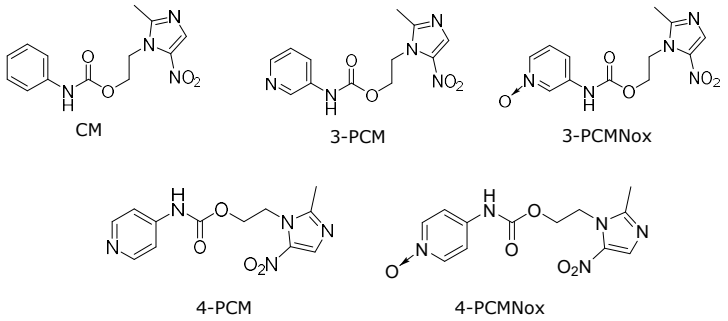

Figure 1. Chemical structures of the compounds.

2.2. Gelation studies

The gelation properties of all the compounds were tested in a wide range of solvents (Table S1, see supporting information). The gelation test was carried out following a trivial method, where the gelator (10.0 mg) was dispersed in a suitable solvent (1.0 mL) in a sealed vial (1.0 wt/v%) via sonication, and heated to give a transparent solution. The vial was left undisturbed, and the gel formation was confirmed by a vial inversion test. Gelation tests revealed that all the compounds were insoluble in non-polar aromatic solvents such as xylenes, mesitylene, and toluene (Table S1). Crystalline compounds were obtained for CM and 3-PCM in alcohols, while the compounds 4-PCM and *N*-oxides precipitated out. We have also observed that the functional group modification has induced hydrogelation in 3-PCMNox at 4.0 wt%, whereas crystals were obtained for 4-PCMNox in water. Gelation tests were also performed in 1:1 (v/v) aqueous mixtures of ethylene glycol, DMF, DMSO, and

EtOH. This showed that 3-PCM formed gel in the aqueous mixtures (1:1, v/v) of EG and DMSO, while the compounds CM, 4-PCM and 4-PCMNox were found to be non-gelators.

The minimum amount of the gelator required to form a self-standing gel is known as the minimum gelator concentration (MGC). The 3-PCMNox gelled at a minimum concentration of 3.8 wt%, while 3-PCM formed stable gel at 3.8 and 4.5 wt/v% in EG/water and DMSO/water (1:1, v/v) (Table S2).

2.3. Thermal stability

The gel-sol transition temperature (T_{gel}) is marked by the conversion of a gel to its solution state, which can be used to calculate the thermal stability of the gel. We have studied the thermal stability of the 3-PCM gels prepared in the aqueous mixtures (1:1, v/v) of EG and DMSO at 5.0 wt/v% and the transitions were observed at 86.2 and 75.1 °C, respectively. The hydrogelator showed a gel-sol transition temperature of 67.9 °C at 4.0 wt/v% (Table S3).

2.4. Metallogelation

We have studied coordination-induced metallogelation studies with all the compounds using various transition metal salts. The metallogelation experiments were performed in a standard 7.0 mL vial with DMF/water (1:1, v/v) at 1:2 metal-to-ligand ratio. The corresponding amount of ligand was dissolved in 0.5 mL of DMF by sonication and slow heating followed by the addition of the metal solution in water (0.5 mL). The vial was then sealed and kept undisturbed to test gelation. The metallogelation experiments with CM showed that the ligand precipitated out in all cases (Table S4). This highlights the importance of specific functional groups such as pyridyl/*N*-oxide moieties, for coordination-driven self-assembly. We then studied the metallogelation with 3-PCM and the metallogelation studies with copper(II) salts formed a precipitate, but an opaque gel was obtained with cadmium(II) chloride. The MGC of the 3-PCM+$CdCl_2$ gel was observed to be 4.3 wt/v% of the ligand, and it formed a thermo irreversible gel. The compound 4-PCM was observed to be a non-gelator upon metal coordination. The hydrogelator 3-PCMNox did not form a metallogels; however, by tuning the solvent composition, DMF/water (1:9, v/v) metallogel was obtained with silver(I) nitrate. Meanwhile, its isomer 4-PCMNox formed a green gel with copper(II) sulfate. The analysis of MGC revealed that the 3-PCMNox+$AgNO_3$ and 4-PCMNox+$CuSO_4$ gelled at a minimum concentration of 6.1 wt/v% of the corresponding ligands (Table S4).

2.5. Mechanical stability

Understanding the physiological properties of a gel is a key factor in analyzing the solid-like characteristic of the gel network [46, 47]. Rheology is used to quantify the deformation and flow characteristics of supramolecular gels, and rheological experiments provide information about the gel structural characteristics [48-50]. Initially, oscillatory rheological measurement (amplitude-sweep tests) was conducted to determine the linear viscoelastic region (LVR) at a constant frequency of 1.0 Hz. The storage modulus (G') dominates over the viscous modulus (G'') within the LVR region, and the elastic component is independent of the applied strain. The 3-PCM based gels made at 5.0 wt/v% in EG/water and DMSO/water (1:1, v/v) showed an LVR of about 0.05%, while the 3-PCMNox hydrogel at 4.0 wt% showed an LVR of 0.02% (Figure S11-S12). The cross-over point at which the gel completely breaks into solution was observed to be 1.0 -10.0 % in the above cases.

Frequency sweep experiments were performed within a range of 0.1- 10 Hz at a constant strain of 0.02 %. These materials can be called true gels since the elastic (G') is a magnitude higher than the viscous (G") moduli under varying frequencies. The 3-PCM gel prepared in EG/water (1:1, v/v) showed better mechanical strength than the gel obtained from DMSO/water (1:1, v/v), and the trend was

consistent with thermal stability (Figure S13). The hydrogel based on 3-PCMNox also formed a stable gel at 4.0 wt% (Figure S14). These results indicates the importance of functional group modification in tuning the gelation properties. We further investigated the mechanical properties of the three metallogels (3-PCM+$CdCl_2$, 3-PCMNox+$AgNO_3$, and 4-PCMNox+$CuSO_4$) by performing the amplitude sweep to study the stability of the gels. These metallogels showed an LVR of about 0.05% of strain and revealed a cross-over point near 1.0-12.0 % of strain (Figure S15). Analyzing the frequency sweep experiments showed that the 4-PCMNox+$CuSO_4$ gel was stiffer, and the 3-PCMNox+$AgNO_3$ gel showed a weak gel network (Figure 2). The difference in mechanical strength can be attributed to the favorable interaction between the specific functionality and the metal salts, which leads to coordination-driven self-assembly.

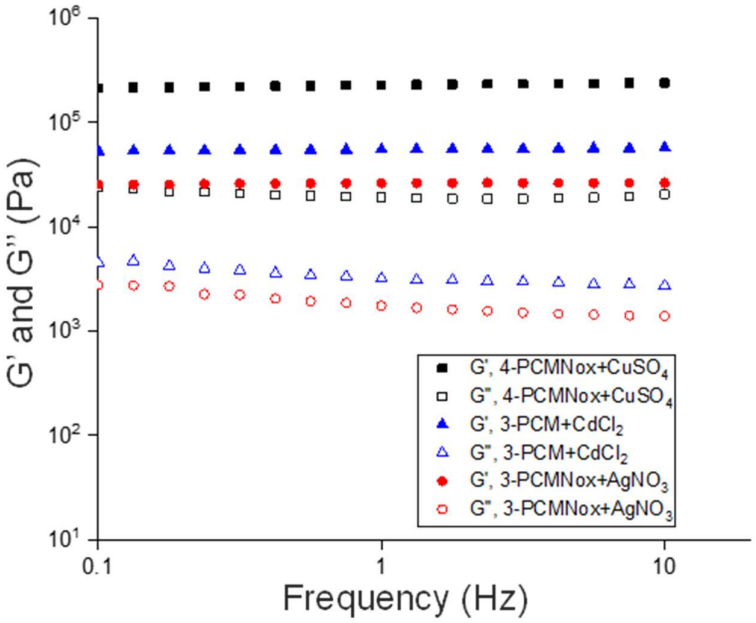

Figure 2. Frequency sweep experiments with 3-PCM+$CdCl_2$ gel (5.8 wt/v% of ligand) and 4-PCMNox+$CuSO_4$ gel (6.1 wt/v% of ligand) in DMF/water 1:1, v/v, and 3-PCMNox+$AgNO_3$ gel (6.1 wt/v% of ligand) in DMF/water 1:9, v/v, at 1:2 metal to ligand ratio and at 20.0 °C measured at a constant strain of 0.02%.

2.6. Scanning electron microscopy

Scanning electron microscopy (SEM) is a powerful technique for understanding the surface morphology of solid materials. The obtained gels were filtered and air-dried to prepare the xerogels for the SEM studies. SEM performed on the dried gels of all the 3-PCM gels (5.0 wt/v%) obtained from DMSO/water (1:1, v/v) revealed a fibrous network with long rod-shaped fibers (width ranging 0.5-1.5 μm) (Figure S16a). On the other hand, its xerogel based on EG/water (1:1, v/v) displayed flaked-shaped morphology with irregular shapes (Figure S16b). The dried gel based on the hydrogel of 3-PCMNox revealed plate-shaped or flake-shaped morphologies (Figure S17). We have also analyzed the xerogels prepared from the metallogels to study the coordination-induced self-assembly by analyzing the change in morphology of the gel fibers. The dried gel of 3-PCM+$CdCl_2$ showed thin and dense fibers with fiber width ranging (0.1-0.6 μm) (Figure 3a). The 3-PCMNox+$AgNO_3$-based dried gel displayed rod-shaped fiber morphology (fiber width ranging 0.6-3.3 μm) (Figure 3b). The 4-PCMNox+$CuSO_4$ based xerogel exhibited tiny flake-shaped morphology (Figure S18).

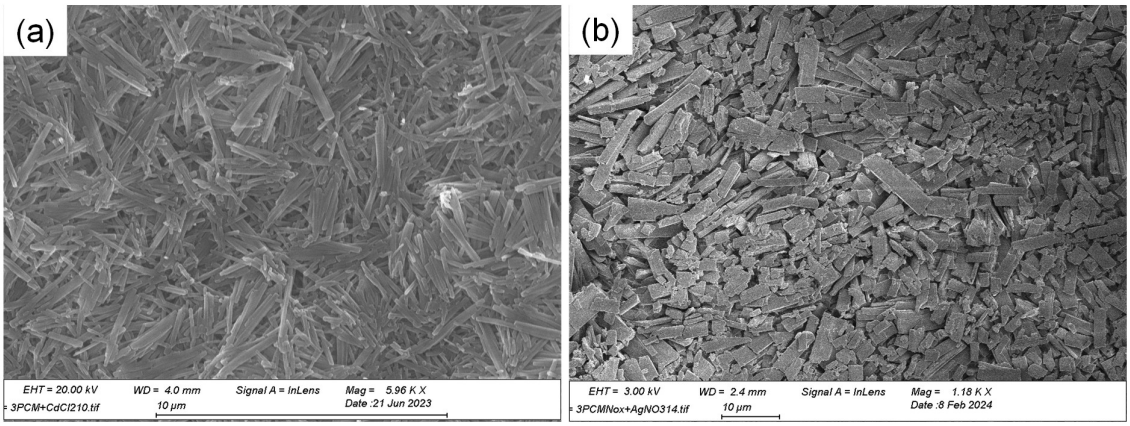

Figure 3. SEM images of the xerogel of (a) 3-PCM+$CdCl_2$ gel (5.8 wt/v% of ligand) in DMF/water (1:1, v/v), and (b) 3-PCMNox+$AgNO_3$ gel (6.1 wt/v% of ligand) in DMF/water (1:9, v/v), at 1:2 metal to ligand ratio.

2.7. X-ray crystallography

The solid-state structural analysis helps to identify the specific non-covalent interactions that play a key role in the self-assembly process of supramolecular materials. Our group have extensively used X-ray diffraction techniques to understand the non-covalent interactions observed in the solid state and the relative gel strength [51-53]. The ligands 3-PCM, 4-PCM, and 3-PCMNox crystallized in a triclinic *P*-1 space group, while the compound CM crystallized in a monoclinic $P2_1/n$ space group (Table S5 and S6). The compound CM exhibited a 0-D hydrogen bonding with its neighboring molecules via N—H···N hydrogen bonding between the carbamate functionality and metronidazole moiety and a similar kind of hydrogen bonding was also observed in 3-PCM and 4-PCM. The ligand 3-PCMNox crystallized with one water molecule. Although the N—H···N hydrogen bonding interaction was similar to 3-PCMNox, the water molecule displayed a bifurcated hydrogen bonding interaction with the *N*-oxide (O–H···O interaction) and carbamate carbonyl functionalities (O–H···O interaction) resulting in a 1-D hydrogen bonded chain. The 3-PCMNox+$AgNO_3$ and 3-PCM+$AgNO_3$ complexes crystallized in monoclinic $P2_1/c$ space group, while 3-PCMNox+$CdCl_2$ crystallized in monoclinic $C2/c$ space group and 4-PCM+$CdCl_2$ complex crystallized in a triclinic *P*-1 space group (Table S5 and S6). A one-dimensional coordination polymer was observed with 3-PCMNox+$CdCl_2$ and 4-PCM+$CdCl_2$ with the cadmium(II) central atom displaying octahedral geometry. Two-dimensional coordination polymers were obtained with both 3-PCMNox+$AgNO_3$ and 3-PCM+$AgNO_3$. Single crystal analysis with the 3-PCM+$AgNO_3$ coordination polymer revealed a silver-silver metallic bond and a non-coordinated nitrate counter anion. On the other hand, the single crystals of 3-PCMNox+$AgNO_3$ revealed distorted tetrahedral geometry with the central silver atom coordinated with two *N-oxide* functionalities, free nitrogen of the metronidazole group and the nitrate counter anion. The *N-oxide* functionality in this complex acts as a bridging ligand between two silver atoms.

2.8. Powder X-ray Diffraction

The phase purity of the crystals was validated by comparing the powder X-ray diffraction (PXRD) pattern of the bulk crystal and dried gels (xerogels) with the simulated pattern obtained from the crystal structure [52, 54-56]. The drying process of the gel could result in artefacts [57], however, this approach gives valuable insight into the self-assembly process in LMWGs [11, 51, 52, 54-56, 58]. We have analyzed the PXRD pattern of bulk crystals of all ligands and complexes, and also with the xerogels to compare the solid state properties with that of the gel state. The bulk crystals of CM,

obtained by dissolving in ethanol and DMSO/water (1:1, v/v) at 50 mg/mL showed pattern matching with the simulated pattern of the crystal data (Figure S19). PXRD pattern of the xerogels of 3-PCM (5.0 wt/v%) from EG/water and DMSO/water (1:1, v/v) matched the simulated pattern of 3-PCM confirming similar kind of interactions or packing in the solid form and dried gel states (Figure S20). The xerogel of the metallogel 3-PCM+$CdCl_2$ showed a different powder pattern compared to the simulated pattern of the 3-PCM, suggesting a different mode of packing due to metal coordination (Figure S20). The powder pattern of the crystals obtained via metal complexation of 3-PCM with silver(I) nitrate in a 1:1 aqueous mixture of DEA/DMA revealed that most of the peaks were matching with the simulated pattern of the single crystal of 3-PCM+$AgNO_3$ complex data (Figure S21). The PXRD pattern of the *N*-oxide compounds were performed with the bulk crystals (10.0 mg/mL) and xerogel (40.0 mg/mL) of 3-PCMNox from water and the results indicated that the PXRD pattern matched exactly with the simulated pattern of 3-PCMNox obtained from the single crystal data (Figure S22). We have also prepared the metal complexes of 3-PCMNox with silver(I) nitrate and cadmium(II) chloride. The 3-PCMNox+$AgNO_3$ xerogel obtained from DMF/water (1:9, v/v) at 6.1 wt/v% of ligand and 1:2 metal to ligand ratio revealed a matching powder pattern with the simulated pattern of 3-PCMNox+$AgNO_3$ complex, which revealed similar packing in solid-sate and dried gel state (Figure S23). The powder pattern of the bulk crystals of 3-PCMNox+$CdCl_2$ and 4-PCM+$CdCl_2$ matched exactly with the corresponding simulated pattern (Figure S24 & S25), suggesting the phase purity of the bulk samples. The xerogel prepared from the 4-PCMNox+$CuSO_4$ gel (6.1 wt/v% of ligand) in DMF/water (1:1, v/v), at 1:2 metal to ligand ratio showed a different powder pattern compared to the simulated pattern of the 4-PCMNox (Figure S26) confirming the metal complexation in 4-PCMNox+$CuSO_4$ gel.

2.8. Antibacterial activity

2.8.1. Well Diffusion Assay

The antibacterial activity of the prepared complexes and compounds were prepared in 0.1M acetic acid and tested against *E. coli* and *S. aureus*. The initial antibacterial experiments with the ligands 3-PCM, 4-PCM, 3-PCMNox and 4-PCMNox were negative i.e. there was no zone of inhibition against both the bacteria. Further, the antibacterial experiments on complexes such as -3-PCM+$CdCl_2$ (**C1**) 4-PCM+$CdCl_2$ (**C2**), 3-PCMNox+$CdCl_2$ (**C3**), 4-PCMNox+$CdCl_2$ (**C4**), 3-PCM+$AgNO_3$ (**C5**), 4-PCM+$AgNO_3$ (**C6**), 3-PCMNox+$AgNO_3$ (**C7**), 4-PCMNox+$AgNO_3$ (**C8**) were analyzed. The results revealed that the solution of complexes **C1-C7** and **C7 gel** showed zone of inhibition against both gram-negative (*E. coli*) and gram-positive (*S. aureus*) strains in the well diffusion method. **C1**, **C2**, **C3**, **C7** and **C7** gel showed better antibacterial activity in both the strains with ZOI of 10 ± 3 mm and complexes **C4**, **C5** and **C6** showed less antibacterial activity with ZOI 4 ± 2 mm (Figure 4). The positive control used in this study was amikacin sulfate against both strains, and the negative control was 0.1 M acetic acid, which did not inhibit both strains. The 0.1 M acetic acid was used to improve the solubility of the ligands and the complexes in water, and it was observed that the acetic acid concentration at 0.1 M did not kill the bacteria. The 4-PCMNox based cadmium and silver complexes showed very minimal or no antibacterial activity in comparison with its isomeric 3-PCMNOx based complexes, which highlights the importance of the specific role of functional groups.

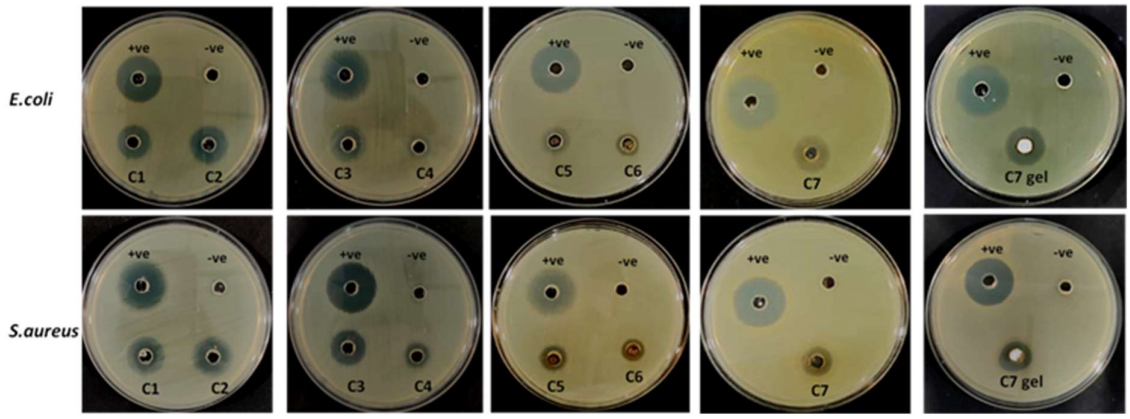

Figure 4. The images of plates showing antibacterial activity against *S. aureus* and *E. coli.*

2.8.2. Antibacterial studies by SEM analysis

The antibacterial activity of **C1-C7** and **C7 gel** complexes were visualized under SEM as shown in (Figures 5 and 6). Few bacterial disrupted or broken kinds of morphology were observed and marked in the figures showing their inhibition against these complexes. The results correlate with the zone of inhibition in 2.8.1 and we can see a reduction in bacterial number in all the complexes when compared to the control group i.e. bacteria alone sample of both the strains.

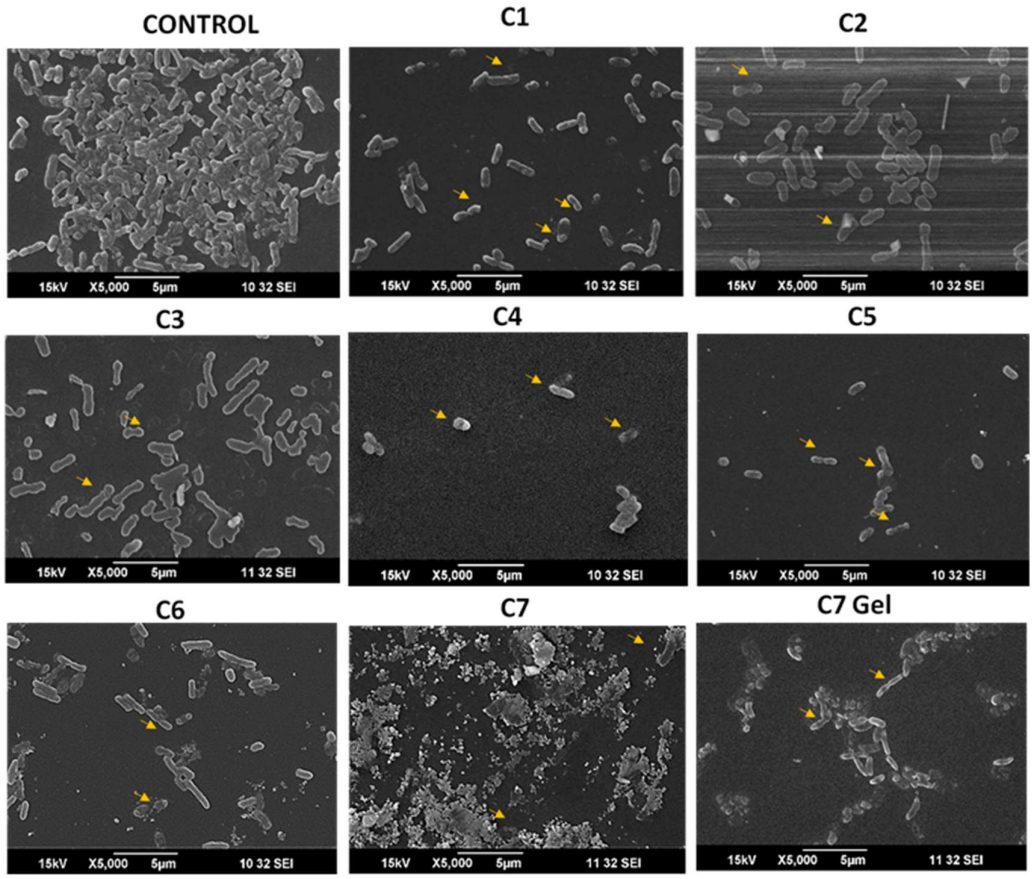

Figure 5. SEM images showing antibacterial activity via membrane disruption of *E.coli* by various complexes.

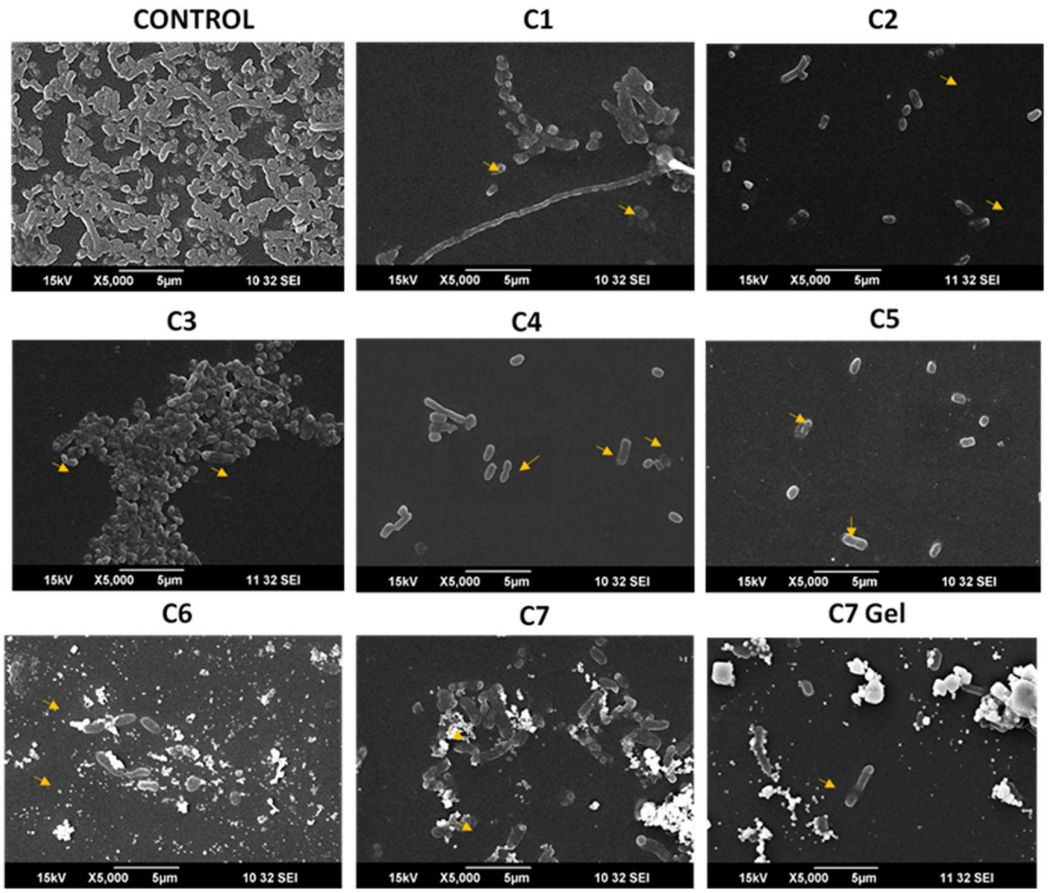

Figure 6. SEM images showing antibacterial activity via membrane disruption of *S.aureus* by various complexes

3. Materials and Methods

All the starting materials, reagents, and solvents were commercially available (Sigma Aldrich, Fluorochem and TCI Europe) and used as supplied. The metronidazole was purchased from Accel Pharmtech, USA. ^{1}H and ^{13}C NMR spectra (Figure S1-S10, see supporting information) were recorded on a Bruker AVANCE 400 spectrometer (Rheinstetten, Germany) and SEM was performed on a Leo Supra 25 microscope (Carl Zeiss, Oberkochen, Germany). The rheological experiments were performed on Anton Paar modular compact rheometer MCR 302 (Graz, Austria). SCXRD and powder X-ray diffraction (PXRD) were carried out using Bruker D8 venture (Karlsruhe, Germany) and PANalytical instrument (Almelo, Netherlands).

3.1. Synthesis of Ligands

3.1.1. Synthesis of 2-(2-methyl-5-nitro-1H-imidazol-1-yl)ethyl phenylcarbamate (CM): A solution of metronidazole (1.00 g, 5.8 mmol) in THF (40.0 mL) was added dropwise to a mixture of isocyanatobenzene (0.64 mL, 5.8 mmol) and triethylamine (0.89 mL, 6.4 mmol) in dry THF (50 mL) and was refluxed overnight under a nitrogen atmosphere. It was then cooled to room temperature and the white precipitate formed was filtered and washed with water and diethyl ether dried in air to obtain the product as a white solid. The compound was recrystallized from ethyl acetate. Yield: 1.45 g, 85.8%.^{1}H NMR (400 MHz, DMSO-d_6) δ 9.64 (s, 1H), 8.05 (s, 1H), 7.38 (d, J = 8.0 Hz, 2H), 7.31 – 7.22

(m, 2H), 7.00 (tt, *J* = 7.3, 1.2 Hz, 1H), 4.59 (t, *J* = 5.1 Hz, 2H), 4.46 (t, *J* = 5.1 Hz, 2H), 2.48 (s, 3H). $^{13}C\{^{1}H\}$ NMR (101 MHz, DMSO-d_6) δ 152.94, 151.67, 138.71, 138.49, 133.13, 128.73, 122.71, 118.52, 62.19, 45.39, 13.94. HRMS (APCI): calcd for $C_{13}H_{14}N_4O_4Na$ $[M + Na]^+$, 313.0907; found, 313.0909.

3.1.2. Synthesis of 2-(2-methyl-5-nitro-1H-imidazol-1-yl)ethyl pyridin-3-ylcarbamate (3-PCM): A solution of nicotinoyl azide (2.96 g, 20.0 mmol) in toluene (50 mL) was refluxed for 2.0 hours under a nitrogen atmosphere and cooled to room temperature. A solution of metronidazole (3.42 g, 20.0 mmol) and triethylamine (3.06 mL, 21.9 mmol) in 40 mL THF was added dropwise to the reaction mixture at room temperature. The resulting mixture was further refluxed overnight, and the white precipitate formed was filtered. The residue was washed with hot water and dried in air to obtain the product as a white solid. The product was further purified by recrystallizing in ethyl acetate. Yield: 4.65 g, 80.0 %. ^{1}H NMR (400 MHz, DMSO-d_6) δ 9.87 (s, 1H), 8.56 (d, *J* = 2.8 Hz, 1H), 8.22 (dd, *J* = 4.8, 1.5 Hz, 1H), 8.05 (s, 1H), 7.80 (d, *J* = 9.0 Hz, 1H), 7.31 (dd, *J* = 8.3, 4.7 Hz, 1H), 4.61 (t, 2H), 4.48 (t, 2H), 2.49 (s, 3H). $^{13}C\{^{1}H\}$ NMR (101 MHz, DMSO-d_6) δ 153.56, 152.13, 144.26, 140.83, 138.99, 135.93, 133.61, 125.88, 124.09, 63.08, 45.74, 14.43. HRMS (APCI): calcd for $C_{12}H_{13}N_5O_4Na$ $[M + Na]^+$, 314.0860; found, 314.0857.

3.1.3. Synthesis of 2-(2-methyl-5-nitro-1H-imidazol-1-yl)ethyl pyridin-4-ylcarbamate (4-PCM): A similar procedure was followed as in the case of 3-PCM, isonicotinoyl azide (1.48 g, 10.0 mmol), metronidazole (1.71 g, 10.0 mmol) and triethylamine (1.53 mL, 10.9 mmol). The crude compound was recrystallized from ethanol/water (1:1, v/v). Yield: 2.20 g, 75.9 %. ^{1}H NMR (400 MHz, DMSO-d_6) δ 10.09 (s, 1H), 8.38 – 8.32 (m, 2H), 8.03 (s, 1H), 7.39 – 7.33 (m, 2H), 4.60 (t, 2H), 4.48 (t, 2H), 2.47 (s, 3H). $^{13}C\{^{1}H\}$ NMR (101 MHz, DMSO-d_6) δ 152.58, 151.63, 150.26, 145.71, 138.51, 133.13, 112.45, 62.75, 45.17, 13.96. HRMS (APCI): calcd for $C_{12}H_{13}N_5O_4$ $[M + H]^+$, 292.1040; found, 292.1031.

3.1.4. Synthesis of 3-(((2-(2-methyl-5-nitro-1H-imidazol-1-yl)ethoxy)carbonyl)amino)pyridine 1-oxide (3-PCMNox): To a solution of 3-PCM (3.00 g, 10.3 mmol) in 30.0 mL DMF, 3–chloroperoxybenzic acid (3.91 g, 22.6 mmol) was added in portions, and the solution was stirred overnight at room temperature. The solution was then dried to obtain the crude product. The product was then purified by column chromatography using 10.0-20.0% of methanol/DCM as the eluent. The product was purified further by recrystallization from hot water. Yield: 2.32 g, 73.4 %. ^{1}H NMR (400 MHz, DMSO-d_6) δ 10.08 (s, 1H), 8.36 (t, *J* = 1.9 Hz, 1H), 8.05 (s, 1H), 7.91 (dt, *J* = 5.8, 1.6 Hz, 1H), 7.36 – 7.28 (m, 2H), 4.61 (t, *J* = 5.1 Hz, 2H), 4.49 (t, *J* = 5.1 Hz, 2H), 2.47 (s, 3H). $^{13}C\{^{1}H\}$ NMR (101 MHz, DMSO-d_6) δ 152.71, 151.64, 138.53, 138.22, 133.25, 133.14, 129.23, 126.22, 115.05, 62.97, 45.14, 13.96. HRMS (APCI): calcd for $C_{12}H_{13}N_5O_5Na$ $[M + Na]^+$, 330.0809; found, 330.0811.

3.1.5. Synthesis of 4-(((2-(2-methyl-5-nitro-1H-imidazol-1-yl)ethoxy)carbonyl)amino)pyridine 1-oxide (4-PCMNox): A similar procedure was followed as in the case of 3-PCMNox, 4-PCM (2.00 g, 6.9 mmol) and 3–chloroperoxybenzic acid (1.71 g, 15.1 mmol). Yield: 1.55 g, 73.4 %. ^{1}H NMR (400 MHz, DMSO-d_6) δ 10.20 (s, 1H), 8.10 – 8.04 (m, 2H), 8.02 (s, 1H), 7.40 – 7.32 (m, 2H), 4.59 (t, *J* = 5.1 Hz, 2H), 4.50 – 4.43 (m, 2H), 2.45 (s, 3H). $^{13}C\{^{1}H\}$ NMR (101 MHz, DMSO-d_6) δ 152.57, 151.63, 138.91, 138.51, 136.26, 133.14, 115.07, 62.88, 45.13, 13.97. HRMS (APCI): calcd for $C_{12}H_{13}N_5O_5Na$ $[M + Na]^+$, 330.0809; found, 330.0805.

3.2. Gelation Details

About 10.0 mg of the compound and 1.0 mL of the corresponding solvent was added to a standard 7.0 mL vial with an inner diameter of 15.0 mm. The vial was sealed, and the mixture was then sonicated and slowly heated to obtain a clear solution. The solution was left undisturbed for gelation and a vial-

inversion test was performed to confirm gelation. The experiments were repeated at higher concentrations up to 60.0 mg of the compound where needed to test the gelation property.

3.2.1. Minimum gelation concentration (MGC)

The gel was prepared following the above procedure by dissolving the compounds in 1.0 mL of solvent. Incremental quantities of the solvent were added, and the gelation procedure was repeated until a minuscule amount of the solvent was detected on the surface of the gel. The concentration slightly above which a stable gel is obtained is observed to be the MGC of the gelator.

3.3. Metallogelation studies

The mixture was prepared by dissolving the corresponding ligand in DMF (0.5 mL) and mixing with the transition metal salt dissolved in water (0.5 mL) at a 1:2 metal: ligand ratio. A clear solution was observed initially and allowed to stand undisturbed for about 24.0 h to confirm gelation.

3.4. Thermal stability

The required amount of the gelator was taken in a standard 7.0 mL vial, followed by 1.0 mL of solvent was added. The mixture was sonicated and gradually heated to dissolve and left undisturbed. A tiny spherical glass ball was placed delicately on top of the gel after 24 hours and the vial was sealed. It was then immersed carefully in an oil bath fitted with a thermosensor and magnetic stirrer. The temperature of the oil bath was increased consistently at a rate of 10.0 °C per minute. At some point, the glass ball slowly slides down, and the temperature at which the glass ball touched the bottom of the vial was recorded as T_{gel}.

3.5. Mechanical stability

The mechanical strength of the gel was measured using an MCR 302 Anton Paar modular compact rheometer equipped with a 2.5 cm stainless steel parallel plate geometry with a measuring gap of 1.00 mm. Rheological experiments were performed in (1:1, v/v) EG/water and DMSO/water at 5.0 wt/v% with 3-PCM and at 5.0 wt% with the aqueous gel of 3-PCMNox. Metallogels were prepared with 3-PCM and cadmium(II) chloride (at 2:1 ligand to metal ratio) at 5.8 wt/v% of ligand in DMF/water (1:1, v/v). We have also prepared metallogels with 3-PCMNox and silver(I) nitrate (at 2:1 ligand to metal ratio) at 6.2 wt/v% of ligand in DMF/water (1:9, v/v). The metallogels based on 4-PCMNox and copper sulfate (at 2:1 ligand to metal ratio) at 6.2 wt/v% of ligand was prepared in DMF/water (1:1, v/v). The experiments were conducted carefully by placing an approximately 1.0 mL gel on the plate. To prevent solvent evaporation and ensure a consistent temperature of 20.0 °C during frequency and amplitude sweeps, a Peltier temperature control hood was employed. Amplitude sweeps were conducted at a constant frequency of 1.0 Hz and logarithmic ramp strain (γ) ranging from 0.01% to 100%. Frequency sweeps were performed between 0.1 and 10.0 Hz within the linear viscoelasticity range (at a strain of 0.02%).

3.6. Scanning electron microscopy (SEM)

The surface morphologies of the xerogels were examined using SEM. Gels of compounds 3-PCM in (1:1, v/v) EG/water and DMSO/water at 5.0 wt/v% and the aqueous gel of 3-PCMNox (5.0 wt%) were prepared and the gel was filtered after 24 h, dried in air to obtain the xerogel. Similarly, the xerogels from the metallogels (at 1:2 metal to ligand ratio) were prepared with 3-PCM+$CdCl_2$ (DMF/water (1:1, v/v)), 3-PCMNox+$AgNO_3$ (DMF/water (1:9, v/v)), 4-PCMNox+$CuSO_4$ (DMF/water, (1:1, v/v)). A tiny portion of the xerogel was placed on a pin mount, with the carbon tab positioned on top. The mount was then coated with a layer of gold for a duration of 5-6 minutes to obtain a thickness of gold coating

about 9.0-12.0 nm. Subsequently, the mount was loaded onto a Leo Supra 25 microscope, which was operated at a voltage of 3.0 kilovolts and a working distance of 3.0-4.0 millimeters. The SEM pictures were recorded using an in-lens detector.

3.7. Single crystal X-ray Diffraction

Single crystals of the ligand CM were obtained by the slow evaporation of 20.0 mg/mL of the corresponding compounds in ethyl acetate, resulting in colorless rhombus-shaped crystals. The 3-PCM crystal was obtained by the slow evaporation of 20.0 mg/mL of the corresponding compounds in ethanol, resulting in colorless block-shaped crystals, while 3-PCMNox crystals were obtained similarly by crystallizing from water to obtain block-shaped crystals. Similarly, block-shaped X-ray quality crystals of 4-PCM were obtained by the slow evaporation of 20.0 mg of the corresponding compounds in 1.0 mL DMF. The block-shaped single crystals of complex 3-PCMNox+$CdCl_2$ were obtained by dissolving 30.7 mg of the ligand 3-PCMNox in 0.5 mL of methanol and mixing it with 9.2 mg of cadmium(II) chloride dissolved in 0.5 mL of water. The 4-PCM+$CdCl_2$ complex was crystallized by the slow evaporation of DMF solution (2.0 mL) of ligand 4-PCM (14.5 mg) and cadmium(II) chloride (4.6 mg) to obtain block-shaped crystals. X-ray quality plate-shaped crystals of 3-PCM+$AgNO_3$ were obtained by treating a DMSO (1.5 mL) solution of 3-PCM (14.5 mg) with silver(I) nitrate (4.2 mg) dissolved in 0.5 mL of water and keeping it over a week, while needle-shaped single crystals of 3-PCMNox+$AgNO_3$ were obtained by dissolving 15.3 mg of the ligand 3-PCMNox in 0.5 mL of diethyl acetamide and mixing it with silver(I) nitrate (4.2 mg) dissolved in 0.5 mL of water, and obtained the crystals over 2-3 days. X-ray analysis was conducted on a Bruker D8 Venture (Photon100 CMOS detector) diffractometer implemented with Cryostream (Oxford Cryosystems) open-flow nitrogen cryostats. The crystal data were collected at room temperature (302(2) K or 305(2) K) using MoKα radiation (λ = 0.71073 Å). A 2015 apex-III software suite (Bruker AXS: Madison, WI) is used for unit cell determination, data collection, data reduction, structure solution/refinement, and empirical absorption correction. All structures were solved using the direct method and refined by the full-matrix least-squares on *F2* for all data using SHELXTL. All non-disordered non-hydrogen atoms were refined anisotropically. All the hydrogen atoms were placed in calculated positions and refined using a riding model. Crystallographic data for the structures are deposited to Cambridge Crystallographic Data Centre as supplementary publication (CCDC no: 2414629-2414636).

3.7. Powder X-ray Diffraction

The PXRD of all the obtained crystals of ligands and complexes were ground to fine powder and about 20.0 mg of the sample was used to record PXRD. We have also recorded the PXRD of the xerogels, prepared in a similar manner for SEM. The PXRD experiments were recorded on a PANalytical instrument with 2θ ranging from 4.0−60.0^0 with a step size of 0.025.

3.8. Antibacterial activity of prepared gels

The Luria Bertani (LB) broth was used for inoculating the bacteria (either *S. aureus* and *E. coli*) and the inoculated cultures were overnight incubated at 37°C. After the overnight incubation, the turbid grown culture was set to 0.5 (1.5×10^8 CFU/mL) as per McFarland standard. This was used for all the experiments. The experiment was conducted to assess the antibacterial activity of the sample against one gram-positive (*S. aureus*) and one gram-negative (*E. coli*) bacterium. 100 µL of the cultures were spread on LB agar plates. Using an agar puncher, wells of diameter 8.0 mm were punched, and 100mg of prepared gel (in acetic acid) was added to the wells. The drug vancomycin or amikacin was kept as positive control, and 0.1 M acetic acid is kept as a negative control. The plates were then incubated at

37.0 °C in upright position. After 24 h of incubation, the zone of inhibition was observed, and images of the plates were taken (Bio-Rad Gel Doc, USA) [59].

3.9. Membrane disruption studies by SEM analysis

The antibacterial activity of prepared complexes and compounds were assessed visually using SEM (JEOL JSM-690LA) with an acceleration voltage of 15KV. In 24 well plate, coverslip was added, and 20µL bacterial culture (*E. coli* and *S. aureus*) were added individually. Further, 1.0 mL LB broth and 100µL prepared compounds and complexes were added and incubated overnight at 37°C. The control was bacterial culture along with Lb broth without the samples. After incubation, the wells were washed with PBS and dried for 1 hour. Further,the coverslips were fixed with 2.0% glutaraldehyde and dehydrated with a series of ethanol washes from (50-100%). The samples were dried and given for SEM analysis.

Conclusions

We have synthesized various metronidazole incorporated carbamate-based pyridyl *N*-oxides. Gelation studies revealed that the 3-pyridyl *N*-oxide formed hydrogel, while the 4-pyridyl *N*-oxide moiety was a non-gelator. The 3-PCM formed gel in 1:1 (v/v) aqueous mixtures of ethyelene glycol and DMSO. Metallogealtion experiments of all the compounds with various transition metal salts revealed that gels were obtained for 3-PCM+$CdCl_2$ (5.8 wt/v% of ligand), 4-PCMNox+$CuSO_4$ (6.1 wt/v% of ligand) in DMF/water 1:1, v/v, and 3-PCMNox+$AgNO_3$ gel (6.1 wt/v% of ligand) in DMF/water 1:9 (v/v), at 1:2 metal to ligand ratio. The mechanical strength analysis using frequency sweep experiments showed that the 4-PCMNox+$CuSO_4$ gel was stiffer compared to 3-PCM+$CdCl_2$-based gel, and the 3-PCMNox+$AgNO_3$ gel showed a weak gel network, which can be attributed to the nature of the metal-ligand coordination-driven self-assembly in the metallogels. The fibre-like morphology of the xerogels based on ligand and metallogels was analysed using SEM studies. The antibacterial studies with all the prepared ligands and cadmium(II) and silver(I)-based metal complexes revealed that the cadmium(II) and silver(I) complexes showed activity against gram-positive and gram-negative bacteria.

Declaration

The authors declare no conflict of interest.

Acknowledgments

We thank University of Iceland Research Fund and Science Institute for funding. S.S.J. thanks the University of Iceland for the Doctoral research grant. We also acknowledge Dr. Sigríður Jónsdóttir and Dr. Fridrick Magnus, University of Iceland for NMR/Mass spectroscopy and powder X-ray diffraction analysis, respectively. We thank Rannís Iceland for infrastructure grants (150998–0031 & 191763–0031) for a single crystal X-ray diffractometer and Rheometer.

Appendix A. Supplementary material

Supplementary data to this article can be found online at xxxxxxxxxxxxxxxx. Crystallographic information for the CM, 3-PCM, 4-PCM, 3-PCMNox, 3-PCMNox+$CdCl_2$, 4-PCM+$CdCl_2$, 3-PCMNox+$AgNO_3$, 3-PCM+$AgNO_3$ structure has been deposited to the Cambridge Crystallographic Data Centre as supplementary data (CCDC no: 2414629-2414636).

References

[1] D. Ma, T. Wu, J. Zhang, M. Lin, W. Mai, S. Tan, W. Xue, X. Cai, Sci. Adv. Mater. 5 (2013) 1400.

[2] N. Nandi, K. Gayen, S. Ghosh, D. Bhunia, S. Kirkham, S.K. Sen, S. Ghosh, I.W. Hamley, A. Banerjee, Biomacromolecules 18 (2017) 3621.
[3] W.T. Truong, Y. Su, J.T. Meijer, P. Thordarson, F. Braet, Chem. Asian J. 6 (2011) 30.
[4] D.K. Kumar, J.W. Steed, Chem. Soc. Rev. 43 (2014) 2080.
[5] J.A. Foster, K.K. Damodaran, A. Maurin, G.M. Day, H.P. Thompson, G.J. Cameron, J.C. Bernal, J.W. Steed, Chem. Sci. 8 (2017) 78.
[6] A. Dawn, Int. J. Mol. Sci. 20 (2019) 781.
[7] Z. Riaz, S. Baddi, C.-L. Feng, Supramol. Mater. (2024) 100064.
[8] P. Dastidar, U. Manna, S. Ghosh, A. Pharas, N. Roy, P. Pal, Chem. Eur. J. e202403999.
[9] S. Sidiq, G. Ahanger, N. Nazir, M. Iqbal Zargar, A. Ahmad Dar, J. Mol. Liq. 409 (2024) 125341.
[10] S. Banerjee, R.K. Das, U. Maitra, J. Mater. Chem. 19 (2009) 6649.
[11] P. Dastidar, Chem. Soc. Rev. 37 (2008) 2699.
[12] M. de Loos, B.L. Feringa, J.H. van Esch, Eur. J. Org. Chem. 2005 (2005) 3615.
[13] L.A. Estroff, A.D. Hamilton, Chem. Rev. 104 (2004) 1201.
[14] M. George, R.G. Weiss, Acc. Chem. Res. 39 (2006) 489.
[15] P.R.A. Chivers, D.K. Smith, Nat. Rev. Mater. 4 (2019) 463.
[16] J. Cui, A. Liu, Y. Guan, J. Zheng, Z. Shen, X. Wan, Langmuir 26 (2010) 3615.
[17] X. Huang, P. Terech, S.R. Raghavan, R.G. Weiss, J. Am. Chem. Soc. 127 (2005) 4336.
[18] H. Huang, X. Zhu, L. Su, H. Wang, Y. Yang, RSC Adv. 3 (2013) 11854.
[19] T. Naota, H. Koori, J. Am. Chem. Soc. 127 (2005) 9324.
[20] S. Basak, J. Nanda, A. Banerjee, J. Mater. Chem. 22 (2012) 11658.
[21] C.D. Jones, J.W. Steed, Chem. Soc. Rev. 45 (2016) 6546.
[22] S.S. Jayabhavan, J.W. Steed, K.K. Damodaran, Cryst. Growth Des. 21 (2021) 5383.
[23] G. Kuppadakkath, S.S. Jayabhavan, K.K. Damodaran, Molecules 29 (2024) 2149.
[24] S. Sudhakaran Jayabhavan, G. Kuppadakkath, K.K. Damodaran, ChemPlusChem 88 (2023) e202300302.
[25] D.K. Smith, Soft Matter (2024).
[26] L. Li, J.M. Scheiger, P.A. Levkin, Adv. Mater. 31 (2019) 1807333.
[27] S. Sudhakaran Jayabhavan, D. Ghosh, K.K. Damodaran, Molecules 26 (2021) 6420.
[28] D. Ghosh, P. Chaudhary, A. Pradeep, S. Singh, J. Rangasamy, K.K. Damodaran, J. Mol. Liq. 382 (2023) 122023.
[29] K. Nepali, H.-Y. Lee, J.-P. Liou, J. Med. Chem. 62 (2019) 2851.
[30] D. Shinn, The Lancet 279 (1962) 1191.
[31] F.P. Tally, V.L. Sutter, S.M. Finegold, California medicine 117 (1972) 22.
[32] F.P. Tally, V.L. Sutter, S.M. Finegold, Antimicrob Agents Chemother. 7 (1975) 672.
[33] S. Löfmark, C. Edlund, C. Nord, Clin. Infect. Dis. 50 Suppl 1 (2010) S16.
[34] K.J. McClellan, S. Noble, Am. J. Clin. Dermatol. 1 (2000) 191.
[35] R. Sobel, J.D. Sobel, Expert Opin. Pharmacother. 16 (2015) 1109.
[36] S. Duggal, S. Sharma, N. Rai, D. Chauhan, V. Upadhyay, S. Srivastava, K. Porwal, C. Kulkarni, A.K. Trivedi, J.R. Gayen, P.R. Mishra, N. Chattopadhyay, S. Pal, Biomedicines 12 (2024) 1603.
[37] J. Kang, V.K.R. Tangadanchu, L. Gopala, W.-W. Gao, Y. Cheng, H.-B. Liu, R.-X. Geng, S. Li, C.-H. Zhou, Chin. Chem. Lett. 28 (2017) 1369.
[38] N. Kumar, R.K. Rohilla, N. Roy, D.S. Rawat, Bioorg. Med. Chem. Lett. 19 (2009) 1396.
[39] Monika, Meenakshi, M. Brahma, M. Maruthi, S. Selvakumar, A. Ansari, M.K. Gupta, Chem. Biodiversity 21 (2024) e202400105.
[40] S. Sebastian, E. Yadav, P. Bhardwaj, M. Maruthi, D. Kumar, M.K. Gupta, J. Mater. Chem. B 11 (2023) 9975.
[41] D. Satapathy, D. Biswas, B. Behera, S.S. Sagiri, K. Pal, K. Pramanik, J. Appl. Polym. Sci. 129 (2013) 585.
[42] C. Venkataramaiah, N. Sreedhar, C.N. Raju, RSC Adv. 11 (2021) 3897.

[43] T.H.S. Kumara, K.M. Mahadevan, H.N. Harishkumar, B. Padmashali, G. Naganagowda, Phosphorus, Sulfur, Silicon Relat. Elem. 184 (2009) 1866.
[44] M. Moniruzzaman, P.R. Sundararajan, Langmuir 21 (2005) 3802.
[45] C.D. Freeman, N.E. Klutman, K.C. Lamp, Drugs 54 (1997) 679.
[46] Rheology for Chemists: An Introduction (2), The Royal Society of Chemistry, 2008, p. 1-13.
[47] J.-M. Guenet, Organogels: Thermodynamics, structure, solvent role, and properties. Springer, 2016.
[48] A. Dawn, H. Kumari, Chem. Eur. J. 24 (2018) 762.
[49] S. Sathaye, A. Mbi, C. Sonmez, Y. Chen, D.L. Blair, J.P. Schneider, D.J. Pochan, Wiley Interdiscip. Rev.: Nanomed. Nanobiotechnology 7 (2015) 34.
[50] E.R. Draper, D.J. Adams, Chem 3 (2017) 390.
[51] D.A. Tómasson, D. Ghosh, M.R.P. Kurup, M.T. Mulvee, K.K. Damodaran, CrystEngComm 23 (2021) 617.
[52] D. Ghosh, R. Bjornsson, K.K. Damodaran, Gels 6 (2020) 41.
[53] D. Ghosh, M.T. Mulvee, K.K. Damodaran, Molecules 24 (2019) 3472.
[54] D. Ghosh, K. Ferfolja, Ž. Drabavičius, J.W. Steed, K.K. Damodaran, New J. Chem. 42 (2018) 19963.
[55] D. Ghosh, A.D. Farahani, A.D. Martin, P. Thordarson, K.K. Damodaran, Chem. Mater. 32 (2020) 3517.
[56] D. Ghosh, I. Lebedytė, D.S. Yufit, K.K. Damodaran, J.W. Steed, CrystEngComm 17 (2015) 8130.
[57] D.J. Adams, Gels 4 (2018) 32.
[58] G. Yu, X. Yan, C. Han, F. Huang, Chem. Soc. Rev. 42 (2013) 6697.
[59] M.N. Sundaram, V. Krishnamoorthi Kaliannagounder, V. Selvaprithiviraj, M. K. Suresh, R. Biswas, A.K. Vasudevan, P.K. Varma, R. Jayakumar, ACS Sustain. Chem. Eng. 6 (2018) 7826.

SUPPORTING INFORMATION

Evaluating the Self-Assembly and Antibacterial Activity of Tailored Supramolecular Gels

Sreejith Sudhakaran Jayabhavan, Arthi Chandramouli, Jayakumar Rangasamy, and Krishna K. Damodaran*

Contents

1. Synthetic scheme

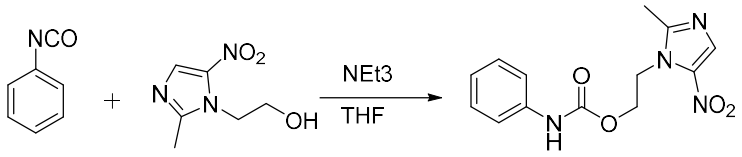

Scheme S1. Synthetic route for CM.

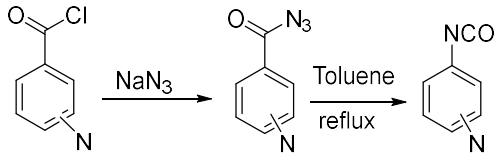

Scheme S2. Synthetic route for 3/4-pyridyl-isocyanate.

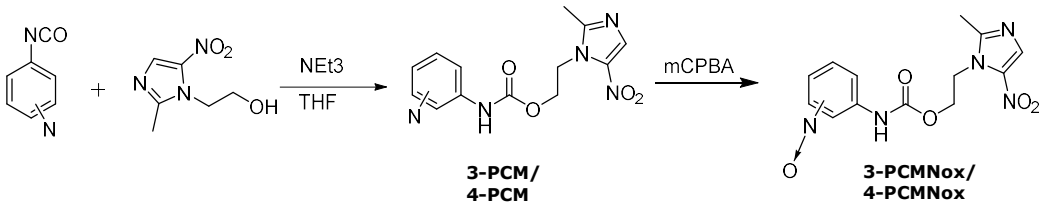

Scheme S3. Synthetic route for *N*-oxides.

2. NMR spectra

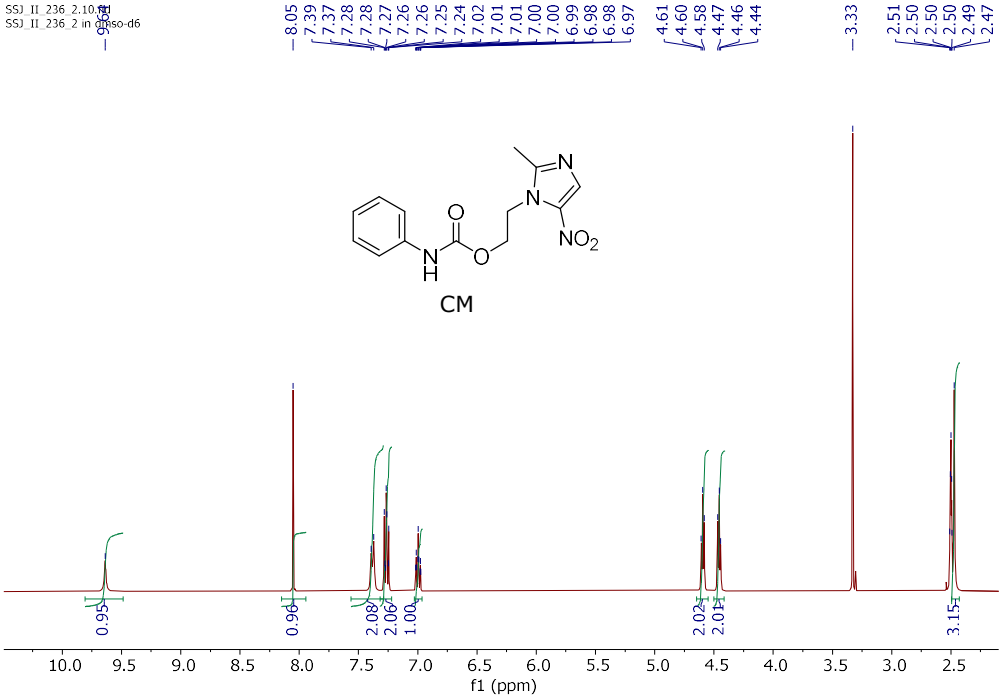

Figure S1. ^{1}H NMR spectrum of CM.

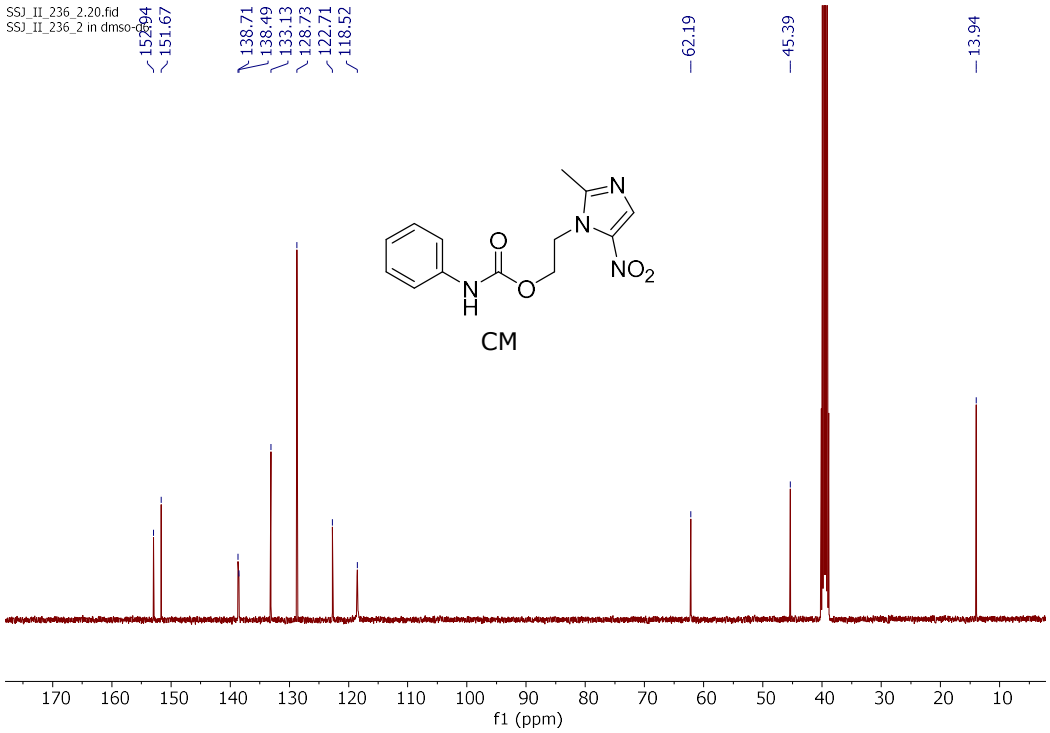

Figure S2. ^{13}C NMR spectrum of CM.

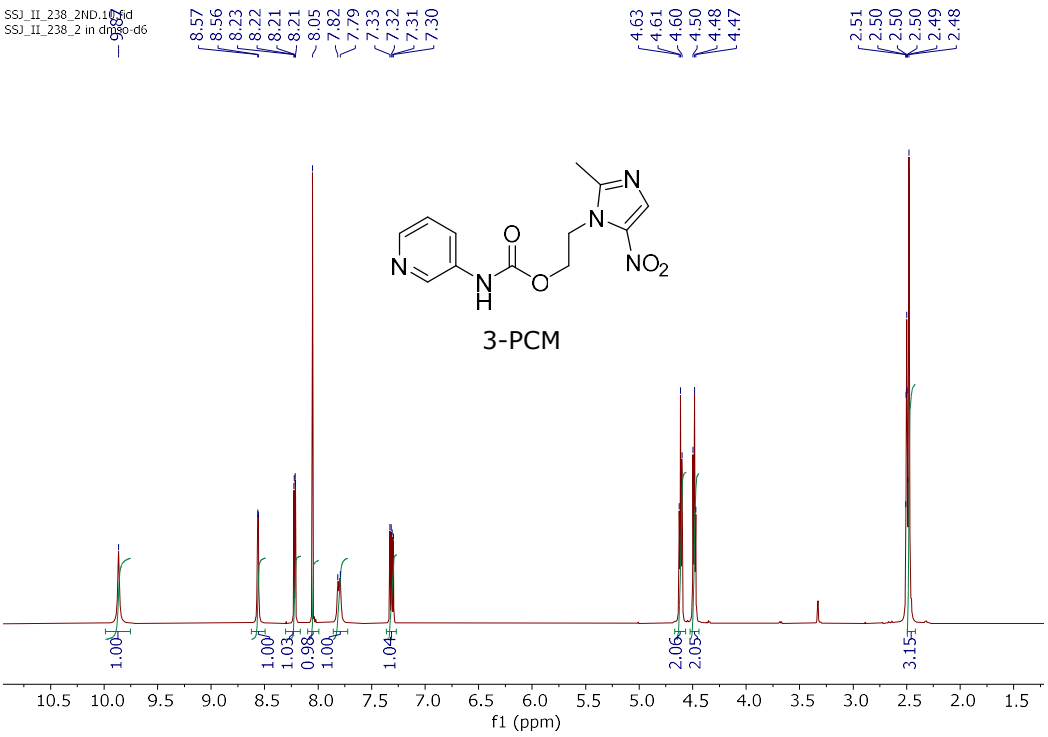

Figure S3. ^{1}H NMR spectrum of 3-PCM.

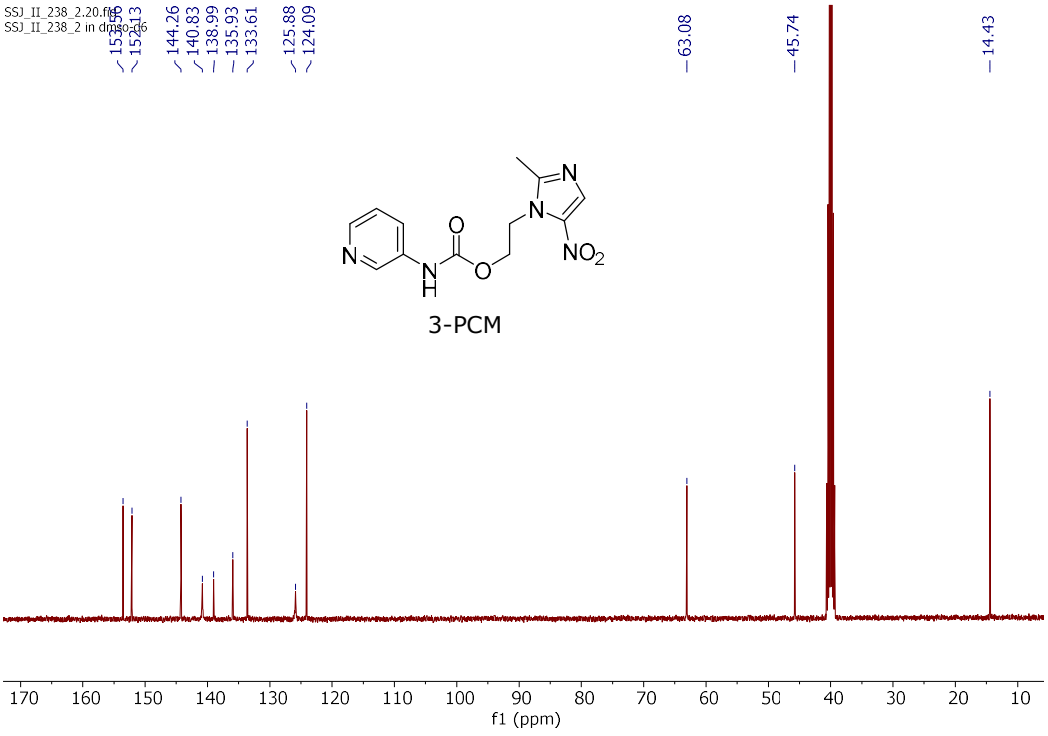

Figure S4. ^{13}C NMR spectrum of 3-PCM.

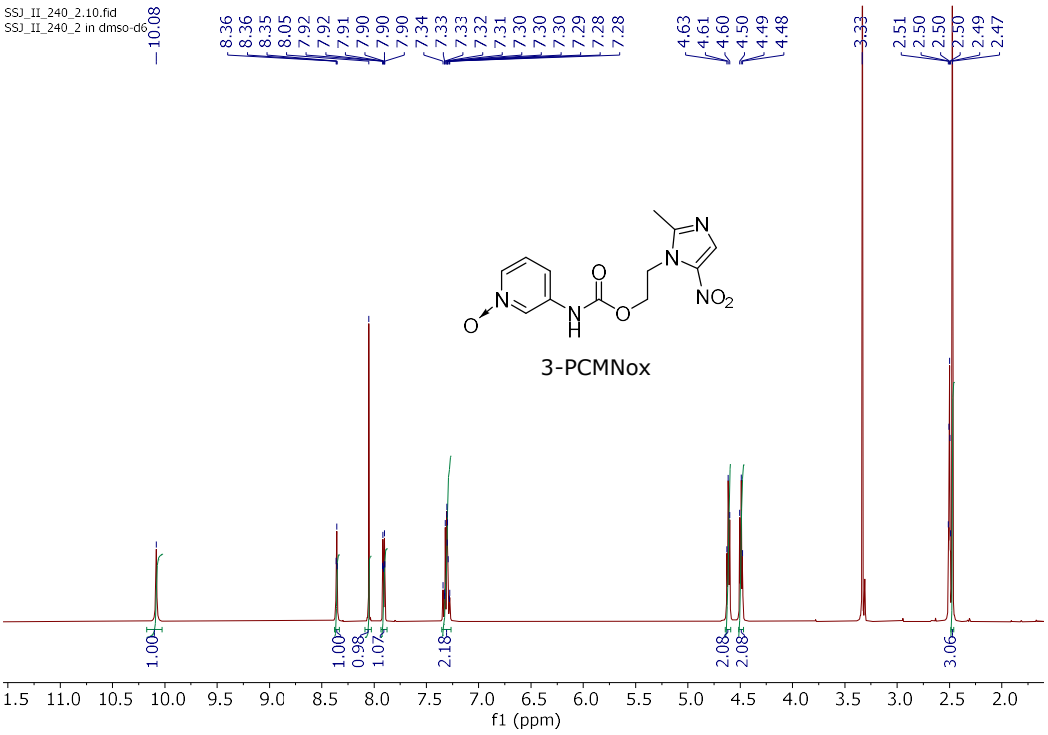

Figure S5. ^{1}H NMR spectrum of 3-PCMNox.

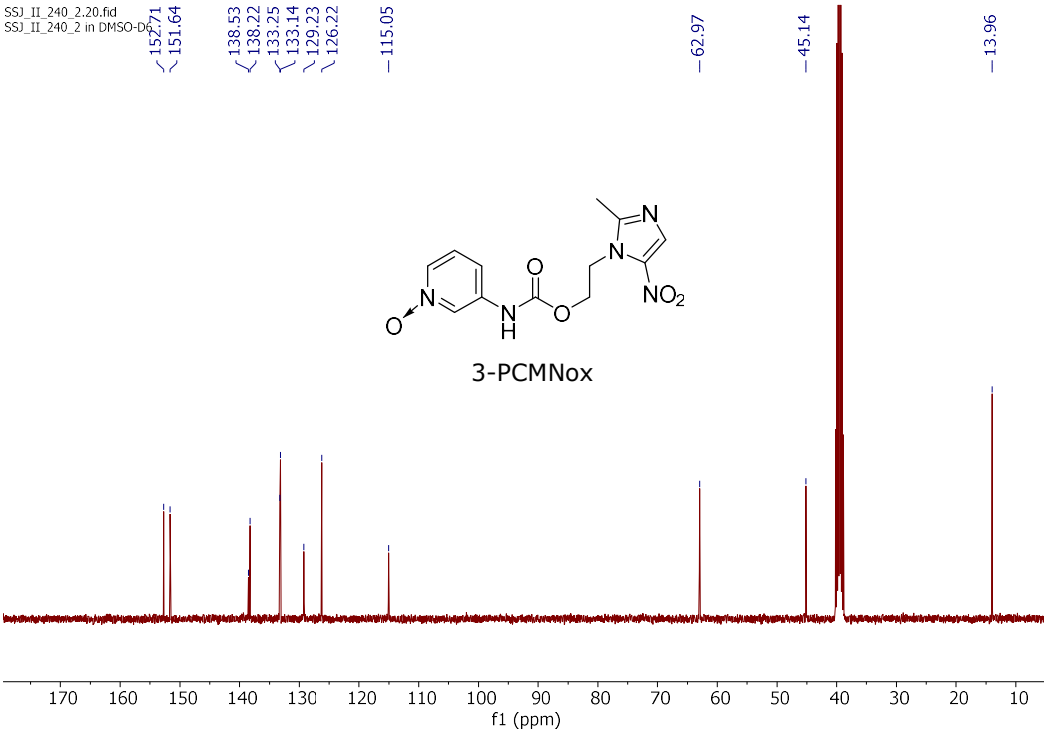

Figure S6. ^{13}C NMR spectrum of 3-PCMNox.

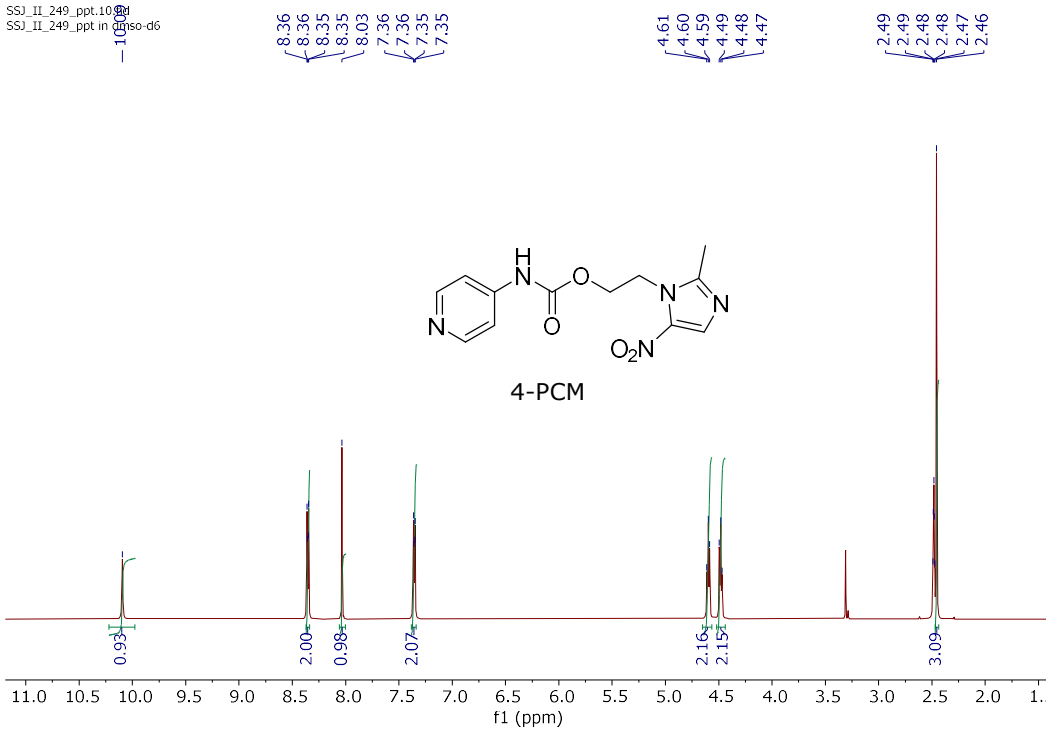

Figure S7. ^{1}H NMR spectrum of 4-PCM.

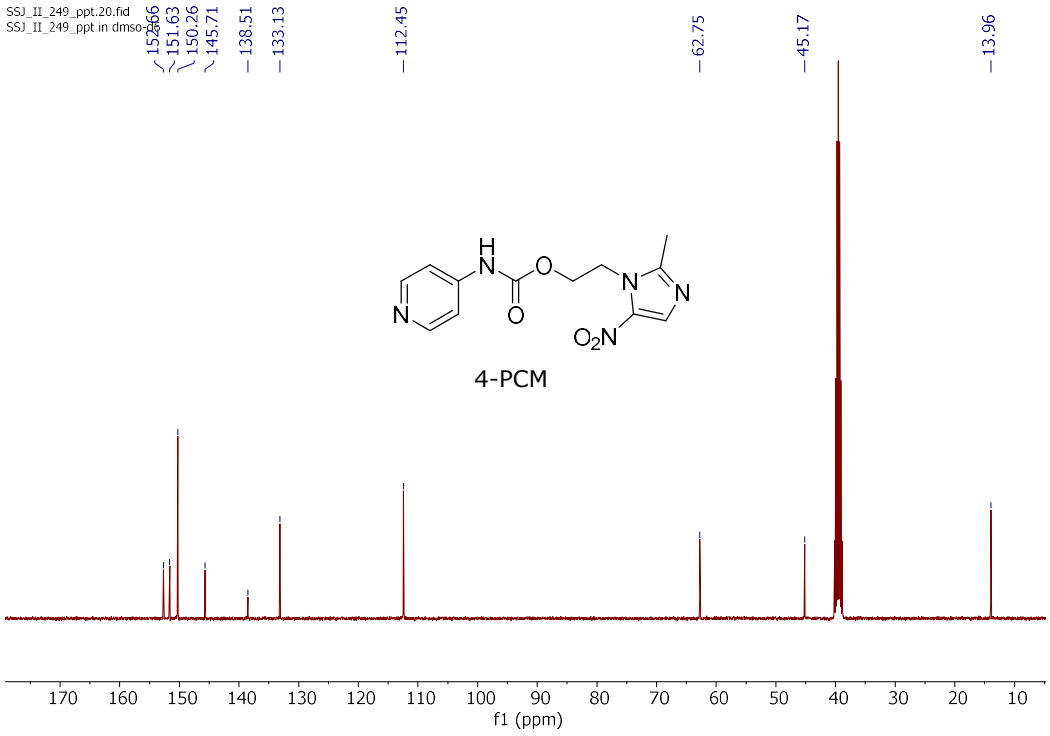

Figure S8. ^{13}C NMR spectrum of 4-PCM.

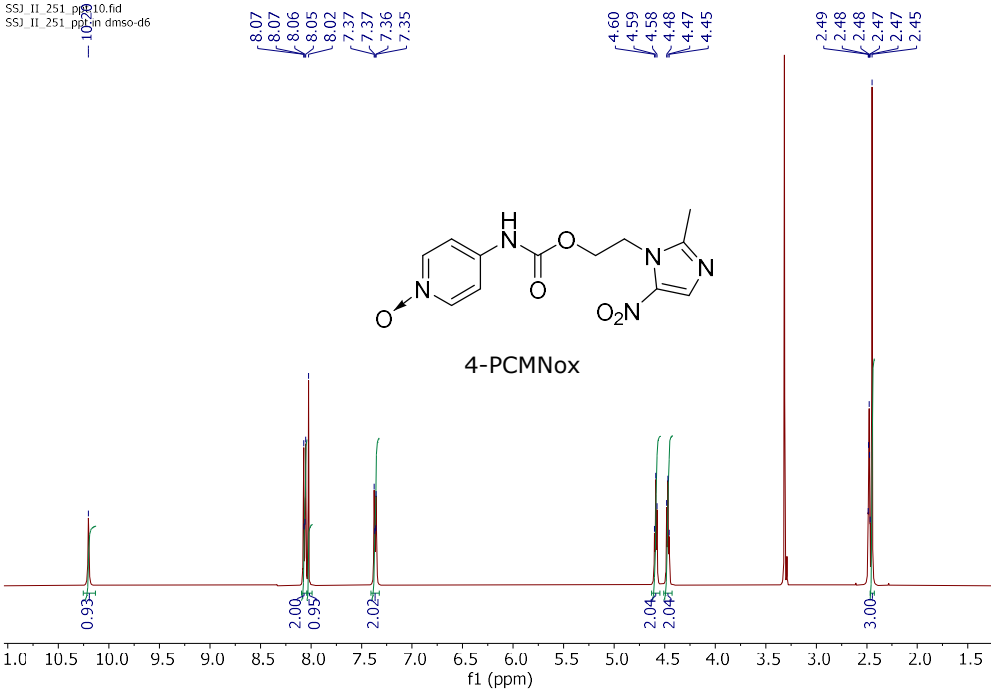

Figure S9. ^{1}H NMR spectrum of 4-PCMNox.

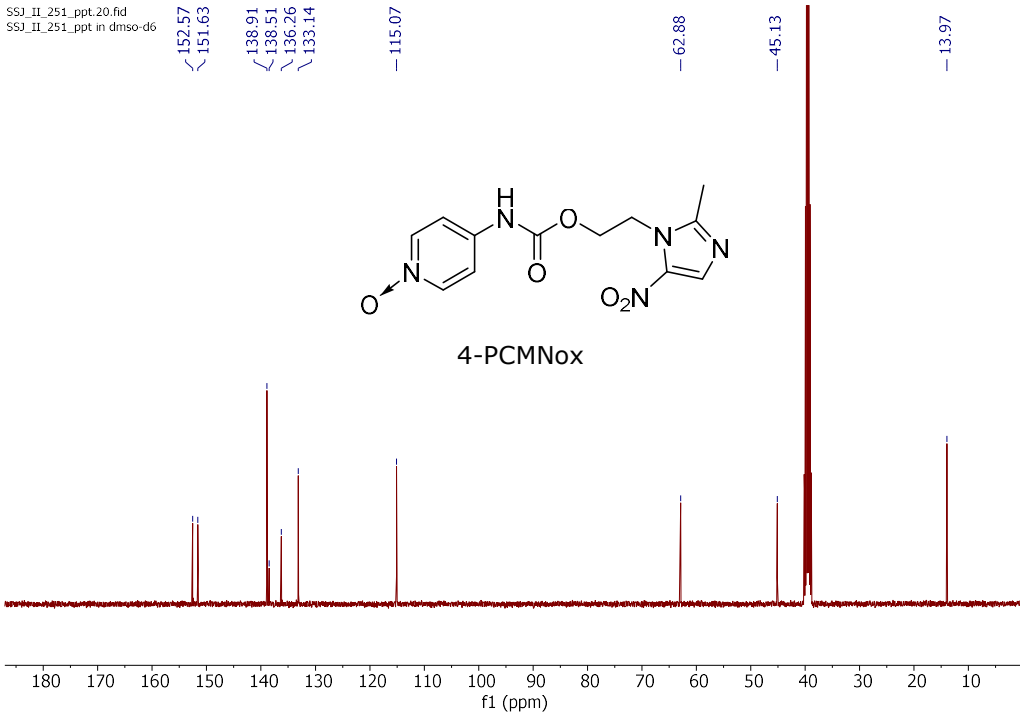

Figure S10. ^{13}C NMR spectrum of 4-PCMNox.

3. Gelation studies

Table S1. Gelation Experiments with compounds at 1.0 wt/v%

Sl No.	**Solvent**	CM	3-PCM	4-PCM	3-PCMNox	4-PCMNox
1	*o*-xylene	I	I	I	I	I
2	*m*-xylene	I	I	I	I	I
3	*p*-xylene	I	I	I	I	I
4	toluene	I	I	I	I	I
5	mesitylene	I	I	I	I	I
6	n-butanol	Cry	Cry	Ppt	Ppt	Ppt
7	EtOH	Cry	Cry	Ppt	Ppt	Ppt
8	water	I	I	I	**G**[#]	Cry
9	chlorobenzene	Cry	Ppt	I	I	I
10	Nitrobenzene	S	Cry	Ppt	Ppt	Ppt
11	EG:water	Coll*	**G***	Ppt*	S*	Coll*
12	DMF:water	Coll*	Ppt*	Cry*	Ppt*	Coll*
13	DMSO:water	Cry*	**G***	Ppt*	Ppt*	Coll*
14	EtOH/water	Ppt	Cry	Ppt	Ppt	Ppt

G= gel, [#]= 4.0 wt/v%, *= 5.0 wt/v%, Ppt= precipitate, Coll= Colloid, I= Insoluble, and aqueous mixtures were taken at 1:1, v/v.

Table S2. Minimum gelator concentration (MGC) studies

MGC (wt/v%)			
Sl No.	**Solvent**	3-PCM	3-PCMNox
1	water	---	3.8
2	EG:water	3.8	---
3	DMSO:water	4.5	---

Table S3. Determination of Sol-gel Transition Temperature (T_{gel})

T_{gel} (°C)				
Sl No.	**Solvent**	Wt/v%	3-PCM	3-PCMNox
1	water	4.0	---	67.9
2	EG:water	5.0	86.2	---
3	DMSO:water	5.0	75.1	---

Table S4. Metallogelation studies at 1:2 metal-to-ligand ratio in DMF/water (1:1, v/v)

Metal salts	CM (5.8 wt/v%)	3-PCM (5.8 wt/v%)	4-PCM (5.8 wt/v%)	3-PCMNox (6.1 wt/v%)	4-PCMNox (6.1 wt/v%)
$Cu(NO_3)_2.3H_2O$	Blue sol- Ppt (ligand)	Blue sol- Ppt	Blue sol- Ppt	Green sol-Ppt	Green sol-Coll
$CuSO_4.5H_2O$	Blue sol- Ppt (ligand)	Blue sol- Ppt	Blue sol- Ppt	Blue sol-Ppt	Green sol-**Green gel**
$Cu(OAc)_2.2H_2O$	Blue sol- Ppt (ligand)	Blue sol- Cry	Blue sol- Ppt	Blue sol	Blue sol- Cry
$CuCl_2$	Blue sol- Ppt (ligand)	Blue sol- Ppt	Blue sol- Ppt	Green sol-Cry	Green sol-Coll
$CdCl_2$	Sol- Ppt (ligand)	Sol- **Gel**	Sol-Ppt	Sol-Cry	Sol-Ppt
$CoCl_2$	Pink sol- Ppt (ligand)	Pink sol- Cry	Pink sol-Ppt	Pink sol-Ppt	Pink sol-Coll
$ZnCl_2$	Sol- Ppt (ligand)	Sol- Ppt	Sol-Ppt	Sol-Ppt	Sol-Microcry
$Ni(NO_3)_2$	Green sol- Ppt (ligand)	Green sol-Ppt	Green sol-Ppt	Green sol-Ppt	Green sol-Ppt
$Fe(NO_3)_3$	Yellow sol- Ppt (ligand)	Red sol- Coll	Red sol-Ppt	Red sol-Ppt	Red sol- Coll
$AgNO_3$*	Sol-Ppt	Sol-Ppt	Sol-Ppt	Sol-**Gel**	Sol-Ppt

Ppt- precipitate, Sol- solution, Cry- crystalline, Coll- colloid, *- DMF/water (1:9, v/v)

4. Rheology

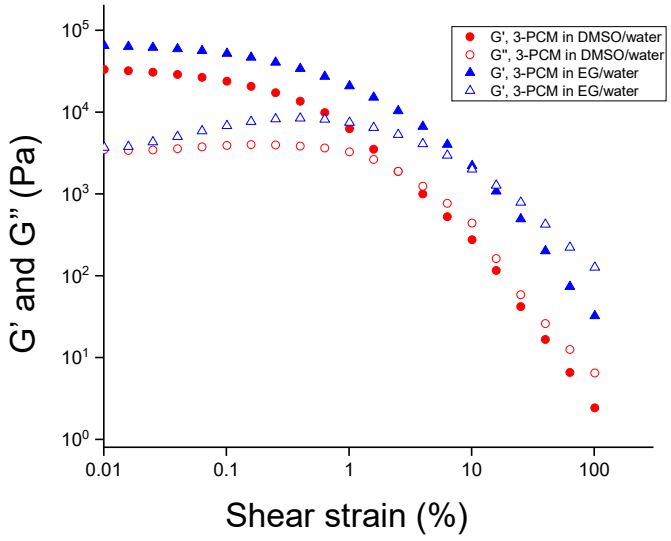

Figure S11. Strain sweep experiments with 3-PCM based gels (5.0 wt/v%) in DMSO/water and EG/water 1:1, v/v, at 20.0 °C measured at a constant frequency of 1.0 Hz.

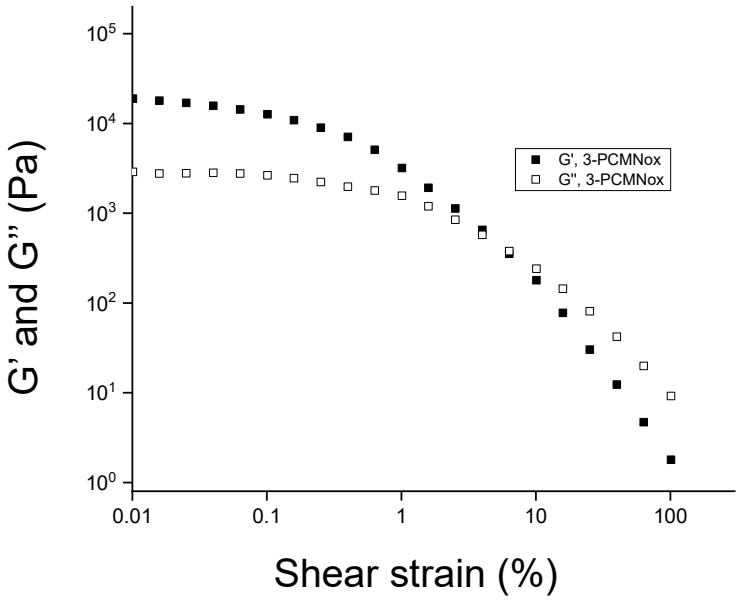

Figure S12. Strain sweep experiments with 3-PCMNox based gels (4.0 wt%) in water, at 20.0 °C measured at a constant frequency of 1.0 Hz.

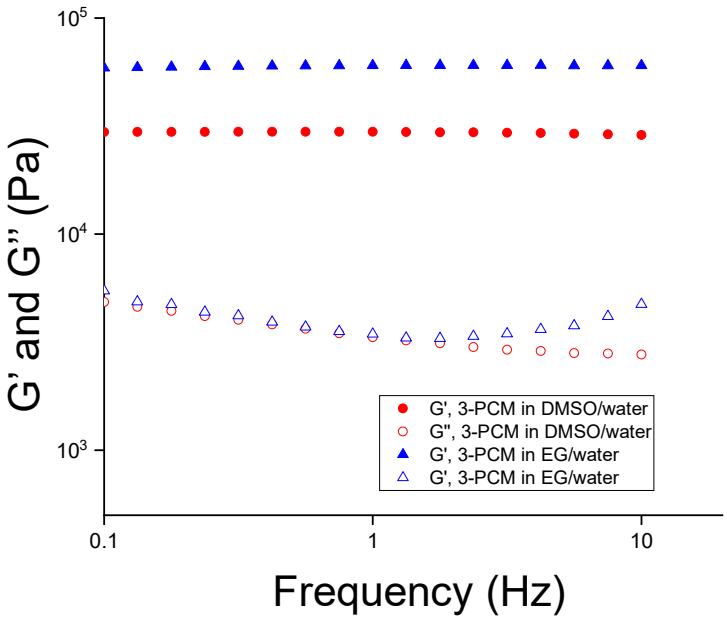

Figure S13. Frequency sweep experiments with 3-PCM based gels (5.0 wt/v%) in DMSO/water and EG/water 1:1, v/v, at 20.0 °C measured at a constant strain of 0.02%.

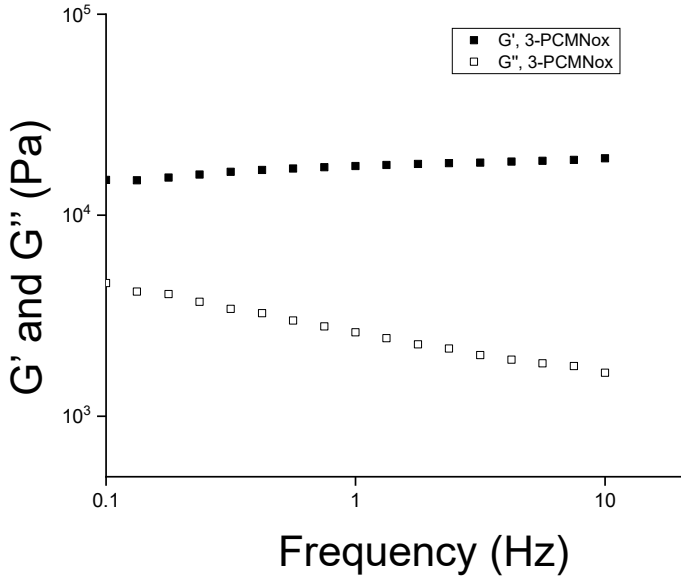

Figure S14. Frequency sweep experiments with 3-PCMNox based gels (4.0 wt%) in water, at 20.0 °C measured at a constant frequency of 1.0 Hz.

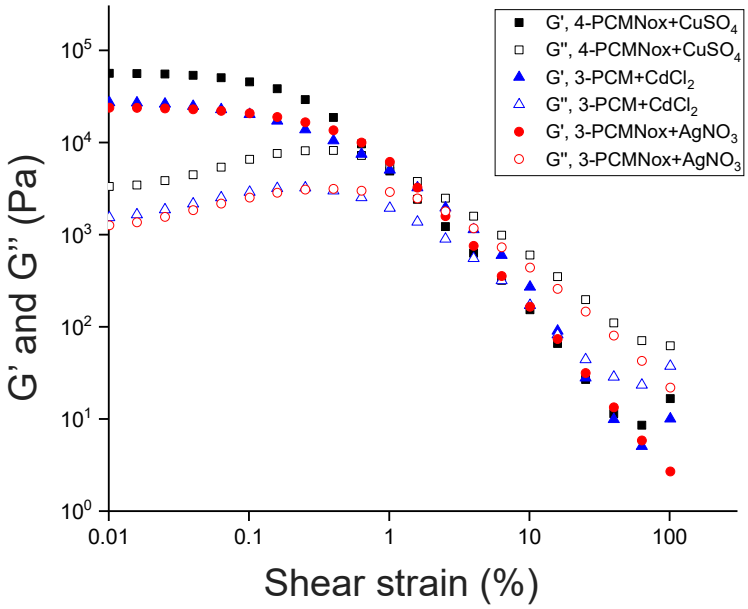

Figure S15. Strain sweep experiments with 3-PCM+$CdCl_2$ gel (5.8 wt/v% of ligand) and 4-PCMNox+$CuSO_4$ gel (6.1 wt/v% of ligand) in DMF/water 1:1, v/v, and 3-PCMNox+$AgNO_3$ gel (6.1 wt/v% of ligand) in DMF/water 1:9, v/v, at 1:2 metal to ligand ratio and at 20.0 °C measured at a constant frequency of 1.0 Hz.

5. Scanning electron microscopy

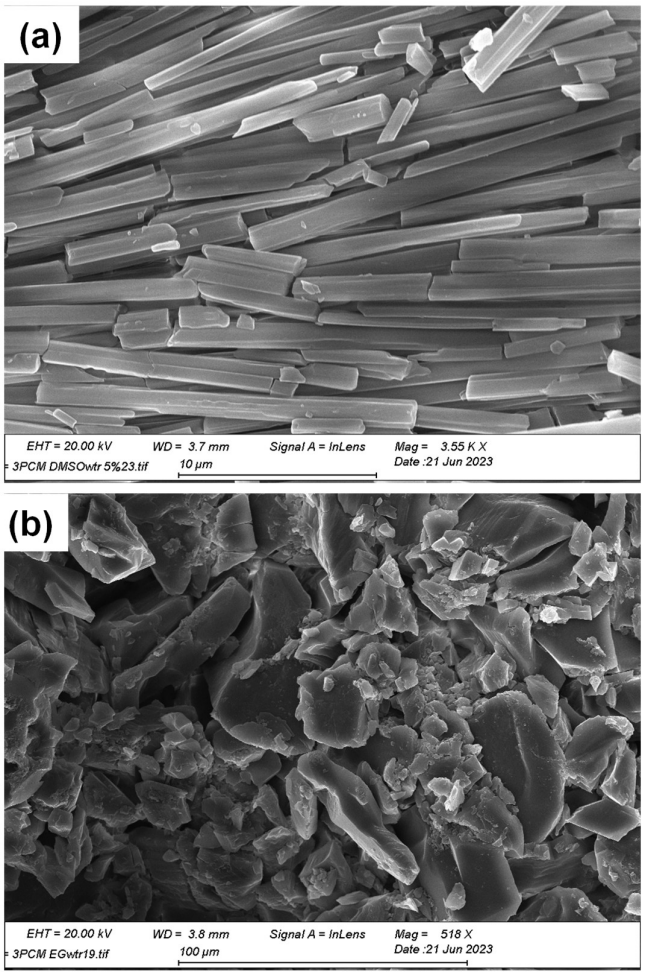

Figure S16. SEM images of the xerogels obtained from 3-PCM based gels (5.0 wt/v%) in (a) DMSO/water, and (b) EG/water 1:1, v/v.

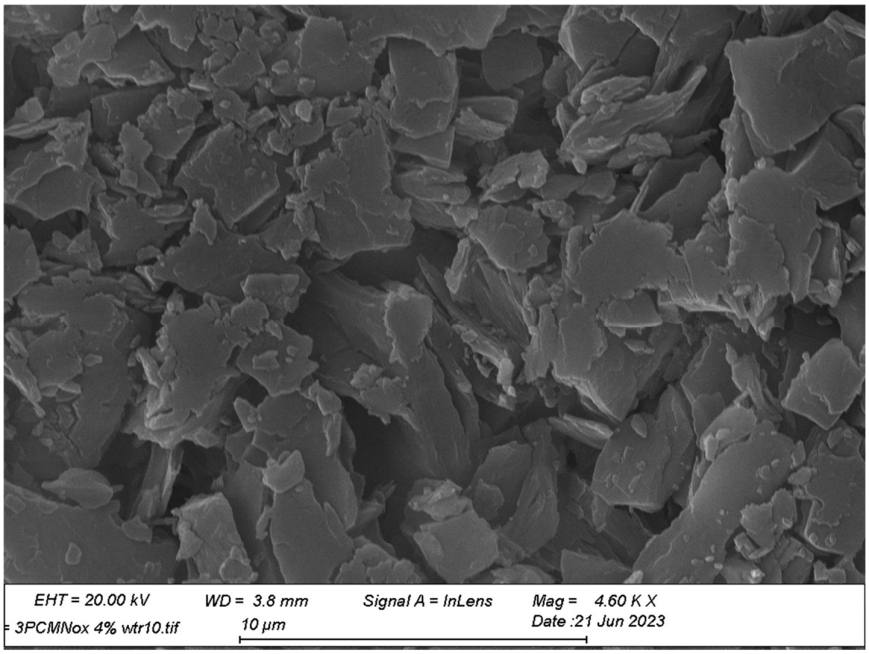

Figure S17. SEM images of the xerogel of 3-PCMNox obtained from water (4.0 wt%).

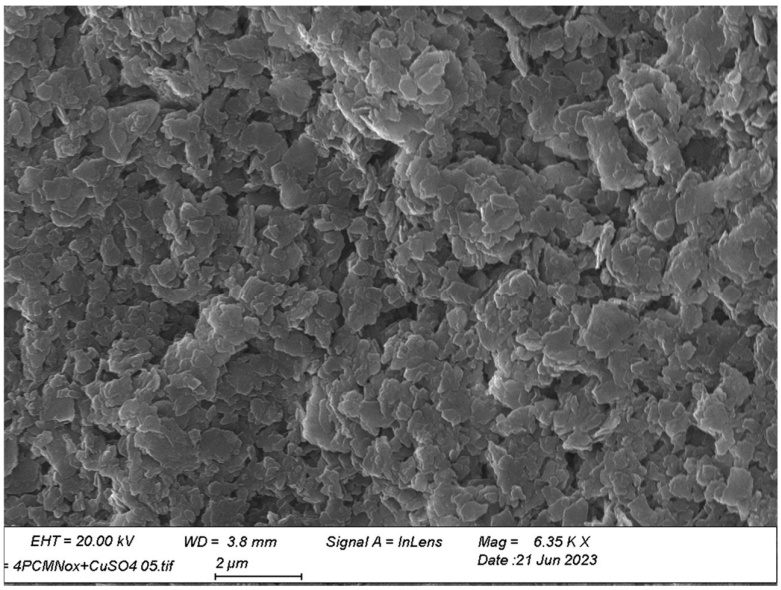

Figure S18. SEM images of the xerogel of 4-PCMNox+$CuSO_4$ gel (6.1 wt/v% of ligand) in DMF/water (1:1, v/v), at 1:2 metal to ligand ratio.

6. Single crystal X-ray diffraction

Table S5: Crystal data

Crystal data	CM	3-PCM	4-PCM	3-PCMNox
File name	SSJ_II_236_EA	SSJ_II_241_EtOH	SSJ_III_128_4	SSJ_II_240_H2O
Empirical formula	$C_{13}H_{14}N_4O_4$	$C_{12}H_{13}N_5O_4$	$C_{12}H_{13}N_5O_4$	$C_{12}H_{15}N_5O_6$
Color	Colorless	Colorless	Colorless	Colorless
Formula weight	290.28	291.27	291.27	325.29
Crystal size (mm)	0.250 x 0.200 x 0.080	0.190 x 0.130 x 0.070	0.230 x 0.170 x 0.040	0.190 x 0.060 x 0.040
Crystal system	Monoclinic	Triclinic	Triclinic	Triclinic
Space group	$P2_1/n$	P-1	P-1	P-1
a (Å)	10.3896(8)	7.5761(5)	9.1319(7)	6.8390(5)
b (Å)	10.9685(8)	8.6966(6)	9.4856(7)	9.0647(6)
c (Å)	11.9682(9)	10.3852(7)	9.8024(6)	12.4965(9)
α (°)	90	91.211(2)	102.462(2)	103.598(2)
β (°)	94.640(3)	103.529(2)	98.962(2)	102.087(2)
γ (°)	90	91.437(2)	106.185(2)	104.118(2)
Volume (Å^3)	1359.41(18)	664.79(8)	774.84(10)	700.39(9)
Z	4	2	2	2
$D_{calc.}$(g/cm^3)	1.418	1.455	1.248	1.542
F(000)	608	304	304	340
μ (mm^{-1}) MoK_α	0.108	0.113	0.097	0.126
Temperature (K)	305(2)	305(2)	305(2)	302(2)
Reflections collected/ unique/observed [I>2σ(I)]	49154/6634/ 4068	36735/4626/ 3367	30396/3865 / 3107	27092/3085/ 2371
Data/restraints/parameters	6634/0/195	4626/0/195	3865/0/191	3085/0/221
Goodness of fit on F^2	1.015	1.044	1.196	1.034
Final R indices [I>2σ(I)]	R_1 = 0.0555 wR_2 = 0.1475	R_1 = 0.0487 wR_2 = 0.1325	R_1 = 0.0634 wR_2 = 0.2038	R_1 = 0.0402 wR_2 = 0.0918
R indices (all data)	R_1 = 0.0960 wR_2 = 0.1721	R_1 = 0.0753 wR_2 = 0.1468	R_1 = 0.0775 wR_2 = 0.2119	R_1 = 0.0597 wR_2 = 0.1008

Table S5: continued

Crystal data	3-PCMNox+$CdCl_2$	4-PCM+$CdCl_2$	3-PCMNox+$AgNO_3$	3-PCM+$AgNO_3$
File name	SSJ_II_261_7	SSJ_III_113_5	SSJ_III_129_5	SSJ_III_116_9
Empirical formula	$C_{24}H_{26}N_{10}O_{10}Cl_2Cd$	$C_{30}H_{40}N_{12}O_{10}Cl_2Cd$	$C_{12}H_{13}N_6O_8Ag$	$C_{12}H_{13}N_6O_7Ag$
Color	Colorless	Colorless	Colorless	Colorless
Formula weight	797.85	912.04	477.15	461.15
Crystal size (mm)	0.190 x 0.060 x 0.030	0.180 x 0.070 x 0.040	0.150 x 0.060 x 0.030	0.200 x 0.150 x 0.040
Crystal system	Monoclinic	Triclinic	Monoclinic	Monoclinic
Space group	*C*2/c	*P*-1	$P2_1/c$	$P2_1/c$
a (Å)	20.8635(17)	8.1465(5)	9.866(6)	13.9969(9)
b (Å)	10.6648(10)	11.3696(7)	22.853(12)	8.7113(6)
c (Å)	14.7496(13)	11.9926(7)	7.455(4)	13.1115(8)
α (°)	90	65.277(2)	90	90
β (°)	107.959(3)	76.226(2)	103.59(2)	96.835(2)
γ (°)	90	72.751(2)	90	90
Volume ($Å^3$)	3122.0(5)	955.22(10)	1633.9(15)	1587.34(18)
Z	4	1	4	4
$D_{calc.}$(g/cm^3)	1.697	1.585	1.940	1.930
F(000)	1608	466	952	920
μ (mm^{-1}) MoK_α	0.942	0.782	1.294	1.323
Temperature (K)	302(2)	302(2)	305(2)	302(2)
Reflections collected/ unique/observed [I>2σ(I)]	65687/3695/ 3044	40717/4197/ 3555	53843/3361/ 2346	50676/3664/ 2976
Data/restraints/parameters	3695/0/219	4197/0/253	3361/0/245	3664/0/240
Goodness of fit on F^2	1.073	1.086	1.065	1.129
Final R indices [I>2σ(I)]	R_1 = 0.0263 wR_2 =0.0519	R_1 = 0.0304 wR_2 = 0.0602	R_1 = 0.0499 wR_2 = 0.0603	R_1 = 0.0374 wR_2 = 0.1014
R indices (all data)	R_1 = 0.0403 wR_2 = 0.0559	R_1 = 0.0419 wR_2 = 0.0636	R_1 = 0.0887 wR_2 = 0.0653	R_1 = 0.0515 wR_2 = 0.1077

Table S6: Hydrogen bonding parameters

Compound CM						
No.	Donor–H···Acceptor	D–H/Å	H···A/Å	D···A/Å	∠D–H···A/°	Symmetry operation
1	N(7A)–H(7A)···N(19A)	0.918(18)	2.137(17)	3.0133(14)	161.1(15)	1-x,-y,1-z
2	C(12A)–H(12B)···O(9A)	0.97	2.50	3.1265(15)	122	1/2-x,-1/2+y,1/2-z
3	C(21A)–H(21A)···O(16A)	0.96	2.40	3.2278 (19)	144	1/2-x,-1/2+y,1/2-z
Compound 3-PCM						
No.	Donor–H···Acceptor	D–H/Å	H···A/Å	D···A/Å	∠D–H···A/°	Symmetry operation
1	N(7C)–H(2)···N(16C)	0.896(17)	2.146(17)	3.0296(15)	168.9(15)	-x,-y,1-z
Compound 3-PCMNox						
No.	Donor–H···Acceptor	D–H/Å	H···A/Å	D···A/Å	∠D–H···A/°	Symmetry operation
1	N(8C)–H(2A)···N(17C)	0.859(19)	2.184(18)	3.0287(19)	167.8(19)	x,2-y,1-z
2	O(23C)–H(1)···O(10C)	0.90(3)	2.01(3)	2.899(2)	171(2)	1-x,1-y,-z
3	O(23C)–H(2)···O(4C)	0.89(3)	1.84(3)	2.729(2)	173(3)	x,y,z
4	C(7C)–H(7C)···O(21C)	0.93	2.50	3.079(2)	120	1+x,1+y,z
5	C(12C)–H(12B)···O(4C)	0.97	2.45	3.349(2)	154	x,1-y,-z
6	C(18C)–H(18C)···O(23C)	0.93	2.35	3.221(2)	155	1+x,y,1+z
Compound 4-PCM						
No.	Donor–H···Acceptor	D–H/Å	H···A/Å	D···A/Å	∠D–H···A/°	Symmetry operation
1	N(7)–H(7)···N(16)	0.86	2.08	2.931(3)	171	1-x,-y,1-z
2	C(17)–H(17)···O(9)	0.93	2.53	3.385(3)	153	x,y,1+z
6	C(18)–H(18)···O(1)	0.95	2.55	3.281(3)	134	1/2-x,2-y,1/2+z
7	C(27)–H(27A)···O(11)	0.98	2.45	3.389(3)	161	1-x,-1/2+y,1/2-z
Compound 3-PCMNox+$CdCl_2$						
No.	Donor–H···Acceptor	D–H/Å	H···A/Å	D···A/Å	∠D–H···A/°	Symmetry operation
1	N(8)–H(8)···Cl(23)	0.81(2)	2.61(2)	3.3890(19)	163(2)	1-x,y,1/2-z
2	C(5)–H(5)···O(21)	0.93	2.56	3.172(3)	124	1-x,y,1/2-z
3	C(7)–H(7)···Cl(23)	0.93	2.76	3.586(2)	148	1-x,y,1/2-z
4	C(16)–H(16A)···Cl(23)	0.96	2.74	3.622(2)	154	1/2+x,-1/2+y,z
5	C(16)–H(16B)···O(4)	0.96	2.54	3.451(3)	158	1/2+x,3/2-y,1/2+z

Compound 4-PCM+$CdCl_2$						
No.	Donor–H···Acceptor	D–H**/Å**	H···A**/Å**	D···A**/Å**	∠D–H···A**/°**	Symmetry operation
1	N(7G)–H(7G)···O(22G)	0.86	2.02	2.858(3)	165	x,y,z
2	C(12G)–H(12B)···O(20G)	0.97	2.52	3.170(3)	124	2-x,1-y,2-z
3	C(15G)–H(15B)···Cl(27)	0.96	2.57	3.521(3)	169	1-x,1-y,1-z
4	C(17G)–H(17G)···Cl(27)	0.93	2.74	3.332(3)	123	x,-1+y,1+z
Compound 3-PCMNox+$AgNO_3$						
No.	Donor–H···Acceptor	D–H**/Å**	H···A**/Å**	D···A**/Å**	∠D–H···A**/°**	Symmetry operation
1	N(8P)–H(8P)···O(24P)	0.86	2.09	2.918(4)	162	x,y,z
2	C(5P)–H(5P)···O(22P)	0.93	2.59	3.336(4)	138	-1+x,3/2-y,1/2+z
3	C(7P)–H(7P)···O(25P)	0.93	2.43	3.341(5)	167	x,y,z
4	C(13P)–H(13B)···O(22P)	0.97	2.47	3.429(4)	171	x,y,1+z
5	C(16P)–H(16B)···O(22P)	0.96	2.55	3.437(4)	153	x,y,1+z
6	C(16P)–H(16C)···O(26P)	0.96	2.51	3.463(4)	174	-x,1-y,1-z
Compound 3-PCM+$AgNO_3$						
No.	Donor–H···Acceptor	D–H**/Å**	H···A**/Å**	D···A**/Å**	∠D–H···A**/°**	Symmetry operation
1	N(7)–H(7)···O(24)	0.98(4)	2.28(4)	3.168(6)	151(3)	x,y,z
2	C(2)–H(2)···O(24)	0.93	2.60	3.256(6)	128	x,y,z
3	C(4)–H(4)···0(25)	0.93	2.38	3.105(6)	135	x,3/2-y,-1/2+z
4	C(18)–H(18)···O(23)	0.93	2.36	3.140(6)	141	1-x,1-y,1-z

7. Powder X-ray diffraction

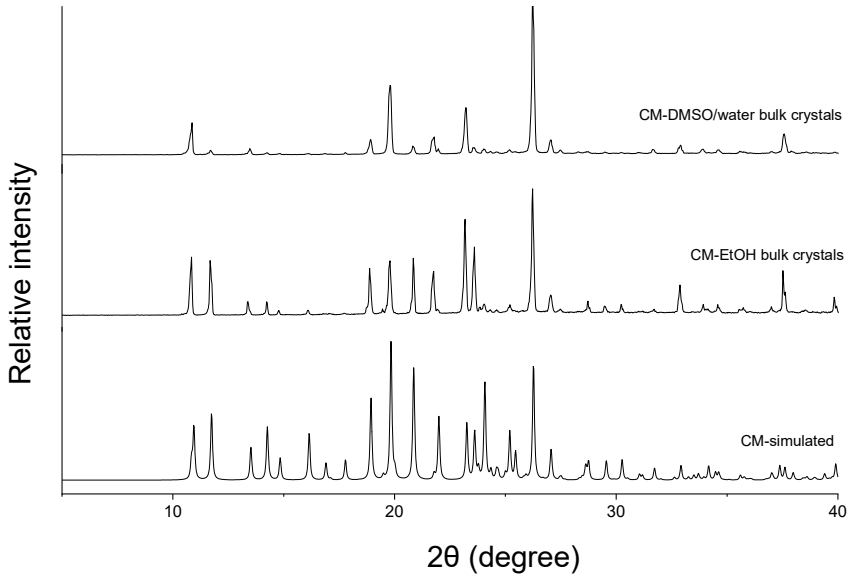

Figure S19. Comparison of PXRD pattern of the crystals of CM obtained from EtOH and DMSO/water 1:1, v/v) at 2.0 wt/v% with that of the simulated pattern obtained from the single crystal X-ray structure of the CM.

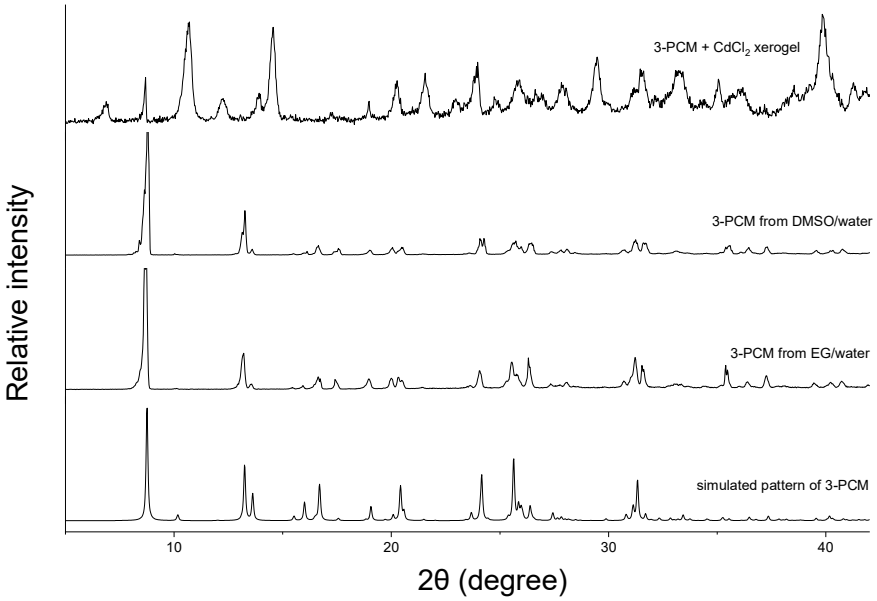

Figure S20. Comparison of PXRD pattern; simulated pattern of 3-PCM, xerogel of 3-PCM obtained from EG/water and DMSO/water (1:1, v/v) at 5.0 wt/v% and the xerogel 3-PCM+CdCl2 gel (5.8 wt/v% of ligand) in DMF/water (1:1, v/v), at 1:2 metal to ligand ratio.

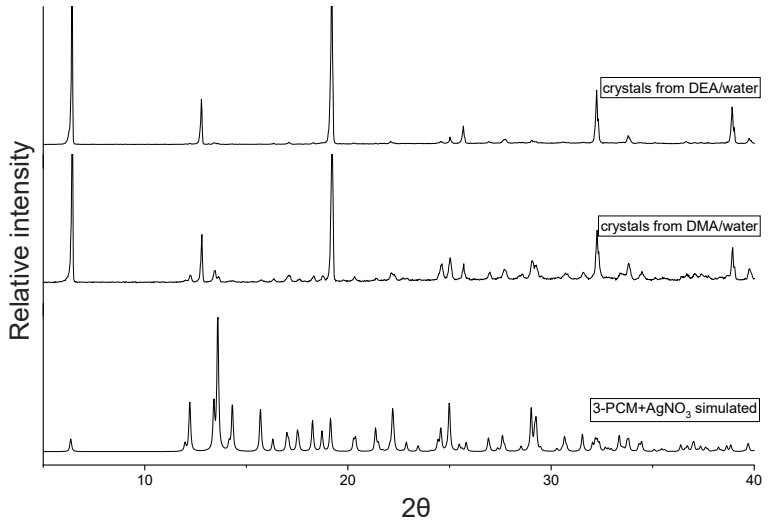

Figure S21. Comparison of PXRD pattern; simulated pattern of 3-PCM+$AgNO_3$, and the corresponding 3-PCM+$AgNO_3$ crystals obtained via layering a DMA/DEA solution of 3-PCM (10.0 mg/mL) with $AgNO_3$ dissolved in water, at 1:2 metal to ligand ratio.

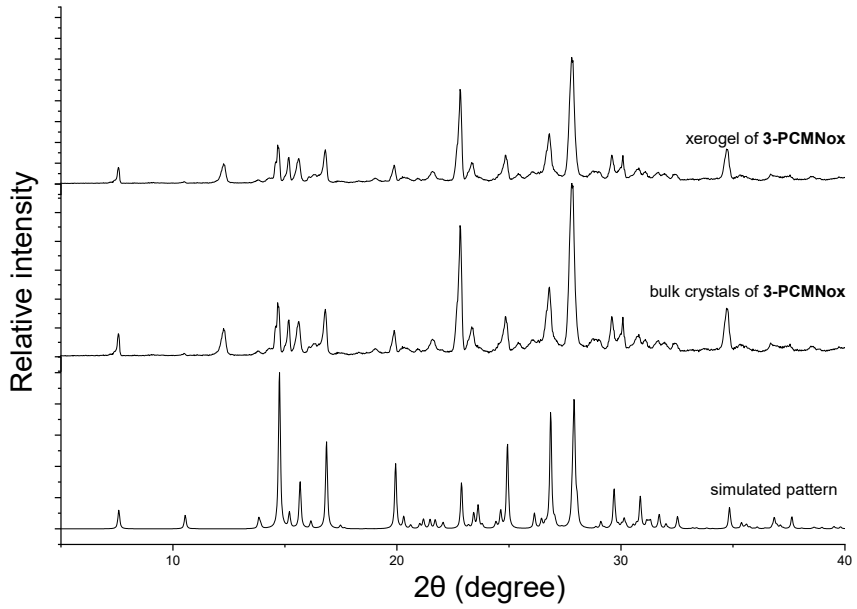

Figure S22. Comparison of PXRD pattern: simulated pattern of 3-PCMNox, bulk crystals obtained via crystallising in water (20.0 mg/mL), and xerogels obtained from the hydrogel prepared at 4.0 wt/v%.

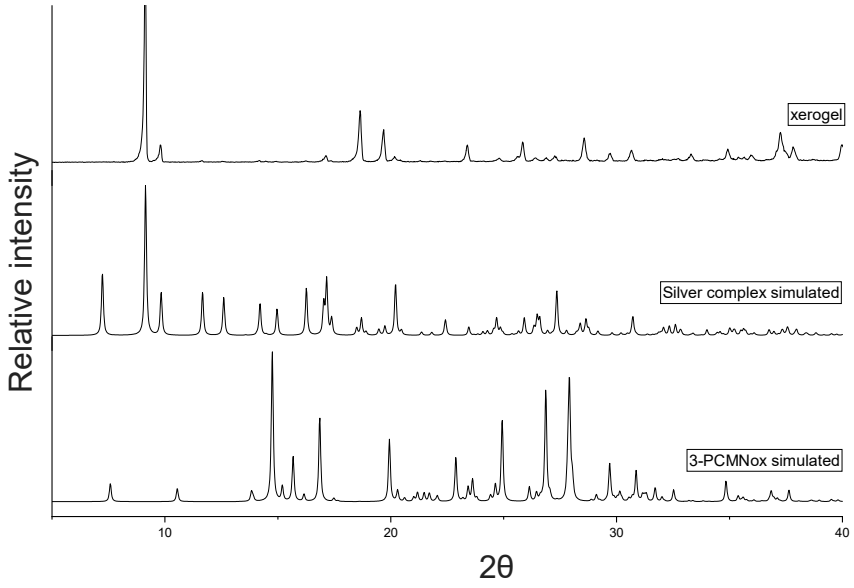

Figure S23. Comparison of PXRD pattern: simulated pattern of 3-PCMNox, simulated pattern of 3-PCMNox+$AgNO_3$ complex, and the xerogel obtained from 3-PCMNox+$AgNO_3$ gel (6.1 wt/v% of ligand) in DMF/water (1:9, v/v), at 1:2 metal to ligand ratio.

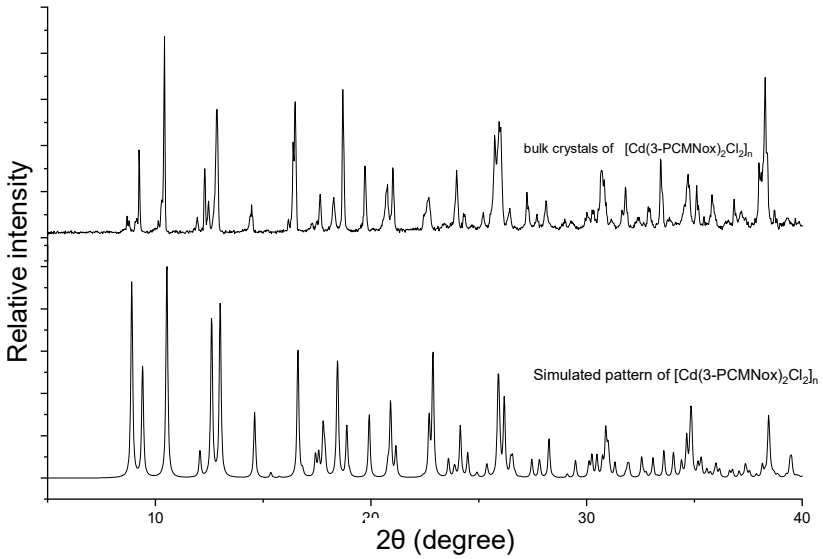

Figure S24. Comparison of PXRD pattern; simulated pattern of 3-PCMNox+$CdCl_2$, and the bulk crystals obtained via layering a DMF solution of 3-PCMNox (61.0 mg/mL) with $CdCl_2$ dissolved in water, at 1:2 metal to ligand ratio.

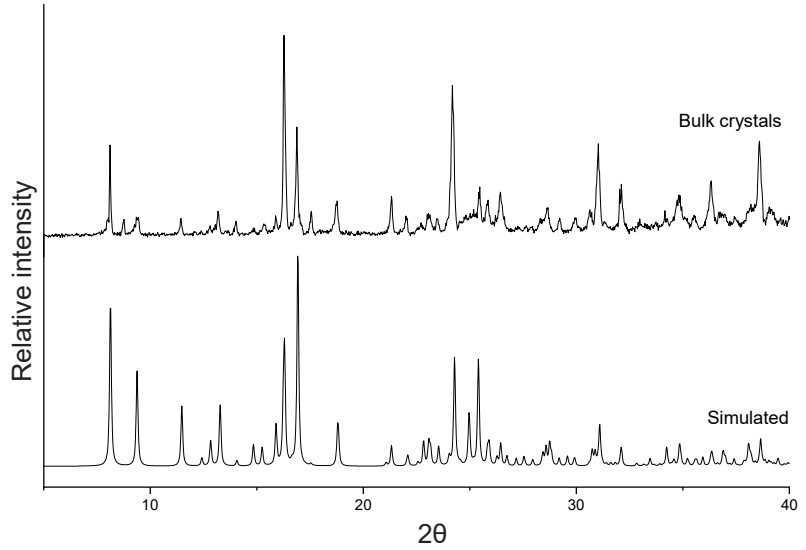

Figure S25. Comparison of PXRD pattern: simulated pattern of 4-PCM+$CdCl_2$, with the bulk crystals obtained from 1.0 mL DMF with 29.1 mg of 4-PCM and 1:2 metal to ligand ratio.

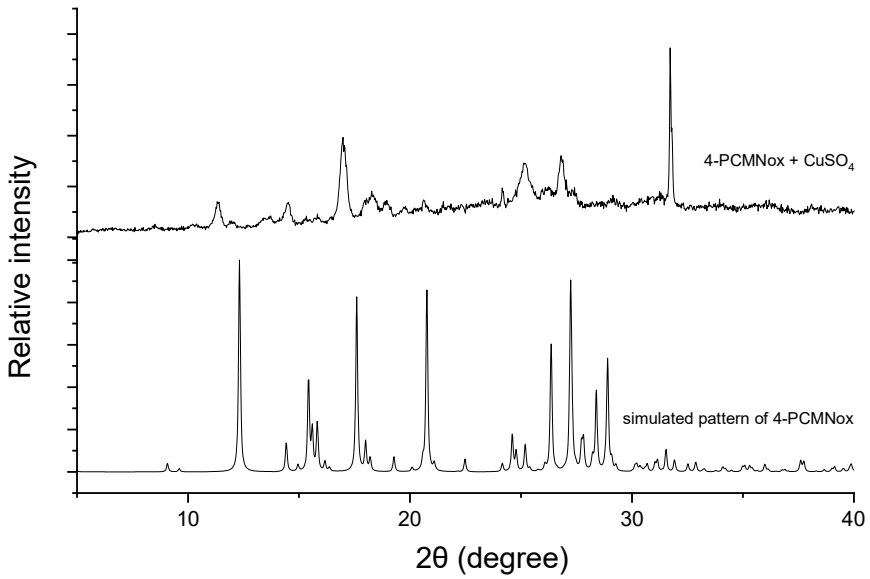

Figure S26. Comparison of PXRD pattern: simulated pattern of 4-PCMNox, with the xerogel of 4-PCMNox+$CuSO_4$ gel (6.1 wt/v% of ligand) in DMF/water (1:1, v/v), at 1:2 metal to ligand ratio.

4.0 Role of functional groups on the self-assembly process in multi-component gels

Multi-component gels are formed by mixing two or more entities such as a gelator, a gelator and a non-gelator, or even a combination of two non-gelators. Multi-component gels based on mixing chiral compounds tagged with electron-rich (donor) or electron-deficient (acceptor) moieties will form fascinating material with potential application in optoelectronic devices. These molecules could interact either constructively or destructively to undergo self-sorting or co-assembled network, which mainly depends on various parameters (gelator structure, the spatial orientation of the functional groups and solvent system, etc.).

In this chapter, we are evaluating the role of the individual component's molecular structure on the self-assembly process of multi-component systems by analysing the gelation properties of chiral multicomponent gels with structurally similar (enantiomers) and non-similar donor or acceptor moieties. We have designed chiral donor-acceptor system to analyze the effect of enantiomeric donor and acceptor in the self-assembly process in multi-component gels and to study the charge-transfer (CT) interaction mediated alternate stacking of donor-acceptor molecules. The self-assembly process in these multi-component systems based on the multifunctional chiral LMWGs depends on either hydrogen bonding or charge transfer interactions, or both.

4.1 Analyzing the self-assembly modes in chiral multi-component systems based on individual components with structurally similar (enantiomers) and non-similar (donor or acceptor moieties) functionalities to evaluate the role of specific functional groups on the self-assembly modes.

Article-VI

The self-assembly process in multi-component systems was examined by analyzing the gelation properties of chiral multi-component systems. The influence of structural similarity among individual components was analyzed by using structurally similar (enantiomers) and non-similar (donor or acceptor) moieties. The gelation properties of individual enantiomers, mixed enantiomers, and mixed chiral donor-acceptor compounds were examined in different solvents. The analysis of mechanical strength indicated that the mixed chiral gels had greater strength compared to other gels in mesitylene; however, an opposite tendency was found with thermal stability. Scanning electron microscopy (SEM) of the desiccated gels composed of mixed enantiomers and mixed chiral donor-acceptor systems revealed morphological alterations indicative of distinct self-assembly mechanisms. Powder X-ray examination indicated that a co-assembled mode was observed in the mixed gels containing structurally similar components. The mixed chiral donor-acceptor gel revealed self-sorting nature, with the charge transfer interaction between the donor and acceptor significantly influencing the self-assembly of these mixed gels. We conducted computational analyses in order to predict the electronic distribution within the chiral compounds. The results indicate that modifying the structural characteristics of individual components is a critical factor influencing the self-assembly patterns of multi-component systems.

Article-VI

This project is published in a peer-reviewed journal and included as published. Minor variations may arise from the original article owing to formatting issues.

Publication details:

"**Analyzing the self-assembly modes in chiral multi-component gels based on donor and acceptor moieties**"

Sreejith S. Jayabhavan, H. Myneni, M. Riedel, and Krishna K. Damodaran*

Supramol. Chem., **2024**, 1-13.

Author contributions:

S.S.J. and K.K.D planned and designed the research; **S.S.J.** synthesized the gelators, performed characterizations, and evaluated gelation properties. H.M. carried out the computational calculations and M.R. confirmed the results. **S.S.J.** and K.K.D. wrote the initial manuscript draft and all authors reviewed the main manuscript.

Supramolecular Chemistry

ISSN: (Print) (Online) Journal homepage: www.tandfonline.com/journals/gsch20

Analysing the self-assembly modes in chiral multi-component gels based on donor and acceptor moieties

Sreejith Sudhakaran Jayabhavan, Hemanadhan Myneni, Morris Riedel & Krishna K. Damodaran

To cite this article: Sreejith Sudhakaran Jayabhavan, Hemanadhan Myneni, Morris Riedel & Krishna K. Damodaran (22 Aug 2024): Analysing the self-assembly modes in chiral multi-component gels based on donor and acceptor moieties, Supramolecular Chemistry, DOI: 10.1080/10610278.2024.2394465

To link to this article: https://doi.org/10.1080/10610278.2024.2394465

SUPRAMOLECULAR CHEMISTRY
https://doi.org/10.1080/10610278.2024.2394465

Analysing the self-assembly modes in chiral multi-component gels based on donor and acceptor moieties

Sreejith Sudhakaran Jayabhavan[a], Hemanadhan Myneni[b], Morris Riedel[b,c] and Krishna K. Damodaran[a]

[a]Department of Chemistry, Science Institute, University of Iceland, Reykjavík, Iceland; [b]The Faculty of Industrial Engineering, Mechanical Engineering, and Computer Science, University of Iceland, Reykjavík, Iceland; [c]Large-Scale Data Science Division, Juelich Supercomputing Centre, Jülich, Germany

ABSTRACT

The role of the structural similarity in the individual components on the self-assembly process of multi-component systems was studied by analysing the gelation properties of chiral multi-component gels with structurally similar (enantiomers) and non-similar donor or acceptor moieties. The gelation properties of the individual enantiomers, mixed enantiomers, and mixed chiral donor-acceptor compounds were analysed in various solvents. Analysis of the mechanical strength revealed that the mixed chiral gels were stronger compared to other gels in mesitylene; however, a reverse trend was observed for thermal stability. Scanning electron microscopy (SEM) of the dried gels of the mixed enantiomeric and mixed chiral donor-acceptor gels showed morphological changes indicating different self-assembly modes. Powder X-ray analysis revealed that a co-assembled mode was observed for the mixed gels with structurally similar components. However, a self-sorting nature was observed for the mixed chiral donor-acceptor gel, and the charge transfer interaction between the donor and acceptor played a major role in the self-assembly of these mixed gels. We performed computational studies to predict the electronic distribution in the individual chiral molecules. These results demonstrate that altering the structural features of the individual components is one of the key parameters that control the self-assembly modes of multi-component systems.

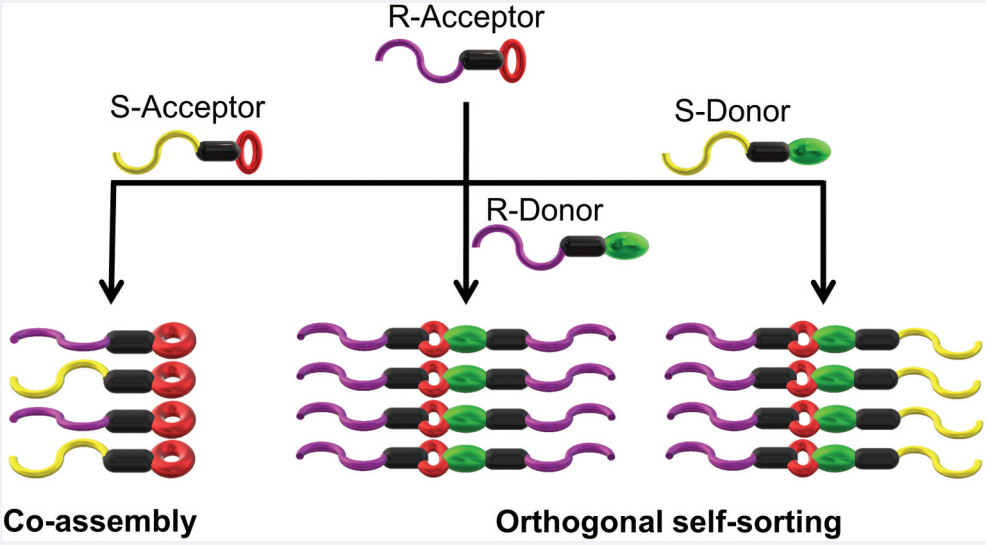

ARTICLE HISTORY
Received 10 June 2024
Accepted 15 August 2024

KEYWORDS
Multi-component gels; amides; chirality; donor-acceptor; self-assembly

1. Introduction

Nature has successfully assembled simple building blocks such as amino acids and sugars to generate multi-component systems and complex architectures (*e.g.*, biopolymers) that characterise life on Earth. Inspired by nature, several supramolecular materials based on multi-component systems with intriguing properties have been developed [1]. Multi-component systems based on low molecular weight gelators (LMWGs) [2–7] are an excellent class of soft materials to analyse the

CONTACT Krishna K. Damodaran krishna@hi.is Department of Chemistry, Science Institute, University of Iceland, Dunhagi 3, 107, Reykjavík, Iceland
Supplemental data for this article can be accessed online at https://doi.org/10.1080/10610278.2024.2394465

mechanism of the self-assembly process because the self-assembly in LMWGs can be tuned by several external and internal factors such as heat, light, sound, salts, pH, nature of functionality, gelator structure, and so forth. In multi-component gels, one of the components or both can be gelator, or all components are non-gelators, but mixing induces the gelation [8,9]. The advantage of multi-component systems based on mixing two gelators is that the self-assembly process can be analysed by correlating the non–covalent interactions between individual and the mixed gelator molecules [10–13]. The self-assembly of multi-component gels is driven by hydrogen bonding, π-π interactions, charge transfer interactions, etc., and the self-assembly based on charge transfer interactions has been studied extensively owing to their excellent prospects in organic photovoltaics, sensing, ferroelectricity, and semiconductors [14–16].

Charge-transfer complexation has been used in the design of many supramolecular architectures, such as organogels, rotaxanes, catenanes, and liquid crystalline materials [17–19]. The self-assembly in the donor-acceptor pair arises due to the charge transfer (CT) interaction between the highest occupied molecular orbital (HOMO) of the donor to the lowest unoccupied molecular orbital (LUMO) of the acceptor [20]. Charge-transfer interactions induced gelation in multi-component systems based on bile acids and trinitrofluorenone was first reported in 1999 by Maitra's group and showed that the structure of the donor unit on the bile acid backbone played a crucial role in gelation [18]. The self-assembly process in the multi-component gels arises from constructive or destructive interactions between individual gelators, resulting in a specific co-assembly of well-ordered fibres with both gelators, self-sorted individual gelators or a mixture of both (random co-assembly) [9]. Several reports were brought into light, with the co-assembly via CT by the alternate stacking of the donor-acceptor chromophores [21]. Qui *et al*. reported a co-assembled donor-acceptor based gel with the ability to sense complex chemical environments, and the purple sponge-like gel obtained by mixing derivatives of triphenylene and hexaazatriphenylene triimide was stable in the presence of non-polar solvents, but dissociated in the presence of polar solvents [22]. Zhibo Li's group studied the effects of conjugated aromatic core in the donor and acceptor, which influenced the co-assembly via CT interactions [23].

Self-sorting phenomenon [24] between the donor and acceptor moieties is of greater importance, which could lead to separate bundles of fibres with *p*-type and *n*-type characteristics for effective electron transfer and transport of charge carriers [25]. Raju and co-workers investigated the co-assembly of pyrene derivatives with trinitrofluorenone (TNF) and observed that pyrene derivatives without hydrogen-bonding groups exhibit charge transfer (CT) gelation; however, derivatives with amide, urethane, or urea groups tend to undergo self-sorting rather than co-assembly with TNF [26]. Ghosh *et al*. reported a series of bis-amide functionalised donor and acceptor moieties and studied the effect of the spacer length on self-assembly and gelation. When the distance between the bis-amide does not match, the donor-acceptor (D-A) pair undergoes self-sorting, probed by π-π stacking and hydrogen bonding interaction between amide functionality of D-D or A-A [27]. The same group also reported the self-sorting of naphthalene-diimide (NDI) acceptor and dialkoxy-naphthalene (DAN) donor organogelators, using symmetrical and unsymmetrical amide hydrogen bonding functionality design in the donor (DAN) and the acceptor (NDI) moieties, respectively. Due to the stronger nature of hydrogen bonding compared to CT interaction, self-sorting was observed for the donor-acceptor system [25].

These results indicate that the formation of self-sorted or co-assembled networks is one of the main factors that determines the properties of the multi-component gels. However, predicting the formation of self-sorted or co-assembled networks is challenging because the self-assembly of the individual components depends on various factors such as gelation environment, pH, temperature, and chemical structure [7–9]. The structural similarity of individual gelators is an important criterion for tuning the self-assembly of the multi-component system. Multi-component systems based on structurally similar components, such as enantiomers, prefer co-assembly over self-sorting [10–13,28–37], and we have shown that mixing enantiomeric gels leads to co-assembled networks [10–13]. The self-assembly of multi-component gels based on donor and acceptor systems is well understood, but studies on the self-assembly modes of chiral multi-component gels based on mixing chiral-donor and -acceptor systems are rare [21,38–40]. In this work, we investigate the self-assembly process of multifunctional chiral LMWGs based on chiral-donor and -acceptor equipped with hydrogen bonding moieties such as amides and amino acid derivatives. Amide moieties are well known for their ability to display complementary hydrogen bonding between the amide functionalities to form *β*-sheets, resulting in gel fibrils with intriguing characteristics [41,42]. The self-assembly process of the multi-component systems based on the multifunctional chiral LMWGs depends

on either hydrogen bonding or charge transfer interactions, or both. To the best of our knowledge, there are no reports on the correlation of these non-bonding interactions towards the self-assembly modes in multi-component gels based on chiral donor and acceptor systems.

2. Materials and methods

The commercially available solvents and starting materials were bought from Fluorochem UK, TCI-Europe (Boereveldseweg, Belgium), and Sigma-Aldrich (MEDOR ehf, Reykjavik, Iceland). The gelation tests were conducted using deionised water. The ^{1}H and ^{13}C NMR spectra (see Figure S1-S8) obtained with a Bruker Avance 400 spectrometer (Rheinstetten, Germany), and the SEM images (Carl Zeiss, Oberkochen, Germany) obtained with a Leo Supra 25 microscope were used to characterise the xerogels. The modular compact rheometer MCR 302 (Graz, Austria) manufactured by Anton Paar was used for the rheological studies. Using a PANalytical device (Almelo, The Netherlands), powder X-ray diffraction (PXRD) analysis was carried out with bulk compounds and xerogel.

2.1. Synthesis of ligands

2.1.1. General synthesis of amides

To a suspension of *R* or *S*-based 4-((1-methoxy-3-methyl-1-oxobutan-2-yl)carbamoyl)benzoic acid (1.0 g, 3.6 mmol) in 10.0 mL of dry DCM, about 2.2 mL (1.70 g, 14.3 mmol) of thionyl chloride was added under a nitrogen atmosphere, and the mixture was allowed to stir at 45.0°C overnight. A clear solution was observed, and the solvents were evaporated to yield the corresponding acid chloride, which was washed with *n*-hexane and decanted to obtain a white solid powder. To this powder, 50 mL of dried DCM was added, and N^{1}-(naphthalen-1-yl)ethane-1,2-diamine dihydrochloride (1.04 g, 3.6 mmol) or 2-(2-aminoethyl)isoindoline-1,3-dione trifluoroacetate (1.09 g, 3.6 mmol) was subsequently added to a mixture under nitrogen atmosphere. A solution of 2.0 mL (1.9 g, 14.3 mmol) of triethylamine in dry DCM (40.0 mL) was added dropwise to the mixture at 0°C and stirred overnight at room temperature. The mixture was dried to obtain the crude TAD or TAA-based compounds. The TAD compound was purified by column chromatography (silica gel, eluent: petroleum ether/ethyl acetate, 3:1, v/v) and further recrystallised in 1:1 (v/v) aqueous ethanol. However, the TAA compounds were purified by crystallising the crude compound in ethanol three times.

2.1.2. Methyl (4-((2-(naphthalen-1-ylamino)ethyl) carbamoyl)benzoyl)-D-valinate (R-TAD)

Yield 1.20 g, 72.2%. ^{1}H NMR (400 MHz, Chloroform-*d*) δ (ppm): 7.91–7.82 (m, 1 H), 7.80–7.76 (m, 1 H), 7.75 (s, 4 H), 7.49–7.38 (m, 2 H), 7.38–7.29 (m, 1 H), 7.27–7.20 (m, 1 H), 6.81 (t, J = 6.1 Hz, 1 H), 6.70 (d, J = 8.6 Hz, 1 H), 6.60 (d, J = 8.8 Hz, 1 H), 5.16 (s, 1 H), 4.74 (dd, J = 8.6, 4.9 Hz, 1 H), 3.87 (q, J = 5.9 Hz, 2 H), 3.77 (s, 3 H), 3.54 (t, J = 5.6 Hz, 2 H), 2.34–2.21 (m, 1 H), 0.99 (t, J = 6.8 Hz, 6 H).^{13}C {^{1}H} NMR (100 MHz, Chloroform-*d*) δ (ppm): 172.61, 168.07, 166.67, 143.46, 137.26, 136.89, 134.46, 128.71, 127.46, 126.67, 125.99, 125.05, 123.52, 120.32, 117.63, 103.90, 57.77, 52.48, 45.03, 39.77, 31.70, 19.14, 18.16. HRMS (APCI): calcd. for $C_{26}H_{29}N_3O_4Na$ [M + Na]+, 470.2050; found, 470.2046.

2.1.3. Methyl (4-((2-(naphthalen-1-ylamino)ethyl) carbamoyl)benzoyl)-L-valinate (S-TAD)

Yield 1.25 g, 75.2%. ^{1}H NMR (400 MHz, Chloroform-*d*) δ (ppm): 7.91–7.84 (m, 1 H), 7.80–7.77 (m, 1 H), 7.76 (s, 4 H), 7.49–7.38 (m, 2 H), 7.38–7.29 (m, 1 H), 7.27–7.19 (m, 1 H), 6.79 (t, J = 6.0 Hz, 1 H), 6.69 (d, J = 8.6 Hz, 1 H), 6.60 (d, J = 6.5 Hz, 1 H), 5.16 (s, 1 H), 4.75 (dd, J = 8.6, 5.0 Hz, 1 H), 3.87 (q, J = 5.9 Hz, 2 H), 3.77 (s, 3 H), 3.55 (t, J = 5.6 Hz, 2 H), 2.34–2.21 (m, 1 H), 0.99 (t, J = 6.9 Hz, 6 H). ^{13}C {^{1}H} NMR (100 MHz, Chloroform-*d*) δ (ppm): 172.61, 168.05, 166.64, 143.46, 137.26, 136.90, 134.46, 128.71, 127.47, 126.66, 125.99, 125.06, 123.53, 120.32, 117.64, 103.90, 57.76, 52.48, 45.03, 39.78, 31.71, 19.13, 18.16. HRMS (APCI): calcd. for $C_{26}H_{29}N_3O_4Na$ [M + Na]+, 470.2050; found, 470.2027.

2.1.4. Methyl (4-((2-(1,3-dioxoisoindolin-2-yl)ethyl) carbamoyl)benzoyl)-D-valinate (R-TAA)

Yield 1.05 g, 64.8%. ^{1}H NMR (400 MHz, Chloroform-*d*) δ (ppm): 7.85 (dd, *J* = 5.4, 3.1 Hz, 2 H), 7.82 (s, 4 H), 7.72 (dd, *J* = 5.6, 3.1 Hz, 2 H), 7.09 (t, *J* = 5.3 Hz, 1 H), 6.68 (d, *J* = 8.6 Hz, 1 H), 4.76 (dd, *J* = 8.6, 4.9 Hz, 1 H), 4.05–3.98 (m, 2 H), 3.78 (s, 3 H), 3.75–3.65 (m, 2 H), 2.34–2.22 (m, 1 H), 1.00 (t, *J* = 7.1 Hz, 6 H). ^{13}C {^{1}H} NMR (100 MHz, Chloroform-*d*) δ (ppm): 172.67, 169.02, 166.80, 166.64, 137.13, 136.86, 134.46, 131.96, 127.50, 127.47, 123.70, 57.69, 52.47, 40.54, 37.57, 31.76, 19.14, 18.14. HRMS (APCI): calcd. for $C_{24}H_{25}N_3O_6Na$ [M + Na]+, 474.1636; found, 474.1636.

2.1.5. Methyl (4-((2-(1,3-dioxoisoindolin-2-yl)ethyl) carbamoyl)benzoyl)-L-valinate (S-TAA)

Yield 1.15 g, 70.9%. ^{1}H NMR (400 MHz, Chloroform-*d*) δ (ppm): 7.85 (dd, J = 5.4, 3.1 Hz, 2 H), 7.82 (s, 4 H), 7.72 (dd, J = 5.4, 3.1 Hz, 2 H), 7.10 (t, J = 5.2 Hz, 1 H), 6.68 (d, J = 8.6 Hz, 1 H), 4.76 (dd, J = 8.6, 4.9 Hz, 1 H), 4.05–3.97 (m, 2 H), 3.78 (s, 3 H), 3.76–3.70 (m, 2 H), 2.34–2.22 (m, 1 H), 1.00 (t, J = 7.1 Hz, 6 H). ^{13}C {^{1}H} NMR (100 MHz, Chloroform-*d*) δ (ppm): 172.65, 169.00, 166.78, 166.63, 137.13, 136.84, 134.44, 131.96, 127.49, 127.46, 123.69, 57.68, 52.46,

40.53, 37.57, 31.75, 19.13, 18.13. HRMS (APCI): calcd. for $C_{24}H_{25}N_3O_6Na$ [M + Na]+, 474.1636; found, 474.1639.

2.2. Gelation studies

The gelation abilities of the enantiomeric compounds were assessed in different solvents. This was done by measuring 10.0 mg of each molecule in a standard 7.0 mL vial (with an inner diameter of 15.0 mm). Then, 1.0 mL of the solvent was poured into the vial, which was then sealed. The mixture was sonicated and gradually heated to get a transparent solution, which was then allowed to settle without disturbance. A vial inversion test was performed to confirm gelation. Additionally, the gelation experiments were performed in various mixed aqueous systems. About 10.0 mg of the compound was dissolved in 0.5 mL of the suitable solvent within a standard 7.0 mL vial. Subsequently, 0.5 mL of deionised water was added. The gelation ability was tested using the method mentioned above. Finally, we conducted multi-component gelation experiments with mesitylene and *p*-xylene by combining enantiomers in a 1:1 equimolar ratio, using the same procedure outlined for gelation with individual enantiomeric compounds. The studies were also performed with higher concentrations of the compounds (up to 50.0 mg/mL) to test the gelation ability.

2.2.1. Minimum gelator concentration (MGC)

The MGC experiment was performed with enantiomeric gels in various solvents/solvent mixtures. We have also studied the MGCs of multi-component gels obtained from mesitylene and *p*-xylene in a standard 7.0 mL vial and adding 1.0 mL of solvent. The mixture was sonicated and slowly heated for the complete dissolution of the compounds. Subsequently, the solution was maintained at room temperature to allow gel formation, and the MGC was recorded when solvent drops were not oozing out of the gel during the inversion test. The MGC can be defined as the smallest quantity of gelator needed to form a stable gel.

2.2.2. T_{gel} experiments

The T_{gel} experiments were conducted in mesitylene using equimolar mixed gels with a concentration of 2.0 wt/v% to study the mixed gel's thermal stability. In a 7.0 mL standard vial, the 2.0 wt/v% of gelator and 1.0 mL of mesitylene were added. The mixture underwent sonication, which was heated to dissolve and kept for gel formation. A ball-drop procedure was conducted after 24 hours to observe the gel-to-sol transition temperature, known as the gel–sol transition temperature (T_{gel}). A spherical glass sphere was delicately positioned on the surface of the gel, and the vial was sealed and submerged in an oil bath. A magnetic stirrer and a thermometer were employed to monitor the temperature while gradually heating the oil bath at a rate of 10.0°C per minute. As the temperature rises, the glass ball gradually becomes submerged in the gels, and the temperature at which the ball makes contact with the bottom of the vial is measured as T_{gel}.

2.3. Rheology

A rheometer model MCR 302 from Anton Paar was utilised to perform rheological measurements. A stainless steel parallel plate design with a distance of 2.5 cm between the plates was employed to measure the mechanical strength. Measurements were conducted at a constant temperature of 20.0°C in all instances. A Peltier temperature control hood was utilised as a solvent trap to sustain a temperature of 20.0°C during frequency and amplitude sweeps. The mixed gels of the chiral compounds were made by dissolving an equimolar amount of the corresponding compounds in 1.0 mL of mesitylene at a concentration of 2.0 wt/v%. Similarly, we have also prepared the enantiomeric and equimolar enantiomeric mixed gels based on the acceptor moieties in mesitylene at 2.0 wt/v%. The oscillatory amplitude sweep was conducted 24 hours later by transferring approximately 1.0 mL portion of gel onto the plate. A constant frequency of 1.0 Hz was maintained while doing an amplitude sweep using a logarithmic ramp strain (Y) ranging from 0.01% to 100%. A frequency sweep was conducted within the linear viscoelasticity range (0.02% strain) from 0.1 to 10.0 Hz.

2.4. Scanning electron microscopy (SEM)

The surface morphologies of the xerogels were investigated using SEM using a Leo Supra 25 microscope. The TAA-based gels of enantiomers and the mixed gel (R-TAA+S-TAA) were made from mesitylene at 2.0 wt/v %. Equimolar mixed gels were prepared by dissolving an appropriate quantity of the respective compounds in 1.0 mL of mesitylene, with a concentration of 2.0 wt/v %. After 24 hours, the gels were filtered under vacuum and then dried under a fume hood to obtain the xerogel. A small fraction of the xerogel was positioned on a pin mount, with the carbon tab on top. The surface was then coated with gold for 5–6 minutes (12–15 nm thickness) to avoid the accumulation of electric charge on the surface. Subsequently, the sample was loaded, and images were captured at an operating voltage of 3.0 kV and a working distance of 3–4 mm. An in-lens detector was

utilised to capture the scanning electron microscope (SEM) images.

2.5. Circular dichroism (CD)

The solution state CD experiments were carried out with the enantiomeric and equimolar chiral compounds at different concentrations (0.01, 0.02, and 0.03 wt/v%). The optimal concentration for CD experiments was 0.02 wt/v %, where the high tension (HT) value was optimal. The data was collected using a JASCO J-1100 CD spectrometer, with a scanning range of 200 to 400 nm and a scanning rate of 20.0 nm per minute. The spectrometer had a bandwidth of 1.0 nm and operated in continuous scanning mode.

2.6. Powder X-ray diffraction (PXRD)

We have dissolved 2.0 wt/v% of enantiomeric and equimolar mixed chiral donor-acceptor compounds in mesitylene. The precipitate observed for the enantiomeric compounds based on donor moieties was filtered and dried for PXRD analysis. The gels obtained were filtered and dried under a fume hood in all the other cases. The purpose was to compare the powder pattern with the enantiomers to study the nature of self-assembly. The studies were conducted using PANalytical equipment (Almelo, Netherlands) equipped with a Cu anode. The measurements were taken within the 2θ range of 4.0 to 50.0, with a step size of 0.025.

2.7. UV–visible spectroscopy

Agilent Cary UV-vis Multicell Peltier spectrometer was utilised to study UV absorption. We have prepared the solutions of TAD enantiomers at a concentration of 9.3×10^{-5} M in mesitylene. The equimolar solution of the TAD enantiomers was also prepared, such that the total concentration is 9.3×10^{-5} M in mesitylene. Similarly, all the mixed systems (TAD+TAA) were prepared at a 1:1 molar ratio with the concentration of TAD made at 9.3×10^{-5} M in mesitylene. The data was collected at a bandwidth of 2.0 nm.

2.8. Computational studies

All the quantum chemical calculations were performed using the ORCA software package, version 5.0.4 [43,44]. The density functional theory-based protocol consisted of the wB97X-D3 functional (including the D3 dispersion correction [45] and the def2-SVP basis set [46]). The RIJCOSX [47,48] approximation was used to calculate Coulomb and Exchange integrals using the def2/J auxiliary basis set by Weigend *et al.* [49]. All structures were fully optimised, both in the gas-phase and including the mesitylene solvent, without constraints and confirmed to be minima on the potential energy surface through frequency calculations.

3. Results and discussion

3.1. Design and synthesis

The self-assembly process of multi-component enantiomeric gels has been analysed by various analytical methods [50,51], and X-ray diffraction techniques have been used to distinguish between self-sorted and co-assembled networks in multi-component gels [11,12,51–56]. We have used single crystal X-ray diffraction (SCXRD) to show the crystallographic evidence of specific co-assembly in the mixed enantiomeric gel of valine methyl ester-based terephthalic amide (TAV) [11], and the rigidity of the terephthalic moiety and amide functionalities were crucial for the self-assembly process. The diamides exhibit β-tape-like self-assembly, forming a well-defined fibrous network in both enantiomeric and mixed gel forms. In this work, we have replaced one of the valine methyl esters of TAV [11] with a donor (naphthalene-based) or an acceptor (phthalimide-

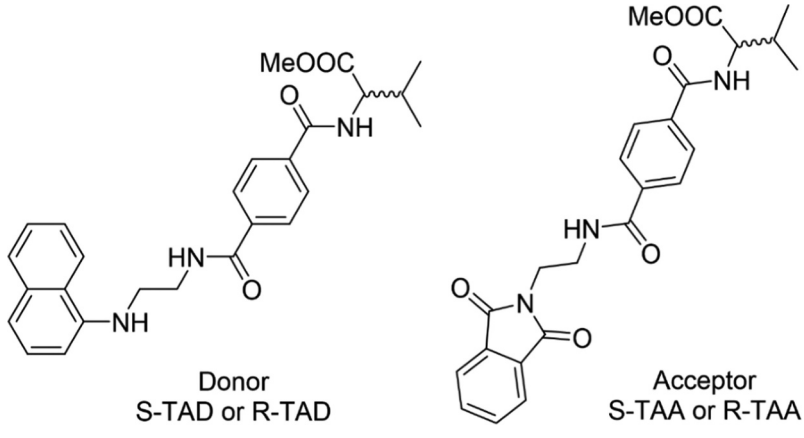

Figure 1. Chemical structure of the enantiomeric (*R*- or S-) donor and acceptor molecules.

based) moiety to develop enantiomeric donor (TAD) and acceptor (TAA) compounds (Figure 1). The starting material (monoacid) was synthesised using a protocol previously reported by our group [11] (see Scheme S1). The TAD compounds were synthesised by reacting the acid chloride of 4-((1-methoxy-3-methyl-1-oxobutan-2-yl)carbamoyl)-benzoic acid (R or S) with N^1-(naphthalen-1-yl) ethane-1,2-diamine dihydrochloride in DCM in the presence of triethyl amine. Similarly, the reaction of the monoacid with acceptor-based amine salt 2-(2-aminoethyl)isoindoline-1,3-dione trifluoroacetate [57] resulted in enantiomeric TAA compounds (see Scheme S2 and S3). The gelation experiments were performed with multi-component systems obtained by mixing enantiomers or donor-acceptor compounds to analyse the interactions (hydrogen bonding or charge transfer interactions) that control the self-assembly modes.

3.2. Gelation experiments

We performed gelation experiments with the enantiomers of TAD or TAA in various solvents/solvent mixtures. The trivial gelation test was followed by dissolving an appropriate amount of the compound in the respective solvent in a standard vial, left undisturbed for gel formation. Gelation tests with enantiomers of TAD revealed precipitation in various aromatic solvents such as xylenes, toluene, and mesitylene and in alcohols such as ethanol and n-butanol (see Table S1). The gelation test was further tested in a 1:1 aqueous mixture (v/v), which revealed that the TAD enantiomers gelled in aqueous mixtures of ethylene glycol and ethanol. TAD enantiomers were also found to gel in chlorobenzene at 5.0 wt/v %. The TAA enantiomers were observed to be versatile (Table S1), as they formed supergelators in xylenes, toluene, and mesitylene and an aqueous mixture of ethanol (1:1, v/v). The TAA enantiomers also formed gel at 1.0 wt/v% in ethylene glycol in aqueous mixtures (1:1, v/v) of ethylene glycol, DMSO, and at 2.0 wt/v% in 1:1 (v/v) DMF/water (see Table S1). Gelation tests were conducted up to 5.0 wt/v% of TAA to confirm the gel formation in all cases where solubility of the compound was possible.

The gelation tests were performed with the multi-component enantiomeric system obtained by mixing equimolar enantiomeric donor or acceptor compounds in mesitylene and *p*-xylene (see Table S2). These solvents were selected due to their non-polar nature, higher boiling points, and the probability of π-π interaction with the terephthalic core. The equimolar donor system R-TAD +S-TAD precipitated out in both the solvents (see Figure S9) and similar results were observed in experiments at higher concentrations (5.0 wt/v%). The mixed acceptor system R-TAA+S-TAA was observed to form gels in both mesitylene and *p*-xylene. The minimum gelator concentration (MGC) of the mixed gels was evaluated and compared with the individual enantiomeric gels. The R-TAA+S-TAA gelled in *p*-xylene at 0.7 wt/v%, slightly higher than its corresponding enantiomers (0.4 wt/v%). Similarly, the mixed gel gelled at a higher concentration of 1.0 wt/v% in mesitylene than the enantiomers.

Analysis of gelation tests with the mixed chiral donor-acceptor system in mesitylene revealed R-TAD+S-TAA and R-TAA+S-TAD formed gels at 1.4 wt/v% and R-TAD +R-TAA and S-TAD+S-TAA gelled at 2.0 wt/v%. The gel formation was accompanied by a colour change from a colourless solution to a yellow gel upon cooling, which

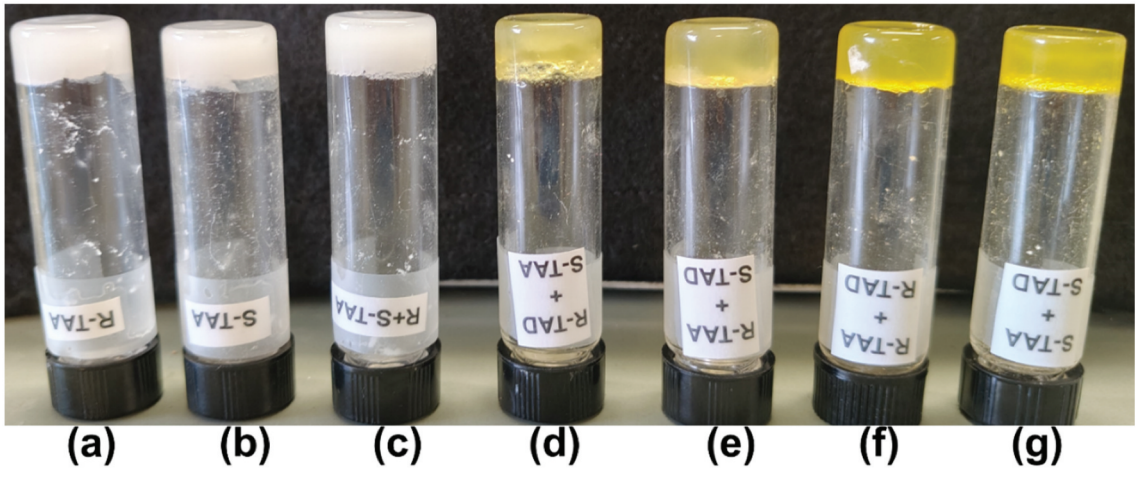

Figure 2. TAD and TAA-based gels in mesitylene at 2.0 wt/v%; (a) R-TAA, (b) S-TAA, (c) R-TAA+S-TAA, (d) R-TAD+S-TAA, (e) R-TAA +S-TAD, (f) R-TAA+R-TAD, and (g) S-TAA+S-TAD.

was not observed in individual and mixed enantiomeric gels (Figure 2 and see Figure S10). This may be due to the charge transfer interaction between the donor and acceptor-based compounds.

Gelation tests performed in p-xylene resulted in yellow gels similar to the gels in mesitylene. The MGC of R-TAD+S-TAA and R-TAA+S-TAD was 1.4 wt/v%, while the R-TAD+R-TAA and S-TAD+S-TAA gelled at a slightly higher concentration (1.7 wt/v%). The analysis of MGC revealed that the mixed chiral donor-acceptor system gelled at higher concentrations compared to mixed enantiomeric gels, which may be due to the alteration of the non-covalent interaction arising from the donor-acceptor charge transfer interactions.

3.3. Thermal stability

Analysis of the gel-sol transition temperature provides information about the thermal strength of the supramolecular gels, which is known as T_{gel}. The thermal stability (T_{gel}) of the enantiomeric TAA gels in mesitylene at 2.0 wt/v% was found to be 165.0°C, which matches with the boiling point of mesitylene. Therefore, we performed the T_{gel} experiments for enantiomeric TAA gels at lower concentrations because the thermal stability depends on the concentration of the gelator, and the T_{gel} values were found to be 158.8°C and 164.2°C at 1.0 wt/v% and 1.5 wt/v %), respectively. We have analysed the T_{gel} of the mixed enantiomeric and chiral donor-acceptor based gels in mesitylene at 2.0 wt/v%. Since the solubility of R-TAD+S-TAA and R-TAA+S-TAD in *p*-xylene was poor, we were unable to find an optimum concentration with *p*-xylene to compare the T_{gel}. The thermal strength analysis revealed that the thermal strength of the mixed enantiomeric gel (R-TAA+S-TAA) was slightly stronger than the corresponding mixed chiral donor-acceptor based gels (see Table S3). The comparison of the thermal strengths of the mixed chiral donor-acceptor based gels indicated that the R-TAD +S-TAA and R-TAA+S-TAD showed slightly higher than the R-TAD+R-TAA and S-TAA+S-TAD gels, presumably due to the existence of a different self-assembly mode due to structurally non-similar individual components in mixed R+S donor-acceptor systems.

3.4. Rheology

Rheology can be utilised to study the self-assembly process in supramolecular gels, which can be used to evaluate both the solid and liquid-like properties of the viscoelastic gel [58]. We have used rheology to study the self-assembly modes in multi-component gels by tuning the functional groups [12]. For the rheological experiments, a strain sweep was conducted initially to identify the linear viscoelastic region (LVR), which is the range of strain where the elastic modulus (G′) remains constant regardless of the applied strain. The LVR ensured that the gels experienced reversible deformation during the studies; this will allow us to compare the structural properties of the gels. Gels were made in mesitylene at 2.0 wt/v% with enantiomeric and mixed enantiomeric gels of TAA and mixed chiral donor-acceptor gels. The strain sweep measurement indicated that all the gels maintained a consistent G′ up to a strain of 0.1% (see Figure S11). The gel networks transitioned from a solid to a liquid phase, which occurred at strains ranging from around 1.0% to 15.0%.

Frequency sweep experiments were performed at a constant strain of 0.02%, over the 0.1–10 Hz range, and have observed that the G′ > G″, and the frequency was independent of the applied strain. The individual enantiomeric gels of TAA were stronger than the equimolar mixed gel (R-TAA+S-TAA) in mesitylene at 2.0 wt/v %. However, the mixed chiral donor-acceptor based gels (R-TAD+S-TAA, R-TAD+R-TAA, S-TAD+R-TAA, and S-TAD +S-TAA) in mesitylene at 2.0 wt/v% showed higher mechanical strength than the TAA-based gels (Figure 3), which confirms that the self-assembly modes are different in mixed enantiomeric and mixed chiral donor-acceptor gels.

3.5. Gel morphology

The hierarchical structure of self-assembled fibres in multi-component gels has been studied using scanning electron microscopy (SEM), transmission electron microscopy (TEM), cryogenic TEM, atomic force microscopy (AFM), and confocal laser scanning microscopy. SEM can be considered as an effective method in the analysis of the surface morphology of organic and inorganic materials on a nanometre to micrometre (μm) scale [10,11,51], and we used SEM to analyse the morphologies of the dried gel fibres, which can be correlated to the self-assembly modes. For example, the morphology of the dried gel fibre of the co-assembled system may differ in fibre morphology compared to the corresponding individual xerogels [10,13]. SEM analysis performed on the xerogels (2.0 wt/v%) from mesitylene revealed fibrous morphology in all cases. The dried gels of enantiomeric R-TAA and S-TAA showed thin and long fibres with fibre widths ranging from 0.2–2.0 μm (Figure 4(a,b)), but the morphology of the mixed enantiomeric dried gel (R-TAA+S-TAA) was slightly different from the individual

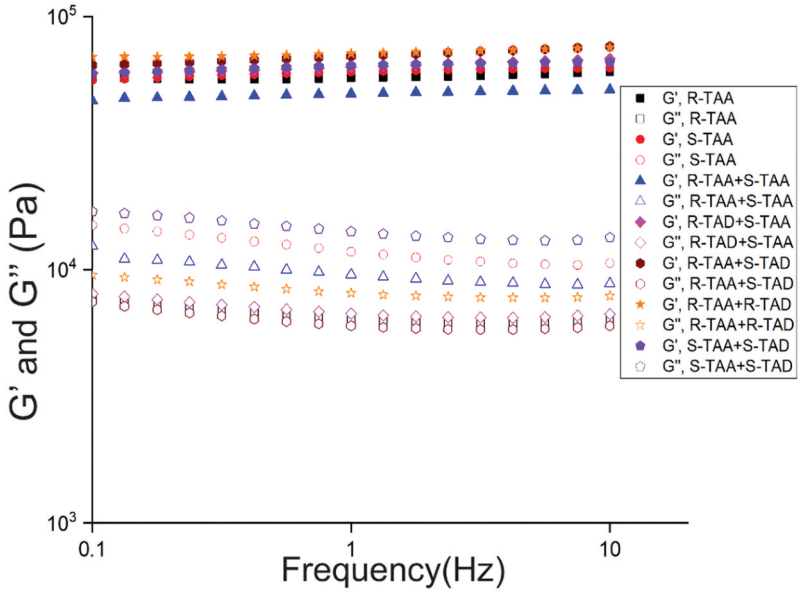

Figure 3. Frequency sweep of enantiomeric and equimolar enantiomeric and mixed chiral donor-acceptor gels based on donor or acceptor systems (2.0 wt/v%) in mesitylene at 20.0°C measured at a constant strain of 0.02%.

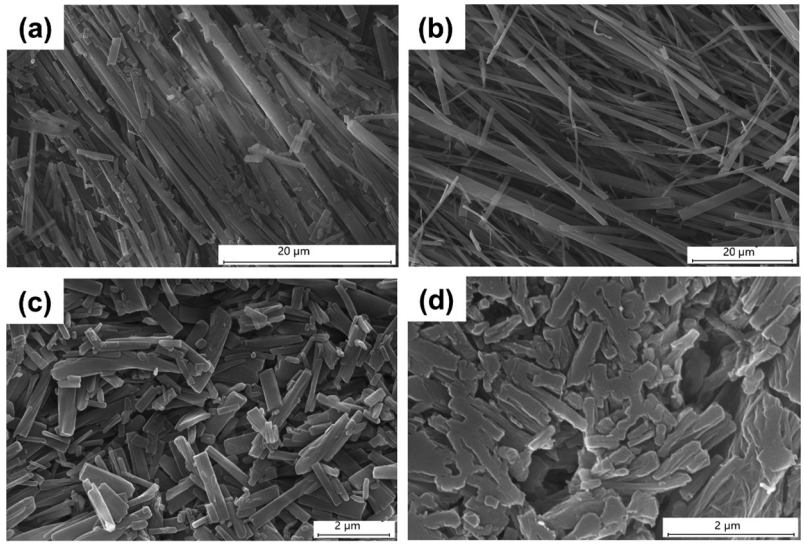

Figure 4. SEM images of the xerogel obtained from mesitylene at 2.0 wt/v% with (a) R-TAA, (b) S-TAA, (c) R-TAA+S-TAA, and (d) R-TAA +S-TAD.

enantiomers displaying discrete rectangular blocks (0.1–1.0 µm thickness) indicating a different self-assembly mode (Figure 4(c)).

The analysis of the dried gels of mixed chiral donor-acceptor gels (R-TAD+S-TAA, R-TAD+R-TAA, S-TAD+R-TAA, and S-TAD+S-TAA) revealed a thin and plate-shaped fibre morphology (Figure 4(d) and see Figure S12), which was not similar to the individual and mixed enantiomeric gels, indicating the formation of a different self-assembly mode, presumably arising from both the hydrogen bonding and donor-acceptor charge transfer interactions.

3.6. Circular dichroism

Circular dichroism (CD) experiments help to understand the structural information of the self-assembled chiral architectures [10–12,59]. The chirality of the enantiomeric TAA and TAD compounds and the mixed enantiomers were studied in absolute ethanol using solution-state CD experiments. The optimal concentration for the CD studies was observed to be 0.02 wt/v%, where the HT value was observed to be optimal. Performing CD experiments was challenging for wavelengths below

210 nm, where the absorbance tends to change abruptly due to the presence of the chromophores in addition to the contributions from solvents. In the solution state, the CD spectra for R-TAD displayed positive maxima around 227 nm and negative maxima around 248 nm, and a mirror image was observed for S-TAD (see Figure S13). The CD spectra for R-TAA showed a positive maxima around 226 nm and a negative maxima around 250 nm, and the corresponding enantiomeric S-TAA showed a mirror image (see Figure S14). The equimolar mixed enantiomers (R-TAA+S-TAA or R-TAD+S-TAD) showed linear signals due to external compensation. The peak detected at a wavelength of 228 nm could likely indicate the β-conformation structure found in self-assembled gels of short peptides, which may be attributed to the hydrogen bonding in amides and the π-π stacking interactions [60,61]. The equimolar donor-acceptor mixture based on chiral compounds R-TAD+S-TAA and S-TAD +R-TAA showed linear signals, presumably due to the presence of chiral compounds in the equimolar ratio. However, the mixed R-TAD+R-TAA showed positive maxima around 247 nm and negative maxima around 251 nm, but S-TAD+S-TAA displayed a slightly different mirror image (see Figure S15).

3.7. Powder X-ray diffraction (PXRD)

PXRD can be used as a tool to compare the molecular packing in the dried gel state with that of the simulated powder pattern obtained from the single crystal data [11,50,62–64], even though the drying process of gel could result in artefacts [65]. In the absence of single crystal data, PXRD can also be used to compare the xerogel of enantiomers and the mixed gel to study the self-assembly modes [13,66]. The PXRD pattern of the xerogels of enantiomers of TAA in mesitylene at 2.0 wt/v % displayed superimposable patterns, but the PXRD pattern of the mixed enantiomeric TAA was different from the individual enantiomers (see Figure S16). This indicated that the self-assembly modes were not similar, and the enantiomers interacted with each other to form a different network, presumably a co-assembled network. The PXRD experiments for the enantiomers and mixed compounds of the non-gelator TAD were performed with the residue obtained from mesitylene, which was filtered and dried to record the PXRD. The comparison of the PXRD patterns revealed a similar trend as TAA xerogels, suggesting co-assembly in mixed enantiomeric TAD compound (see Figure S17). Finally, we have recorded PXRD with the dried gels of mixed chiral donor-acceptor system (R-TAD+S-TAA, R-TAD+R-TAA, S-TAD+R-TAA, and S-TAD+S-TAA) prepared from mesitylene at 2.0 wt/v%. A similar powder pattern, comparable with the added powder pattern of both the enantiomers, was observed for all the cases (Figure 5 and see Figure S18), indicating that the individual components were self-sorted. The difference in thermal stability and the morphology of the chiral gels

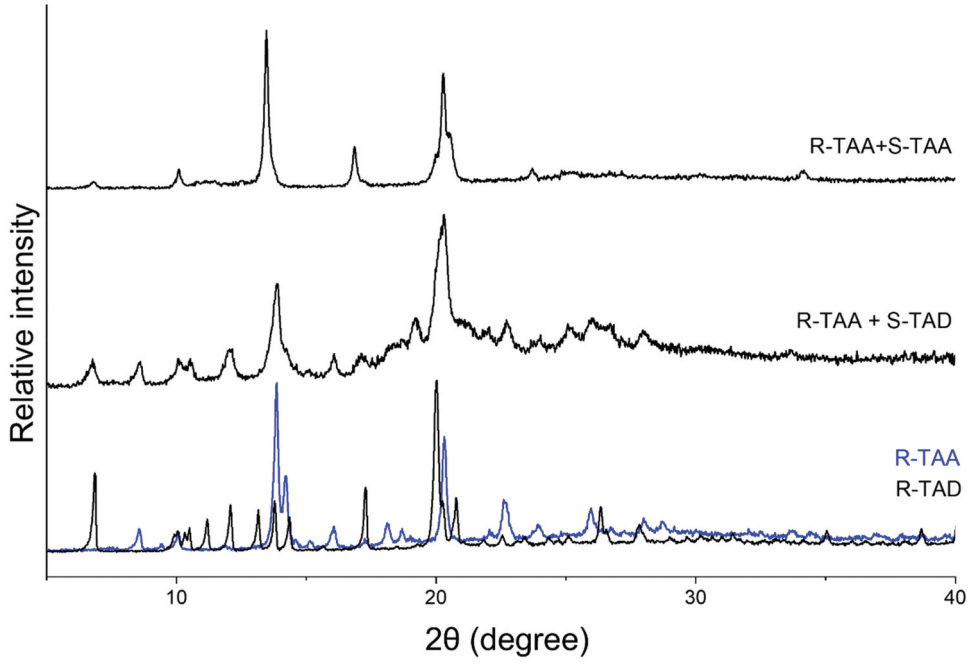

Figure 5. PXRD studies with the xerogels obtained from R-TAA, R-TAA+S-TAA, R-TAA+S-TAD and the precipitate with R-TAD from mesitylene at 2.0 wt/v%.

compared to the individual enantiomeric gels suggest that the self-sorted donor may interact with the self-sorted acceptor chains leading to orthogonal self-sorting [67].

3.8. UV-visible spectroscopy

The UV-vis studies were performed with the enantiomers of TAD and TAA and the mixed R-TAD+S-TAD and R-TAA+S-TAA systems in mesitylene at 9.3×10^{-5} M concentration of TAD and TAA, respectively. The absorbance spectra of enantiomeric TAD and the mixed R-TAD+S-TAD were identical (see Figure S19). The TAA enantiomers did not show absorbance in the UV range 290–800 nm, and the data below 290 nm could not be measured because of the solvent absorbance (see Figure S20). Therefore, we prepared the equimolar mixed chiral donor-acceptor systems (TAD+TAA) using 9.3×10^{-5} M TAD and TAA in mesitylene. The maximum absorbance was observed at 335 nm in all the cases. We have observed a colour change from colourless to yellow in the solution and gel state with the mixed chiral donor-acceptor system (TAD+TAA), indicating a charge transfer interaction. However, there was no shift in the maximum absorbance, but a hypochromic shift with chiral mixtures (TAD+TAA) of about 60.0–70.0% was observed. We were unable to perform the gel state UV-vis experiments due to the opaque nature of the gels, which is evident from the transmittance spectra (see Figure S21).

3.9. Computational studies

Computational studies were carried out to investigate the nature of interactions between the donor and acceptor enantiomeric molecules, both in the gas phase and in the presence of the solvent mesitylene (Table 1 and see Table S4). To verify the nature of the stationary points and to ensure that the optimised structures correspond to minima on the potential energy surface, numerical frequency calculations (NumFreq) were performed. All the optimised structures exhibited no imaginary frequencies, confirming that they are the true minima.

Comparing the total energy gap between the highest occupied molecular orbital (HOMO) and lowest unoccupied molecular orbital (LUMO) of the donor and acceptor enantiomers in the gas phase and with mesitylene, the energy difference increased in all cases (ranging from 0.005 to 0.275 eV, see Table S5 and S6). Analysis of the HOMO-LUMO energy gap of monomers revealed that the HOMO and LUMO energy levels of the acceptor moieties were lower than the corresponding HOMO and LUMO of the donor moieties (Table S5 and S6). This may suggest that an effective interaction between the donor-acceptor pairs (R-TAD or S-TAD with R-TAA or S-TAA) is possible, as expected.

4. Conclusions

We have designed and synthesised various enantiomeric donor and acceptor moieties (R-TAD, S-TAD, R-TAA, and S-TAA) to study the self-assembly modes in the multi-component system. The gelation properties of the individual enantiomeric compounds and the mixed enantiomeric and chiral gels were studied in various solvent/solvent mixtures. The enantiomeric acceptor moieties formed a white opaque gel in xylenes and mesitylene, but the enantiomeric donor moieties were found to be non-gelators. Enantiomeric multi-component gels were prepared by mixing equimolar acceptor-based enantiomers (structurally similar), and mixed chiral donor-acceptor gels (structurally non-similar components) were obtained by mixing the donor-acceptor moieties in mesitylene and *p*-xylene, respectively. Analysis of the mechanical strength

Table 1. HOMO and LUMO distribution with the solvent mesitylene.

	R-TAD	S-TAD	R-TAA	S-TAA
LUMO	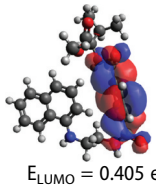 E_{LUMO} = 0.405 eV	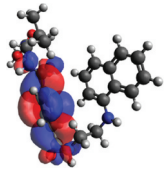 E_{LUMO} = 0.394 eV	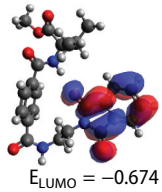 E_{LUMO} = −0.674 eV	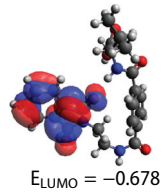 E_{LUMO} = −0.678 eV
HOMO	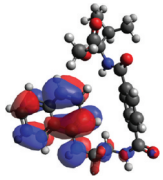 E_{HOMO} = −7.409 eV	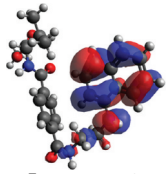 E_{HOMO} = −7.314 eV	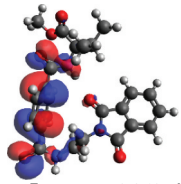 E_{HOMO} = −9.269 eV	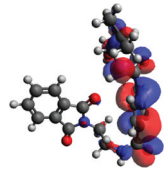 E_{HOMO} = −9.246 eV

revealed that the mixed chiral donor-acceptor gels were stronger than the mixed acceptor-based enantiomeric gels and individual enantiomers, but a reverse trend was observed for thermal stability. SEM analysis revealed that the morphologies of the mixed enantiomeric and chiral gels were different, indicating a different self-assembly mode. The preservation of chirality was evaluated using solution state CD experiments. PXRD studies revealed the presence of co-assembled networks in the mixed enantiomeric system, but self-sorting was observed for the mixed chiral donor-acceptor gels. The hypochromic shift in the UV absorbance after mixing the chiral donor and acceptor moieties confirmed the donor-acceptor interactions in mixed chiral donor-acceptor gels. Computational studies were performed with all the monomers to obtain the minimum energy potential in each case. These results demonstrate that the self-assembly modes depend on the individual component's structure, which is one of the key parameters that could control the nature of non-bonding interactions, such as hydrogen bonding or charge transfer interactions, that will be useful to generate complex multi-component architecture with intriguing properties.

Acknowledgment

We thank the University of Iceland Research Fund and The Icelandic Center for Research Fund, Rannís Iceland (IRF-228902-051) for funding. We thank Dr. Sigríður Jónsdóttir Jónsdóttir and Dr. Fridrik Magnus from the University of Iceland for NMR and mass spectrometry, powder X-ray diffraction analysis, and the Biochemistry department for the circular dichroism investigations. We thank Geethanjali Kuppadakkath, University of Iceland for the help with UV-experiments and Sverrir Guðmundsson, University of Iceland for the help with short path length cuvettes for UV-experiments. S.S.J. is thankful to the University of Iceland for the doctoral research grant. We thank Rannís Iceland infrastructure funds (191763-0031) for the rheometer and (210521-901) for the UV-vis spectrometer. The computational study performed by H.M. is co-financed by the EUROCC2 project funded by the European High-Performance Computing Joint Undertaking (JU) and EU/EEA states under grant agreement No 101101903. H.M. and M.R. have also been supported by the European Digital Innovation Hub (EDIH) of Iceland (EDIH-IS), funded in parts by the Digital Europe Programme under grant agreement No 101083762. The computational resources used in this work were provided by the Icelandic Research e-Infrastructure project, funded by the Icelandic Centre of Research Infrastructure fund.

Disclosure statement

No potential conflict of interest was reported by the author(s).

Funding

This research was funded by the Icelandic Research Fund, Rannís Iceland [IRF- 228902-051] and the University of Iceland Research Fund. European High Performance Computing Joint Undertaking [No 101101903]; European Digital Innovation Hub [No 101083762]; Háskóli Íslands [KKD-RS_2023]; Icelandic Centre for Research [191763-0031].

ORCID

Krishna K. Damodaran http://orcid.org/0000-0002-9741-2997

References

[1] Okesola BO, Mata A. Multicomponent self-assembly as a tool to harness new properties from peptides and proteins in material design. Chem Soc Rev. **2018**;47 (10):3721–3736. doi: 10.1039/C8CS00121A

[2] de Loos M, Feringa BL, van Esch JH. Design and application of self-assembled low molecular weight hydrogels. Eur J Org Chem. **2005**;2005(17):3615–3631. doi: 10.1002/ejoc.200400723

[3] Kumar DK, Steed JW. Supramolecular gel phase crystallization: orthogonal self-assembly under non-equilibrium conditions. Chem Soc Rev. **2014**;43 (7):2080–2088. doi: 10.1039/C3CS60224A

[4] Steed JW. Anion-tuned supramolecular gels: a natural evolution from urea supramolecular chemistry. Chem Soc Rev. **2010**;39(10):3686–3699. doi: 10.1039/b926219a

[5] Smith DK. Supramolecular gels – a panorama of low-molecular-weight gelators from ancient origins to next-generation technologies. Soft Matter. **2024**;20(1):10–70. doi: 10.1039/D3SM01301D

[6] Adams DJ. Personal perspective on understanding low molecular weight gels. J Am Chem Soc. **2022**;144 (25):11047–11053. doi: 10.1021/jacs.2c02096

[7] Chu C-W, Schalley CA. Recent advances on supramolecular gels: from stimuli-responsive gels to Co-assembled and self-sorted Systems. Org Mater. **2021**;3(01):025–040. doi: 10.1055/s-0040-1722263

[8] Buerkle LE, Rowan SJ. Supramolecular gels formed from multi-component low molecular weight species. Chem Soc Rev. **2012**;41(18):6089–6102. doi: 10.1039/c2cs35106d

[9] Raeburn J, Adams DJ. Multicomponent low molecular weight gelators. Chem Commun. **2015**;51 (25):5170–5180. doi: 10.1039/C4CC08626K

[10] Tómasson DA, Ghosh D, Kržišnik Z, et al. Enhanced mechanical and thermal strength in mixed-enantiomers-based supramolecular gel. Langmuir. **2018**;34 (43):12957–12967. doi: 10.1021/acs.langmuir.8b02729

[11] Ghosh D, Farahani AD, Martin AD, et al. Unraveling the self-assembly modes in multicomponent supramolecular gels using single-crystal X-ray diffraction. Chem Mater. **2020**;32(8):3517–3527. doi: 10.1021/acs.chemmater.0c00475

[12] Sudhakaran Jayabhavan S, Kuppadakkath G, Damodaran KK. The role of functional groups in tuning the self-assembly modes and physical properties of

multicomponent gels. ChemPluschem. **2023**;88(8): e202300302. doi: 10.1002/cplu.202300302
[13] Gudmundsson TA, Kuppadakkath G, Ghosh D, et al. Nanoscale assembly of enantiomeric supramolecular gels driven by the nature of solvents. Nanoscale. **2024**;16(18):8922–8930. doi: 10.1039/D4NR00204K
[14] Barman S, Pal A, Mukherjee A, et al. Supramolecular organic ferroelectric materials from donor–acceptor systems. Chem Eur J. **2024**;30(8):e202303120. doi: 10.1002/chem.202303120
[15] Pandeeswar M, Senanayak SP, Narayan K, et al. Multi-stimuli-responsive charge-transfer hydrogel for room-temperature organic ferroelectric thin-film devices. J Am Chem Soc. **2016**;138(26):8259–8268. doi: 10.1021/jacs.6b03811
[16] Mathur C, Gupta R, Bansal RK. Organic Donor-Acceptor Complexes As Potential Semiconducting Materials. Chem Eur J. **2024**;30(23):e202304139. doi: 10.1002/chem.202304139
[17] Vignon SA, Jarrosson T, Iijima T, et al. Switchable neutral Bistable Rotaxanes. J Am Chem Soc. **2004**;126 (32):9884–9885. doi: 10.1021/ja048080k
[18] Maitra U, Vijay Kumar P, Chandra N. First donor–acceptor interaction promoted gelation of organic fluids. Chem Commun. **1999**;(7):595–596. doi: 10.1039/a809821b
[19] Cougnon FBL, Au-Yeung HY, Pantoş GD, et al. Exploring the formation pathways of Donor–Acceptor catenanes in aqueous dynamic combinatorial libraries. J Am Chem Soc. **2011**;133(9):3198–3207. doi: 10.1021/ja111407m
[20] Das A, Ghosh S. Supramolecular assemblies by charge-transfer interactions between donor and acceptor chromophores. Angew Chem Int Ed. **2014**;53 (8):2038–2054. doi: 10.1002/anie.201307756
[21] Wang F, Shen C, Gan F, et al. Tunable multicolor circularly polarized luminescence via Co-assembly of one chiral electron acceptor with various donors. CCS Chem. **2023**;5(7):1592–1601. doi: 10.31635/ccschem.022.202202024
[22] Li C, Shen C, Nie J, et al. Multi-responsive supramolecular gels based on charge transfer interactions. Chem Asian J. **2018**;13(13):1678–1682. doi: 10.1002/asia.201800572
[23] Wang K, Guo Z, Zhang L, et al. Co-assembly of donor and acceptor towards organogels tuned by charge transfer interaction strength. Soft Matter. **2017**;13 (10):1948–1955. doi: 10.1039/C6SM02691E
[24] Safont-Sempere MM, Fernández G, Würthner F. Self-sorting phenomena in complex supramolecular systems. Chem Rev. **2011**;111(9):5784–5814. doi: 10.1021/cr100357h
[25] Das A, Ghosh S. A generalized supramolecular strategy for self-sorted assembly between donor and acceptor gelators. Chem Commun. **2011**;47(31):8922–8924. doi: 10.1039/c1cc12915e
[26] Babu P, Sangeetha NM, Vijaykumar P, et al. Pyrene-derived novel one- and two-component organogelators. Chem Eur J. **2003**;9(9):1922–1932. doi: 10.1002/chem.200204459
[27] Molla MR, Das A, Ghosh S. Self-sorted assembly in a mixture of donor and acceptor chromophores. Chem Eur J. **2010**;16(33):10084–10093. doi: 10.1002/chem.201000596
[28] Foster JA, Edkins RM, Cameron GJ, et al. Blending gelators to tune gel structure and probe anion-induced disassembly. Chem Eur J. **2014**;20(1):279–291. doi: 10.1002/chem.201303153
[29] Das RK, Kandanelli R, Linnanto J, et al. Langmuir. **2010**;26(20):16141–16149. doi: 10.1021/la1029905
[30] Koga T, Matsuoka M, Higashi N. Structural control of self-assembled nanofibers by artificial β-sheet peptides composed of d - or l -isomer. J Am Chem Soc. **2005**;127 (50):17596–17597. doi: 10.1021/ja0558387
[31] Hirst AR, Smith DK, Feiters MC, et al. Two-component dendritic Gel: effect of stereochemistry on the supramolecular chiral assembly. Chem Eur J. **2004**;10 (23):5901–5910. doi: 10.1002/chem.200400502
[32] Nagy-Smith K, Beltramo PJ, Moore E, et al. Molecular, local, and network-level basis for the enhanced stiffness of hydrogel networks formed from coassembled racemic peptides: predictions from Pauling and Corey. ACS Cent Sci. **2017**;3(6):586–597. doi: 10.1021/acscentsci.7b00115
[33] Li H, Han L, Li Q, et al. Hierarchical chiral supramolecular nanoarchitectonics with molecular detection: helical structure controls upon self-assembly and coassembly. Macromol Rapid Commun. **2022**;43(14):2100690. doi: 10.1002/marc.202100690
[34] Patterson AK, El-Qarra LH, Smith DK. Chirality-directed hydrogel assembly and interactions with enantiomers of an active pharmaceutical ingredient. Chem Commun. **2022**;58(24):3941–3944. doi: 10.1039/D1CC06942J
[35] McAulay K, Dietrich B, Su H, et al. Using chirality to influence supramolecular gelation. Chem Sci. **2019**;10 (33):7801–7806. doi: 10.1039/C9SC02239B
[36] Yang X, Lu H, Tao Y, et al. Controlling supramolecular filament chirality of hydrogel by co-assembly of enantiomeric aromatic peptides. J Nanobiotechnology. **2022**;20(1):77. doi: 10.1186/s12951-022-01285-0
[37] Swanekamp RJ, Welch JJ, Nilsson BL. Proteolytic stability of amphipathic peptide hydrogels composed of self-assembled pleated β-sheet or coassembled rippled β-sheet fibrils. Chem Commun. **2014**;50(70):10133–10136. doi: 10.1039/C4CC04644G
[38] Liao R, Wang F, Guo Y, et al. Chirality-controlled supramolecular donor–acceptor copolymerization with distinct energy transfer efficiency. J Am Chem Soc. **2022**;144(22):9775–9784. doi: 10.1021/jacs.2c02270
[39] Wang Y-F, Lu H-Y, Chen C, et al. 1,8-naphthalimide-based circularly polarized TADF enantiomers as the emitters for efficient orange-red OLEDs. Org Electron. **2019**;70:71–77. doi: 10.1016/j.orgel.2019.03.020
[40] Kumar S, Maurya YK, Lis T, et al. Synthesis of a donor–acceptor heterodimer via trifunctional completive self-sorting. Nat Commun. **2022**;13(1):3204. doi: 10.1038/s41467-022-30859-7
[41] Weiss RG, and Terech P, editors. Molecular gels: materials with self-assembled fibrillar networks. Dordrecht, Zuid-Holland, Netherlands: Springer; 2006.
[42] Fages F, Voegtle F, Zinic M. Top. Curr Chem. **2005**;256:77–131.
[43] Neese F. The ORCA program system. WIREs Comput Mol Sci. **2012**;2(1):73–78. doi: 10.1002/wcms.81
[44] Neese F. Software update: the ORCA program system—version 5.0. WIREs Comput Mol Sci. **2022**;12(5):e1606. doi: 10.1002/wcms.1606

[45] Chai J-D, Head-Gordon M. Systematic optimization of long-range corrected hybrid density functionals. J Chem Phys. **2008**;128(8):128. doi: 10.1063/1.2834918
[46] Weigend F, Ahlrichs R. Balanced basis sets of split valence, triple zeta valence and quadruple zeta valence quality for H to Rn: design and assessment of accuracy. Phys Chem Chem Phys. **2005**;7(18):3297–3305. doi: 10.1039/b508541a
[47] Neese F, Wennmohs F, Hansen A, et al. Efficient, approximate and parallel hartree–Fock and hybrid DFT calculations. A 'chain-of-spheres' algorithm for the hartree–Fock exchange. Chem Phys. **2009**;356(1–3):98–109. doi: 10.1016/j.chemphys.2008.10.036
[48] Izsák R, Neese F. An overlap fitted chain of spheres exchange method. J Chem Phys. **2011**;135(14):135. doi: 10.1063/1.3646921
[49] Weigend F. Accurate coulomb-fitting basis sets for H to Rn. Phys Chem Chem Phys. **2006**;8(9):1057–1065. doi: 10.1039/b515623h
[50] Yu G, Yan X, Han C, et al. Characterization of supramolecular gels. Chem Soc Rev. **2013**;42(16):6697–6722. doi: 10.1039/c3cs60080g
[51] Draper ER, Adams DJ. How should multicomponent supramolecular gels be characterised? Chem Soc Rev. **2018**;47(10):3395–3405. doi: 10.1039/C7CS00804J
[52] Morris KL, Chen L, Raeburn J, et al. Chemically programmed self-sorting of gelator networks. Nat Comm. **2013**;4(1):1480. doi: 10.1038/ncomms2499
[53] Džolić Z, Wolsperger K, Žinić M. Synergic effect in gelation by two-component mixture of chiral gelators. New J Chem. **2006**;30(10):1411–1419. doi: 10.1039/B609642E
[54] Shigemitsu H, Fujisaku T, Tanaka W, et al. An adaptive supramolecular hydrogel comprising self-sorting double nanofibre networks. Nat Nanotechnol. **2018**;13(2):165–172. doi: 10.1038/s41565-017-0026-6
[55] Onogi S, Shigemitsu H, Yoshii T, et al. In situ real-time imaging of self-sorted supramolecular nanofibres. Nat Chem. **2016**;8(8):743. doi: 10.1038/nchem.2526
[56] McAulay K, Dietrich B, Su H, et al. Using chirality to influence supramolecular gelation. Chem Sci. **2019**;10(33):7801–7806. doi: 10.1039/C9SC02239B
[57] Mori M, Dasso Lang MC, Saladini F, et al. Synthesis and evaluation of Bifunctional Aminothiazoles as antiretrovirals targeting the HIV-1 nucleocapsid protein. ACS Med Chem Lett. **2018**;10(4):463–468. doi: 10.1021/acsmedchemlett.8b00506
[58] Guenet J-M. Organogels: thermodynamics, structure, solvent role, and properties. Cham, Switzerland: Springer; 2016.
[59] Gottarelli G, Lena S, Masiero S, et al. The use of circular dichroism spectroscopy for studying the chiral molecular self-assembly: an overview. Chirality. **2008**;20(3–4):471–485. doi: 10.1002/chir.20459
[60] Qin S-Y, Pei Y, Liu X-J, et al. Hierarchical self-assembly of a β-amyloid peptide derivative. J Mater Chem B. **2013**;1(5):668–675. doi: 10.1039/C2TB00105E
[61] Shin S, Lim S, Kim Y, et al. Supramolecular switching between flat sheets and helical tubules triggered by coordination interaction. J Am Chem Soc. **2013**;135(6):2156–2159. doi: 10.1021/ja400160j
[62] Jayabhavan SS, Steed JW, Damodaran KK. Crystal habit modification of metronidazole by supramolecular gels with complementary functionality. Cryst Growth Des. **2021**;21(9):5383–5393. doi: 10.1021/acs.cgd.1c00659
[63] Ghosh D, Lebedytė I, Yufit DS, et al. Selective gelation of N-(4-pyridyl)nicotinamide by copper(ii) salts. Cryst Eng Comm. **2015**;17(42):8130–8138. doi: 10.1039/C5CE00901D
[64] Ghosh D, Deepa, Damodaran KK, et al. Metal complexation induced supramolecular gels for the detection of cyanide in water. Supramol Chem. **2020**;32(4):276–286. doi: 10.1080/10610278.2020.1751845
[65] Adams DJ. Does drying affect gel networks? Gels. **2018**;4(2):32. doi: 10.3390/gels4020032
[66] Kuppadakkath G, Jayabhavan SS, Damodaran KK. Supramolecular gels based on C3-symmetric amides: application in Anion-Sensing and removal of dyes from water. Molecules. **2024**;29(9):2149. doi: 10.3390/molecules29092149
[67] Fleming S, Debnath S, Frederix PWJM, et al. Insights into the coassembly of hydrogelators and surfactants based on aromatic peptide amphiphiles. Biomacromolecules. **2014**;15(4):1171–1184. doi: 10.1021/bm401720z

SUPPORTING INFORMATION

Analyzing the Self-Assembly Modes in Chiral Multi-Component Gels Based on Donor and Acceptor Moieties

Sreejith Sudhakaran Jayabhavan[a], Hemanadhan Myneni[b], Morris Riedel[b,c], and Krishna K. Damodaran[a*]

1. Synthetic scheme

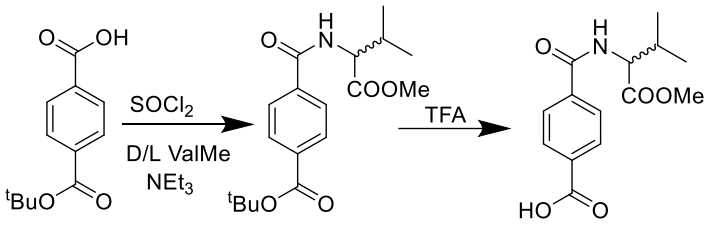

Scheme S1. Synthetic route for mono-acid.

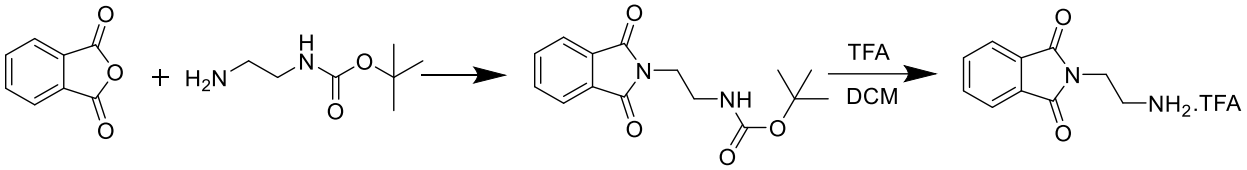

Scheme S2. Synthetic route for acceptor amine.

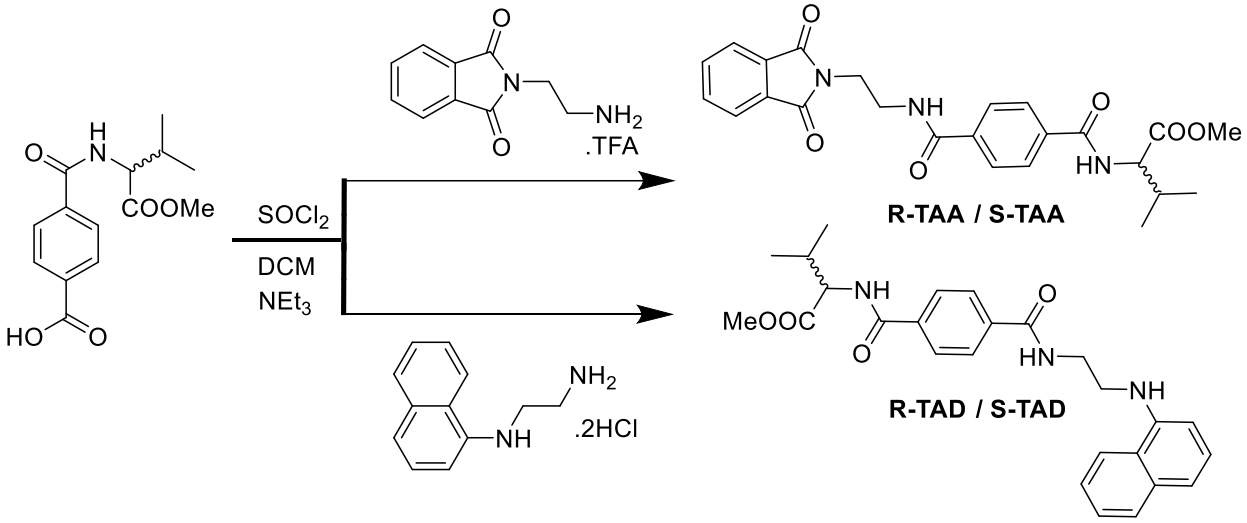

Scheme S3. Synthetic route for donor or acceptor based bisamides.

2. NMR spectra

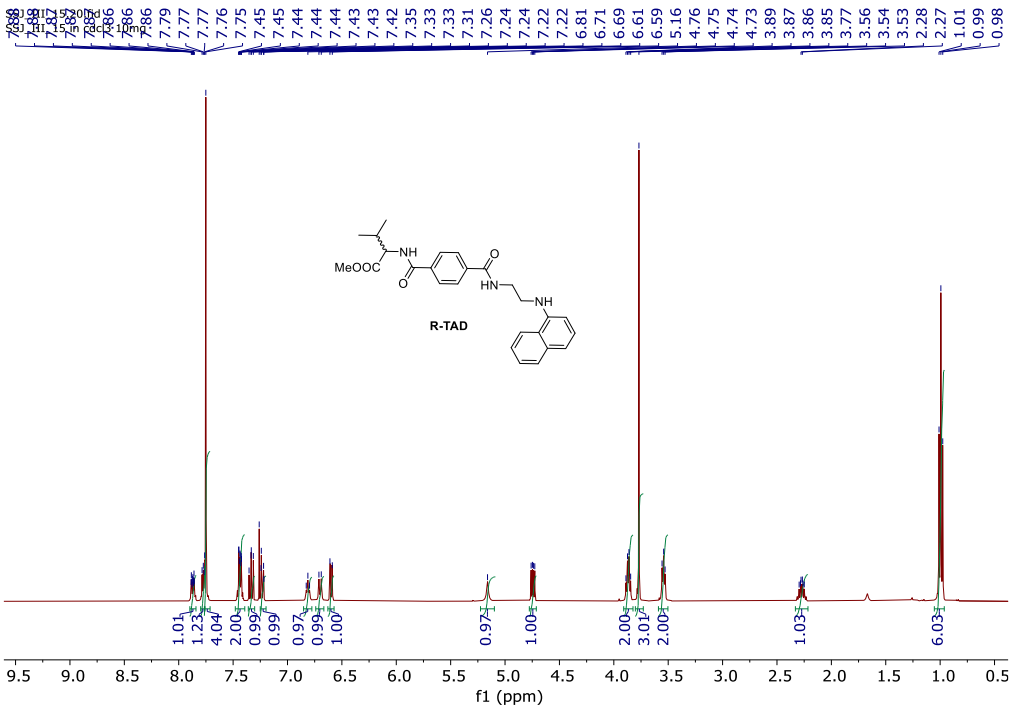

Figure S1. ^{1}H NMR spectrum of R-TAD.

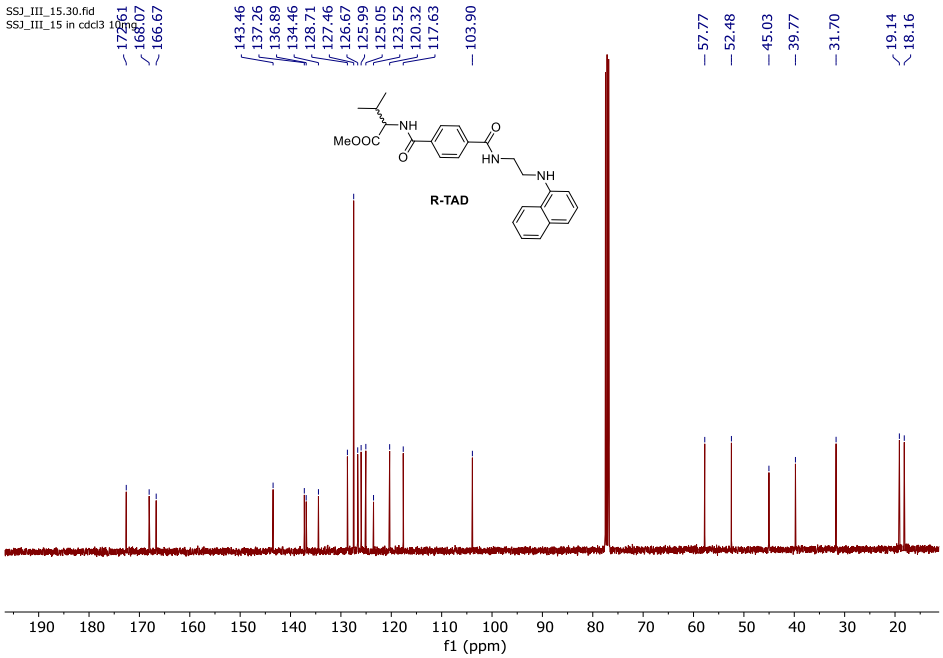

Figure S2. ^{13}C NMR spectrum of R-TAD.

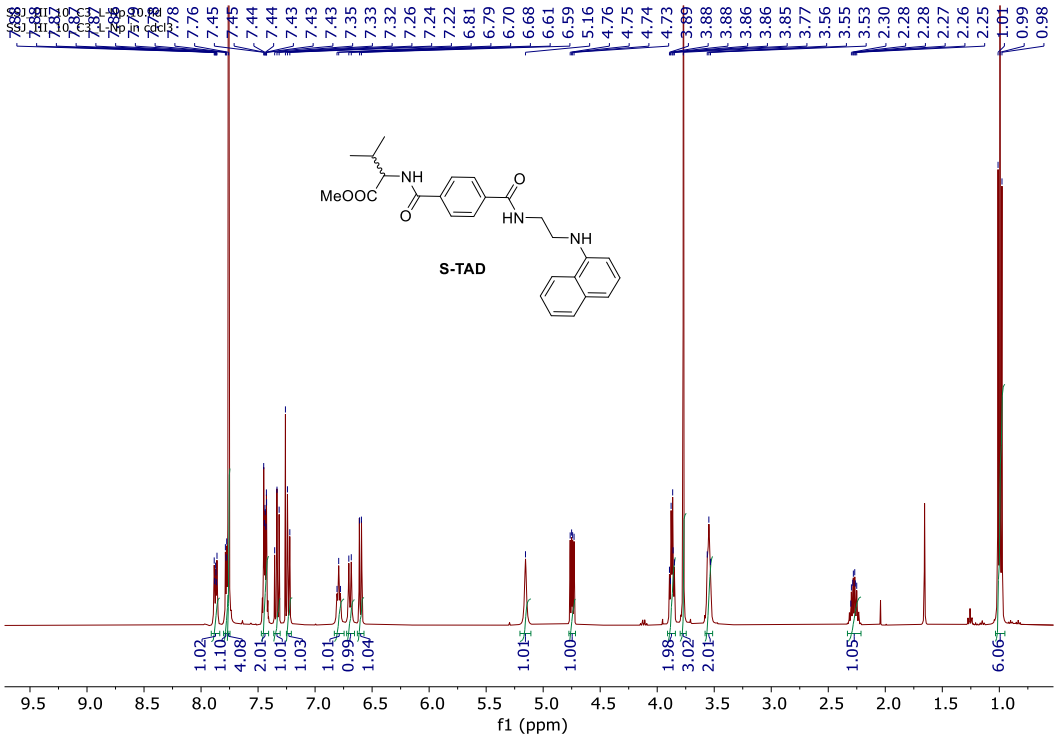

Figure S3. ^{1}H NMR spectrum of S-TAD.

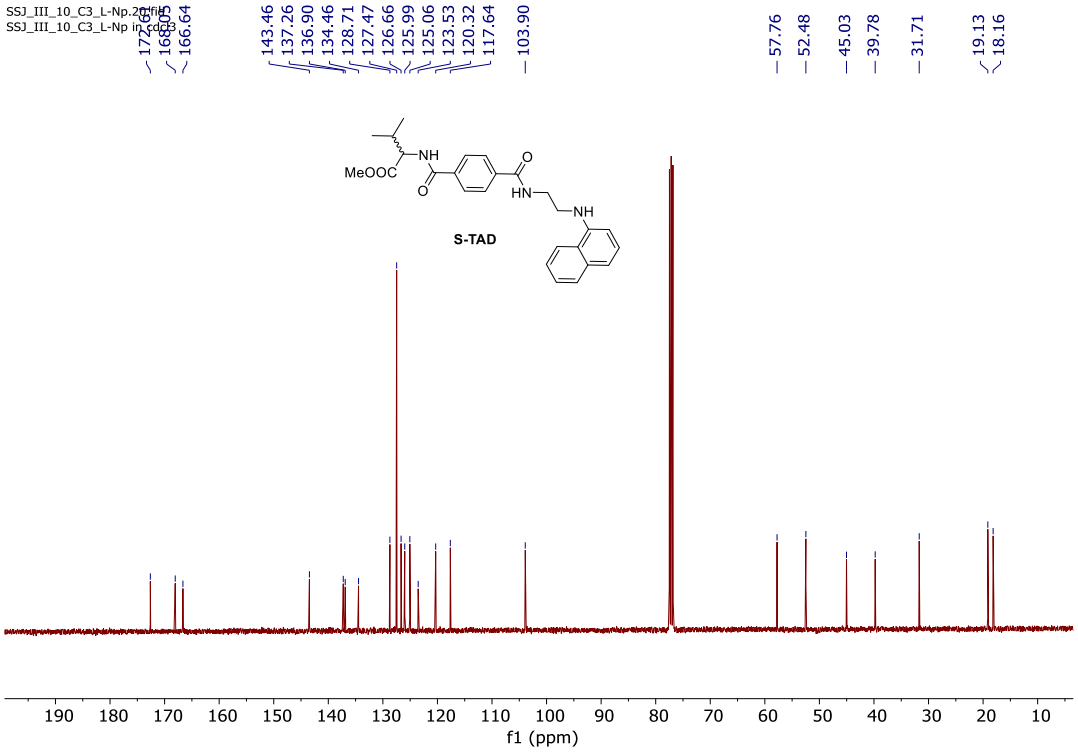

Figure S4. ^{13}C NMR spectrum of S-TAD.

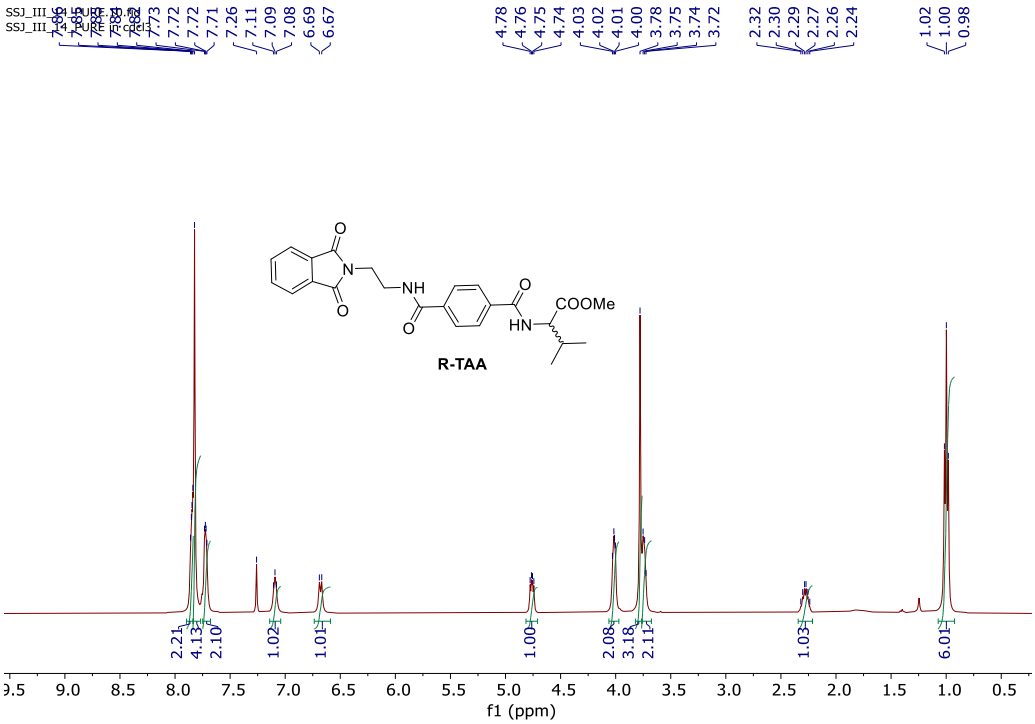

Figure S5. ^{1}H NMR spectrum of R-TAA.

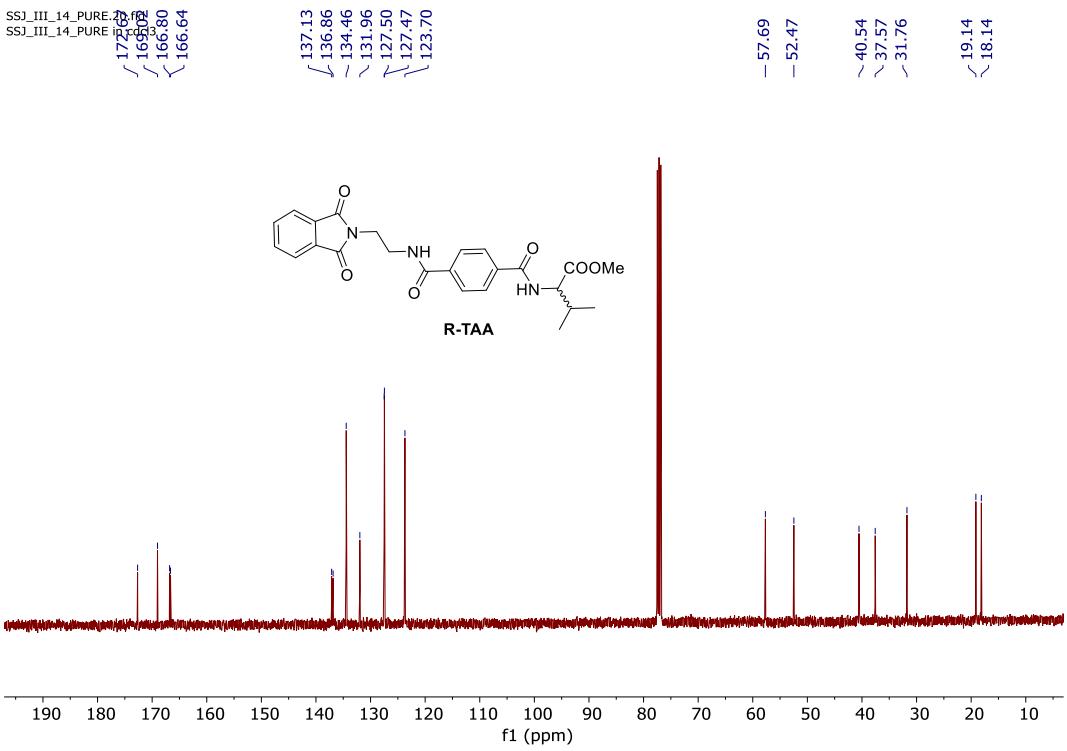

Figure S6. ^{13}C NMR spectrum of R-TAA.

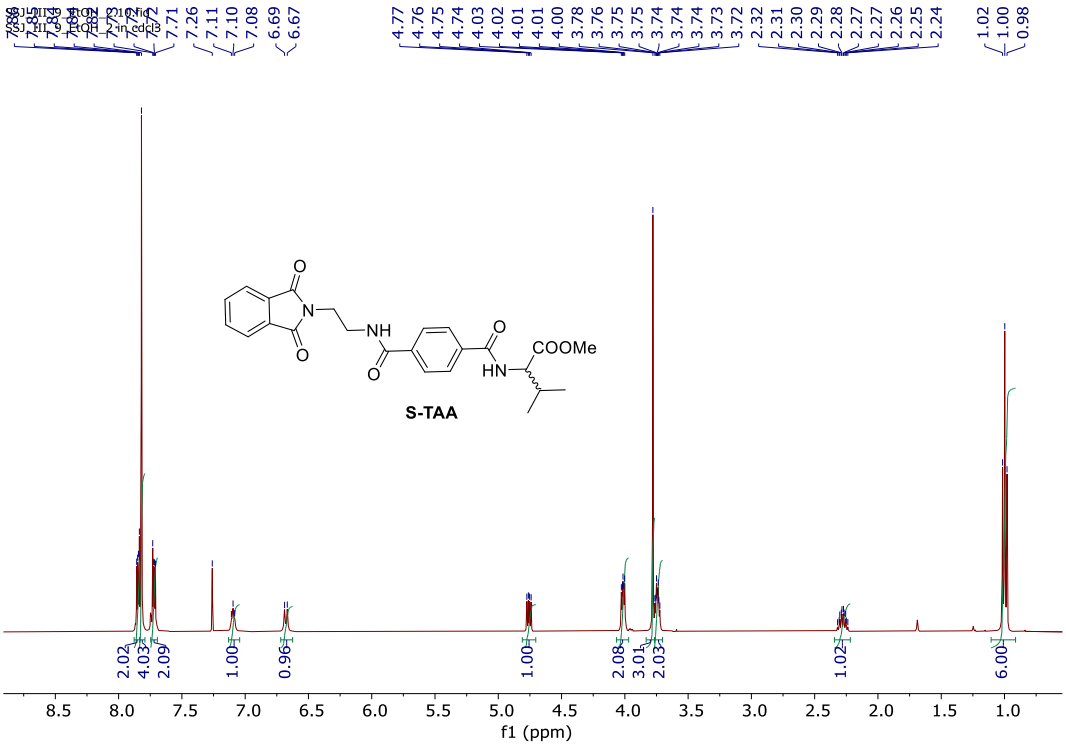

Figure S7. ^{1}H NMR spectrum of S-TAA.

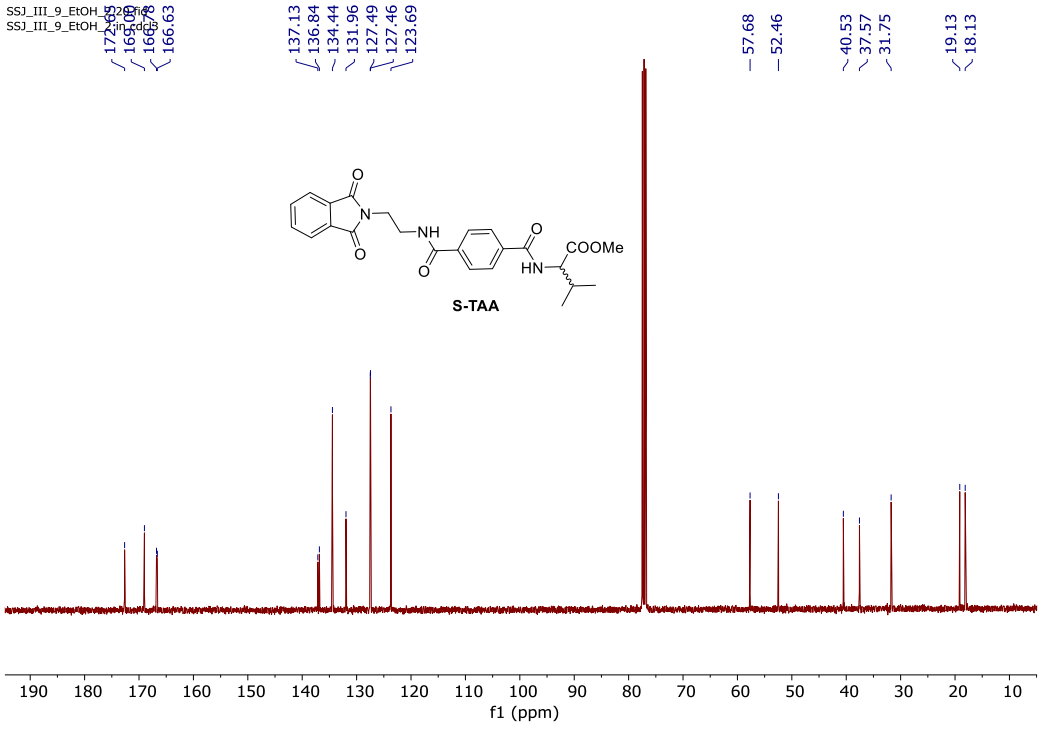

Figure S8. ^{13}C NMR spectrum of S-TAA.

3. Gelation studies

Table S1. Gelation Experiments with enantiomeric compounds

Sl No.	**Solvent**	R-TAD	S-TAD	R-TAA	S-TAA
1	*o*-xylene	Ppt	Ppt	G$^{\$}$	G$^{\$}$
2	*m*-xylene	Ppt	Ppt	G$^{\$}$	G$^{\$}$
3	*p*-xylene	Ppt	Ppt	G$^{\$}$	G$^{\$}$
4	toluene	Ppt	Ppt	G$^{\$}$	G$^{\$}$
5	mesitylene	Ppt	Ppt	G$^{\$}$	G$^{\$}$
6	n-butanol	C	C	Ppt	Ppt
7	EG	Ppt	Ppt	G	G
8	ACN	Ppt	Ppt	Ppt	Ppt
9	nitromethane	Ppt	Ppt	Ppt	Ppt
10	chlorobenzene	Gel***	Gel***	C	C
11	ethanol	Ppt	Ppt	Ppt	Ppt
12	Nitrobenzene	C	C	C	C
14	EG:water	G*	G*	G	G
15	DMF:water	Ppt	Ppt	G*	G*
16	DMSO:water	Ppt	Ppt	G	G
17	EtOH/water	G*	G*	G$^{\$}$	G$^{\$}$
18	ACN/water	Ppt	Ppt	Ppt	Ppt
19	THF/water	Ppt	Ppt	Ppt	Ppt

G= gel at 1.0 wt/v%, $^{\$}$= super gelators (0.5 wt/v%), *= 2.0 wt/v%, Ppt= precipitate, C= Colloid, and aqueous mixtures were taken at 1:1, v/v.

Table S2. Gelation experiments with multicomponent system with minimum gelator concentration (MGC)

		MGC (wt/v%)					
Sl No.	**Solvent**	R-TAA + S-TAD	R-TAD + S-TAA	R-TAA + R-TAD	S-TAA + S-TAD	R-TAA + S-TAA	R-TAD + S-TAD
1	*p*-xylene	G*	G*	G$^{\#\#\#}$	G$^{\#\#\#}$	G***	Ppt**
2	mesitylene	G*	G*	G$^{\#\#}$	G$^{\#\#}$	G	Ppt**

G= gel at 1.0 wt/v%, $^{\#\#}$= 2.0 wt/v%, $^{\#\#\#}$=1.7 wt/v%, *= 1.4 wt/v%, **= 5.0 wt/v%, ***=0.7 wt/v%, Ppt= precipitate.

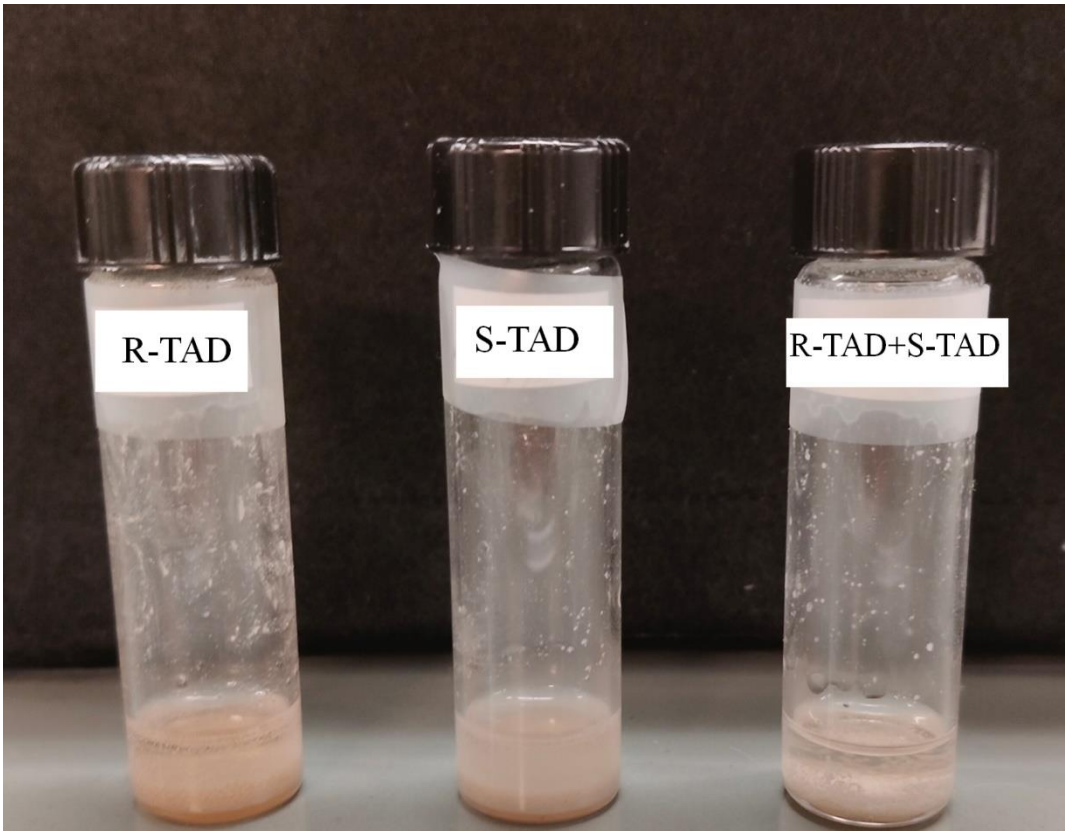

Figure S9. Gelation experiments with TAD-based compounds in mesitylene at 2.0 wt/v.

Table S3. Determination of Sol-gel Transition Temperature (T_{gel})

		T_{gel} (°C)				
Sl No.	**Solvent**	R-TAA + S-TAD	R-TAD + S-TAA	R-TAA + R-TAD	S-TAA + S-TAD	R-TAA + S-TAA
1	Mesitylene	152.8	150.3	146.5	142.2	156.3

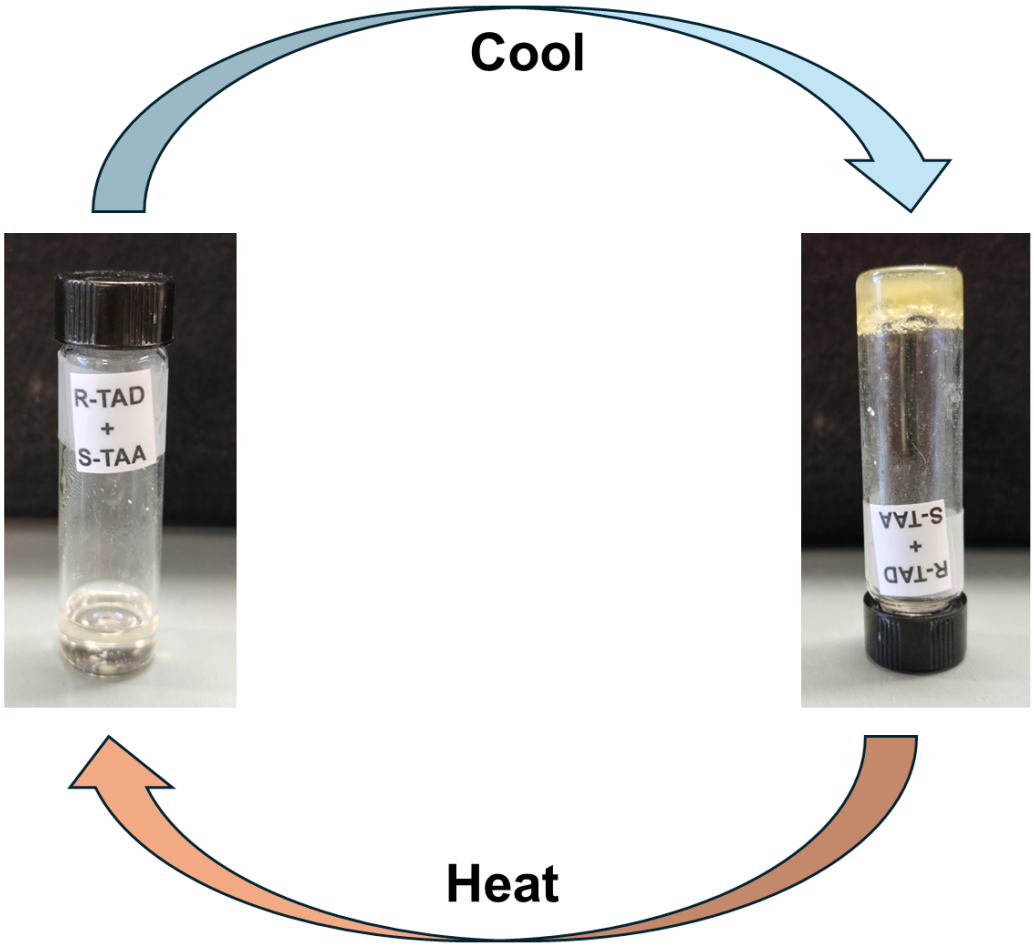

Figure S10. Sol-gel transition with a color change in chiral donor-acceptor based mixed gels.

3. Rheology

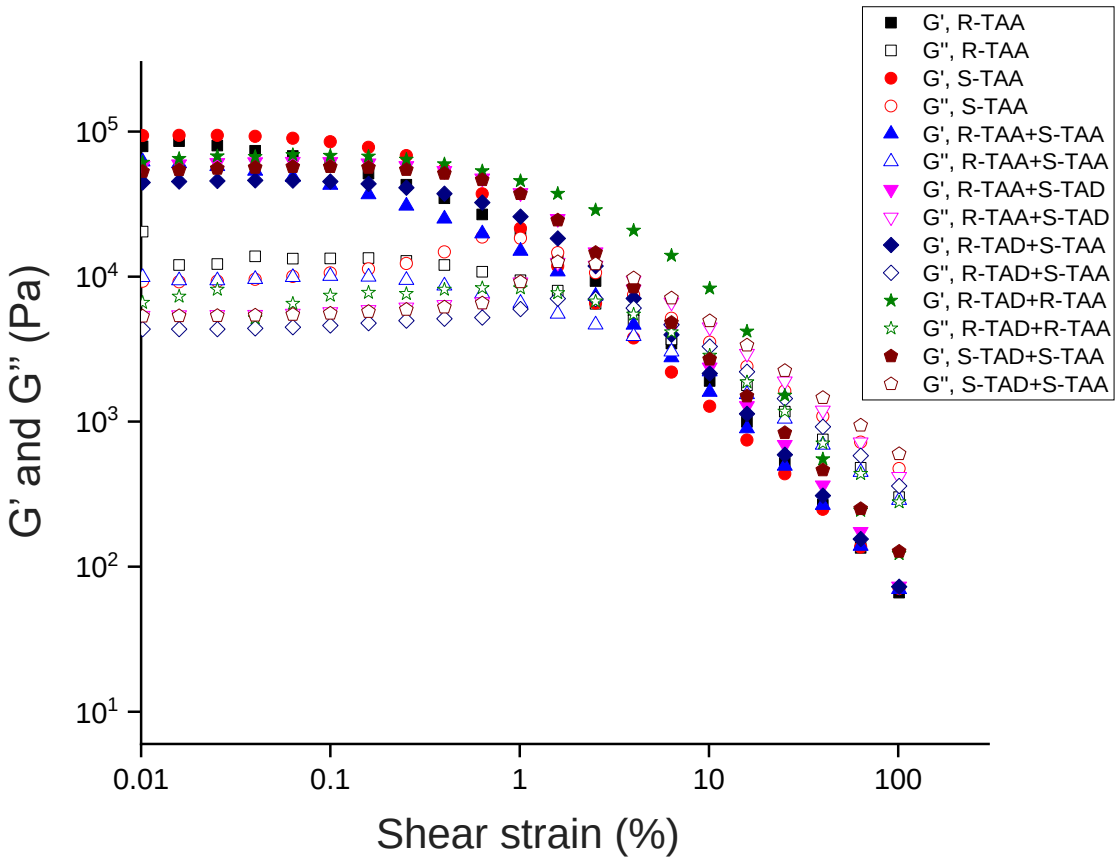

Figure S11. Strain sweep experiments with TAD and TAA-based gels at 20.0 °C measured at a constant frequency of 1.0 Hz.

4. Scanning electron microscopy

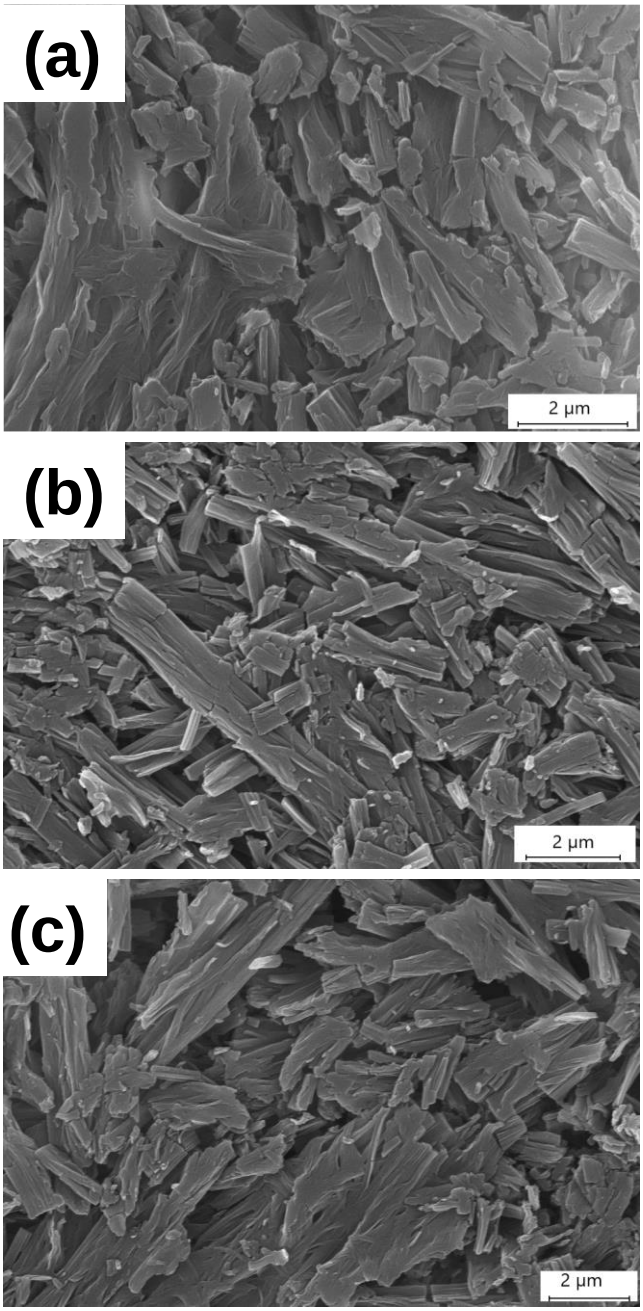

Figure S12. SEM images of (a) R-TAD+S-TAA, (b) R-TAD+R-TAA, and (c) S-TAD+S-TAA xerogels obtained from mesitylene at 2.0 wt/v%.

5. Circular dichroism

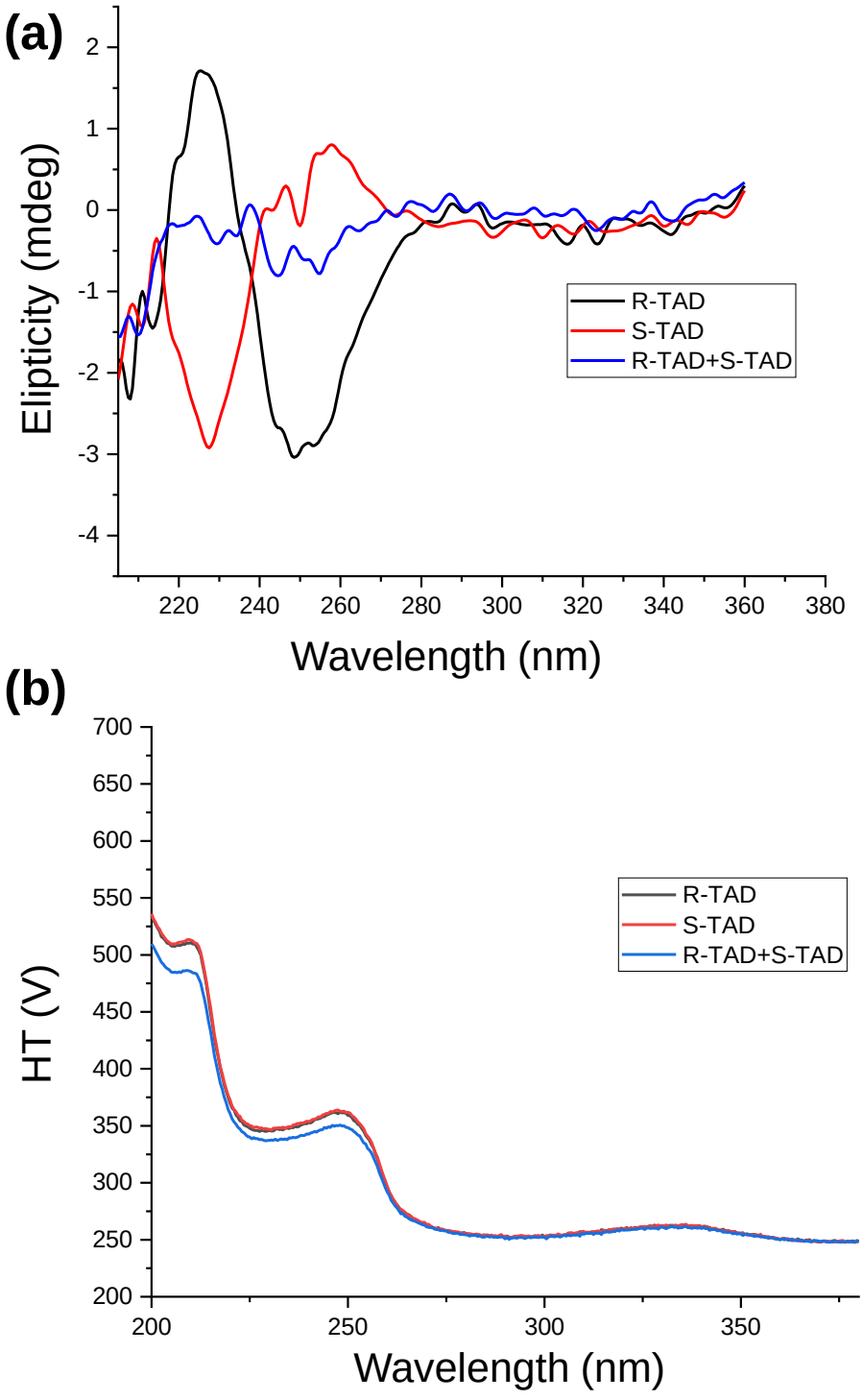

Figure S13. (a) CD spectra of R-TAD, S-TAD, and R-TAD+S-TAD in solution state at 0.02 wt/v% in absolute ethanol and (b) HT data for the CD spectra.

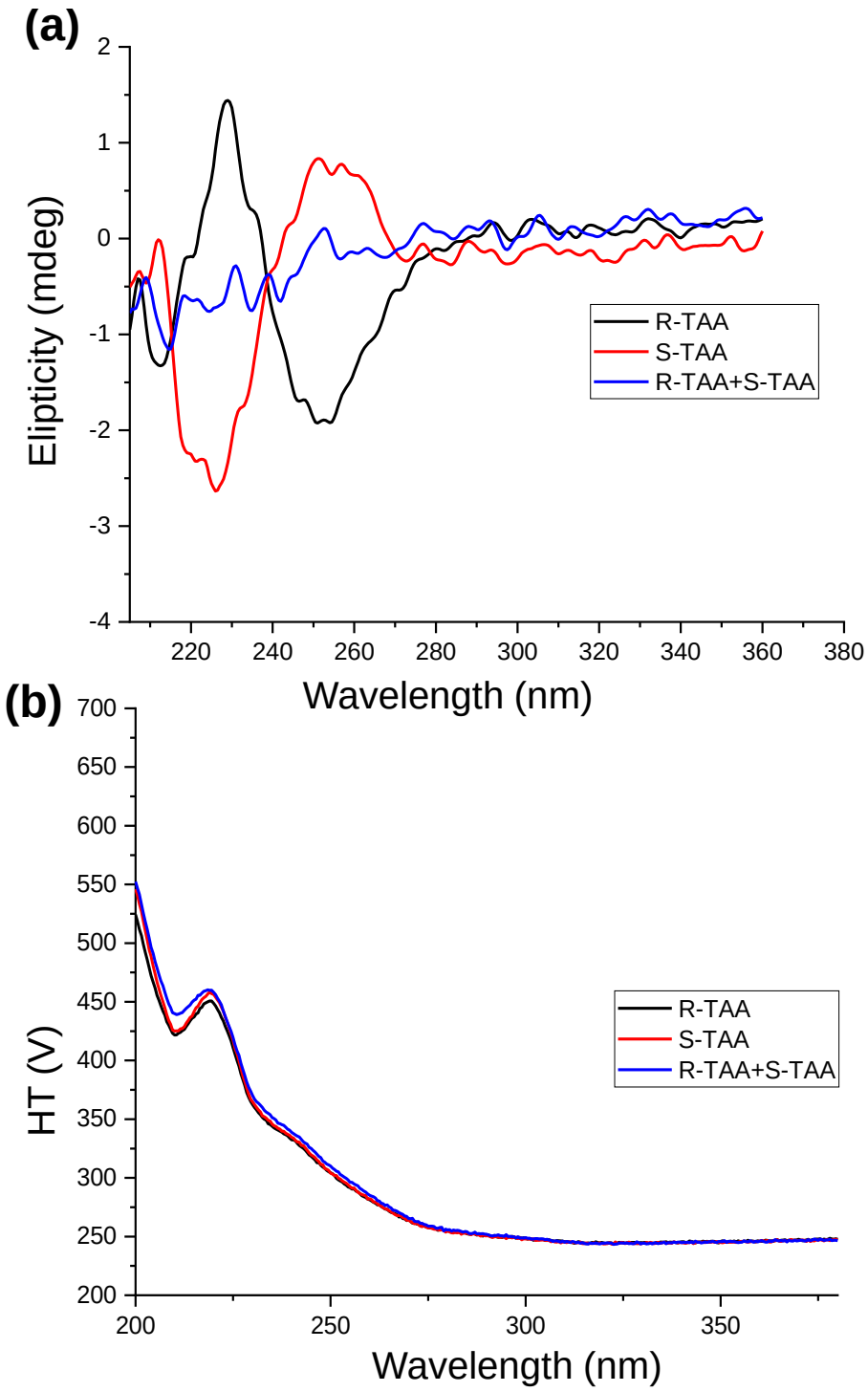

Figure S14. (a) CD spectra of R-TAA, S-TAA, and R-TAA+S-TAA in solution state at 0.02 wt/v% in absolute ethanol and (b) HT data for the CD spectra.

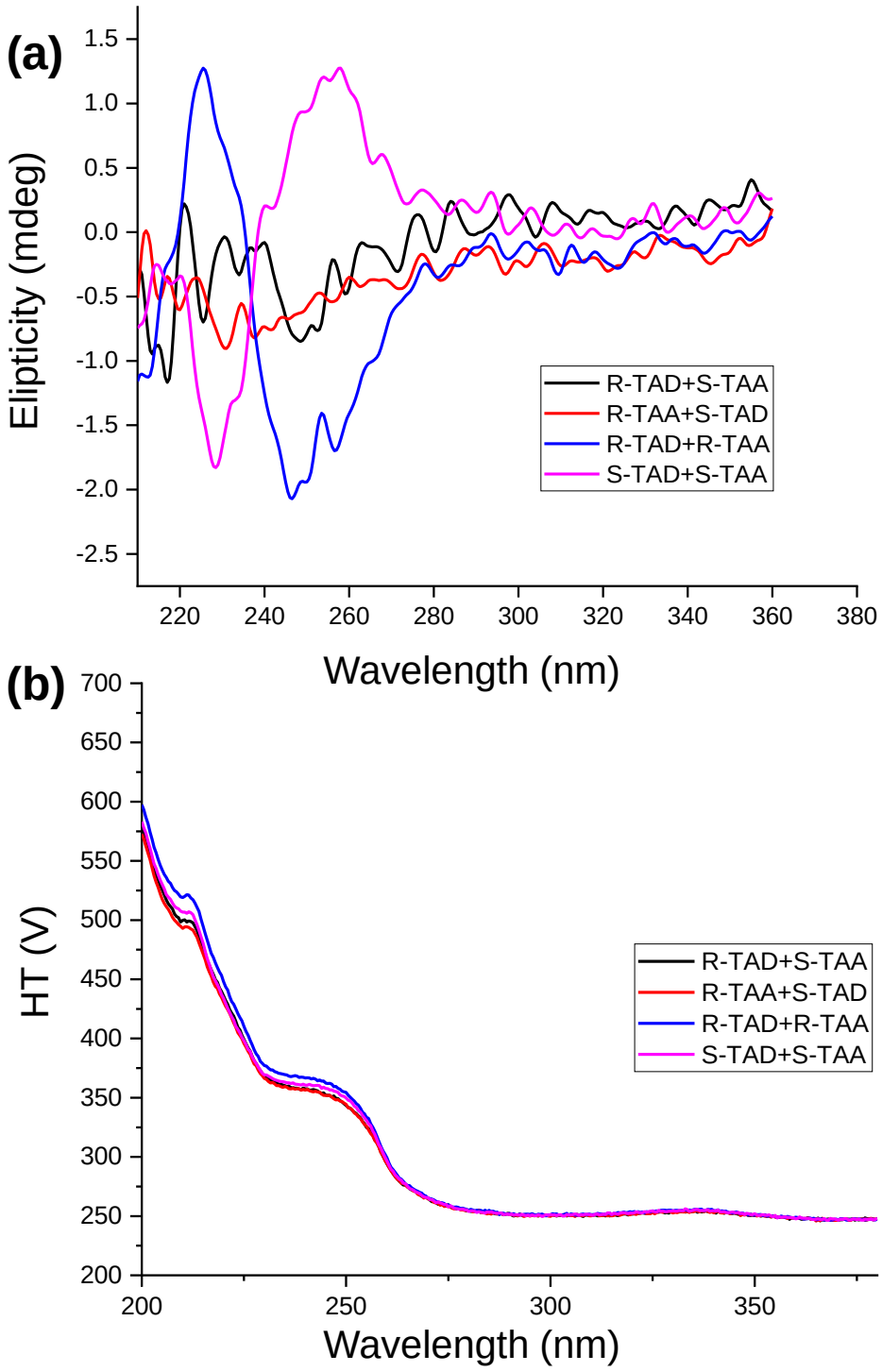

Figure S15. (a) CD spectra of mixed chiral donor-acceptor gels (R-TAD+S-TAA, R-TAD+R-TAA, S-TAD+R-TAA, and S-TAD+S-TAA) in solution state at 0.02 wt/v% in absolute EtOH and (b) HT data for the CD spectra.

6. Powder X-ray diffraction

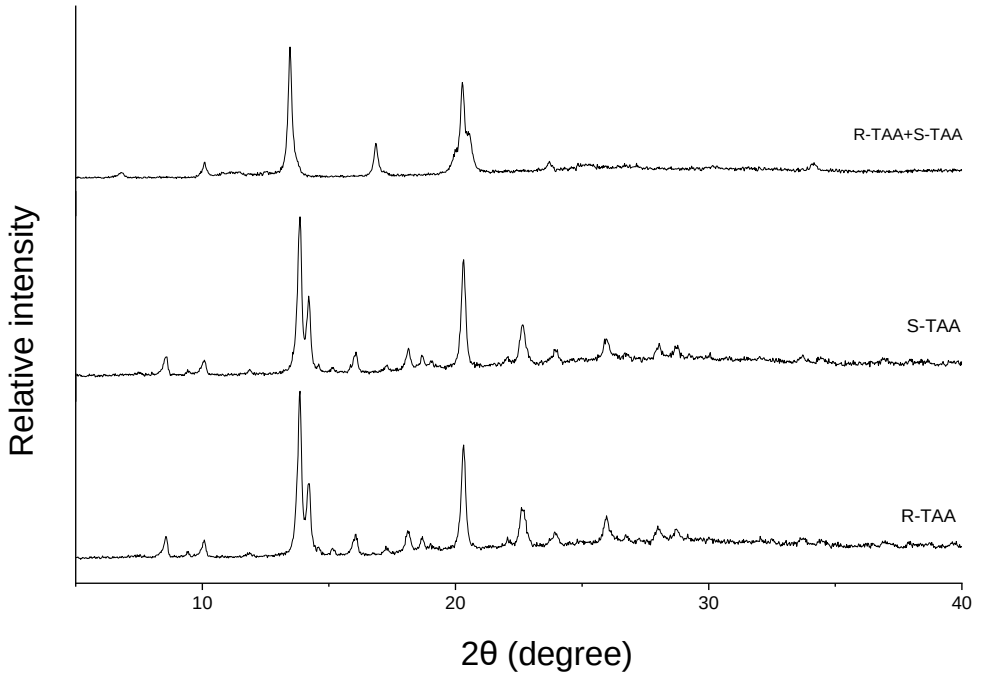

Figure S16. Comparison of PXRD pattern of the xerogel of R-TAA, S-TAA and R-TAA+S-TAA, obtained from mesitylene at 2.0 wt/v%.

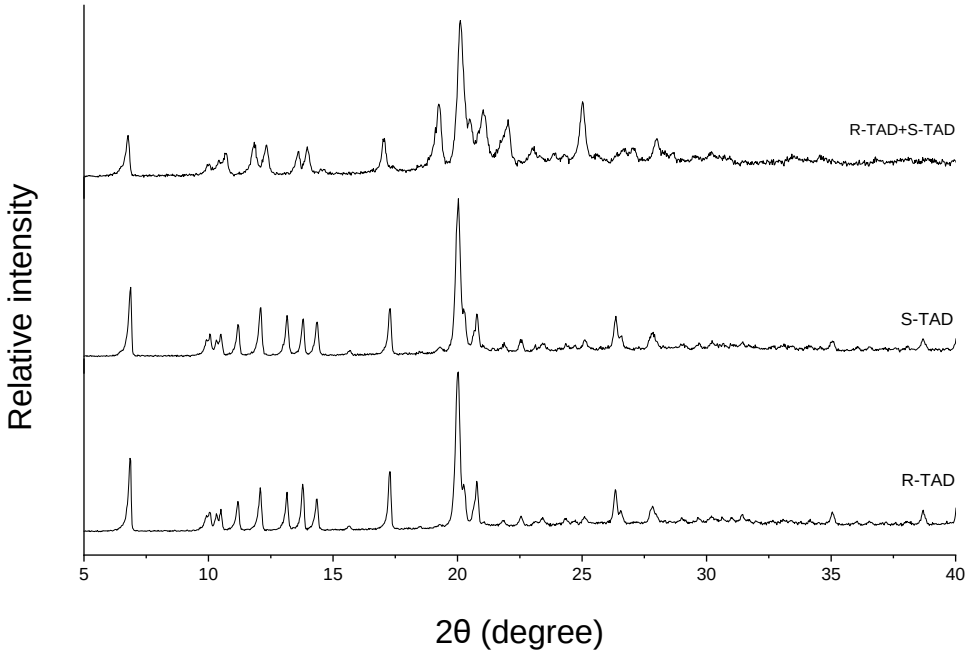

Figure S17. Comparison of PXRD pattern of the precipitate of R-TAD, S-TAD and R-TAD+S-TAD, obtained from mesitylene at 2.0 wt/v%.

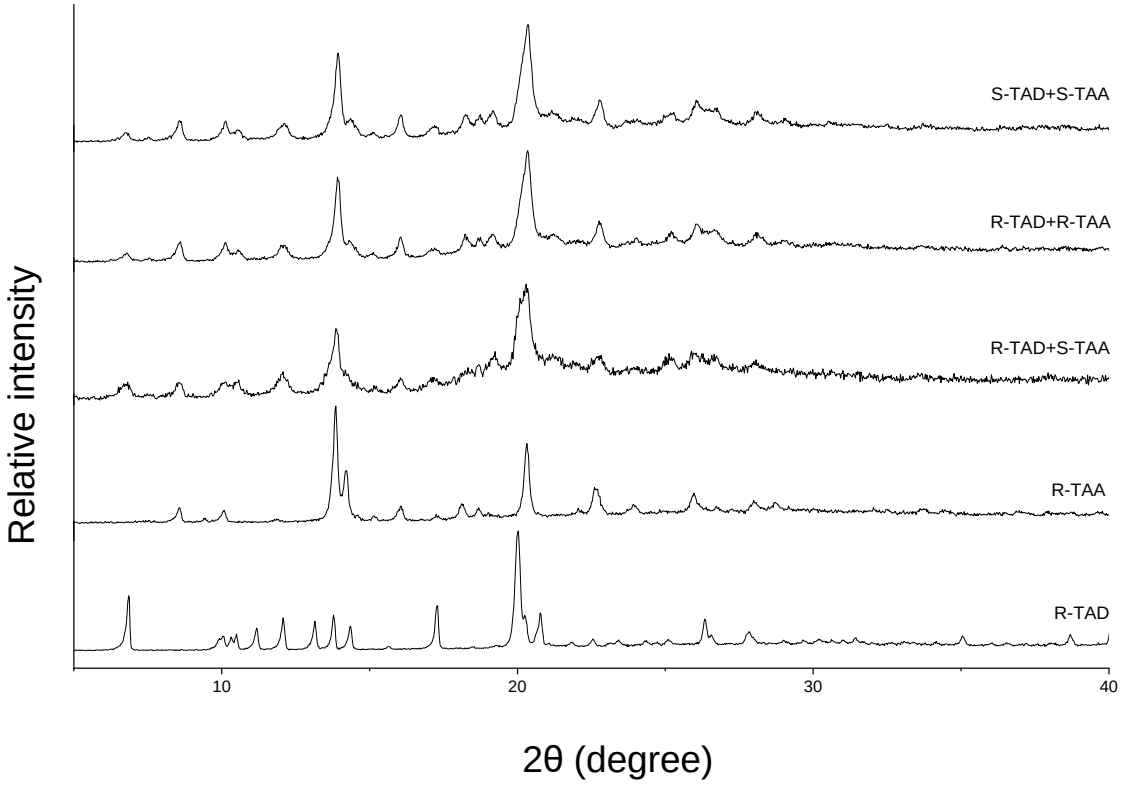

Figure S18. Comparison of PXRD pattern of the precipitate of R-TAD, and xerogels obtained from R-TAA and TAD+TAA mixed gels, obtained from mesitylene at 2.0 wt/v%.

7. UV-visible spectroscopy

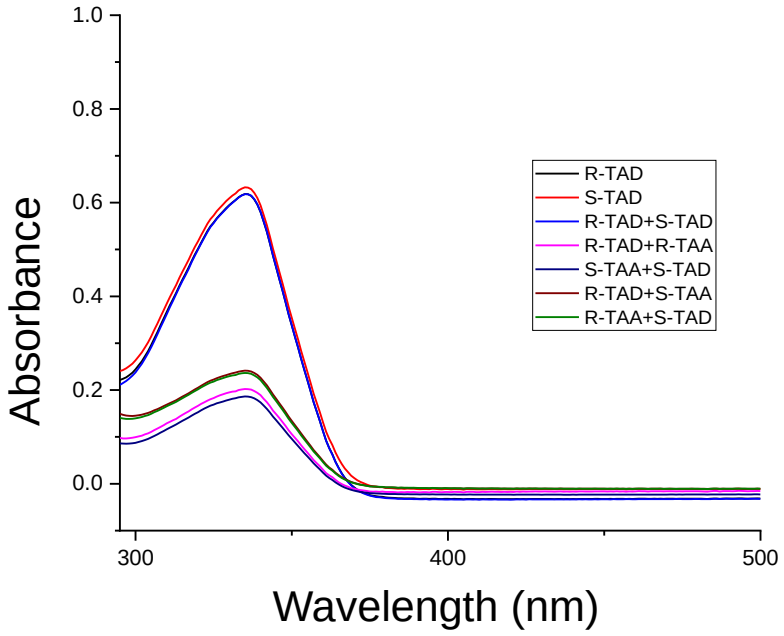

Figure S19. UV-vis studies with TAD (enantiomeric and mixed) and equimolar mixed chiral systems (TAD+TAA) at a TAD concentration of 9.3 X 10^{-5} M in mesitylene.

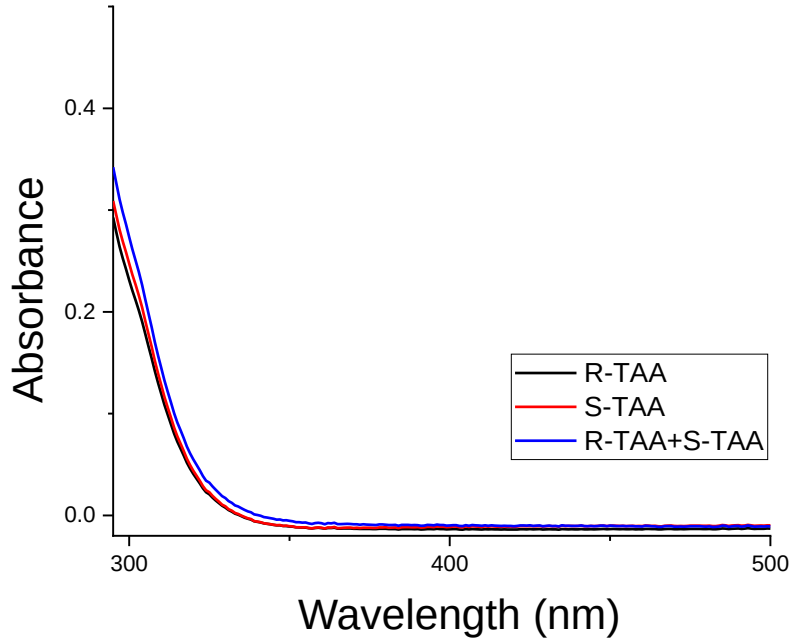

Figure S20. UV-vis studies with enantiomeric and equimolar mixed TAA at a concentration of 9.3 X 10^{-5} M in mesitylene.

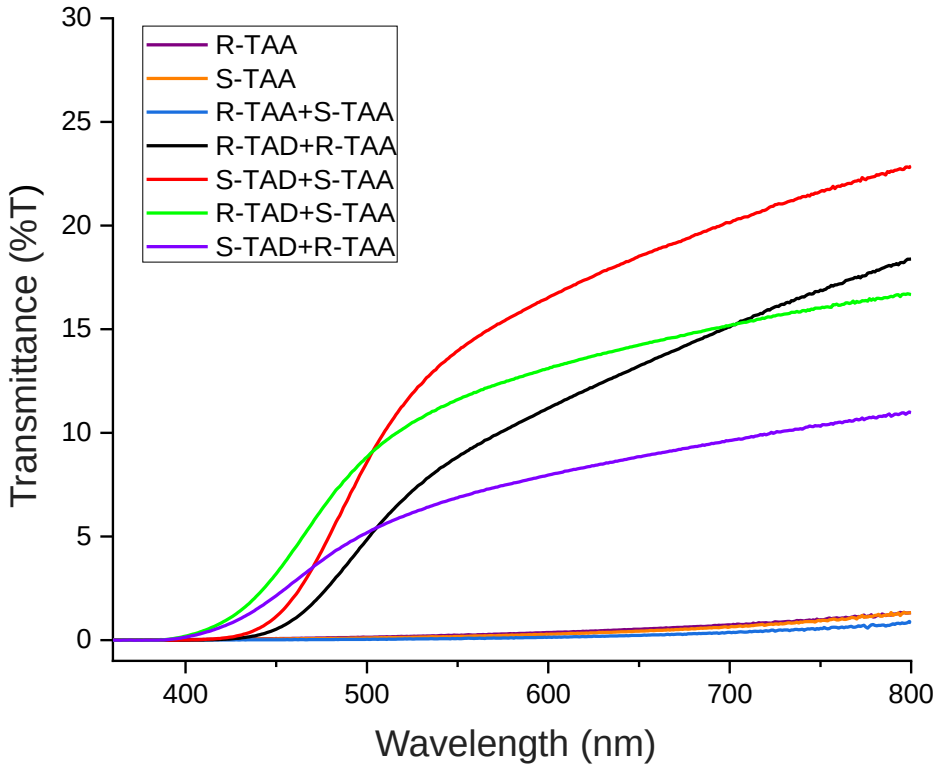

Figure S21. UV-vis studies performed in gel state at 1.4 wt/v% in mesitylene showing the opaque nature of the gels.

8. Computational studies

Table S4. HOMO and LUMO distribution in the gas phase

	R-TAD	S-TAD	R-TAA	S-TAA
LUMO	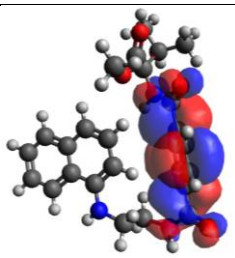 E_{lumo}= 0.311	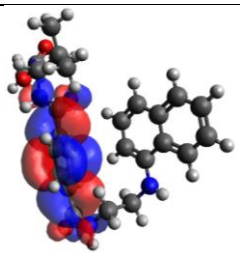 E_{lumo}= 0.318	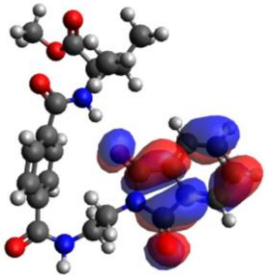 E_{lumo}= -0.897	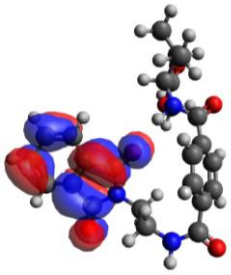 E_{lumo}= -0.900
HOMO	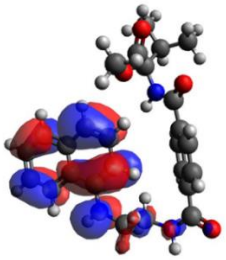 E_{homo}= -7.498	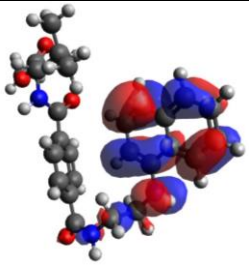 E_{homo}= -7.295	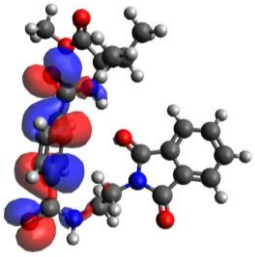 E_{homo}= -9.217	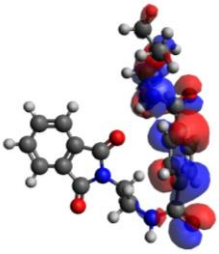 E_{homo}= -9.193

Table S5. Computational studies with monomers in gas phase

Gas phase	**HOMO (eV)**	**LUMO (eV)**	**Energy gap (eV)**
R-TAD	-7.498	0.311	7.809
S-TAD	-7.295	0.318	7.613
R-TAA	-9.217	-0.897	8.32
S-TAA	-9.193	-0.900	8.293

Table S6. Computational studies with monomers in the solvent mesitylene

In mesitylene	**HOMO (eV)**	**LUMO (eV)**	**Energy gap (eV)**
R-TAD	-7.409	0.405	7.814
S-TAD	-7.314	0.394	7.708
R-TAA	-9.269	-0.674	8.595
S-TAA	-9.246	-0.678	8.568

5.0 Role of functional groups on the self-assembly process in enantiomeric multi-component gels

Multi-component gels are prepared by combining two or more components in a specific stoichiometry, leading to either constructive or destructive mode of self-assembly in mixed gels. We are interested in two-component based multi-component systems due to their ease of control and low complexity. Mixing the two components leads to self-recognition at the molecular level, such that the individual components can be assembled separately (self-sorting), or randomly (random co-assembly), or combined in a specific fashion (specific co-assembly) to construct a new network mode. The structural similarity of the individual components plays a major role in the self-sorting or co-assembly behavior of the multi-component system. Structurally similar components tend to form a co-assembled network over self-sorting.

In this chapter, we are analyzing the role of functional groups in the self-assembly process in multicomponent gels with structurally similar components. As a result, we have chosen to use enantiomeric compounds to study the properties of multi-component systems. We have selected bis(amide) as hydrogen bonding moieties due to their efficacy as low molecular weight gelators (LMWGs) and their ability to generate both hydro- and organogels. Chirality was created by using methyl ester-protected amino acids, which was reacted with a diacid of choice to form the bis(amide) moiety. Amino acids were utilized because they are available in both enantiomeric and racemic forms and are cost-effective. Our prime question was, how does the ligand structure and the nature of functionalities tune the gelation properties in multi-component gels? We investigated the impact of rigid and flexible linkers of the enantiomers on the self-assembly modes in multi-component gels. To study the effect of functionality, we have compared multi-component gels with structurally similar individual components (enantiomers) with varying functionalities.

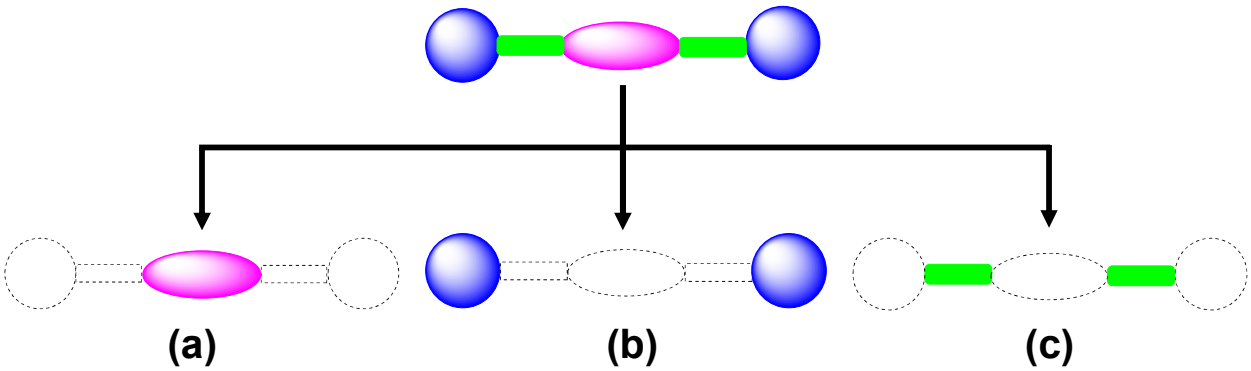

Scheme 5.1. Different ways to modify the bis-amide amino acid compounds: (a) central core (purple), (b) functional amino acid groups (blue) and (c) linker functionality (green).

This chapter is divided into three sections.

5.1 Analyzing the role of rigid and flexible core functionalities on the self-assembly modes.

In this work, we have chosen enantiomeric bis(amides) based on a bi-phenyl system tagged with valine methyl ester. We envisioned studying the role of flexibility between the bi-phenyl system in tuning the gel state properties in the mixed gel. The self-assembly modes were analyzed by comparing the thermal and mechanical stability of the enantiomeric gels with the equimolar mixed gel. This revealed that the presence of a rigid core (alkynyl functionality) could enhance the gel strength in mixed gels in comparison to its corresponding individual enantiomeric gels. Hence, studying the specific role of functionalities in multi-component gels based on enantiomers will enable us to design gelators with particular applications. However, due to the lack of crystal structures, the nature of self-assembly in these individual and mixed systems could not be analyzed. Moreover, the enhanced gel strength with the mixed system was only observed with one rigid core (alkynyl), while the other rigid cores (phenyl- and alkenyl) did not show a similar trend with the mixed gels. This made us concentrate on understanding the self-assembly in enantiomeric bis(amides) based on a bi-phenyl system with varying functionalities at the tail ends, detailed in this section's second part.

5.2 Analyzing the role of functional groups on the self-assembly modes of enantiomeric multi-component gels based on alanine and phenyl alanine methyl esters

Article VII

We analyzed the role of specific functional groups on the self-assembly mechanisms and physical properties of multi-component gels made up of structurally similar individual components. The gelation characteristics of individual and mixed enantiomeric compounds of biphenyl bis-(amides) of alanine (BPA) or phenylalanine (BPP) methyl ester were examined in various solvent/solvent mixtures. Multi-component gels are produced by combining the enantiomeric BPP molecules at a lower concentration, whereas a higher amount was necessary for the mixed alanine-based BPA gels. The analysis of the mechanical strength of individual and mixed BPP compounds revealed that the mixed BPP gels exhibited improved mechanical strength (about 2-fold increase) in *p*-xylene, but a lower gel strength was noted in DMSO/water. A contrary tendency was noted with mixed BPA gels, highlighting the significance of functional groups in the formation of the gel network. X-ray diffraction investigation of the gelator and xerogels in the solid state verified the co-assembled networks in mixed enantiomeric gels. The stability of the gels in relation to anions was assessed by examining their anion-induced stimuli-responsive properties. These results indicate the effect of specific functionality of the individual components could lead to multi-component gels with smart properties.

5.3. Evaluating the role of linker functionalities in the enantiomeric multi-component gels.

Article VIII

Understanding the nature of self-assembly in multi-component supramolecular gels is a complex task, as molecular assembly is governed by the geometry and spatial configuration of functional groups, which determine the non-bonding interactions. We have synthesized many enantiomers derived from bis(amides) of valine methyl ester with an aromatic core. We envision the flexible and rigid atmosphere between the aromatic core and the bis(amides) to tune the gelation properties in the individual enantiomeric and the equimolar mixed form. The self-assembly modes were investigated by studying the thermal and mechanical stability of the enantiomeric gels in

comparison with the equimolar mixed gel. The chirality preservation was confirmed using CD experiments in solution and dispersed gel state. SEM studies were performed to study the morphology of self-assembled fibers. We have examined the self-assembly mechanism in multi-component gels, providing crystallographic proof of specific co-assembly using single-crystal X-ray diffraction. Analysis of self-assembly revealed a transition from an orthogonal-self-assembly to a specifically co-assembled network. We have studied the self-assembly transformation using X-ray diffraction and observed that the nature of the solvent influences the change in self-assembly in these multi-component gels based on enantiomers. Analyzing such transition in the gel state will enable us to dictate the gel formation; hence, these soft materials can be served for multiple applications.

5.1 Analyzing the role of rigid and flexible core functionalities on the self-assembly modes

Multi-component systems based on low molecular weight gelators (LMWGs) have captured significant attention in recent years due to their remarkable properties and wide range of applications in numerous fields, including biomedicine and industry.[1-5] These gels are formed from two or more components, each of which can be a gelator or a non-gelator.[6-9] The interaction of these diverse components leads to distinctive properties that single-component gels cannot achieve. The self-assembly process in multi-component gels based on LMWGs relies on various non-covalent interactions, including hydrogen bonding, π-π stacking, and charge transfer interactions. These interactions can be modulated by external factors such as temperature, pH, light, and ionic strength, enabling precise control over the properties of the system.[6-9] This tunability is a key advantage of multi-component systems, which has facilitated the development of multi-component gels for diverse applications, such as drug delivery systems, tissue engineering, environmental remediation, and oil spill recovery. Multi-component gels can undergo either self-sorting or co-assembly (specific or random). However, the nature of the self-assembly has been known to be tuned by the nature of the individual components.[10] Structural similarity of the individual components favors co-assembly over self-sorting due to the effective interaction between the individual components, such as enantiomers.[10-31] Enantiomers can promote self-assembly processes, resulting in the formation of complex and organized structures. This can improve the mechanical characteristics and stability of the gel. Chiral gels are known to exhibit optical properties, chiral recognition, and biological properties. The use of simple amino acids will serve the purpose, as both the enantiomers are easily available and are cost-effective in nature.[32] MacLachlan and coworkers have recently reported that multi-component gel shows co-assembly when individual components show structural similarity, and this was confirmed with results from SEM, DSC, and SAXS.[33] However, predicting the self-assembly is still a challenging task, as the other structural features, such as rigidity or flexibility of the linker core, can influence the self-assembly. The core helps to maintain the structural integrity of the gelator by providing a network that holds different functionalities together. In this work, we are interested in analyzing the role of linkers between two phenyl moieties tagged with enantiomeric bis(amides). The role of central core will be evaluated by analyzing the self-assembly modes of enantiomeric bis-(amide) compounds with different flexible and rigid groups.

5.1.1 Results and Discussion

The spatial arrangement of the functional groups in the individual components may influence the physical properties of multi-component gels. Altering the functional moieties can modify the mechanical and thermal stabilities, morphologies, and self-assembly behaviors of multi-component gels.[34-36] The significance of functional groups in determining the self-assembly mechanisms of multi-component enantiomeric gels remains a challenging task to understand. In this context, we planned to study the effect of rigidity or flexibility in the linker core in the multi-component system based on enantiomers. We have designed and synthesized various bis(amides) (1-6) with varying flexibility in the linker core (*Figure 5.1.1*).

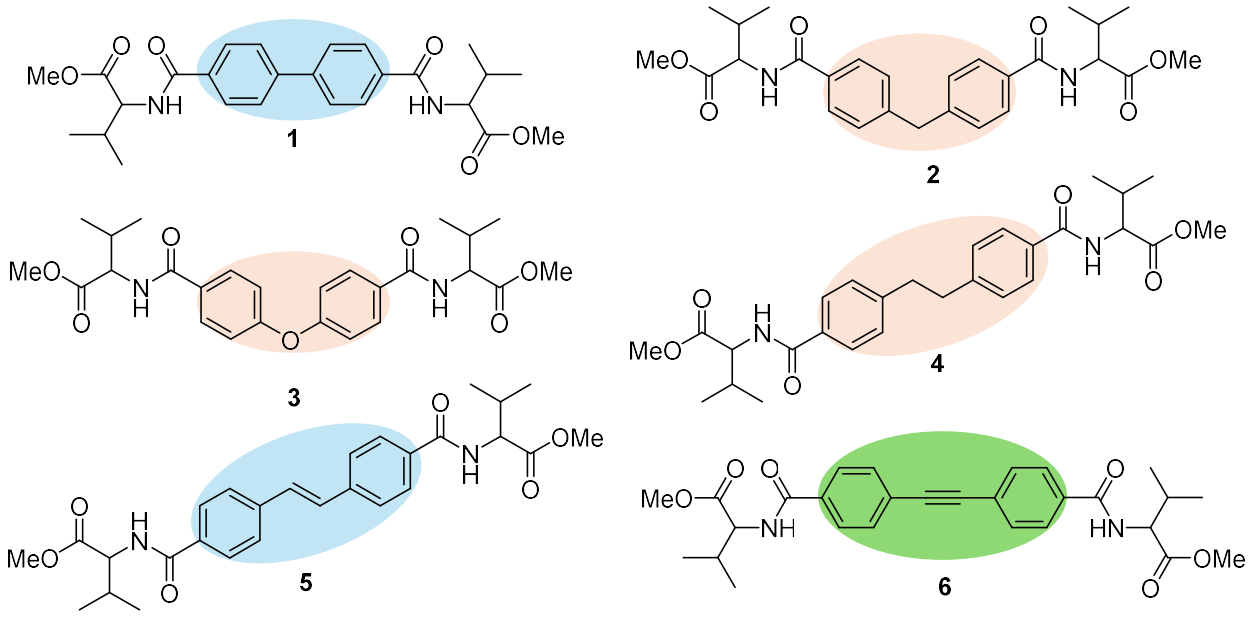

Figure 5.1.1. Chemical structures of the bis(amides), blue color-linker with a relatively rigid core, red color-linker with flexible core, green color- a rigid core linker.

We envision the linker core plays a significant role in the self-assembly of multi-component gels. The 1-diacid, 3-diacid, and 5-diacids were commercially purchased and followed a trivial method for synthesizing bis(amides). The 2-diacid and 4-diacid were synthesized using a reported protocol, and the analytical data matched with the reported data (*Scheme 5.1.1 & 5.1.2*).[37, 38]

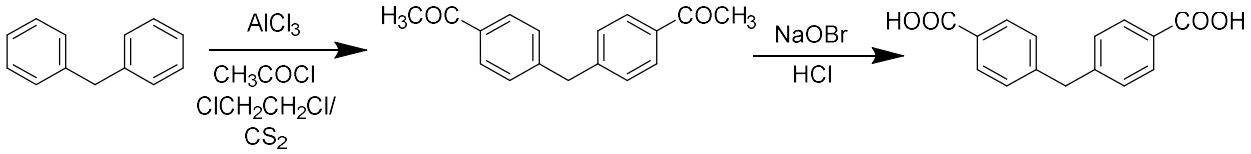

Scheme 5.1.1. Synthetic route for 2-diacid.

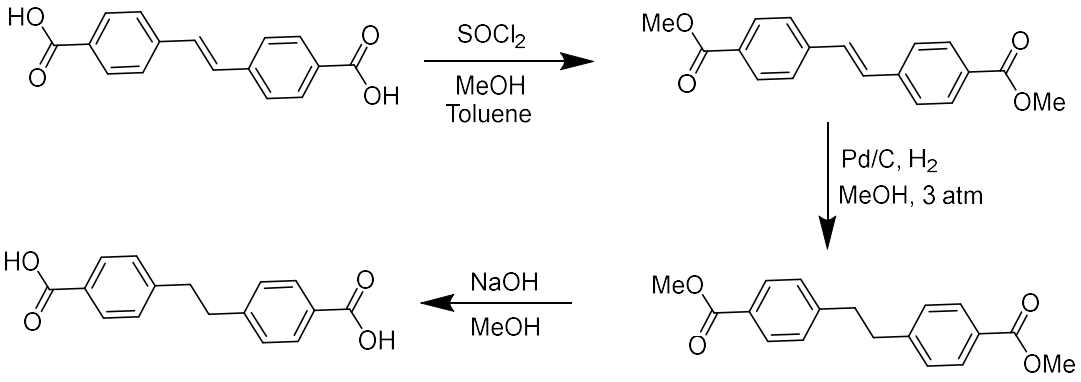

Scheme 5.1.2. Synthetic route for 4-diacid.

The 6-diacid was synthesized using sonogashira coupling, such that the 4-ethynylbenzoic acid and 4-iodobenzoic acid were reacted in the presence of dichlorobis(triphenylphosphine)palladium catalyst and piperidine as the base for the ease of the reaction (Scheme *5.1.*3).[39] These diacids were then reacted with thionyl chloride to form the corresponding acid chlorides and were treated with methyl valine esters to obtain the final enantiomeric bis(amides).

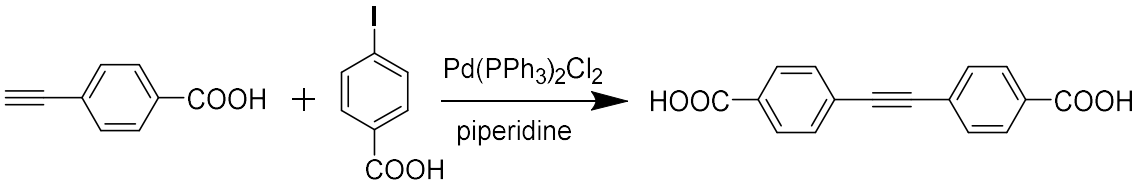

Scheme 5.1.3. Synthetic route for 6-diacid.

The gelation properties of all the individual and equimolar mixture of enantiomeric molecules were tested in various solvents/solvent mixtures (Table 5.1.1 & 5.1.2). Enantiomers of 1 and 5 formed gel in most of the organic solvents and aqueous mixtures. These enantiomers gelled in aqueous mixtures at a lower concentration (below 1.0 wt/%) and can be considered as supergelators. The 1-RR+SS gelled only in DMSO/water (1:1, v/v), while 5-RR+SS gelled in most of the solvents (Table 5.1.1 & 5.1.2). The enantiomers of 2 gelled only in aqueous mixtures, while the 2-RR+SS did not form any gel. The system 3 seems to be a non-gelator in both enantiomeric and mixed forms.

Table 5.1.1. Gelation Experiments

Solvent	Gelation test at 1.0-5.0 wt/v%								
	1-RR	1-SS	1-RR+SS	2-RR	2-SS	2-RR+SS	3-RR	3-SS	3-RR+SS
o-xylene	G**	G**	Ppt	Ppt	Ppt	Ppt	Coll	Coll	Coll
m-xylene	G**	G**	Ppt	Ppt	Ppt	Ppt	Coll	Coll	Coll
p-xylene	G**	G**	PG	PG	PG	Ppt	Coll	Coll	Coll
toluene	G***	G***	Ppt	Ppt	Ppt	Ppt	Coll	Coll	Coll

mesitylene	G**	G**	Ppt	Ppt	Ppt	Ppt	Coll	Coll	Coll
MeOH/water	G	G	Coll	G	G	C	Ppt	Ppt	Ppt
EtOH/water	G	G	Coll	G	G	C	Ppt	Ppt	Ppt
DMF/water	G	G	S	G**	G**	C	Ppt	Ppt	Ppt
DMSO/water	G	G	G	G	G	C	Ppt	Ppt	Ppt

Ppt= precipitate, Cry= Crystals, Coll=colloid, I= Insoluble, PG- partial gel, and aqueous mixtures were taken at 1:1, v/v, G-gel at 1.0 wt/v%, *-2.0 wt/v%, **- 3.0 wt/v%, ***- 4.0 wt/v%.

The flexible compound 4 (both enantiomeric and mixed form) gelled in aqueous mixtures of methanol, ethanol and DMSO (1:1, v/v) at 2.0 wt/v% (Table 5.1.2).. The semi rigid linker-based moiety 6 gelled in all the aqueous mixtures at 1.0 wt/v% in both the enantiomeric and equimolar mixed forms. It formed gel in DMF/water at a very low concentration of 0.6 wt/v%. The gelation studies showed the versatile gelation ability of compounds with rigid linkers compared to those with flexible linkers.

Table 5.1.2. Gelation Experiments

Solvent	Gelation test at 1.0-5.0 wt/v%								
	4-RR	4-SS	4-RR+SS	5-RR	5-SS	5-RR+SS	6-RR	6-SS	6-RR+SS
o-xylene	Coll**	Coll**	Coll**	G*	G*	G*	Ppt**	Ppt**	Ppt**
m-xylene	Coll**	Coll**	Coll**	G*	G*	G*	Ppt**	Ppt**	Ppt**
p-xylene	Coll**	Coll**	Coll**	G	G	G	Ppt**	Ppt**	Ppt**
toluene	Coll**	Coll**	Coll**	G*	G*	G*	Ppt**	Ppt**	Ppt**
mesitylene	Coll**	Coll**	Coll**	G*	G*	G*	Ppt**	Ppt**	Ppt**
MeOH/water	G*	G*	G*	G$^{\#\#}$	G$^{\#\#}$	G$^{\#\#}$	G	G	G
EtOH/water	G*	G*	G*	G$^{\#\#}$	G$^{\#\#}$	G$^{\#\#}$	G	G	G
DMF/water	Coll*	Coll*	Coll*	G	G	G	G$^{\#}$	G$^{\#}$	G$^{\#}$
DMSO/water	G*	G*	G*	G$^{\#\#}$	G$^{\#\#}$	G$^{\#\#}$	G	G	G

Ppt= precipitate, Cry= Crystals, Coll=colloid, I= Insoluble, PG- partial gel, and aqueous mixtures were taken at 1:1, v/v, G-gel at 1.0 wt/v%, *-2.0 wt/v%, **- 3.0 wt/v%, $^{\#}$- 5.0 wt/v%, $^{\#\#}$- 0.6 wt/v%.

The analysis of gel strength was performed using rheological studies. Rheology is an excellent tool for comparing the mechanical strength and even studying self-healing properties of semi-solid materials.[40-42] Frequency sweep experiments were performed with 1, 4, and 6-enantiomeric and mixed gel in DMSO/water (1:1, v/v) at constant strain of 0.02% at their corresponding gelling concentration. The mechanical strength of the enantiomeric gels of 1 at 2.0 wt/v% showed a 10-fold increase in storage modulus compared to the equimolar mixed gel (1+RR+SS) (*Figure 5.1.2a*).

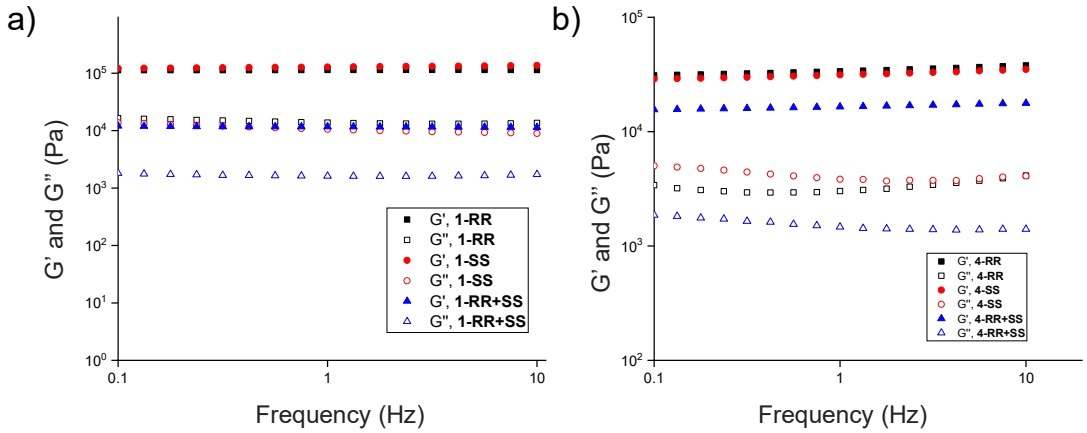

Figure 5.1.2. Frequency sweep experiment with gels at 2.0 wt/v% in DMSO/water (1:1, v/v) at 20.0 °C with a) 1-RR, 1-SS, and 1-RR+SS gels and b) 4-RR, 4-SS, and 4-RR+SS.

Similar results were also observed with the enantiomeric gels of 4 (3-fold increase) compared to the mixed gel 4-RR+SS (*Figure 5.1.2b*). The mixed gel 5-RR+SS showed slightly lower mechanical strength than their corresponding enantiomeric gels prepared at 2.0 wt/v% in *p*-xylene (*Figure 5.1.3a*).

However, the mechanical strength of the mixed gel based on 6-RR+SS at 1.0 wt/v% in DMSO/water (1:1, v/v) showed better mechanical strength than the corresponding enantiomeric gels (*Figure 5.1.3b*), which shows the importance of rigid linkers in tuning the gelation properties in multi-component gels based on enantiomers.

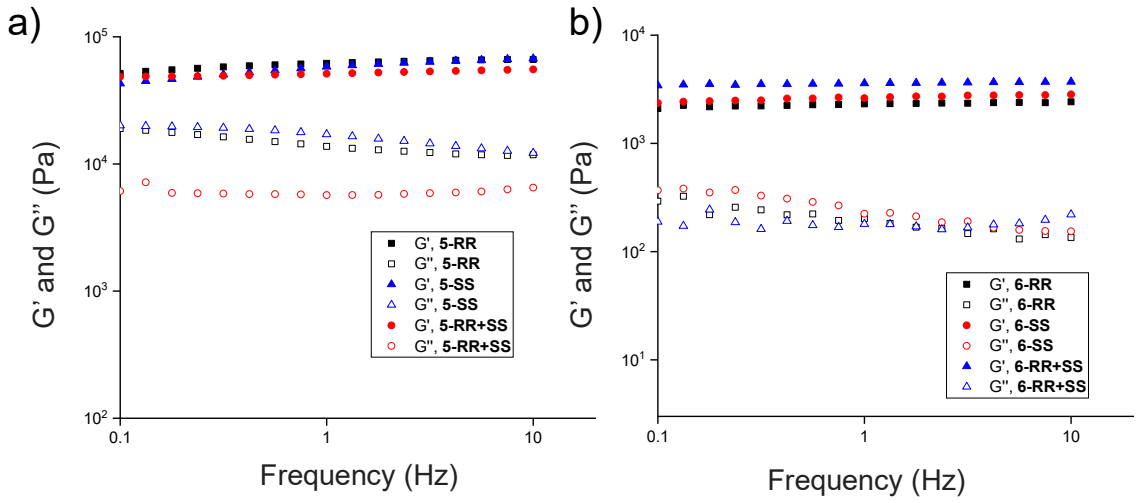

Figure 5.1.3. Frequency sweep experiment at 20.0 °C with a) 5-RR, 5-SS, and 5-RR+SS gels (2.0 wt/v%) in *p*-xylene and b) 6-RR, 6-SS, and 6-RR+SS gels (1.0 wt/v%) in DMSO/water (1:1, v/v).

5.1.2 Experimental section

Material and Methods

Starting materials and solvents were ordered from Sigma-Aldrich (MEDOR ehf, Reykjavik, Iceland), TCI-Europe (Boereveldseweg, Belgium), and Fluorochem (Glossop, UK), and utilized as received. All experiments utilized deionized water. The compounds were characterized using ^{1}H and ^{13}C NMR spectroscopy, recorded on a Bruker Avance 400 spectrometer (Rheinstetten, Germany). Rheological investigations were performed with an Anton Paar modular compact rheometer MCR 302 (Graz, Austria). X-ray diffraction analyses were conducted using Bruker D8 (Karlsruhe, Germany) for single-crystal (SCXRD) and PANalytical (Almelo, Netherlands) for powder (PXRD) diffraction.

Synthesis

Synthesis of 6-diacid: In a two-neck round bottom flask, under a nitrogen atmosphere, both 4-ethynylbenzoic acid (0.3 g, 2.05 mmol) and 4-iodobenzoic acid (0.5 g, 2.05 mmol) were introduced and added with piperidine (3.1 mL, 20.5 mmol) and dichlorobis(triphenylphosphine)palladium (58 mg, 0.08 mmol) and was stirred at 85 °C for 2.3-3.0 hours. The reaction mixture was concentrated, and then water (20.0 mL) and ethyl acetate (30.0 mL) was added. The aqueous layer was separated and acidified with 2.0 M hydrochloric acid. The corresponding 6-diacid precipitated and dried under vacuum to obtain the product as a whitish powder. Yield: 0.41 g, 78.1%. ^{1}H NMR (400 MHz, dmso-d_6) δ 13.18 (broad s, 2H), 7.99 (d, J = 8.4 Hz, 4H), 7.70 (d, J = 8.4 Hz, 4H). ^{13}C {^{1}H} NMR (100 MHz, dmso-d_6) δ 166.66, 131.73, 131.04, 129.62, 126.05, 91.07.

General method of synthesis of the bis(amides): Thionyl chloride (20 equiv.) and 2.0-3.0 drops of DMF were added to a two-neck RB flask containing the corresponding diacid (1.0 equiv.), and the mixture was refluxed overnight. The solution was evaporated to dryness by distillation to yield the corresponding acid chloride, which was used in the next step without any further purification. The amino acid ester (S or R)-methyl valinate hydrochloride (2.1 equiv.) was added to the flask under a dry nitrogen atmosphere at 0 °C, followed by the addition of DCM (100.0 mL). A solution of triethylamine (4.5 equiv.) in DCM (50.0 mL) was added dropwise to the above solution, and the mixture was stirred overnight at room temperature. The solution was then concentrated in a rotary vapor and kept in the hood overnight and then DCM (100.0 mL) was added to this solution, which was washed with 3.0% $NaHCO_3$ (2 x 80.0 mL) and 0.05 M HCl (2 x 80.0 mL), followed by brine. The organic layer dried over sodium sulfate was evaporated to yield the desired amide as the white solid. The crude was recrystallized from a 1:1 ethanol/water solvent mixture combination to yield crystalline material.

1-RR: Yield 1.55 g, 80.3 %. ^{1}H NMR (400 MHz, Chloroform-d) δ 7) δ 7.91 (d, J = 8.4 Hz, 4H), 7.68 (d, J = 8.4 Hz, 4H), 6.70 (d, J = 8.6 Hz, 2H), 4.81 (dd, J = 8.6, 4.9 Hz, 2H), 3.79 (s, 6H), 2.38 – 2.24 (m, 2H), 1.02 (dd, J = 8.9, 6.9 Hz, 12H). ^{13}C {^{1}H} NMR (100 MHz, Chloroform-d) δ 172.80, 166.91, 143.41, 133.65, 127.88, 127.55, 57.60, 52.43, 31.81, 19.15, 18.13. HRMS (APCI): calcd for $C_{26}H_{32}N_2O_6Na$ [M + Na]+, 491.2153; found, 491.2156.

1-SS: Yield 1.61 g, 83.4 %. ^{1}H NMR (400 MHz, Chloroform-d) δ 7.91 (d, J = 8.6 Hz, 4H), 7.68 (d, J = 8.8 Hz, 4H), 6.70 (d, J = 8.6 Hz, 2H), 4.81 (dd, J = 8.7, 4.9 Hz, 2H), 3.79 (s, 6H), 2.36 –

2.24 (m, 2H), 1.02 (dd, *J* = 8.9, 6.9 Hz, 12H). ^{13}C {^{1}H} NMR (100 MHz, Chloroform-d) δ 172.81, 166.93, 143.42, 133.64, 127.88, 127.55, 57.61, 52.44, 31.81, 19.15, 18.13. HRMS (APCI): calcd for for $C_{26}H_{32}N_2O_6Na$ [M + Na]+, 491.2153; found, 491.2133.

2-RR: Yield 1.08 g, 57.4 %. ^{1}H NMR (400 MHz, Chloroform-d) δ 7.74 (d, *J* = 8.4 Hz, 4H), 7.25 (d, *J* = 8.4 Hz, 4H), 6.59 (d, *J* = 8.8 Hz, 2H), 4.77 (dd, *J* = 8.6, 4.9 Hz,2H), 4.07 (s, 2H), 3.77 (s, 6H), 2.33 – 2.20 (m, 2H), 0.99 (dd, *J* = 9.9, 6.9 Hz, 12H). ^{13}C {^{1}H} NMR (100 MHz, Chloroform-d) δ 172.82, 167.14, 144.44, 132.47, 129.12, 127.57, 57.51, 52.39, 41.71, 31.79, 19.13, 18.09. HRMS (APCI): calcd for $C_{27}H_{34}N_2O_6Na$ [M + Na]+, 505.2309; found, 505.2257.

2-SS: Yield 1.18 g, 62.8 %. ^{1}H NMR (400 MHz, Chloroform-d) δ 7.74 (d, *J* = 8.4 Hz, 4H), 7.25 (d, *J* = 8.4 Hz, 4H), 6.59 (d, *J* = 8.8 Hz, 2H), 4.77 (dd, *J* = 8.6, 4.9 Hz, 2H), 4.07 (s, 2H), 3.77 (s, 6H), 2.33 – 2.18 (m, 2H), 0.98 (dd, *J* = 9.9, 6.9 Hz, 12H). ^{13}C {^{1}H} NMR (100 MHz, Chloroform-d) δ 172.81, 167.13, 144.44, 132.46, 129.30, 127.57, 57.51, 52.39, 41.70, 31.78, 19.13, 18.09. HRMS (APCI): calcd for $C_{27}H_{34}N_2O_6Na$ [M + Na]+, 505.2309; found, 505.2313.

3-RR: Yield 1.43 g, 76.1 %. ^{1}H NMR (400 MHz, Chloroform-d) δ 7.83 (d, J = 8.8 Hz, 4H), 7.07 (d, J = 8.8 Hz, 4H), 6.59 (d, J = 14.1 Hz, 2H), 4.78 (dd, J = 8.6, 4.9 Hz, 2H), 3.78 (s, 6H), 2.34 – 2.20 (m, 2H), 1.00 (dd, J = 9.8, 6.9 Hz, 12H). ^{13}C {^{1}H} NMR (100 MHz, Chloroform-d) δ 172.85, 166.58, 159.48, 129.76, 129.34, 119.00, 57.58, 52.43, 31.79, 19.15, 18.11. HRMS (APCI): calcd for $C_{26}H_{32}N_2O_7Na$ [M + Na]+, 507.2102; found, 507.2095.

3-SS: Yield 1.52 g, 80.8 %. ^{1}H NMR (400 MHz, Chloroform-d) δ 7.82 (d, J = 8.8 Hz, 4H), 7.07 (d, J = 8.8 Hz, 4H), 6.60 (d, J = 8.6 Hz, 2H), 4.78 (dd, J = 8.6, 5.0 Hz, 2H), 3.78 (s, 6H), 2.34 – 2.21 (m, 2H), 1.00 (dd, J = 9.5, 6.9 Hz, 12H). ^{13}C {^{1}H} NMR (100 MHz, Chloroform-d) δ 172.85, 166.59, 159.47, 129.74, 129.35, 118.99, 57.59, 52.43, 31.78, 19.14, 18.11. HRMS (APCI): calcd for $C_{26}H_{32}N_2O_7Na$ [M + Na]+, 507.2102; found, 507.2103.

4-RR: Yield 1.55 g, 84.2 %. ^{1}H NMR (400 MHz, Chloroform-d) δ 7.71 (d, J = 8.4 Hz, 4H), 7.20 (d, J = 8.3 Hz, 4H), 6.61 (d, J = 8.6 Hz, 2H), 4.77 (dd, J = 8.7, 4.9 Hz, 2H), 3.77 (s, 6H), 2.98 (s, 4H), 2.27 (pd, J = 6.9, 4.9 Hz, 2H), 0.99 (dd, J = 9.3, 6.9 Hz, 12H). ^{13}C {^{1}H} NMR (100 MHz, Chloroform-d) δ 172.86, 167.25, 145.33, 132.08, 128.89, 127.34, 57.48, 52.39, 37.42, 31.77, 19.14, 18.11. HRMS (APCI): calcd for $C_{28}H_{36}N_2O_6Na$ [M + Na]+, 519.2466; found, 519.2461.

4-SS: Yield 1.60 g, 86.9 %. ^{1}H NMR (400 MHz, Chloroform-d) δ 7.71 (d, J = 8.4 Hz, 4H), 7.20 (d, J = 8.4 Hz, 4H), 6.61 (d, J = 8.6 Hz, 2H), 4.77 (dd, J = 8.6, 5.0 Hz, 2H), 3.77 (s, 6H), 2.98 (s, 4H), 2.27 (pd, J = 6.9, 4.9 Hz, 2H), 0.99 (dd, J = 9.3, 6.9 Hz, 12H). ^{13}C {^{1}H} NMR (100 MHz, Chloroform-d) δ 172.86, 167.25, 145.33, 132.08, 128.89, 127.34, 57.48, 52.39, 37.42, 31.77, 19.14, 18.11. HRMS (APCI): calcd for $C_{28}H_{36}N_2O_6Na$ [M + Na]+, 519.2466; found, 519.2460.

5-RR: Yield 1.53 g, 83.1 %. ^{1}H NMR (400 MHz, Chloroform-d) δ 7.82 (d, J = 8.5 Hz, 4H), 7.60 (d, J = 8.5 Hz, 4H), 7.21 (s, 2H), 6.65 (d, J = 8.6 Hz, 2H), 4.80 (dd, J = 8.6, 4.9 Hz, 2H), 3.79 (s, 6H), 2.36 – 2.23 (m, 2H), 1.01 (dd, J = 8.4, 6.9 Hz, 12H). ^{13}C {^{1}H} NMR (100 MHz, Chloroform-d) δ 172.85, 166.86, 140.33, 133.44, 129.70, 127.74, 126.95, 57.57, 52.42, 31.83, 19.15, 18.15. HRMS (APCI): calcd for $C_{28}H_{34}N_2O_6Na$ [M + Na]+, 517.2309; found, 517.2324.

5-SS: Yield 1.63 g, 88.6 %. ^{1}H NMR (400 MHz, Chloroform-d) δ 7.82 (d, J = 8.5 Hz, 4H), 7.59 (d, J = 8.5 Hz, 4H), 7.20 (s, 2H), 6.65 (d, J = 8.6 Hz, 2H), 4.80 (dd, J = 8.6, 4.9 Hz, 2H), 3.79 (s,

6H), 2.36 – 2.23 (m, 2H), 1.01 (dd, J = 8.3, 6.8 Hz, 12H). ^{13}C {^{1}H} NMR (100 MHz, Chloroform-d) δ 172.85, 166.86, 140.32, 133.43, 129.70, 127.74, 126.95, 57.57, 52.42, 31.82, 19.14, 18.14. HRMS (APCI): calcd for $C_{28}H_{34}N_2O_6Na$ [M + Na]+, 517.2309; found, 517.2297.

6-RR: Yield 0.79 g, 42.7 %. ^{1}H NMR (400 MHz, Chloroform-d) δ 7.81 (d, J = 8.5 Hz, 4H), 7.62 (d, J = 8.5 Hz, 4H), 6.65 (d, J = 8.6 Hz, 2H), 4.79 (dd, J = 8.6, 4.9 Hz, 2H), 3.79 (s, 6H), 2.37 – 2.23 (m, 2H), 1.01 (dd, J = 8.4, 6.9 Hz, 12H). ^{13}C {^{1}H}} NMR (100 MHz, Chloroform-d) δ 172.76, 166.61, 133.98, 132.03, 127.30, 126.44, 90.99, 57.64, 52.46, 31.81, 19.14, 18.14. HRMS (APCI): calcd for $C_{28}H_{32}N_2O_6Na$ [M + Na]+, 515.2153; found, 515.2143.

6-SS: Yield 0.86 g, 46.5 %. ^{1}H NMR (400 MHz, Chloroform-d) δ 7.81 (d, J = 8.6 Hz, 4H), 7.62 (d, J = 8.6 Hz, 4H), 6.65 (d, J = 8.6 Hz, 2H), 4.79 (dd, J = 8.6, 4.9 Hz, 2H), 3.79 (s, 6H), 2.35 – 2.23 (m, 2H), 1.01 (dd, J = 8.4, 6.9 Hz, 12H). ^{13}C {^{1}H} NMR (100 MHz, Chloroform-d) δ 172.76, 166.61, 133.98, 132.03, 127.30, 126.44, 90.99, 57.64, 52.46, 31.81, 19.14, 18.14. HRMS (APCI): calcd for $C_{28}H_{32}N_2O_6Na$ [M + Na]+, 515.2153; found, 515.2139.

Gelation Details

A trivial gelation technique was followed to test the gelation ability with these enantiomeric and mixed enantiomers. Approximately 10.0 mg of the chemical compounds and 1.0 mL of the corresponding solvent were introduced into a standard 7.0 mL vial with an inner diameter of 15.0 mm. The vial was sealed, and the mixture was then sonicated and slowly heated to obtain a clear solution. The solution was allowed to stay undisturbed for gelation, and a vial-inversion test was performed to confirm gelation. The trials were repeated with increased quantities, reaching up to 5.0 wt/v%.

Rheology

The mechanical strength of the gel was evaluated using an MCR 302 Anton Paar modular compact rheometer with a 2.5 cm stainless steel parallel plate geometry and a measuring gap of 1.00 mm. The studies were conducted by putting approximately 1.0 mL of gel onto the plate. A Peltier temperature control hood was employed to restrict the solvent evaporation and sustain a consistent temperature of 20.0 °C during frequency and amplitude sweeps. Frequency sweeps were performed from 0.1 to 10.0 Hz within the linear viscoelasticity range at a strain of 0.02%. Gels were prepared with 1, 4, and 6-enantiomeric and mixed forms in DMSO/water (1:1, v/v) and gels of 5 from *p*-xylene at their corresponding wt/v%.

5.1.3 Conclusions

We have synthesized various enantiomeric bis(amides) based on a bi-phenyl system tagged with valine methyl ester to analyze the role of flexibility in the bi-phenyl core in tuning the gel state properties. We have incorporated various flexible and rigid functionalities between the phenyl moieties to understand the role of the nature of the central core in dictating the gelation properties in multi-component gels based on enantiomers. Gelation properties were studied in various solvents/solvent mixtures. The self-assembly modes were analyzed by comparing the mechanical stability of the enantiomeric gels with the equimolar mixed gel. This revealed the presence of a rigid core (alkynyl functionality) that enhanced the gel strength in mixed gels in comparison to its

corresponding individual enantiomeric gels. However, in all the other cases where gels were obtained, the enantiomeric gels showed enhanced mechanical strength compared to the mixed gel. We are currently analyzing of the nature of self-assembly in these enantiomeric multi-component gels. However, the absence of crystal structures restricted the analysis of self-assembly in these individual and mixed systems. Furthermore, the improved gel strength in the mixed system was solely seen with one rigid core (alkynyl), but the other rigid cores (phenyl and alkenyl) did not exhibit a comparable trend with the mixed gels. This prompted us to focus on comprehending the self-assembly of enantiomeric bis(amides) derived from a bi-phenyl framework, with varying functionalities at the terminal ends, and is elaborated in the following sections.

References

(1) Li, Y.; Liu, Y.; Ma, R.; Xu, Y.; Zhang, Y.; Li, B.; An, Y.; Shi, L. A G-Quadruplex Hydrogel via Multicomponent Self-Assembly: Formation and Zero-Order Controlled Release. *ACS Appl. Mater. Interfaces* **2017**, *9* (15), 13056-13067.

(2) Wong Po Foo, C. T. S.; Lee, J. S.; Mulyasasmita, W.; Parisi-Amon, A.; Heilshorn, S. C. Two-component protein-engineered physical hydrogels for cell encapsulation. *Proc. Natl. Acad. Sci.* **2009**, *106* (52), 22067-22072.

(3) Cross, E. R.; Sproules, S.; Schweins, R.; Draper, E. R.; Adams, D. J. Controlled Tuning of the Properties in Optoelectronic Self-Sorted Gels. *J. Am. Chem. Soc.* **2018**, *140* (28), 8667-8670.

(4) Zhou, M.; Smith, A. M.; Das, A. K.; Hodson, N. W.; Collins, R. F.; Ulijn, R. V.; Gough, J. E. Self-assembled peptide-based hydrogels as scaffolds for anchorage-dependent cells. *Biomaterials* **2009**, *30* (13), 2523-2530.

(5) Alakpa, Enateri V.; Jayawarna, V.; Lampel, A.; Burgess, Karl V.; West, Christopher C.; Bakker, Sanne C. J.; Roy, S.; Javid, N.; Fleming, S.; Lamprou, Dimitris A.; et al. Tunable Supramolecular Hydrogels for Selection of Lineage-Guiding Metabolites in Stem Cell Cultures. *Chem* **2016**, *1* (2), 298-319.

(6) Buerkle, L. E.; Rowan, S. J. Supramolecular gels formed from multi-component low molecular weight species. *Chem. Soc. Rev.* **2012**, *41* (18), 6089-6102.

(7) Chu, C.-W.; Schalley, C. A. Recent Advances on Supramolecular Gels: From Stimuli-Responsive Gels to Co-Assembled and Self-Sorted Systems. *Organic Materials* **2021**, *03* (01), 025-040.

(8) Raeburn, J.; Adams, D. J. Multicomponent low molecular weight gelators. *Chem. Commun.* **2015**, *51* (25), 5170-5180, 10.1039/C4CC08626K.

(9) Smith, D. K. Lost in translation? Chirality effects in the self-assembly of nanostructured gel-phase materials. *Chem Soc Rev* **2009**, *38* (3), 684-694, From Nlm.

(10) Tómasson, D. A.; Ghosh, D.; Kržišnik, Z.; Fasolin, L. H.; Vicente, A. A.; Martin, A. D.; Thordarson, P.; Damodaran, K. K. Enhanced Mechanical and Thermal Strength in Mixed-Enantiomers-Based Supramolecular Gel. *Langmuir* **2018**, *34* (43), 12957-12967.

(11) Swanekamp, R. J.; Welch, J. J.; Nilsson, B. L. Proteolytic stability of amphipathic peptide hydrogels composed of self-assembled pleated β-sheet or coassembled rippled β-sheet fibrils. *Chem. Commun.* **2014**, *50* (70), 10133-10136, 10.1039/C4CC04644G.

(12) Patterson, A. K.; El-Qarra, L. H.; Smith, D. K. Chirality-directed hydrogel assembly and interactions with enantiomers of an active pharmaceutical ingredient. *Chem. Commun.* **2022**, *58* (24), 3941-3944, 10.1039/D1CC06942J.

(13) Yang, X.; Lu, H.; Tao, Y.; Zhang, H.; Wang, H. Controlling supramolecular filament chirality of hydrogel by co-assembly of enantiomeric aromatic peptides. *J. Nanobiotechnology* **2022**, *20* (1), 77.
(14) Das, R. K.; Kandanelli, R.; Linnanto, J.; Bose, K.; Maitra, U. Supramolecular Chirality in Organogels: A Detailed Spectroscopic, Morphological, and Rheological Investigation of Gels (and Xerogels) Derived from Alkyl Pyrenyl Urethanes. *Langmuir* **2010**, *26* (20), 16141-16149.
(15) Swanekamp, R. J.; DiMaio, J. T.; Bowerman, C. J.; Nilsson, B. L. Coassembly of enantiomeric amphipathic peptides into amyloid-inspired rippled β-sheet fibrils. *J. Am. Chem. Soc.* **2012**, *134* (12), 5556-5559.
(16) Koga, T.; Matsuoka, M.; Higashi, N. Structural control of self-assembled nanofibers by artificial β-sheet peptides composed of D-or L-isomer. *J. Am. Chem. Soc.* **2005**, *127* (50), 17596-17597.
(17) Hirst, A. R.; Smith, D. K.; Feiters, M. C.; Geurts, H. P. Two-Component Dendritic Gel: Effect of Stereochemistry on the Supramolecular Chiral Assembly. *Chem. Eur. J.* **2004**, *10* (23), 5901-5910.
(18) Ghosh, D.; Farahani, A. D.; Martin, A. D.; Thordarson, P.; Damodaran, K. K. Unraveling the Self-Assembly Modes in Multicomponent Supramolecular Gels Using Single-Crystal X-ray Diffraction. *Chem. Mater.* **2020**, *32* (8), 3517-3527.
(19) Nagy-Smith, K.; Beltramo, P. J.; Moore, E.; Tycko, R.; Furst, E. M.; Schneider, J. P. Molecular, Local, and Network-Level Basis for the Enhanced Stiffness of Hydrogel Networks Formed from Coassembled Racemic Peptides: Predictions from Pauling and Corey. *ACS Cent Sci* **2017**, *3* (6), 586-597, From Nlm.
(20) Zhu, X.; Li, Y.; Duan, P.; Liu, M. Self-assembled ultralong chiral nanotubes and tuning of their chirality through the mixing of enantiomeric components. *Chem. Eur. J.* **2010**, *16* (27), 8034-8040.
(21) Liu, Z.; Sun, J.; Zhou, Y.; Zhang, Y.; Wu, Y.; Nalluri, S. K. M.; Wang, Y.; Samanta, A.; Mirkin, C. A.; Schatz, G. C. Supramolecular Gelation of Rigid Triangular Macrocycles through Rings of Multiple C–H⋯ O Interactions Acting Cooperatively. *J. Org. Chem.* **2016**, *81* (6), 2581-2588.
(22) Li, H.; Han, L.; Li, Q.; Lai, H.; Fernández-Trillo, P.; Tian, L.; He, F. Hierarchical Chiral Supramolecular Nanoarchitectonics with Molecular Detection: Helical Structure Controls upon Self-Assembly and Coassembly. *Macromol. Rapid Commun.* **2022**, *43* (14), 2100690.
(23) McAulay, K.; Dietrich, B.; Su, H.; Scott, M. T.; Rogers, S.; Al-Hilaly, Y. K.; Cui, H.; Serpell, L. C.; Seddon, A. M.; Draper, E. R. Using chirality to influence supramolecular gelation. *Chem. Sci.* **2019**, *10* (33), 7801-7806.
(24) Nagy, K. J.; Giano, M. C.; Jin, A.; Pochan, D. J.; Schneider, J. P. Enhanced Mechanical Rigidity of Hydrogels Formed from Enantiomeric Peptide Assemblies. *J. Am. Chem. Soc.* **2011**, *133* (38), 14975-14977.
(25) Messmore, B. W.; Sukerkar, P. A.; Stupp, S. I. Mirror image nanostructures. *J. Am. Chem. Soc.* **2005**, *127* (22), 7992-7993.
(26) Adhikari, B.; Nanda, J.; Banerjee, A. Multicomponent hydrogels from enantiomeric amino acid derivatives: helical nanofibers, handedness and self-sorting. *Soft Matter* **2011**, *7* (19), 8913-8922, 10.1039/C1SM05907F.
(27) Cicchi, S.; Ghini, G.; Lascialfari, L.; Brandi, A.; Betti, F.; Berti, D.; Baglioni, P.; Di Bari, L.; Pescitelli, G.; Mannini, M. Self-sorting chiral organogels from a long chain carbamate of 1-benzyl-pyrrolidine-3, 4-diol. *Soft Matter* **2010**, *6* (8), 1655-1661.

(28) Lascialfari, L.; Pescitelli, G.; Brandi, A.; Mannini, M.; Berti, D.; Cicchi, S. Urea vs. carbamate groups: a comparative study in a chiral C2 symmetric organogelator. *Soft Matter* **2015**, *11* (42), 8333-8341, 10.1039/C5SM01684C.
(29) Yang, Z.; Liang, G.; Ma, M.; Gao, Y.; Xu, B. Conjugates of naphthalene and dipeptides produce molecular hydrogelators with high efficiency of hydrogelation and superhelical nanofibers. *J. Mater. Chem.* **2007**, *17* (9), 850-854, 10.1039/B611255B.
(30) Shen, J.-S.; Mao, G.-J.; Zhou, Y.-H.; Jiang, Y.-B.; Zhang, H.-W. A ligand-chirality controlled supramolecular hydrogel. *Dalton Trans.* **2010**, *39* (30), 7054-7058, 10.1039/C0DT00364F.
(31) Foster, J. A.; Edkins, R. M.; Cameron, G. J.; Colgin, N.; Fucke, K.; Ridgeway, S.; Crawford, A. G.; Marder, T. B.; Beeby, A.; Cobb, S. L.; Steed, J. W. Blending Gelators to Tune Gel Structure and Probe Anion-Induced Disassembly. *Chem. Eur. J.* **2014**, *20* (1), 279-291.
(32) Suzuki, M.; Hanabusa, K. L-Lysine-based low-molecular-weight gelators. *Chem. Soc. Rev.* **2009**, *38*, 967-975.
(33) Loos, J. N.; Boott, C. E.; Hayward, D. W.; Hum, G.; MacLachlan, M. J. Exploring the Tunable Optical and Mechanical Properties of Multicomponent Low-Molecular-Weight Gelators. *Langmuir* **2021**, *37* (1), 105-114.
(34) Fleming, S.; Debnath, S.; Frederix, P. W. J. M.; Hunt, N. T.; Ulijn, R. V. Insights into the Coassembly of Hydrogelators and Surfactants Based on Aromatic Peptide Amphiphiles. *Biomacromolecules* **2014**, *15* (4), 1171-1184.
(35) Chan, A. S. W.; Sundararajan, P. R. Co-Assembly and Self-Sorting Effects in Gels of Blends of Polyurethane Model Compounds. *ChemistrySelect* **2017**, *2* (3), 1149-1157.
(36) Loos, J. N.; D'Acierno, F.; Vijay Mody, U.; MacLachlan, M. J. Manipulating the Self-Assembly of Multicomponent Low Molecular Weight Gelators (LMWGs) through Molecular Design. *ChemPlusChem* **2022**, *87* (4), e202200026.
(37) Jeong, W.; Khazi, M. I.; Lee, D. G.; Kim, J.-M. Intrinsically Porous Dual-Responsive Polydiacetylenes Based on Tetrahedral Diacetylenes. *Macromolecules* **2018**, *51* (24), 10312-10322.
(38) Marshall, R. J.; Richards, T.; Hobday, C. L.; Murphie, C. F.; Wilson, C.; Moggach, S. A.; Bennett, T. D.; Forgan, R. S. Postsynthetic bromination of UiO-66 analogues: altering linker flexibility and mechanical compliance. *Dalton Trans.* **2016**, *45* (10), 4132-4135, 10.1039/C5DT03178H.
(39) Crosignani, S.; Prêtre, A.; Jorand-Lebrun, C.; Fraboulet, G.; Seenisamy, J.; Augustine, J. K.; Missotten, M.; Humbert, Y.; Cleva, C.; Abla, N.; et al. Discovery of Potent, Selective, and Orally Bioavailable Alkynylphenoxyacetic Acid CRTH2 (DP2) Receptor Antagonists for the Treatment of Allergic Inflammatory Diseases. *J. Med. Chem.* **2011**, *54* (20), 7299-7317.
(40) Goodwin, J. W.; Hughes, R. W. *Rheology for chemists: an introduction*; Royal Society of Chemistry, 2008.
(41) Guenet, J.-M. *Organogels: Thermodynamics, structure, solvent role, and properties*; Springer, 2016.
(42) Jayabhavan, S. S.; Myneni, H.; Riedel, M.; Damodaran, K. K. Analysing the self-assembly modes in chiral multi-component gels based on donor and acceptor moieties. *Supramol. Chem.* **2023**, *34* (9-10), 414-426.

Article-VII

This project is published in a peer-reviewed journal and included as published. Minor variations may arise from the original article due to formatting issues.

Publication details:

"**The Role of Functional Groups in Tuning the Self-Assembly Modes and Physical Properties of Multi-component Gels**"

Sreejith S. Jayabhavan, G. Kuppadakkath and Krishna K. Damodaran*

ChemPlusChem, **2023**, *88* (8), e202300302.

Author contributions:

SSJ and KKD planned and designed the research; **SSJ** synthesised the gelators, performed characterisations, and evaluated gelation properties. GK carried out the crystallisation experiments. **SSJ** and KKD wrote the initial manuscript draft, and all authors reviewed the main manuscript.

ChemPlusChem

Research Article
doi.org/10.1002/cplu.202300302

Chemistry Europe
European Chemical Societies Publishing

www.chempluschem.org

The Role of Functional Groups in Tuning the Self-Assembly Modes and Physical Properties of Multicomponent Gels

Sreejith Sudhakaran Jayabhavan,[a] Geethanjali Kuppadakkath,[a] and Krishna K. Damodaran*[a]

We have analyzed the nature and role of functional groups on the self-assembly modes and the physical properties of multicomponent gels with structurally similar individual components. The gelation properties of individual and mixed enantiomeric compounds of biphenyl bis-(amides) of alanine (BPA) or phenylalanine (BPP) methyl ester were analyzed in various solvent/solvent mixtures. Multicomponent gels were formed by mixing the enantiomeric BPP compounds at a lower concentration, but a higher concentration was required for mixed alanine-based BPA gels. The comparison of the mechanical strength of the individual and mixed BPP compounds indicated that the mixed BPP gels displayed enhanced mechanical strength (~2-fold increase) in *p*-xylene, but a weaker gel was observed in DMSO/water. However, a reverse trend was observed for BPA gels, indicating the role of functional groups in the gel network formation. X-ray diffraction analysis of the gelator and the xerogels in the solid state confirmed the formation of co-assembled networks in mixed enantiomeric gels. The stability of the gels towards anions was evaluated by analyzing the anion induced stimuli-responsive properties. These results indicate the effective modeling of the functional groups of the individual components could lead to multicomponent gels with tunable properties.

Introduction

Multicomponent supramolecular gels based on low molecular weight gelators (LMWGs)[1] are an excellent class of soft materials with intriguing potential applications and tunable properties.[2] The components of these LMWGs can be a gelator or non-gelator, which forms a gel upon mixing in a specified stoichiometry. Adding external entities such as surfactants, polymers, nanoparticles, or metal complexes to the individual system can also induce gelation.[3] Multicomponent gels obtained by mixing individual gelators have gained widespread interest over the last decade because the gelation properties of the individual gelators can be correlated to mixed gels. This will help to unravel the key parameters that influence the self-assembly modes of the multicomponent systems.[3] The individual gelators could interact each other to form a co-assembled network (specific or random), but non-favorable interactions between the components lead to self-sorted networks.[3c] However, predicting the self-assembly modes, is challenging because the self-assembly modes of individual gelators for example, the formation of a self-sorted or co-assembled network depend on the molecular structure and various parameters such as the gelation condition, mutual interaction, pH, and temperature.[3] Structural similarity is a key parameter that plays a crucial role in controlling the mutual interaction between individual components in multicomponent gels. Mixing enantiomeric gels can induce self-recognition at the molecular level due to the structural similarity of individual components resulting in gels with better packing and favorable properties[4] that are not accessed by individual enantiomeric gels. Multicomponent systems based on enantiomeric compounds tend to favor co-assembly over self-sorting,[4a–n] but self-sorted fibers are obtained if the components with identical conformation display favorable interaction[4o–r] leading to conglomerates (Scheme 1).

Multicomponent enantiomeric gels with both co-assembled and self-sorted fibers are rare.[4s–u] Adams *et al.* showed that mixing functionalized dipeptide enantiomers leads to co-assembled structures in water. We have shown that mixing

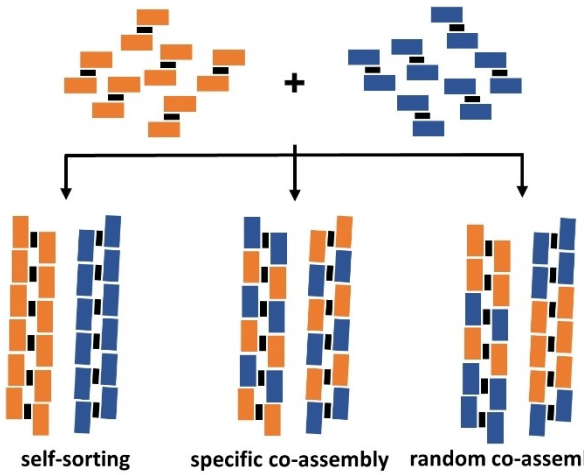

Scheme 1. Various modes of self-assembly. Color code, orange-*R*-amino acid based, blue- *S*-amino acid based, and linker is shown in black color.

[a] *S. Sudhakaran Jayabhavan, G. Kuppadakkath, Prof. K. K. Damodaran*
Department of Chemistry
University of Iceland
Dunhagi 3
107 Reykjavík (Iceland)
E-mail: krishna@hi.is

Supporting information for this article is available on the WWW under https://doi.org/10.1002/cplu.202300302

enantiomeric components leads to specific co-assembly in multicomponent gels and reported the structural evidence of co-assembled gelators using X-ray diffraction analysis in mixed enantiomeric gels.[4h] The co-assembled gels based on terephthalic bis-(amide) of valine methyl ester displayed enhanced thermal and mechanical stability compared to the individual gels due to the better packing arising from the favorable interaction between individual components.[4h] Adams and co-workers reported that the self-assembly modes of the multicomponent systems could be switched between self-sorted and co-assembled fibers using the pH-switch method.[5] These results indicate the necessity of additional studies for a better understanding of the self-assembly process, which will enable to control and predict the self-assembly modes in multicomponent gels.

The nature and spatial orientation of the functional groups of the individual components could affect the physical properties of multicomponent gels. For example, varying the functional moieties can alter the mechanical/thermal stabilities, morphologies, and self-assembly modes of multicomponent gels.[6] However, the importance of non-hydrogen bonding functional moieties/groups in dictating the self-assembly modes of multicomponent enantiomeric gels are not known. In this work, we are investigating the influence of non-hydrogen bonding functional groups on the physical properties and the self-assembly modes of multicomponent enantiomeric gels. The role of non-hydrogen bonding functional groups will be evaluated by analyzing the self-assembly modes of enantiomeric bis-(amide) compounds with different amino acid groups. We have selected bis-(amide) of amino acid derivatives because they are inexpensive, crystalline, easily modified, and available in both enantiomeric forms.[7] Furthermore, the diamides display β-tape-like self-assembly to form a well-defined fibrous network in enantiomeric and mixed gel forms. The gelation properties of the individual and mixed materials were evaluated and compared with other amino acid ester compounds to evaluate the role of functional groups on the self-assembly modes and gelation properties.

Results and Discussion

Supramolecular gels based on chiral LMWGs display potential applications in various fields, including asymmetric catalysis, chiral nanomaterials, and chiral recognition.[8] We have shown that chiral LMWGs based on amide and urea moieties are excellent candidates for analyzing the self-assembly modes of multicomponent gels and reported the crystallographic evidence for specific co-assembly in a multicomponent gel based on enantiomers.[4h,s] The structural analysis of the enantiomeric and mixed gelators based on the terephthalic amide of valine methyl ester indicated that the rigid aromatic core plays a crucial role in the self-assembly process.[4h] The role of the non-hydrogen bonding functional groups on the gelation properties and the self-assembly mode in enantiomeric multicomponent gels can be analyzed by replacing the end groups of a C_2-symmetric amide linker with different amino acid derivatives.

In this work, we have designed four bis-(amides) of two different amino acid esters such as alanine (RR- and SS-BPA) and phenylalanine (RR- and SS-BPP), with a biphenyl spacer to evaluate the structural parameters of the non-hydrogen bonding functional groups on the self-assembly modes of multicomponent gels. Alanine has the shortest alkyl chain, which is the simplest chiral amino acid and phenylalanine was selected to evaluate the role of hydrophobic phenyl groups on the gel state properties. The four enantiomeric bis-(amides) were synthesized by reacting biphenyl-4,4′-dicarboxylic acid chloride with *R* or *S*-methyl ester hydrochloride of alanine and phenylalanine (Scheme 2) and were characterized using NMR and mass spectrometry. Multicomponent gels were prepared by mixing equimolar *R* and *S* enantiomers, and the gelation properties of the individual and mixed enantiomers were evaluated in a series of solvents and solvent systems using standard gelation techniques.

Gelation Studies

The gelation test was performed by dissolving a calculated amount of the compound in an appropriate solvent by sonication followed by heating. After cooling to room temperature, the solution was left undisturbed, and a vial inversion test confirmed the gel formation (Figure S1, see Supporting Information). The gelation experiments were carried out with the individual and the mixed enantiomers in various solvent and solvent mixtures (Table S1, see Supporting Information). The enantiomeric compounds based on RR- and SS-BPA was observed to gel in *p*-xylenes and *m*-xylene at 2.6 wt/v%, and at 3.0 wt/v% in *o*-xylene and mesitylene. The mixed compound (RR + SS-BPA) also formed gel in similar solvents but at a higher concentration in *p*-xylenes and *m*-xylene (3.0 wt/v%), *o*-xylene (3.6 wt/v%), and mesitylene (3.8 wt/v%), respectively. We tested the gelation properties in aqueous mixtures (1:1, v/v) of ethanol, DMF, and DMSO, and gels were formed at 3.0 wt/v% for both enantiomeric and mixed compounds. The enantiomeric (RR- and SS-BPP) and the mixed enantiomers (RR + SS-BPP) of phenylalanine-based compounds formed gels in xylenes and mesitylene (Table S1, see Supporting Information). The experiments performed in the aqueous mixtures (1:1, v/v) of DMF or DMSO solution at 1.0 wt/v% revealed gel formation for the enantiomers. The gelation experiment failed for RR + SS-BPP mixture due to their poor solubility and gelation was not observed for experiments performed at lower concentrations of RR + SS-BPP mixture. This prompted us to check the gelation

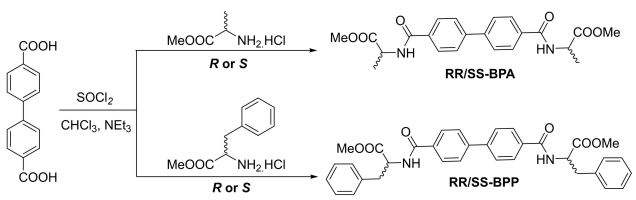

Scheme 2. Synthesis of enantiomeric BPA and BPP compounds.

properties by increasing the solubilizing agent. The experiments performed with all four enantiomers and the mixed compounds at higher concentrations of DMSO revealed gel formation in 3:2 (v/v) DMSO/water mixture. Gelation was observed for the enantiomeric and mixed compounds of BPA compounds at 3.0 wt/v% and at 2.0 wt/v% for BPP compounds in DMSO/water (3:2, v/v), respectively.

The minimum amount of the gelator required to entrap the whole solvent to form a stable gel is the minimum gelator concentration (MGC). Analysis of the MGC values revealed that the enantiomeric compounds (RR- and SS-BPA) gelled xylenes and mesitylene at a lower concentration than the mixed RR+SS-BPA. (Table S2, see Supporting Information). A similar trend was observed for aqueous mixtures (1:1, v/v) of ethanol and DMSO, v/v) but the MGC for DMF/water (1:1, v/v) and DMSO/water (3:2, v/v) were the same. The enantiomeric gels (RR- and SS-BPP) in xylenes and mesitylene had MGC values ranging from 2.5 to 5.0 wt/v%, but a lower MGC was observed for the mixed gels RR+SS-BPP in the corresponding solvents (Table S2, see Supporting Information), which may be due to the better packing of the gel network upon mixing the enantiomers. However, the mixed RR+SS-BPP gelled at a higher concentration compared to individual enantiomers in DMSO/water (3:2, v/v) at 2.0 wt/v% presumably due to the higher solubility of the mixed gels in DMSO.

Thermal Stability

The gel-to-solution-phase transition temperature (T_{gel}) was measured using the standard "dropping ball" technique to analyze the thermal stability of the gel network. The T_{gel} analysis of alanine-based enantiomeric gels (RR- and SS-BPA) and mixed gels (RR+SS-BPA) in *p*-xylene and *o*-xylene indicated that the thermal stability of the enantiomeric gels was higher than the mixed RR+SS-BPA gel. The experiments performed with RR- and SS-BPA and mixed gels in aqueous DMSO solution at 4.0 wt/v% (1:1, v/v) and 3.0 wt/v% (3:2, v/v) showed that the enantiomeric and equimolar mixed gel showed similar thermal strength (Table S3, see Supporting Information). The thermal stability of phenylalanine-based gels in *p*-xylenes, *m*-xylene, and mesitylene at 3.0 wt/v% revealed that the mixed gel (RR+SS-BPP) displayed a thermally stable network in comparison with the individual enantiomeric gels (RR- and SS-BPP). The higher thermal stability in the mixed gel is presumably due to the favorable interactions between the enantiomers leading to a better gel network (Table S3, see Supporting Information), and similar results were also obtained with the BPP gels in DMSO/water (3:2, v/v) at 1.8 wt/v%.

Mechanical Strength

The deformation and flow characteristics of supramolecular gels can be studied using rheology, which is a smart tool for characterizing the strength of the gel network.[9] Rheological measurements were carried out to evaluate the solid-like properties and mechanical strength of the individual and mixed enantiomeric gels. We have performed rheological experiments in *p*-xylene with enantiomeric (RR- and SS-BPA) gels at 2.6 wt/v% and the mixed RR+SS-BPA gel at 3.5 wt/v% because the enantiomeric gels were not soluble above 2.7 wt/v% concentration in *p*-xylene. The linear viscoelastic region (LVR) was measured using the strain sweep experiments at a constant frequency of 1.0 Hz.[4h,s,10] Amplitude sweep experiments revealed a gradual decrease in G′ after 0.02% of strain, and the gel network collapsed around 5.0–15.0% of strain (Figure S2, see Supporting Information). Frequency sweep experiments showed that the enantiomeric (RR- and SS-BPA) gels in *p*-xylene (2.6 wt/v%) were comparatively stronger than the mixed RR+SS-BPA gel in *p*-xylene at 3.5 wt/v% (Figure 1a).

The experiments conducted with enantiomeric (RR- and SS-BPA) and mixed (RR+SS-BPA) gels in DMSO/water mixtures at 4.0 wt/v% (1:1, v/v) and 3.0 wt/v% (3:2, v/v) showed that the elastic modulus G′ tends to decrease after 0.02% of strain, and the gel network collapsed at the crossover point (1.0–10.0% strain, Figure S3, see Supporting Information). The frequency sweep experiments with the above gels within LVR (0.1–10.0 Hz) at a constant strain of 0.02% revealed that the mixed enantiomeric gel was mechanically stronger than the enantiomeric gels in DMSO/water mixtures (Figure S4, see Supporting Information).

Rheological experiments performed on phenylalanine-based enantiomeric (RR- and SS-BPP) and the mixed (RR+SS-BPP) gels in *p*-xylene at 3.0 wt/v% showed a narrow LVR, as the elastic modulus decreased after 0.02% of strain and the crossover point were within the range of 8.0–15.0% of the shear strain (Figure S5, see Supporting Information). Frequency sweep experiments were performed with RR- and SS-BPP and the mixed RR+SS-BPP gels (3.0 wt/v%) in *p*-xylene in the range of 0.1–10.0 Hz (within LVR) at a constant strain of 0.02%. The results indicated that the mixed enantiomeric gel was mechanically stronger (~2-fold) compared to the enantiomeric gels (Figure 1b). The enhanced thermal and mechanical strength of the mixed enantiomeric gels based on BPP can be attributed to the co-assembly in the mixed system, which provides sufficient cross-links to form a better gel network. However, the RR- and SS-BPP gels were stiffer than the mixed enantiomeric RR+SS-BPP gels in DMSO/water (3:2, v/v) presumably due to the increased solubility of the mixed gels[4h] arising from the

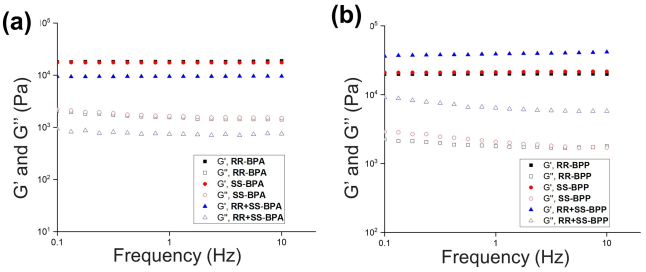

Figure 1. Frequency sweep experiments in *p*-xylene with (a) BPA compounds (SS- and RR-BPA at 2.6 wt/v%) and RR+SS-BPA at 3.5 wt/v%) and (b) BPP compounds (3.0 wt/v%) at a constant strain of 0.02%, at 20.0 °C.

favorable interaction of the self-assembled enantiomers with hydrogen bonding solvents (Figure S6, see Supporting Information).

The role of the non-hydrogen bonding functional group on the gelation properties of multicomponent gels was analyzed by comparing the mechanical and thermal stabilities of the mixed gels. The phenylalanine-based compounds showed better solubility compared to the alanine-based compounds in aromatic solvents due to the favorable interaction of the phenyl groups with the aromatic solvents. The enhanced mechanical and thermal stabilities of BPP gels compared to BPA gels indicate the role of phenyl groups on the gelation properties. This is presumably due to the enhanced hydrophobic interactions of phenyl moieties in aqueous mixtures leading to better gel network formation.

Gel Morphology

The morphology of the dried gels was analyzed using scanning electron microscopy (SEM). SEM analysis can provide insight into the self-assembly modes by analyzing the morphologies of the xerogels.[11] The difference in the fiber morphology of the individual and mixed fibrils can be correlated to the self-assembly modes in the mixed enantiomeric gels.[4h] Xerogels were prepared from *p*-xylene and DMSO/water at a similar concentration (above MGC) for the enantiomeric and mixed gels. SEM performed on the dried gels of RR- and SS-BPA enantiomers in *p*-xylene at 2.7 wt/v% revealed the presence of thick needle-shaped fibers with dimensions of 0.1 to 2.0 μm (Figure 2a and 2b). The xerogels of RR-BPP and SS-BPP obtained from *p*-xylene (3.0 wt/v%) showed fibrous networks with twisted fibers of corresponding handedness, which revealed the chirality of the molecule was observed to be transferred to the hierarchical aggregates, and the fiber width ranged 0.3 to 1.2 μm (Figure 2c and 2d).

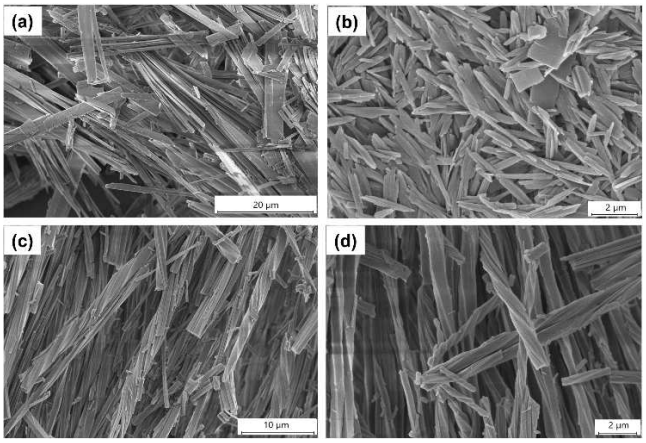

Figure 2. SEM images of the xerogels from *p*-xylene (a) RR-BPA and (b) SS-BPA at 2.7 wt/v% and (c) RR-BPP and (d) SS-BPP at 3.0 wt/v%.

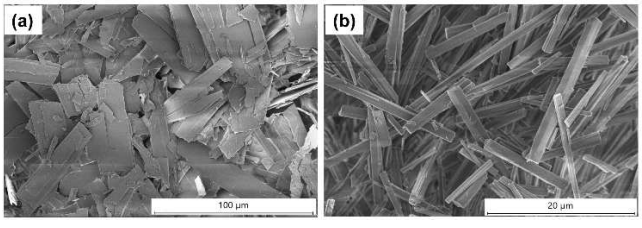

Figure 3. SEM images of the mixed xerogels from *p*-xylene of (a) RR + SS-BPA at 3.5 wt/v% and (b) RR + SS-BPP at 3.0 wt/v%.

The xerogels of mixed RR + SS-BPA (3.5 wt/v%) displayed plate-like morphology with dimensions 2.5–15.0 μm (Figure 3a) but the equimolar RR + SS-BPP showed flake-like morphology with fiber dimensions of 0.3 to 2.2 μm (Figure 3b) in *p*-xylene, respectively. The difference may be attributed to co-assembled enantiomeric fibers in the mixed enantiomeric gels.

SEM images recorded for the enantiomeric (RR-BPA and SS-BPA) and mixed RR + SS-BPA xerogels from DMSO/water (1:1, v/v) displayed plate-shaped morphology with dimensions ranging from 2.0 to 16.0 μm (Figure S7, see Supporting Information. SEM analysis of the BPP xerogels from DMSO/water (1:1, v/v) at 1.2 wt/v% revealed the presence of twisted fibers for both RR-BPP and SS-BPP xerogels (Figure S8, see Supporting Information). For comparison, the morphology of the mixed RR + SS-BPP compound was performed by a drop-cast method, and the result indicated the absence of twisted fibers, presumably due to co-assembled enantiomers in mixed gels (Figure S9, see Supporting Information). We have also analyzed the morphologies of the RR-BPP, SS-BPP, and mixed RR + SS-BPP xerogels from DMSO/water (3:2, v/v) at 1.8 wt/v% for comparison, and the results were similar to the DMSO/water (1:1, v/v) xerogels (Figure S10, see Supporting Information).

Circular Dichroism

CD experiments provide valuable structural information of the self-assembly processes that lead to chiral supramolecular architectures,[12] which will allow us to understand the structural information of the hierarchical structure. The chirality of the four enantiomeric compounds and the mixed enantiomers were confirmed using solution-state CD experiments performed in absolute ethanol at different concentrations (0.020 to 0.030 wt/v%) and 0.025 wt/v% was selected as the optimum concentration. The CD spectra for RR-BPA displayed positive maxima around 233 nm and negative maxima around 265 nm, which was found to be a mirror image of SS-BPA (Figure 4a and Figure S11, see Supporting Information). The peak at 233 nm may correspond to the β-conformation architecture as observed in self-assembled gels of short peptides, presumably due to the hydrogen bonding in amides and π-π stacking interactions.[13] The corresponding mixed system RR + SS-BPA showed a linear CD signal, indicating the existence of both the enantiomers as the CD signal cancels out due to external compensation.

The solution state CD experiments with enantiomeric phenylalanine-based compounds indicated that the SS-BPP displayed a positive maxima at 219 nm and a negative maxima around 280 nm, which can be associated with the π-π stacking interactions from the phenyl groups (Figure S12, see Supporting

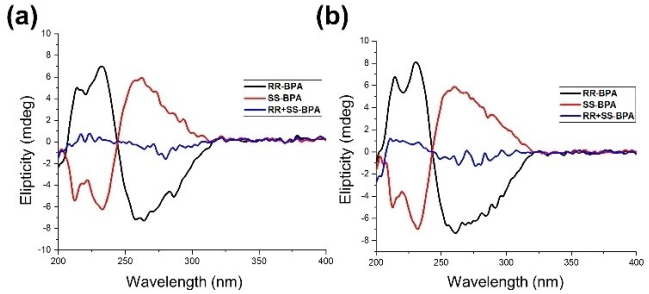

Figure 4. CD spectra of RR-, SS-, and RR + SS-BPA at 0.025 wt/v % in (a) solution state in EtOH and (b) dispersed gel state in EtOH/water (1 : 1 v/v).

Information). The CD spectrum of RR-BPP showed the mirror image of SS-BPP, but the mixed RR + SS-BPP displayed a linear signal, similar to the mixed BPA compound (Figure S12, see Supporting Information).

The CD experiments performed in the dispersed gel state with the BPA gels obtained from ethanol/water (1 : 1, v/v) at 3.0 wt/v % at various concentrations and 0.025 wt/v % was found to be the optimum concentration. We have observed positive signal maxima around 260 nm and negative signal maxima around 232 nm and 214 nm with SS-BPA, and the RR-BPA exhibited the mirror image (Figure 4b and Figure S11, see Supporting Information). The mixed RR + SS-BPA gel displayed a linear signal, which shows the existence of both the enantiomers in the gel state, which cancels out the CD signal.

Single Crystal X-ray Diffraction

The self-assembly modes in multicomponent gels can be analyzed by various spectroscopies[4v,14] and X-ray diffraction techniques.[4m,15] We used single-crystal X-ray diffraction (SCXRD) to elucidate the structural evidence of the co-assembled network in the multicomponent enantiomeric gel.[4h] SCXRD is an excellent tool to correlate the key interactions in the solid-state structure to the gel state, which will help to evaluate the role of these interactions in controlling the self-assembly modes. The self-sorting modes in multicomponent dipeptides gels were confirmed by SCXRD,[16] and X-ray diffraction has been used to get insight into the packing modes of gel fibers of the enantiomers.[17] The crystallization experiments with the four enantiomers and the mixed enantiomeric compounds were performed in various solvents/solvent mixtures. However, we could only isolate X-ray quality single crystals of alanine-based compounds (RR-BPA). Single crystals of RR-BPA were isolated from EtOH/$CHCl_3$ mixture (1 : 1, v/v), and the structural analysis revealed that the compound crystallized in a triclinic *P*1 space group (Table S4 and S5, see Supporting Information) with one BPA molecule in the asymmetric unit (Figure 5a).

One of the oxygen atoms of the alanine ester and the phenyl moieties were found to be disordered. The amide moieties displayed complementary N–H···C=O interactions with adjacent molecules to form a one-dimensional hydrogen-bonded chain (Figure 5b), and these 1-D chains are considered

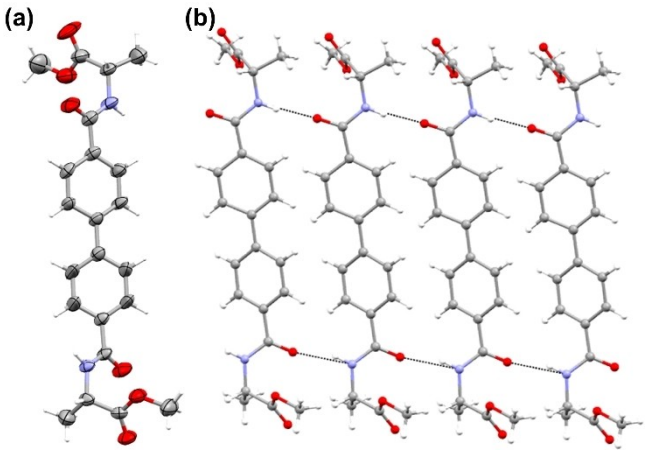

Figure 5. (a) Thermal ellipsoidal plot of RR-BPA, and (b) amide moieties displaying complementary hydrogen bonding via N–H···C=O interactions, disordered atoms are omitted for clarity.

to be one of the crucial parameters for supramolecular gel network formation.[1b]

Powder X-ray Diffraction

Powder X-ray diffraction (PXRD) is an important tool to confirm the phase purity of the material and analyze the molecular packing by comparing the simulated pattern of the single-crystal data with the PXRD pattern of the bulk material or the xerogels.[1b,4h,10b,11,18] PXRD analysis helps to understand the self-assembly in LMWGs, but this method has some flaws due to possible artifacts during the drying process to prepare the xerogels.[10a,19] We have performed PXRD of the bulk materials and xerogels of the enantiomers and mixed compounds. The bulks crystals of the RR-BPA obtained from ethanol (by dissolving 20.0 mg/mL) matched with the simulated pattern of RR-BPA obtained from the crystal structure (Figure S13, see Supporting Information). The PXRD pattern for the bulk crystals and the xerogels from DMSO/water (3 : 2, v/v, 3.0 wt/v %) of both the enantiomers were identical revealing the similarity of the hierarchical assembly in the solid-state and xerogel (Figure S14, see Supporting Information). A slightly different pattern was observed for the xerogels obtained from *p*-xylene (2.6 wt/v %) compared to the bulk crystals but the major peaks were matching with the bulk crystals (Figure S15, see Supporting Information). The comparison of the simulated pattern of RR-BPA with the powder pattern of the xerogels of RR-BPA and mixed RR + SS-BPA from DMSO/water (3 : 2, v/v, 3.0 wt/v %) revealed that the PXRD pattern of the mixed xerogels were not similar to the simulated/enantiomeric xerogels. This indicates the presence of an alternate packing presumably due to the self-assembled network (Figure 6) and similar results were obtained for *p*-xylene xerogels (Figure S16, see Supporting Information).

PXRD experiments performed with the xerogels of enantiomeric BPP compounds in *p*-xylene (3.0 wt/v %) and DMSO/water

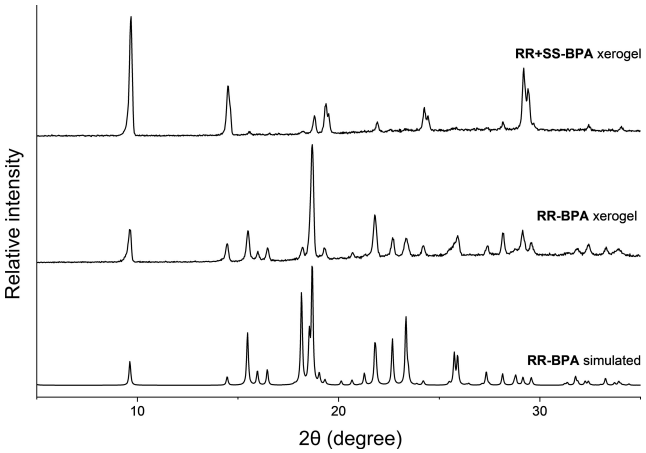

Figure 6. Comparison of simulated pattern RR-BPA with the PXRD pattern of the xerogels of RR-BPA and mixed RR + SS-BPA in DMSO/water (3 : 2, v/v) at 3.0 wt/v %.

(3 : 2, v/v) at 1.8 wt/v % revealed identical powder pattern (Figure S17 and S18, see Supporting Information). However, the mixed RR + SS-BPP xerogel obtained DMSO/water (3 : 2, v/v) at 1.8 wt/v %, displayed a different powder pattern from the enantiomeric xerogels (Figure S17, see Supporting Information) and similar results were observed for *p*-xylene xerogels (3.0 wt/v %, Figure S18, see Supporting Information). This is presumably due to the self-assembled enantiomeric components in the mixed gel leading to a different gel network.

Anion Sensing

Supramolecular gels are an excellent class of stimuli-responsive materials because the gelation process can be turned ON/OFF in the presence of external stimuli such as pH, light, sound, redox, and by the addition of an external entity, for example, salts/ions.[20] The amide moieties are excellent candidates for anions sensing and we have reported the anion sensing properties of LMWGs based on amide moieties.[10b,21] This prompted us to study the stimuli-responsive properties of multicomponent enantiomeric gels towards anions, which will help to evaluate the effect of functional groups on the anion sensing properties. The stimuli-responsive properties of the individual and mixed enantiomeric gels were analyzed by treating the gels with various potassium salts, such as KF, KCl, KBr, KI, KCN, and CH_3CO_2K at MGC. The potassium salts (1.0 equiv.) were added to the BPA compounds (3.0 wt/v %) and BPP compounds (1.8 wt/v %) in DMSO/water mixture (3 : 2, v/v), respectively. The results indicated that the gel network collapsed, resulting in colloids for the individual RR- and SS-BPA compounds. The experiments performed with mixed RR + SS-BPA compounds also resulted in colloids except for KBr and KI salts, where partial gels were observed. Similar results were observed for experiments performed at higher gelator concentrations (4.0 wt/v %) of BPA compounds. The anion sensing studies performed with the individual and mixed BPP compounds (1.8 wt/v %) indicated that the gel network was intact in the presence of anions except for KCN. The effect of anions on the thermal stability of the gel network was analyzed by T_{gel} experiments and the mixed enantiomeric gels were thermally stronger compared to the individual components (Table S6, see Supporting Information). The comparison of T_{gel} values with the corresponding native gels indicated that anions slightly lowered the thermal stability of the gels, which may be attributed to the enhanced solubility of the gelator in the presence of anions. The mechanical strength of the BPP gels was evaluated by performing the frequency sweep experiments in the presence of 1.0 equivalents of potassium salts, which revealed that the enantiomeric gels were more robust than the mixed gels in the presence of anions (Figure S19–S21, see Supporting Information). Analysis of the results revealed that the presence of potassium salts did not show any profound effect on the mechanical strength of the BPP gels except for KCN, where the gel network collapsed. These results indicate that the presence of a hydrophobic phenyl group in BPP gels compared to BPA gels is crucial for generating a robust gel network towards anions.

Conclusions

The self-assembly modes of mixed enantiomeric gels based on bis-(amides) of alanine and phenylalanine with biphenyl linker were analyzed to evaluate the role of non-hydrogen bonding functional groups on gelation properties. Gelation was observed for the individual and mixed gels in various solvent/solvent mixtures. Analysis of the MGC values revealed that the enantiomeric gels of RR- and SS-BPA were slightly less than the equimolar mixed gels, but a reverse trend was observed for the BPP compounds. The sol-gel transition temperature analysis and rheology experiments indicated that the mechanical and thermal strength of the RR- and SS-BPA enantiomeric gels were comparatively more robust than the mixed gel in xylenes. However, the mixed RR + SS-BPA gel displayed better mechanical stabilities in DMSO/water mixtures. These results indicate that the non-hydrogen bonding functional group plays an important role in the physical properties of multicomponent gels. SEM analysis of the dried gels from *p*-xylene revealed that the mixed gels displayed different morphologies compared to the enantiomers, which indicates the formation of co-assembled enantiomers in the mixed gel. The structural analysis of RR-BPA revealed a 1-D hydrogen-bonded chain, which was compared to the PXRD pattern of the xerogels to evaluate the self-assembly modes. The PXRD pattern of the enantiomeric and mixed xerogels of BPP was compared to confirm the self-assembly modes in mixed gels. The stimuli-responsive properties of the individual and mixed enantiomeric gels revealed that the nature of non-hydrogen bonding functional groups play an important role on the gel stability towards anions. This study shows that the elegant choice of functional groups is crucial for generating multicomponent gels with tunable properties. These results will provide a better understanding of the role of non-hydrogen bonding functional groups on gelation properties,

which will help supramolecular chemists to design LMWGs with specific functional groups to develop multicomponent systems with predictable properties.

Experimental Section

The precursors for organic reactions, reagents and solvents were commercially available (TCI-Europe, Fluorochem and Sigma-Aldrich) and were used as received. The circular dichroism and gelation experiments were performed in freshly distilled ethanol and deionized water. The enantiomeric methyl ester hydrochloride salts of alanine and phenylalanine were synthesized using the reported procedure.[22] Bruker AVANCE 400 spectrometer was used to record the NMR spectra (^{1}H and ^{13}C NMR) (Figure S22–S29, see Supporting Information). The mechanical stability of the gels was evaluated in MCR 302 modular compact rheometer from Anton Paar, and circular dichroism (CD) experiments were performed using JASCO J-1100 CD spectrometer. The morphologies of the dried gels (xerogel) were analyzed using a scanning electron microscope (SEM) with a Leo Supra 25 Microscope, and powder X-ray diffraction (PXRD) was performed on a Malvern Panalytical diffractometer.

Synthesis

General procedure. Biphenyl-4,4′-dicarboxylic acid (1.0 g, 4.1 mmol) was taken in a two-neck RB flask and 10.0 mL (137.8 mmol) thionyl chloride was added, and a catalytic amount of dry DMF (2.0–3.0 drops) was added later. The reaction mixture was refluxed for 12 hours, cooled to room temperature, and evaporated to dryness by distillation to yield the acid chloride, which was used in the subsequent step without any further purification. The corresponding methyl ester hydrochloride (*S* or *R*) of alanine/phenylalanine (8.4 mmol) and 50.0 mL of $CHCl_3$ were added into this RB flask at 0 °C under a dinitrogen atmosphere. A solution of $CHCl_3$ (40.0 mL) with triethylamine (16.4 mmol) was added dropwise to the mixture and was stirred at room temperature for 12.0 hours before being heated to 60 °C for 2.0 hours. It was concentrated, and DCM (50.0 mL) was added and washed with 3.0% $NaHCO_3$ (2×40.0 mL) and 0.05 M HCl (2×40.0 mL), followed by brine. Dried Na_2SO_4 was used to dry the organic layer, and the mixture was filtered and evaporating the solution yielded the desired bis-(amide) as a white solid.

RR-BPA. Yield 1.48 g, 87.6%. ^{1}H NMR (400 MHz, Chloroform-*d*) δ 7.93–7.83 (m, 4H), 7.69–7.62 (m, 4H), 6.85 (d, *J* = 7.3 Hz, 2H), 4.89–4.76 (m, 2H), 3.80 (s, 6H), 1.55 (d, *J* = 7.1 Hz, 6H). ^{13}C {^{1}H} NMR (100 MHz, Chloroform-*d*) δ 173.85, 166.44, 143.34, 133.39, 127.86, 127.47, 52.76, 48.67, 18.79. HRMS (APCI): calcd. for $C_{22}H_{24}N_2O_6Na$ [M + Na]$^+$, 435.1527; found, 435.1511.

SS-BPA. Yield 1.50 g, 88.8%. ^{1}H NMR (400 MHz, Chloroform-*d*) δ 7.93–7.83 (m, 4H), 7.69–7.59 (m, 4H), 6.85 (d, *J* = 7.3 Hz, 2H), 4.89–4.76 (m, 2H), 3.80 (s, 6H), 1.55 (d, *J* = 7.3 Hz, 6H).^{13}C {^{1}H} NMR (100 MHz, Chloroform-*d*) δ 173.86, 166.44, 143.34, 133.39, 127.86, 127.47, 52.76, 48.67, 18.78. HRMS (APCI): calcd. for $C_{22}H_{24}N_2O_6Na$ [M + Na]$^+$, 435.1527; found, 435.1520.

RR-BPP. Yield 1.85 g, 79.7%. ^{1}H NMR (400 MHz, Chloroform-*d*) δ 7.85–7.77 (m, 4H), 7.68–7.61 (m, 4H), 7.35–7.21 (m, 6H), 7.18–7.08 (m, 4H), 6.65 (d, *J* = 7.6 Hz, 2H), 5.16–5.07 (m, 2H), 3.78 (s, 6H), 3.37–3.18 (m, 4H). ^{13}C {^{1}H} NMR (100 MHz, Chloroform-*d*) δ 172.18, 166.44, 143.40, 135.95, 133.38, 129.48, 128.79, 127.82, 127.53, 127.38, 53.69, 52.61, 38.03. HRMS (APCI): calcd. for $C_{34}H_{32}N_2O_6Na$ [M + Na]$^+$, 587.2153; found, 587.2140.

SS-BPP. Yield 1.93 g, 83.2%. ^{1}H NMR (400 MHz, Chloroform-*d*) δ 7.87–7.79 (m, 4H), 7.72–7.63 (m, 4H), 7.37–7.23 (m, 6H), 7.20–7.10 (m, 4H), 6.66 (d, *J* = 7.6 Hz, 2H), 5.18–5.07 (m, 2H), 3.80 (s, 6H), 3.37–3.24 (m, 4H).^{13}C {^{1}H} NMR (100 MHz, Chloroform-*d*) δ 172.18, 166.44, 143.41, 135.94, 133.38, 129.48, 128.80, 127.82, 127.53, 127.38, 53.69, 52.61, 38.03. HRMS (APCI): calcd. for $C_{34}H_{32}N_2O_6Na$ [M + Na]$^+$, 587.2153; found, 587.2137.

Gelation Details

Gelation Test. The necessary quantity of gelator was charged into a standard vial (7.0 mL) with an inner diameter of 1.5 cm along with 1.0 mL of solvent. The mixed RR + SS compounds were prepared by adding an equimolar ratio of individual RR- and SS-compounds, and the solvent/solvent mixture was added. The vial was sealed, heated slowly, and gently shaken to produce a clear solution, and the solution was left undisturbed. After 24.0 hours, an inversion test was carried out to verify the gel formation.

Minimum Gelator Concentration (MGC). Following the above technique, the gel was prepared by dissolving the corresponding compound in the solvent/solvent mixture (1.0 mL). The solvent was added in increments, the heating-cooling cycle was repeated, and the sample vial was inverted after 24.0 h to ensure there was no solvent dropping off from the gel. This was repeated until a small quantity of the solvent/solvent mixture was visible on the gel surface, and the concentration slightly above this point at which a stable gel was detected after one day was noted as the MGC.

T_{gel} Experiment. An appropriate amount of the gelator and the solvent (1.0 mL) were charged into a standard vial (7.0 mL). The mixture was sonicated and heated to produce a transparent solution, then left undisturbed to gel. After 24 hours, a tiny spherical glass ball (100.0 mg) was gently placed on the top surface of the gel. The vial was then sealed and submerged into an oil bath with a temperature sensor and magnetic stirrer. The oil bath temperature was gradually raised (~10 °C per minute), and the temperature when the glass ball reached the bottom of the standard vial was noted as T_{gel}.

Rheology

The mechanical strengths of gels from DMSO/water (1:1, and 3:2, v/v, respectively) and *p*-xylene were determined using a stainless-steel parallel plate geometry design in MCR 102 Anton Paar modular compact rheometer. Rheological experiments were performed at a gap height of 1.0 mm. Gels of RR- and SS-BPA were prepared at 40.0 mg of the corresponding gelator in 1.0 mL of DMSO/water (1:1, v/v) and at 30.0 mg in DMSO/water (3:2, v/v). The RR + SS-BPA gel in DMSO/water (1:1, v/v) was prepared by dissolving a mixture of 20.0 mg of RR-BPA and SS-BPA in 1.0 mL of the solvent mixture and 15.0 mg of RR-BPA and SS-BPA were used for 3:2 DMSO/water (v/v) mixture. In a similar manner, gels were prepared with RR-, SS-, and equimolar RR + SS-BPP in *p*-xylene at 3.0 wt/v% and in DMSO/water (3:2, v/v) at 1.8 wt/v%. The measurements were carried out by scoping the gel (~1.0 mL portion) on the parallel plate. At a constant temperature of 20.0 °C, oscillatory measurements were performed to analyze the viscoelastic properties. Amplitude sweeps were performed between the log ramp strain (γ) = 0.01–100% at a constant frequency (1.0 Hz), while the frequency sweeps were determined within the linear viscoelasticity domain (0.02% strain) between 0.1 and 10.0 Hz. We have used the Peltier temperature control hood to maintain the temperature at 20.0 °C and to avoid evaporation during frequency/amplitude sweeps.

Scanning Electron Microscopy (SEM)

We have prepared gels with enantiomeric compounds in *p*-xylene (2.7 wt/v%) and mixed compounds of BPA in *p*-xylene (3.5 wt/v%) and DMSO/water (1:1, v/v, 4.0 wt/v%). Gels with BPP compounds were made from *p*-xylene (3.0 wt/v%), and in 1:1, v/v DMSO/water at 1.2 wt/v% and at 1.8 wt/v% in 3:2, v/v DMSO/water. All the gels obtained were filtered after a span of 24 h. After air-drying for a certain period, a small part of the xerogel was placed on a pin mount with the carbon tab on top and coated with gold for 2.0–3.0 min for about 12–15 nm thickness. Dried gel morphologies were investigated on a Leo Supra 25 microscope with an in-lens detector at 3.0 kV and a 3.0–4.0 mm working distance.

Circular Dichroism (CD)

A JASCO J-1100 CD spectrometer was used to collect the data in a continuous scanning mode with a wavelength range of 200 to 400 nm at 50.0 nm/minute rate and 1.0 nm bandwidth. The solution state experiments with RR-, and SS-, BPA/BPP were performed by dissolving 10.0 mg of the corresponding compound in 3.0 mL of absolute ethanol, while the equimolar RR+SS- BPA/BPP was prepared by dissolving 5.0 mg of each enantiomer in 3.0 mL of absolute ethanol. The experiments were performed at various concentrations (0.025, 0.03, and 0.035 wt/v%), and the best results were obtained at 0.025 wt/v%, which was taken as the optimum concentration. The dispersed gel state CD experiments were also performed with BPA compounds at an optimum concentration of 0.025 wt/v%, and mixed BPP compounds did not form gel in EtOH/water.

Single Crystal X-ray Diffraction (SCXRD)

A Bruker D8 Venture diffractometer with a Photon100 CMOS detector and Cryostream (Oxford Cryosystems) open-flow nitrogen cryostats was used for the X-ray study. X-ray quality crystals were isolated and immersed in a paratone oil and then mounted. The apex-III software was used to determine the unit cell, gather data, reduce data, solve/fine-tune the structure, and correct the empirical absorption (Bruker AXS: Madison, WI, 2015). The structures were resolved using the direct methods, and all data were then refined using SHELXTL's full-matrix least squares on $F^{2,}$ and anisotropic refinement was performed on every non-disordered atom other than hydrogen atoms. The disordered atoms were refined using free variable (FVAR) and all hydrogen atoms were put in their calculated locations and refined using a riding model.

Deposition Number 2255444 (for RR-BPA), contains the supplementary crystallographic data for this paper. These data are provided free of charge by the joint Cambridge Crystallographic Data Centre and Fachinformationszentrum Karlsruhe Access Structures service.

Powder X-ray Diffraction (PXRD)

We have performed PXRD on the bulk crystals of enantiomeric (RR- and SS-BPA) obtained from ethanol (by dissolving 20.0 mg/mL). PXRD analysis was performed on the enantiomeric (RR- and SS-BPA) and mixed RR+SS-BPA obtained from the corresponding gels made in DMSO/water (3:2, v/v) at 3.0 wt/v% and with the xerogels of RR-, and SS-BPA obtained from *p*-xylene at 2.7 wt/v% and 3.5 wt/v% with RR+SS-BPA. In a similar manner, Gels were prepared with RR-, SS-, and equimolar RR+SS-BPP in *p*-xylene at 3.0 wt/v% and at 1.8 wt/v% DMSO/water (3:2, v/v) to obtain the corresponding xerogels. A Panalytical instrument with Cu anode with 2θ ranging from 4.0 to 50.0° and 0.025° step size was used for the PXRD analysis.

Anion Sensing

Anion sensing studies were performed in DMSO/water mixture (3:2, v/v) for both the BPP and BPA compounds. The individual and mixed enantiomeric compounds of BPP (18.0 mg) and BPA (30.0 or 40.0 mg) were taken in a 7.0 mL standard vial and DMSO (600 μL) was added to dissolve the gelator, followed by the addition of 1.0 equivalents of corresponding potassium salts in water (400 μL). The vial was sealed, and gently heated to obtain a clear solution, and was left undisturbed for a period of 24.0 hours. A vial inversion test was performed to check the effect of anions on gelation. T_{gel} and rheological experiments were performed with the BPP gels after a span of 24.0 hours.

Acknowledgements

This research was funded by the Icelandic Research Fund (IRF-228902-051), Rannís Iceland and the University of Iceland Research Fund. We thank Dr. Sigríður Jónsdóttir Jónsdóttir and Dr, Fridrik Magnus from the University of Iceland for NMR and mass spectrometry, powder X-ray diffraction analysis, and the Biochemistry department for the circular dichroism investigations. S.S.J. is thankful to the University of Iceland for the doctoral research grant. We thank Rannís Iceland infrastructure funds (150998-0031 and 191763-0031) for a single crystal X-ray diffractometer and rheometer.

Conflict of Interests

The authors declare no conflict of interest.

Data Availability Statement

The data that support the findings of this study are available in the supplementary material of this article.

Keywords: amino acids · enantiomers · multicomponent gels · self-assembly · sensing

[1] a) S. Banerjee, R. K. Das, U. Maitra, *J. Mater. Chem.* **2009**, *19*, 6649–6687; b) P. Dastidar, *Chem. Soc. Rev.* **2008**, *37*, 2699–2715; c) M. de Loos, B. L. Feringa, J. H. van Esch, *Eur. J. Org. Chem.* **2005**, *2005*, 3615–3631; d) L. A. Estroff, A. D. Hamilton, *Chem. Rev.* **2004**, *104*, 1201–1218; e) M. George, R. G. Weiss, *Acc. Chem. Res.* **2006**, *39*, 489–497; f) D. K. Kumar, J. W. Steed, *Chem. Soc. Rev.* **2014**, *43*, 2080–2088; g) P. R. A. Chivers, D. K. Smith, *Nat. Rev. Mater.* **2019**, *4*, 463–478.

[2] a) Y. Li, Y. Liu, R. Ma, Y. Xu, Y. Zhang, B. Li, Y. An, L. Shi, *ACS Appl. Mater. Interfaces* **2017**, *9*, 13056–13067; b) C. T. S. Wong Po Foo, J. S. Lee, W. Mulyasasmita, A. Parisi-Amon, S. C. Heilshorn, *Proc. Natl. Acad. Sci. USA* **2009**, *106*, 22067–22072; c) E. R. Cross, S. Sproules, R. Schweins, E. R. Draper, D. J. Adams, *J. Am. Chem. Soc.* **2018**, *140*, 8667–8670; d) M. Zhou, A. M. Smith, A. K. Das, N. W. Hodson, R. F. Collins, R. V. Ulijn, J. E. Gough, *Biomaterials* **2009**, *30*, 2523–2530; e) E. V. Alakpa, V. Jayawarna, A. Lampel, K. V. Burgess, C. C. West, S. C. J. Bakker, S. Roy, N. Javid, S. Fleming, D. A. Lamprou, J. Yang, A. Miller, A. J. Urquhart, P. W. J. M. Frederix, N. T. Hunt, B. Péault, R. V. Ulijn, M. J. Dalby, *Chem* **2016**, *1*, 298–319.

[3] a) L. E. Buerkle, S. J. Rowan, *Chem. Soc. Rev.* **2012**, *41*, 6089–6102; b) C.-W. Chu, C. A. Schalley, *Org. Mater.* **2021**, *03*, 025–040; c) J. Raeburn, D. J.

Adams, *Chem. Commun.* **2015**, *51*, 5170–5180; d) D. K. Smith, *Chem. Soc. Rev.* **2009**, *38*, 684–694.
[4] a) R. J. Swanekamp, J. J. Welch, B. L. Nilsson, *Chem. Commun.* **2014**, *50*, 10133–10136; b) A. K. Patterson, L. H. El-Qarra, D. K. Smith, *Chem. Commun.* **2022**, *58*, 3941–3944; c) X. Yang, H. Lu, Y. Tao, H. Zhang, H. Wang, *J. Nanobiotechnol.* **2022**, *20*, 77; d) R. K. Das, R. Kandanelli, J. Linnanto, K. Bose, U. Maitra, *Langmuir* **2010**, *26*, 16141–16149; e) R. J. Swanekamp, J. T. DiMaio, C. J. Bowerman, B. L. Nilsson, *J. Am. Chem. Soc.* **2012**, *134*, 5556–5559; f) T. Koga, M. Matsuoka, N. Higashi, *J. Am. Chem. Soc.* **2005**, *127*, 17596–17597; g) A. R. Hirst, D. K. Smith, M. C. Feiters, H. P. Geurts, *Chem. Eur. J.* **2004**, *10*, 5901–5910; h) D. Ghosh, A. D. Farahani, A. D. Martin, P. Thordarson, K. K. Damodaran, *Chem. Mater.* **2020**, *32*, 3517–3527; i) K. Nagy-Smith, P. J. Beltramo, E. Moore, R. Tycko, E. M. Furst, J. P. Schneider, *ACS Cent. Sci.* **2017**, *3*, 586–597; j) X. Zhu, Y. Li, P. Duan, M. Liu, *Chem. Eur. J.* **2010**, *16*, 8034–8040; k) Z. Liu, J. Sun, Y. Zhou, Y. Zhang, Y. Wu, S. K. M. Nalluri, Y. Wang, A. Samanta, C. A. Mirkin, G. C. Schatz, *J. Org. Chem.* **2016**, *81*, 2581–2588; l) H. Li, L. Han, Q. Li, H. Lai, P. Fernández-Trillo, L. Tian, F. He, *Macromol. Rapid Commun.* **2022**, *43*, 2100690; m) K. McAulay, B. Dietrich, H. Su, M. T. Scott, S. Rogers, Y. K. Al-Hilaly, H. Cui, L. C. Serpell, A. M. Seddon, E. R. Draper, *Chem. Sci.* **2019**, *10*, 7801–7806; n) K. J. Nagy, M. C. Giano, A. Jin, D. J. Pochan, J. P. Schneider, *J. Am. Chem. Soc.* **2011**, *133*, 14975–14977; o) B. W. Messmore, P. A. Sukerkar, S. I. Stupp, *J. Am. Chem. Soc.* **2005**, *127*, 7992–7993; p) B. Adhikari, J. Nanda, A. Banerjee, *Soft Matter* **2011**, *7*, 8913–8922; q) S. Cicchi, G. Ghini, L. Lascialfari, A. Brandi, F. Betti, D. Berti, P. Baglioni, L. Di Bari, G. Pescitelli, M. Mannini, *Soft Matter* **2010**, *6*, 1655–1661; r) L. Lascialfari, G. Pescitelli, A. Brandi, M. Mannini, D. Berti, S. Cicchi, *Soft Matter* **2015**, *11*, 8333–8341; s) D. A. Tómasson, D. Ghosh, Z. Kržišnik, L. H. Fasolin, A. A. Vicente, A. D. Martin, P. Thordarson, K. K. Damodaran, *Langmuir* **2018**, *34*, 12957–12967; t) Z. Yang, G. Liang, M. Ma, Y. Gao, B. Xu, *J. Mater. Chem.* **2007**, *17*, 850–854; u) J.-S. Shen, G.-J. Mao, Y.-H. Zhou, Y.-B. Jiang, H.-W. Zhang, *Dalton Trans.* **2010**, *39*, 7054–7058; v) J. A. Foster, R. M. Edkins, G. J. Cameron, N. Colgin, K. Fucke, S. Ridgeway, A. G. Crawford, T. B. Marder, A. Beeby, S. L. Cobb, J. W. Steed, *Chem. Eur. J.* **2014**, *20*, 279–291.
[5] S. Panja, B. Dietrich, A. J. Smith, A. Seddon, D. J. Adams, *ChemSystemsChem* **2022**, *4*, e202200008.
[6] a) S. Fleming, S. Debnath, P. W. J. M. Frederix, N. T. Hunt, R. V. Ulijn, *Biomacromolecules* **2014**, *15*, 1171–1184; b) A. S. W. Chan, P. R. Sundararajan, *ChemistrySelect* **2017**, *2*, 1149–1157; c) J. N. Loos, F. D'Acierno, U. Vijay Mody, M. J. MacLachlan, *ChemPlusChem* **2022**, *87*, e202200026.
[7] M. Suzuki, K. Hanabusa, *Chem. Soc. Rev.* **2009**, *38*, 967–975.
[8] a) S. S. Babu, V. K. Praveen, A. Ajayaghosh, *Chem. Rev.* **2014**, *114*, 1973–2129; b) L. Zhang, Q. Jin, M. Liu, *Chem. Asian J.* **2016**, *11*, 2642–2649.
[9] a) J. W. Goodwin, R. W. Hughes, *Rheology for chemists: an introduction*, Royal Society of Chemistry **2008**; b) J.-M. Guenet, *Organogels: Thermodynamics, structure, solvent role, and properties*, Springer **2016**.
[10] a) S. S. Jayabhavan, J. W. Steed, K. K. Damodaran, *Cryst. Growth Des.* **2021**, *21*, 5383–5393; b) S. S. Jayabhavan, B. Kristinsson, D. Ghosh, C. Breton, K. K. Damodaran, *Gels* **2023**, *9*, 89.
[11] G. Yu, X. Yan, C. Han, F. Huang, *Chem. Soc. Rev.* **2013**, *42*, 6697–6722.
[12] G. Gottarelli, S. Lena, S. Masiero, S. Pieraccini, G. P. Spada, *Chirality* **2008**, *20*, 471–485.
[13] a) S.-Y. Qin, Y. Pei, X.-J. Liu, R.-X. Zhuo, X.-Z. Zhang, *J. Mater. Chem. B* **2013**, *1*, 668–675; b) S. Shin, S. Lim, Y. Kim, T. Kim, T.-L. Choi, M. Lee, *J. Am. Chem. Soc.* **2013**, *135*, 2156–2159.
[14] a) P. Xing, H. P. Tham, P. Li, H. Chen, H. Xiang, Y. Zhao, *Adv. Sci.* **2018**, *5*, 1700552; b) M. Halperin-Sternfeld, M. Ghosh, R. Sevostianov, I. Grigoriants, L. Adler-Abramovich, *Chem. Commun.* **2017**, *53*, 9586–9589; c) G. Fichman, T. Guterman, L. Adler-Abramovich, E. Gazit, *CrystEngComm* **2015**, *17*, 8105–8112; d) M. M. Smith, D. K. Smith, *Soft Matter* **2011**, *7*, 4856–4860; e) D. Li, Y. Shi, L. Wang, *Chin. J. Chem.* **2014**, *32*, 123–127; f) A. Das, S. Ghosh, *Chem. Commun.* **2011**, *47*, 8922–8924; g) K. L. Morris, L. Chen, J. Raeburn, O. R. Sellick, P. Cotanda, A. Paul, P. C. Griffiths, S. M. King, R. K. O'Reilly, L. C. Serpell, D. J. Adams, *Nat. Commun.* **2013**, *4*, 1480; h) S. Onogi, H. Shigemitsu, T. Yoshii, T. Tanida, M. Ikeda, R. Kubota, I. Hamachi, *Nat. Chem.* **2016**, *8*, 743.
[15] a) Z. Džolić, K. Wolsperger, M. Žinić, *New J. Chem.* **2006**, *30*, 1411–1419; b) H. Shigemitsu, T. Fujisaku, W. Tanaka, R. Kubota, S. Minami, K. Urayama, I. Hamachi, *Nat. Nanotechnol.* **2018**, *13*, 165–172; c) E. R. Draper, D. J. Adams, *Chem. Soc. Rev.* **2018**, *47*, 3395–3405.
[16] C. Colquhoun, E. R. Draper, E. G. B. Eden, B. N. Cattoz, K. L. Morris, L. Chen, T. O. McDonald, A. E. Terry, P. C. Griffiths, L. C. Serpell, D. J. Adams, *Nanoscale* **2014**, *6*, 13719–13725.
[17] J. R. Engstrom, A. J. Savyasachi, M. Parhizkar, A. Sutti, C. S. Hawes, J. M. White, T. Gunnlaugsson, F. M. Pfeffer, *Chem. Sci.* **2018**, *9*, 5233–5241.
[18] a) D. Ghosh, R. Bjornsson, K. K. Damodaran, *Gels* **2020**, *6*, 41; b) D. A. Tómasson, D. Ghosh, M. R. P. Kurup, M. T. Mulvee, K. K. Damodaran, *CrystEngComm* **2021**, *23*, 617–628; c) D. Ghosh, I. Lebedytė, D. S. Yufit, K. K. Damodaran, J. W. Steed, *CrystEngComm* **2015**, *17*, 8130–8138.
[19] a) D. J. Adams, *Gels* **2018**, *4*, 32; b) S. Sudhakaran Jayabhavan, D. Ghosh, K. K. Damodaran, *Molecules* **2021**, *26*, 6420.
[20] a) S. Panja, D. J. Adams, *Chem. Soc. Rev.* **2021**, *50*, 5165–5200; b) M.-O. M. Piepenbrock, G. O. Lloyd, N. Clarke, J. W. Steed, *Chem. Rev.* **2010**, *110*, 1960–2004.
[21] a) D. Ghosh, Deepa, K. K. Damodaran, *Supramol. Chem.* **2020**, *32*, 276–286; b) A. Ghosh, P. Das, R. Kaushik, K. K. Damodaran, D. A. Jose, *RSC Adv.* **2016**, *6*, 83303–83311.
[22] a) T. P. Day, D. Sil, N. M. Shukla, A. Anbanandam, V. W. Day, S. A. David, *Mol. Pharm.* **2011**, *8*, 297–301; b) B. Kaptein, W. L. Noorduin, H. Meekes, W. J. P. van Enckevort, R. M. Kellogg, E. Vlieg, *Angew. Chem. Int. Ed.* **2008**, *47*, 7226–7229.

Manuscript received: June 23, 2023
Revised manuscript received: July 3, 2023
Accepted manuscript online: July 5, 2023
Version of record online: ■■, ■■

ChemPlusChem

Supporting Information

The Role of Functional Groups in Tuning the Self-Assembly Modes and Physical Properties of Multicomponent Gels

Sreejith Sudhakaran Jayabhavan, Geethanjali Kuppadakkath, and Krishna K. Damodaran*

Table of Contents

1. Gelation studies

Figure S1. Photos of individual (RR- & SS-) and mixed (RR+SS-) gels of BPA and BPP compounds obtained from *p*-xylene.

Table S1. Gelation Experiments

Solvent	Gelation test at 1.0 wt/v%					
	RR-BPA	**SS-BPA**	**RR+SS-BPA**	**RR-BPP**	**SS-BPP**	**RR+SS-BPP**
Methanol	Ppt	Ppt	Ppt	Ppt	Ppt	Ppt
Ethanol	Ppt	Ppt	Ppt	Ppt	Ppt	Ppt
p-xylene	G^{*}	G^{*}	G^{**}	$G^{\$}$	$G^{\$}$	G^{*}
m-xylene	G^{*}	G^{*}	G^{**}	$G^{\$}$	$G^{\$}$	$G^{\$\$}$
o-xylene	$G^{\$}$	$G^{\$}$	$G^{\#}$	$G^{\#\#}$	$G^{\#\#}$	$G^{\$}$
toluene	C	C	C	Ppt	Ppt	Ppt
mesitylene	$G^{\$}$	$G^{\$}$	$G^{\#}$	$G^{\$}$	$G^{\$}$	$G^{\$}$
Ethanol/water (1:1, v/v)	$G^{\$}$	$G^{\$}$	$G^{\$}$	I	I	I
DMF/water (1:1, v/v)	$G^{\$}$	$G^{\$}$	$G^{\$}$	G	G	I
DMSO/water (1:1, v/v)	$G^{\$}$	$G^{\$}$	$G^{\$}$	G	G	I
DMSO/water (3:2, v/v)	$G^{\$}$	$G^{\$}$	$G^{\$}$	G^	G^	G^

Ppt = precipitate, G= gel, C= colloid, I= insoluble, G^{*}= 2.6 wt/v%, G^{**}= 3.5 wt/v%, $G^{\$}$= 3.0 wt/v%, $G^{\$\$}$= 2.2 wt/v%, $G^{\#}$= 4.0 wt/v%, $G^{\#\#}$= 5.0 wt/v% and G^= 2.0 wt/v%.

Table S2. Determination of Minimum Gel Concentration (MGC)

Solvent	MGC (wt/v%)					
	RR-BPA	**SS-BPA**	**RR+SS-BPA**	**RR-BPP**	**SS-BPP**	**RR+SS-BPP**
p-xylene	2.5	2.5	2.9	3.0	3.0	2.5
m-xylene	2.5	2.5	2.9	3.0	3.0	2.2
o-xylene	2.8	2.9	3.6	5.0	5.0	2.5
mesitylene	3.0	2.9	3.8	2.5	2.5	2.0
ethanol/water (1:1, v/v)	2.7	2.7	2.9	----	----	----
DMF/water (1:1, v/v)	3.0	3.0	3.0	1.0	0.9	----
DMSO/water (1:1, v/v)	2.7	2.7	2.8	0.9	0.9	----
DMSO/water (3:2, v/v)	2.8	2.8	2.8	1.2	1.2	1.8

Table S3. Determination of Sol-gel Transition Temperature (T_{gel})

Solvent	T_{gel} (°C)					
	RR-BPA	**SS-BPA**	**RR+SS-BPA**	**RR-BPP**	**SS-BPP**	**RR+SS-BPP**
p-xylene	142.8*	143.9*	139.9**	108.6$^{\$}$	110.1$^{\$}$	138.2$^{\$}$
m-xylene	138.4*	138.4*	137.9**	106.3$^{\$}$	104.9$^{\$}$	142.1$^{\$}$
o-xylene	144.7$^{\$}$	146.5$^{\$}$	140.9$^{\$\$}$	----	----	----
mesitylene	----	----	----	118.2$^{\$}$	117.1$^{\$}$	150.2$^{\$}$
DMSO/water (1:1, v/v)	121.3$^{\$\$}$	120.9$^{\$\$}$	120.6$^{\$\$}$	----	----	----
DMSO/water (3:2, v/v)	91.1$^{\$}$	92.3$^{\$}$	89.9$^{\$}$	107.3$^{\#}$	108.2$^{\#}$	121.6$^{\#}$

*= 2.7 wt/v%, **= 3.2 wt/v%, $^{\$}$= 3.0 wt/v%, $^{\$\$}$= 4.0 wt/v%, $^{\#}$= 1.8 wt/v%.

2. Rheology

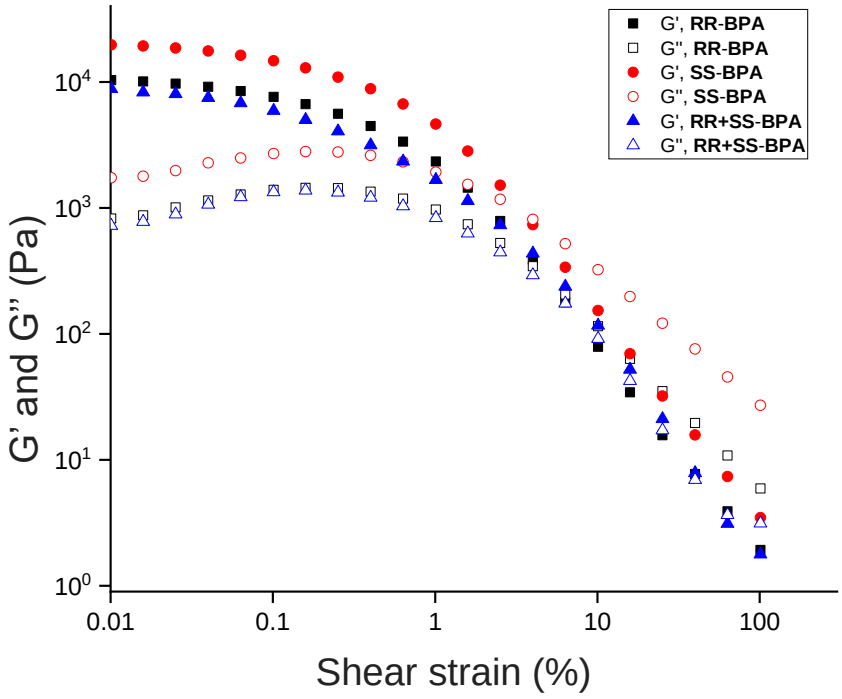

Figure S2. Strain sweep experiments with RR- and SS-BPA (2.6 wt/v%) and RR+SS-BPA (3.5 wt/v%) in *p*-xylene at a constant frequency of 1.0 Hz at 20.0 °C.

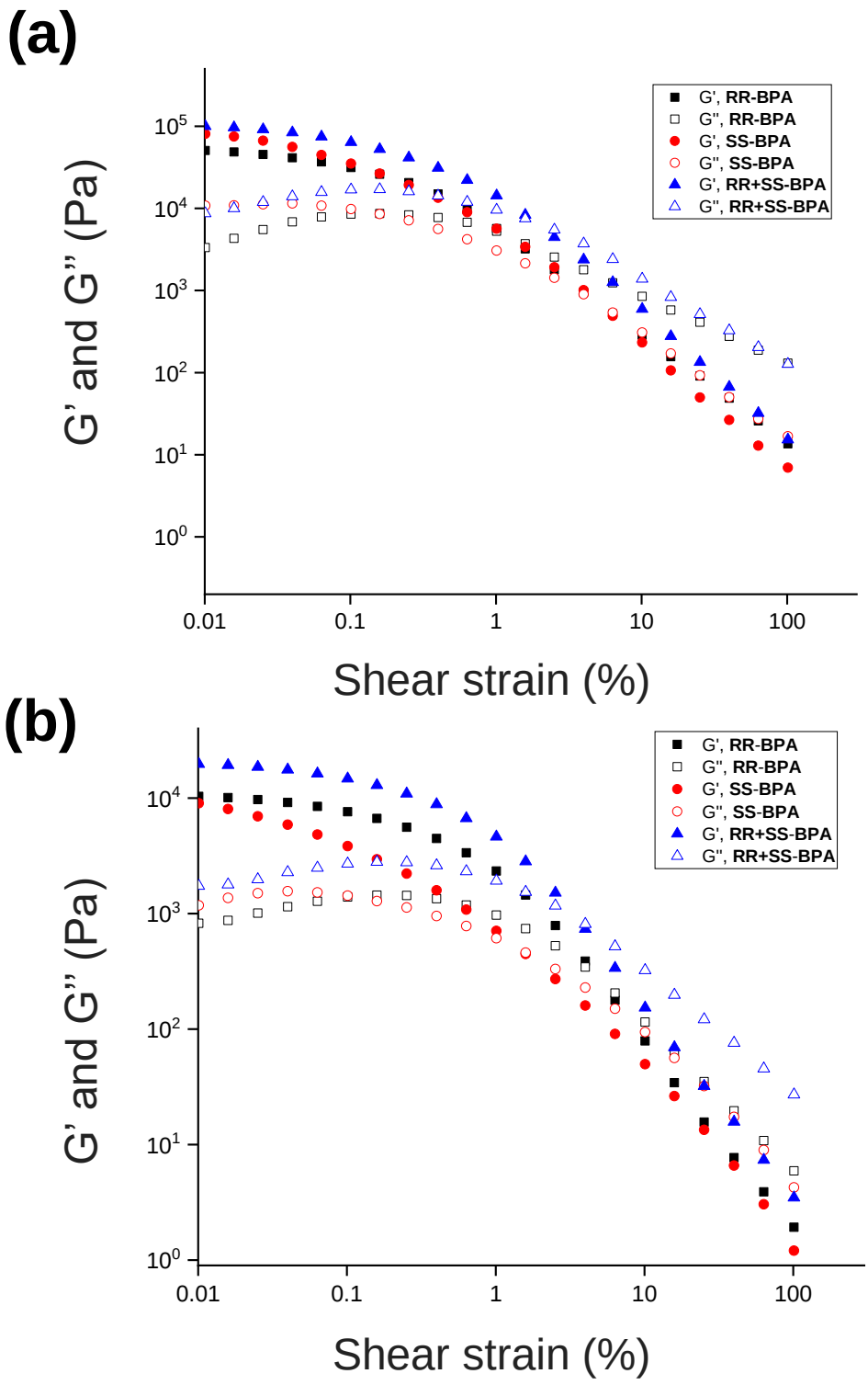

Figure S3. Strain sweep experiments at 20.0 °C with BPA compounds in DMSO/water (a) at 4.0 wt/v% (1:1, v/v), and (b) at 3.0 wt/v% (3:2, v/v), measured at a constant frequency of 1.0 Hz.

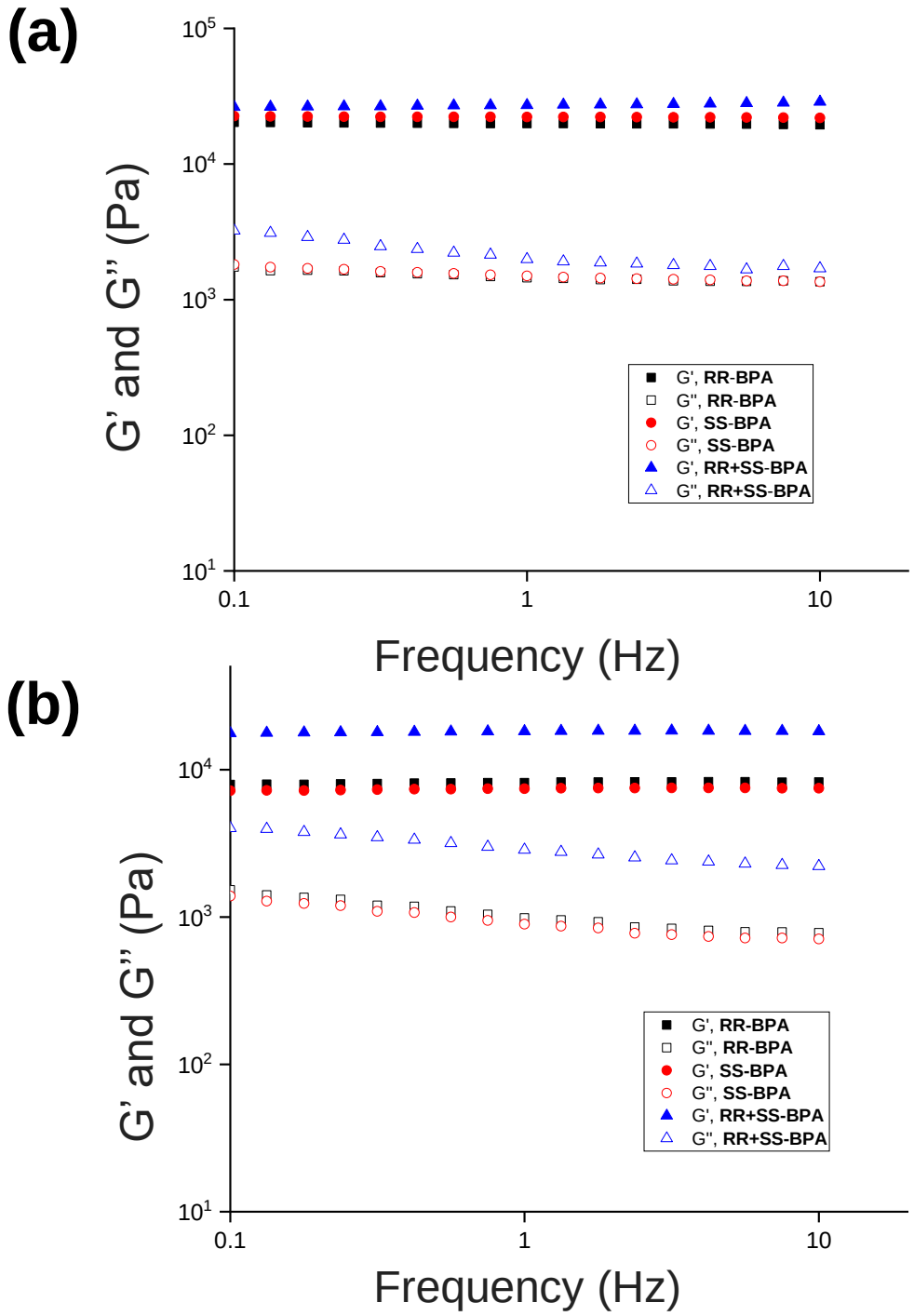

Figure S4. Frequency sweep experiments at 20.0 °C with BPA compounds in DMSO/water (a) at 4.0 wt/v% (1:1, v/v), and (b) at 3.0 wt/v% (3:2, v/v), measured at a constant strain of 0.02%.

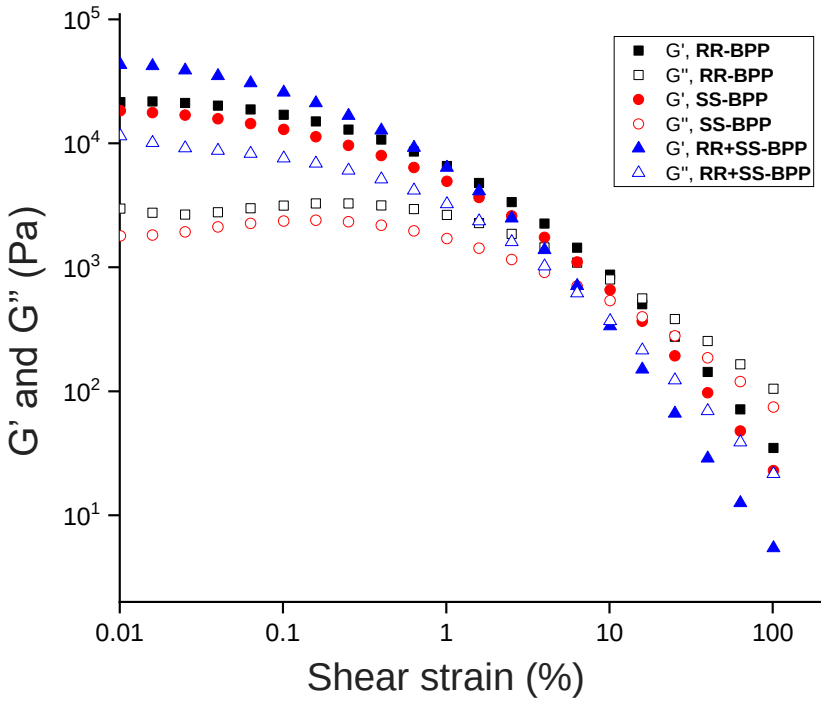

Figure S5. Strain sweep experiments with gels of BPP compounds (3.0 wt/v%) in *p*-xylene at 20.0 °C measured at a constant frequency of 1.0 Hz.

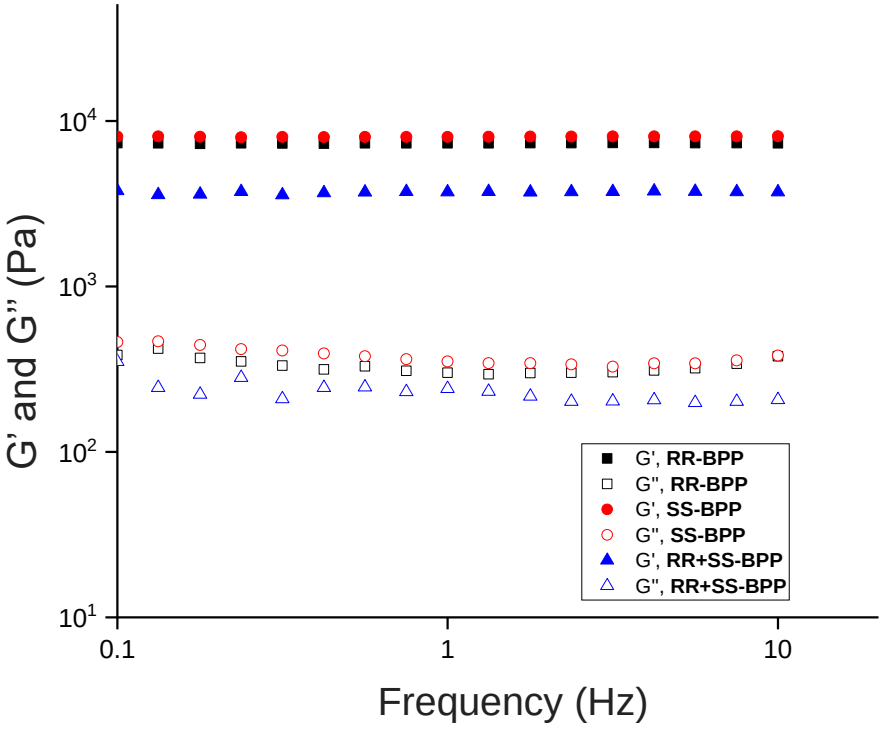

Figure S6. Frequency sweep experiments with gels of BPP compounds at 1.8 wt/v% in DMSO/water (3:2, v/v) at 20.0 °C measured at a constant strain of 0.02 %.

3. Scanning Electron Microscopy (SEM)

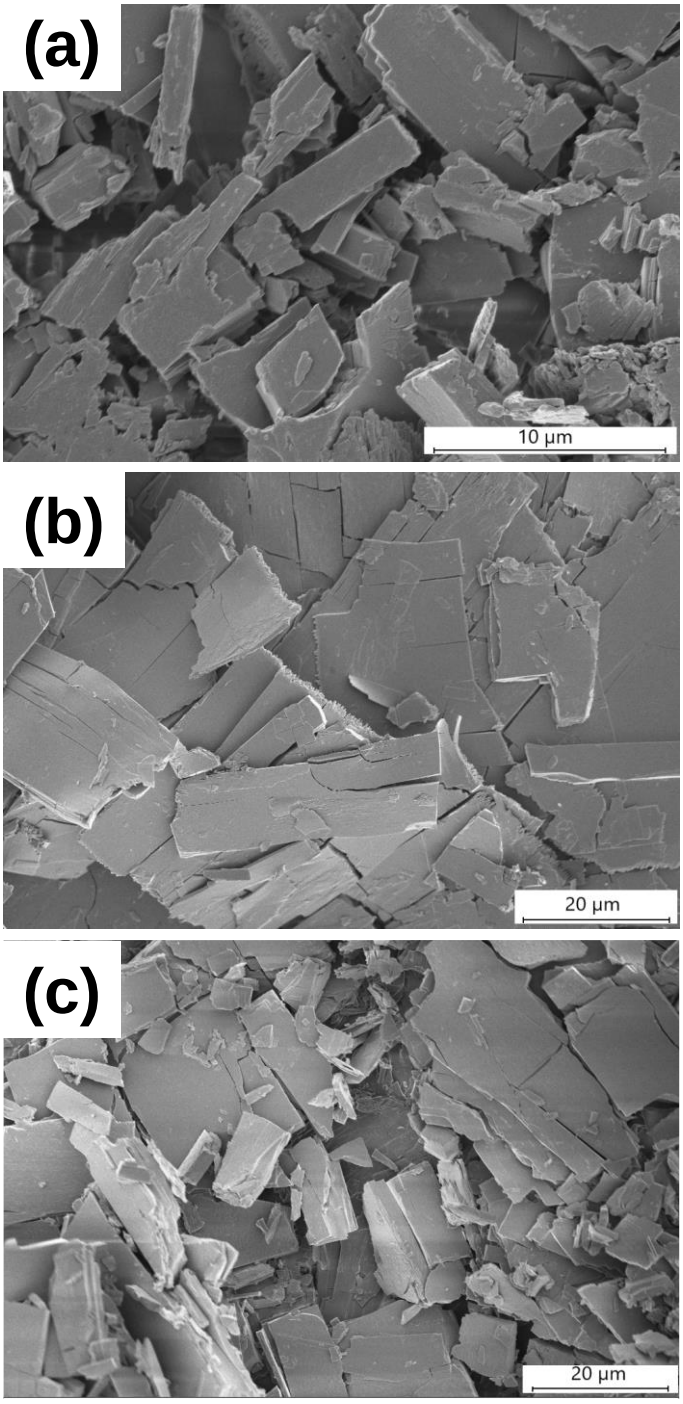

Figure S7. SEM images of the xerogels of (a) RR-BPA, (b) SS-BPA, and (c) RR+SS-BPA gelators prepared from DMSO/water (1:1, v/v) at 4.0 wt/v%.

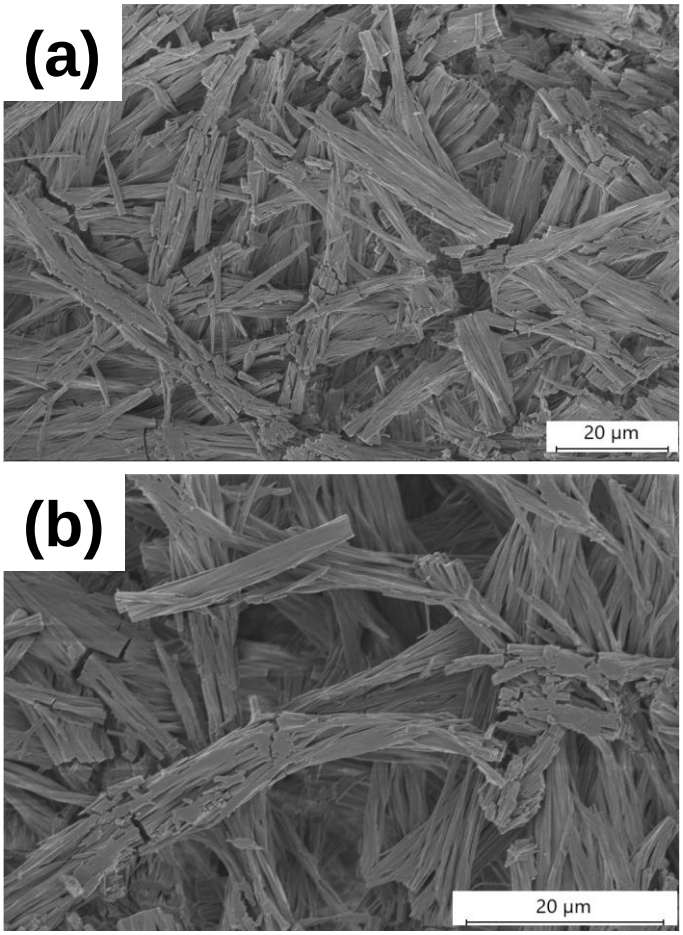

Figure S8. SEM images of the xerogels of (a) RR-BPP, and (b) SS-BPP gelators prepared from DMSO/water (1:1, v/v) at 1.2 wt/v%.

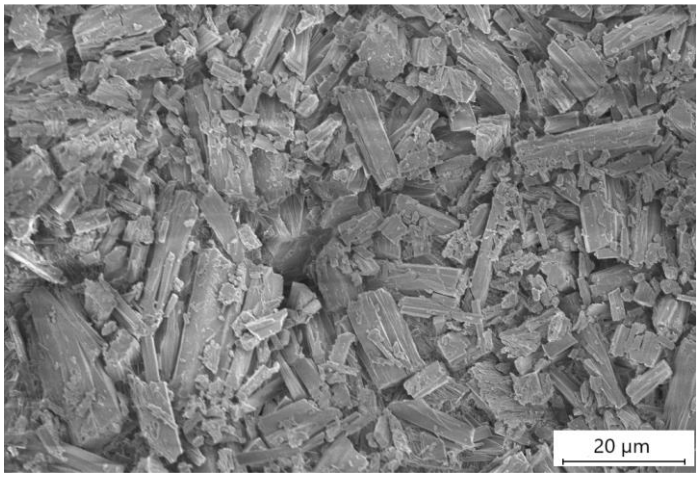

Figure S9. SEM images of the mixed compound RR+SS-BPP prepared by drop-cast method in DMSO/water (1:1, v/v) at 1.2 wt/v%.

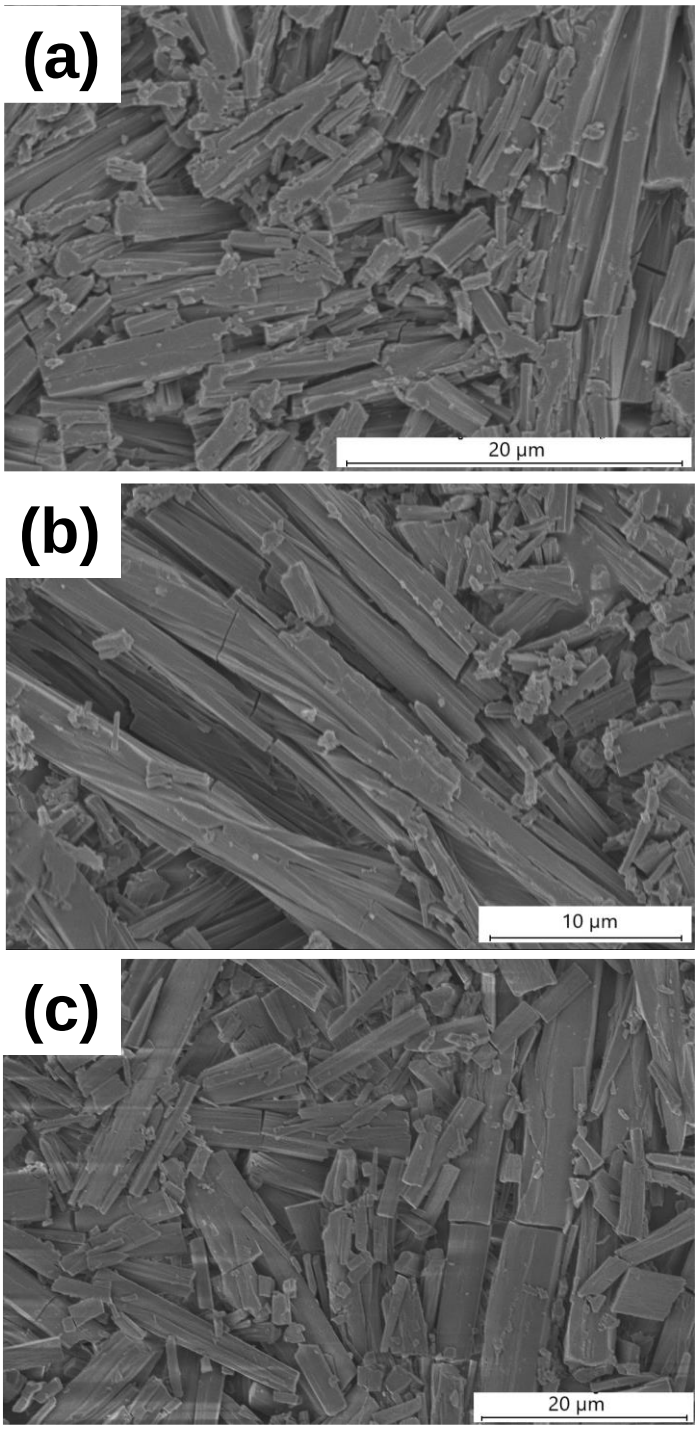

Figure S10. SEM images of the xerogels of (a) RR-BPP, (b) SS-BPP, and (c) RR+SS-BPP gelators prepared from DMSO/water (3:2, v/v) at 1.8 wt/v%.

4. Circular dichroism (CD)

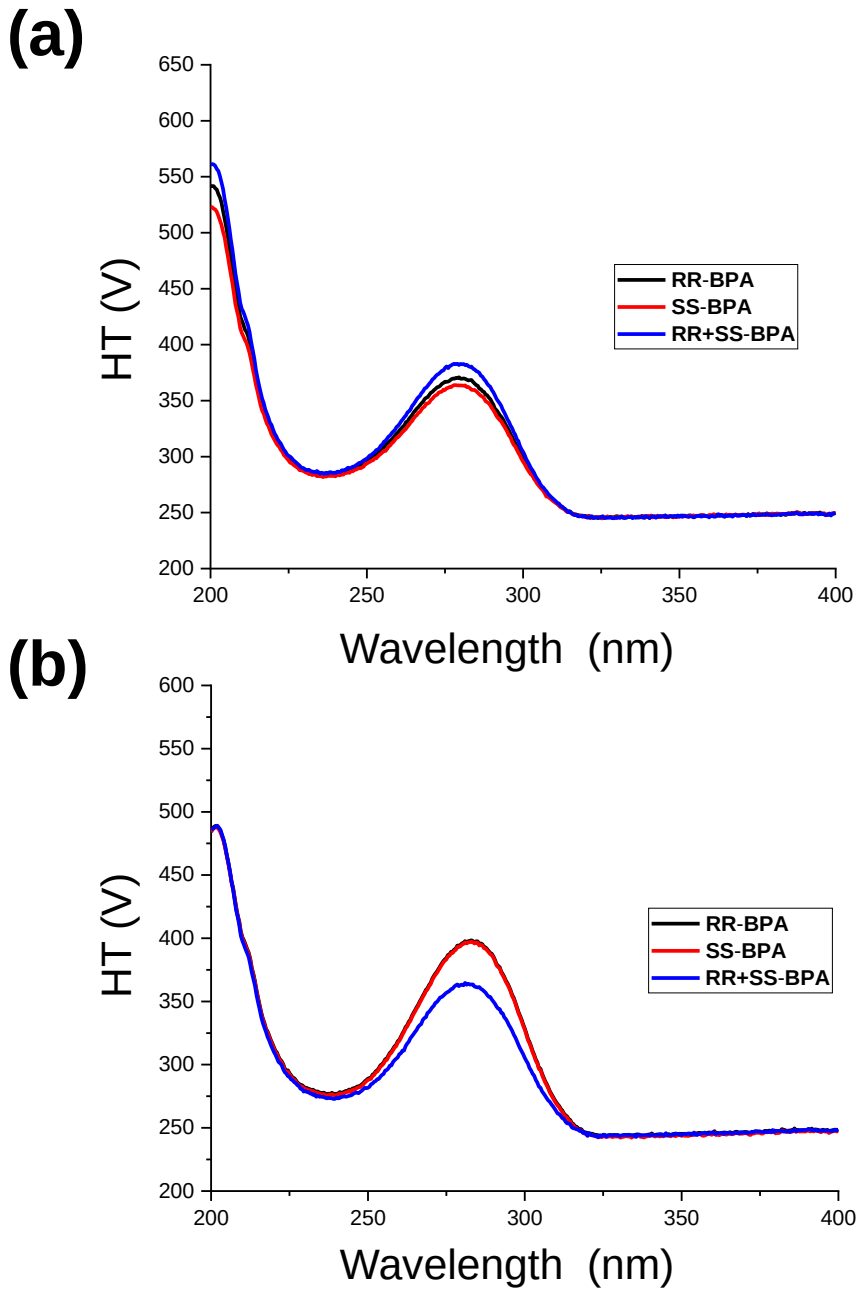

Figure S11. HT data for the CD spectra of BPA compounds shown in Figure 4 (main text): (a) solution state at 0.025 wt/v% in absolute EtOH, and (b) dispersed gel state at 0.025 wt/v% in EtOH/water (1:1 v/v).

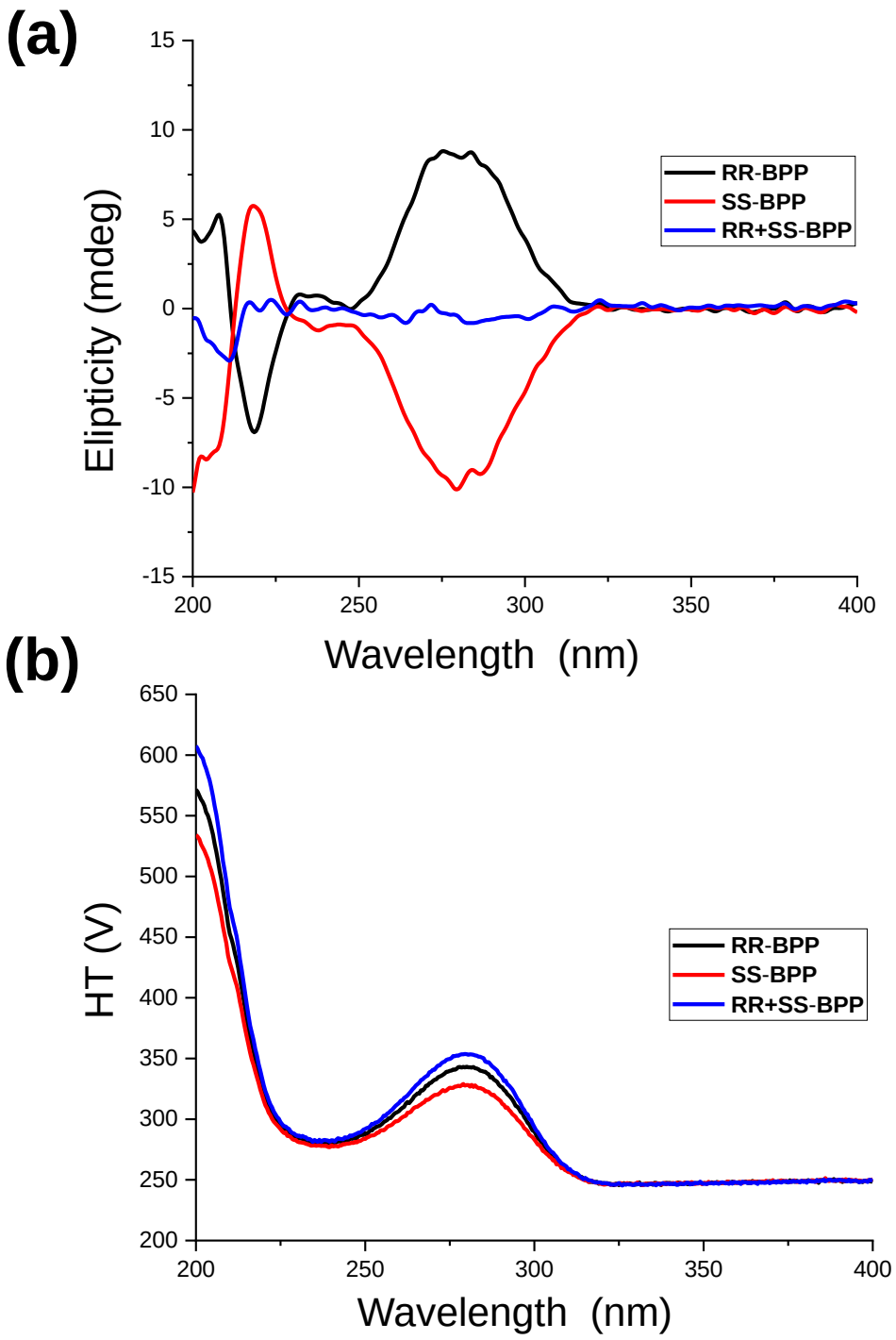

Figure S12. (a) CD spectra for the BPP compounds, and (b) the corresponding HT data in solution state at 0.025 wt/v% in absolute EtOH.

5. X-ray crystallography

Table S4: Crystal data

Crystal data	**RR-BPA**
Empirical formula	$C_{22}H_{24}N_2O_6$
Color	Colorless
Formula weight	412.43
Crystal size (mm)	0.35 x 0.13 x 0.05
Crystal system	Triclinic
Space group	*P*1
a (Å)	4.99830(10)
b (Å)	5.8581(2)
c (Å)	18.4025(5)
α (°)	92.4630(10)
β (°)	92.4380(10)
γ (°)	101.9980(10)
Volume (Å^3)	525.85(3)
Z	1
$D_{calc.}$(g/cm^3)	1.302
F(000)	218
μ (mm^{-1}) CuK_α	0.792
Temperature (K)	302(2)
Reflections collected/ unique/observed [I>2σ(I)]	19611/ 4260/4005
Data/restraints/parameters	4260/3/361
Goodness of fit on F^2	1.048
Final R indices [I>2σ(I)]	R_1 = 0.0365 wR_2 = 0.0986
R indices (all data)	R_1 = 0.0389 wR_2 = 0.1010

Table S5: Hydrogen bonding parameters

Compound RR-BPA						
No.	Donor–H···Acceptor	D–H/Å	H···A/Å	D···A/Å	∠D–H···A/°	Symmetry operation
1	N(7)–H(7)···O(9)	0.86	2.01	2.830(3)	160	1+x,y,z
2	N(24)–H(24)···O(23)	0.86	2.13	2.964(3)	164	-1+x,y,z
3	C(4)–H(4A)···O(30)	0.96	2.58	3.23(3)	126	-1+x,1+y,-1+z
4	C(4)–H(4C)···O(1)	0.96	2.48	3.399(4)	160	x,-1+y,z
5	C(5)–H(5)···O(1)	0.98	2.55	3.532(3)	178	1+x,y,z
6	C(6)–H(6A)···O(3)	0.96	2.59	3.361(4)	137	x,1+y,z
7	C(26)–H(26B)···O(30)	0.96	2.42	3.36(3)	163	-1+x,y,z
8	C(29)–H(29A)···O(30)	0.96	2.46	3.416(18)	172	x,1+y,z

6. Powder X-ray diffraction

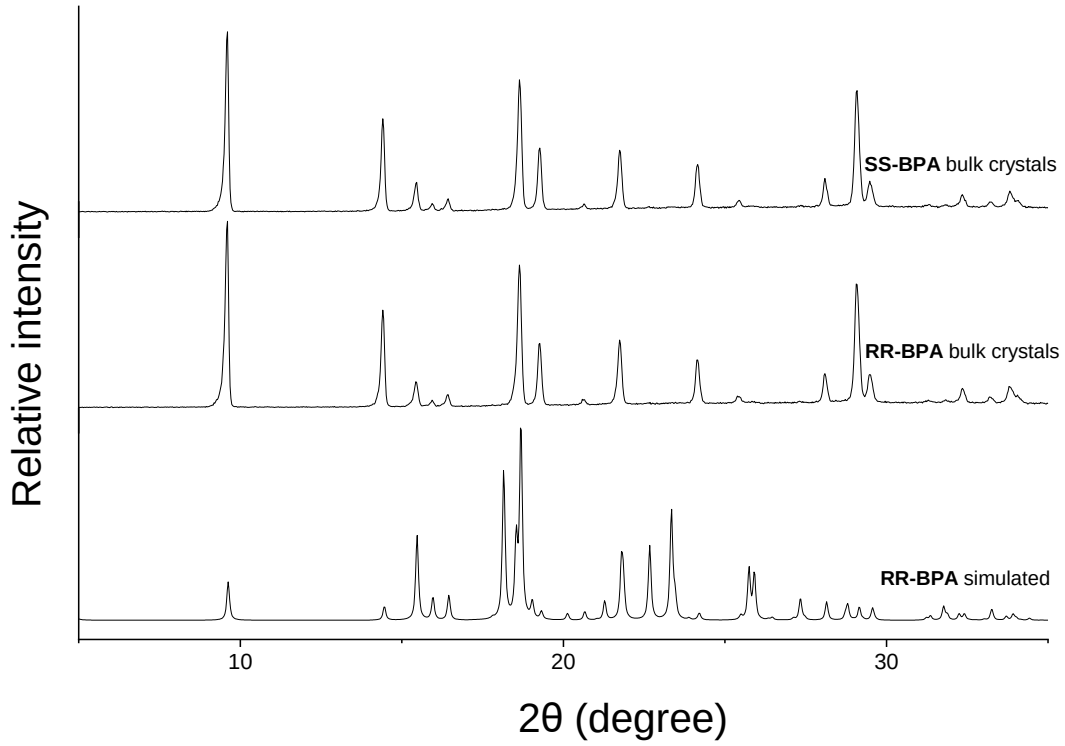

Figure S13. Comparison of the simulated pattern of RR-BPA obtained from the crystal structure with the PXRD pattern the bulk crystals of RR-BPA and SS-BPA prepared from ethanol (20.0 mg/mL).

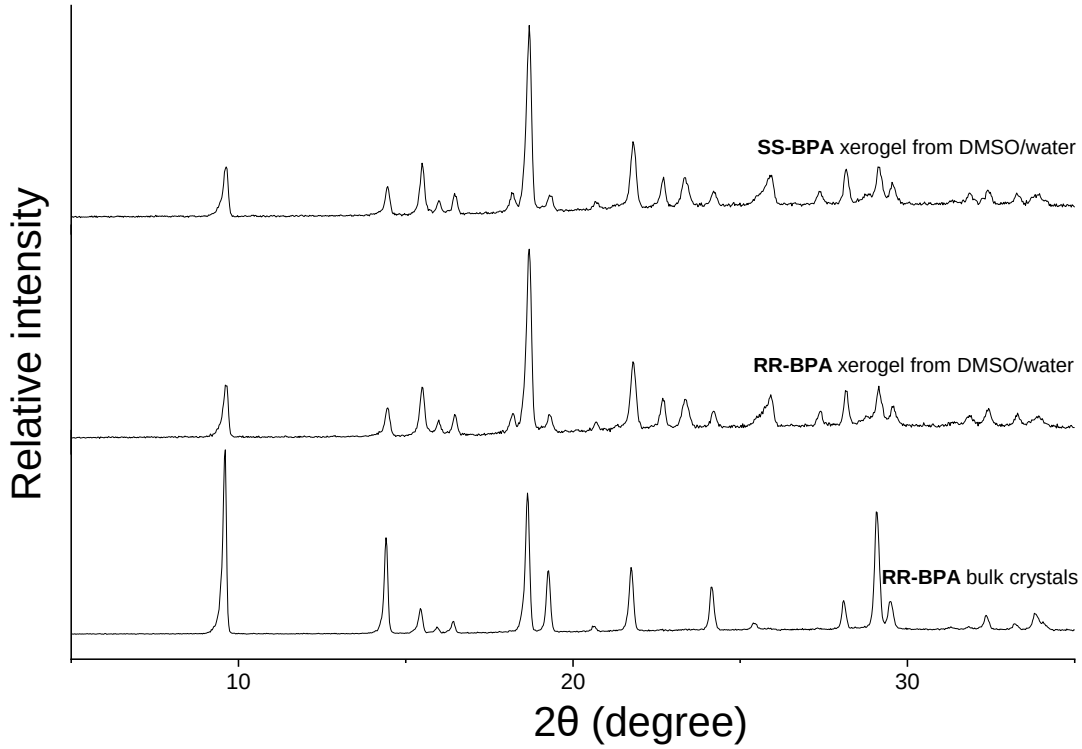

Figure S14. Comparison of PXRD pattern of the bulk crystals of RR-BPA with the xerogels of RR-BPA and SS-BPA prepared from DMSO/water (3:2, v/v), at 3.0 wt/v%.

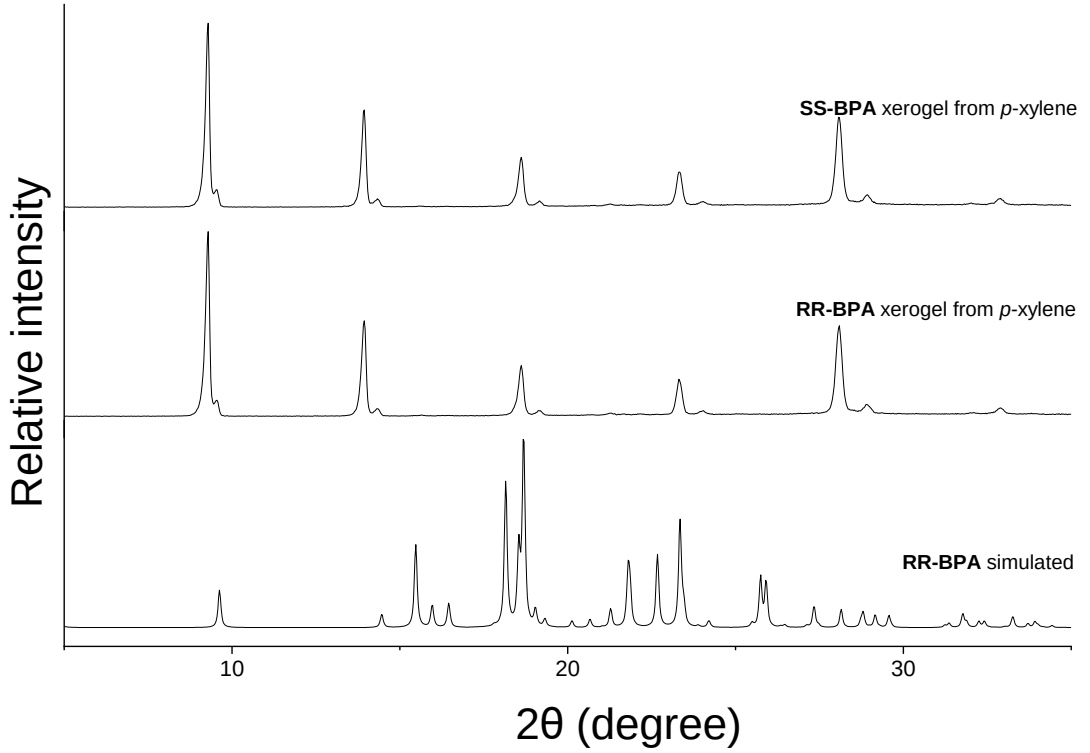

Figure S15. Comparison of the simulated pattern of RR-BPA with the PXRD pattern of RR-BPA and SS-BPA xerogel prepared from *p*-xylene at 2.6 wt/v%, respectively.

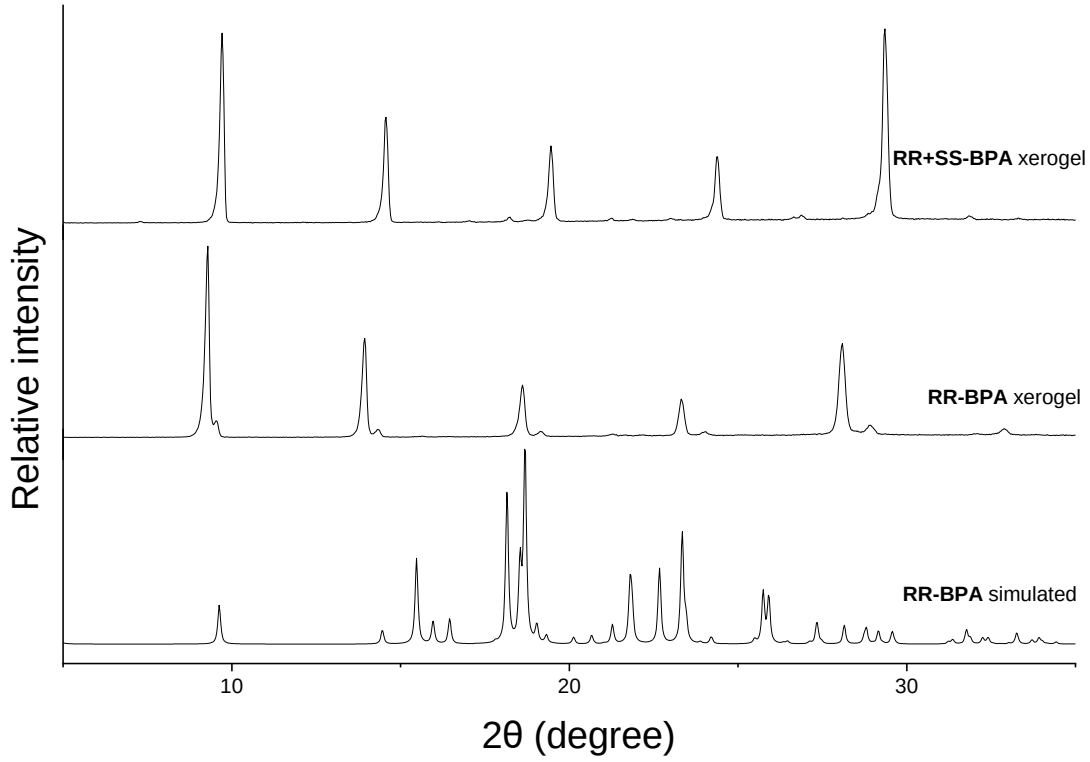

Figure S16. Comparison of simulated pattern of RR-BPA with the PXRD pattern of RR-BPA (2.6 wt/v%) and RR+SS-BPA (3.5 wt/v%) xerogels from *p*-xylene.

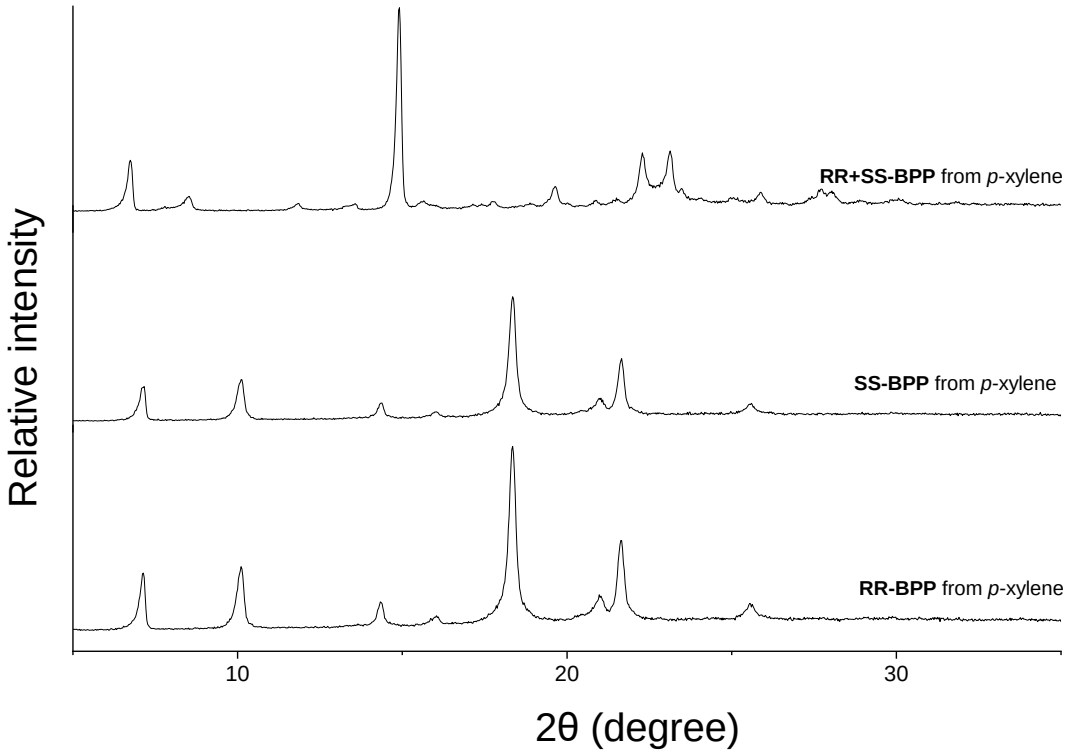

Figure S17. Comparison of PXRD pattern of xerogels of BPP compounds prepared in *p*-xylene at 3.0 wt/v%.

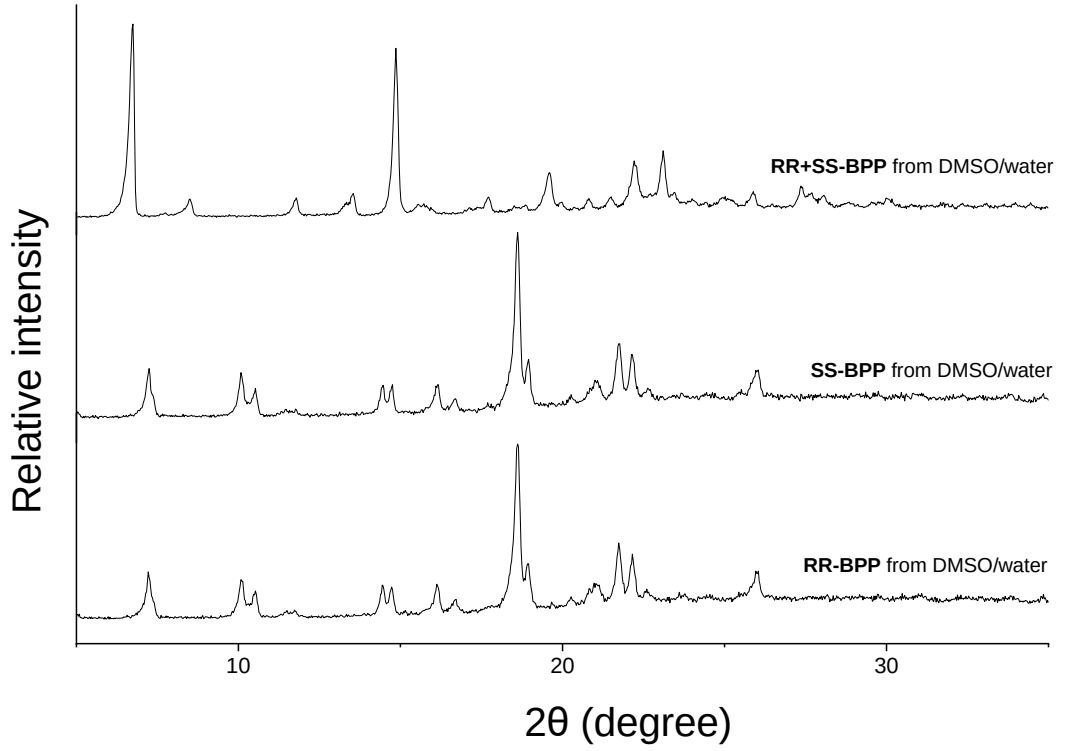

Figure S18. Comparison of PXRD pattern of xerogels of BPP compounds prepared in DMSO/water (3:2, v/v), at 1.8 wt/v%.

7. Anion Sensing

Table S6: T_{gel} studies with the BPP-gels in the presence of 1.0 equivalents of various potassium salts

	T_{gel} (°C)					
	Without anions	KF	KCl	KBr	KI	CH_3CO_2K
RR-BPP	105.9	104.6	106.9	103.3	105.2	101.1
SS-BPP	107.9	108.1	104.2	102.6	103.9	100.3
RR+SS-BPP	120.0	114.1	118.4	116.0	117.0	113.3

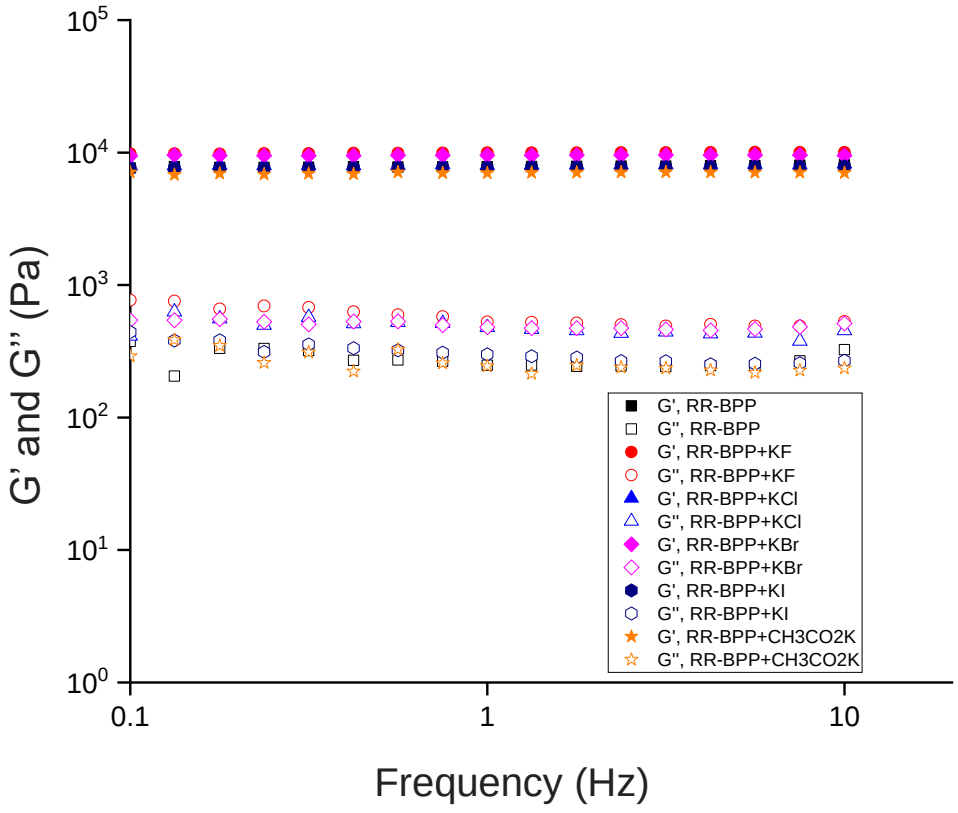

Figure S19. Frequency sweep experiments with gels of RR-BPP compounds at 1.8 wt/v% in the presence 1.0 equivalents of various potassium salts in DMSO/water (3:2, v/v) at 20.0 °C, measured at a constant strain of 0.02 %.

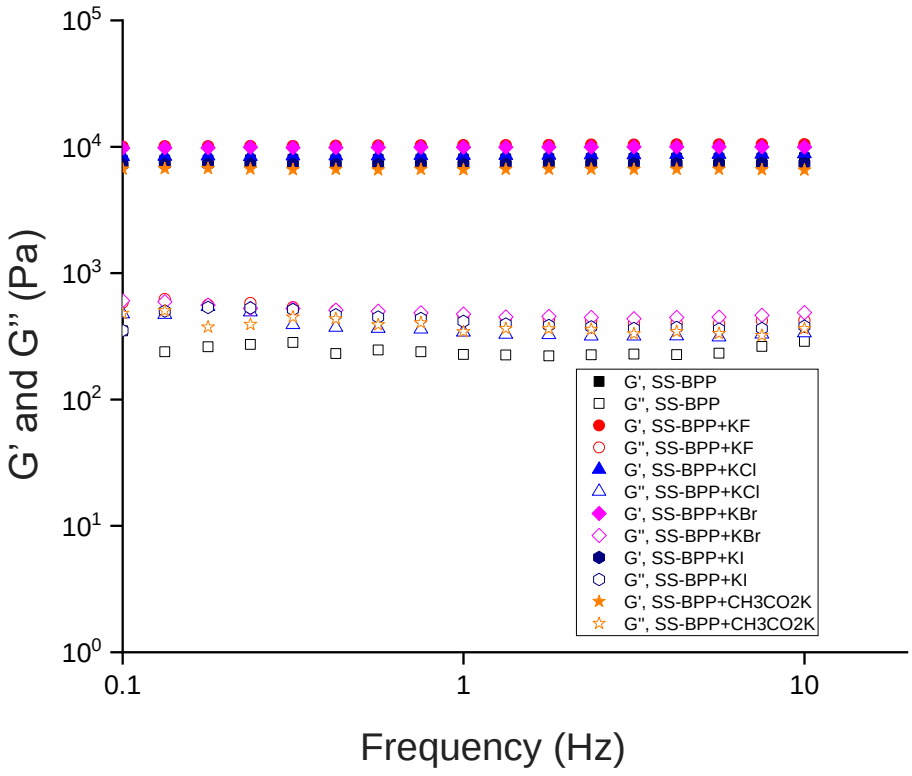

Figure S20. Frequency sweep experiments with gels of SS-BPP compounds at 1.8 wt/v% in the presence 1.0 equivalents of various potassium salts in DMSO/water (3:2, v/v) at 20.0 °C, measured at a constant strain of 0.02 %.

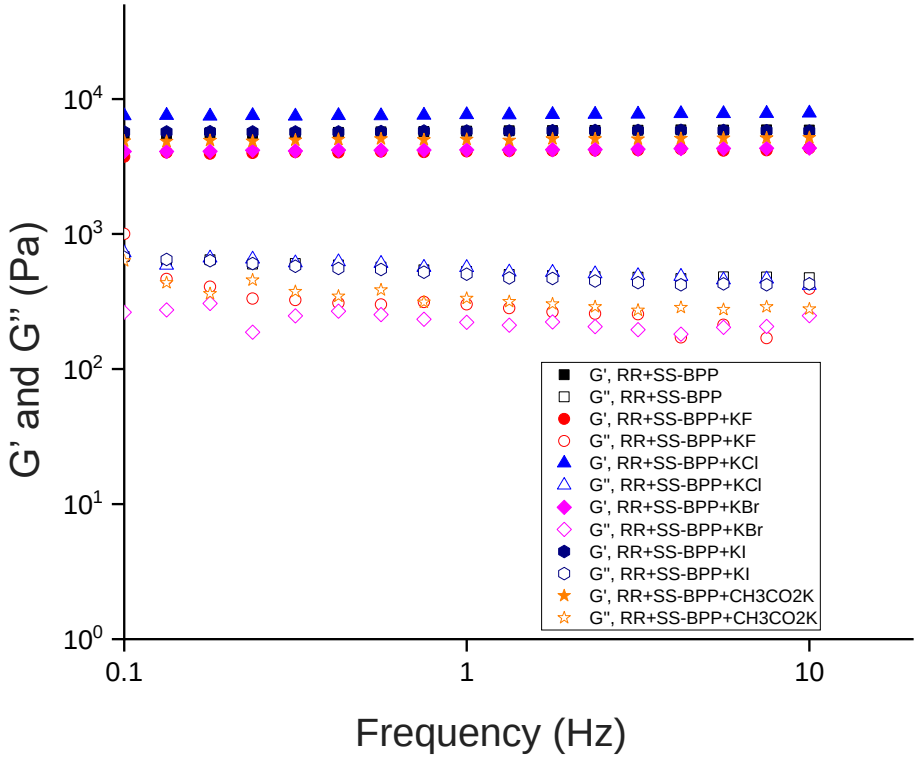

Figure S21. Frequency sweep experiments with gels of RR-BPP compounds at 1.8 wt/v% in the presence 1.0 equivalents of various potassium salts in DMSO/water (3:2, v/v) at 20.0 °C, measured at a constant strain of 0.02 %.

8. NMR spectra

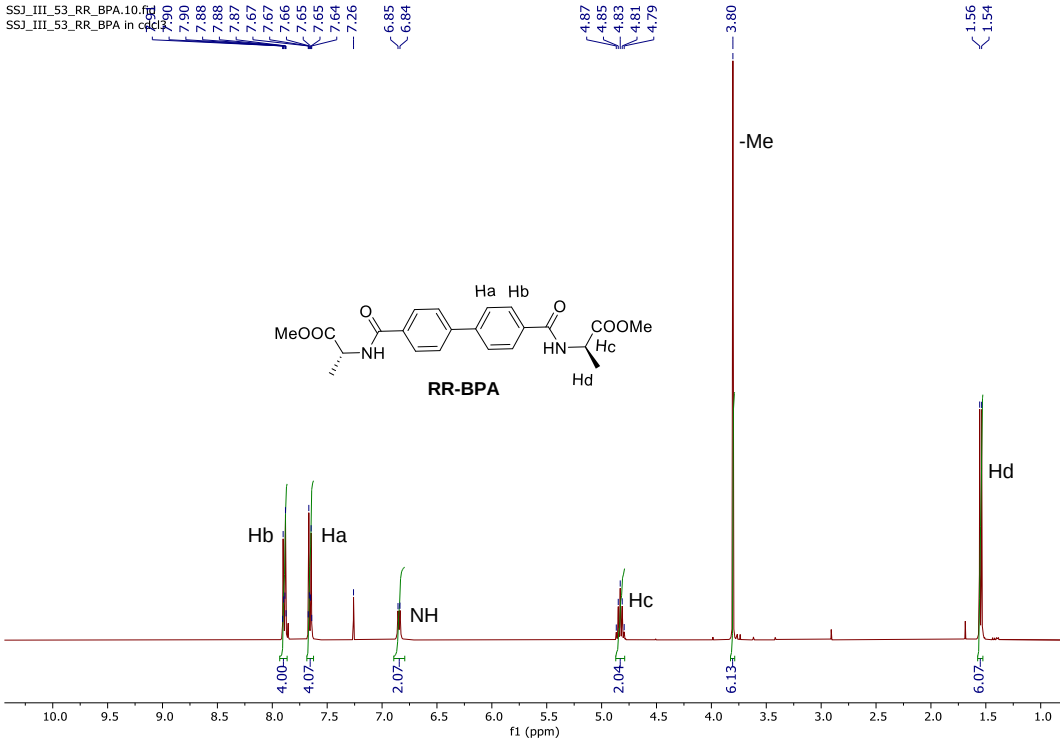

Figure S22. ^{1}H NMR spectrum of RR-BPA.

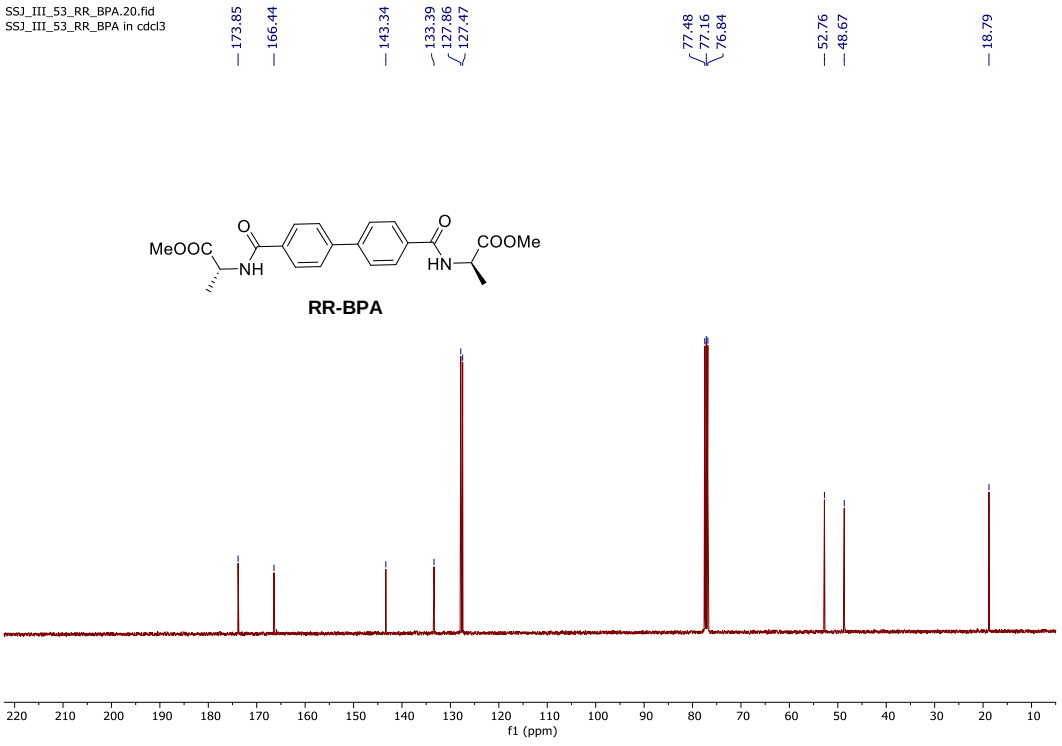

Figure S23. ^{13}C NMR spectrum of RR-BPA.

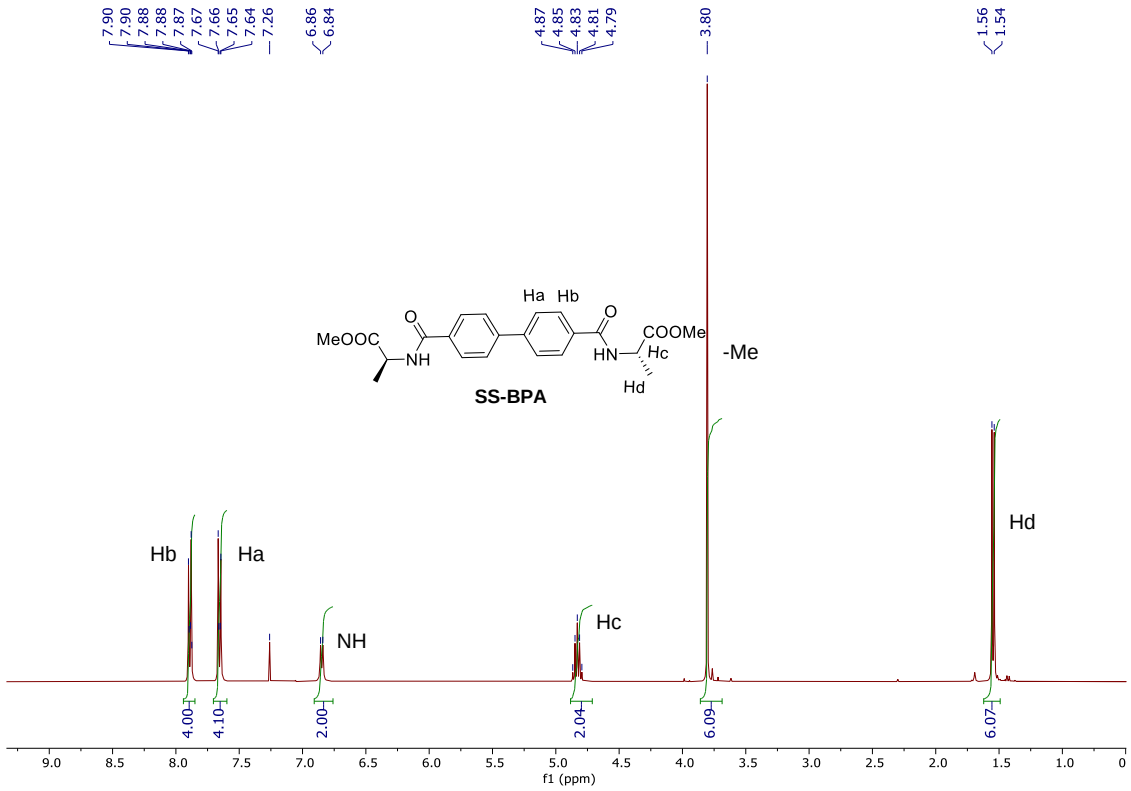

Figure S24. ^{1}H NMR spectrum of SS-BPA.

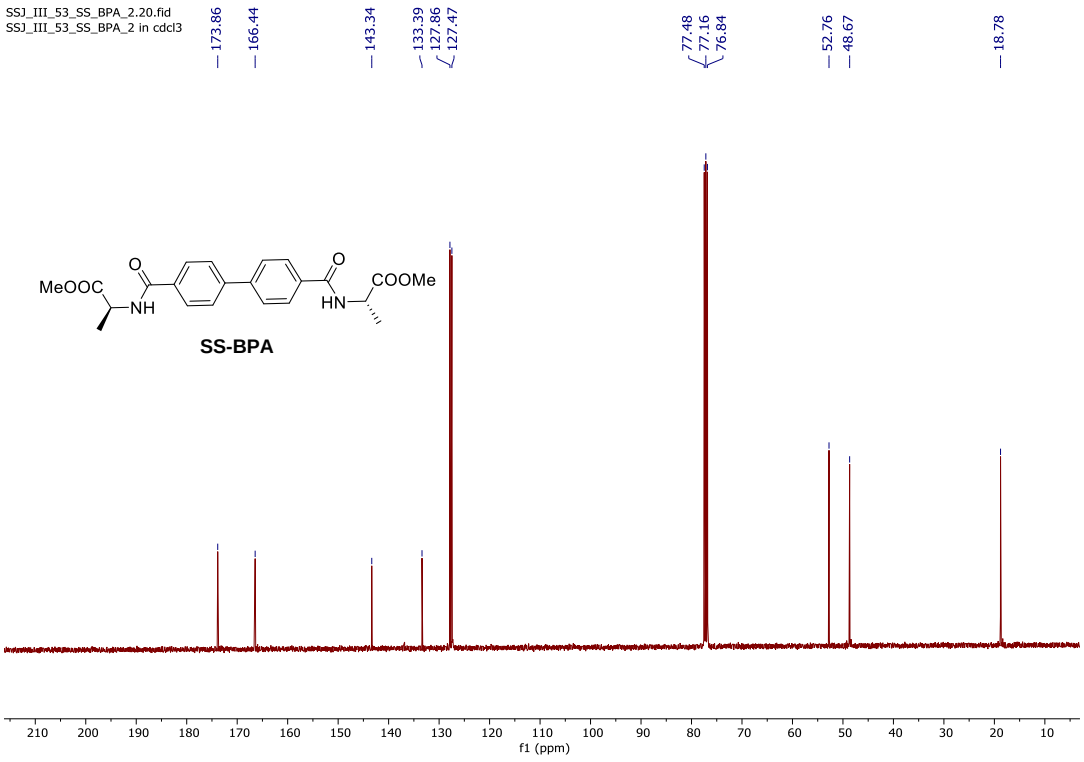

Figure S25. ^{13}C NMR spectrum of SS-BPA.

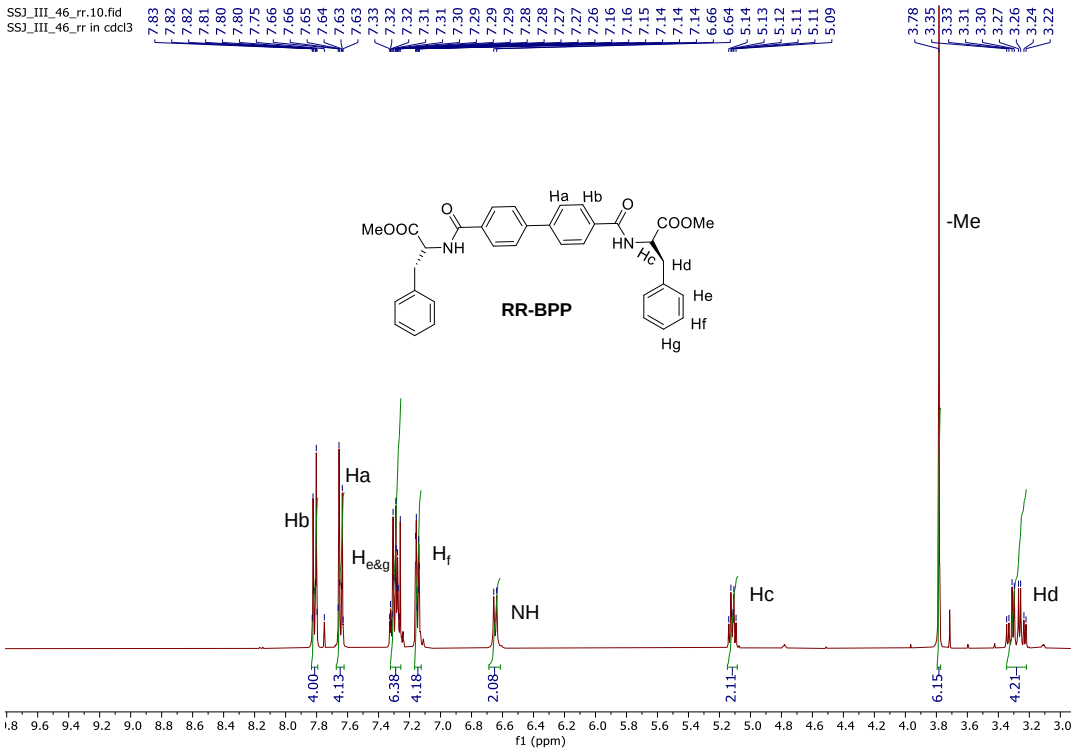

Figure S26. ^{1}H NMR spectrum of RR-BPP.

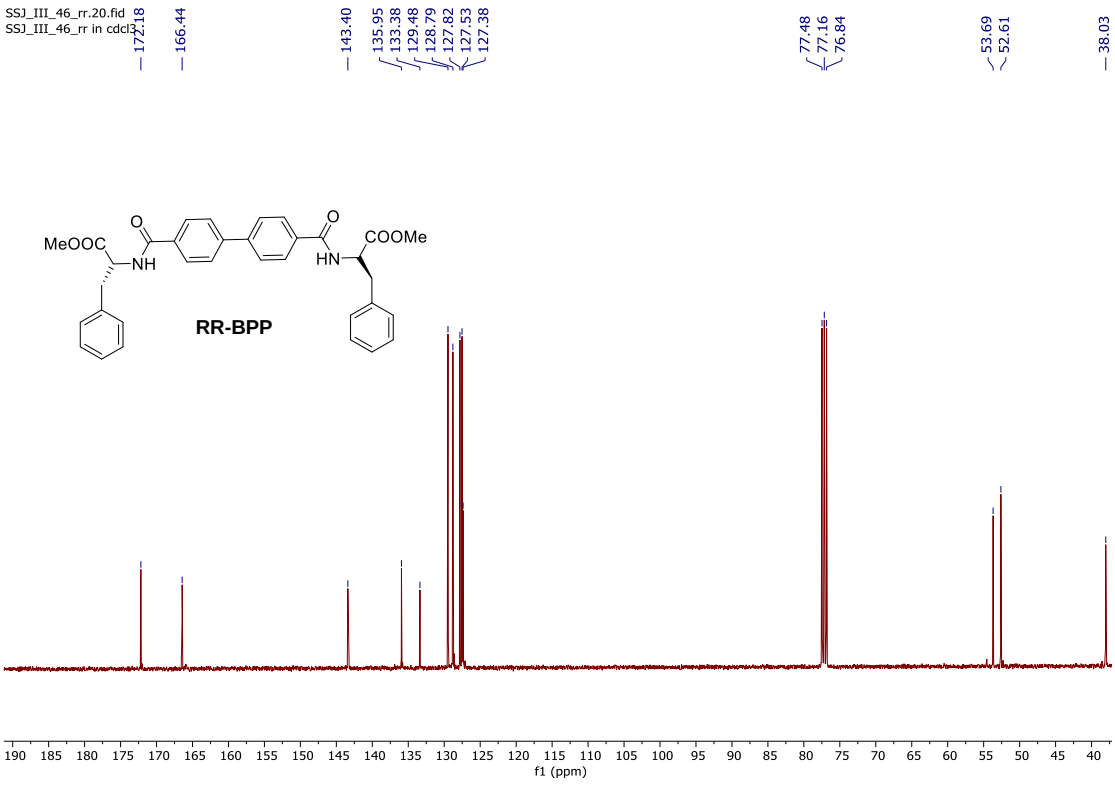

Figure S27. ^{13}C NMR spectrum of RR-BPP.

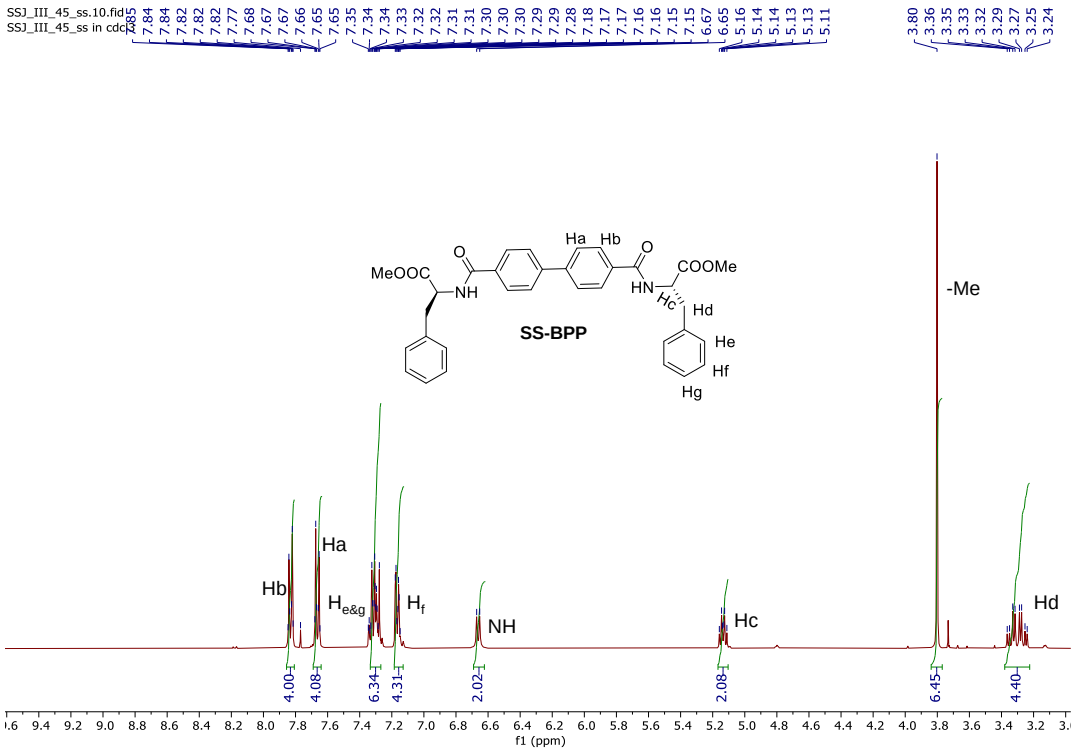

Figure S28. ^{1}H NMR spectrum of SS-BPP.

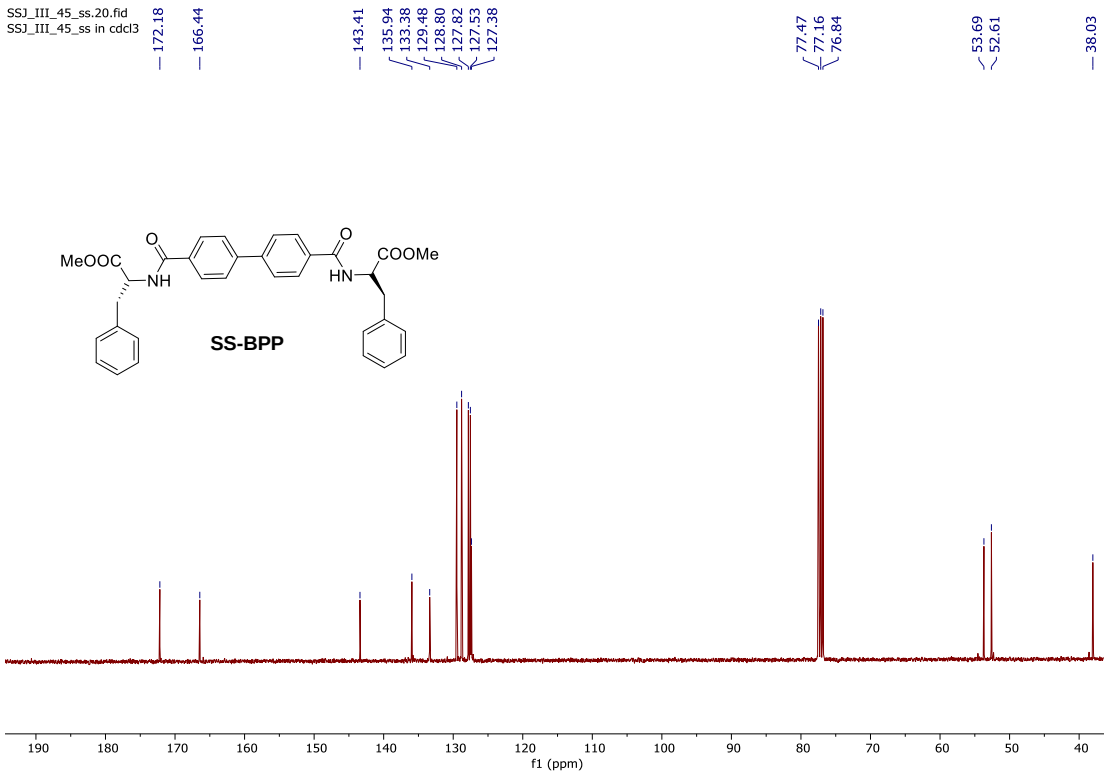

Figure S29. ^{13}C NMR spectrum of SS-BPP.

Article-VIII

This manuscript is in its final form and is preparing for submission to a peer-reviewed journal. It is presented as the current version.

Publication details:

"**Flexibility of Linkers: An Important Factor in Tuning the Gelation Properties in Multi-component Based Gels**"

Sreejith S. Jayabhavan and Krishna K. Damodaran*

Author contributions:

SSJ and KKD planned and designed the research; **SSJ** synthesised the gelators, performed characterisations, solved single crystal structures and evaluated gelation properties. **SSJ** and KKD wrote the initial draft, and the authors reviewed the main manuscript.

RESEARCH ARTICLE

Flexibility of Linkers: An Important Factor in Tuning the Gelation Properties in Multi-component Based Gels

Sreejith Sudhakaran Jayabhavan,[a] and Krishna K. Damodaran *[a]

[a] Department of Chemistry, Science Institute, University of Iceland, Dunhagi 3, 107 Reykjavík, Iceland, E-mail: krishna@hi.is; Fax: +354-552-8911

Supporting Information for this article is given via a link at the end of the document.

Abstract: The physio-chemical properties of multi-component systems highly depend on the molecular self-assembly. Understanding the self-assembly process in multi-component supramolecular gels is a challenging task because the molecular assembly is influenced mostly by the geometry and spatial arrangement of the functional groups, which dictate the non–bonding interactions. We have synthesized various enantiomers based on bis-(amides) of valine methyl ester with an aromatic core. We envision that the flexiblity between the aromatic core and the bis-(amides) could play an important role in tuing the gelation properties of the individual enantiomeric in mixed enantiomeric system. We have observed that flexibility favored the enantiomeric compounds to be better gelators, while it ceased gelation when they were mixed in equal proportion in most cases. However, mixing enantiomers with a rigid core induced gelation upon mixing. The self-assembly was investigated by studying the thermal and mechanical stability of the enantiomeric gels in comparison with the equimolar mixed gel. The chirality preservation was confirmed using CD experiments in solution and dispersed gel state. The self-assembled fibers were visualized using scanning electron microscopy (SEM). We have also addressed the self-assembly mode in multi-component gels with crystallographic evidence of specific co-assembly using single-crystal X-ray diffraction. The transformation of self-assembly modes in mixed gel based on the flexible linker was analyzed using X-ray diffraction techniques and concluded that the precise design of the gelator core plays a major role in the self-assembly of multi-component gels based on enantiomers.

Introduction

Self-assembly in multi-component systems is a fundamental phenomenon having enormous impacts across several domains, including materials science, nanotechnology, and biology. Multi-component systems can generate unique architectures and functionalities via self-assembly. The development of supramolecular materials utilizing multi-component systems will enhance our understanding of the self-assembly mechanism, hence facilitating the development of multi-component materials with remarkable features. Numerous biological processes depend on self-assembly, including the production of cell membranes, proteins, and DNA. Comprehending these processes can motivate the creation of biomimetic materials and systems in engineering and medicine. Multi-component systems based on low molecular weight gelators (LMWGs)[1] fall under this category because the self-assembly modes depend on the dynamic nature of the non–bonding interactions. Multi-component self-assembly in LMWGs arises through various non–bonding interactions, which can lead to highly ordered structures with properties that are not achieved by individual counterparts.[2] The individual materials can be gelators, non-gelators or a mixture of both, when mixed in a particular ratio, results in the formation of a gel. Mixing distinct gelators offers a better framework for analyzing the self-assembly mechanism in multi-component gels,[3] attainable by correlating the gelation characteristics of both individual and mixed gels.[2-4] In mixed gels, the individual moieties could remain as self-sorted entities (orthogonal co-assembly), or they could interact constructively or destructively to form specific or random co-assembly of the entities (Scheme 1).

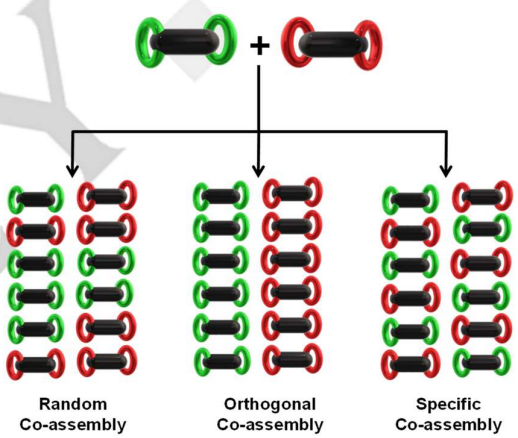

Scheme 1. Various modes of co-assembled multi-component systems and enantiomers are shown in green and red.

A primary issue in these multi-component systems is to control the nature of the self-assembly process, as interactions among individual components from the molecular to the macroscopic scale are extremely complex. The self-assembly process is influenced by several experimental parameters, including solvent choice, sonication, pH, gelator architecture, and temperature.[2] The molecular architecture of individual gelators is pivotal in the self-assembly process. Therefore, combining structurally similar components, such as enantiomers, generates favorable interactions among the components, and reduce the complexity in understanding the self-assembly process, and thus yielding multi-component gels with fascinating properties.[4] Self-recognition at the molecular level can be achieved due to the presence of structurally similar functionalities in the individual gelators and structurally similar gelators tend to favor co-assembly over self-sorting.[4a-j] Our group have shown that the self-assembly of multi-component gels can be controlled by

incorporating structural similarity in individual components and mixing enantiomeric gels will lead to specific co-assembly.[4b] Self-sorted enantiomeric gels[4k-m] are observed when the interactions between identical conformation are favored, resulting in the formation of conglomerates and in some cases, a mixture of self-sorted and co-assembly fibers are also observed.[4n] Adam and colleagues have demonstrated that altering hydrophobicity and pH, can regulate self-sorting or co-assembly in multi-component gels based on a dipeptide gelator and a non-gelling amphiphile.[4o] Thus, predicting the formation of self-sorted or co-assembled gels in enantiomeric multi-component systems is challenging because predicting whether the interactions between individual components or the enantiomers are favored is hard.

The self-assembly process of multi-component enantiomeric gels can be analyzed by various analytical methods.[3d-k] X-ray diffraction techniques have been used to differentiate the self-sorted and co-assembled networks in multi-component gels.[3k, 4c, 5] We have used single crystal X-ray diffraction (SCXRD) to show the crystallographic evidence of specific co-assembly in the mixed enantiomeric gel of terephthalic amide tagged with a valine methyl ester.[4b] The structural analysis revealed that the aromatic core connected to the rigid amide functionality plays a crucial role in self-assembly. This prompted us to evaluate the role of the molecular structure and their spatial orientation in the self-assembly process of multi-component enantiomeric gels by adding flexible linkers between the aromatic core and the amide moieties. Adams's group has studied the effect of hydrophobic spacer length on the non-gelling additive in altering the properties of multi-component systems at a higher pH.[6] We have shown that the effective modeling of the functional groups in enantiomeric compounds leads to multi-component systems with tunable properties.[7] The effect of linkers and their spatial orientation in the self-assembly process have been reported for structurally different components,[8] and to the best of our knowledge, the importance of these factors in the self-assembly process is not studied in enantiomeric multi-component gels. The structural similarity of the individual components will help us to identify the crucial role of the linkers in dictating the self-assembly modes, enabling the design of multi-component systems with tunable properties. In this work, we report the self-assembly modes of chiral LMWGs based on enantiomeric multi-component gels by connecting bis-(amides) of valine methyl ester to the aromatic platform (1,4-phenyl core) with rigid and flexible linkers.

Results and Discussion

We have selected C_2-symmetric chiral bis-(amide) of methyl valinate with rigid and flexible linkers between the aromatic core and the amide functionality (Scheme 2) because of their intriguing applications as multifunctional biomaterials.[9] Chiral LMWGs based on amino acid derivatives are excellent candidates to unravel the self-assembly process of multi-component enantiomeric gels because of their availability in both enantiomeric and racemic forms and amino acids are cheap with easily modifiable functional groups.[10] Furthermore, the diamides display β-tape type self-assembly to form a well-defined fibrous network[11], both in enantiomeric and mixed gel forms, leading to organo/hydrogels.[4b] We have designed a series of C_2-symmetric chiral bis-(amides) by introducing methylene, ethylene and methine groups between the aromatic core and the carbonyl group of terephthalic bis-(methyl valinate amide) (TAV)[4b] resulting in chiral bis-(amides) with rigid and flexible groups (Scheme 2). The enantiomeric 1,4-phenylene based bis-(amides) of valine methyl ester with rigid and flexible linkers were synthesized and characterized using standard analytical techniques and the structural analysis was performed by SCXRD.

Scheme 2. Chemical structure of TAV and compounds **1-3.**

The introduction of methylene group to terephthalic bis-(methyl valinate amide)[4b] resulted in compound **1** and enantiopure **1**-RR and **1**-SS compounds were synthesized by reacting the acid chloride of 1,4- phenylene diacetic acid with *R*- or *S*-methyl valinate hydrochloride in $CHCl_3$ in the presence of triethylamine. The 1,4- phenylene diacetic acid was synthesized according to

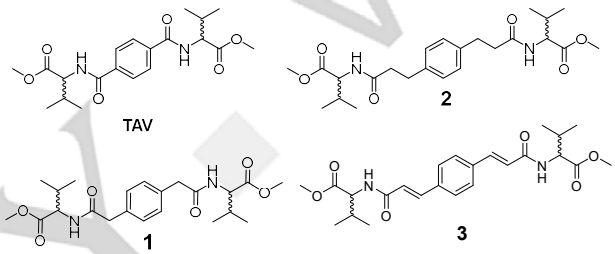

the reported procedures (Scheme S1, see Supporting Information).[3m, 12] The addition of ethylene and methine groups to terephthalic bis-(methyl valinate amide)[4b] resulted in compounds **2** and **3**, respectively. The enantiomeric compounds of **2** and **3** were synthesized by reacting *R*- or *S*-methyl valinate hydrochloride with 1,4-phenylenediacrylic acid (Scheme S2, see Supporting Information)[8f] and with 1,4-phenylenedipropionic acid (Scheme S3, see Supporting Information), respectively. The compounds were characterized using NMR, mass spectrometry, and SCXRD. Circular dichroism (CD) experiments were performed to confirm the chiral behavior of the compounds, and the gelation properties were evaluated in a series of solvents and solvent systems using standard gelation techniques.

Gelation studies

Gelation experiments were performed by heating the sample and a suitable solvent in a sealed vial, followed by sonication to dissolve, and left undisturbed overnight. A vial inversion test confirmed the gel formation. The experiments were performed with the enantiomers (RR and SS) and an equimolar mixture (1:1, v/v) of the enantiomers (RR+SS) for the flexible (**1** and **2**) and rigid (**3**) compounds in various alcohols, and aliphatic and aromatic solvents (Table S1, see Supporting Information). Gelation was observed for the enantiomeric and mixed compound **1** in higher alcohols, but crystalline materials were obtained with lower alcohols, such as methanol and ethanol. The experiments performed in aromatic solvents revealed that enantiomeric and mixed systems of **1** also formed gel in toluene, *o*-xylene, *m*-xylene, *p*-xylene, and mesitylene, but colloidal solutions were observed in benzene, chlorobenzene, and nitrobenzene. The enantiomeric

compounds **1**-RR and **1**-SS formed a gel at a lower concentration compared to the mixed **1**-(RR+SS) system in all the cases. The gelation experiments with the enantiomeric and mixed compounds of **2** indicated that gel formation was observed for enantiomeric compounds (**2**-RR and **2**-SS**)** in aromatic solvents such as xylenes, mesitylene, and toluene, but the mixed system **2**-(RR+SS) failed to form gel. However, the mixed system **2**-(RR+SS) formed gel at 12.0 wt/v% in xylenes, mesitylene, and toluene. Similarly, gelation experiments with the compounds of **3** in various solvent/solvent mixtures revealed that the enantiomeric compounds (**3**-RR and **3**-SS) failed to form gels (Table S1, see Supporting Information), but the mixed system **3**-(RR+SS) formed gel at 2.0 wt/v% in *m*-xylene and *o*-xylene.

The ability of these compounds to gel aqueous mixtures was analyzed by performing experiments in aqueous mixtures of various solvents (1:1, v/v) due to their limited solubility in water. The compounds were dissolved in polar solvents (methanol, ethanol, DMSO or DMF), followed by the addition of water, and the mixture was heated to dissolve, cooled and left undisturbed for gel formation. The individual enantiomeric compounds formed gel in 1:1 (v/v) of DMF/water, DMSO/water, methanol/water, and ethanol/water. The mixed compound **1**-(RR+SS) formed gel at a higher wt/v% in comparison with the individual enantiomers. For compound **2**, gels were obtained for both enantiomeric and mixed systems at 5.0 wt/v% in DMSO/water (1:1, v/v). The experiments performed with **3** indicated that the enantiomeric compounds failed to gel aqueous mixtures, but the mixed compound **3**-(RR+SS) formed gel at 5.0 wt/v% in in DMSO/water (1:1, v/v).

The minimum gel concentration (MGC), which is the minimum quantity of a compound required to form a stable gel, was recorded for the compounds in corresponding solvents. The MGC of the enantiomeric gels were similar (Table S2, see Supporting Information) but different from the mixed gels. For compound **1**, the MGC for the mixed gel **1**-(RR+SS) was comparatively higher in most of the solvents. The minimum gel concentration of the mixed gels of **1** in the aqueous mixtures also displayed higher MGCs compared to the enantiomers. We have compared the MGCs of the mixed gels (**TAV**, **1**, **2** and **3**) in DMSO/water (1:1, v/v) to evaluate the role of the rigid and flexible linkers and the results indicated that the MGCs are lower for TAV mixed gel, while the MGC for **2**-(RR+SS), was observed to be slightly less than both **1**-(RR+SS) and **3**-(RR+SS).higher for flexible linkers.

Thermal Stability

The gel-to-solution-phase transition temperature (T_{gel}) was evaluated to analyze the thermal stability of the gel network. The T_{gel} experiments performed in various solvents revealed that the enantiomers displayed similar thermal stability in most of the cases, presumably due to the similar gel network of the enantiomers (Table S3, see Supporting Information). The thermal stability of the mixed **1**-(RR+SS) gels was lower than its individual enantiomers. Similar results were observed in DMSO/water (1:1, v/v) at 5.0 wt/v% for the mixed **1**-(RR+SS) and **2**-(RR+SS) gels. The comparison of the thermal stabilities of the gelators indicated that the gel with rigid linkers such as TAV and **3**-(RR+SS) displayed better thermal stability (100.7 & 115.3 °C, respectively) compared to the flexible gels in 1:1 (v/v) DMSO/water (Table S3, see Supporting Information), presumably due to the enhanced solubility of the flexible system in DMSO/water (1:1, v/v) mixture.

Mechanical strength

Rheology is a tool for analyzing the deformation and flow characteristics of supramolecular gels,[13] which could provide key insights into the structural characteristics of the gel network. Rheological measurements were carried out to evaluate the solid-like properties and mechanical strength of the enantiomeric and mixed gels. The experiments were performed with the gels of **1**-**3** in the corresponding solvents. A strain sweep was performed at a constant frequency of 1.0 Hz to determine the linear viscoelastic region (LVR), where the elastic modulus (G′) is independent of the applied strain, and the gel undergoes reversible deformation within this region. The strain sweep measurement with the gels of the enantiomers of **1** and **2** and the mixed gels of **1**-**2** in *o*-xylene (7.0 wt/v%), *m*-xylene (7.0 wt/v%) and DMSO/water (1:1, v/v) at (5.0 wt/v%), and the mixed gels of **3** in *o*-xylene (2.0 wt/v%), *m*-xylene (2.0 wt/v%) and DMSO/water (1:1, v/v) at (5.0 wt/v%) displayed a constant G′ up to 0.02% of strain (Figure S1-S6, see Supporting Information). The gel networks collapsed to the solution phase at around 0.1-1.0 % of strain, which is known as the cross-over point.

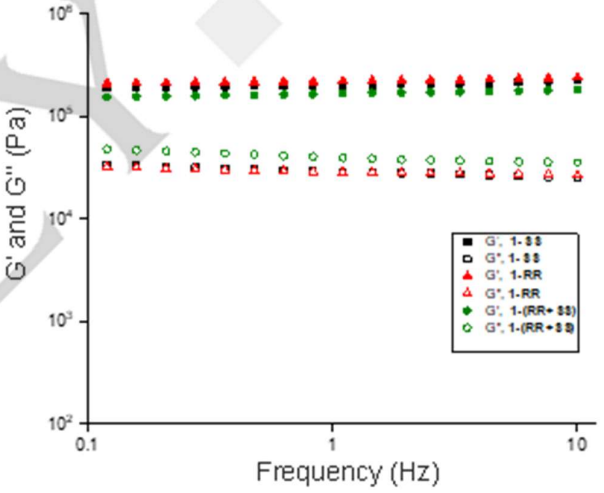

Figure 1. Frequency sweep of gels of compound **1** (6.0 wt/v%) in ethanol/water (1:1, v/v) at 25.0 °C measured at a constant strain of 0.02%.

Frequency sweep experiments were performed within the limit of the linear viscoelastic region between 0.1-10 Hz at a constant strain of 0.02%. The gelation behavior was validated by a constant elastic (G′) and viscous (G″) moduli under varying frequencies, and experiments showed that the enantiomeric gels were mechanically stronger than the corresponding mixed gels. (Figure S7-S14, see Supporting Information). For example, the enantiomers of **1** displayed a 5-fold increase in mechanical strength compared to the mixed **1**-(RR+SS) gel in DMSO/water (1:1, v/v), and similar results were observed for **2**. The comparison of the mechanical strength of the mixed gels at 5.0 wt/v% in DMSO/water (1:1, v/v) indicated that mixed gel of **3**-(RR+SS) displayed a weaker network in comparison with the **1**-(RR+SS) and **2**-(RR+SS) gel in DMSO/water composition. The mixed gels based on **1**-(RR+SS) and **2**-(RR+SS) in *o*-xylene and *m*-xylene

showed very low mechanical strength in comparison with its corresponding enantiomeric gels. The **3**-(RR+SS) gel obtained from *o*-xylene was stronger than the *m*-xylene based gel. We have performed the rheological studies for the enantiomeric and mixed gels of **1** in various solvents/solvent mixture such as *p*-xylene, *n*-butanol, and ethanol/water (1:1, v/v) mixture to evaluate the role of solvents. The enantiomeric gels of **1** obtained from ethanol/water (1:1, v/v) at 6.0 wt/v% showed enhanced mechanical strength compared to the **1**-(RR+SS) gel (Figure 1). Similar results were obtained with other solvents, and the enantiomeric gels (**1**-RR and **1**-SS) were found to be stiffer in comparison with the mixed **1**-(RR+SS) gel (Figure S15-S20, see Supporting Information). These results indicate that the mechanical strength of the mixed gels was not affected by the nature of the solvent.

Gel Morphology

Scanning electron microscopy (SEM) is an efficient tool to analyze the nature and the morphology of the self-assembled fibrous network in LMWGs.[14] SEM can be used to differentiate the self-assembly modes, such as self-sorting or co-assembly in multi-component gels, by analyzing the morphological difference in individual and mixed gels.[3b] SEM images of the individual and mixed LMWGs were recorded to visualize the morphological changes of the fibrous network due to the self-assembly process. We have performed SEM to analyze the surface morphology of the dried gels of **1**-RR and **1**-SS in *m*-xylene, and needle-shaped morphology with diameter ranges 2.0-10.0 μm (Figure 2a & Figure S21a, see Supporting Information) was observed. The mixed **1**-(RR+SS) xerogel displayed plate shaped morphology (Figure 2c) and similar morphologies were observed for the xerogels of **1** in *o*-xylene and *p*-xylene (Figure S21-22, see Supporting Information).

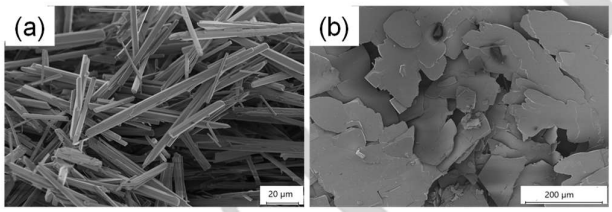

Figure 2. SEM images of the xerogels of (a) **1-RR**, and (b) equimolar **1**-(RR+SS) gelators from *m*-xylene prepared at 7.0 wt/v%.

The enantiomers of **2** displayed needle and tape-like morphologies (diameter range 0.5-6.0 μm) in *o*-xylene and *m*-xylene and needle shaped morphologies were observed for the mixed gels (Figure S23-24, see Supporting Information). The surface morphology of the dried gels of **3**-(RR+SS) from *o*-xylene and *m*-xylene at 2.0 wt/v% revealed the fibrous network with diameters ranging from 100-400 nm (Figure S25, see Supporting Information). SEM images of the dried gels of **1**-RR and **1**-SS from DMSO/water (1:1, v/v) at 5.0 wt/v% displayed stick-shaped fibers (width ranges 1.0-10.0 μm), and the mixed **1**-(RR+SS) xerogel also showed similar fiber morphology; however, the length of the fibers was shorter in comparison with the dried gels of the enantiomers (Figure S26, see Supporting Information). A plate-shaped morphology was observed for the dried gels of **2**-RR, **2**-SS, and the mixed **2**-(RR+SS) in DMSO/water (1:1, v/v), which suggests the absence of morphological change upon mixing the enantiomers (Figure S27, see Supporting Information). The dried gel from DMSO/water (1:1, v/v) of the mixed **3**-(RR+SS) at 5.0 wt/v% displayed flake-shaped morphology (Figure S28, see Supporting Information). SEM images of the xerogels of **1** from various solvents such as toluene, *n*-butanol, and ethanol/water (1:1, v/v) confirmed that the individual and mixed gels displayed similar morphologies (Figure S29-31, see Supporting Information), which shows that the nature of the solvents does not affect the morphology of the fibrous network.

Circular dichroism

The self-assembly process of chiral supramolecular architectures can be monitored by CD experiments, which could provide vital information about the chirality-driven self-assembly process. [15] The comparison of the CD signal of the individual and self-assembled gel will help us to elucidate the structural Information of the hierarchical structure. The chirality of the enantiomeric and mixed compounds of **1**-**3** was confirmed using solution-state CD experiments, which were performed in absolute ethanol at different concentrations, and 0.03 wt/v% was found to be the optimum concentration (Figure S32-S37, see Supporting Information). The CD spectrum for **1**-SS displayed positive maxima around 216 nm arising from the π−π stacking interactions and negative maxima around 236 nm, and a mirror image of the CD spectrum was observed for **1**-RR (Figure S32, see Supporting Information). The peak at 236 nm may correspond to the *β*-conformation architecture as observed in LMWGs of short peptides, which corresponds to the hydrogen bonding in amides.[16] The CD spectra of the enantiomers of **2** compounds exhibited closer correspondence with **1** (Figure S34, see Supporting Information), probably due to the structural similarity of the network in flexible-based linkers. The CD spectrum of the rigid linker **3**-SS was found to be a mirror image of **3**-RR (Figure S36, see Supporting Information). The rigid linker **3**-SS also displayed CD signals similar to **1**-SS, suggesting the *β*-conformation architecture,[16] but a broad peak around 290-350 nm was observed, which may be attributed to the n-π* transition associated with the α,β-unsaturated amide. [16b, 17]

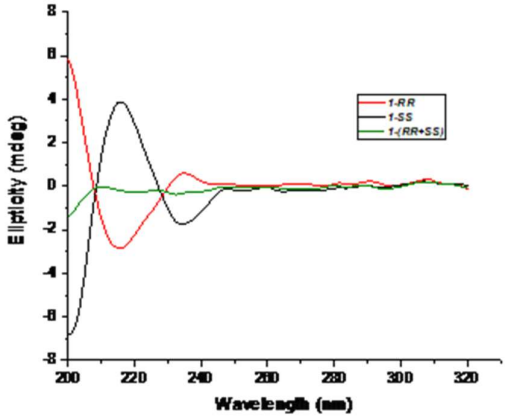

Figure 3. CD spectra of **1-RR**, **1-SS**, and equimolar **1-(RR+SS)** in dispersed gel state at 0.03 w/v% in ethanol/water (1:1, v/v).

The CD spectra of enantiomers of the flexible (**1** and **2**) and rigid linkers (**TAV**[4b] and **3**) displayed ellipticity in opposite phases (Figure S32-S37, see Supporting Information), presumably due to the confirmational changes arising from rigid and flexible networks. The equimolar mixture of the enantiomers of **1**-**3** displayed a linear signal, respectively, indicating the presence of both enantiomers in the equimolar ratio (Figure S32-S37, see Supporting Information).

The gel state CD experiments were performed with dispersed gels of **1** in ethanol/water (1:1, v/v) with an absorption cut-off around 190-200 nm, and other organic solvents were discarded due to background absorption. The aqueous mixture gel of **1** (6.0 wt/v%) obtained from ethanol/water (1:1, v/v) mixture was homogeneously dispersed in a diluted solution (0.03 wt/v%) of the same solvent mixture, and the CD experiments revealed that the chiral supramolecular architectures were similar to the solution state of **1** (Figure 3, and Figure S38, see Supporting Information). The mixed gel of equimolar amounts of **1**-RR and **1**-SS resembled a linear signal, which indicates the presence of both enantiomers in the equimolar ratio. We have also performed CD experiments by varying the ratio of **1**-RR and **1**-SS in the mixed compound in solution and gel state to confirm the enantiomeric excess of individual compounds (Figure S39-S42, see Supporting Information).

Single crystal X-ray diffraction

Single-crystal X-ray diffraction (SCXRD) is an excellent tool to analyze the key interactions in the solid-state structure of the gelator[18], and correlating these interactions with the gel state will help to identify the role of these interactions in the self-assembly modes. SCXRD has been used to get an insight into the packing modes of the gel fibers of enantiomers by comparing them to its non-gelator racemate[19] or by isolating the crystals of one of the components to prove the self-sorting modes in multi-component dipeptides gels.[4p] However, the comparison of such interactions is limited in enantiomeric multi-component gels due to the unavailability of the crystal structures of the individual and mixed enantiomers. We have compared the solid-state structures of individual and mixed enantiomeric gelators of **TAV** and reported the structural evidence for the specific co-assembly in enantiomeric multi-component gels.[4b] This prompted us to perform the crystallization experiments of the individual and mixed enantiomers of compounds **1**-**3** to evaluate the self-assembly modes using SCXRD. X-ray quality single crystals of the enantiomeric compounds (**1**-RR, **1**-SS, **2**-RR, and **2**-SS), the equimolar **1**-(RR+SS) and **3**-(RR+SS) mixed systems were obtained as needle-shaped crystals by the slow evaporation from ethanol/water (1:1, v/v) over 1-2 days. The slow evaporation of an acetonitrile solution of the enantiomers of **3** resulted in block-shaped crystals in 1-2 days. The pre-assembled **2**-(RR+SS) from *p*-xylene (5.0 wt/v%) were re-crystallized in ethanol/water (1:1, v/v) to yield needle-shaped crystals. The crystallographic details and hydrogen-bonding parameters of the compounds are summarized in Table S5-S7 & Table S8-S10 (see Supporting Information), respectively.

The enantiomers **1**-RR and **1**-SS were crystallized in the orthorhombic chiral $P2_12_12_1$ space group (Figure S43, see Supporting Information). The bis-(amides) of the gelators showed *syn*-conformation with respect to the aromatic plane (Figure 43), and the amide moieties displayed complementary hydrogen bonding via N−H···O interactions with the adjacent molecule to form a 1-D hydrogen-bonded network (Figure S44, see Supporting Information). The amide moieties were pointing downwards from the aromatic plane, leading to a bent structure. The mixed enantiomeric gelator **1**-(RR+SS) crystallized in a triclinic centrosymmetric *P*-1 space group with one of the enantiomers in the asymmetric unit, which was related to the other enantiomer via an inversion center. The bis-(amides) displayed *anti*-conformation (Figure 4a), and the nearly orthogonal orientation of the amide moieties resulted in an elongated twisted structure compared to the enantiomers. The complementary amide hydrogen bonding of amide moieties of the enantiomers resulted in a 1-D hydrogen-bonded tape with a sequence of −(R−R)−(S−S)−(R−R)−(S−S)−, proved the specific co-assembly of the enantiomers (Figure 4b). The comparison of the solid-sate structures revealed that adjacent phenyl rings displayed an edge-to-face π-π interaction in the enantiomers, but an offset face-to-face interaction (Figure S45, see Supporting Information) was observed in mixed **1**-(RR+SS). Since the gelation ability is highly dependent on the spatial arrangement of functional groups, this could be correlated to the better gelation ability of the enantiomeric compounds.

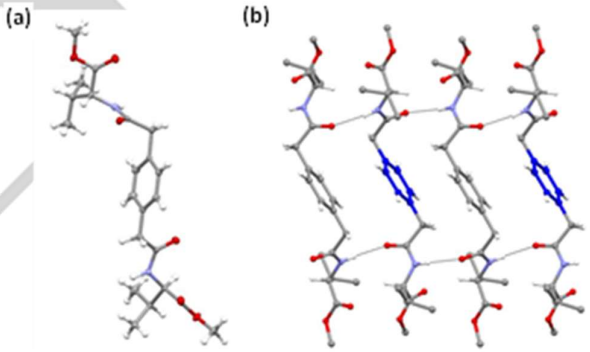

Figure 4. Crystal structure of equimolar **1-(RR+SS)** (a) asymmetric unit, (b) formation of 1-D hydrogen bonded architecture (hydrogen atoms are omitted for clarity), black dotted lines represent hydrogen bonding.

The enantiomers (**2**-RR and **2**-SS) crystallized in an orthorhombic chiral $P2_12_12_1$ space group. The molecular structures were different from the enantiomers of **1,** and the amide moieties displayed *anti*-conformation (Figure S46, see Supporting Information), presumably due to the additional flexibility (methylene group) in the molecule leading to an antiparallel orientation of the amide moieties with respect to the aromatic plane. The amide groups displayed hydrogen-bonding interactions with four adjacent molecules to form a hydrogen-bonded 2-D corrugated sheet (Figure S47, see Supporting Information). The crystallization of the mixed **2**-(RR+SS) resulted in enantiomers, but recrystallizing the compounds from xylenes in ethanol/water produced **2**-(RR+SS), which was confirmed by X-ray analysis. The mixed **2**-(RR+SS) crystallized in the triclinic centrosymmetric *P*-1 space group similar to **1**-(RR+SS) with amide moieties displaying *anti*-conformation (Figure S48a, see

Supporting Information). However, the amide groups were not orthogonal to each other (78.81°), leading to a twisted confirmation. The amide moieties showed complementary hydrogen bonding with the adjacent molecule via N−H···O interactions to form a 1-D hydrogen-bonded chain, which confirmed the specific co-assembly between the two enantiomers (Figure S48b, see Supporting Information).

Similarly, the SXCRD analysis of enantiomeric compounds of **3** revealed that **3**-RR and **3**-SS were crystallized in the orthorhombic chiral $P2_12_12_1$ space group. The bis-(amides) of the gelators showed *anti*-conformation (Figure S49, see Supporting Information) and were slightly planar but bent downwards with respect to the aromatic core. The hydrogen bonding patterns were similar to the enantiomers of **2,** but a 3-D hydrogen-bonded network was observed presumably due to the due to the rigid linkers. The mixed **3**-(RR+SS) crystallized in a centrosymmetric monoclinic $P2_1/n$ space group. The molecular structure of **3**-(RR+SS) was similar to the enantiomers, but the bis-(amides) of the gelators were slightly planar and twisted upwards with respect to the aromatic core (Figure S50a, see Supporting Information). The enantiomers displayed complementary amide hydrogen bonding to form a dimer, and these dimers were further hydrogen bonded to four adjacent dimers via N−H···O interaction of the amide functionalities to form a 2-D hydrogen bonded corrugated sheet-like architecture (Figure S50b, see Supporting Information). The gelation ability of the mixed form compared to the enantiomers may be attributed to the hydrogen-bonded sheet-like architecture. The comparison of solid-state structures of the enantiomers and the reported **TAV** revealed that methylene groups did not alter the hydrogen bonding pattern, but the introduction of ethylene and methine groups resulted in a hydrogen-bonded corrugated 2-D sheet and 3-D networks in **2** and **3**, respectively, which highlights the importance of functional groups on the self-assembly process. The mixed gels with flexible linkers (**1** and **2**) displayed 1-D hydrogen-bonded chains, but the hydrogen-bonded dimers of the rigid linker **3**-(RR+SS) were propagated to form a 2-D corrugated sheet-like architecture.

Powder X-ray Diffraction (PXRD)

The phase purity of the compounds was analyzed using powder X-ray diffraction (PXRD).[14, 20] The PXRD patterns of the bulk crystals and xerogels were compared with the simulated pattern of the single-crystal structures of the corresponding gelators, which could help us to identify the role of various non–bonding interactions in the gel state.[4b, 14, 20-21] This approach is a promising technique to get an insight into the self-assembly process in LMWGs,[4b, 14, 20-21] but the preparation of xerogel can also result in a change in morphology or polymorphic phase transition.[22] The enantiomeric and mixed gels of **1** were prepared in *o*-xylene, *m*-xylene, *p*-xylene, ethanol/water (1:1, v/v) and DMSO/water (1:1, v/v) was filtered after 24 h and dried in air to obtain the xerogel.

The PXRD pattern of the bulk crystals and the xerogels of the individual enantiomers **1**-RR and **1**-SS and the mixed **1**-(RR+SS) matched with the simulated pattern of the corresponding crystal structure (Figure 5 and S51-S53, see Supporting Information), which suggests that the crystal structure and the hierarchical assembly of the xerogel network are similar.

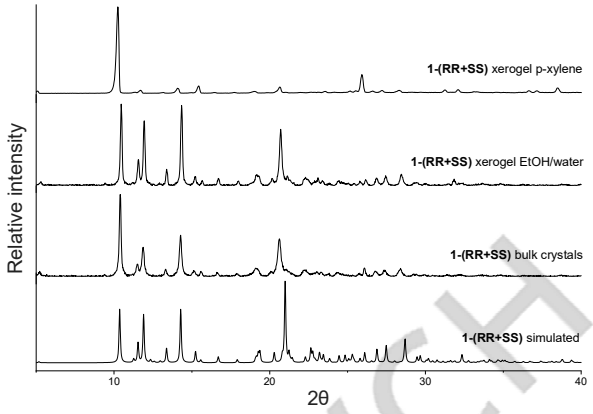

Figure 5. Comparison of PXRD pattern of equimolar **1-(RR+SS)**: simulated, bulk crystals obtained from ethanol/water and xerogel at 6.0 wt/v% obtained from ethanol/water (1:1, v/v) and at 7.0 wt/v% in p-xylene.

The *p*-xylene xerogels were weakly diffracting, presumably due to the poor crystallinity and low order of the dried gels compared to the crystalline state (Figure 5 and S51-S53, see Supporting Information).[4b] The PXRD pattern of the mixed **1**-(RR+SS) xerogels matched with the simulated pattern were different from the individual enantiomers, which confirms specific co-assembly in mixed gels (Figure 5).

The PXRD experiments with the enantiomers of **2** were performed with xerogels from *o*-xylene, *m*-xylene, *p*-xylene, and DMSO/water (1:1, v/v). The PXRD of the bulk crystals and the xerogels of **2**-RR and **2**-SS matched well, but the peaks were slightly shifted towards the lower 2θ value compared to the simulated pattern (Figure S54-S55, see Supporting Information). However, PXRD of the xerogels of the mixed **2**-(RR+SS) obtained by mixing enantiomers in DMSO/water (1:1, v/v) was slightly from the simulated pattern of **2**-(RR+SS) crystal structure, which can be attributed to the orthogonal self-assembly (Figure S56, see Supporting Information). This prompted us to evaluate the self-assembly modes of **2**-(RR+SS) in various solvents by crystallizing the mixture in *p*-xylene, methanol, ethanol, DMF, DMSO, and aqueous mixtures of ethanol, DMF and DMSO followed by PXRD analysis.

The PXRD pattern showed specific co-assembly in *p*-xylene, DMF and DMSO (Figure S57, see Supporting Information), but orthogonal co-assembly was observed for alcohols and aqueous mixtures after a week (Figure S58, see Supporting Information). We monitored the self-assembly of **2**-(RR+SS) in *p*-xylene by performing PXRD of samples dried at different time intervals, and the results indicated that the self-assembly process was not kinetically favored, which required a week to complete the self-assembly process. (Figure S59, see Supporting Information). Similar results were obtained in DMF and DMSO, but the self-assembly process was much faster, and specific co-assembly was observed within 4.0 hours (Figure S60-S61, see Supporting Information), which was performed by adding water at regular intervals to the DMF or DMSO solution of **2**-(RR+SS). The addition of water at different intervals resulted in a specific co-assembled (>24.0 hrs) network or orthogonal co-assembled (<12.0 hrs) systems (Figure S60-61, see Supporting Information).

The stability of the co-assembled network was analyzed by performing gelation experiments in DMSO/water (1:1, v/v) using **2**-(RR+SS) crystals and the PXRD pattern confirmed the retention of the self-assembled network (Figure S62, see Supporting Information) and similar results were obtained in aqueous mixtures of EtOH and DMF (Figure S63, see Supporting Information). The time-delayed self-assembly process in **2**-(RR+SS) may be attributed to the extended flexibility of the linkers, which requires large-scale conformational changes to form the co-assembled network.

The PXRD patterns of the bulk crystals of the enantiomers of **3** matched with the corresponding simulated patterns (Figure S64-65, see Supporting Information). The PXRD pattern of the bulk crystals of **3**-(RR+SS**)** and the xerogels obtained from DMSO/water (1:1, v/v) at 5.0 wt/v% matched perfectly well with the simulated pattern, confirming specific co-assembly Figure S66, see Supporting Information). PXRD patterns of the xerogels from *o*-xylene and *m*-xylene were less crystalline in nature with broader peaks, but the major peaks matched with the simulated pattern. Figure S67, see Supporting Information.

The analysis of the PXRD results of the xerogel of mixed gels (**1**-**3**) confirmed the formation of specific co-assembly in enantiomeric multi-component gels. Furthermore, we could monitor the kinetics of the self-assembly process in the mixed gel of **2** using PXRD analysis. The products obtained from the time-dependent self-assembly process of **2**-(RR+SS) were analyzed to support the findings. The T_{gel} experiments performed at 5.0 wt/v% in DMSO/water (1:1, v/v) with specifically co-assembled and the orthogonally co-assembled systems of **2**-(RR+SS) revealed that orthogonally co-assembled systems were thermally weaker (83.7 °C) than specifically co-assembled gels (91.1 °C). The frequency sweep experiments revealed that the mechanical strength, specifically co-assembled gel network was stronger compared to the orthogonally co-assembled gel but weaker than the individual enantiomeric gels (Figure S68, see Supporting Information), which was consistent with the thermal stability and similar results were obtained for xylene gels. These results were corroborated with the solid-state structures, indicating that the adjacent phenyl rings in **2**-(RR+SS) specific co-assembled displayed an offset face-to-face interaction. However, an edge-to-face π-π interaction was observed in the enantiomers, and the better gelation ability of the enantiomeric compounds may be attributed to the spatial arrangement of these functional groups.

Conclusion

We have synthesized and characterized a series of C_2-symmetric chiral bis-(amides) of methyl valinate appended to an aromatic platform (1,4-phenyl core) with rigid (**3**) and flexible linkers (**1** & **2**). The gelation properties of the enantiomers were compared with the corresponding multi-component gels obtained by mixing equimolar enantiomeric components. The enantiomers with flexible linkers formed a better gelation network at lower concentrations compared to the mixed enantiomeric compounds but mixing the gelators induced gelation for compounds with rigid linkers (**3**) or formed gels below the MGC of the enantiomers (TAV). The rheological experiments showed that the mechanical strength of the individual enantiomers with flexible linkers was higher compared to the mixed gels, but a reverse phenomenon was observed for rigid TAV gels, which was consistent with the thermal stabilities in most of the cases. The SEM images of the dried gels did not show drastic morphological changes for the enantiomeric and mixed gels, indicating that the chirality was not transferred to the fibrous network. We have proved that mixed gelators displayed specific co-assembly irrespective of the flexibility/rigidity of the linkers using single crystal X-ray diffraction. The self-assembly of the mixed gel with the more flexible linker (**2**) depends on the solvents and duration of the crystallization to attain thermodynamic equilibrium, yielding orthogonal self-assembly in the beginning and slowly transforming into specific co-assembly. We have analyzed the time-delayed self-assembly process in the mixed system of **2** using X-ray diffraction analysis. In summary, we have shown that different self-assembly modes are possible for a multi-component gel with flexible linkers, which was confirmed by X-ray crystallography. This will provide a key insight into the self-assembling nature of enantiomeric multi-component gels, which will help to design multi-component systems with tunable properties.

Experimental Section

The starting materials and solvents were commercially purchased from Sigma-Aldrich and TCI-Europe and were used as supplied, except for 1,4-bis(bromomethyl)benzene, which was purchased from Accel Pharmtech, USA. The circular dichroism and gelation experiments were performed using deionized water and freshly distilled ethanol. Enantiomeric (S or R)-methyl valinate hydrochloride salt was synthesized using the reported procedure. **1-RR** and **1-SS** were synthesized by following a protocol as reported by our group in our earlier work. The 1,4-phenylene diacetic acid, 3,3'-(1,4-phenylene)diacrylic acid, and 3,3'-(1,4-phenylene)dipropionic acid were synthesized following the literature (See supporting Information). ^{1}H and ^{13}C NMR spectra were recorded on a Bruker AVANCE 400 spectrometer (Figure S69-S80, see Supporting Information). Attenuated total reflectance−Fourier transform infrared (ATR−FTIR) was measured in a Nicolet iZ10, and circular dichroism was performed in a JASCO J-1100 CD spectrometer, respectively. The morphology of the xerogel was analyzed using a scanning electron microscope (SEM) with a Leo Supra 25 Microscope, while a Bruker D8 venture and Bruker D8 Focus instrument were used to carry out the single-crystal X-ray diffraction (SCXRD) and powder X-ray diffraction (PXRD).

Synthesis

1-RR and **1**-SS: Thionyl chloride (20.0 mL, 275.0 mmol) was added to a two-neck RB flask containing 1,4-phenylene diacetic acid (0.84 g, 4.3 mmol), and the mixture was refluxed overnight. The solution was evaporated to dryness by distillation to yield the corresponding acid chloride, which was used in the next step without any further purification. The amino acid ester (*S* or *R*)-methyl valinate hydrochloride (1.45 g, 10.0 mmol) was added to the flask under a dry N_2 atmosphere at 0 °C followed by the addition of $CHCl_3$ (40.0 mL). A solution of triethylamine (2.6 mL, 21.5 mmol) in $CHCl_3$ (25.0 mL) was added dropwise to the above solution, and the mixture was stirred overnight at room temperature. The solution was refluxed for 4.0 hrs, cooled to room temperature, and concentrated in a rotary vapor. DCM (50.0 mL) was added to this solution, which was washed with 3.0% $NaHCO_3$ (2 x 40.0 mL) and 0.05 M HCl (2 x 40.0 mL), followed by brine. The organic layer dried over Na_2SO_4 was evaporated to yield the desired amide as the white solid. The crude was recrystallized from a 1:1 ethanol/water solvent mixture combination to yield crystalline material.

1-SS: Yield 1.61 g, 88.0 %. ^{1}H NMR (400 MHz, Chloroform-*d*) δ 7.28 (s, 4H), 5.92 (d, *J* = 9.2 Hz, 2H), 4.57 – 4.49 (m, 2H), 3.69 (s, 6H), 3.60 (d, *J* = 1.5 Hz, 4H), 2.14 – 2.01 (m, 2H), 0.85 (d, *J* = 6.9 Hz, 6H), 0.77 (d, *J* = 6.8 Hz, 6H). ^{13}C {^{1}H} NMR (100 MHz, Chloroform-*d*) δ 172.47, 170.71, 133.98, 130.08, 57.16, 52.25, 43.47, 31.34, 19.03, 17.82. HRMS (APCI): calcd for $C_{22}H_{32}N_2O_6Na$ [M + Na]$^+$, 443.2158; found, 443.2153.

1-RR: Yield 1.58 g, 86.0 %. ^{1}H NMR (400 MHz, Chloroform-*d*) δ 7.28 (s, 4H), 5.91 (d, *J* = 8.8 Hz, 2H), 4.57 – 4.49 (m, 2H), 3.69 (s, 6H), 3.60 (d, *J* = 1.4 Hz, 4H), 2.17 – 2.01 (m, 2H), 0.85 (d, *J* = 6.9 Hz, 6H), 0.77 (d, *J* = 6.9 Hz, 6H). ^{13}C {^{1}H} NMR (100 MHz, Chloroform-*d*) δ 172.46, 170.69, 133.98, 130.07, 57.15, 52.25, 43.46, 31.33, 19.03, 17.82. HRMS (APCI): calcd for $C_{22}H_{32}N_2O_6Na$ [M + Na]$^+$, 443.2158; found, 443.2153.

2-RR and **2**-SS: The experimental procedure was similar to **1**. 3,3'-(1,4-phenylene)dipropionic acid (1.14 g, 5.1 mmol), thionyl chloride (20.0 mL), (*S* or *R*)-methyl valinate hydrochloride (1.71 g, 10.2 mmol) and triethtylamine 2.8 mL (2.1 g, 20.4 mmol).

2-SS: Yield 1.97 g, 86.1 %. ^{1}H NMR (400 MHz, Chloroform-*d*) δ 7.08 (s, 4H), 6.02 (d, *J* = 8.9 Hz, 2H), 4.59 – 4.51 (m, 2H), 3.72 (s, 6H), 2.92 (t, *J* = 7.2 Hz, 4H), 2.57 – 2.45 (m, 4H), 2.12 – 1.98 (m, 2H), 0.89 – 0.78 (m, 12H). ^{13}C {^{1}H} NMR (100 MHz, Chloroform-*d*) δ 172.78, 172.15, 138.70, 128.62, 56.98, 52.21, 38.65, 31.51, 31.47, 18.94, 17.93. HRMS (APCI): calcd for $C_{24}H_{36}N_2O_6Na$ [M + Na]$^+$, 471.2466; found, 471.2458.

2-RR: Yield 1.89 g, 82.9 %. ^{1}H NMR (400 MHz, Chloroform-*d*) δ 7.08 (s, 4H), 6.03 (d, *J* = 8.8 Hz, 2H), 4.59 – 4.51 (m, 2H), 3.72 (s, 6H), 2.92 (t, *J* = 7.9 Hz, 4H), 2.57 – 2.45 (m, 4H), 2.12 – 1.99 (m, 2H), 0.87 – 0.78 (m, 12H). ^{13}C {^{1}H} NMR (100 MHz, Chloroform-*d*) δ 172.78, 172.15, 138.70, 128.61, 56.97, 52.20, 38.64, 31.50, 31.46, 18.93, 17.93. HRMS (APCI): calcd for $C_{24}H_{36}N_2O_6Na$ [M + Na]$^+$, 471.2466; found, 471.2457.

3-RR and **3**-SS: The experimental procedure was similar to the **1**. 3,3'-(1,4-phenylene)diacrylic acid (1.28 g, 5.9 mmol), thionyl chloride (20.0 mL), (*S* or *R*)-methyl valinate hydrochloride (1.97 g, 11.7 mmol) and triethtylamine 3.3 mL (2.4 g, 23.5 mmol).

3-SS: Yield 1.92 g, 73.6 %.^{1}H NMR (400 MHz, Chloroform-*d*) δ 7.61 (d, *J* = 15.6 Hz, 2H), 7.49 (s, 4H), 6.50 (d, *J* = 15.6 Hz, 2H), 6.26 (d, *J* = 8.8 Hz, 2H), 4.76 – 4.68 (m, 2H), 3.76 (s, 6H), 2.29 – 2.16 (m, 2H), 1.01 – 0.92 (m, 12H). ^{13}C {^{1}H} NMR (100 MHz, Chloroform-*d*) δ 172.82, 165.62, 140.94, 136.17, 128.43, 121.16, 57.36, 52.39, 31.67, 19.10, 18.04. HRMS (APCI): calcd for $C_{24}H_{32}N_2O_6Na$ [M + Na]$^+$, 467.2153; found, 467.2142.

3-RR: Yield 1.83 g, 70.1 %. ^{1}H NMR (400 MHz, Chloroform-*d*) δ 7.61 (d, *J* = 15.5 Hz, 2H), 7.48 (s, 2H), 6.51 (d, *J* = 15.6 Hz, 2H), 6.29 (d, *J* = 8.8 Hz, 2H), 4.77 – 4.68 (m, 2H), 3.76 (s, 6H), 2.29 – 2.16 (m, 2H), 1.01 – 0.92 (m, 12H). ^{13}C {^{1}H} NMR (100 MHz, Chloroform-*d*) δ 172.83, 165.64, 140.94, 136.18, 128.43, 121.16, 57.36, 52.40, 31.67, 19.10, 18.04. HRMS (APCI): calcd for $C_{24}H_{32}N_2O_6Na$ [M + Na]$^+$, 467.2153; found, 467.2130.

Gelation Details

Gelation Test: In a standard 7.0 mL vial with an inner diameter of 1.5 cm, an appropriate amount of gelator was taken, and 1.0 mL of solvent was added. An equimolar ratio of individual RR- and SS- compounds was mixed to prepare the (RR+SS), followed by adding the solvent/solvent mixture. The vial was closed, slowly heated, and gently shaken to get a clear solution and was left undisturbed for gelation. An inversion test was performed after 24.0 h to confirm the gel formation.

Minimum Gel Concentration (MGC): The gel was prepared following the above procedure by dissolving the compounds in 1.0 mL of the solvent. An additional amount of the solvent was added portion-wise, the heating-cooling process was repeated, and the sample vial was inverted to observe no flow of the solvent. This was repeated until a small amount of the solvent was observed on the top of the gel, and the concentration just above this point where we observed a stable gel after 24.0 h was recorded as the MGC.

T_{gel} Experiment: In a standard 7.0 mL vial, the appropriate amount of the gelator was taken, and 1.0 mL of solvent was added. The mixture was sonicated and heated to obtain a clear solution and left undisturbed for gelation. A tiny spherical glass ball (106.0 mg) was carefully put on top of the gel after 24 hrs. The vial was immersed in an oil bath fitted with a thermosensor and magnetic stirrer. The oil bath temperature was gradually raised by around 10.0 °C per minute. At a certain temperature, the glass ball slowly immerses into the gel, and the temperature at which the glass ball touched the bottom of the vial was noted as the T_{gel}.

Rheology

The mechanical strengths of the gels formed were measured using a stainless-steel parallel plate geometry design with a diameter of 25.0 mm in an MCR 102 Anton Paar modular compact rheometer. Rheological experiments were performed at a gap height of 1.0 mm, and experiments were carried out by scoping a ~1.0 mL portion of gel on the plate. Oscillatory measurements were performed to evaluate the viscoelastic properties at a constant temperature of 25.0 °C. Amplitude sweeps were performed with a constant frequency (f) of 1.0 Hz and log ramp strain (γ) = 0.01−100%, while the frequency sweeps were carried out between 0.01 and 10.0 Hz within the linear viscoelasticity domain (0.02% strain). A Peltier temperature control hood was used to avoid evaporation and maintain a temperature of 25.0 °C for frequency and amplitude sweeps.All of the amplitude sweep experiments were performed at a constant frequency of 1.0 Hz, while the frequency sweep experiments were performed at a constant shear strain of 0.02 %. Gels of **1**-RR and **1**-SS were prepared at 6.0 wt/v% of the corresponding gelator in 1.0 mL of ethanol/water, and the **1**-(RR+SS) gel was prepared by dissolving a mixture of 30.0 mg of **1**-RR and 30.0 mg of **1**-SS in 1.0 mL of ethanol/water (1:1, v/v). Similarly, we performed the frequency sweep experiments of gelators **1** in *n*-butanol and *p*-xylene at 6.0 and 7.0 wt/v%, respectively. Rheological experiments were also performed with **2**-RR, **2**-SS, and mixed **2**-(RR+SS) gels in DMSO/water (1:1, v/v) at 5.0 wt/v%. We have also analyzed the rheological properties of the individual enantiomeric gels of **2**-RR and **2**-SS in xylenes at 5.0 wt/v%. The mechanical strength of the equimolar mixed **3**-(RR+SS) gel in *o*-xylene and *m*-xylene was measured at 2.0 wt/v%.

Scanning Electron Microscopy (SEM)

The enantiomeric and the mixed gels of **1** were prepared at 6.0 wt/v% in 2-propanol, *n*-butanol, ethanol/water (1:1, v/v), and 7.0 wt/v% in toluene and xylenes. The gels of **2**-RR and **2**-SS were obtained at 5.0 wt/v% in xylenes, mesitylene, and toluene. Similarly, gels of equimolar **3**-(RR+SS) in *o*-xylene and *m*-xylene were prepared at 2.0 wt/v%. The gels obtained were filtered after a span of 24 hrs. It was then dried in air to obtain the xerogel, and a small portion of the xerogel was placed on a pin mount with the carbon tab on top and coated with gold for 2.0-3.0 min. On a Leo Supra 25 microscope with an in-lens detector at an operating voltage of 3.0 kV and a working distance of 3.0-4.0 mm, the morphologies of the dried gels were examined.

Circular Dichroism (CD)

A JASCO J-1100 CD spectrometer was used to collect the data between 200 and 320 nm wavelengths at a 20.0 nm per minute rate, with a bandwidth of 1.0 nm, and in a continuous scanning mode. The enantiomeric (**1**-RR and **1**-SS) and the equimolar mixed **1**-(RR+SS) gels were prepared at 6.0 wt/v% in ethanol/water (1:1, v/v). After 24 h, the gels were dispersed in ethanol/water (1:1, v/v) to obtain various concentrations (0.025, 0.03, and 0.035 wt/v%), and 0.03 wt/v% was the optimum concentration. The solution state experiments with gelators **1**-**3** were performed by dissolving 10.0 mg of the corresponding gelator in 3.0 mL of

absolute ethanol, and it was diluted ten times in the same solvent to conduct the CD experiments.

Crystallography

Single-crystal X-ray Diffraction (SCXRD): Single crystals of all the enantiomers and mixed compounds of **1** were obtained by the slow evaporation of 10.0 mg/mL of the corresponding compounds in ethanol/water (1:1, v/v), resulting in colorless needle-shaped crystals. Similarly, needle-shaped X-ray quality crystals of **2**-RR and **2**-SS were obtained by the slow evaporation of 30.0 mg of the corresponding compounds in 1.0 mL acetonitrile. The crystallization of **3**-RR and **3**-SS by the slow evaporation of 10.0 mg of the compound in 2.0 mL of acetonitrile yielded colorless block-shaped crystals. The experiments performed by dissolving 10.0 mg of equimolar **3**-(RR+SS) in 2.0 mL ethanol/water (1:1, v/v) mixture resulted in needle-shaped single crystals. The crystallization experiments with mixed **2**-(RR+SS) were challenging, and the initial trials did not yield good crystals suitable for SCXRD. The crystals obtained in (1:1, v/v) ethanol/water and DMF/water yielded poor-quality crystals. The unit cell matched with the individual enantiomers (2-RR and 2-SS), indicating self-sorting or random co-assembly. We recrystallized the air-dried colloid (obtained at 5.0 wt/v% in *p*-xylene) in 2.0 mL ethanol/water (1:1, v/v) to yield **2**-(RR+SS) crystals. X-ray analysis was conducted on a Bruker D8 Venture (Photon100 CMOS detector) diffractometer implemented with Cryostream (Oxford Cryosystems) open-flow nitrogen cryostats. The crystal data were collected at 150(2) K using CuK_α radiation (λ = 1.542 Å) for all the crystals except for the equimolar **2**-(RR+SS) with MoK_α radiation (λ = 0.71073 Å). The unit cell determination, data collection, data reduction, structure solution/refinement, and empirical absorption correction were performed in apex-III software (Bruker AXS: Madison, WI, 2015). All structures were solved using the direct method and refined by the full-matrix least-squares on F^2 for all data using SHELXTL. All non-disordered non-hydrogen atoms were refined anisotropically. All the hydrogen atoms were placed in the calculated positions and refined using a riding model. Crystallographic data for the structures are deposited to Cambridge Crystallographic Data Centre as supplementary publication (CCDC no: 2414646-2414654).

Powder X-ray Diffraction (PXRD)

The crystalline bulk compounds of **1**-**2** were obtained by the slow evaporation of the solution of the corresponding compounds (40.0 mg) in 2.0 mL of ethanol/water (1:1, v/v). The bulk crystals of **3**-RR, **3**-SS, and equimolar **3**-(RR+SS) were obtained by the slow evaporation of the 20.0 mg of the compounds in 2.0 mL of acetonitrile. The obtained crystals were filtered, vacuum-dried, and ground to a fine powder. PXRD was also performed on the xerogels of **1** obtained from the corresponding gels made in ethanol/water (1:1, v/v) at 6.0 wt/v% and *p*-xylene at 7.0 wt/v%. The **2**-RR and **2**-SS xerogels were obtained from 5.0 wt/v% gels in *o*-xylene, *m*-xylene, and DMSO/water (1:1, v/v) and **2**-(RR+SS) xerogels were prepared from DMSO/water (1:1, v/v) at 5.0 wt/v%. Similarly, the mixed **3**-(RR+SS) xerogels were prepared from *o*-xylene and *m*-xylene at 2.0 wt/v% and DMSO/water (1:1, v/v) at 5.0 wt/v%. All the xerogels were prepared following the sample preparation procedure for SEM analysis. The PXRD experiments were carried out in a PANalytical instrument with Cu anode, between 2θ from 4.0 to 50.0, and a step size of 0.025.

Acknowledgments

We thank the University of Iceland Research Fund and Icelandic Research Fund (IRF-228902-051) Rannís Iceland for funding. We acknowledge Sigrídur Jónsdóttir, University of Iceland, for NMR and mass spectrometry, and Fridrik Magnus, University of Iceland, for powder X-ray diffraction analysis, and Department of Biochemistry for the circular dichroism experiments. S.S.J. thanks the University of Iceland for the doctoral research grant. We thank Rannís Iceland for infrastructure grants (150998-0031 and 191763-0031) for a single crystal X-ray diffractometer and rheometer.

Conflict of interest

The authors declare no conflict of interest.

Keywords: self-assembly• multi-component gels • specific co-assembly • rigid and flexible linker • single-crystal X-ray diffraction.

References

[1] a) S. Banerjee, R. K. Das and U. Maitra, *Journal of Materials Chemistry* **2009**, *19*, 6649-6687; b) P. Dastidar, *Chemical Society Reviews* **2008**, *37*, 2699-2715; c) M. de Loos, B. L. Feringa and J. H. van Esch, *European Journal of Organic Chemistry* **2005**, *2005*, 3615-3631; d) L. A. Estroff and A. D. Hamilton, *Chemical Reviews* **2004**, *104*, 1201-1218; e) M. George and R. G. Weiss, *Accounts of Chemical Research* **2006**, *39*, 489-497; f) D. K. Kumar and J. W. Steed, *Chemical Society Reviews* **2014**, *43*, 2080-2088; g) P. R. A. Chivers and D. K. Smith, *Nature Reviews Materials* **2019**, *4*, 463-478.

[2] a) L. E. Buerkle and S. J. Rowan, *Chemical Society Reviews* **2012**, *41*, 6089-6102; b) C.-W. Chu and C. A. Schalley, *Organic Materials* **2021**, *03*, 025-040; c) J. Raeburn and D. J. Adams, *Chemical Communications* **2015**, *51*, 5170-5180; d) D. K. Smith, *Chem Soc Rev* **2009**, *38*, 684-694.

[3] a) P. Duan, H. Cao, L. Zhang and M. Liu, *Soft Matter* **2014**, *10*, 5428-5448; b) J. R. Moffat and D. K. Smith, *Chemical Communications* **2009**, 316-318; c) W. Edwards and D. Smith, *Gels* **2018**, *4*, 31; d) P. Xing, H. P. Tham, P. Li, H. Chen, H. Xiang and Y. Zhao, *Advanced Science* **2018**, *5*, 1700552; e) M. Halperin-Sternfeld, M. Ghosh, R. Sevostianov, I. Grigoriants and L. Adler-Abramovich, *Chemical Communications* **2017**, *53*, 9586-9589; f) G. Fichman, T. Guterman, L. Adler-Abramovich and E. Gazit, *CrystEngComm* **2015**, *17*, 8105-8112; g) M. M. Smith and D. K. Smith, *Soft Matter* **2011**, *7*, 4856-4860; h) D. Li, Y. Shi and L. Wang, *Chinese Journal of Chemistry* **2014**, *32*, 123-127; i) J. A. Foster, R. M. Edkins, G. J. Cameron, N. Colgin, K. Fucke, S. Ridgeway, A. G. Crawford, T. B. Marder, A. Beeby, S. L. Cobb and J. W. Steed, *Chemistry – A European Journal* **2014**, *20*, 279-291; j) A. Das and S. Ghosh, *Chemical Communications* **2011**, *47*, 8922-8924; k) K. L. Morris, L. Chen, J. Raeburn, O. R. Sellick, P. Cotanda, A. Paul, P. C. Griffiths, S. M. King, R. K. O'Reilly, L. C. Serpell and D. J. Adams, *Nature Communications* **2013**, *4*, 1480; l) P. Sahoo, K. Damdoaran, S. Raghavan and P. Dastidar, *Chemistry, an Asian journal* **2011**, *6*, 1038-1047; m) G. Radau, *Monatshefte für Chemie/Chemical Monthly* **2003**, *134*, 1159-1166; n) A. Brizard, R. Oda and I. Huc, *Topics in current chemistry* **2005**, *256*, 167-218.

[4] a) A. K. Patterson, L. H. El-Qarra and D. K. Smith, *Chemical Communications* **2022**, *58*, 3941-3944; b) D. Ghosh, A. D. Farahani, A. D. Martin, P. Thordarson and K. K. Damodaran, *Chemistry of Materials* **2020**, *32*, 3517-3527; c) K. McAulay, B. Dietrich, H. Su, M. T. Scott, S. Rogers, Y. K. Al-Hilaly, H. Cui, L. C. Serpell, Annela M. Seddon, E. R. Draper and D. J. Adams, *Chemical Science* **2019**, *10*, 7801-7806; d) K. Nagy-Smith, P. J. Beltramo, E. Moore, R. Tycko, E. M. Furst and J. P. Schneider, *ACS Cent Sci* **2017**, *3*, 586-597; e) Z. Liu, J. Sun, Y. Zhou, Y. Zhang, Y. Wu, S. K. M. Nalluri, Y. Wang, A. Samanta, C. A. Mirkin, G. C. Schatz and J. F. Stoddart, *The Journal of Organic Chemistry* **2016**, *81*, 2581-2588; f) R. J. Swanekamp, J. T. M. DiMaio, C. J. Bowerman and B. L. Nilsson, *Journal of the American Chemical Society* **2012**, *134*, 5556-5559; g) K. J. Nagy, M. C. Giano, A. Jin, D. J. Pochan and J. P. Schneider, *Journal of the American Chemical Society* **2011**, *133*, 14975-14977; h) R. K. Das, R. Kandanelli, J. Linnanto, K. Bose and U. Maitra, *Langmuir*

2010, *26*, 16141-16149; i) X. Zhu, Y. Li, P. Duan and M. Liu, *Chemistry – A European Journal* **2010**, *16*, 8034-8040; j) A. R. Hirst, D. K. Smith, M. C. Feiters and H. P. M. Geurts, *Chemistry – A European Journal* **2004**, *10*, 5901-5910; k) B. Adhikari, J. Nanda and A. Banerjee, *Soft Matter* **2011**, *7*, 8913-8922; l) S. Cicchi, G. Ghini, L. Lascialfari, A. Brandi, F. Betti, D. Berti, P. Baglioni, L. Di Bari, G. Pescitelli, M. Mannini and A. Caneschi, *Soft Matter* **2010**, *6*, 1655-1661; m) L. Lascialfari, G. Pescitelli, A. Brandi, M. Mannini, D. Berti and S. Cicchi, *Soft Matter* **2015**, *11*, 8333-8341; n) D. A. Tómasson, D. Ghosh, Z. Kržišnik, L. H. Fasolin, A. A. Vicente, A. D. Martin, P. Thordarson and K. K. Damodaran, *Langmuir* **2018**, *34*, 12957-12967; o) S. Panja, B. Dietrich, A. J. Smith, A. Seddon and D. J. Adams, *ChemSystemsChem* **2022**, *4*, e202200008; p) C. Colquhoun, E. R. Draper, E. G. B. Eden, B. N. Cattoz, K. L. Morris, L. Chen, T. O. McDonald, A. E. Terry, P. C. Griffiths, L. C. Serpell and D. J. Adams, *Nanoscale* **2014**, *6*, 13719-13725.

[5] a) Z. Džolić, K. Wolsperger and M. Žinić, *New Journal of Chemistry* **2006**, *30*, 1411-1419; b) H. Shigemitsu, T. Fujisaku, W. Tanaka, R. Kubota, S. Minami, K. Urayama and I. Hamachi, *Nature Nanotechnology* **2018**, *13*, 165-172; c) S. Onogi, H. Shigemitsu, T. Yoshii, T. Tanida, M. Ikeda, R. Kubota and I. Hamachi, *Nature Chemistry* **2016**, *8*, 743; d) E. R. Draper and D. J. Adams, *Chemical Society Reviews* **2018**, *47*, 3395-3405.

[6] S. Panja, B. Dietrich, A. Trabold, A. Zydel, A. Qadir and D. J. Adams, *Chemical Communications* **2021**, *57*, 7898-7901.

[7] S. Sudhakaran Jayabhavan, G. Kuppadakkath and K. K. Damodaran, *ChemPlusChem* **2023**, *88*, e202300302.

[8] a) S. Guo, M. Song, X. Gao, L. Dong, T. Hou, X. Lin, W. Tan, Y. Cao, M. Rogers and Y. Lan, *Food & Function* **2020**, *11*, 7651-7660; b) S. Fleming, S. Debnath, P. W. J. M. Frederix, N. T. Hunt and R. V. Ulijn, *Biomacromolecules* **2014**, *15*, 1171-1184; c) A. S. W. Chan and P. R. Sundararajan, *ChemistrySelect* **2017**, *2*, 1149-1157; d) J. N. Loos, F. D'Acierno, U. Vijay Mody and M. J. MacLachlan, *ChemPlusChem* **2022**, *87*, e202200026; e) F. Aparicio, E. Matesanz and L. Sánchez, *Chemistry–A European Journal* **2014**, *20*, 14599-14603; f) J. Liu, F. Yuan, X. Ma, D. i. Y. Auphedeous, C. Zhao, C. Liu, C. Shen and C. Feng, *Angew. Chem. Int. Ed* **2018**, *130*, 6585-6589.

[9] a) N. Mehwish, X. Dou and C. Feng, *European Polymer Journal* **2019**, *117*, 236-253; b) D. Yuan, X. Du, J. Shi, N. Zhou, J. Zhou and B. Xu, *Angewandte Chemie International Edition* **2015**, *54*, 5705-5708.

[10] M. Suzuki and K. Hanabusa, *Chemical Society reviews* **2009**, *38*, 967-975.

[11] a) F. Fages, F. Vögtle and M. Žinic in *Systematic Design of Amide- and Urea-Type Gelators with Tailored Properties*, Springer Berlin Heidelberg, Berlin, Heidelberg, **2005**, pp. 77-131; b) M. Sarkar and K. Biradha, *Chemical Communications* **2005**, 2229-2231.

[12] C. Kaiser, A. Schmiedel, M. Holzapfel and C. Lambert, *The Journal of Physical Chemistry C* **2012**, *116*, 15265-15280.

[13] a) J. W. Goodwin and R. W. Hughes, *Rheology for chemists: an introduction*, Royal Society of Chemistry, **2008**, p; b) J.-M. Guenet, *Organogels: Thermodynamics, structure, solvent role, and properties*, Springer, **2016**, p.

[14] G. Yu, X. Yan, C. Han and F. Huang, *Chemical Society Reviews* **2013**, *42*, 6697-6722.

[15] G. Gottarelli, S. Lena, S. Masiero, S. Pieraccini and G. P. Spada, *Chirality* **2008**, *20*, 471-485.

[16] a) S.-Y. Qin, Y. Pei, X.-J. Liu, R.-X. Zhuo and X.-Z. Zhang, *Journal of Materials Chemistry B* **2013**, *1*, 668-675; b) S. Shin, S. Lim, Y. Kim, T. Kim, T.-L. Choi and M. Lee, *Journal of the American Chemical Society* **2013**, *135*, 2156-2159.

[17] M. Gupta, A. Bagaria, A. Mishra, P. Mathur, A. Basu, S. Ramakumar and V. S. Chauhan, *Advanced Materials* **2007**, *19*, 858-861.

[18] a) D. K. Kumar, D. A. Jose, A. Das and P. Dastidar, *Chemical Communications* **2005**, 4059-4061; b) S. Abraham, Y. Lan, R. S. H. Lam, D. A. S. Grahame, J. J. H. Kim, R. G. Weiss and M. A. Rogers, *Langmuir* **2012**, *28*, 4955-4964; c) Y. Xu, C. Kang, Y. Chen, Z. Bian, X. Qiu, L. Gao and Q. Meng, *Chemistry – A European Journal* **2012**, *18*, 16955-16961; d) Y. Wang, L. Tang and J. Yu, *Crystal Growth & Design* **2008**, *8*, 884-889; e) D. Braga, S. d'Agostino, E. D'Amen and F. Grepioni, *Chemical Communications* **2011**, *47*, 5154-5156; f) P. Byrne, G. O. Lloyd, L. Applegarth, K. M. Anderson, N. Clarke and J. W. Steed, *New Journal of Chemistry* **2010**, *34*, 2261-2274; g) P. Dastidar, R. Roy, R. Parveen and K. Sarkar, *Advanced Therapeutics* **2019**, *2*, 1800061; h) D. K. Kumar, D. A. Jose, P. Dastidar and A. Das, *Langmuir* **2004**, *20*, 10413-10418.

[19] J. R. Engstrom, A. J. Savyasachi, M. Parhizkar, A. Sutti, C. S. Hawes, J. M. White, T. Gunnlaugsson and F. M. Pfeffer, *Chemical Science* **2018**, *9*, 5233-5241.

[20] a) D. Ghosh, I. Lebedytė, D. S. Yufit, K. K. Damodaran and J. W. Steed, *CrystEngComm* **2015**, *17*, 8130-8138; b) S. Sudhakaran Jayabhavan, D. Ghosh and K. K. Damodaran, *Molecules* **2021**, *26*, 6420.

[21] a) D. Ghosh, M. T. Mulvee and K. K. Damodaran, *Molecules* **2019**, *24*, 3472; b) D. Ghosh, Deepa and K. K. Damodaran, *Supramolecular Chemistry* **2020**, *32*, 276-286.

[22] D. J. Adams, *Gels* **2018**, *4*, 32.

Entry for the Table of Contents

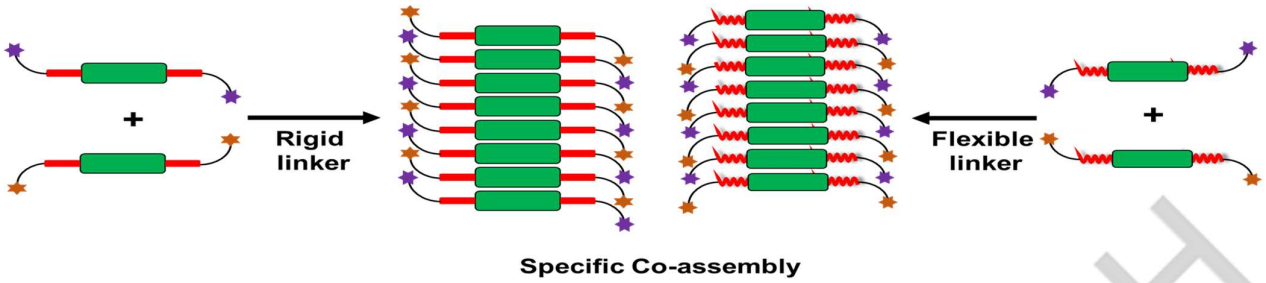

We have examined the role of the flexible and rigid core of the gelator structure in their self-assembly modes in multi-component gels based on enantiomers. The equimolar mixed gels based on the rigid linker formed specific co-assembled network with ease, however, the equimolar mixed gels based on flexible linkers had to undergo structural transformation to achieve the thermodynamically favored specific co-assembly.

SUPPORTING INFORMATION

Flexibility of Linkers: An Important Factor in Tuning the Gelation Properties in Multi-Component Based Gels

Sreejith Sudhakaran Jayabhavan, and Krishna K. Damodaran*

Contents

1. Synthetic Scheme

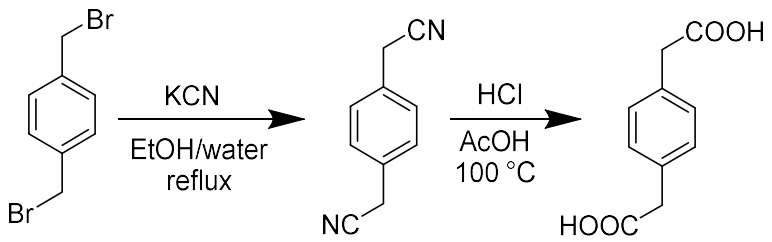

Scheme S1. Synthetic route for 1,4-phenylenediacetic acid.

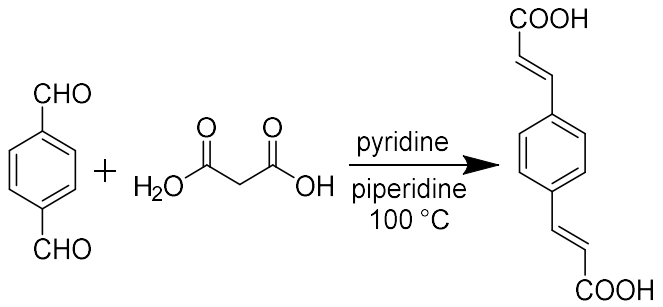

Scheme S2. Synthetic route for 1,4-phenylenediacrylic acid.

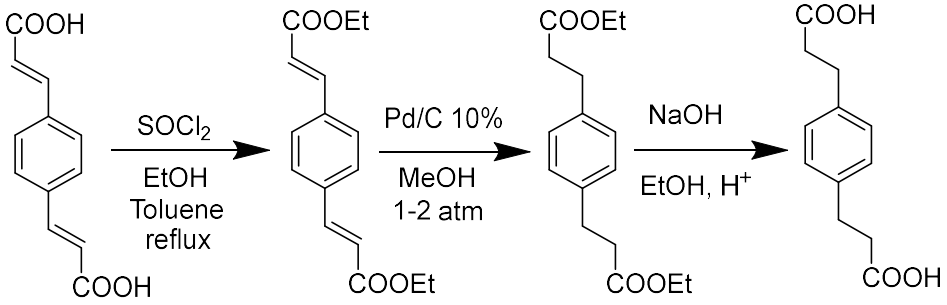

Scheme S3. Synthetic route for 1,4-phenylenedipropionic acid.

2. Gelation studies

Table S1. Gelation Experiments

Solvent	Gelation test at 1.0 wt/v%								
	1-RR	**1-SS**	**1-(RR+SS)**	**2-RR**	**2-SS**	**2-(RR+SS)**	**3-RR**	**3-SS**	**3-(RR+SS)**
2-propanol	$G^{\#\#}$	$G^{\#\#}$	$G^{\$}$	$Cry^{\#\#}$	$Cry^{\#\#}$	$Cry^{\#\#}$	$Ppt^{\#\#}$	$Ppt^{\#\#}$	$Ppt^{\#\#}$
n-butanol	$G^{\#\#}$	$G^{\#\#}$	$G^{\$}$	$Cry^{\#\#}$	$Cry^{\#\#}$	$Cry^{\#\#}$	$Ppt^{\#\#}$	$Ppt^{\#\#}$	$Ppt^{\#\#}$
2-butanol	$G^{\#\#}$	$G^{\#\#}$	$G^{\$}$	$Cry^{\#\#}$	$Cry^{\#\#}$	$Cry^{\#\#}$	$Ppt^{\#\#}$	$Ppt^{\#\#}$	$Ppt^{\#\#}$
pentanol	$G^{\#\#}$	$G^{\#\#}$	$G^{\$}$	$Cry^{\#\#}$	$Cry^{\#\#}$	$Cry^{\#\#}$	$Ppt^{\#\#}$	$Ppt^{\#\#}$	$Ppt^{\#\#}$
2-pentanol	$G^{\#\#}$	$G^{\#\#}$	$G^{\$}$	$Cry^{\#\#}$	$Cry^{\#\#}$	$Cry^{\#\#}$	$Ppt^{\#\#}$	$Ppt^{\#\#}$	$Ppt^{\#\#}$
ethylene glycol	$G^{\#}$	$G^{\#}$	$G^{\#\#}$	$Cry^{\#\#}$	$Cry^{\#\#}$	$Cry^{\#\#}$	$Ppt^{\#\#}$	$Ppt^{\#\#}$	$Ppt^{\#\#}$
p-xylene	$G^{\#\#}$	$G^{\#\#}$	$G^{\$\$}$	$G^{\#\#}$	$G^{\#\#}$	$C^{\$\$}$	C*	C*	C*
m-xylene	$G^{\#\#}$	$G^{\#\#}$	$G^{\$\$}$	$G^{\#\#}$	$G^{\#\#}$	$C^{\$\$}$	C*	C*	G*
o-xylene	$G^{\#\#}$	$G^{\#\#}$	$G^{\$\$}$	$G^{\#\#}$	$G^{\#\#}$	$C^{\$\$}$	C*	C*	G*
toluene	$G^{\#\#}$	$G^{\#\#}$	$G^{\$\$}$	$G^{\#\#}$	$G^{\#\#}$	$C^{\$\$}$	C*	C*	C*
mesitylene	$G^{\#\#}$	$G^{\#\#}$	$G^{\$\$}$	$G^{\#\#}$	$G^{\#\#}$	$C^{\$\$}$	C*	C*	C*
methanol/water (1:1, v/v)	$G^{\#}$	$G^{\#}$	$G^{\#\#}$	$Cry^{\#\#}$	$Cry^{\#\#}$	$Cry^{\#\#}$	Cry*	Cry*	Cry*
ethanol/water (1:1, v/v)	$G^{\#\#}$	$G^{\#\#}$	$G^{\#\#}$	$Cry^{\#\#}$	$Cry^{\#\#}$	$Cry^{\#\#}$	Cry*	Cry*	Cry*
DMF/water (1:1, v/v)	$G^{\#\#}$	$G^{\#\#}$	$G^{\#\#}$	$PG^{\$\$}$	$PG^{\$\$}$	$Cry^{\$\$}$	$C^{\#\#}$	$C^{\#\#}$	$C^{\#\#}$
DMSO/water (1:1, v/v)	$G^{\#}$	$G^{\#}$	$G^{\#\#}$	$G^{\#\#}$	$G^{\#\#}$	$G^{\#\#}$	$C^{\#\#}$	$C^{\#\#}$	$G^{\#\#}$

G= gel, G^{*}= 2.0 wt/v%, G^{**}= 3.0 wt/v%, $G^{\#}$= 4.0 wt/v%, $G^{\#\#}$= 5.0 wt/v%, $G^{\$}$= 6.0 wt/v%, $G^{\$\$}$= 7.0 wt/v%, S= solution, Cry= crystals, C= colloid, PG= partial gel.

Table S2. Determination of Minimum Gel Concentration (MGC)

Solvent	MGC (wt/v%)								
	1-RR	**1**-SS	**1**-(RR+SS)	**2**-RR	**2**-SS	**2**-(RR+SS)	**3**-RR	**3**-SS	**3**-(RR+SS)
2-propanol	4.8	4.6	5.8	----	----	----	----	----	----
2-butanol	4.8	4.8	5.8	----	----	----	----	----	----
n-butanol	4.8	4.6	5.8	----	----	----	----	----	----
2-pentanol	5.0	4.8	6.0	----	----	----	----	----	----
ethylene glycol	3.6	3.6	4.5	----	----	----	----	----	----
p-xylene	4.5	4.5	7.0	2.8	2.8	----	----	----	----
m-xylene	4.6	4.6	6.8	4.0	3.8	----	----	----	1.8
o-xylene	4.5	4.5	7.0	3.0	2.8	----	----	----	1.6
toluene	4.8	4.6	6.8	4.2	4.0	----	----	----	----
mesitylene	4.6	4.4	6.6	3.0	3.0	----	----	----	----
methanol/water (1:1, v/v)	4.0	4.0	4.8	----	----	----	----	----	----
ethanol/water (1:1, v/v)	3.8	3.8	4.5	----	----	----	----	----	----
DMF/water (1:1, v/v)	4.8	4.6	5.0	----	----	----	----	----	----
DMSO/water (1:1, v/v)	4.0	4.0	4.5	4.2	4.0	4.2	----	----	4.7

Table S3. Determination of Sol-gel Transition Temperature (T_{gel})

Solvent	T_{gel} (°C)								
	1-RR	**1**-SS	**1**-(RR+SS)	**2**-RR	**2**-SS	**2**-(RR+SS)	**3**-RR	**3**-SS	**3**-(RR+SS)
2-butanol	64.6$^{\$}$	64.2$^{\$}$	62.2$^{\$}$	----	----	----	----	----	----
n-butanol	63.9$^{\$}$	64.5$^{\$}$	61.9$^{\$}$	----	----	----	----	----	----
2-pentanol	69.6$^{\$}$	68.8$^{\$}$	64.6$^{\$}$	----	----	----	----	----	----
p-xylene	108.1$^{\$\$}$	109.4$^{\$\$}$	99.8$^{\$\$}$	92.8$^{\#\#}$	94.3$^{\#\#}$	----	----	----	----
m-xylene	110.4$^{\$\$}$	112.2$^{\$\$}$	102.3$^{\$\$}$	96.5$^{\#\#}$	99.2$^{\#\#}$	----	----	----	108.1*
o-xylene	108.3$^{\$\$}$	108.6$^{\$\$}$	100.2$^{\$\$}$	97.2$^{\#\#}$	98.1$^{\#\#}$	----	----	----	142.7*
toluene	105.2$^{\$\$}$	104.5$^{\$\$}$	94.8$^{\$\$}$	90.8$^{\#\#}$	87.1$^{\#\#}$	----	----	----	----
mesitylene	113.8$^{\$\$}$	116.4$^{\$\$}$	109.0$^{\$\$}$	105.4$^{\#\#}$	108.8$^{\#\#}$	----	----	----	----
methanol/water (1:1, v/v)	65.2$^{\$}$	65.0$^{\$}$	60.5$^{\$}$	----	----	----	----	----	----
ethanol/water (1:1, v/v)	66.3$^{\$}$	66.1$^{\$}$	64.9$^{\$}$	----	----	----	----	----	----
DMF/water (1:1, v/v)	94.4$^{\$}$	95.1$^{\$}$	91.4$^{\$}$	----	----	----	----	----	----
DMSO/water (1:1, v/v)	101.9$^{\$}$	103.6$^{\$}$	93.2$^{\$}$	94.5$^{\#\#}$	96.8$^{\#\#}$	83.7$^{\#\#}$	----	----	115.3

*= 2.0 wt/v%, $^{\#\#}$= 5.0 wt/v%, $^{\$}$= 6.0 wt/v%, $^{\$\$}$= 7.0 wt/v%

3. Rheology

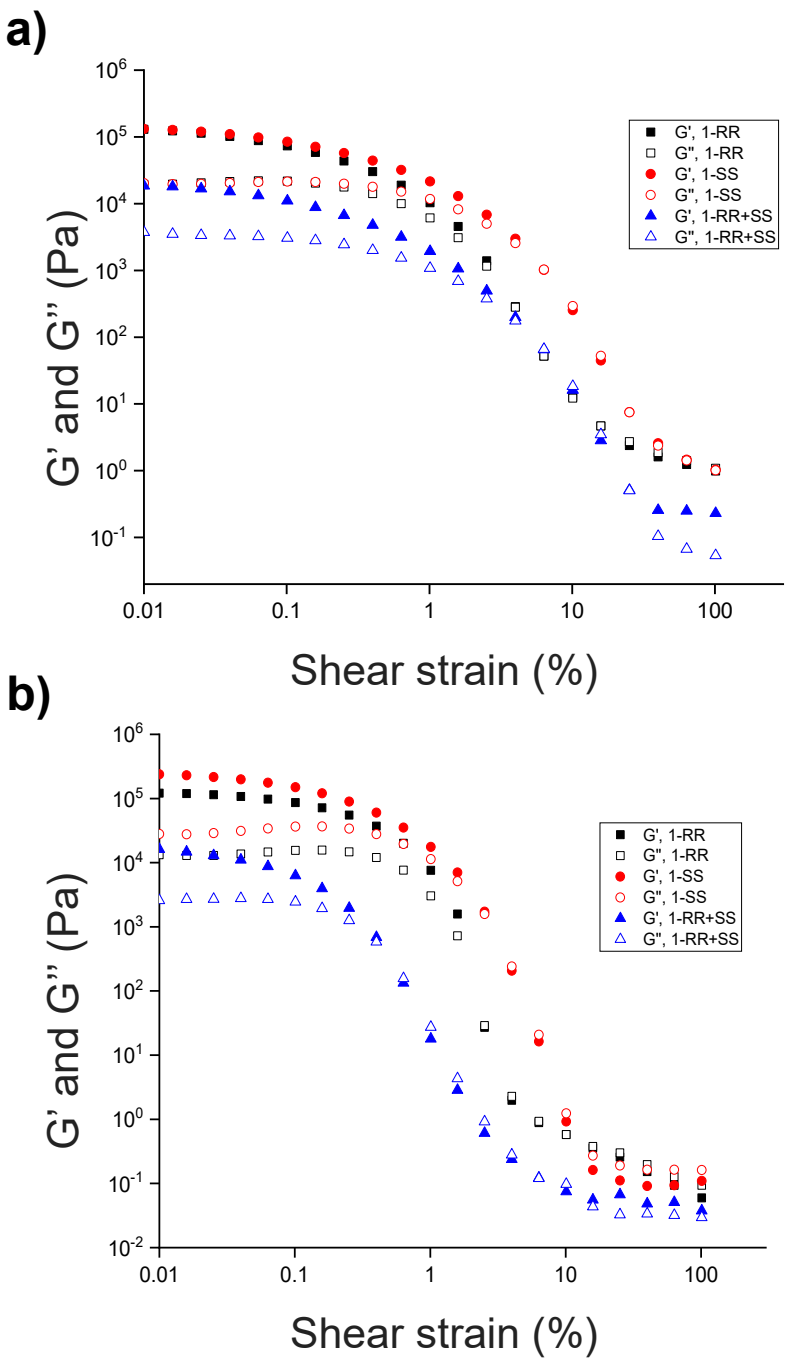

Figure S1. Strain sweep experiments with gels of **1** (7.0 wt/v%) in, (a) *o*-xylene, and (b) *m*-xylene, at 20.0 °C measured at a constant frequency of 1.0 Hz.

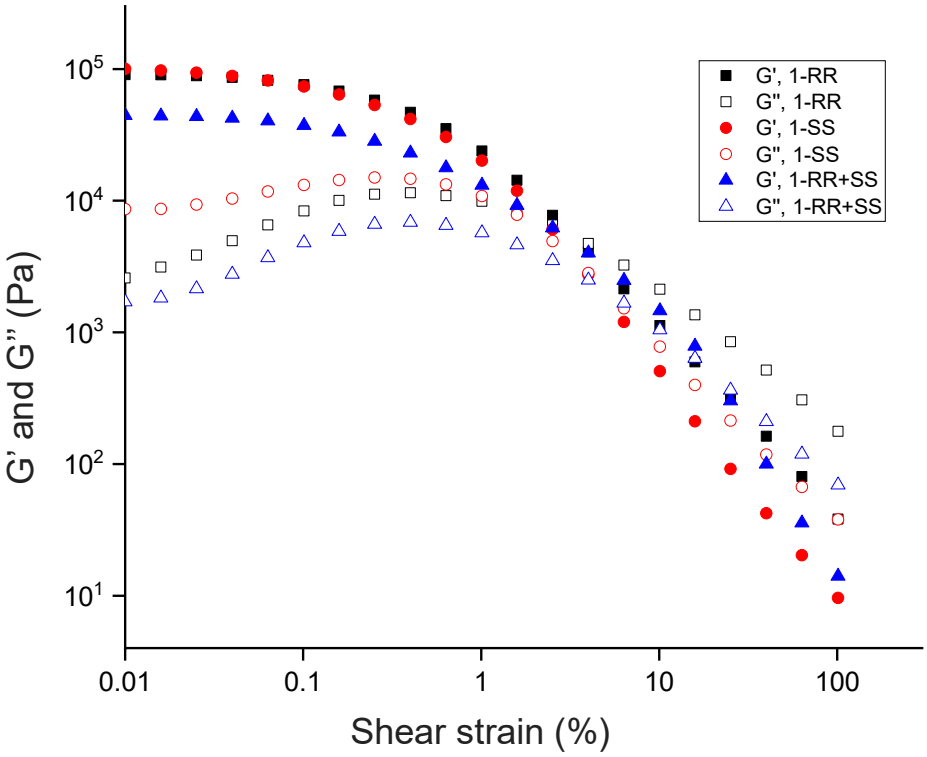

Figure S2. Strain sweep experiments with gels of **1** (5.0 wt/v%) in DMSO/water (1:1, v/v) at 20.0 °C measured at a constant frequency of 1.0 Hz.

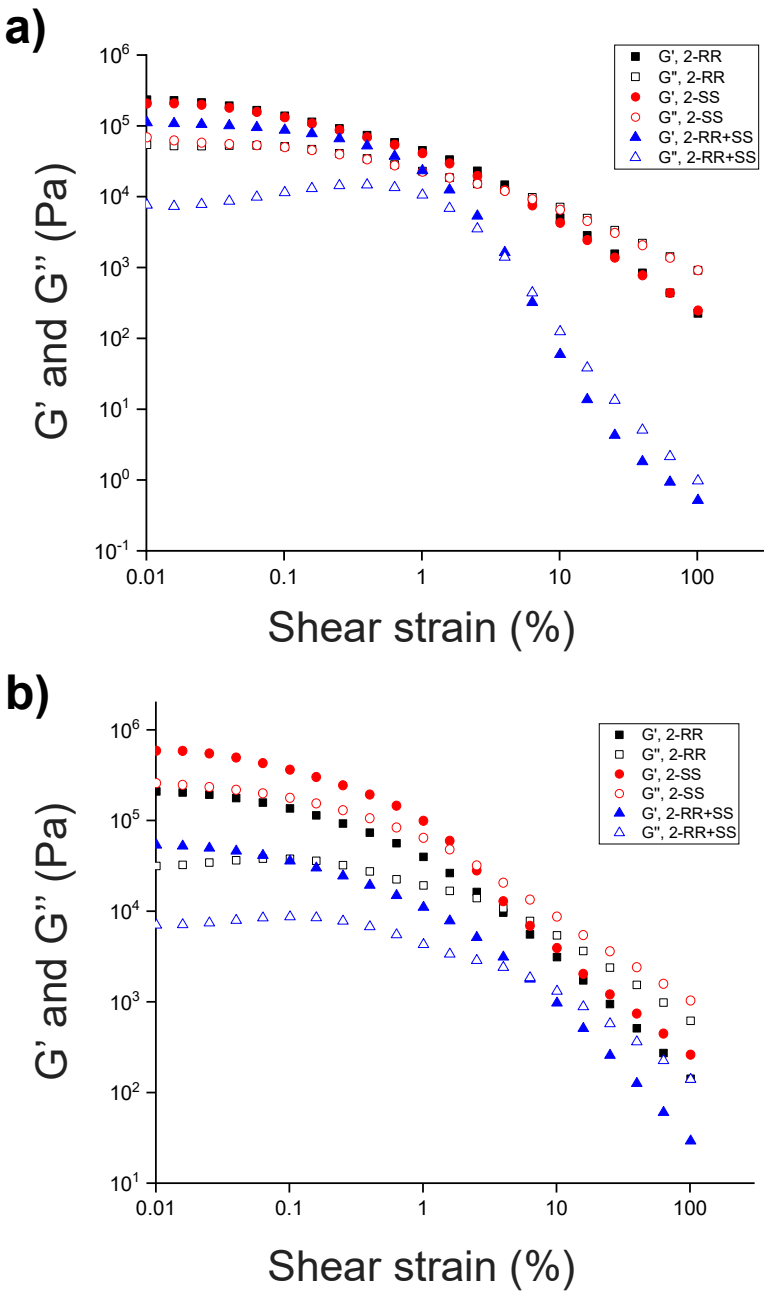

Figure S3. Strain sweep experiments with enantiomeric gels of **2** (7.0 wt/v%) and mixed **2**-(RR+SS) (10.0 wt/v%) in, (a) *o*-xylene, and (b) m-xylene, at 20.0 °C measured at a constant frequency of 1.0 Hz.

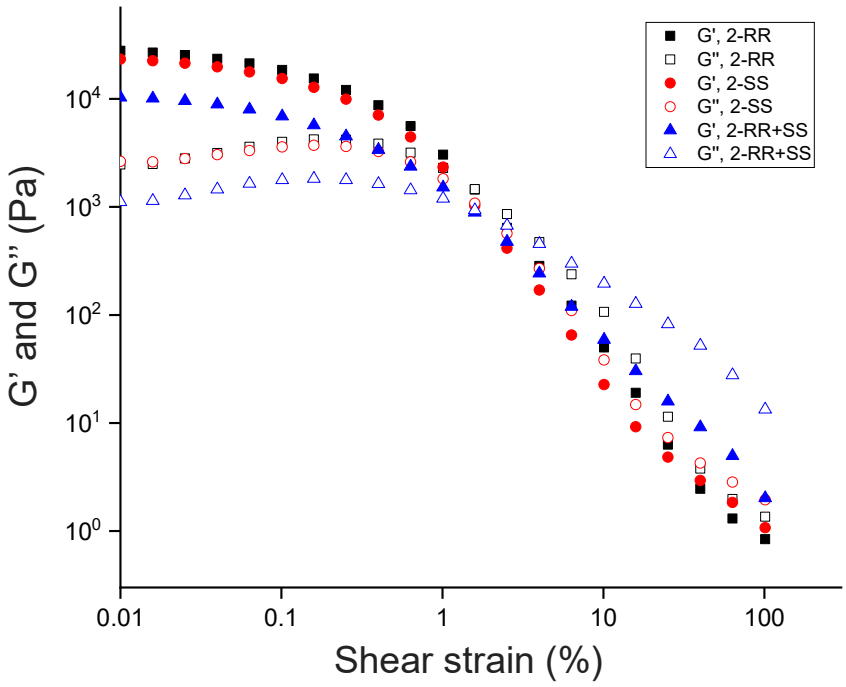

Figure S4. Strain sweep experiments with gels of **2** (5.0 wt/v%) in DMSO/water (1:1, v/v) at 20.0 °C measured at a constant frequency of 1.0 Hz.

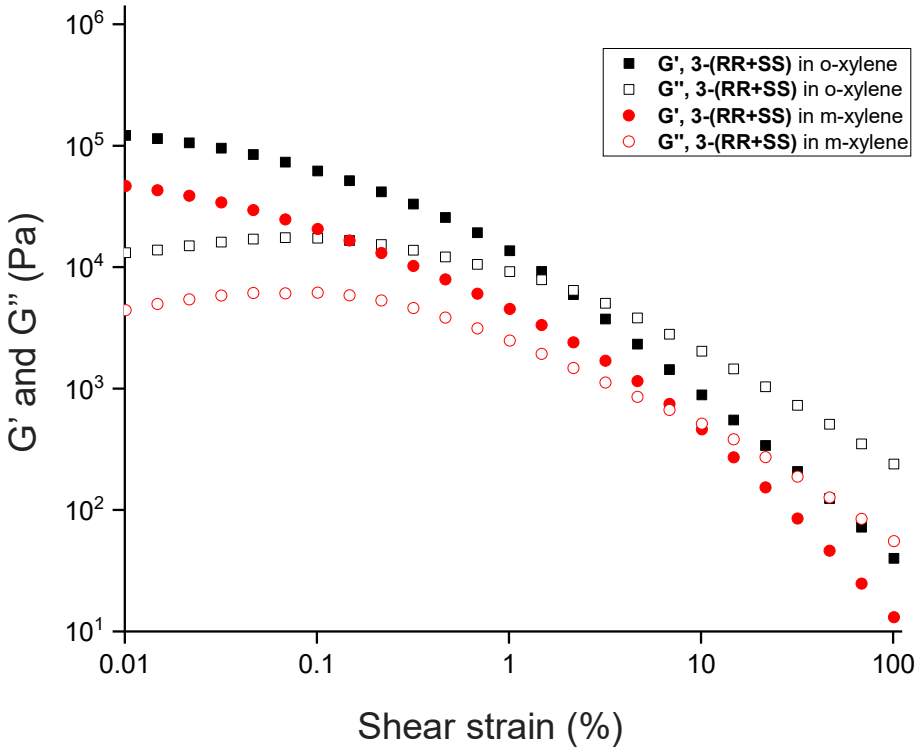

Figure S5. Strain sweep experiments with **3-(RR+SS)** gels (2.0 wt/v%) at 20.0 °C in *o*-xylene and *m*-xylene measured at a constant frequency of 1.0

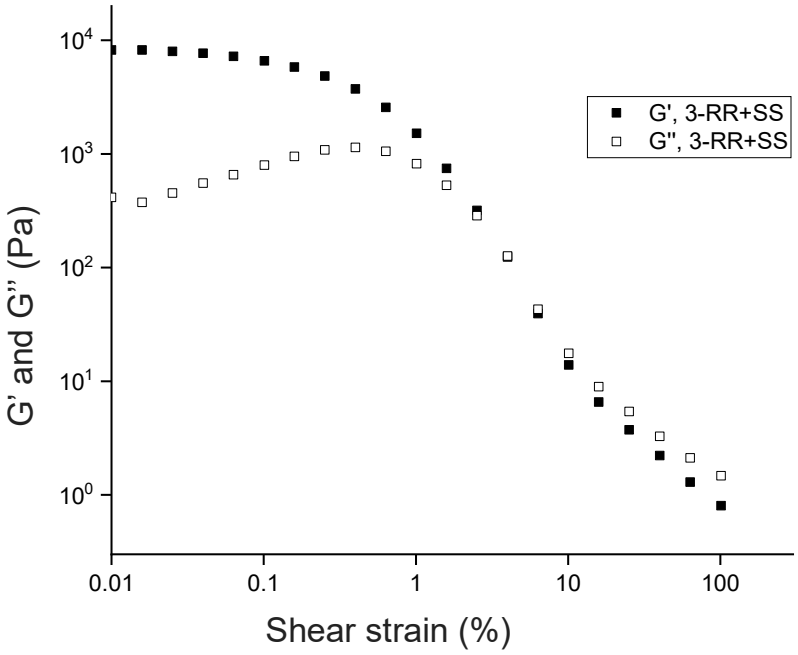

Figure S6. Strain sweep experiments with gels of **3**-(RR+SS) (5.0 wt/v%) in DMSO/water (1:1, v/v) at 20.0 °C measured at a constant frequency of 1.0 Hz.

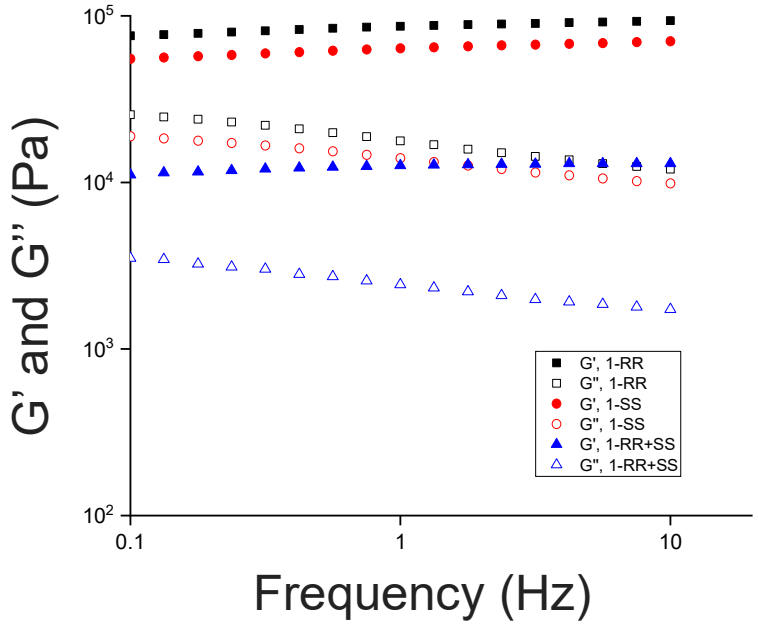

Figure S7. Frequency sweep experiment with **1**-RR, **1**-SS, and **1**-(RR+SS) gels (7.0 wt %) in *o*-xylene, measurements were performed at 20.0 °C, at a constant strain of 0.02%.

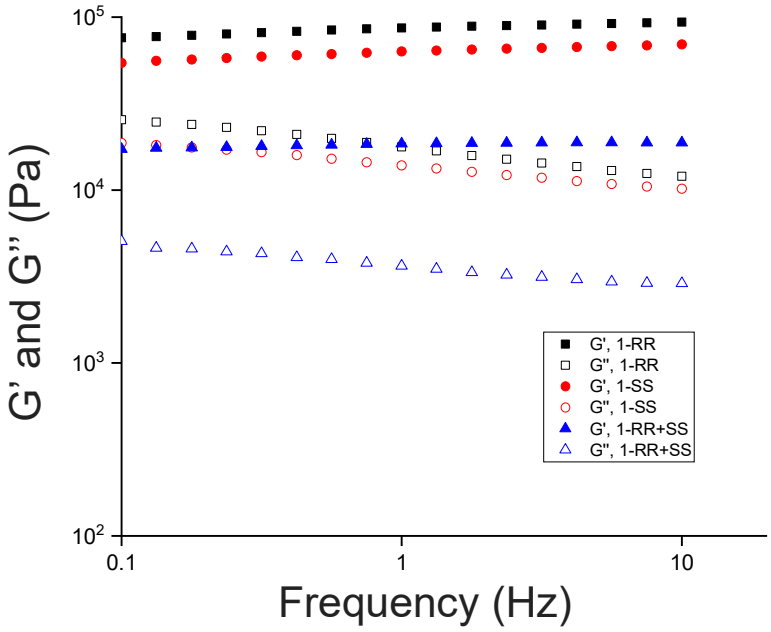

Figure S8. Frequency sweep experiment with **1**-RR, **1**-SS, and **1**-(RR+SS) gels (7.0 wt %) in *m*-xylene, measurements were performed at 20.0 °C, at a constant strain of 0.02%.

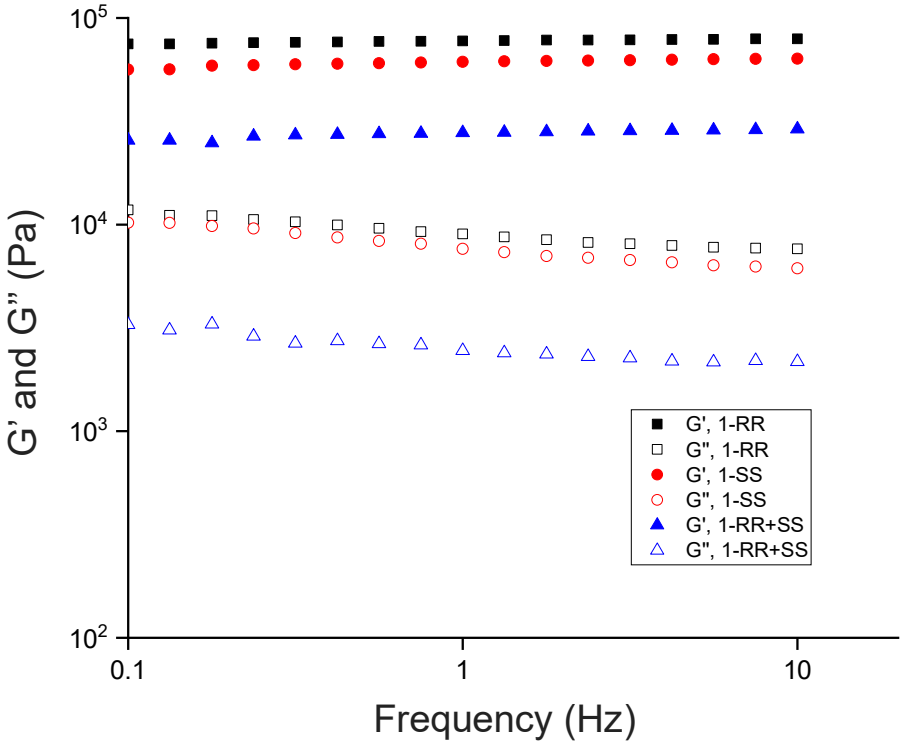

Figure S9. Frequency sweep experiment with **1**-RR, **1**-SS, and **1**-(RR+SS) gels (5.0 wt %) in DMSO/water (1:1, v/v), measurements were performed at 20.0 °C, at a constant strain of 0.02%.

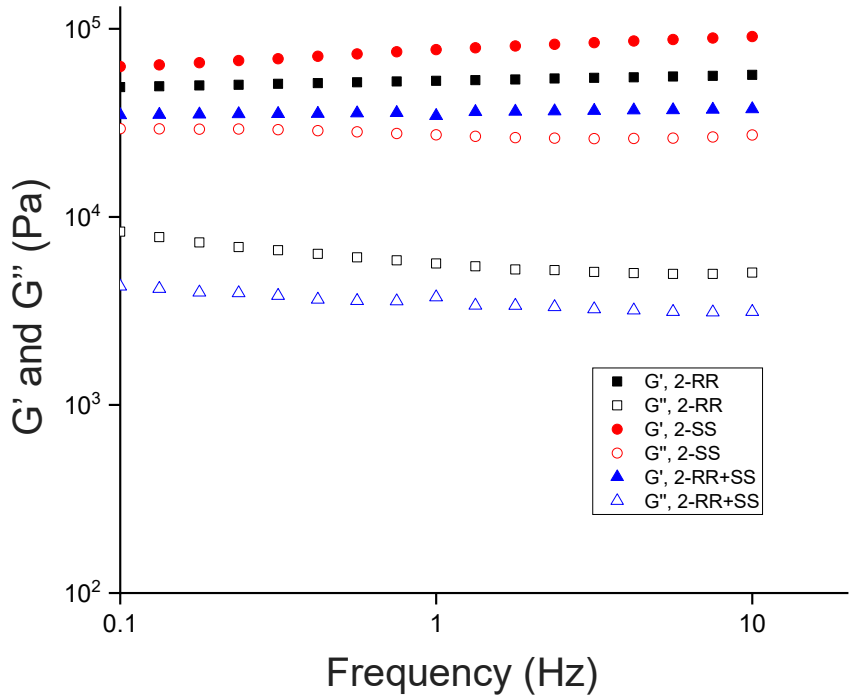

Figure S10. Frequency sweep experiment with enantiomeric gels of **2** (7.0 wt/v%) and mixed **2**-(RR+SS) (12.0 wt/v%) in *o*-xylene, measurements were performed at 20.0 °C, at a constant strain of 0.02%.

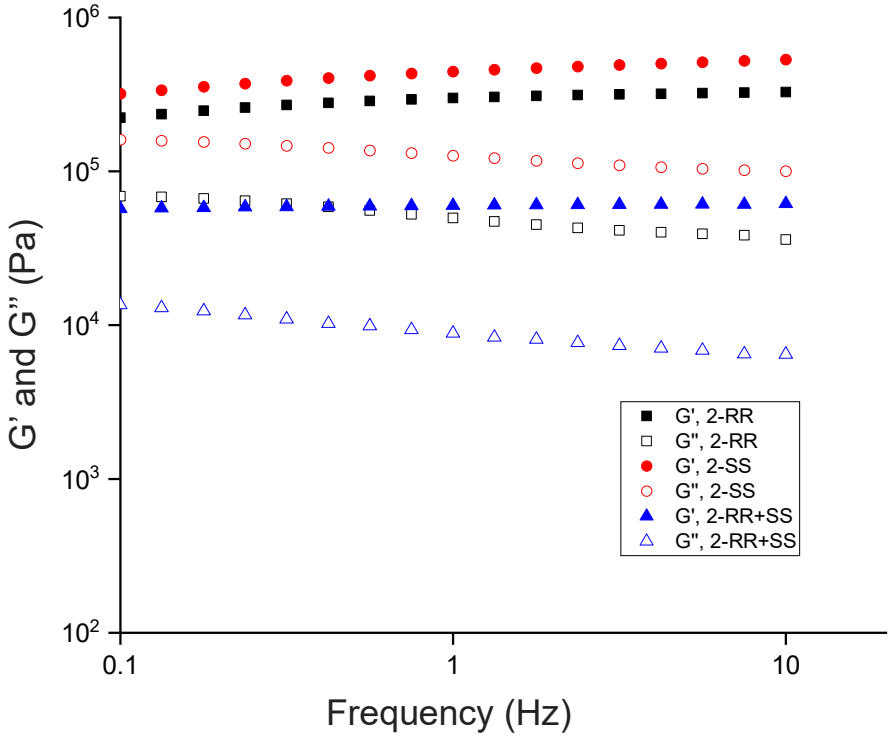

Figure S11. Frequency sweep experiment with enantiomeric gels of **2** (7.0 wt/v%) and mixed **2**-(RR+SS) (12.0 wt/v%) in *m*-xylene, measurements were performed at 20.0 °C, at a constant strain of 0.02%.

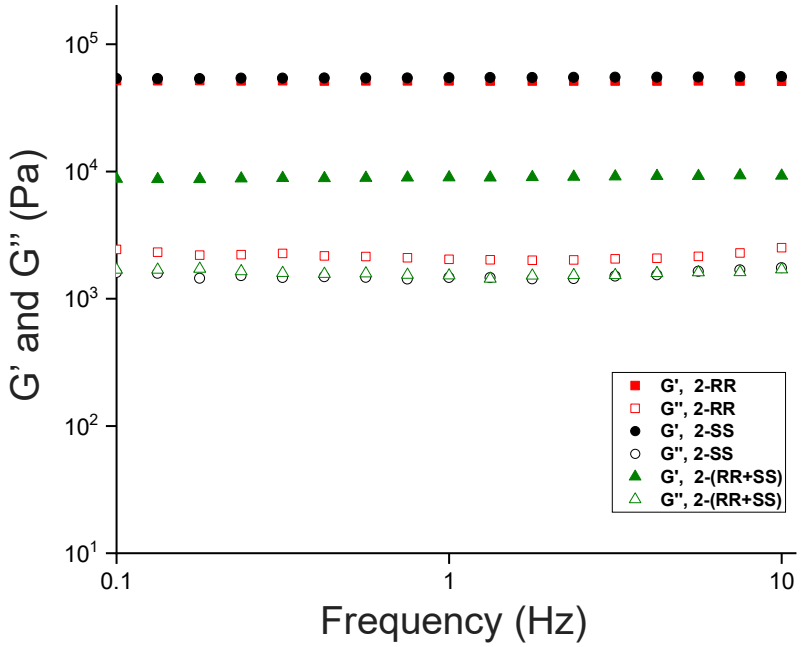

Figure S12. Frequency sweep experiments with gels of **2** (5.0 wt/v%) at 20.0 °C measured at a constant strain of 0.02% in DMSO/water (1:1, v/v).

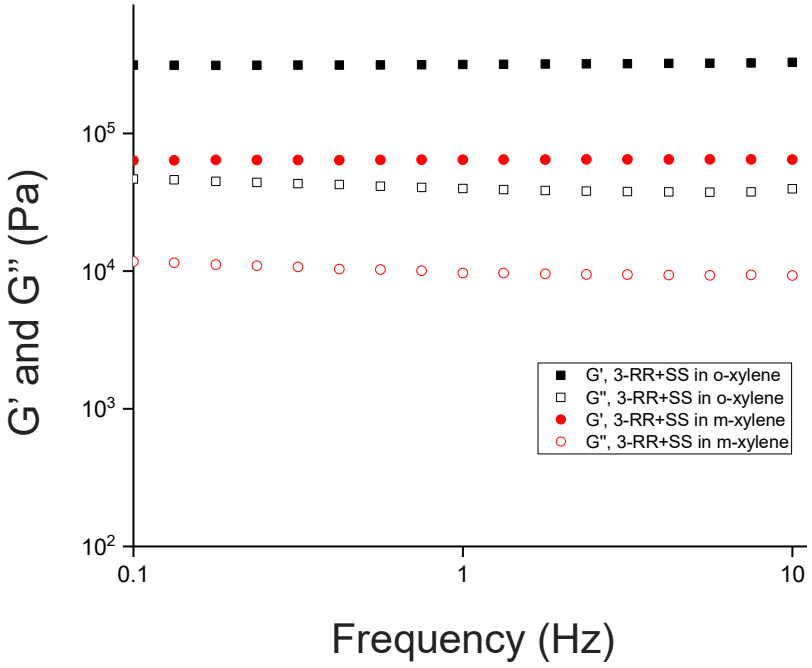

Figure S13. Frequency sweep experiment with mixed **3**-(RR+SS) at 2.0 wt/v% in *o*-xylene and *m*-xylene, measurements were performed at 20.0 °C, at a constant strain of 0.02%.

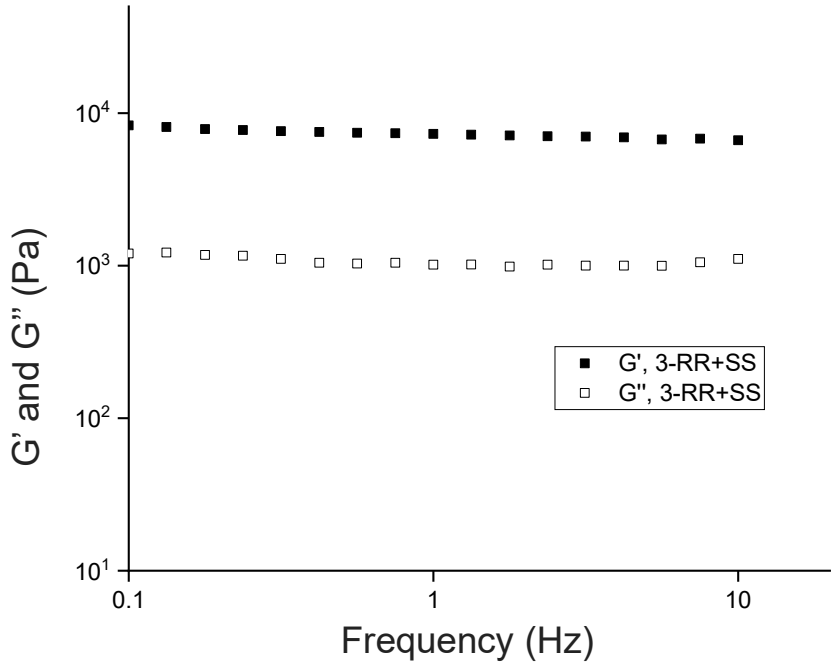

Figure S14. Frequency sweep experiments with gels of mixed **3**-(RR+SS) gels (5.0 wt/v%) at 20.0 °C measured at a constant strain of 0.02% in DMSO/water (1:1, v/v).

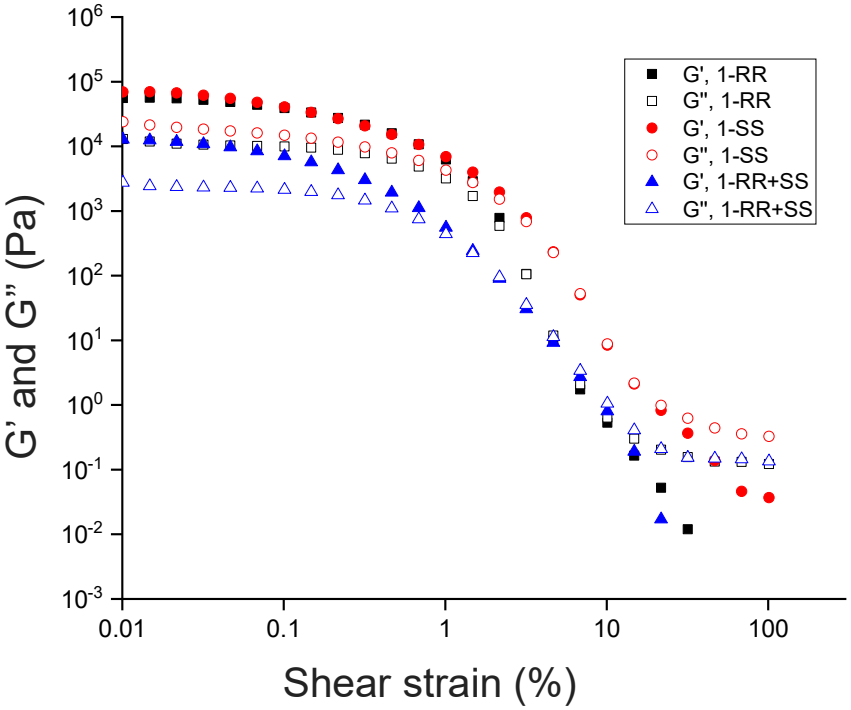

Figure S15. Strain sweep experiments with gels of **1** (7.0 wt %) in *p*-xylene at 20.0 °C and measured at a constant frequency of 1.0 Hz.

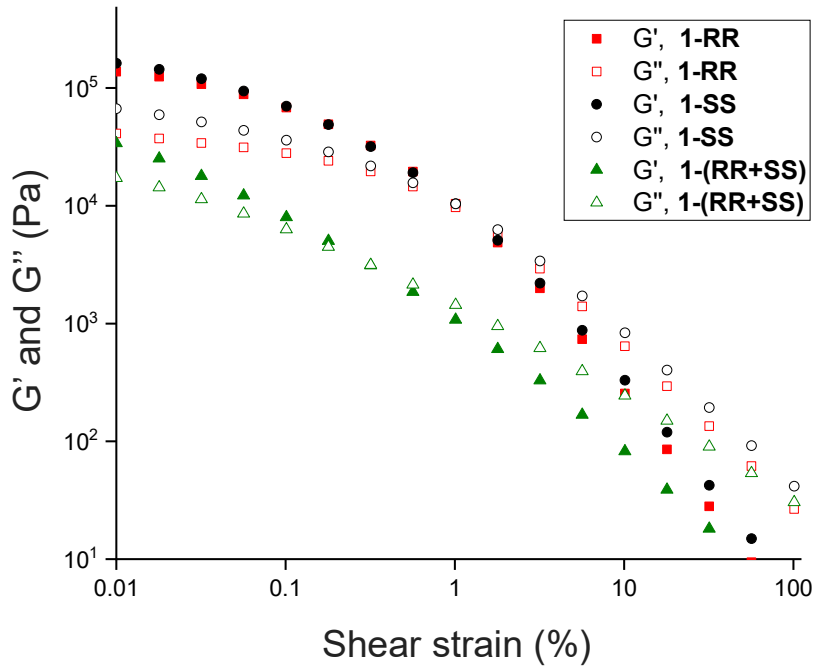

Figure S16. Strain sweep experiments with gels of **1** (6.0 wt/v%) in n-butanol at 20.0 °C and measured at a constant frequency of 1.0 Hz.

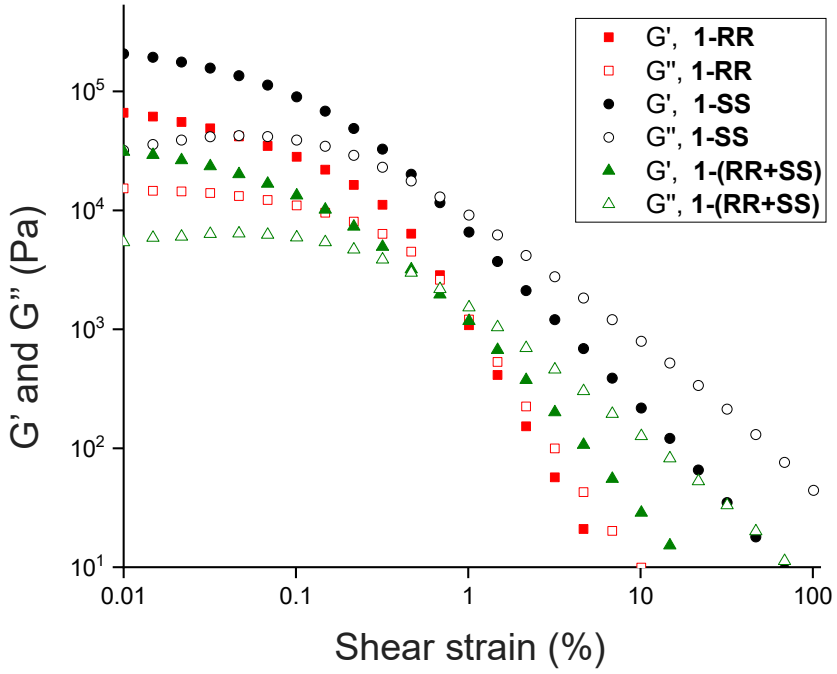

Figure S17. Strain sweep experiments with gels of **1** (6.0 wt/v%) in ethanol/water (1:1, v/v) at 20.0 °C measured at a constant frequency of 1.0 Hz.

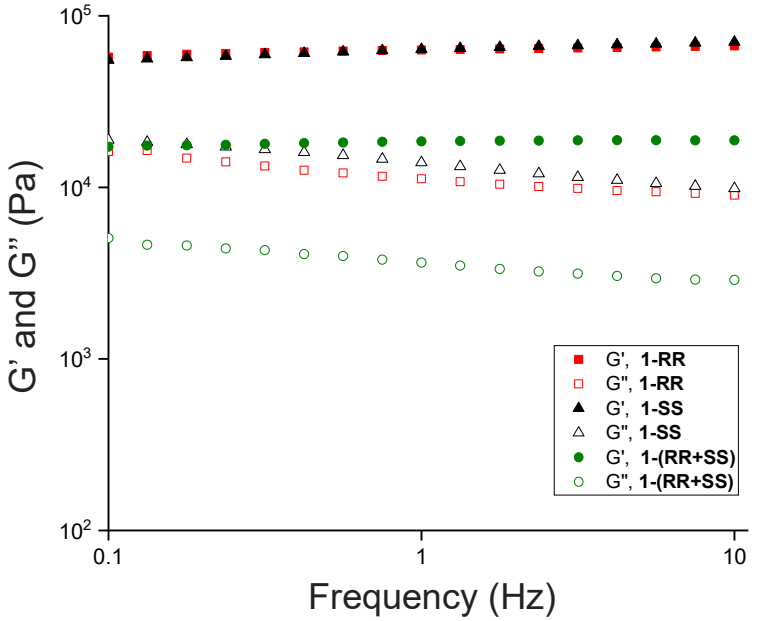

Figure S18. Frequency sweep experiment with gels of **1** (7.0 wt %) in *p*-xylene, measurements were performed at 20.0 °C, at a constant strain of 0.02%.

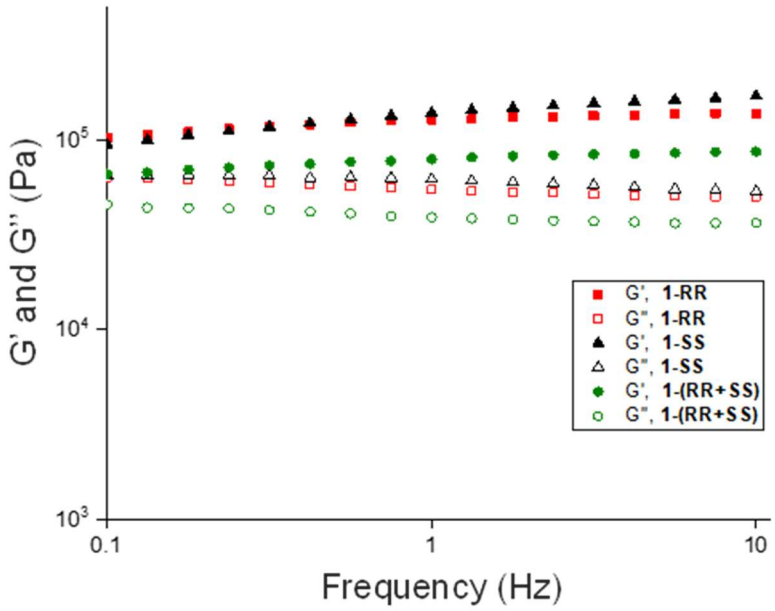

Figure S19. Frequency sweep experiment with **1**-RR, **1-SS**, and **1**-(RR+SS) gels (6.0 wt %) in n-butanol, measurements were performed at 20.0 °C, at a constant strain of 0.02%.

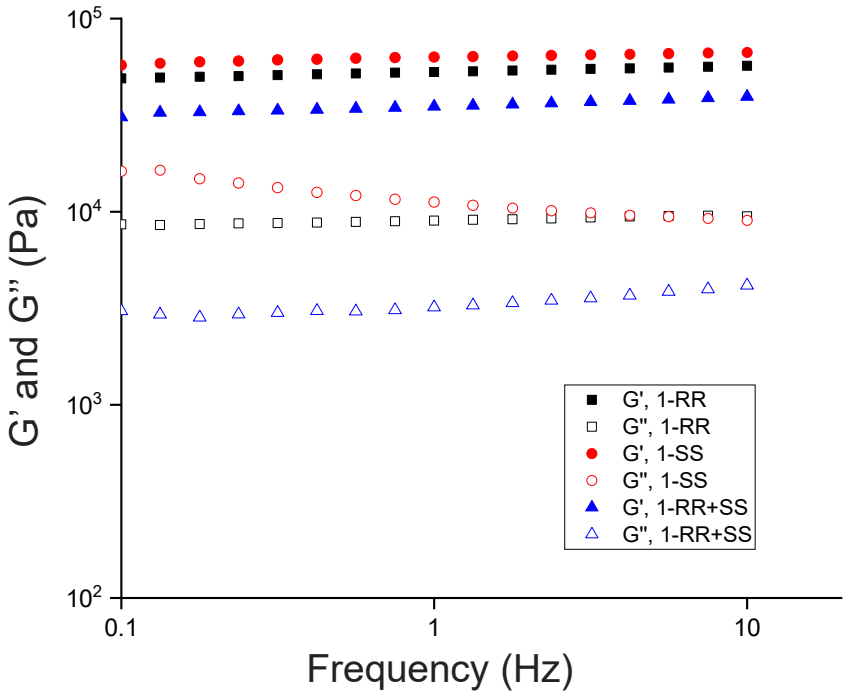

Figure S20. Frequency sweep experiment with gels of **1** (6.0 wt/v%) in ethanol/water (1:1, v/v), measurements were performed at 20.0 °C, at a constant strain of 0.02%.

4. Scanning Electron Microscopy (SEM)

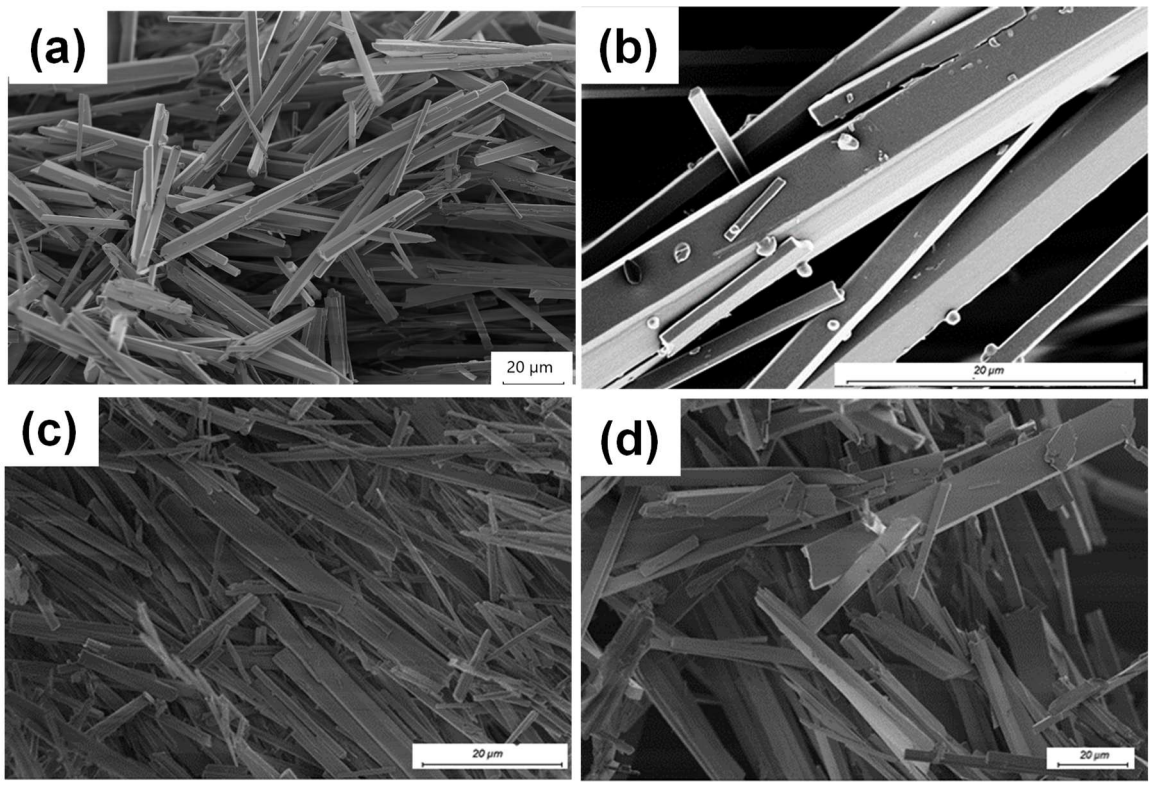

Figure S21. SEM images of the xerogels (7.0 wt/v%) in *m*-xylene prepared with (a) **1**-SS and in *o*-xylene with (b) **1**-RR, (c) **1**-SS, (d) **1**-(RR+SS).

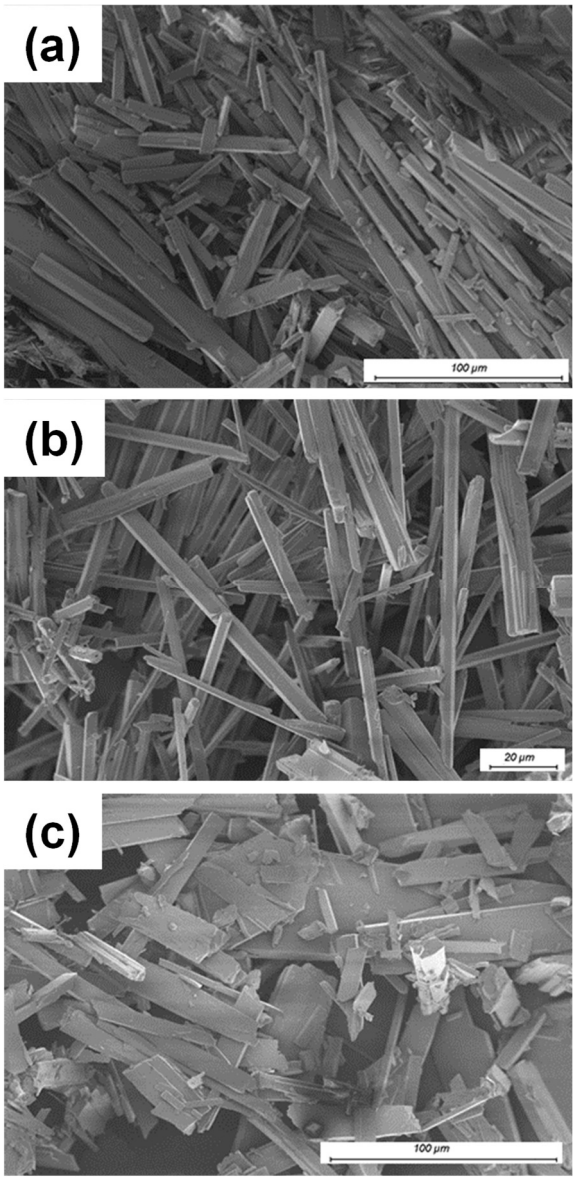

Figure S22. SEM images of the xerogels of (a) **1**-RR, (b) **1**-SS, (c) **1**-(RR+SS) gelators from *p*-xylene prepared at 7.0 wt/v%.

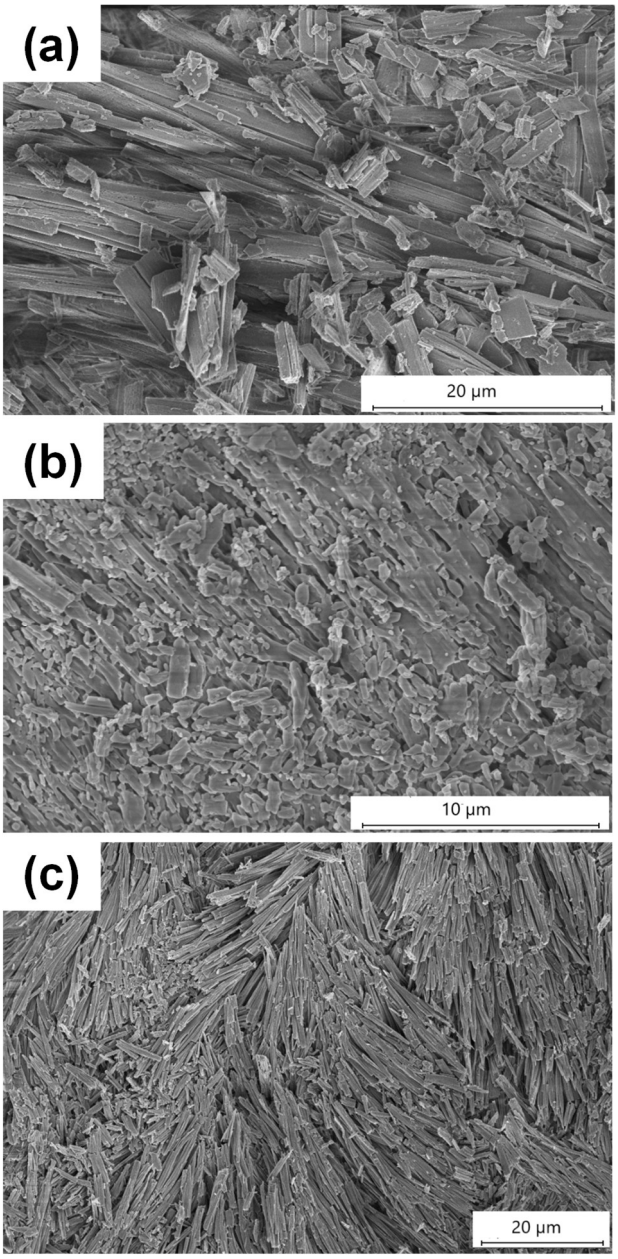

Figure S23. SEM images of the xerogels of enantiomeric gels of **2** (7.0 wt/v%) and mixed **2**-(RR+SS) (12.0 wt/v%) from *o*-xylene.

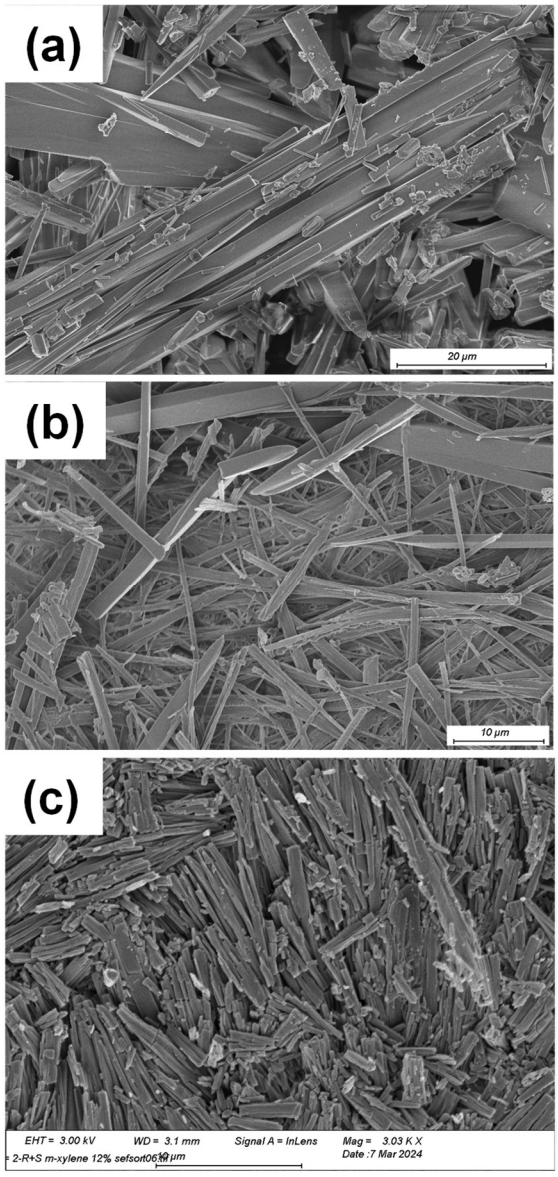

Figure S24. SEM images of the xerogels of enantiomeric gels of **2** (7.0 wt/v%) and mixed **2**-(RR+SS) (12.0 wt/v%) from *m*-xylene.

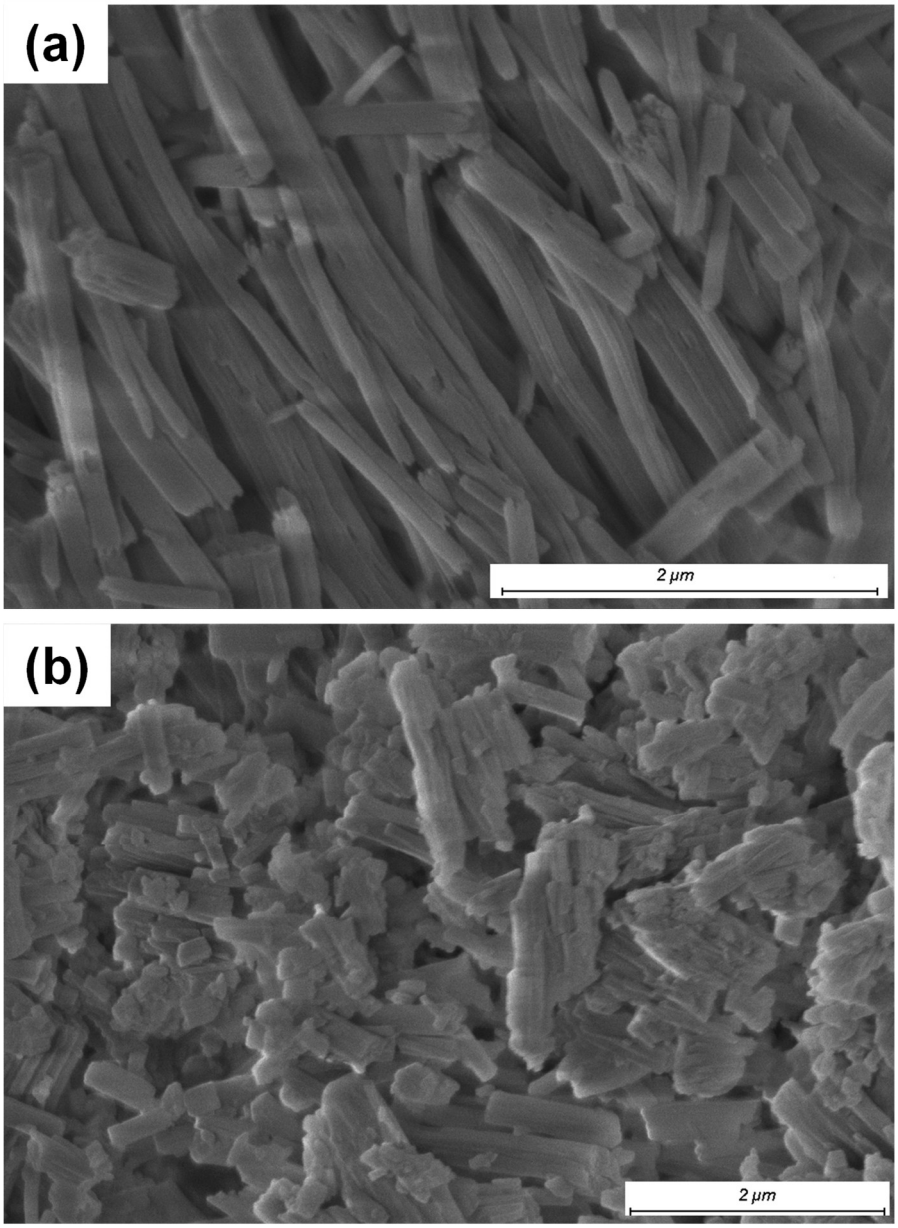

Figure S25. SEM images of the xerogels of **3**-(RR+SS) gelator in (a) *m*-xylene, and (b) *o*-xylene prepared at 2.0 wt/v%.

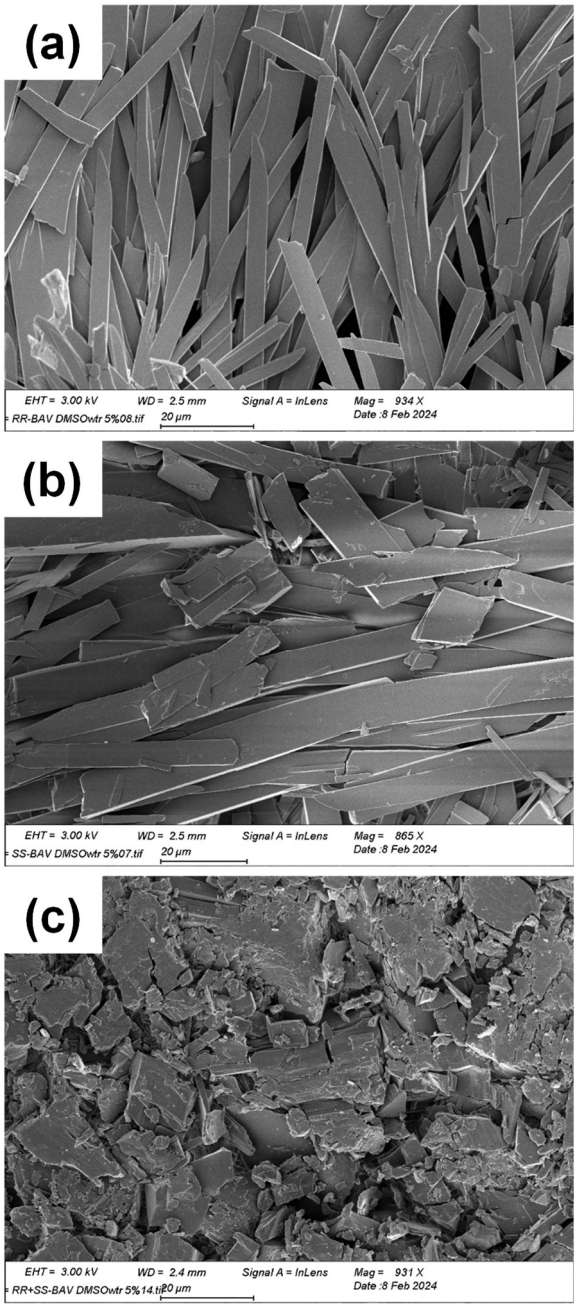

Figure S26. SEM images of the xerogels of (a) **1**-RR, (b) **1**-SS, (c) **1**-(RR+SS) gelators from DMSO/water (1:1, v/v) prepared at 5.0 wt/v%.

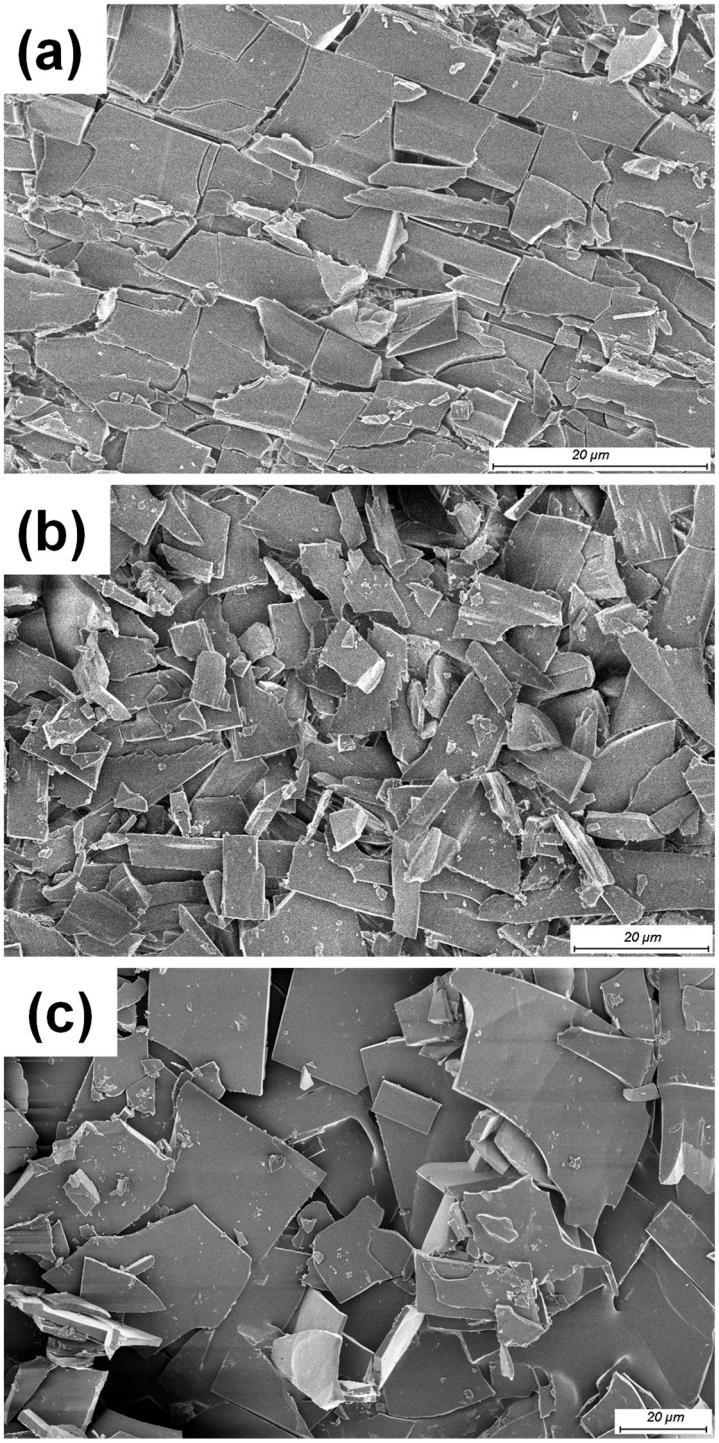

Figure S27. SEM images of the xerogels of (a) **2**-RR**,** (b) **2**-SS**,** and (c) **2**-(RR+SS) gelators from DMSO/water (1:1, v/v) prepared at 5.0 wt/v%.

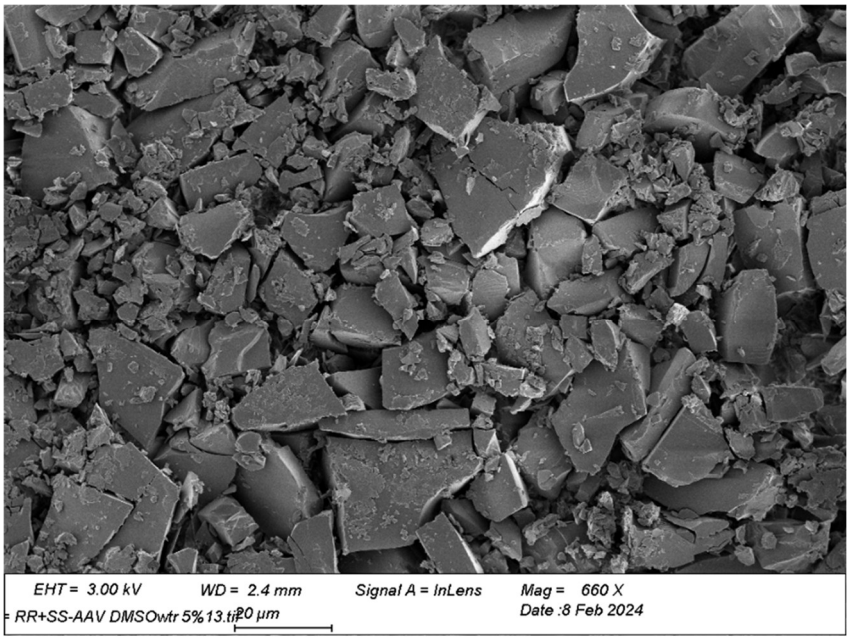

Figure S28. SEM images of the xerogels of mixed 3-(RR+SS) gelators from DMSO/water (1:1, v/v) prepared at 5.0 wt/v%.

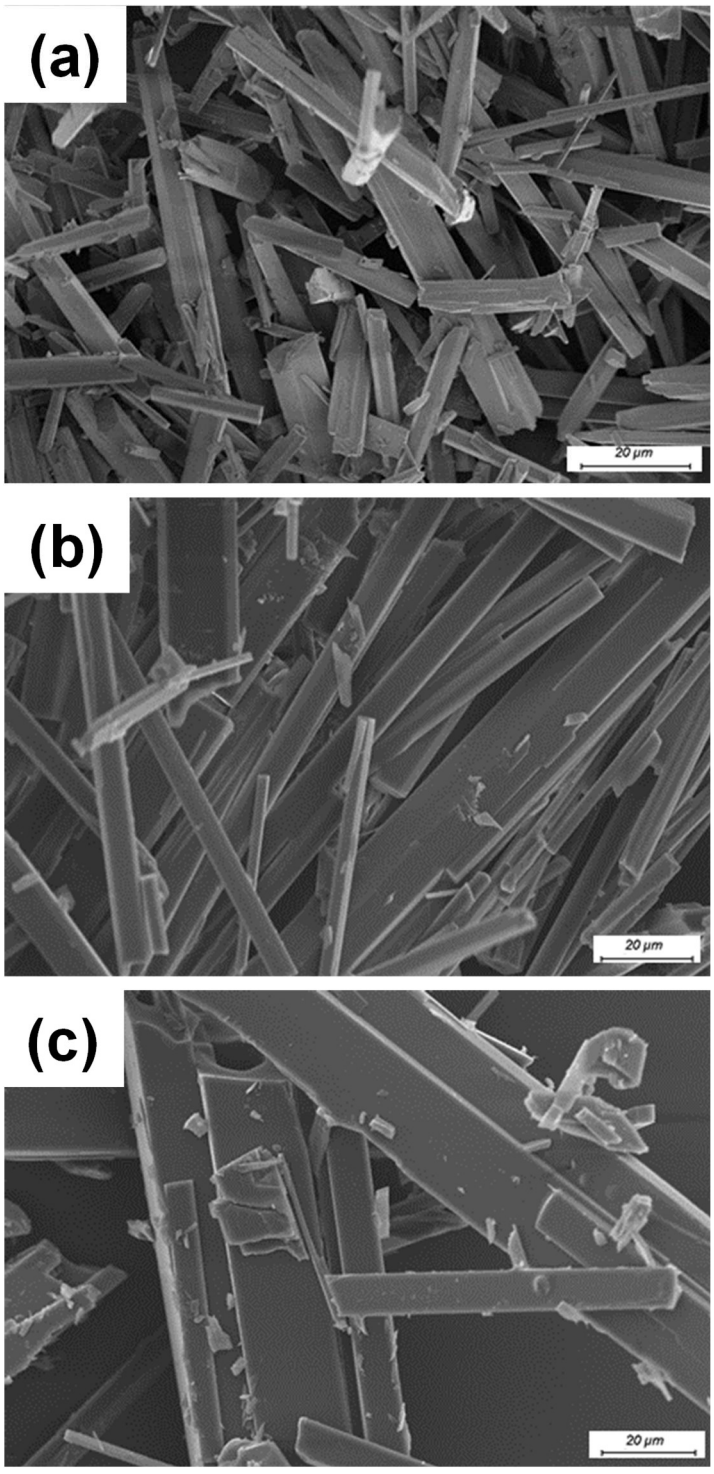

Figure S29. SEM images of the xerogels of (a) **1**-RR, (b) **1**-SS, (c) **1**-(RR+SS) gelators from toluene prepared at 7.0 wt/v%.

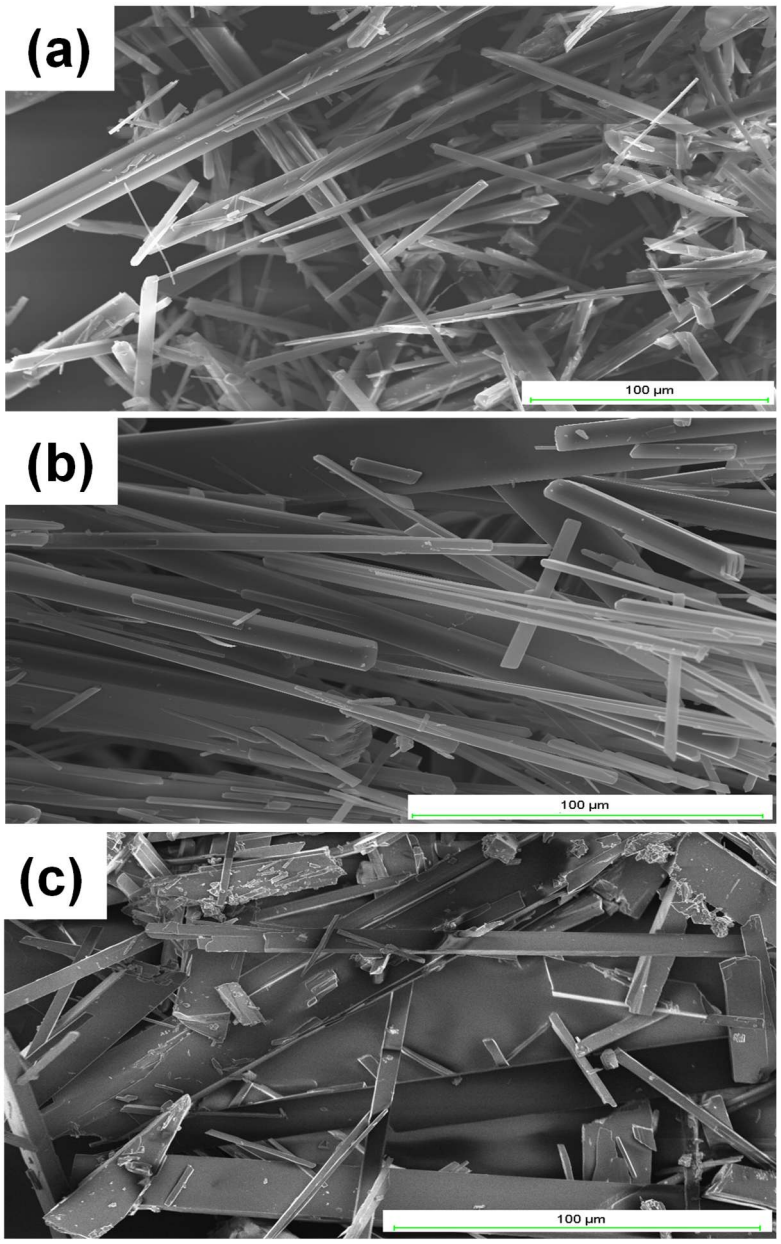

Figure S30. SEM images of the xerogels of (a) **1**-RR, (b) **1**-SS, (c) **1**-(RR+SS) gelators from n-butanol prepared at 6.0 wt/v%.

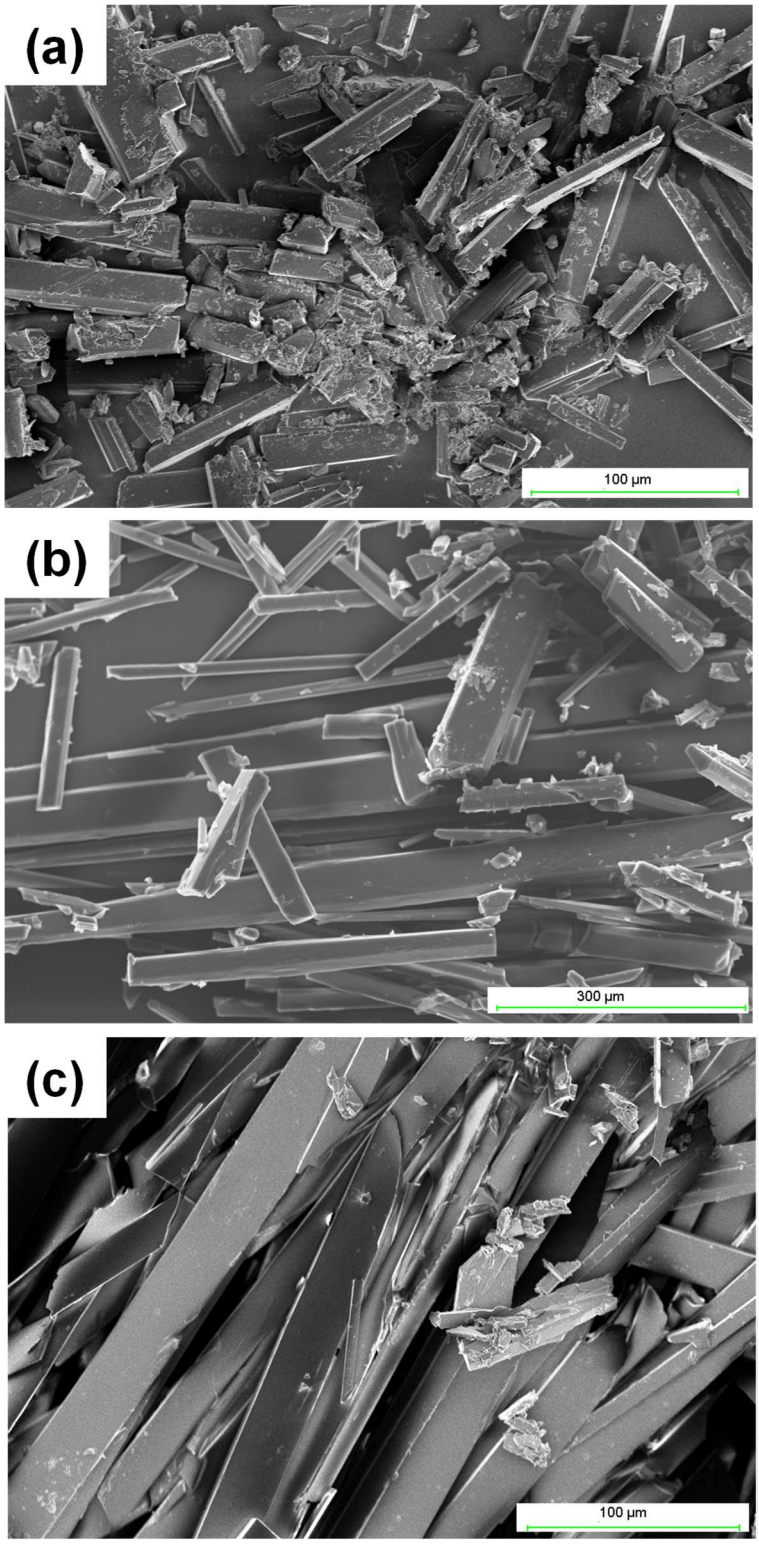

Figure S31. SEM images of the xerogels of (a) **1**-RR, (b) **1**-SS, (c) **1**-(RR+SS) gelators from ethanol/water (1:1, v/v) prepared at 6.0 wt/v%.

5. Circular dichroism (CD)

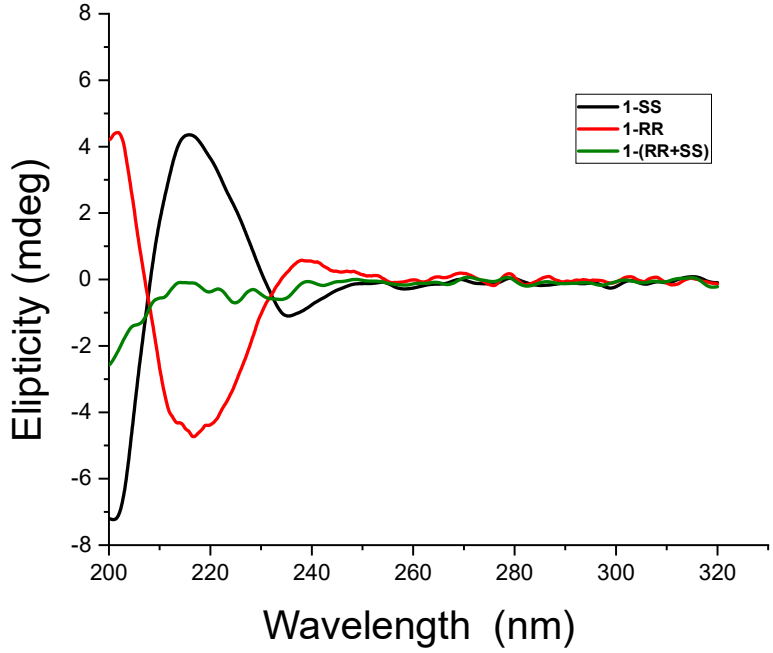

Figure S32. CD spectra of **1**-RR, **1-SS**, and **1**-(RR+SS) in solution state at 0.03 wt/v% in absolute ethanol.

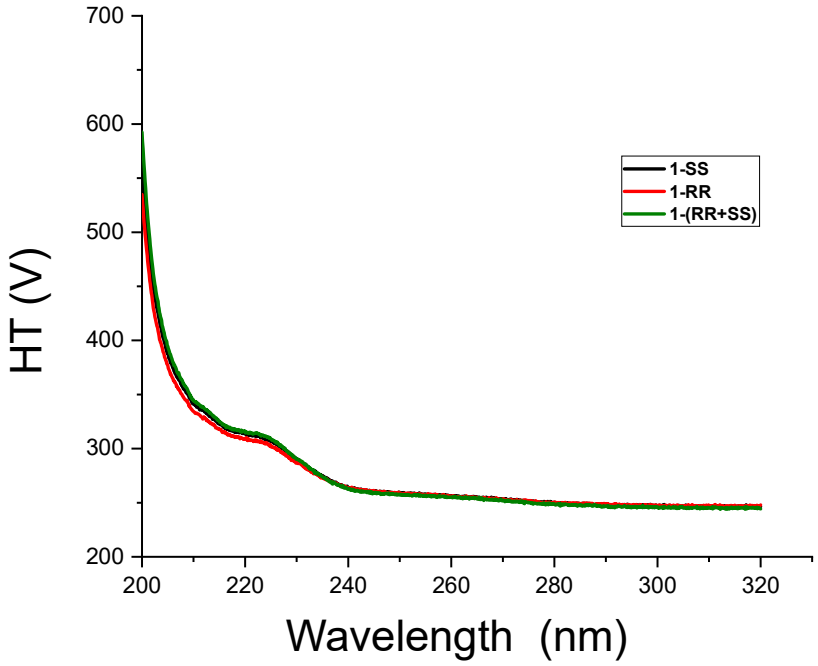

Figure S33. HT data for the CD spectra of **1**-RR, **1-SS**, and **1**-(RR+SS) in solution state at 0.03 wt/v% in absolute ethanol.

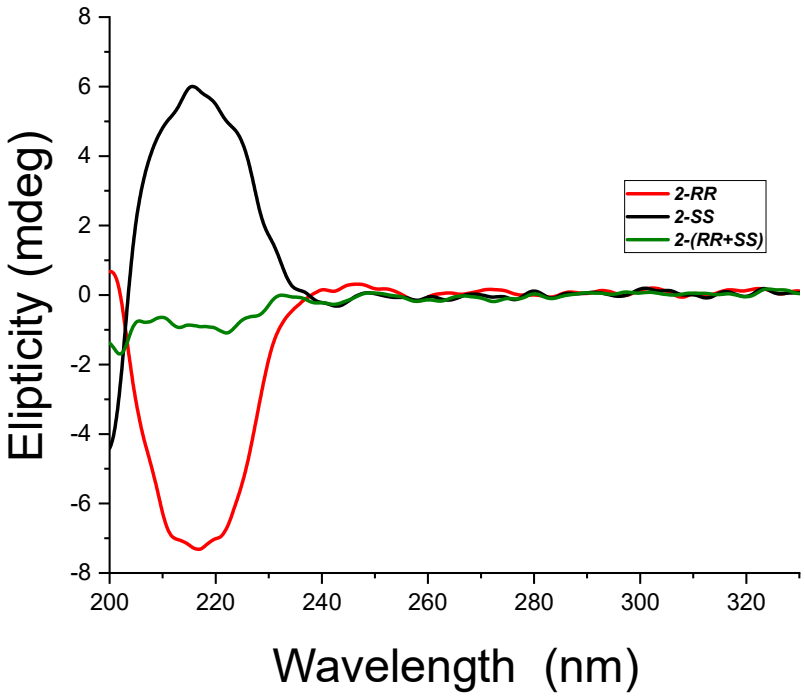

Figure S34. CD spectra of **2**-RR, **2-SS**, and **2**-(RR+SS) in solution state at 0.03 wt/v% in absolute ethanol.

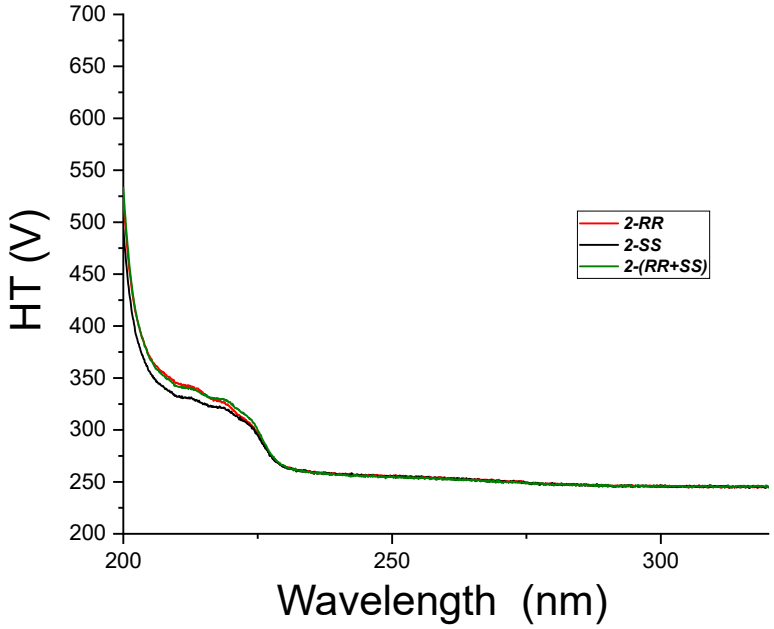

Figure S35. HT data for the CD spectra of **2**-RR, **2-SS**, and **2**-(RR+SS) in solution state at 0.03 wt/v% in absolute ethanol.

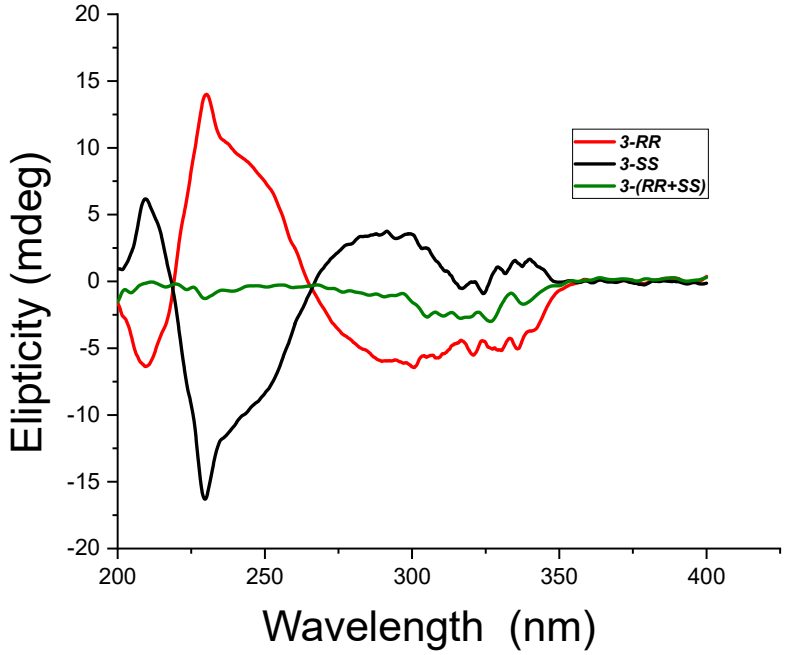

Figure S36. CD spectra of **3**-RR, **3**-SS, and **3**-(RR+SS) in solution state at 0.03 wt/v% in absolute ethanol.

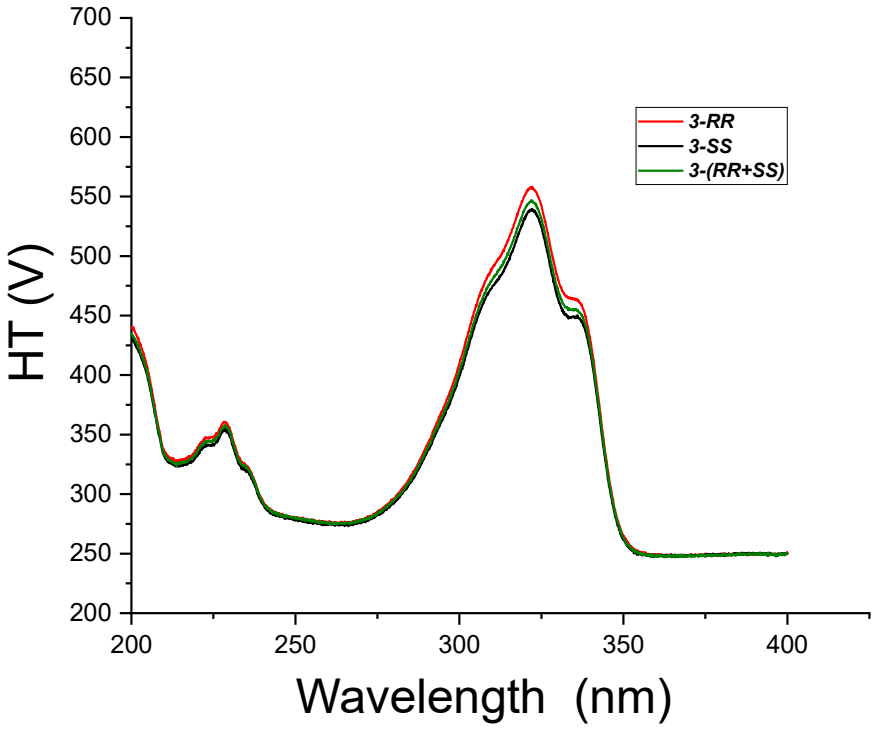

Figure S37. HT data for the CD spectra of **3**-RR, **3**-SS, and **3**-(RR+SS) in solution state at 0.03 wt/v% in absolute ethanol.

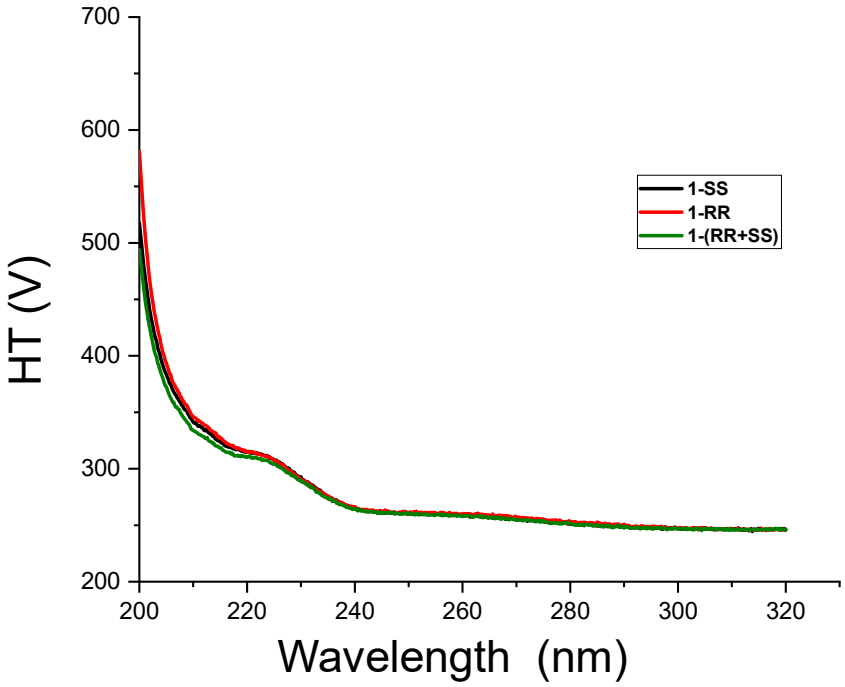

Figure S38. HT data for the CD spectra of **1**-RR, **1-SS**, and **1**-(RR+SS) in dispersed gel state at 0.03 w/v% in ethanol/water (1:1, v/v).

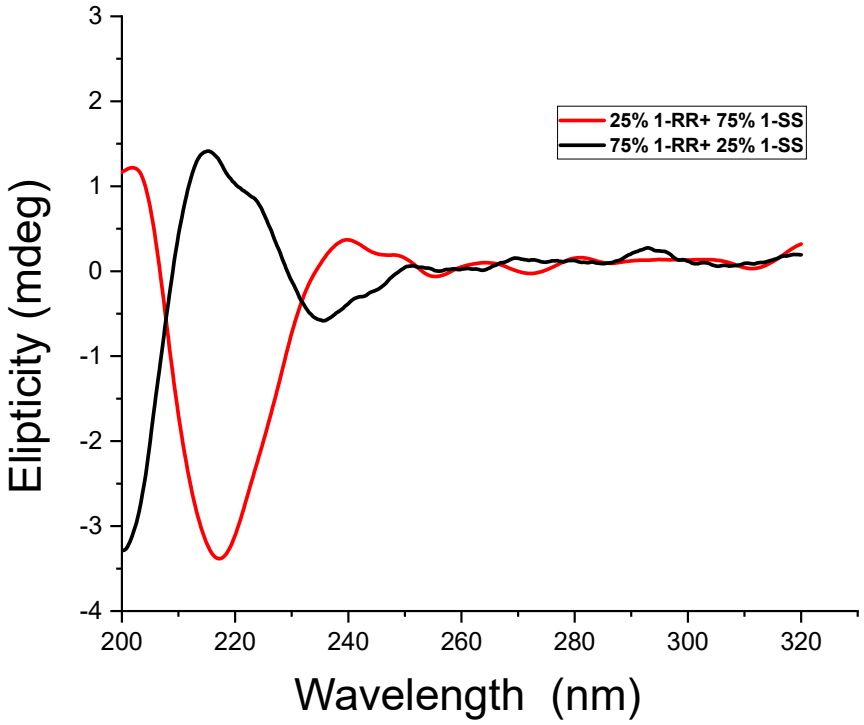

Figure S39. CD spectra of (75% **1**-RR + 25% **1**-SS) and (25% **1**-RR + 75% **1**-SS) mixture in solution state at 0.030 wt/v% in absolute ethanol.

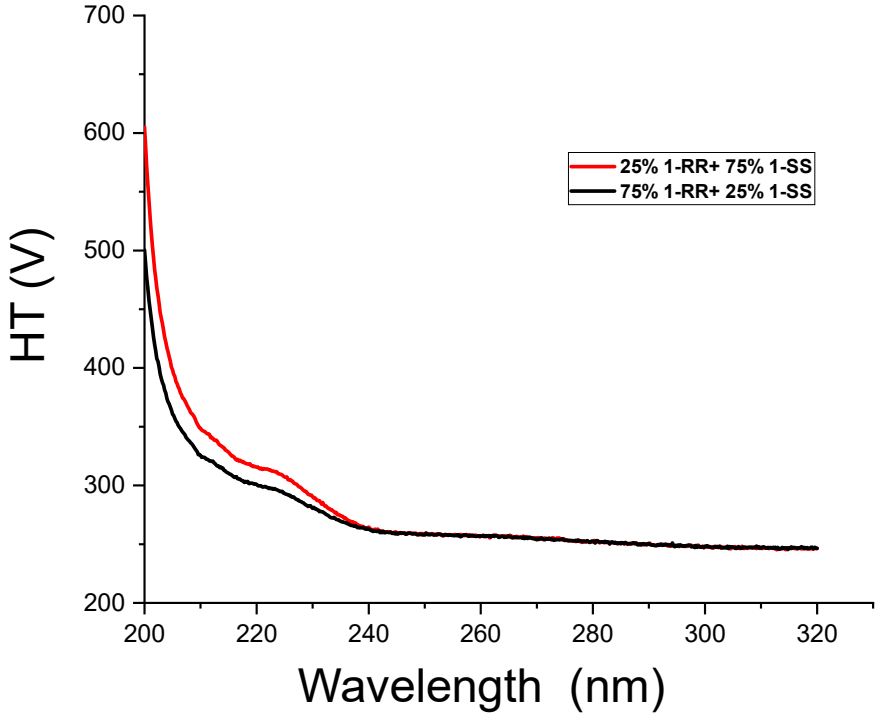

Figure S40. HT data for the CD spectra of (75% **1**-RR + 25% **1**-SS) and (25% **1**-RR + 75% **1**-SS) mixture in solution state at 0.030 wt/v% in absolute ethanol.

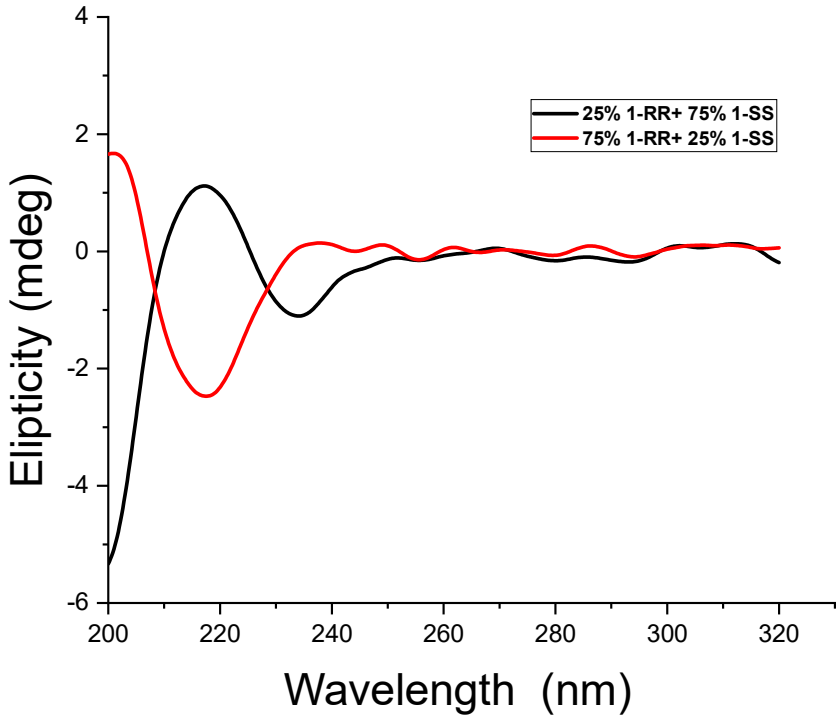

Figure S41. CD spectra of (75% **1**-RR + 25% **1**-SS) and (25% **1**-RR + 75% **1**-SS) mixture in dispersed gel at 0.030 wt/v% in ethanol/water (1:1, v/v).

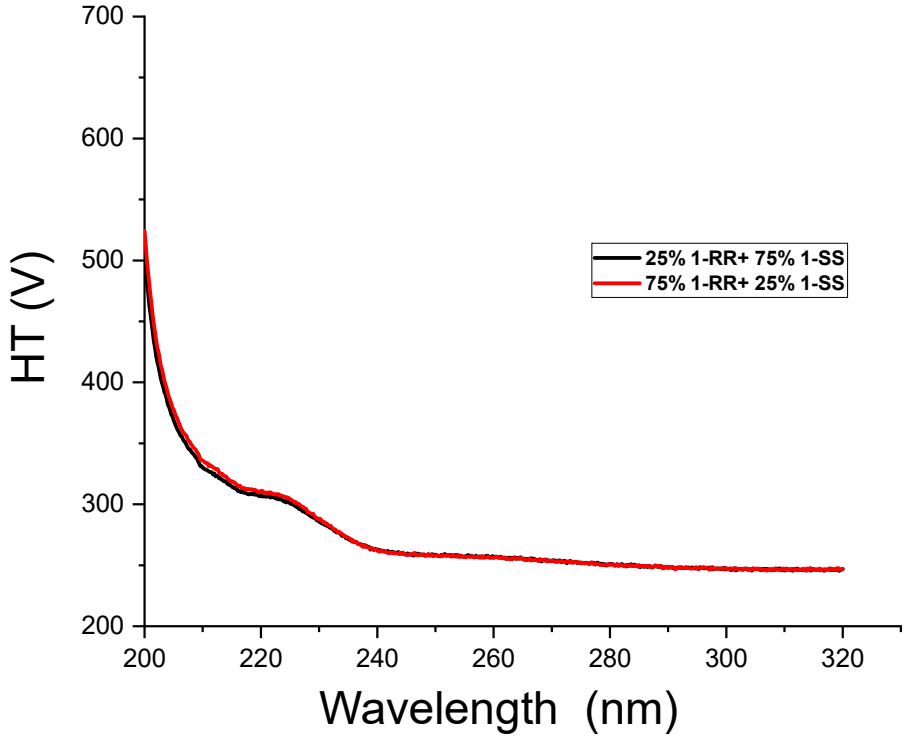

Figure S42. HT Data for the CD spectra of mixture in dispersed gel at 0.030 wt/v% in ethanol/water (1:1, v/v).

6. X-ray crystallography

Table S5. Crystal data for **1**

Crystal data	**1**-RR	**1**-SS	**1**-(RR+SS)
File Name	SSJ_I_180	SSJ_1_98SS	SJ_I_181_2
Empirical formula	$C_{22}H_{32}N_2O_6$	$C_{22}H_{32}N_2O_6$	$C_{22}H_{32}N_2O_6$
Color	Colorless	Colorless	Colorless
Formula weight	420.49	420.49	420.49
Crystal size (mm)	0.600 x 0.095 x 0.055	0.320 x 0.120 x 0.060	0.380 x 0.150 x 0.050
Crystal system	Orthorhombic	Orthorhombic	Triclinic
Space group	$P2_12_12_1$	$P2_12_12_1$	P-1
a (Å)	9.6580(3)	9.6586(3)	8.4379(4)
b (Å)	10.3668(4)	10.3599(3)	8.5542(4)
c (Å)	22.6898(8)	22.6582(6)	17.3003(8)
α (°)	90	90	86.948(2)
β (°)	90	90	80.624(2)
γ (°)	90	90	66.785(2)
Volume (Å^3)	2271.76(14)	2267.23(11)	1132.21(9)
Z	4	4	2
$D_{calc.}$(g/cm^3)	1.229	1.232	1.233
F(000)	904	904	452
μ (mm^{-1}) CuK_α	0.734	0.735	0.736
Temperature (K)	150(2)	150(2)	150(2)
Reflections collected/ unique/observed [I>2σ(I)]	28151/ 4840/4704	43433/ 4458/4284	31297/ 4287/3773
Data/restraints/parameters	4840/0/277	4458/0/277	4287/0/277
Goodness of fit on F^2	1.017	1.056	1.051
Final R indices [I>2σ(I)]	R_1 = 0.0293 wR_2 = 0.0806	R_1 = 0.0281 wR_2 = 0.0705	R_1 0.0361 wR_2 = 0.0949
R indices (all data)	R1 = 0.0305 wR2 = 0.0815	R1 = 0.0298 wR2 = 0.0714	R1 = 0.0417 wR2 = 0.0992

Table S6. Crystal data for **2**

Crystal data	**2**-RR	**2**-SS	**2**-(RR+SS)
File Name	SSJ_II_109_6	SSJ_II_108_12	SSJ_RSPAV_150_3
Empirical formula	$C_{24}H_{36}N_2O_6$	$C_{24}H_{36}N_2O_6$	$C_{24}H_{36}N_2O_6$
Color	Colorless	Colorless	Colorless
Formula weight	448.55	448.55	448.55
Crystal size (mm)	0.320 x 0.060 x 0.050	0.370 x 0.130 x 0.100	0.286 x 0.082 x 0.043
Crystal system	Orthorhombic	Orthorhombic	Triclinic
Space group	$P2_12_12_1$	$P2_12_12_1$	P-1
a (Å)	9.4348(2)	9.4380(4)	8.8556(6)
b (Å)	15.2733(3)	15.2723(6)	9.4093(6)
c (Å)	17.4871(4)	17.4862(7)	16.2415(10)
α (°)	90	90	88.807(2)
β (°)	90	90	88.844(2)
γ (°)	90	90	64.245(2)
Volume (Å^3)	2519.90(9)	2520.46(18)	1218.53(14)
Z	4	4	2
$D_{calc.}$(g/cm^3)	1.182	1.182	1.223
F(000)	968	968	484
μ (mm^{-1}) CuK$_\alpha$	0.691	0.691	μ (mm^{-1}) MoK$_\alpha$=0.087
Temperature (K)	150(2)	150(2)	150(2)
Reflections collected/ unique/observed [I>2σ(I)]	14699/ 4942/4717	19419 /4959/4877	47252/ 5023/3817
Data/restraints/parameters	4942/0/295	4959/0/295	5023/0/295
Goodness of fit on F^2	1.023	1.032	1.019
Final R indices [I>2σ(I)]	R_1 = 0.0305 wR_2 = 0.0797	R_1 = 0.0274 wR_2 = 0.0732	R_1 = 0.0455 wR_2 = 0.0985
R indices (all data)	R1 = 0.0325 wR2 = 0.0814	R1 = 0.0279 wR2 = 0.0736	R1 = 0.0794 wR2 = 0.1058

Table S7. Crystal data for **3**

Crystal data	**3**-RR	**3**-SS	**3**-(RR+SS)
File Name	SSJ_II_80_10_2nd	SSJ_II_76_2	SSJ_RandSAAV
Empirical formula	$C_{24}H_{32}N_2O_6$	$C_{24}H_{32}N_2O_6$	$C_{24}H_{32}N_2O_6$
Color	Colorless	Colorless	Colorless
Formula weight	444.51	444.51	444.51
Crystal size (mm)	0.280 x 0.040 x 0.040	0.150 x 0.040 x 0.030	0.380 x 0.100 x 0.060
Crystal system	Orthorhombic	Orthorhombic	Monoclinic
Space group	$P2_12_12_1$	$P2_12_12_1$	$P2_1/n$
a (Å)	10.7827(4)	10.7781(3)	7.9665(2)
b (Å)	14.4628(5)	14.4702(4)	18.5906(5)
c (Å)	15.8451(5)	15.8639(5)	16.3292(5)
α (°)	90	90	90
β (°)	90	90	96.1540(10)
γ (°)	90	90	90
Volume ($Å^3$)	2471.01(15)	2474.15(12)	2404.45(12)
Z	4	4	4
$D_{calc.}$(g/cm^3)	1.195	1.193	1.228
F(000)	952	952	952
μ (mm^{-1}) CuK_α	0.704	0.703	0.723
Temperature (K)	150(2)	150(2)	150(2)
Reflections collected/ unique/observed [I>2σ(I)]	17513/ 4862/4586	19096/ 4876/4608	34026/ 4738/3887
Data/restraints/parameters	4862/0/295	4876/0/295	4738/0/295
Goodness of fit on F^2	1.062	1.060	1.030
Final R indices [I>2σ(I)]	R_1 = 0.0331 wR_2 = 0.0889	R_1 = 0.0339 wR_2 = 0.0896	R_1 = 0.0566 wR_2 =0.1548
R indices (all data)	R1 = 0.0358 wR2 = 0.0909	R1 = 0.0367 wR2 = 0.0914	R1 = 0.0687 wR2 = 0.1651

Table S8. Hydrogen bonding parameters for **1**

Compound 1-RR						
No.	Donor–H···Acceptor	D–H**/Å**	H···A**/Å**	D···A**/Å**	∠D–H···A**/°**	Symmetry operation
1	N(9)–H(9)···O(21)	0.88	2.01	2.8762(16)	169	-1/2+x,3/2-y,1-z
2	N(22)–H(22)···O(11)	0.88	2.07	2.9273(17)	165	-1/2+x,3/2-y,1-z
3	C(8)–H(8A)···O(28)	0.98	2.54	3.441(2)	153	1/2-x,1-y,-1/2+z
4	C(12)–H(12B)···O(21)	0.99	2.56	3.3604(19)	138	-1/2+x,3/2-y,1-z
5	C(19)–H(19A)···O(11)	0.99	2.50	3.3381(19)	143	-1/2+x,3/2-y,1-z
Compound 1-SS						
No.	Donor–H···Acceptor	D–H**/Å**	H···A**/Å**	D···A**/Å**	∠D–H···A**/°**	Symmetry operation
1	N(9)–H(9)···O(21)	0.88	2.01	2.8771(17)	169	-1/2+x,3/2-y,1-z
2	N(22)–H(22)···O(11)	0.88	2.07	2.9266(17)	165	-1/2+x,3/2-y,1-z
3	C(7)–H(7B)···O(28)	0.98	2.54	3.441(2)	153	1/2-x,1-y,-1/2+z
4	C(12)–H(12B)···O(21)	0.99	2.55	3.358(2)	138	-1/2+x,3/2-y,1-z
5	C(19)–H(19B)···O(11)	0.99	2.50	3.338(2)	143	-1/2+x,3/2-y,1-z
Compound 1-(RR+SS)						
No.	Donor–H···Acceptor	D–H**/Å**	H···A**/Å**	D···A**/Å**	∠D–H···A**/°**	Symmetry operation
1	N(9)–H(9)···O(21)	0.88	2.05	2.8998(14)	162	1-x,-y,1-z
2	N(22)–H(22)···O(11)	0.88	2.06	2.9288(14)	171	1-x,1-y,1-z
3	C(4)–H(4B)···O(21)	0.98	2.54	3.4353(19)	152	2-x,-y,1-z
4	C(5)–H(5)···O(28)	1.00	2.50	3.2810(16)	134	1-x,1-y,1-z
5	C(7)–H(7B)···O(21)	0.98	2.46	3.3950(17)	159	1-x,-y,1-z
6	C(15)–H(15)···O(1)	0.95	2.58	3.4748(17)	157	2-x,-y,1-z
7	C(23)–H(23)···O(1)	1.00	2.47	3.2578(17)	135	1-x,-y,1-z
8	C(26)–H(26A)···O(11)	0.98	2.47	3.3924(19)	157	1-x,1-y,1-z
9	C(30)–H(30B)···O(28)	0.98	2.49	3.3467(18)	146	-x,1-y,2-z

Table S9. Hydrogen bonding parameters for **2**

Compound 2-RR						
No.	Donor–H···Acceptor	D–H**/Å**	H···A**/Å**	D···A**/Å**	∠D–H···A**/°**	Symmetry operation
1	N(9)–H(9)···O(23)	0.88	2.05	2.8822(19)	156	3/2-x,1-y,-1/2+z
2	N(24)–H(24)···O(11)	0.88	2.02	2.8567(18)	158	1/2-x,1-y,1/2+z
3	C(8)–H(8C)···O(3)	0.98	2.58	3.491(3)	154	1/2+x,3/2-y,-z
4	C(21)–H(21B)···O(11)	0.99	2.58	3.184(2)	120	1/2-x,1-y,1/2+z
5	C(31)–H(31B)···O(1)	0.98	2.46	3.343(2)	149	1-x,-1/2+y,3/2-z
Compound 2-SS						
No.	Donor–H···Acceptor	D–H**/Å**	H···A**/Å**	D···A**/Å**	∠D–H···A**/°**	Symmetry operation
1	N(9)–H(9)···O(23)	0.88	2.02	2.8566(16)	158	3/2-x,1-y,-1/2+z
2	N(24)–H(24)···O(11)	0.88	2.05	2.8825(16)	156	1/2-x,1-y,1/2+z
3	C(4)–H(4A)···O(32)	0.98	2.46	3.342(2)	149	1-x,1/2+y,1/2-z
4	C(12)–H(12A)···O(23)	0.99	2.58	3.1833(18)	120	3/2-x,1-y,-1/2+z
5	C(28)–H(28C)···O(30)	0.98	2.58	3.494(2)	154	-1/2+x,1/2-y,2-z
Compound 2-(RR+SS)						
No.	Donor–H···Acceptor	D–H**/Å**	H···A**/Å**	D···A**/Å**	∠D–H···A**/°**	Symmetry operation
1	N(9)–H(9)···O(23)	0.88	2.02	2.9023 (14)	177	-x,2-y,1-z
2	N(24)–H(24)···O(11)	0.88	2.06	2.8836(14)	156	1-x,1-y,1-z
3	C(13)–H(13A)···O(32)	0.99	2.56	3.4443(19)	149	1-x,2-y,1-z

Table S10. Hydrogen bonding parameters for **3**

Compound 3-RR						
No.	Donor–H···Acceptor	D–H**/Å**	H···A**/Å**	D···A**/Å**	∠D–H···A**/°**	Symmetry operation
1	N(9)–H(9)···O(23)	0.88	2.01	2.8680(19)	165	1-x,1/2+y,3/2-z
2	N(24)–H(24)···O(11)	0.88	2.03	2.886(2)	165	1/2+x,1/2-y,1-z
3	C(7)–H(7B)···O(23)	0.98	2.45	3.391(3)	162	1-x,1/2+y,3/2-z
4	C(16)–H(16)···O(1)	0.95	2.48	3.389(3)	160	1/2-x,1-y,1/2+z
5	C(19)–H(19)···O(32)	0.95	2.55	3.280(3)	134	3/2-x,-y,-1/2+z
6	C(21)–H(21)···O(11)	0.95	2.37	3.177(2)	142	1/2+x,1/2-y,1-z
7	C(28)–H(28C)···O(1)	0.98	2.51	3.433(3)	157	3/2+x,1/2-y,1-z
Compound 3-SS						
No.	Donor–H···Acceptor	D–H**/Å**	H···A**/Å**	D···A**/Å**	∠D–H···A**/°**	Symmetry operation
1	N(9)–H(9)···O(23)	0.88	2.03	2.886(2)	165	-1/2+x,3/2-y,1-z
2	N(24)–H(24)···O(11)	0.88	2.01	2.869(2)	165	1-x,-1/2+y,1/2-z
3	C(7)–H(7C)···O(32)	0.98	2.51	3.440(3)	157	-3/2+x,3/2-y,1-z
4	C(12)–H(12)···O(23)	0.95	2.37	3.176(2)	142	-1/2+x,3/2-y,1-z
5	C(15)–H(15)···O(32)	0.95	2.48	3.387(3)	160	3/2-x,1-y,-1/2+z
6	C(18)–H(18)···O(1)	0.95	2.55	3.281(3)	134	1/2-x,2-y,1/2+z
7	C(27)–H(27A)···O(11)	0.98	2.45	3.389(3)	161	1-x,-1/2+y,1/2-z
Compound 3-(RR+SS**)**						
No.	Donor–H···Acceptor	D–H**/Å**	H···A**/Å**	D···A**/Å**	∠D–H···A**/°**	Symmetry operation
1	N(9)–H(9)···O(23)	0.88	2.15	3.008(2)	166	3/2-x,-1/2+y,1/2-z
2	N(24)–H(24)···O(11)	0.88	2.21	3.051(2)	159	1-x,1-y,1-z
3	C(5)–H(5)···O(32)	1.00	2.53	3.350(3)	139	1-x,1-y,1-z
4	C(12)–H(12)···O(23)	0.95	2.49	3.300(2)	144	3/2-x,-1/2+y,1/2-z
5	C(21)–H(21)···O(11)	0.95	2.51	3.309(2)	141	1-x,1-y,1-z
6	C(27)–H(27C)···O(1)	0.98	2.60	3.321(4)	131	3/2-x,1/2+y,1/2-z
7	C(28)–H(28A)···O(23)	0.98	2.55	3.463(3)	155	-1+x,y,z

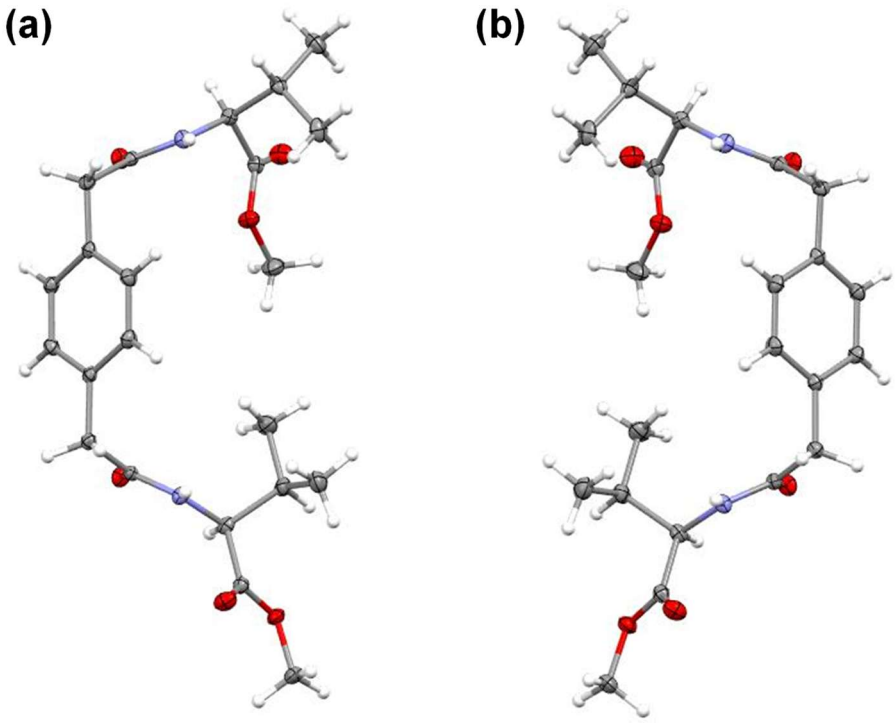

Figure S43. Asymmetric unit of (a) **1**-SS and (b) **1**-RR showing the mirror image of enantiomers.

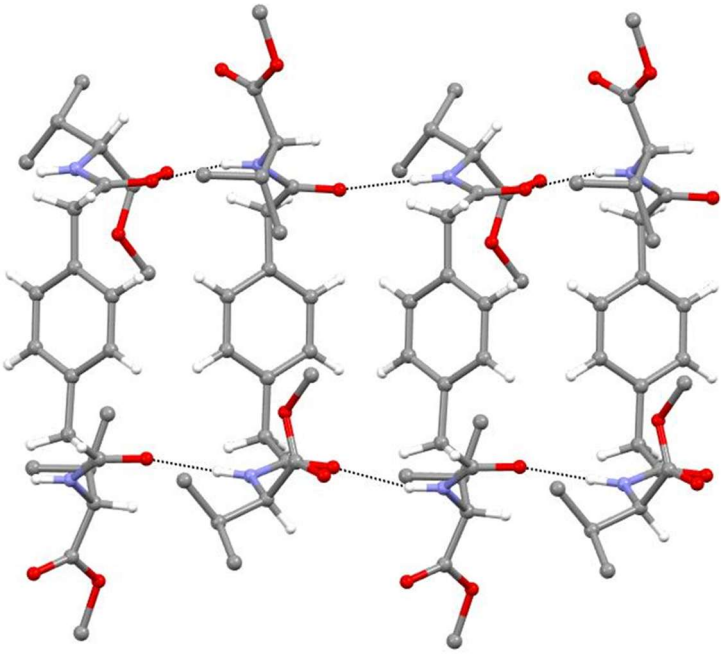

Figure S44. 1-D hydrogen-bonded chain via N−H···O interactions observed in the enantiomers (**1**-RR and **1**-SS).

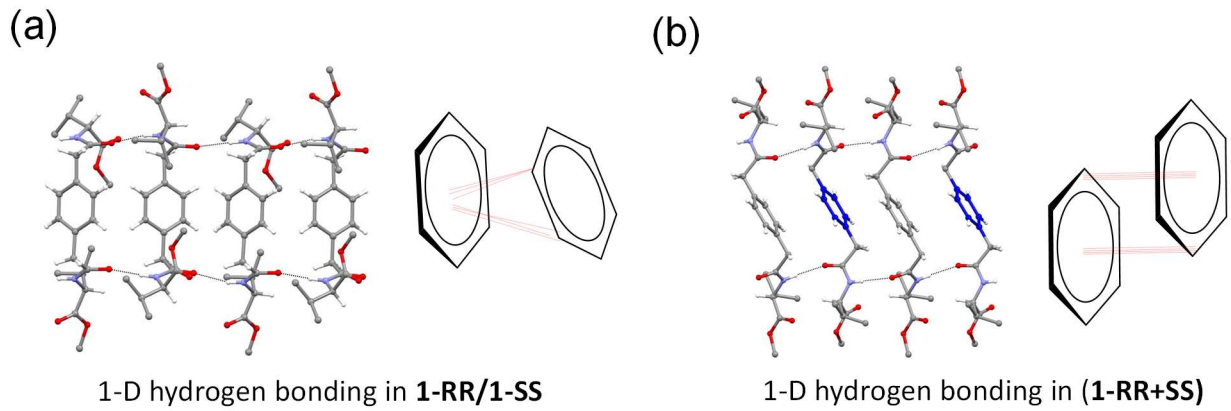

Figure S45. The edge-to-face (a) and offset face-to-face (b) π-π interactions observed in the enantiomers (**1**-RR or **1**-SS)and mixed (**1**-RR+SS) compounds, respectively.

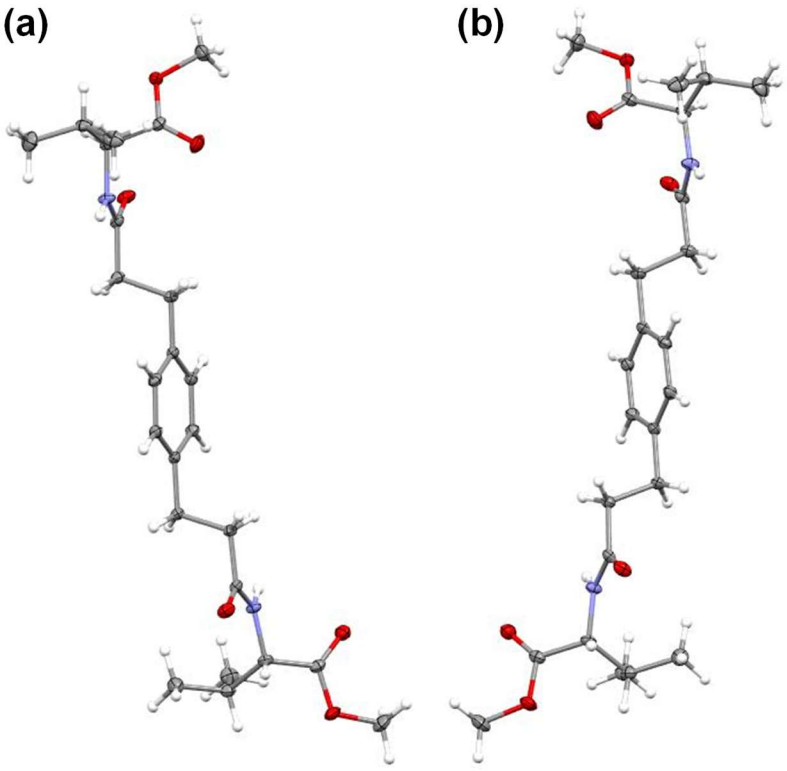

Figure S46. Asymmetric unit of (a) **2**-SS and (b) **2**-RR showing the mirror image of enantiomers.

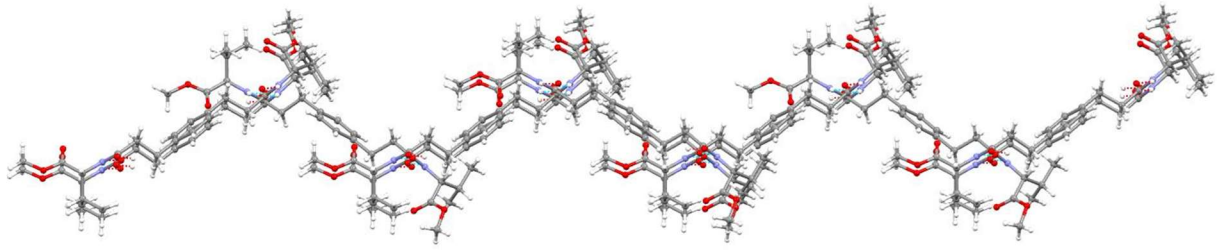

Figure S47. The hydrogen-bonded 2-D corrugated sheet observed in the enantiomers of **2**.

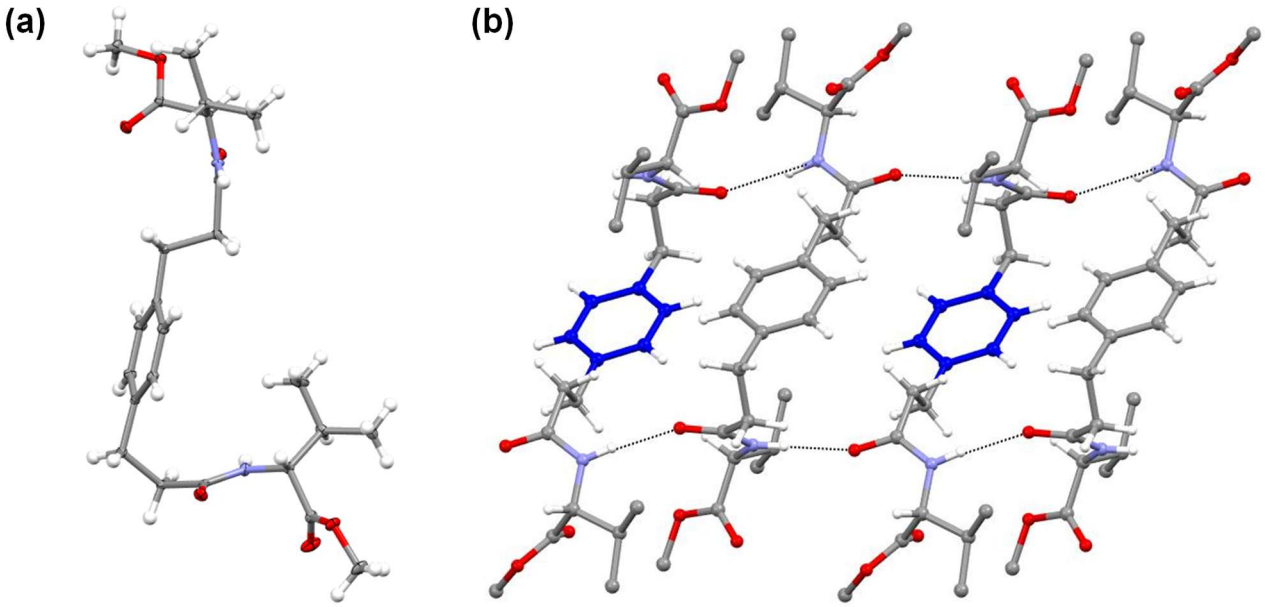

Figure S48. Crystal structure of **2-(RR+SS)** (a) asymmetric unit, (b) formation of 1-D hydrogen bonded architecture (hydrogen atoms of the methyl groups are omitted for clarity).

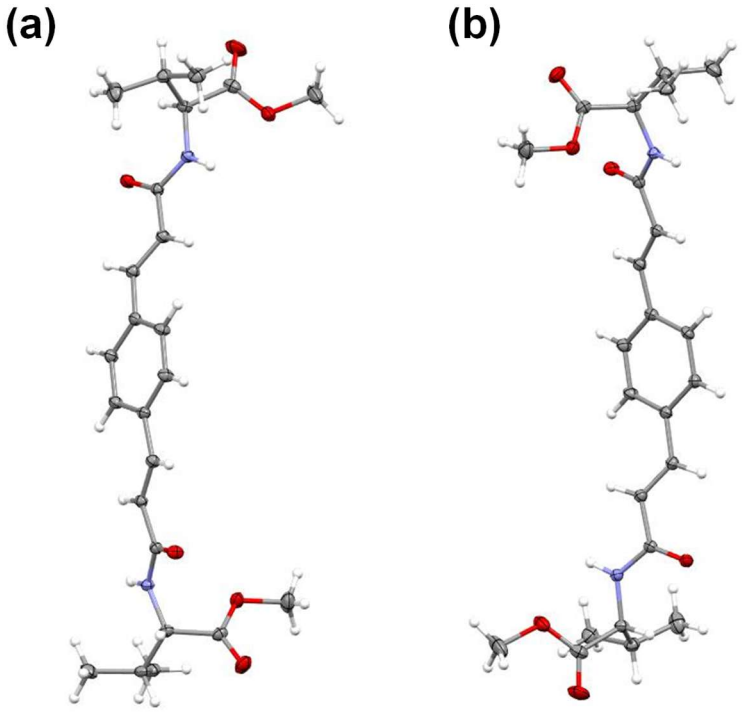

Figure S49. Asymmetric unit of (a) **3-SS** and (b) **3-RR** showing the mirror image of enantiomers.

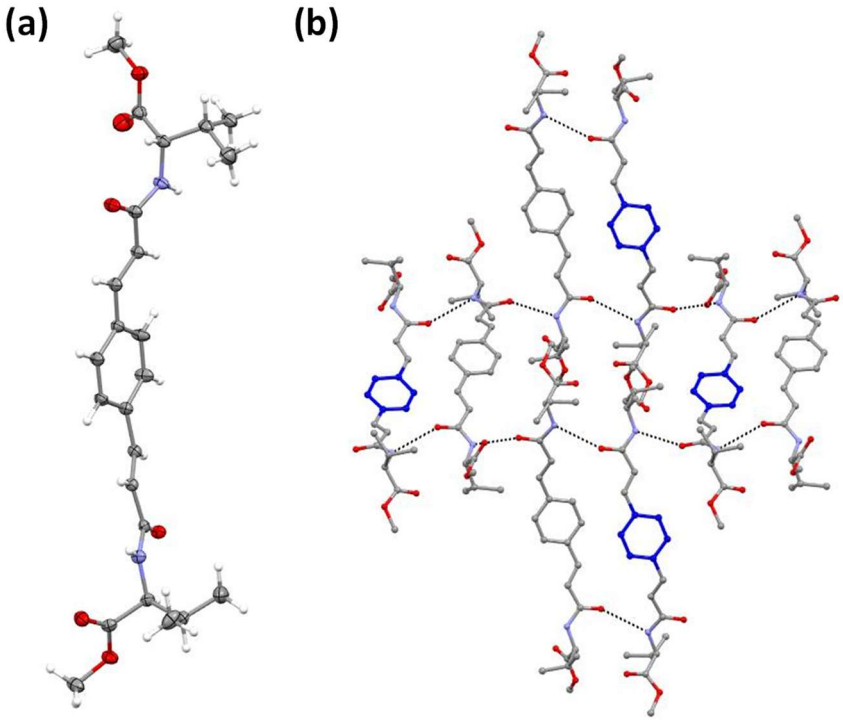

Figure S50. Crystal structure of **3-(RR+SS)** (a) asymmetric unit, (b) formation of 2-D hydrogen bonded architecture (hydrogen atoms are omitted for clarity).

7. Powder X-ray diffraction

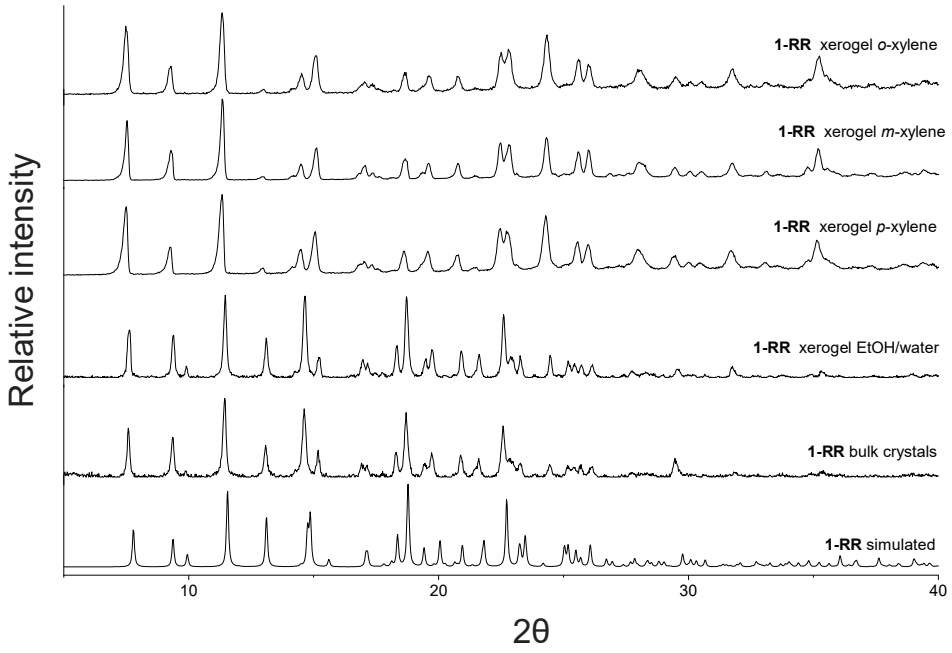

Figure S51. Comparison of PXRD pattern of **1**-RR: simulated, bulk crystals obtained from ethanol/water and xerogel at 6.0 wt/v% obtained from ethanol/water (1:1, v/v) and 7.0 wt/v% in *p*-xylene, *m*-xylene and *o*-xylene.

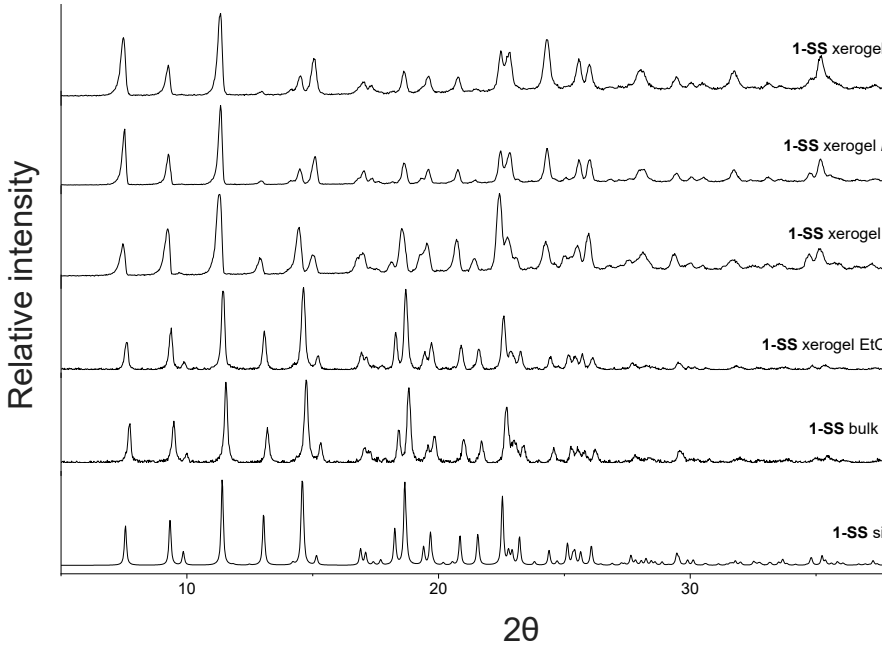

Figure S52. Comparison of PXRD pattern of **1**-SS: simulated, bulk crystals obtained from ethanol/water and xerogel at 6.0 wt/v% obtained from ethanol/water (1:1, v/v) and at 7.0 wt/v% in *p*-xylene, *m*-xylene and *o*-xylene.

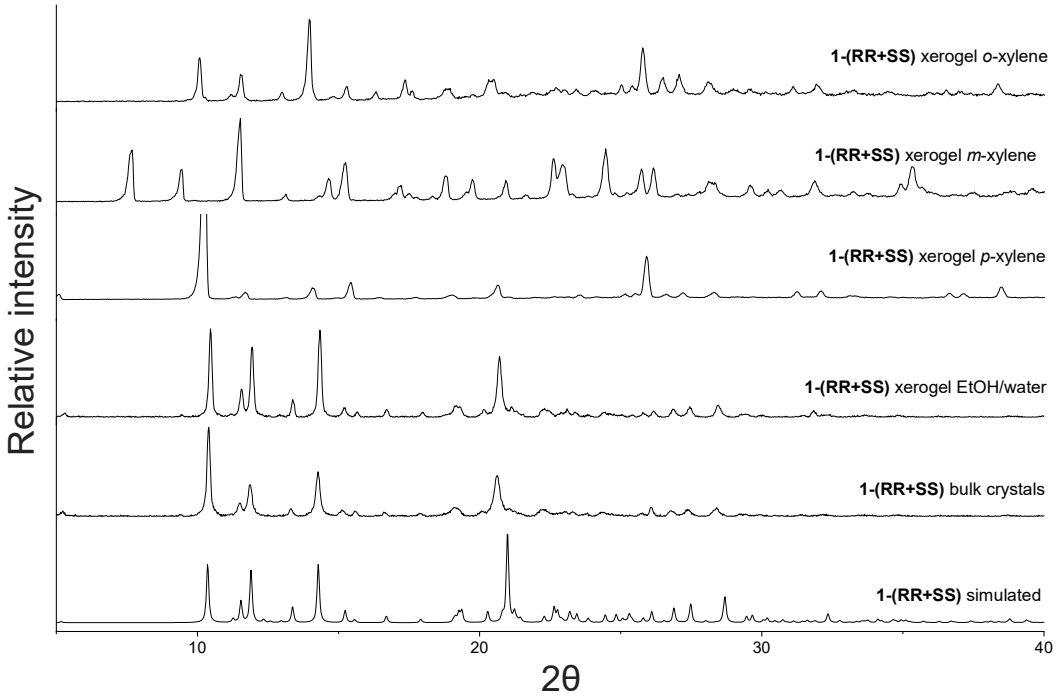

Figure S53. Comparison of PXRD pattern of (**1**-RR+SS): simulated, bulk crystals obtained from ethanol/water and xerogel at 6.0 wt/v% obtained from ethanol/water (1:1, v/v) and at 7.0 wt/v% in *p*-xylene, m-xylene and o-xylene.

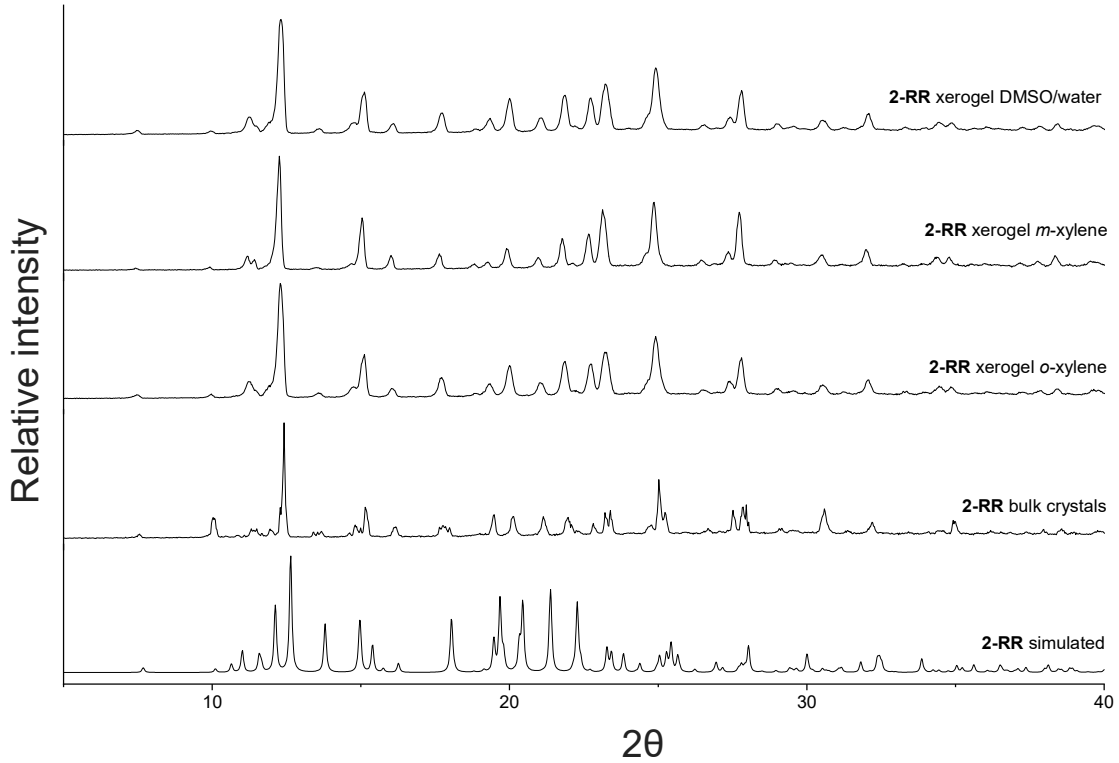

Figure S54. Comparison of PXRD pattern of **2**-RR: simulated, bulk crystals obtained from ethanol/water and xerogel at 5.0 wt/v% obtained from *o*-xylene, *m*-xylene and DMSO/water (1:1, v/v).

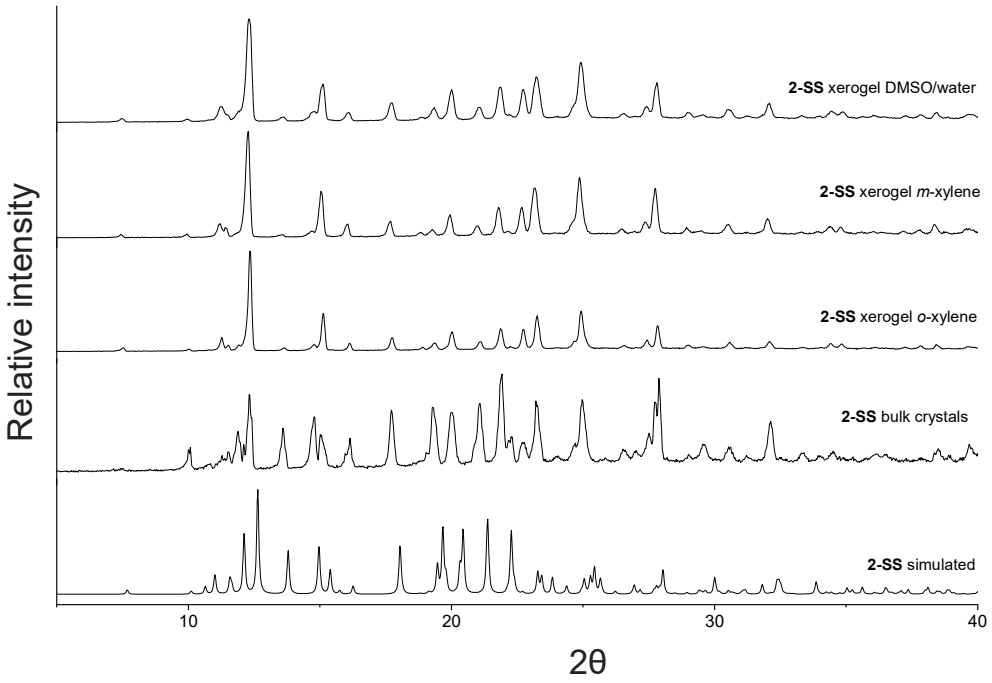

Figure S55. Comparison of PXRD pattern of **2**-SS: simulated, bulk crystals obtained from ethanol/water and xerogel at 5.0 wt/v% obtained from *o*-xylene, *m*-xylene and DMSO/water (1:1, v/v).

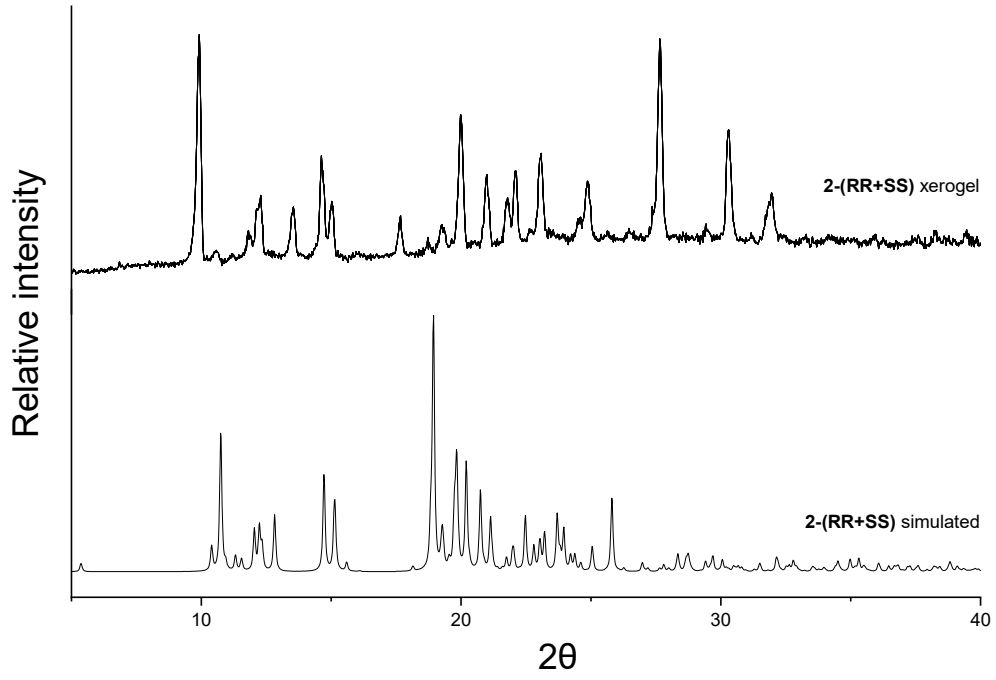

Figure S56. Comparison of PXRD pattern of **2**-(RR+SS): simulated and xerogel at 5.0 wt/v% obtained from DMSO/water (1:1, v/v).

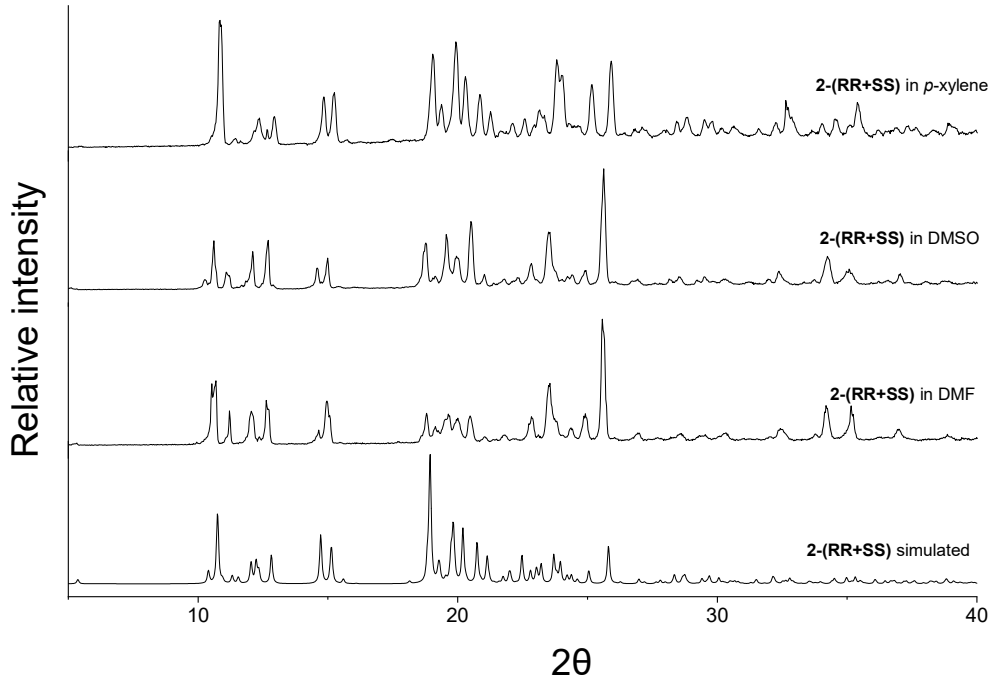

Figure S57. Comparison of PXRD pattern of **2**-(RR+SS): simulated, the dried powder obtained from the solution of DMF and DMSO, and the colloid formed in *p*-xylene, at 5.0 wt/v% over a week.

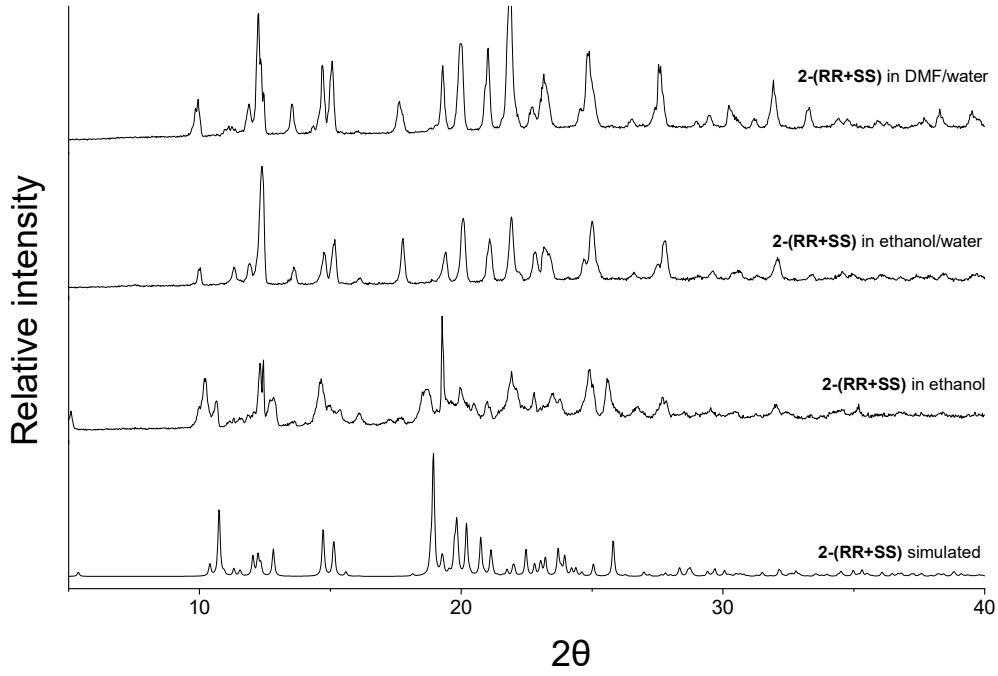

Figure S58. Comparison of PXRD pattern of **2**-(RR+SS): simulated, the dried powder obtained from alcohols and aqueous mixtures after a week.

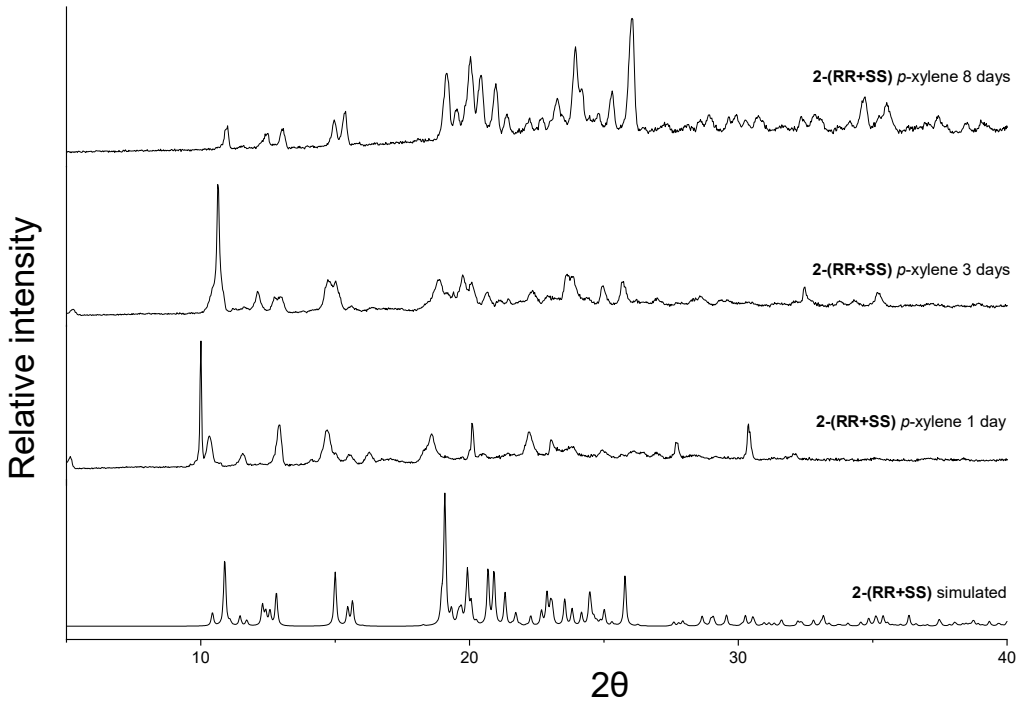

Figure S59. Monitoring self-assembly of **2**-(RR+SS) in *p*-xylene: simulated pattern of **2**-(RR+SS) and dried powder of the colloidal solution obtained by dissolving 20.0 mg of **2**-(RR+SS) in *p*-xylene over a week.

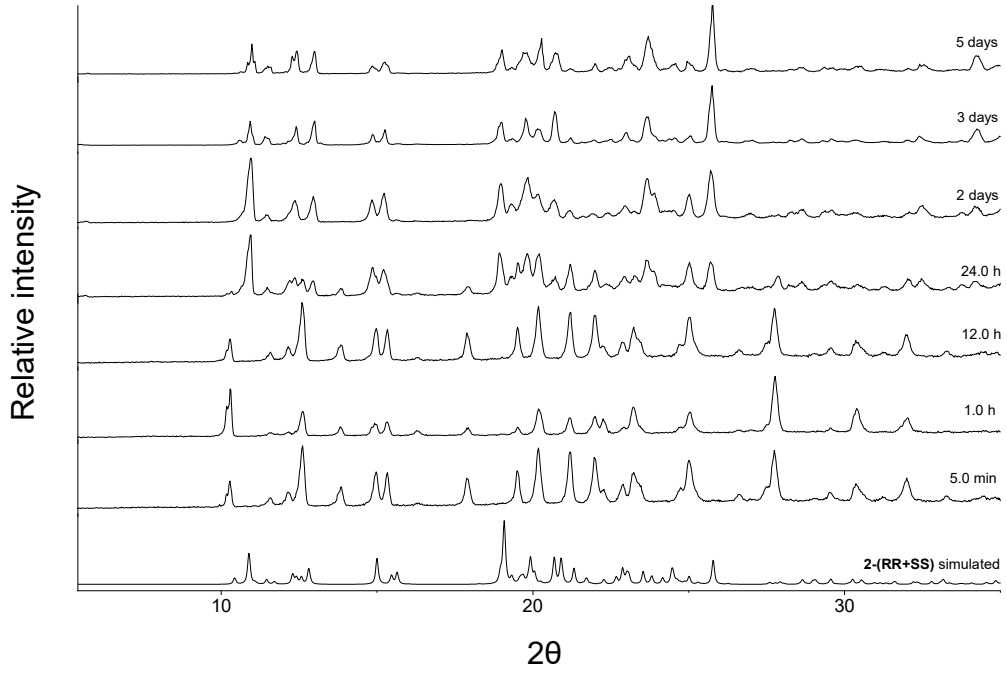

Figure S60. Monitoring self-assembly of **2**-(RR+SS) in DMF: simulated pattern of **2**-(RR+SS) and dried precipitate from DMF solution 20.0 mg of **2**-(RR+SS) via addition of water at various time intervals.

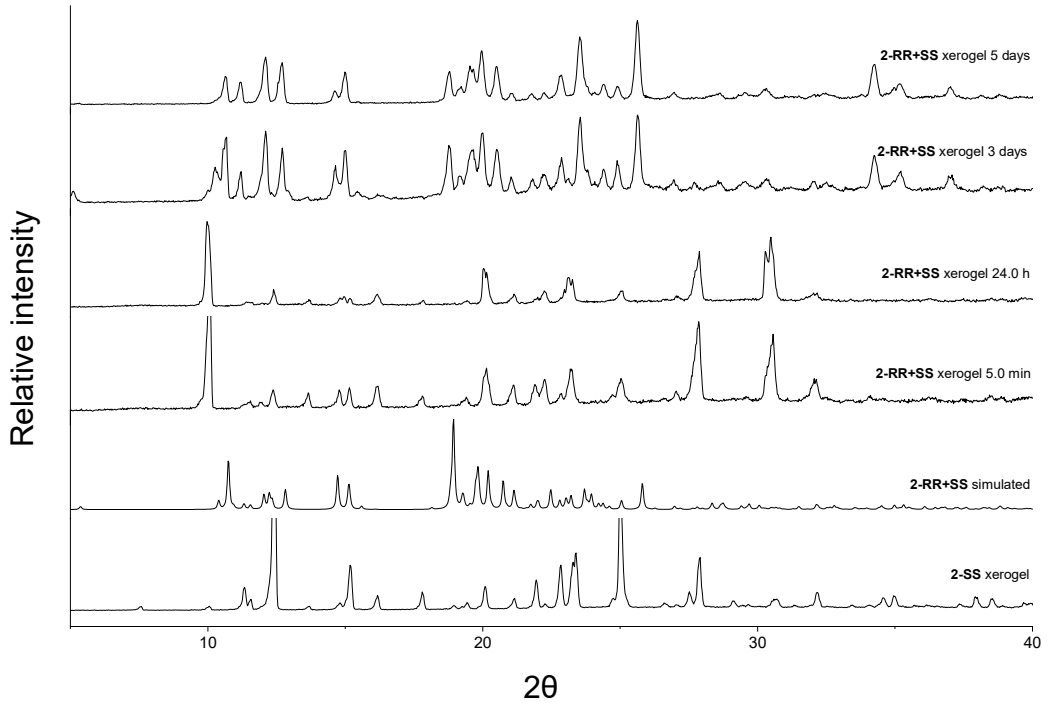

Figure S61. Monitoring self-assembly of **2**-(RR+SS) in DMSO (5.0 wt/v%): **2**-SS xerogel, simulated pattern of **2**-(RR+SS) and the dried gel obtained via addition of water at various time intervals.

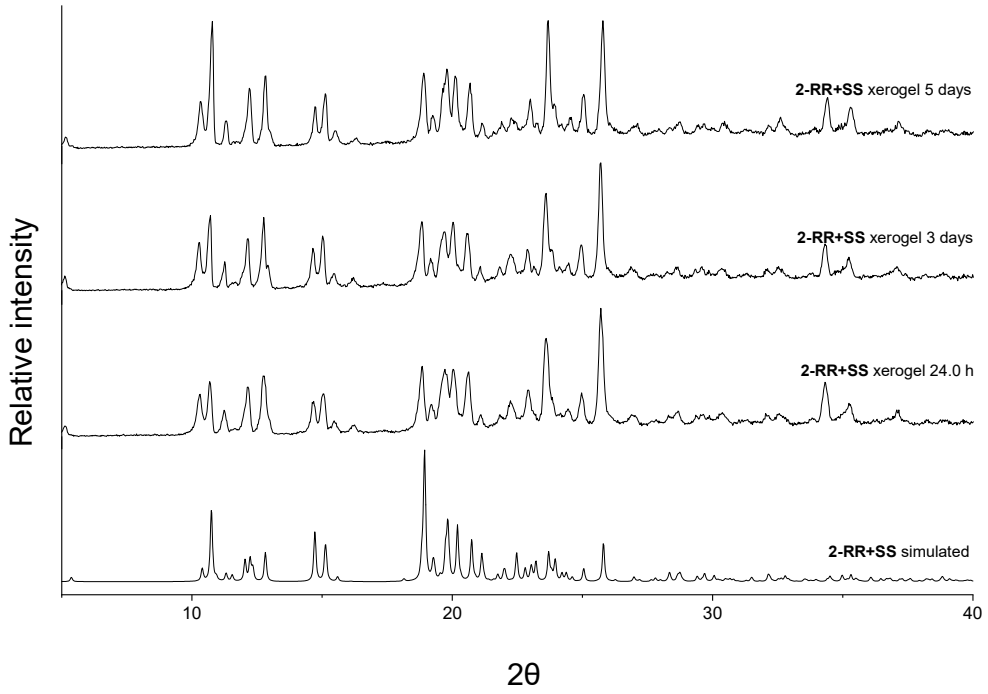

Figure S62. Self-assembly of **2**-(RR+SS) with the preassembled compound at 5.0 wt/v% in DMSO/water (1:1, v/v): Simulated pattern of **2**-(RR+SS), and the dried gel obtained via addition of water at various time intervals.

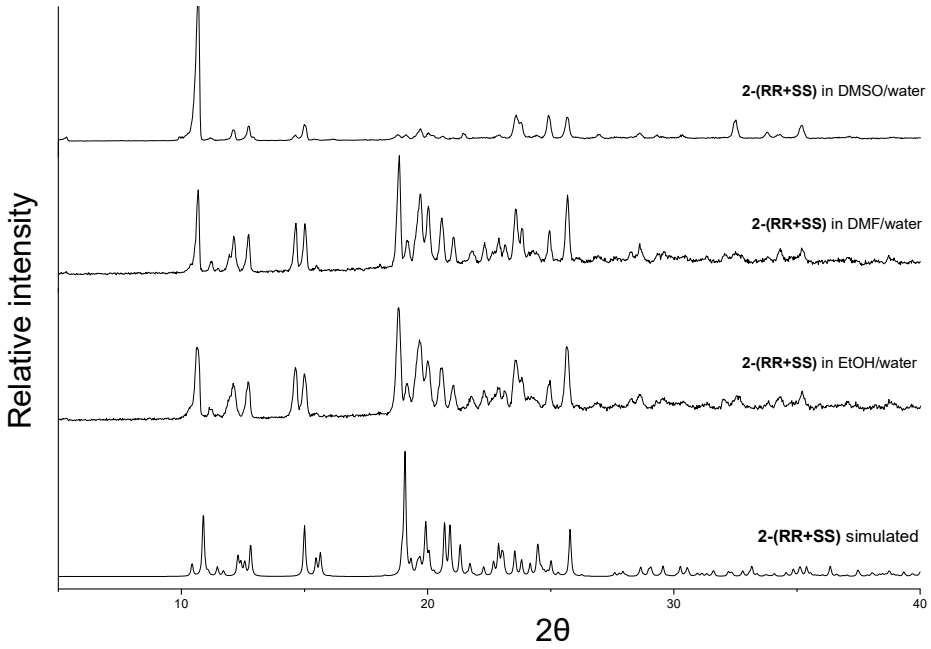

Figure S63. Monitoring self-assembly process in pre-assembled sample of **2-(RR+SS)**: Simulated pattern of **2-(RR+SS)**, and the crystalline material obtained from (1:1, v/v) ethanol/water and DMF/water by dissolving 20.0 mg of the compound in 1.0 mL of the solvent after 7 days and the xerogel obtained from (1:1, v/v) DMSO/water at 5.0 wt/v%.

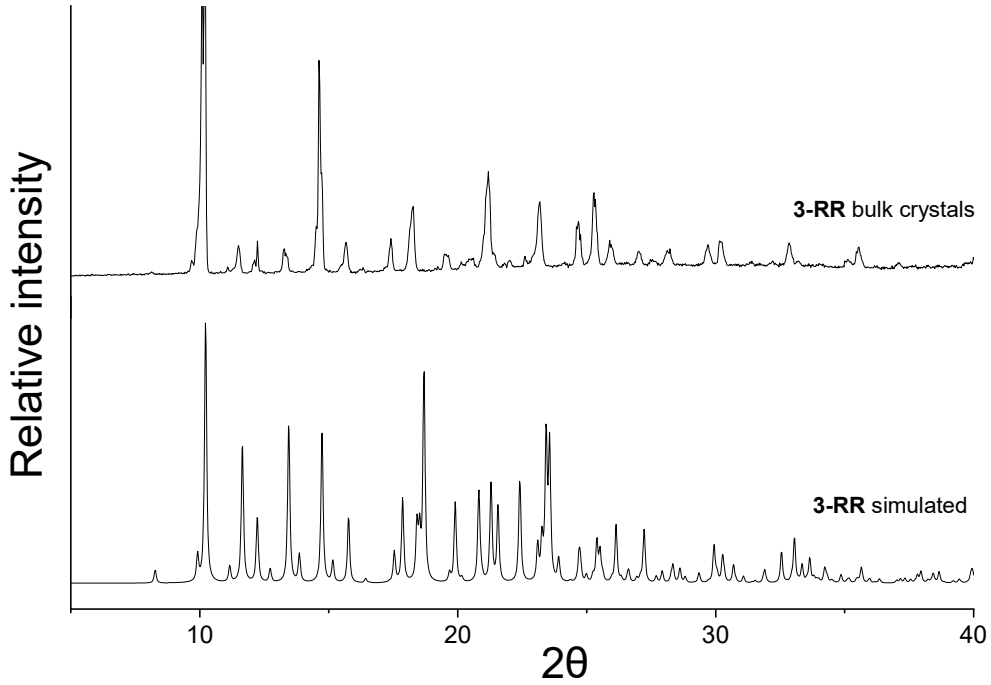

Figure S64. Comparison of PXRD pattern of **3**-RR: simulated, and bulk crystals obtained from acetonitrile.

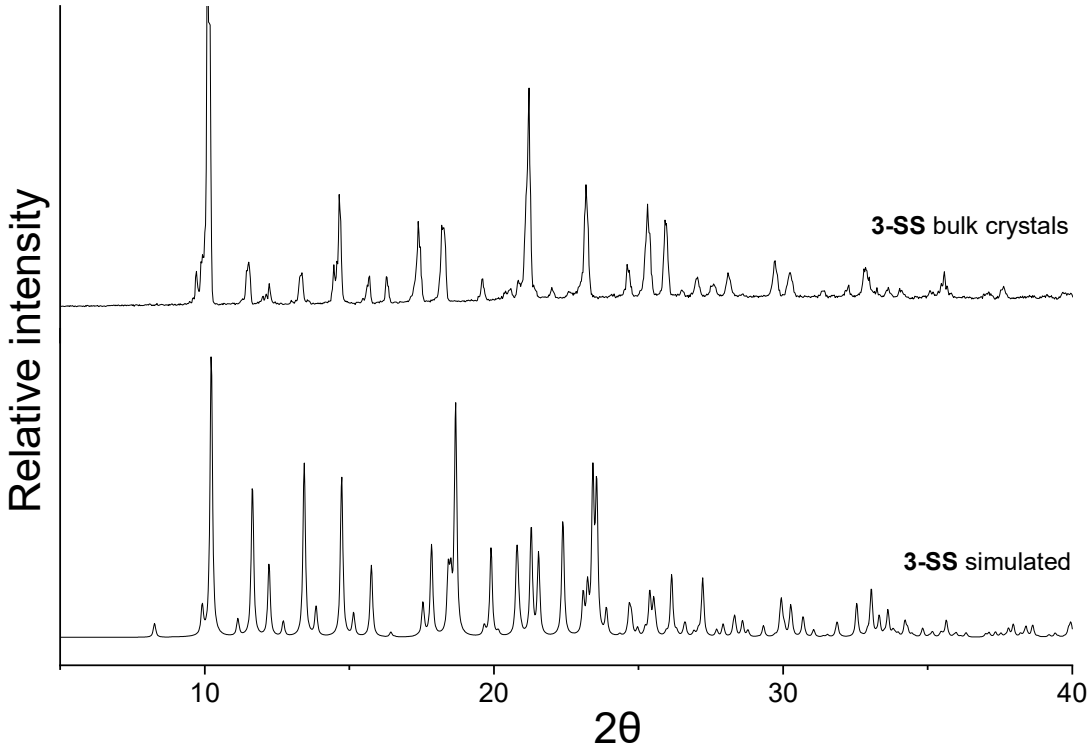

Figure S65. Comparison of PXRD pattern of **3**-SS: simulated, and bulk crystals obtained from acetonitrile.

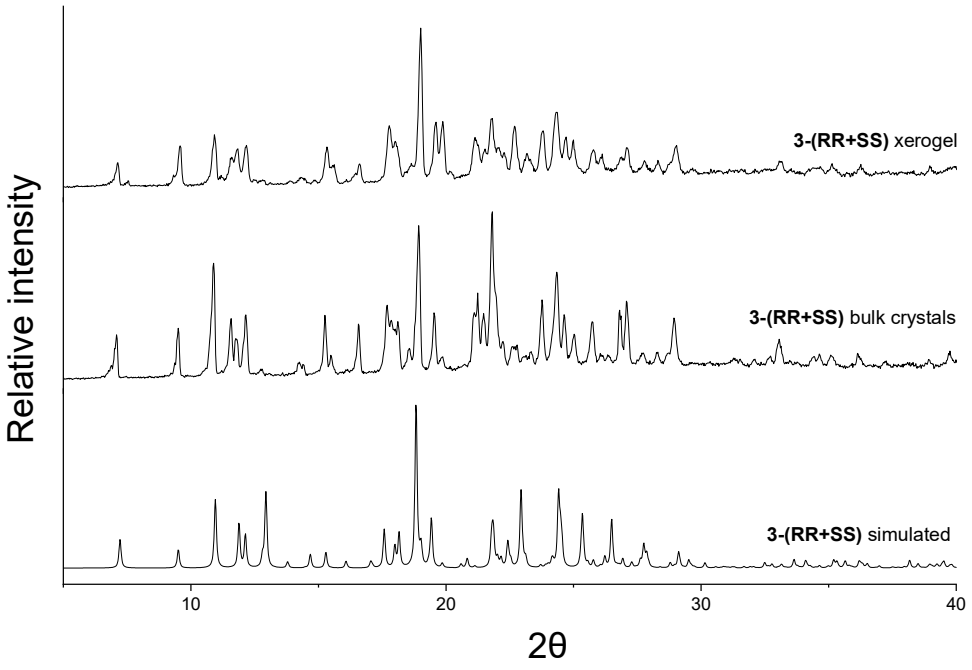

Figure S66. Comparison of PXRD pattern of **3**-(RR+SS): simulated, bulk crystals obtained from acetonitrile, and the xerogels at 5.0 wt/v% obtained DMSO/water (1:1, v/v)

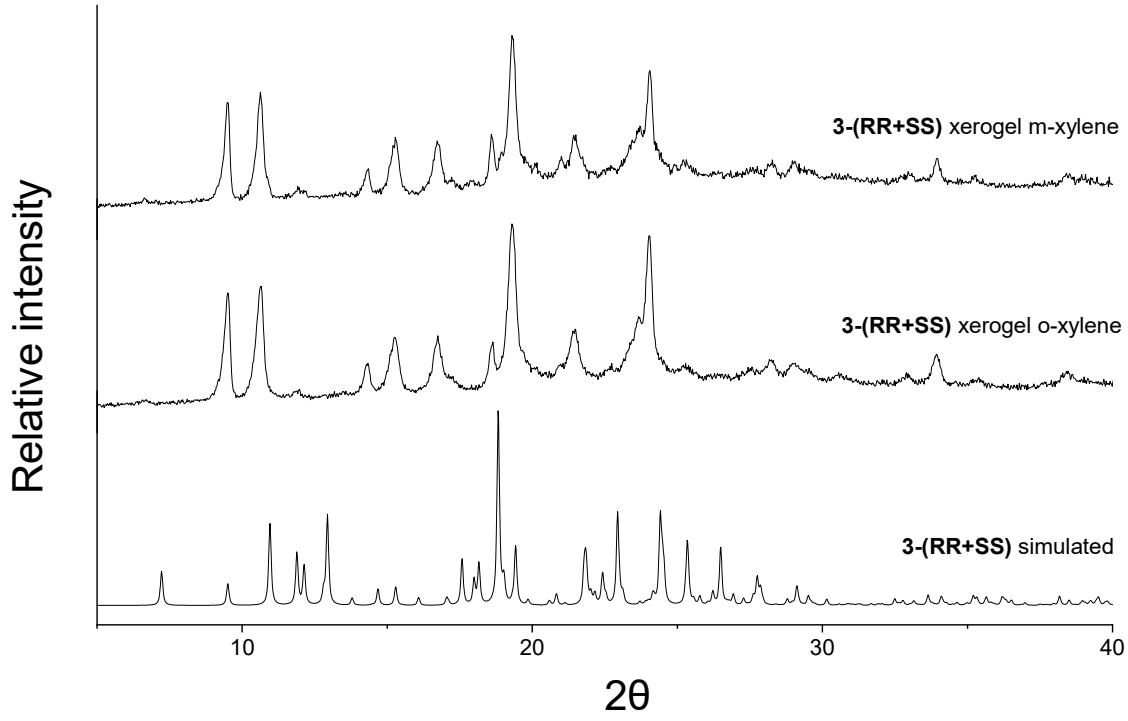

Figure S67. Comparison of PXRD pattern of **3-(RR+SS)**: simulated, and the xerogels at 2.0 wt/v% obtained from *o*-xylene and *m*-xylene.

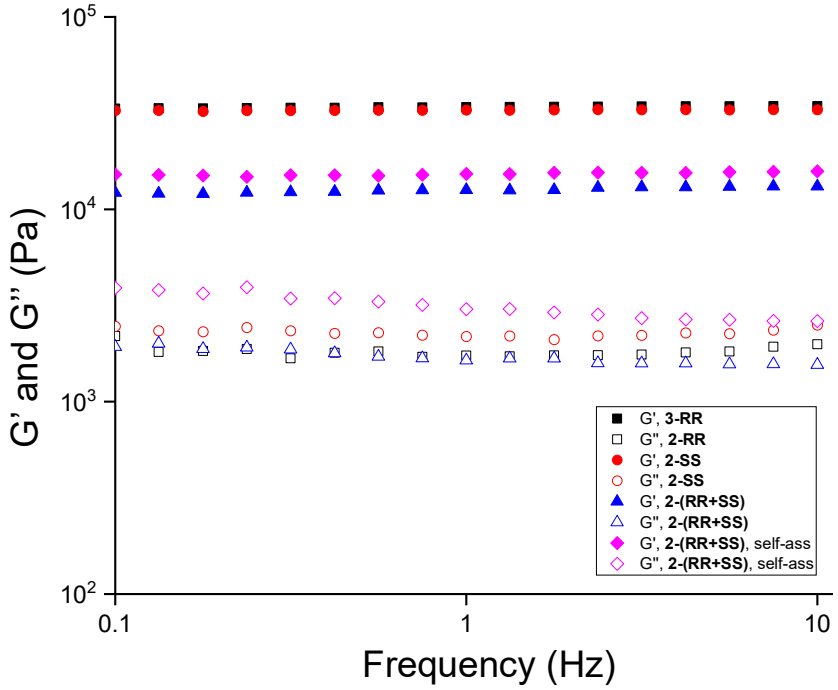

Figure S68. Frequency sweep of gels of **2** (individual, orthogonal co-assembled and also specific co-assembled) (5.0 wt/v%) at 20.0 °C measured at a constant strain of 0.02% in DMSO/water (1:1, v/).

8. NMR spectra

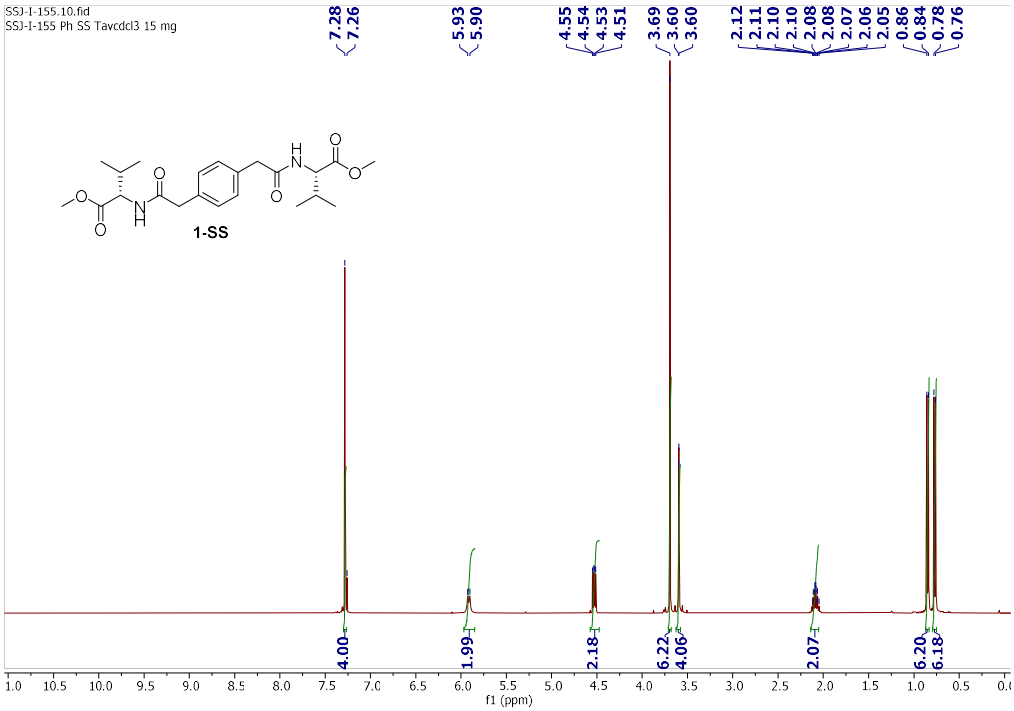

Figure S69. ^{1}H NMR spectrum of **1**-SS.

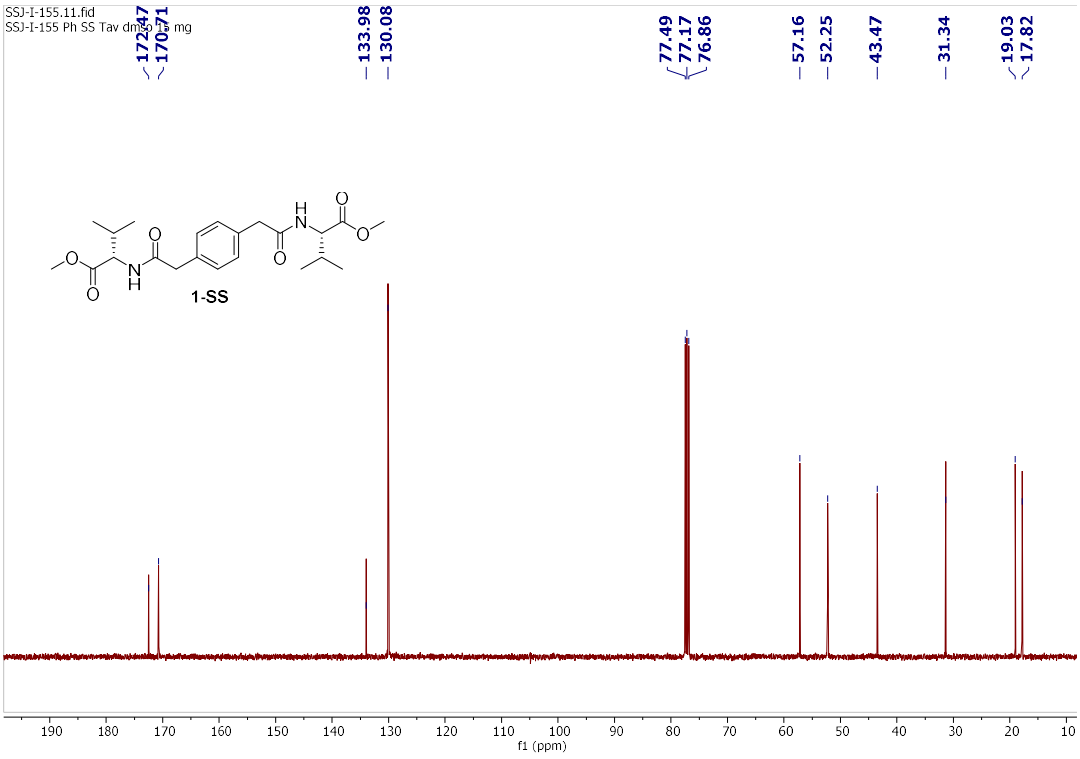

Figure S70. ^{13}C NMR spectrum of **1**-SS.

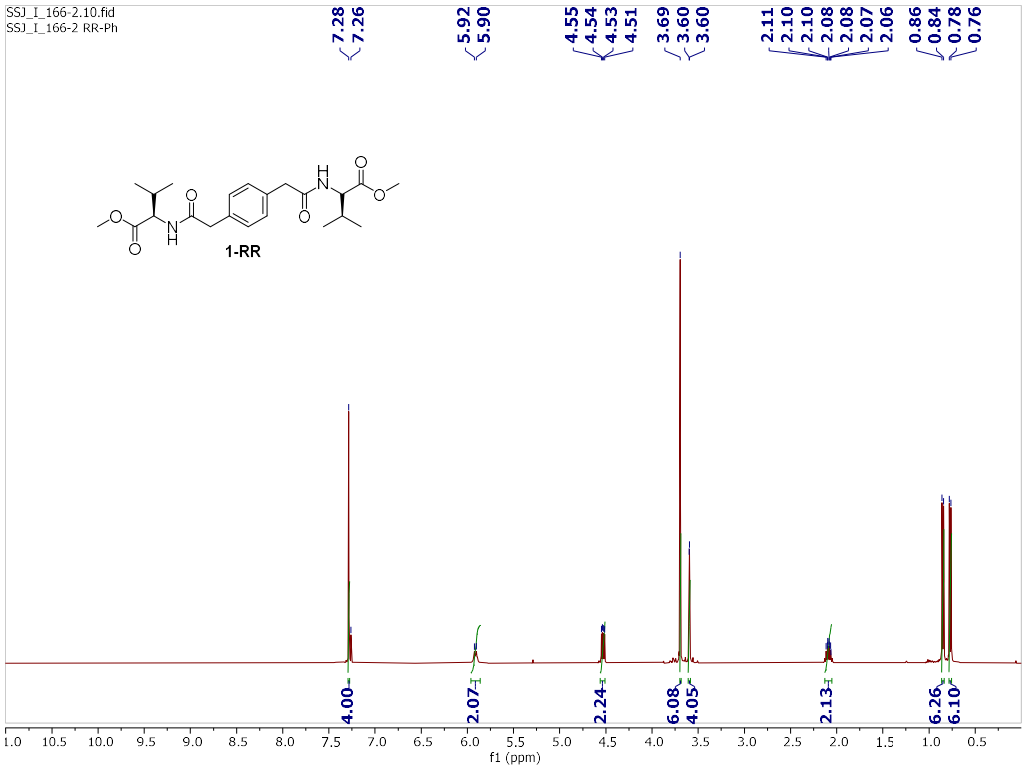

Figure S71. ^{1}H NMR spectrum of **1**-RR.

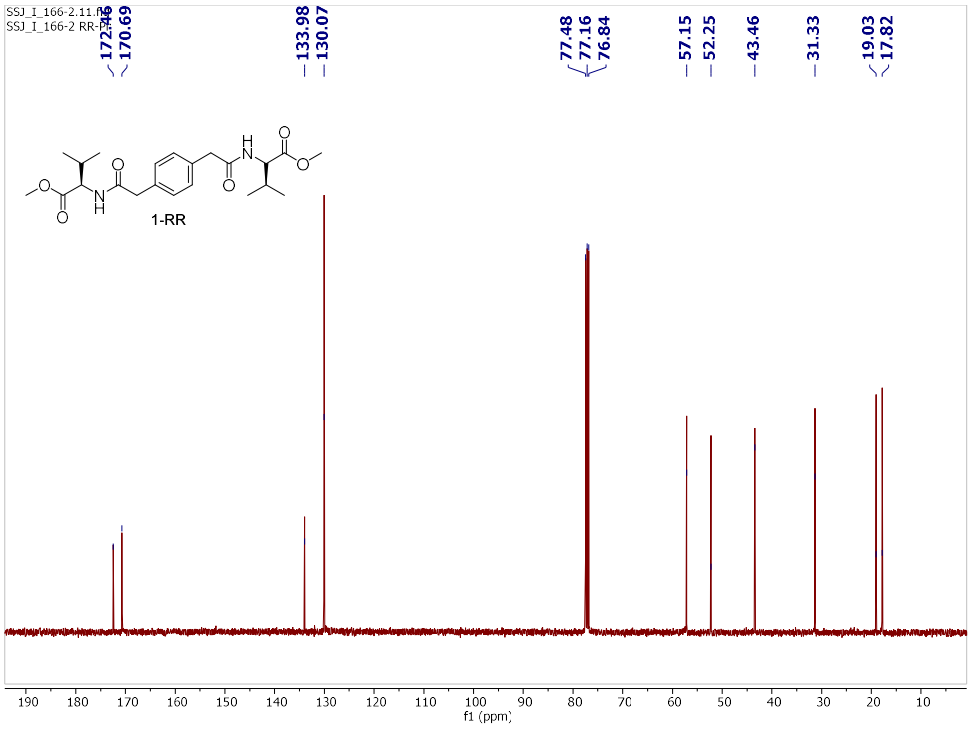

Figure S72. ^{13}C NMR spectrum of **1**-RR.

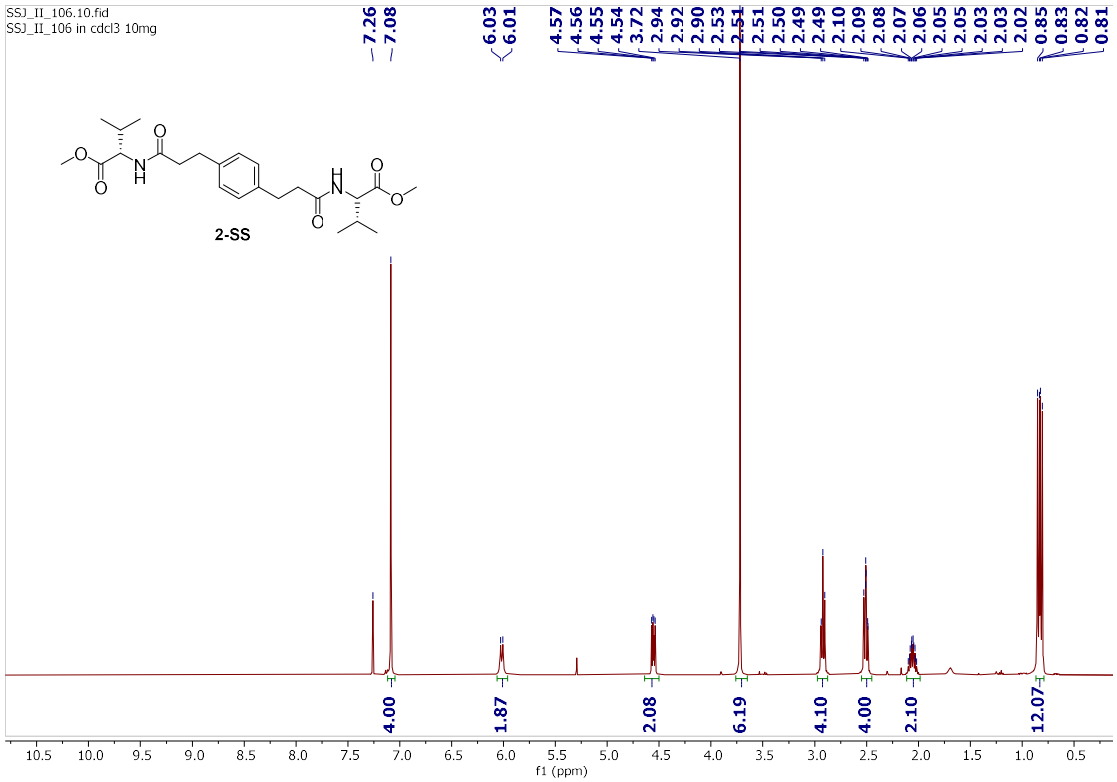

Figure S73. ^{1}H NMR spectrum of **2**-SS.

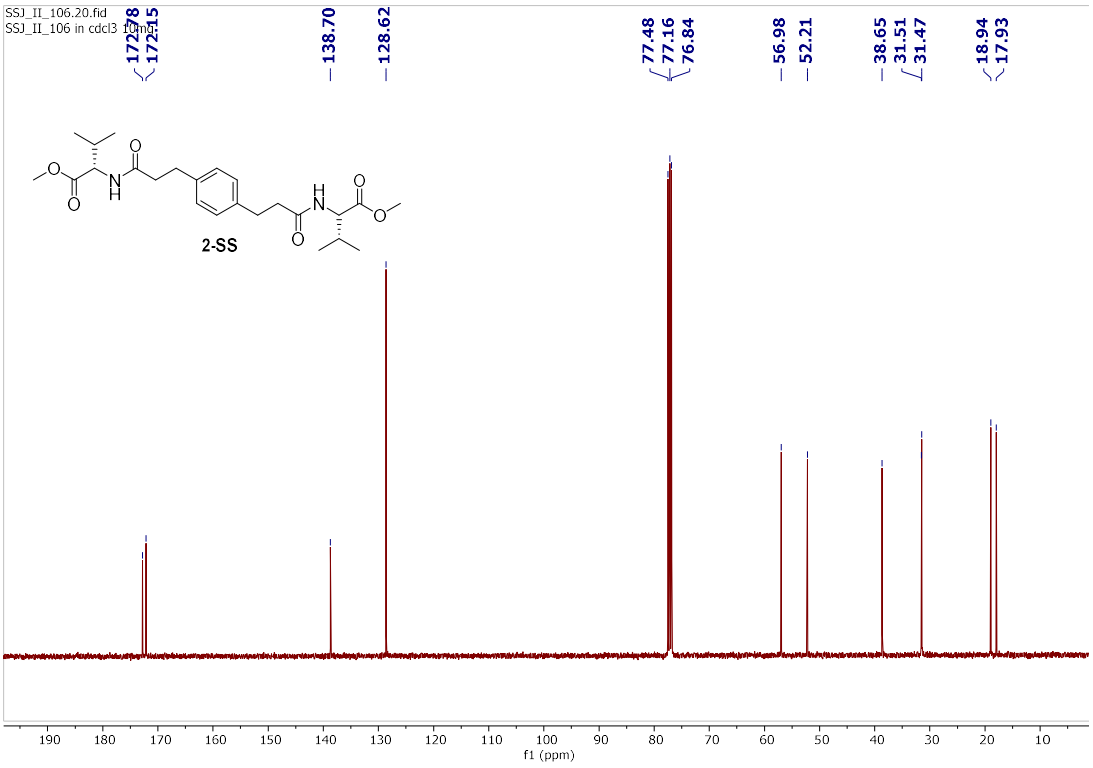

Figure S74. ^{13}C NMR spectrum of **2**-SS.

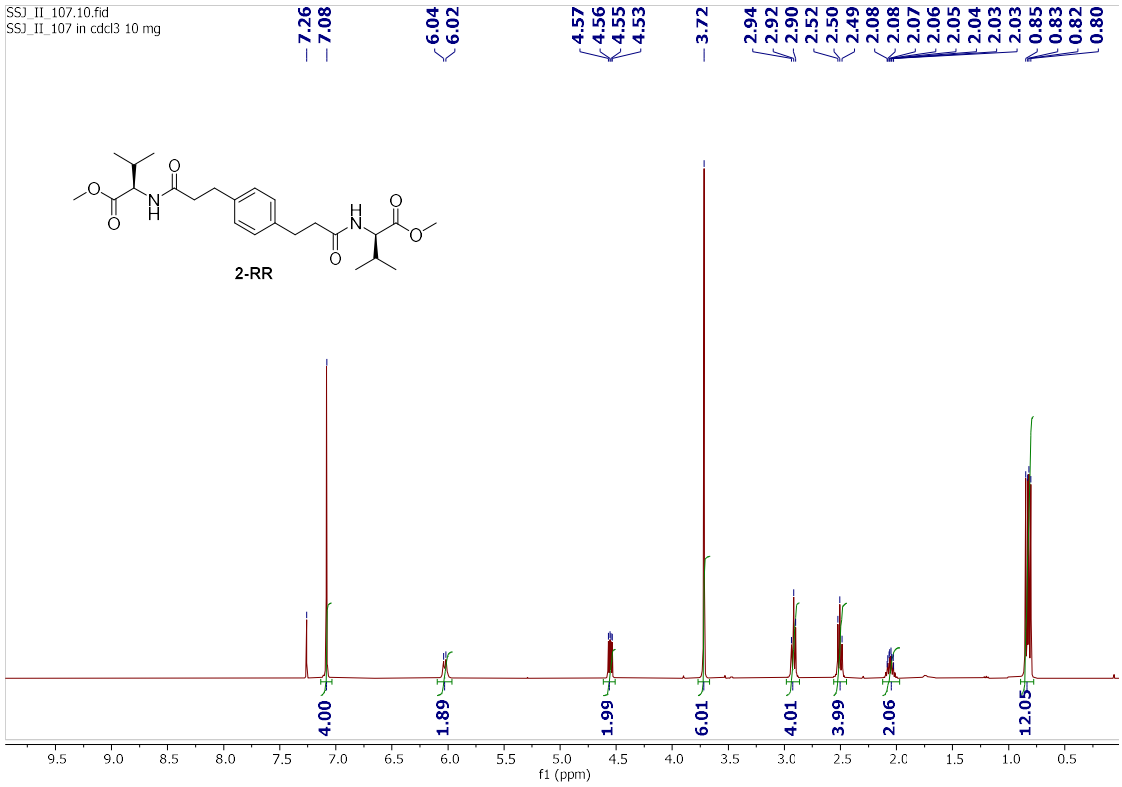

Figure S75. ^{1}H NMR spectrum of **2**-RR.

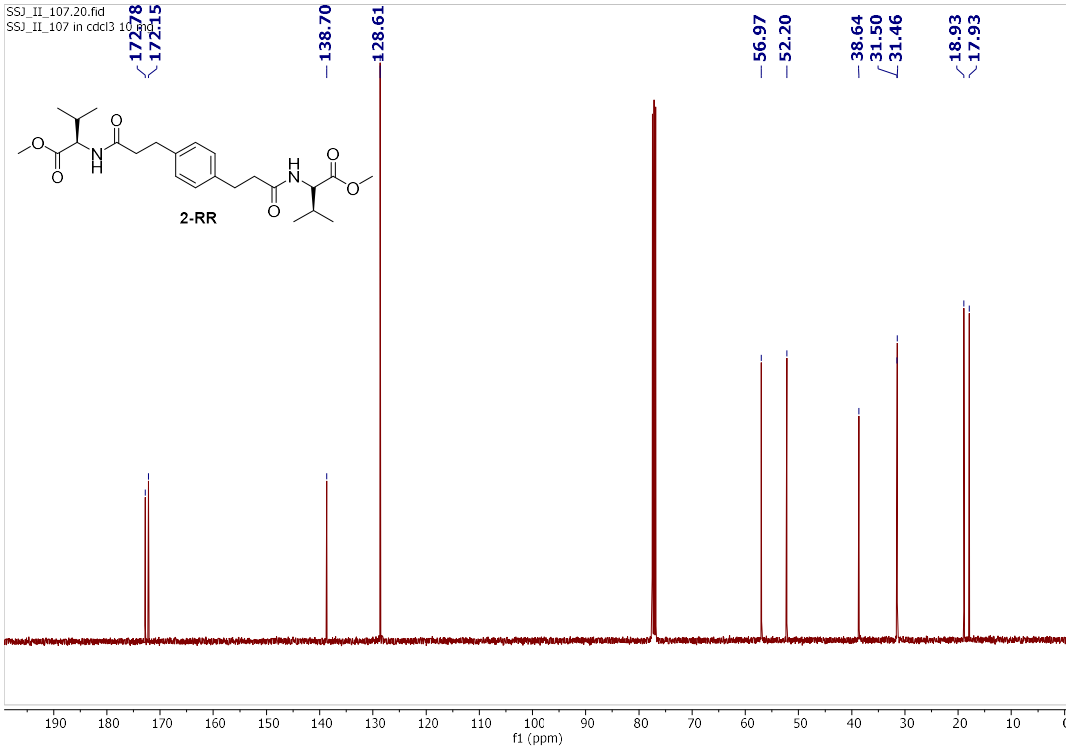

Figure S76. ^{13}C NMR spectrum of **2**-RR.

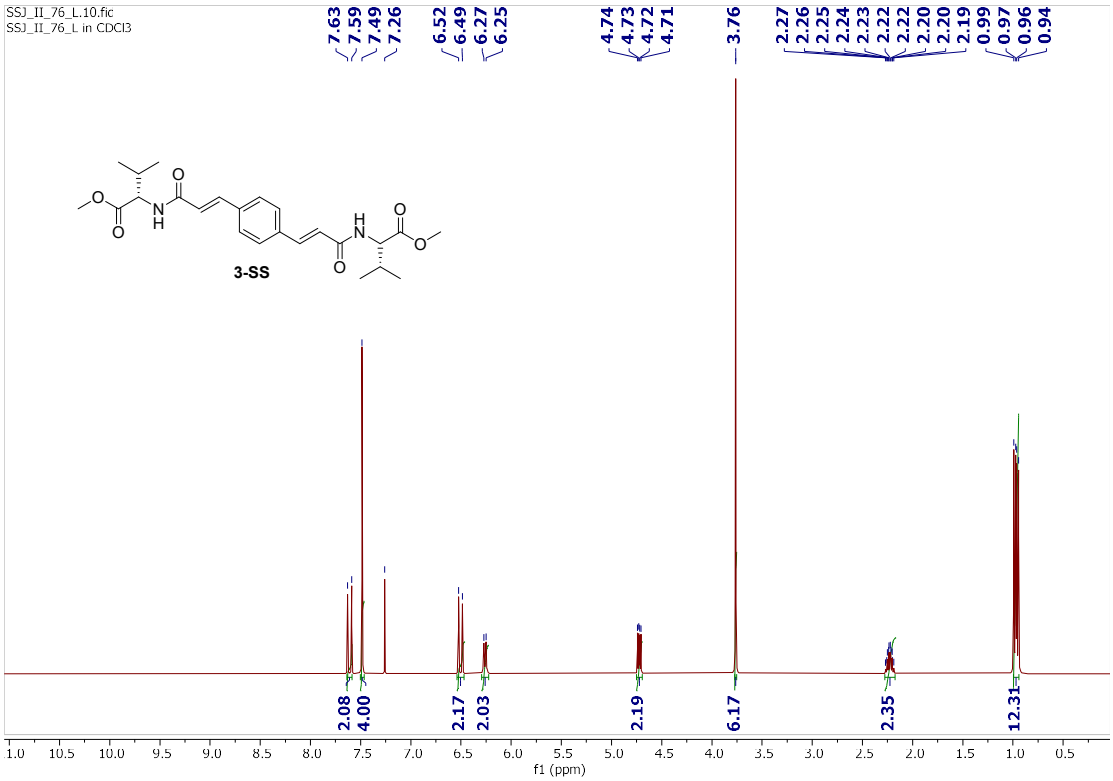

Figure S77. ^{1}H NMR spectrum of **3-**SS.

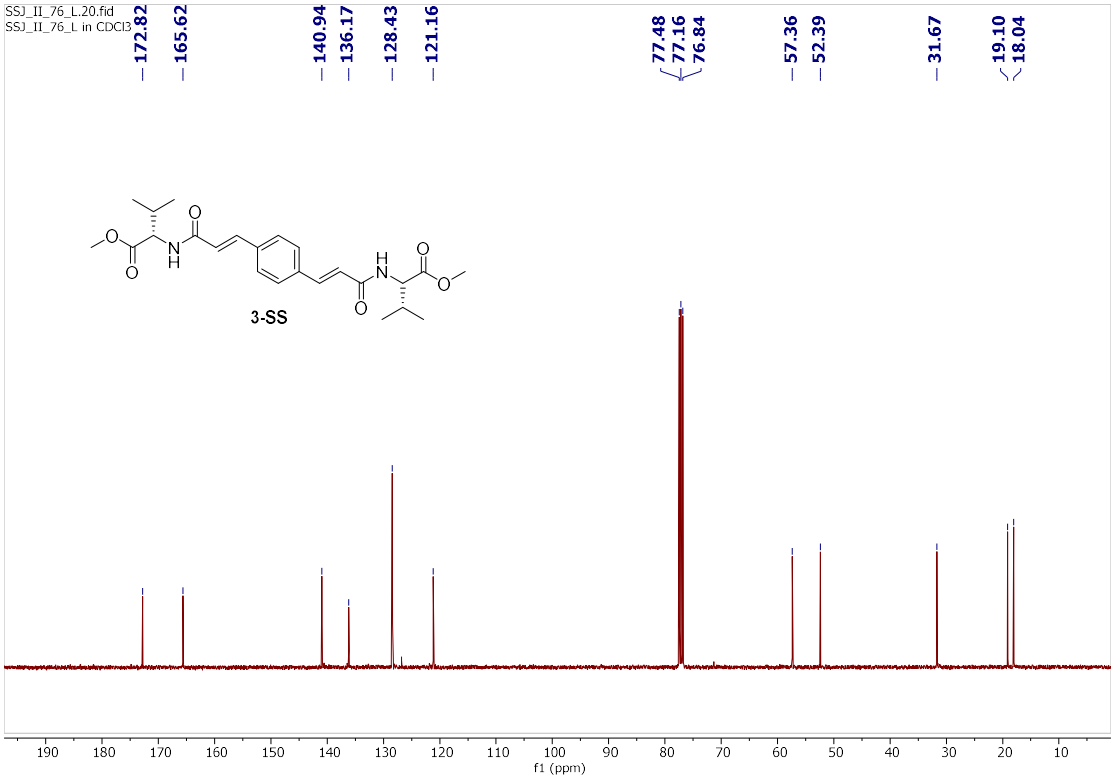

Figure S78. ^{13}C NMR spectrum of **3-**SS.

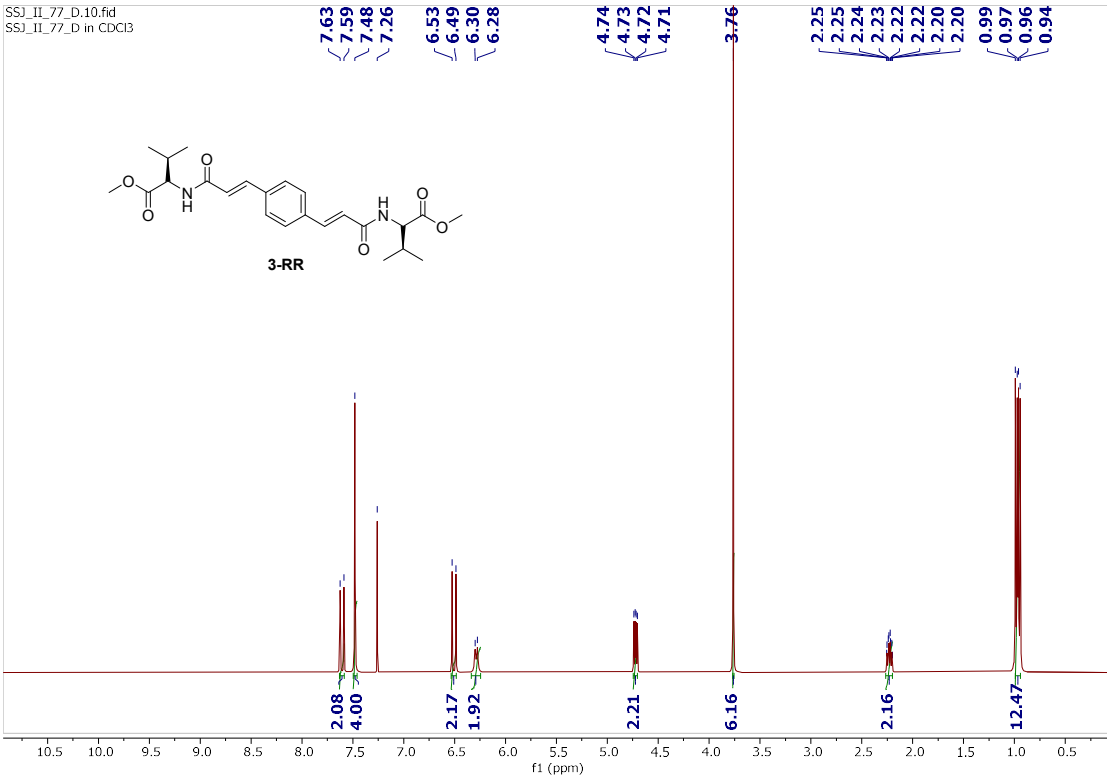

Figure S79. ^{1}H NMR spectrum of **3**-RR.

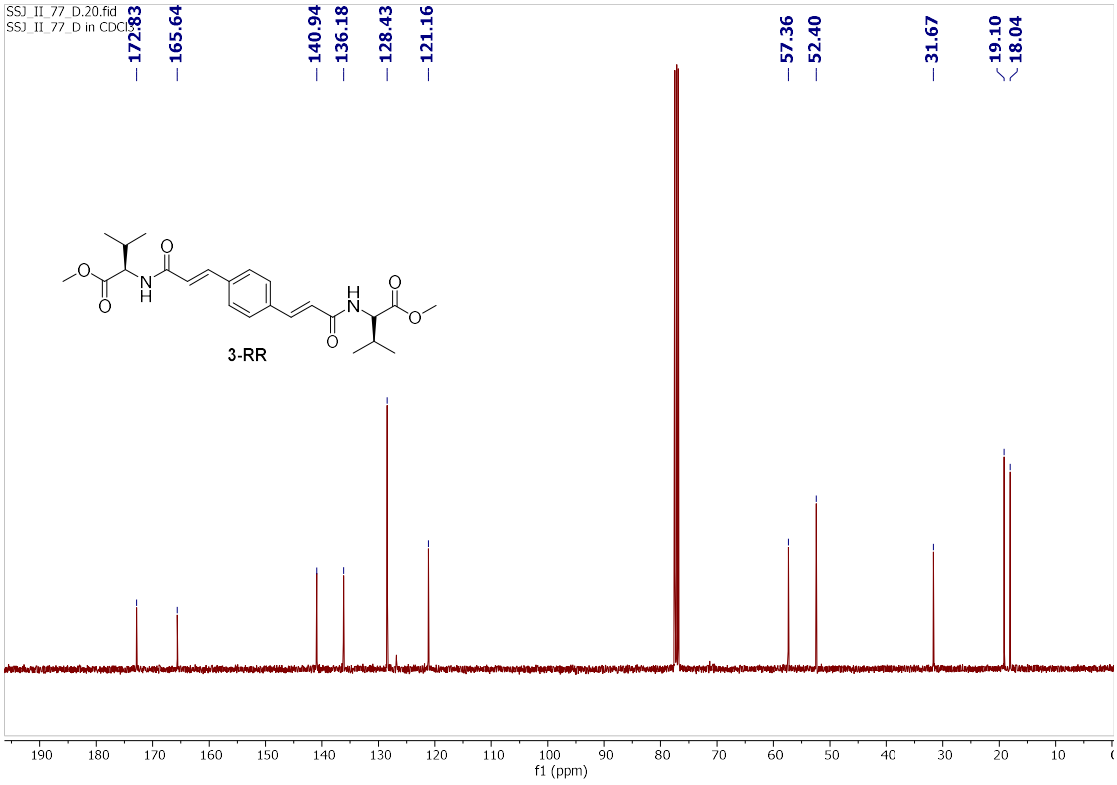

Figure S80. ^{13}C NMR spectrum of **3**-RR.

6 Conclusions

The doctoral study primarily aims to understand the key elements that play a major role in the self-assembly of LMWGs in both individual and multi-component-based gels. The dynamic nature of these systems makes it highly responsive towards an external stimulus. Therefore, comprehending self-assembly in supramolecular gels is an arduous task. In this context, we intended to study self-assembly in individual and multi-component gels to understand the nature and spatial orientation of functional groups in dictating the gelation properties.

Initially, we studied the role of specific functional groups in dictating hydrogelation. We have modified bis(pyridyl urea) compounds to bis(pyridyl-*N*-oxide urea) compounds to induce hydrogelation. Moving forward, we studied the nature of these functional groups in the presence of an external entity like a salt/ion. The modified *N*-oxide compounds showed enhanced gel strength in the presence of salts. We have also found that the modification of functional groups is an excellent strategy to evaluate the role of specific interactions in gel formation. The solid-state interactions were analyzed by X-ray diffraction. The modified compounds showed altered non-covalent interactions, affecting the gelation properties. Comparable results were also obtained upon modifying bis(pyridyl)amide compounds to bis(pyridyl-*N*-oxide)amide compounds. We have thus showcased the potential of using *N*-oxide moieties as stimuli-responsive materials in LMWGs.

We have analyzed the role of the hydrogen bond functionalities in LMWGs by replacing the hydrogen bonding moieties of a non-gelator. We have chosen *N,N'*–bis(pyridyl)urea (3–BPU and 2-BPU), non-gelators, which may be due to the absence of complementary urea tape hydrogen bonding because the nitrogen atom and the carbonyl groups displayed intramolecular interaction with the pyridyl nitrogen atom and C-H moieties. We have replaced the urea with a thiourea group to alter these interactions, which resulted in *N,N'*–bis(pyridyl)thiourea (3-PTU and 2-PTU). We analyzed the gelation properties of thiourea-based compounds and found them to be non-gelators, which prompted us to check whether metal salts could induce the gelation. The metallogelation experiments revealed the selective gelation of 3-PTU and 2-PTU with copper salts. We examined the role of coordination-driven self-assembly in these metallogels using various techniques such as UV-visible spectroscopy and X-ray diffraction.

We then studied the role of positional isomerism in gelation by synthesizing various bis(urea) compounds that mimicked the pharmaceutical drug metronidazole and its isomeric form isometronidazole. The results showed that the metronidazole-mimicking compounds formed gels in nitrobenzene at 1.0 wt/v%, while the isometronidazole-mimicking compounds required higher concentrations for gelation. The gels were used as media for metronidazole crystallization, resulting in crystal habit modification. The study made us understand the impact of drug-mimetic gel on gel-phase crystallization of metronidazole. We showed how the epitaxial crystal growth was influenced by using a drug-mimetic gel. We have also incorporated antibacterial agents in LMWGs to enhance the antibacterial

activity, but the modified compound displayed antibacterial properties only in the presence of metal salts.

Finally, we concentrated towards the self-assembly in the multi-component system based on structurally similar and non-similar components. We analyzed the self-assembly modes of chiral multi-component gels based on donor and acceptor moieties. We have used various analytical methods such as SEM, rheology, CD, PXRD, UV-Vis spectroscopy, and computational studies to investigate the charge transfer interaction in the solution and gel state, which revealed self-sorting in mixed chiral donor-acceptor-based gel. We extended our studies to multi-component gels with structrally similar components to evaluate the role of functional groups in the gelator towards the self-assembly process. We have analyzed the gelation properties in an enantiomeric multi-component system by varying the rigidity/flexibility of the linker core in bi-phenyl bis-amide system to analyze the specific role of rigidity in tuning the gel state properties. We have then studied the role of specific functional groups in multi-component gels by analyzing the gelation properties of individual and mixed enantiomeric compounds of bi-phenyl bis-amides of alanine (BPA) or phenylalanine (BPP) methyl ester in various solvent systems. The conclusion highlights the importance of designing multi-component systems with tunable properties based on understanding molecular interactions between individual gelators. Finally, we have analyzed the role of linkers in tuning the gel state properties in enantiomeric multi-component gels. We have shown that specific-coassembly predominates in structurally similar multi-component systems based on enantiomers. We further examined the transition of self-assembly mechanisms from kinetically favored orthogonal self-assembly to thermodynamically favored co-assembly, influenced by solvent parameters. We have demonstrated the significant importance of the orientation of functional groups in modulating the self-assembly mechanisms in both individual and multi-component gels. We believe these studies will add potential significance towards understanding the self-assembly in LMWGs and will assist chemists in developing smart materials with intriguing properties.

References

(1) Whitesides, G. M.; Boncheva, M. Beyond molecules: Self-assembly of mesoscopic and macroscopic components. *Proc. Natl. Acad. Sci.* **2002**, *99* (8), 4769-4774.
(2) Ball, P. *The Self-Made Tapestry: Pattern Formation in Nature*; Oxford University Press, Inc., 2001.
(3) Jean-Marie, L. Perspectives in Chemistry—Steps towards Complex Matter. *Angew. Chem. Int. Ed.* **2013**, *52* (10), 2836-2850.
(4) Lehn, J.-M. Constitutional Dynamic Chemistry: Bridge from Supramolecular Chemistry to Adaptive Chemistry. In *Constitutional Dynamic Chemistry*, Barboiu, M. Ed.; Springer Berlin Heidelberg, 2012; pp 1-32.
(5) Jean-Marie, L. Perspectives in Chemistry—Aspects of Adaptive Chemistry and Materials. *Angew. Chem. Int. Ed.* **2015**, *54* (11), 3276-3289.
(6) Zhang, M.; Gu, Z.-Y.; Bosch, M.; Perry, Z.; Zhou, H.-C. Biomimicry in metal–organic materials. *Coord. Chem. Rev.* **2015**, *293-294*, 327-356.
(7) Cragg, P. J. *Supramolecular chemistry: from biological inspiration to biomedical applications*; Springer Science & Business Media, 2010.
(8) Noel, M. 'Made in Europe for the World': Making a Claim for a European Chemistry in Publication Programs. The Case of the Supramolecular Chemistry (1987-2005). *Annals of the Fondazione Luigi Einaudi. An Interdisciplinary Journal of Economics, History and Political Science* **2019**, *53*, 2532-4969.
(9) Chakrabarty, R.; Mukherjee, P. S.; Stang, P. J. Supramolecular Coordination: Self-Assembly of Finite Two- and Three-Dimensional Ensembles. *Chem. Rev.* **2011**, *111* (11), 6810-6918.
(10) Steed, J. W.; Atwood, J. L. *Supramolecular chemistry*; John Wiley & Sons, 2022.
(11) Varshey, D. B.; Sander, J. R.; Friščić, T.; MacGillivray, L. R. Supramolecular interactions. *Supramolecular chemistry: from molecules to nanomaterials* **2012**.
(12) Rossow, T.; Seiffert, S. Supramolecular polymer networks: Preparation, properties, and potential. *Supramolecular Polymer Networks and Gels* **2015**, 1-46.
(13) Ariga, K.; Nishikawa, M.; Mori, T.; Takeya, J.; Shrestha, L. K.; Hill, J. P. Self-assembly as a key player for materials nanoarchitectonics. *Science and Technology of Advanced Materials* **2019**, *20* (1), 51-95.
(14) Stupp, S. I.; LeBonheur, V.; Walker, K.; Li, L.-S.; Huggins, K. E.; Keser, M.; Amstutz, A. Supramolecular materials: self-organized nanostructures. *Science* **1997**, *276* (5311), 384-389.
(15) Uhlenheuer, D. A.; Petkau, K.; Brunsveld, L. Combining supramolecular chemistry with biology. *Chem. Soc. Rev.* **2010**, *39* (8), 2817-2826.
(16) Van Arnam, E. B.; Dougherty, D. A. Functional Probes of Drug–Receptor Interactions Implicated by Structural Studies: Cys-Loop Receptors Provide a Fertile Testing Ground: Miniperspective. *J. Med. Chem.* **2014**, *57* (15), 6289-6300.
(17) Pieters, B. J.; Van Eldijk, M. B.; Nolte, R. J.; Mecinović, J. Natural supramolecular protein assemblies. *Chem. Soc. Rev.* **2016**, *45* (1), 24-39.
(18) Kumar, P.; Banerjee, S.; Radha, A.; Firdoos, T.; Sahoo, S. C.; Pandey, S. K. Role of non-covalent interactions in the supramolecular architectures of mercury (II) diphenyldithiophosphates: An experimental and theoretical investigation. *New J. Chem.* **2021**, *45* (4), 2249-2263.
(19) Webber, M. J.; Langer, R. Drug delivery by supramolecular design. *Chem. Soc. Rev.* **2017**, *46* (21), 6600-6620.

(20) Williams, G. T.; Haynes, C. J.; Fares, M.; Caltagirone, C.; Hiscock, J. R.; Gale, P. A. Advances in applied supramolecular technologies. *Chem. Soc. Rev.* **2021**, *50* (4), 2737-2763.
(21) Busseron, E.; Ruff, Y.; Moulin, E.; Giuseppone, N. Supramolecular self-assemblies as functional nanomaterials. *Nanoscale* **2013**, *5* (16), 7098-7140.
(22) ávan Esch, J. H. Catalytic control over the formation of supramolecular materials. *Org. Biomol. Chem.* **2014**, *12* (33), 6292-6296.
(23) Ishiwari, F.; Shoji, Y.; Fukushima, T. Supramolecular scaffolds enabling the controlled assembly of functional molecular units. *Chem. Sci.* **2018**, *9* (8), 2028-2041.
(24) Steed, J. W. Supramolecular gel chemistry: developments over the last decade. *Chem. Commun.* **2011**, *47* (5), 1379-1383, 10.1039/C0CC03293J.
(25) Yamanaka, M. Urea derivatives as low-molecular-weight gelators. *J. Incl. Phenom. Macro.* **2013**, *77* (1), 33-48, journal article.
(26) Lloyd, G. O.; Steed, J. W. Anion-tuning of supramolecular gel properties. *Nat. Chem.* **2009**, *1*, 437, Perspective.
(27) Kumar, D. K.; Steed, J. W. Supramolecular gel phase crystallization: orthogonal self-assembly under non-equilibrium conditions. *Chem. Soc. Rev.* **2014**, *43* (7), 2080-2088, 10.1039/C3CS60224A.
(28) Fang, W.; Zhang, Y.; Wu, J.; Liu, C.; Zhu, H.; Tu, T. Recent Advances in Supramolecular Gels and Catalysis. *Chemistry – An Asian Journal* **2018**, *13* (7), 712-729.
(29) Foster, J. A.; Damodaran, K. K.; Maurin, A.; Day, G. M.; Thompson, H. P. G.; Cameron, G. J.; Bernal, J. C.; Steed, J. W. Pharmaceutical polymorph control in a drug-mimetic supramolecular gel. *Chem Sci* **2017**, *8* (1), 78-84.
(30) Du, X.; Zhou, J.; Shi, J.; Xu, B. Supramolecular Hydrogelators and Hydrogels: From Soft Matter to Molecular Biomaterials. *Chem. Rev.* **2015**, *115* (24), 13165-13307.
(31) Babu, S. S.; Praveen, V. K.; Ajayaghosh, A. Functional π-Gelators and Their Applications. *Chem. Rev.* **2014**, *114* (4), 1973-2129.
(32) Truong, W. T.; Su, Y.; Meijer, J. T.; Thordarson, P.; Braet, F. Self-Assembled Gels for Biomedical Applications. *Chemistry – An Asian Journal* **2011**, *6* (1), 30-42.
(33) Banerjee, S.; Das, R. K.; Maitra, U. Supramolecular gels 'in action'. *Journal of Materials Chemistry* **2009**, *19* (37), 6649-6687, 10.1039/B819218A.
(34) van Bommel, K. J. C.; Stuart, M. C. A.; Feringa, B. L.; van Esch, J. Two-stage enzyme mediated drug release from LMWG hydrogels. *Org. Biomol. Chem.* **2005**, *3* (16), 2917-2920, 10.1039/B507157G.
(35) Buerkle, L. E.; Rowan, S. J. Supramolecular gels formed from multi-component low molecular weight species. *Chem. Soc. Rev.* **2012**, *41* (18), 6089-6102, 10.1039/C2CS35106D.
(36) Chu, C.-W.; Schalley, C. A. Recent Advances on Supramolecular Gels: From Stimuli-Responsive Gels to Co-Assembled and Self-Sorted Systems. *Organic Materials* **2021**, *03* (01), 025-040.
(37) Raeburn, J.; Adams, D. J. Multicomponent low molecular weight gelators. *Chemical Communications* **2015**, *51* (25), 5170-5180, 10.1039/C4CC08626K.
(38) Smith, D. K. Lost in translation? Chirality effects in the self-assembly of nanostructured gel-phase materials. *Chem Soc Rev* **2009**, *38* (3), 684-694, From Nlm.
(39) Rovetta, A.; Emanueli, A.; Nasry, I.; Helmi, A. Ancient Egyptian chariots design and functional aspects. In *International Symposium on History of Machines and Mechanisms Proceedings HMM 2000*, 2000; Springer: pp 149-154.
(40) Rovetta, A.; Nasry, I.; Helmi, A. The chariots of the Egyptian Pharaoh Tut Ankh Amun in 1337 BC: kinematics and dynamics. *Mechanism and machine theory* **2000**, *35* (7), 1013-1031.

(41) Donahue, C. J. Lubricating grease: a chemical primer. *Journal of chemical Education* **2006**, *83* (6), 862.
(42) Fameau, A.-L.; Rogers, M. A. The curious case of 12-hydroxystearic acid—the Dr. Jekyll & Mr. Hyde of molecular gelators. *Current Opinion in Colloid & Interface Science* **2020**, *45*, 68-82.
(43) Yu, G.; Yan, X.; Han, C.; Huang, F. Characterization of supramolecular gels. *Chem. Soc. Rev.* **2013**, *42* (16), 6697-6722, 10.1039/C3CS60080G.
(44) Draper, E. R.; Adams, D. J. Low-molecular-weight gels: the state of the art. *Chem* **2017**, *3* (3), 390-410.
(45) Tomasini, C.; Castellucci, N. Peptides and peptidomimetics that behave as low molecular weight gelators. *Chem. Soc. Rev.* **2013**, *42* (1), 156-172, 10.1039/C2CS35284B.
(46) Dastidar, P. Designing Supramolecular Gelators: Challenges, Frustrations, and Hopes. *Gels* **2019**, *5* (1), 15.
(47) Van Esch, J.; Schoonbeek, F.; De Loos, M.; Marc Veen, E.; Kellogg, R. M.; Feringa, B. L. Low Molecular Weight Gelators for Organic Solvents: From serendipity towards design. *Supramolecular science: where it is and where it is going* **1999**, 233-259.
(48) Frederix, P. W.; Scott, G. G.; Abul-Haija, Y. M.; Kalafatovic, D.; Pappas, C. G.; Javid, N.; Hunt, N. T.; Ulijn, R. V.; Tuttle, T. Exploring the sequence space for (tri-) peptide self-assembly to design and discover new hydrogels. *Nature chemistry* **2015**, *7* (1), 30-37.
(49) Gupta, J. K.; Adams, D. J.; Berry, N. G. Will it gel? Successful computational prediction of peptide gelators using physicochemical properties and molecular fingerprints. *Chem. Sci.* **2016**, *7* (7), 4713-4719.
(50) McConnell, A. J.; Wood, C. S.; Neelakandan, P. P.; Nitschke, J. R. Stimuli-Responsive Metal–Ligand Assemblies. *Chem. Rev.* **2015**, *115* (15), 7729-7793.
(51) Theato, P.; Sumerlin, B. S.; O'Reilly, R. K.; Epps, I. I. I. T. H. Stimuli responsive materials. *Chem. Soc. Rev.* **2013**, *42* (17), 7055-7056, 10.1039/C3CS90057F.
(52) Hajime, S.; Itaru, H. Supramolecular Assemblies Responsive to Biomolecules toward Biological Applications. *Chem. Asian J.* **2015**, *10* (10), 2026-2038.
(53) Segarra-Maset, M. D.; Nebot, V. J.; Miravet, J. F.; Escuder, B. Control of molecular gelation by chemical stimuli. *Chem. Soc. Rev.* **2013**, *42* (17), 7086-7098, 10.1039/C2CS35436E.
(54) Maula, T. A.; Hatch, H. W.; Shen, V. K.; Rangarajan, S.; Mittal, J. Designing molecular building blocks for the self-assembly of complex porous networks. *Molecular Systems Design & Engineering* **2019**, *4* (3), 644-653, 10.1039/C9ME00006B.
(55) Fichman, G.; Gazit, E. Self-assembly of short peptides to form hydrogels: Design of building blocks, physical properties and technological applications. *Acta Biomater.* **2014**, *10* (4), 1671-1682.
(56) Mendes, A. C.; Baran, E. T.; Reis, R. L.; Azevedo, H. S. Self-assembly in nature: using the principles of nature to create complex nanobiomaterials. *Wiley interdisciplinary reviews: nanomedicine and nanobiotechnology* **2013**, *5* (6), 582-612.
(57) Burrows, A. D. The design and applications of multifunctional ligands. *Science progress* **2002**, *85* (3), 199-217.
(58) Yi, W.; Xiao, P.; Liu, X.; Zhao, Z.; Sun, X.; Wang, J.; Zhou, L.; Wang, G.; Cao, H.; Wang, D. Recent advances in developing active targeting and multi-functional drug delivery systems via bioorthogonal chemistry. *Signal Transduction and Targeted Therapy* **2022**, *7* (1), 386.
(59) Piepenbrock, M.-O. M.; Lloyd, G. O.; Clarke, N.; Steed, J. W. Metal-and anion-binding supramolecular gels. *Chem. Rev.* **2010**, *110* (4), 1960-2004.

(60) Wang, W.; Wang, Y.-X.; Yang, H.-B. Supramolecular transformations within discrete coordination-driven supramolecular architectures. *Chem. Soc. Rev.* **2016**, *45* (9), 2656-2693.
(61) Klajn, R.; Stoddart, J. F.; Grzybowski, B. A. Nanoparticles functionalised with reversible molecular and supramolecular switches. *Chem. Soc. Rev.* **2010**, *39* (6), 2203-2237.
(62) Zhou, J.; Li, J.; Du, X.; Xu, B. Supramolecular biofunctional materials. *Biomaterials* **2017**, *129*, 1-27.
(63) McAulay, K.; Dietrich, B.; Su, H.; Scott, M. T.; Rogers, S.; Al-Hilaly, Y. K.; Cui, H.; Serpell, L. C.; Seddon, Annela M.; Draper, E. R.; Adams, D. J. Using chirality to influence supramolecular gelation. *Chem. Sci.* **2019**, *10* (33), 7801-7806, 10.1039/C9SC02239B.
(64) Lou, J.; Mooney, D. J. Chemical strategies to engineer hydrogels for cell culture. *Nat. Rev. Chem.* **2022**, *6* (10), 726-744.
(65) Khan, F.; Atif, M.; Haseen, M.; Kamal, S.; Khan, M. S.; Shahid, S.; Nami, S. A. Synthesis, classification and properties of hydrogels: Their applications in drug delivery and agriculture. *J. Mater. Chem. B* **2022**, *10* (2), 170-203.
(66) Döring, A.; Birnbaum, W.; Kuckling, D. Responsive hydrogels–structurally and dimensionally optimized smart frameworks for applications in catalysis, micro-system technology and material science. *Chem. Soc. Rev.* **2013**, *42* (17), 7391-7420.
(67) Draper, E. R.; Adams, D. J. Responsive Materials by the Self-assembly of Low Molecular Weight Gelators. **2015**.
(68) Dastidar, P. Supramolecular gelling agents: can they be designed? *Chem. Soc. Rev.* **2008**, *37* (12), 2699-2715, 10.1039/B807346E.
(69) Tómasson, D. A.; Ghosh, D.; Kržišnik, Z.; Fasolin, L. H.; Vicente, A. A.; Martin, A. D.; Thordarson, P.; Damodaran, K. K. Enhanced Mechanical and Thermal Strength in Mixed-Enantiomers-Based Supramolecular Gel. *Langmuir* **2018**, *34* (43), 12957-12967.
(70) Lipowitz, v. A. Versuche und Resultate über die Löslichkeit der Harnsäure. *Justus Liebigs Annalen der Chemie* **1841**, *38* (3), 348-355.
(71) Brenzinger, K. Zur Kenntniss des Cystins und des Cystëins.(Mitgetheilt von E. Baumann.). **1892**.
(72) Terech, P.; Weiss, R. G. Low Molecular Mass Gelators of Organic Liquids and the Properties of Their Gels. *Chem. Rev.* **1997**, *97* (8), 3133-3160.
(73) Banerjee, S.; Das, R. K.; Maitra, U. Supramolecular gels 'in action'. *J. Mater. Chem.* **2009**, *19* (37), 6649-6687, 10.1039/B819218A.
(74) Dastidar, P. Supramolecular gelling agents: can they be designed? *Chem. Soc. Rev.* **2008**, *37* (12), 2699-2715, 10.1039/B807346E.
(75) de Loos, M.; Feringa, B. L.; van Esch, J. H. Design and Application of Self-Assembled Low Molecular Weight Hydrogels. *Eur. J. Org. Chem.* **2005**, *2005* (17), 3615-3631.
(76) Estroff, L. A.; Hamilton, A. D. Water Gelation by Small Organic Molecules. *Chem. Rev.* **2004**, *104* (3), 1201-1218.
(77) George, M.; Weiss, R. G. Molecular Organogels. Soft Matter Comprised of Low-Molecular-Mass Organic Gelators and Organic Liquids†. *Acc. Chem. Res.* **2006**, *39* (8), 489-497.
(78) Hirst, A. R.; Escuder, B.; Miravet, J. F.; Smith, D. K. High-Tech Applications of Self-Assembling Supramolecular Nanostructured Gel-Phase Materials: From Regenerative Medicine to Electronic Devices. *Angew. Chem. Int. Ed.* **2008**, *47* (42), 8002-8018.
(79) Kumar, D. K.; Steed, J. W. Supramolecular gel phase crystallization: orthogonal self-assembly under non-equilibrium conditions. *Chem. Soc. Rev.* **2014**, *43* (7), 2080-2088, 10.1039/C3CS60224A.

(80) Piepenbrock, M.-O. M.; Clarke, N.; Steed, J. W. Shear induced gelation in a copper(ii) metallogel: new aspects of ion-tunable rheology and gel-reformation by external chemical stimuli. *Soft Matter* **2010**, *6* (15), 3541-3547, 10.1039/C0SM00313A.
(81) Escuder, B.; Miravet, J. F. *Functional molecular gels*; Royal Society of Chemistry, 2013.
(82) Estroff, L. A.; Hamilton, A. D. Water Gelation by Small Organic Molecules. *Chem. Rev.* **2004**, *104* (3), 1201-1218.
(83) Hirst, A. R.; Smith, D. K. Solvent Effects on Supramolecular Gel-Phase Materials: Two-Component Dendritic Gel. *Langmuir* **2004**, *20* (25), 10851-10857.
(84) Chu, C.-W.; Schalley, C. A. Recent advances on supramolecular gels: From stimuli-responsive gels to co-assembled and self-sorted systems. *Organic Materials* **2021**, *3* (01), 025-040.
(85) Smith, D. K. Supramolecular gels–a panorama of low-molecular-weight gelators from ancient origins to next-generation technologies. *Soft Matter* **2024**.
(86) Xian, S.; Webber, M. J. Temperature-responsive supramolecular hydrogels. *J. Mater. Chem. B* **2020**, *8* (40), 9197-9211.
(87) Wan, Y.; Liu, L.; Yuan, S.; Sun, J.; Li, Z. pH-responsive peptide supramolecular hydrogels with antibacterial activity. *Langmuir* **2017**, *33* (13), 3234-3240.
(88) Cui, J.; Liu, A.; Guan, Y.; Zheng, J.; Shen, Z.; Wan, X. Tuning the Helicity of Self-Assembled Structure of a Sugar-Based Organogelator by the Proper Choice of Cooling Rate. *Langmuir* **2010**, *26* (5), 3615-3622.
(89) Huang, X.; Terech, P.; Raghavan, S. R.; Weiss, R. G. Kinetics of 5α-Cholestan-3β-yl N-(2-Naphthyl)carbamate/n-Alkane Organogel Formation and Its Influence on the Fibrillar Networks. *J. Am. Chem. Soc.* **2005**, *127* (12), 4336-4344.
(90) Huang, H.; Zhu, X.; Su, L.; Wang, H.; Yang, Y. Effect of temperature on self-assembly/disassembly transition of dialkylurea supramolecular gels at high pressure. *RSC Advances* **2013**, *3* (29), 11854-11859, 10.1039/C3RA41540F.
(91) Naota, T.; Koori, H. Molecules That Assemble by Sound: An Application to the Instant Gelation of Stable Organic Fluids. *J. Am. Chem. Soc.* **2005**, *127* (26), 9324-9325.
(92) Basak, S.; Nanda, J.; Banerjee, A. A new aromatic amino acid based organogel for oil spill recovery. *Journal of Materials Chemistry* **2012**, *22* (23), 11658-11664, 10.1039/C2JM30711A.
(93) Maeda, H. Anion-responsive supramolecular gels. *Chem. Eur. J.* **2008**, *14* (36), 11274-11282.
(94) Li, L.; Sun, R.; Zheng, R.; Huang, Y. Anions-responsive supramolecular gels: A review. *Mater. Des.* **2021**, *205*, 109759.
(95) Busschaert, N.; Caltagirone, C.; Van Rossom, W.; Gale, P. A. Applications of supramolecular anion recognition. *Chem. Rev.* **2015**, *115* (15), 8038-8155.
(96) Picci, G.; Mulvee, M. T.; Caltagirone, C.; Lippolis, V.; Frontera, A.; Gomila, R. M.; Steed, J. W. Anion-responsive fluorescent supramolecular gels. *Molecules* **2022**, *27* (4), 1257.
(97) Ha, S.; Lee, J.; Kim, K.-s.; Choi, E. J.; Nhem, P.; Song, C. Anion-responsive thiourea-based gel actuator. *Chem. Mater.* **2019**, *31* (15), 5735-5741.
(98) Gibb, B. C. Hofmeister's curse. *Nature chemistry* **2019**, *11* (11), 963-965.
(99) Abraham, B. L.; Agredo, P.; Mensah, S. G.; Nilsson, B. L. Anion Effects on the Supramolecular Self-Assembly of Cationic Phenylalanine Derivatives. *Langmuir* **2022**, *38* (50), 15494-15505.
(100) Nebot, V. J.; Ojeda-Flores, J. J.; Smets, J.; Fernández-Prieto, S.; Escuder, B.; Miravet, J. F. Rational Design of Heat-Set and Specific-Ion-Responsive Supramolecular Hydrogels

Based on the Hofmeister Effect. *Chemistry – A European Journal* **2014**, *20* (44), 14465-14472.
(101) Offiler, C. A.; Jones, C. D.; Steed, J. W. Metal 'turn-off', anion 'turn-on'gelation cascade in pyridinylmethyl ureas. *Chem. Commun.* **2017**, *53* (12), 2024-2027.
(102) Wang, Y.; Zhan, C.; Fu, H.; Li, X.; Sheng, X.; Zhao, Y.; Xiao, D.; Ma, Y.; Ma, J. S.; Yao, J. Switch from Intra- to Intermolecular H-Bonds by Ultrasound: Induced Gelation and Distinct Nanoscale Morphologies. *Langmuir* **2008**, *24* (15), 7635-7638.
(103) Komiya, N.; Muraoka, T.; Iida, M.; Miyanaga, M.; Takahashi, K.; Naota, T. Ultrasound-Induced Emission Enhancement Based on Structure-Dependent Homo- and Heterochiral Aggregations of Chiral Binuclear Platinum Complexes. *J. Am. Chem. Soc.* **2011**, *133* (40), 16054-16061.
(104) Sambri, L.; Cucinotta, F.; Paoli, G. D.; Stagni, S.; Cola, L. D. Ultrasound-promoted hydrogelation of terpyridine derivatives. *New J. Chem.* **2010**, *34* (10), 2093-2096, 10.1039/C0NJ00391C.
(105) Kotal, A.; Paira, T. K.; Banerjee, S.; Mandal, T. K. Ultrasound-Induced In Situ Formation of Coordination Organogels from Isobutyric Acids and Zinc Oxide Nanoparticles. *Langmuir* **2010**, *26* (9), 6576-6582.
(106) Pappas, C. G.; Frederix, P. W. J. M.; Mutasa, T.; Fleming, S.; Abul-Haija, Y. M.; Kelly, S. M.; Gachagan, A.; Kalafatovic, D.; Trevino, J.; Ulijn, R. V.; Bai, S. Alignment of nanostructured tripeptide gels by directional ultrasonication. *Chem. Commun.* **2015**, *51* (40), 8465-8468, 10.1039/C5CC02049B.
(107) Jones, C. D.; Steed, J. W. Gels with sense: supramolecular materials that respond to heat, light and sound. *Chem. Soc. Rev.* **2016**, *45* (23), 6546-6596.
(108) Draper, E. R.; Adams, D. J. Photoresponsive gelators. *Chem. Commun.* **2016**, *52* (53), 8196-8206, 10.1039/C6CC03485C.
(109) Yang, R.; Peng, S.; Hughes, T. C. Multistimuli responsive organogels based on a reactive azobenzene gelator. *Soft Matter* **2014**, *10* (13), 2188-2196, 10.1039/C3SM53145G.
(110) Piepenbrock, M.-O. M.; Lloyd, G. O.; Clarke, N.; Steed, J. W. Gelation is crucially dependent on functional group orientation and may be tuned by anion binding. *Chem. Commun.* **2008**, (23), 2644-2646, 10.1039/B804259D.
(111) Chivers, P. R.; Smith, D. K. Shaping and structuring supramolecular gels. *Nat. Rev. Mater.* **2019**, *4* (7), 463-478.
(112) Hirst, A. R.; Coates, I. A.; Boucheteau, T. R.; Miravet, J. F.; Escuder, B.; Castelletto, V.; Hamley, I. W.; Smith, D. K. Low-molecular-weight gelators: elucidating the principles of gelation based on gelator solubility and a cooperative self-assembly model. *J. Am. Chem. Soc.* **2008**, *130* (28), 9113-9121.
(113) Das, T.; Häring, M.; Haldar, D.; Díaz, D. D. Phenylalanine and derivatives as versatile low-molecular-weight gelators: Design, structure and tailored function. *Biomater. Sci.* **2018**, *6* (1), 38-59.
(114) Ghosh, D.; Bjornsson, R.; Damodaran, K. K. Role of N–Oxide Moieties in Tuning Supramolecular Gel-State Properties. *Gels* **2020**, *6* (4), 41.
(115) Yu, G.; Yan, X.; Han, C.; Huang, F. Characterization of supramolecular gels. *Chem. Soc. Rev.* **2013**, *42* (16), 6697-6722, 10.1039/C3CS60080G.
(116) Ghosh, D.; Chaudhary, P.; Pradeep, A.; Singh, S.; Rangasamy, J.; Damodaran, K. K. Structural modification induced hydrogelation and antibacterial properties in supramolecular gels. *Journal of Molecular Liquids* **2023**, *382*, 122023.
(117) Cao, X.; Meng, L.; Li, Z.; Mao, Y.; Lan, H.; Chen, L.; Fan, Y.; Yi, T. Large Red-Shifted Fluorescent Emission via Intermolecular π–π Stacking in 4-Ethynyl-1,8-naphthalimide-Based Supramolecular Assemblies. *Langmuir* **2014**, *30* (39), 11753-11760.

(118) Das, U. K.; Banerjee, S.; Dastidar, P. Remarkable Shape-Sustaining, Load-Bearing, and Self-Healing Properties Displayed by a Supramolecular Gel Derived from a Bis-pyridyl-bis-amide of L-Phenyl Alanine. *Chemistry – An Asian Journal* **2014**, *9* (9), 2475-2482.
(119) Li, P.; Dou, X.-Q.; Tang, Y.-T.; Zhu, S.; Gu, J.; Feng, C.-L.; Zhang, D. Gelator-polysaccharide hybrid hydrogel for selective and controllable dye release. *Journal of Colloid and Interface Science* **2012**, *387* (1), 115-122.
(120) Tang, Y.-T.; Dou, X.-Q.; Ji, Z.-A.; Li, P.; Zhu, S.-M.; Gu, J.-J.; Feng, C.-L.; Zhang, D. C2-symmetric cyclohexane-based hydrogels: A rational designed LMWG and its application in dye scavenging. *Journal of Molecular Liquids* **2013**, *177*, 167-171.
(121) Kumar, D. K.; Jose, D. A.; Dastidar, P.; Das, A. Nonpolymeric Hydrogelator Derived from N-(4-Pyridyl)isonicotinamide. *Langmuir* **2004**, *20* (24), 10413-10418.
(122) Kumar, D. K.; Jose, D. A.; Das, A.; Dastidar, P. First snapshot of a nonpolymeric hydrogelator interacting with its gelling solvents. *Chem. Commun.* **2005**, (32), 4059-4061.
(123) Wang, Y.; Tang, L.; Yu, J. Investigation of Spontaneous Transition from Low-Molecular-Weight Hydrogel into Macroscopic Crystals. *Crystal Growth & Design* **2008**, *8* (3), 884-889.
(124) Braga, D.; d'Agostino, S.; D'Amen, E.; Grepioni, F. Polymorphs from supramolecular gels: four crystal forms of the same silver(i) supergelator crystallized directly from its gels. *Chem. Commun.* **2011**, *47* (18), 5154-5156, 10.1039/C1CC10305A.
(125) Ghosh, D.; Lebedytė, I.; Yufit, D. S.; Damodaran, K. K.; Steed, J. W. Selective gelation of N-(4-pyridyl)nicotinamide by copper(ii) salts. *CrystEngComm* **2015**, *17* (42), 8130-8138, 10.1039/C5CE00901D.
(126) Tómasson, D. A.; Ghosh, D.; Kurup, M. R. P.; Mulvee, M. T.; Damodaran, K. K. Evaluating the role of a urea-like motif in enhancing the thermal and mechanical strength of supramolecular gels. *CrystEngComm* **2021**, *23* (3), 617-628, 10.1039/D0CE01194K.
(127) George, M.; Weiss, R. G. Molecular Organogels. Soft Matter Comprised of Low-Molecular-Mass Organic Gelators and Organic Liquids†. *Acc. Chem. Res.* **2006**, *39* (8), 489-497.
(128) Hirst, A. R.; Escuder, B.; Miravet, J. F.; Smith, D. K. High-Tech Applications of Self-Assembling Supramolecular Nanostructured Gel-Phase Materials: From Regenerative Medicine to Electronic Devices. *Angew. Chem. Int. Ed.* **2008**, *47* (42), 8002-8018.
(129) Byrne, P.; Lloyd, G. O.; Applegarth, L.; Anderson, K. M.; Clarke, N.; Steed, J. W. Metal-induced gelation in dipyridyl ureas. *New J. Chem.* **2010**, *34* (10), 2261-2274.
(130) Lloyd, G. O.; Steed, J. W. Anion tuning of the rheology, morphology and gelation of a low molecular weight salt hydrogelator. *Soft Matter* **2011**, *7* (1), 75-84, 10.1039/C0SM00594K.
(131) Lloyd, G. O.; Piepenbrock, M.-O. M.; Foster, J. A.; Clarke, N.; Steed, J. W. Anion tuning of chiral bis(urea) low molecular weight gels. *Soft Matter* **2012**, *8* (1), 204-216, 10.1039/C1SM06448G.
(132) Ghosh, D.; Mulvee, M. T.; Damodaran, K. K. Tuning Gel State Properties of Supramolecular Gels by Functional Group Modification. *Molecules* **2019**, *24* (19), 3472.
(133) Chen, S.; An, Z.; Tong, X.; Chen, Y.; Ma, M.; Shi, Y.; Wang, X. Stronger intermolecular forces or closer molecular spacing? Key impact factor research of gelator self-assembly mechanism. *Langmuir* **2017**, *33* (50), 14389-14395.
(134) Ge, J.; Guo, J.; Yu, X.; Li, Y.; Ma, Z. Structural Tunability on Naphthalimide-Based Dendrimer Gelators via Glaser Coupling Interaction with Tailored Gelation Solvent Polarity and Stimuli-Responsive Properties. *Langmuir* **2021**, *37* (8), 2677-2682.

(135) Ghosh, D.; Ferfolja, K.; Drabavičius, Ž.; Steed, J. W.; Damodaran, K. K. Crystal habit modification of Cu(ii) isonicotinate–N-oxide complexes using gel phase crystallisation. *New J. Chem.* **2018**, *42* (24), 19963-19970, 10.1039/C8NJ05036H.
(136) Desiraju, G. R. Supramolecular Synthons in Crystal Engineering—A New Organic Synthesis. *Angewandte Chemie International Edition in English* **1995**, *34* (21), 2311-2327.
(137) van Esch, J. H.; Feringa, B. L. New Functional Materials Based on Self-Assembling Organogels: From Serendipity towards Design. *Angewandte Chemie International Edition* **2000**, *39* (13), 2263-2266.
(138) Tam, A. Y.-Y.; Yam, V. W.-W. Recent advances in metallogels. *Chem. Soc. Rev.* **2013**, *42* (4), 1540-1567.
(139) Jung, J. H.; Lee, J. H.; Silverman, J. R.; John, G. Coordination polymer gels with important environmental and biological applications. *Chem. Soc. Rev.* **2013**, *42* (3), 924-936.
(140) Dastidar, P.; Ganguly, S.; Sarkar, K. Metallogels from coordination complexes, organometallic, and coordination polymers. *Chemistry–An Asian Journal* **2016**, *11* (18), 2484-2498.
(141) Kim, H.-J.; Lee, J.-H.; Lee, M. Stimuli-Responsive Gels from Reversible Coordination Polymers. *Angewandte Chemie International Edition* **2005**, *44* (36), 5810-5814.
(142) Saha, E.; Karthick, K.; Kundu, S.; Mitra, J. Electrocatalytic Oxygen Evolution in Acidic and Alkaline Media by a Multistimuli-Responsive Cobalt(II) Organogel. *ACS Sustainable Chemistry & Engineering* **2019**, *7* (19), 16094-16102.
(143) Lee, H. H.; Jung, S. H.; Park, S.; Park, K.-M.; Jung, J. H. A metal–organic framework gel with Cd 2+ derived from only coordination bonds without intermolecular interactions and its catalytic ability. *New J. Chem.* **2013**, *37* (8), 2330-2335.
(144) Nicolai, R. P.; Dekker, R. Optimal Maintenance of Multi-component Systems: A Review. In *Complex System Maintenance Handbook*, Kobbacy, K. A. H., Murthy, D. N. P. Eds.; Springer London, 2008; pp 263-286.
(145) Berry, D. J.; Steed, J. W. Pharmaceutical cocrystals, salts and multicomponent systems; intermolecular interactions and property based design. *Adv. Drug Deliv. Rev.* **2017**, *117*, 3-24.
(146) Li, L.; Zheng, R.; Sun, R. Understanding multicomponent low molecular weight gels from gelators to networks. *Journal of Advanced Research* **2024**.
(147) Okesola, B. O.; Wu, Y.; Derkus, B.; Gani, S.; Wu, D.; Knani, D.; Smith, D. K.; Adams, D. J.; Mata, A. Supramolecular self-assembly to control structural and biological properties of multicomponent hydrogels. *Chem. Mater.* **2019**, *31* (19), 7883-7897.
(148) Hanabusa, K.; Miki, T.; Taguchi, Y.; Koyama, T.; Shirai, H. Two-component, small molecule gelling agents. *Journal of the Chemical Society, Chemical Communications* **1993**, (18), 1382-1384.
(149) Hirst, A. R.; Smith, D. K.; Feiters, M. C.; Geurts, H. P. M.; Wright, A. C. Two-Component Dendritic Gels: Easily Tunable Materials. *J. Am. Chem. Soc.* **2003**, *125* (30), 9010-9011.
(150) Basit, H.; Pal, A.; Sen, S.; Bhattacharya, S. Two-component hydrogels comprising fatty acids and amines: structure, properties, and application as a template for the synthesis of metal nanoparticles. *Chem. Eur. J.* **2008**, *14* (21), 6534-6545.
(151) Moffat, J. R.; Smith, D. K. Controlled self-sorting in the assembly of 'multi-gelator'gels. *Chem. Commun.* **2009**, (3), 316-318.
(152) Fuhrhop, J. H.; Svenson, S.; Boettcher, C.; Rössler, E.; Vieth, H. M. Long-lived micellar N-alkylaldonamide fiber gels. Solid-state NMR and electron microscopic studies. *J. Am. Chem. Soc.* **1990**, *112* (11), 4307-4312.

(153) Thiruvengadathan, R.; Korampally, V.; Ghosh, A.; Chanda, N.; Gangopadhyay, K.; Gangopadhyay, S. Nanomaterial processing using self-assembly-bottom-up chemical and biological approaches. *Rep. Prog. Phys.* **2013**, *76* (6), 066501.
(154) Raeburn, J.; Adams, D. J. Multicomponent low molecular weight gelators. *Chem. Commun.* **2015**, *51* (25), 5170-5180, 10.1039/C4CC08626K.
(155) Draper, E. R.; Adams, D. J. How should multicomponent supramolecular gels be characterised? *Chem. Soc. Rev.* **2018**, *47* (10), 3395-3405, 10.1039/C7CS00804J.
(156) Swanekamp, R. J.; Welch, J. J.; Nilsson, B. L. Proteolytic stability of amphipathic peptide hydrogels composed of self-assembled pleated β-sheet or coassembled rippled β-sheet fibrils. *Chem. Commun.* **2014**, *50* (70), 10133-10136.
(157) Onogi, S.; Shigemitsu, H.; Yoshii, T.; Tanida, T.; Ikeda, M.; Kubota, R.; Hamachi, I. In situ real-time imaging of self-sorted supramolecular nanofibres. *Nature chemistry* **2016**, *8* (8), 743-752.
(158) Ardoña, H. A. M.; Draper, E. R.; Citossi, F.; Wallace, M.; Serpell, L. C.; Adams, D. J.; Tovar, J. D. Kinetically Controlled Coassembly of Multichromophoric Peptide Hydrogelators and the Impacts on Energy Transport. *J. Am. Chem. Soc.* **2017**, *139* (25), 8685-8692.
(159) Tangsombun, C.; Smith, D. K. Self-Sorting in Multicomponent Supramolecular Gels Using Different Assembly Triggers and Calcium Ion-Induced Diffusion Patterning. *Chem. Mater.* **2024**, *36* (10), 5050-5062.
(160) Foster, J. A.; Piepenbrock, M.-O. M.; Lloyd, G. O.; Clarke, N.; Howard, J. A.; Steed, J. W. Anion-switchable supramolecular gels for controlling pharmaceutical crystal growth. *Nature chemistry* **2010**, *2* (12), 1037-1043.
(161) Panja, S.; Dietrich, B.; Smith, A. J.; Seddon, A.; Adams, D. J. Controlling Self-Sorting versus Co-assembly in Supramolecular Gels. *ChemSystemsChem* **2022**, *4* (4), e202200008.
(162) Ravarino, P.; Panja, S.; Bianco, S.; Koev, T.; Wallace, M.; Adams, D. J. Controlled Annealing in Adaptive Multicomponent Gels. *Angewandte Chemie International Edition* **2023**, *62* (4), e202215813.
(163) Barman, S.; Pal, A.; Mukherjee, A.; Paul, S.; Datta, A.; Ghosh, S. Supramolecular Organic Ferroelectric Materials from Donor–Acceptor Systems. *Chemistry – A European Journal* **2024**, *30* (8), e202303120.
(164) Pandeeswar, M.; Senanayak, S. P.; Narayan, K.; Govindaraju, T. Multi-stimuli-responsive charge-transfer hydrogel for room-temperature organic ferroelectric thin-film devices. *J. Am. Chem. Soc.* **2016**, *138* (26), 8259-8268.
(165) Mathur, C.; Gupta, R.; Bansal, R. K. Organic Donor-Acceptor Complexes As Potential Semiconducting Materials. *Chemistry – A European Journal* **2024**, *30* (23), e202304139.
(166) Vignon, S. A.; Jarrosson, T.; Iijima, T.; Tseng, H.-R.; Sanders, J. K. M.; Stoddart, J. F. Switchable Neutral Bistable Rotaxanes. *J. Am. Chem. Soc.* **2004**, *126* (32), 9884-9885.
(167) Maitra, U.; Vijay Kumar, P.; Chandra, N.; J. D'Souza, L.; D. Prasanna, M.; R. Raju, A. First donor–acceptor interaction promoted gelation of organic fluids. *Chem. Commun.* **1999**, (7), 595-596, 10.1039/A809821B.
(168) Cougnon, F. B. L.; Au-Yeung, H. Y.; Pantoş, G. D.; Sanders, J. K. M. Exploring the Formation Pathways of Donor−Acceptor Catenanes in Aqueous Dynamic Combinatorial Libraries. *J. Am. Chem. Soc.* **2011**, *133* (9), 3198-3207.
(169) Das, A.; Ghosh, S. Supramolecular assemblies by charge-transfer interactions between donor and acceptor chromophores. *Angewandte Chemie International Edition* **2014**, *53* (8), 2038-2054.
(170) Das, A.; Ghosh, S. A generalized supramolecular strategy for self-sorted assembly between donor and acceptor gelators. *Chem. Commun.* **2011**, *47* (31), 8922-8924.

(171) Wang, K.; Guo, Z.; Zhang, L.; Sun, K.; Yu, P.; Zhou, S.; Wang, W.; Li, Z. Co-assembly of donor and acceptor towards organogels tuned by charge transfer interaction strength. *Soft Matter* **2017**, *13* (10), 1948-1955, 10.1039/C6SM02691E.
(172) Molla, M. R.; Das, A.; Ghosh, S. Self-Sorted Assembly in a Mixture of Donor and Acceptor Chromophores. *Chemistry – A European Journal* **2010**, *16* (33), 10084-10093.
(173) Patterson, A. K.; El-Qarra, L. H.; Smith, D. K. Chirality-directed hydrogel assembly and interactions with enantiomers of an active pharmaceutical ingredient. *Chem. Commun.* **2022**, *58* (24), 3941-3944, 10.1039/D1CC06942J.
(174) Das, R. K.; Kandanelli, R.; Linnanto, J.; Bose, K.; Maitra, U. Supramolecular Chirality in Organogels: A Detailed Spectroscopic, Morphological, and Rheological Investigation of Gels (and Xerogels) Derived from Alkyl Pyrenyl Urethanes. *Langmuir* **2010**, *26* (20), 16141-16149.
(175) Ghosh, D.; Farahani, A. D.; Martin, A. D.; Thordarson, P.; Damodaran, K. K. Unraveling the Self-Assembly Modes in Multicomponent Supramolecular Gels Using Single-Crystal X-ray Diffraction. *Chemistry of Materials* **2020**, *32* (8), 3517-3527.
(176) Nagy, K. J.; Giano, M. C.; Jin, A.; Pochan, D. J.; Schneider, J. P. Enhanced Mechanical Rigidity of Hydrogels Formed from Enantiomeric Peptide Assemblies. *J. Am. Chem. Soc.* **2011**, *133* (38), 14975-14977.
(177) Nagy-Smith, K.; Beltramo, P. J.; Moore, E.; Tycko, R.; Furst, E. M.; Schneider, J. P. Molecular, Local, and Network-Level Basis for the Enhanced Stiffness of Hydrogel Networks Formed from Coassembled Racemic Peptides: Predictions from Pauling and Corey. *ACS Cent Sci* **2017**, *3* (6), 586-597, From Nlm.
(178) Swanekamp, R. J.; DiMaio, J. T.; Bowerman, C. J.; Nilsson, B. L. Coassembly of enantiomeric amphipathic peptides into amyloid-inspired rippled β-sheet fibrils. *J. Am. Chem. Soc.* **2012**, *134* (12), 5556-5559.
(179) Yang, X.; Lu, H.; Tao, Y.; Zhang, H.; Wang, H. Controlling supramolecular filament chirality of hydrogel by co-assembly of enantiomeric aromatic peptides. *Journal of Nanobiotechnology* **2022**, *20* (1), 77.
(180) Koga, T.; Matsuoka, M.; Higashi, N. Structural control of self-assembled nanofibers by artificial β-sheet peptides composed of D-or L-isomer. *J. Am. Chem. Soc.* **2005**, *127* (50), 17596-17597.
(181) Hirst, A. R.; Smith, D. K.; Feiters, M. C.; Geurts, H. P. Two-Component Dendritic Gel: Effect of Stereochemistry on the Supramolecular Chiral Assembly. *Chem. Eur. J.* **2004**, *10* (23), 5901-5910.
(182) Zhu, X.; Li, Y.; Duan, P.; Liu, M. Self-assembled ultralong chiral nanotubes and tuning of their chirality through the mixing of enantiomeric components. *Chem. Eur. J.* **2010**, *16* (27), 8034-8040.
(183) Liu, Z.; Sun, J.; Zhou, Y.; Zhang, Y.; Wu, Y.; Nalluri, S. K. M.; Wang, Y.; Samanta, A.; Mirkin, C. A.; Schatz, G. C. Supramolecular Gelation of Rigid Triangular Macrocycles through Rings of Multiple C–H··· O Interactions Acting Cooperatively. *The Journal of organic chemistry* **2016**, *81* (6), 2581-2588.
(184) Li, H.; Han, L.; Li, Q.; Lai, H.; Fernández-Trillo, P.; Tian, L.; He, F. Hierarchical Chiral Supramolecular Nanoarchitectonics with Molecular Detection: Helical Structure Controls upon Self-Assembly and Coassembly. *Macromolecular Rapid Communications* **2022**, *43* (14), 2100690.
(185) McAulay, K.; Dietrich, B.; Su, H.; Scott, M. T.; Rogers, S.; Al-Hilaly, Y. K.; Cui, H.; Serpell, L. C.; Seddon, A. M.; Draper, E. R. Using chirality to influence supramolecular gelation. *Chem. Sci.* **2019**, *10* (33), 7801-7806.

(186) Messmore, B. W.; Sukerkar, P. A.; Stupp, S. I. Mirror image nanostructures. *J. Am. Chem. Soc.* **2005**, *127* (22), 7992-7993.
(187) Adhikari, B.; Nanda, J.; Banerjee, A. Multicomponent hydrogels from enantiomeric amino acid derivatives: helical nanofibers, handedness and self-sorting. *Soft Matter* **2011**, *7* (19), 8913-8922, 10.1039/C1SM05907F.
(188) Cicchi, S.; Ghini, G.; Lascialfari, L.; Brandi, A.; Betti, F.; Berti, D.; Baglioni, P.; Di Bari, L.; Pescitelli, G.; Mannini, M. Self-sorting chiral organogels from a long chain carbamate of 1-benzyl-pyrrolidine-3, 4-diol. *Soft Matter* **2010**, *6* (8), 1655-1661.
(189) Lascialfari, L.; Pescitelli, G.; Brandi, A.; Mannini, M.; Berti, D.; Cicchi, S. Urea vs. carbamate groups: a comparative study in a chiral C2 symmetric organogelator. *Soft Matter* **2015**, *11* (42), 8333-8341, 10.1039/C5SM01684C.
(190) Yang, Z.; Liang, G.; Ma, M.; Gao, Y.; Xu, B. Conjugates of naphthalene and dipeptides produce molecular hydrogelators with high efficiency of hydrogelation and superhelical nanofibers. *Journal of Materials Chemistry* **2007**, *17* (9), 850-854, 10.1039/B611255B.
(191) Shen, J.-S.; Mao, G.-J.; Zhou, Y.-H.; Jiang, Y.-B.; Zhang, H.-W. A ligand-chirality controlled supramolecular hydrogel. *Dalton Transactions* **2010**, *39* (30), 7054-7058, 10.1039/C0DT00364F.
(192) Foster, J. A.; Edkins, R. M.; Cameron, G. J.; Colgin, N.; Fucke, K.; Ridgeway, S.; Crawford, A. G.; Marder, T. B.; Beeby, A.; Cobb, S. L.; Steed, J. W. Blending Gelators to Tune Gel Structure and Probe Anion-Induced Disassembly. *Chemistry – A European Journal* **2014**, *20* (1), 279-291.
(193) Swanekamp, R. J.; DiMaio, J. T. M.; Bowerman, C. J.; Nilsson, B. L. Coassembly of Enantiomeric Amphipathic Peptides into Amyloid-Inspired Rippled β-Sheet Fibrils. *J. Am. Chem. Soc.* **2012**, *134* (12), 5556-5559.
(194) Zhu, X.; Li, Y.; Duan, P.; Liu, M. Self-Assembled Ultralong Chiral Nanotubes and Tuning of Their Chirality Through the Mixing of Enantiomeric Components. *Chemistry – A European Journal* **2010**, *16* (27), 8034-8040.
(195) Liu, Z.; Sun, J.; Zhou, Y.; Zhang, Y.; Wu, Y.; Nalluri, S. K. M.; Wang, Y.; Samanta, A.; Mirkin, C. A.; Schatz, G. C.; Stoddart, J. F. Supramolecular Gelation of Rigid Triangular Macrocycles through Rings of Multiple C–H···O Interactions Acting Cooperatively. *The Journal of Organic Chemistry* **2016**, *81* (6), 2581-2588.
(196) Gudmundsson, T. A.; Kuppadakkath, G.; Ghosh, D.; Ruether, M.; Seddon, A.; Ginesi, R. E.; Doutch, J.; Adams, D. J.; Gunnlaugsson, T.; Damodaran, K. K. Nanoscale assembly of enantiomeric supramolecular gels driven by the nature of solvents. *Nanoscale* **2024**, 10.1039/D4NR00204K.
(197) Cicchi, S.; Ghini, G.; Lascialfari, L.; Brandi, A.; Betti, F.; Berti, D.; Baglioni, P.; Di Bari, L.; Pescitelli, G.; Mannini, M.; Caneschi, A. Self-sorting chiral organogels from a long chain carbamate of 1-benzyl-pyrrolidine-3,4-diol. *Soft Matter* **2010**, *6* (8), 1655-1661, 10.1039/B918709J.
(198) Hirst, A. R.; Huang, B.; Castelletto, V.; Hamley, I. W.; Smith, D. K. Self-Organisation in the Assembly of Gels from Mixtures of Different Dendritic Peptide Building Blocks. *Chemistry – A European Journal* **2007**, *13* (8), 2180-2188.
(199) Denzer, B. R.; Kulchar, R. J.; Huang, R. B.; Patterson, J. Advanced methods for the characterization of supramolecular hydrogels. *Gels* **2021**, *7* (4), 158.
(200) Iqbal, S.; Rodríguez-LLansola, F.; Escuder, B.; Miravet, J. F.; Verbruggen, I.; Willem, R. HRMAS 1H NMR as a tool for the study of supramolecular gels. *Soft Matter* **2010**, *6* (9), 1875-1878.

(201) Brown, S. P. Advanced solid-state NMR methods for characterising structure and self-assembly in supramolecular chemistry, polymers and hydrogels. *Current Opinion in Colloid & Interface Science* **2018**, *33*, 86-98.
(202) Ramalhete, S. M.; Nartowski, K. P.; Sarathchandra, N.; Foster, J. S.; Round, A. N.; Angulo, J.; Lloyd, G. O.; Khimyak, Y. Z. Supramolecular amino acid based hydrogels: probing the contribution of additive molecules using NMR spectroscopy. *Chem. Eur. J.* **2017**, *23* (33), 8014-8024.
(203) Rutgeerts, L. A. J.; Soultan, A. H.; Subramani, R.; Toprakhisar, B.; Ramon, H.; Paderes, M. C.; De Borggraeve, W. M.; Patterson, J. Robust scalable synthesis of a bis-urea derivative forming thixotropic and cytocompatible supramolecular hydrogels. *Chem. Commun.* **2019**, *55* (51), 7323-7326, 10.1039/C9CC02927C.
(204) Shapiro, Y. E. Structure and dynamics of hydrogels and organogels: An NMR spectroscopy approach. *Progress in Polymer Science* **2011**, *36* (9), 1184-1253.
(205) Strassert, C. A.; Chien, C.-H.; Lopez, M. D. G.; Kourkoulos, D.; Hertel, D.; Meerholz, K.; De Cola, L. Switching on luminescence by the self-assembly of a platinum (II) complex into gelating nanofibers and electroluminescent films. *Angewandte Chemie-International Edition* **2011**, *50* (4), 946-950.
(206) Taira, T.; Suzaki, Y.; Osakada, K. Hydrogels composed of organic amphiphiles and α-cyclodextrin: Supramolecular networks of their pseudorotaxanes in aqueous media. *Chem. Eur. J.* **2010**, *16* (22), 6518-6529.
(207) Ogawa, Y.; Yoshiyama, C.; Kitaoka, T. Helical assembly of azobenzene-conjugated carbohydrate hydrogelators with specific affinity for lectins. *Langmuir* **2012**, *28* (9), 4404-4412.
(208) Sugimoto, T.; Suzuki, T.; Shinkai, S.; Sada, K. A double-stranded helix by complexation of two polymer chains with a helical supramolecular assembly. *J. Am. Chem. Soc.* **2007**, *129* (2), 270-271.
(209) Bhattacharya, S.; Samanta, S. K. Unusual Salt-Induced Color Modulation through Aggregation-Induced Emission Switching of a Bis-cationic Phenylenedivinylene-Based π Hydrogelator. *Chem. Eur. J.* **2012**, *18* (52), 16632-16641.
(210) Kotova, O.; Daly, R.; dos Santos, C. M.; Boese, M.; Kruger, P. E.; Boland, J. J.; Gunnlaugsson, T. Europium-directed self-assembly of a luminescent supramolecular gel from a tripodal terpyridine-based ligand. *Angewandte Chemie International Edition* **2012**, *51* (29), 7208-7212.
(211) Song, Q.; Zhang, R.; Lei, L.; Li, X. Self-assembly of succinated paclitaxel into supramolecular hydrogel for local cancer chemotherapy. *Journal of Biomedical Nanotechnology* **2018**, *14* (8), 1471-1476.
(212) Wu, W.; Zhang, Z.; Xiong, T.; Zhao, W.; Jiang, R.; Chen, H.; Li, X. Calcium ion coordinated dexamethasone supramolecular hydrogel as therapeutic alternative for control of non-infectious uveitis. *Acta Biomater.* **2017**, *61*, 157-168.
(213) Chen, S.; Slattum, P.; Wang, C.; Zang, L. Self-assembly of perylene imide molecules into 1D nanostructures: methods, morphologies, and applications. *Chem. Rev.* **2015**, *115* (21), 11967-11998.
(214) Jeffries, C. M.; Ilavsky, J.; Martel, A.; Hinrichs, S.; Meyer, A.; Pedersen, J. S.; Sokolova, A. V.; Svergun, D. I. Small-angle X-ray and neutron scattering. *Nature Reviews Methods Primers* **2021**, *1* (1), 70.
(215) Gudmundsson, T. A.; Kuppadakkath, G.; Ghosh, D.; Ruether, M.; Seddon, A.; Ginesi, R. E.; Doutch, J.; Adams, D. J.; Gunnlaugsson, T.; Damodaran, K. K. Nanoscale assembly of enantiomeric supramolecular gels driven by the nature of solvents. *Nanoscale* **2024**, *16* (18), 8922-8930.

(216) Kannan, M. Transmission electron microscope—Principle, components and applications. *A textbook on fundamentals and applications of nanotechnology* **2018**, 93-102.
(217) Egerton, R. F. *Physical principles of electron microscopy*; Springer, 2005.
(218) Johnson, D.; Hilal, N.; Bowen, W. R. Basic principles of atomic force microscopy. In *Atomic force microscopy in process engineering*, Elsevier Ltd, 2009; pp 1-30.
(219) Sun, W. Principles of atomic force microscopy. *Atomic Force Microscopy in Molecular and Cell Biology* **2018**, 1-28.
(220) Gottarelli, G.; Lena, S.; Masiero, S.; Pieraccini, S.; Spada, G. P. The use of circular dichroism spectroscopy for studying the chiral molecular self-assembly: an overview. *Chirality* **2008**, *20* (3-4), 471-485, From NLM.
(221) Sakurai, S. SAXS evaluation of size distribution for nanoparticles. *Chapter* **2017**, *5*, 107-134.
(222) Giuri, D.; Marshall, L. J.; Wilson, C.; Seddon, A.; Adams, D. J. Understanding gel-to-crystal transitions in supramolecular gels. *Soft Matter* **2021**, *17* (30), 7221-7226.
(223) Dawn, A.; Mirzamani, M.; Jones, C. D.; Yufit, D. S.; Qian, S.; Steed, J. W.; Kumari, H. Investigating the effect of supramolecular gel phase crystallization on gel nucleation. *Soft Matter* **2018**, *14* (46), 9489-9497.
(224) Melnichenko, Y. B.; Wignall, G. D. Small-angle neutron scattering in materials science: Recent practical applications. *Journal of applied physics* **2007**, *102* (2).
(225) Goodwin, J. W.; Hughes, R. W. *Rheology for chemists: an introduction*; Royal Society of Chemistry, 2008.
(226) Guenet, J.-M. *Organogels: Thermodynamics, structure, solvent role, and properties*; Springer, 2016.
(227) Bianco, S.; Panja, S.; Adams, D. J. Using rheology to understand transient and dynamic gels. *Gels* **2022**, *8* (2), 132.
(228) Abraham, S.; Lan, Y.; Lam, R. S. H.; Grahame, D. A. S.; Kim, J. J. H.; Weiss, R. G.; Rogers, M. A. Influence of Positional Isomers on the Macroscale and Nanoscale Architectures of Aggregates of Racemic Hydroxyoctadecanoic Acids in Their Molecular Gel, Dispersion, and Solid States. *Langmuir* **2012**, *28* (11), 4955-4964.
(229) Xu, Y.; Kang, C.; Chen, Y.; Bian, Z.; Qiu, X.; Gao, L.; Meng, Q. In Situ Gel-to-Crystal Transition and Synthesis of Metal Nanoparticles Obtained by Fluorination of a Cyclic β-Aminoalcohol Gelator. *Chemistry – A European Journal* **2012**, *18* (52), 16955-16961.
(230) Dastidar, P.; Roy, R.; Parveen, R.; Sarkar, K. Supramolecular Synthon Approach in Designing Molecular Gels for Advanced Therapeutics. *Advanced Therapeutics* **2019**, *2* (1), 1800061.
(231) Engstrom, J. R.; Savyasachi, A. J.; Parhizkar, M.; Sutti, A.; Hawes, C. S.; White, J. M.; Gunnlaugsson, T.; Pfeffer, F. M. Norbornene chaotropic salts as low molecular mass ionic organogelators (LMIOGs). *Chem. Sci.* **2018**, *9* (23), 5233-5241, 10.1039/C8SC01798K.
(232) Colquhoun, C.; Draper, E. R.; Eden, E. G. B.; Cattoz, B. N.; Morris, K. L.; Chen, L.; McDonald, T. O.; Terry, A. E.; Griffiths, P. C.; Serpell, L. C.; Adams, D. J. The effect of self-sorting and co-assembly on the mechanical properties of low molecular weight hydrogels. *Nanoscale* **2014**, *6* (22), 13719-13725, 10.1039/C4NR04039B.
(233) Houton, K. A.; Morris, K. L.; Chen, L.; Schmidtmann, M.; Jones, J. T. A.; Serpell, L. C.; Lloyd, G. O.; Adams, D. J. On Crystal versus Fiber Formation in Dipeptide Hydrogelator Systems. *Langmuir* **2012**, *28* (25), 9797-9806.
(234) Mears, L. L. E.; Draper, E. R.; Castilla, A. M.; Su, H.; Zhuola; Dietrich, B.; Nolan, M. C.; Smith, G. N.; Doutch, J.; Rogers, S.; et al. Drying Affects the Fiber Network in Low Molecular Weight Hydrogels. *Biomacromolecules* **2017**, *18* (11), 3531-3540.

(235) Adams, D. J. Does Drying Affect Gel Networks? *Gels* **2018**, *4* (2), 32.
(236) Banerjee, S.; Das, R. K.; Maitra, U. Supramolecular gels 'in action'. *J. Mater. Chem.* **2009**, *19* (37), 6649-6687, 10.1039/B819218A.
(237) Dou, X.-Q.; Li, P.; Zhang, D.; Feng, C.-L. RGD anchored C2-benzene based PEG-like hydrogels as scaffolds for two and three dimensional cell cultures. *J. Mater. Chem. B* **2013**, *1* (29), 3562-3568, 10.1039/C3TB20155D.
(238) Vieira, V. M. P.; Lima, A. C.; de Jong, M.; Smith, D. K. Commercially Relevant Orthogonal Multi-Component Supramolecular Hydrogels for Programmed Cell Growth. *Chem. Eur. J.* **2018**, *24* (56), 15112-15118.
(239) Li, P.; Dou, X.-Q.; Feng, C.-L.; Zhang, D. Mechanical reinforcement of C2-phenyl-derived hydrogels for controlled cell adhesion. *Soft Matter* **2013**, *9* (14), 3750-3757, 10.1039/C3SM27727E.
(240) Forero-Doria, O.; Polo, E.; Marican, A.; Guzmán, L.; Venegas, B.; Vijayakumar, S.; Wehinger, S.; Guerrero, M.; Gallego, J.; Durán-Lara, E. F. Supramolecular hydrogels based on cellulose for sustained release of therapeutic substances with antimicrobial and wound healing properties. *Carbohydrate polymers* **2020**, *242*, 116383.
(241) Sidiq, S.; Ahanger, G.; Nazir, N.; Zargar, M. I.; Dar, A. A. Modulation of mechanical properties of low molecular weight supramolecular hydrogels of calcium cholate by drugs of varying hydrophobicity: Effect on drug release, antioxidant, and antibacterial properties. *Journal of Molecular Liquids* **2024**, *409*, 125341.
(242) Ding, T.; Qi, J.; Zou, J.; Dan, H.; Zhao, H.; Chen, Q. A multifunctional supramolecular hydrogel for infected wound healing. *Biomater. Sci.* **2022**, *10* (2), 381-395.
(243) Suja, S.; Mathiya, S. Supramolecular Gel-Based Materials for Sensing Environmentally Sensitive Molecules. In *Foundation and Growth of Macromolecular Science*, Apple Academic Press, 2024; pp 237-268.
(244) Kuppadakkath, G.; Jayabhavan, S. S.; Damodaran, K. K. Supramolecular Gels Based on C3-Symmetric Amides: Application in Anion-Sensing and Removal of Dyes from Water. *Molecules* **2024**, *29* (9), 2149.
(245) Lochhead, R. The use of polymers in cosmetic products. *Cosmetic science and technology: Theoretical principles and applications* **2017**, *13*, 171-221.
(246) Smith, D. K. Applications of Supramolecular Gels. **2018**.
(247) Pakseresht, S.; Mazaheri Tehrani, M. Advances in multi-component supramolecular oleogels-a review. *Food Reviews International* **2022**, *38* (4), 760-782.
(248) Díaz Díaz, D.; Kühbeck, D.; Koopmans, R. J. Stimuli-responsive gels as reaction vessels and reusable catalysts. *Chem. Soc. Rev.* **2011**, *40* (1), 427-448, 10.1039/C005401C.
(249) Schiaffino, L.; Ercolani, G. Unraveling the Mechanism of the Soai Asymmetric Autocatalytic Reaction by First-Principles Calculations: Induction and Amplification of Chirality by Self-Assembly of Hexamolecular Complexes. *Angew. Chem. Int. Ed.* **2008**, *47* (36), 6832-6835.
(250) Duan, P.; Cao, H.; Zhang, L.; Liu, M. Gelation induced supramolecular chirality: chirality transfer, amplification and application. *Soft Matter* **2014**, *10* (30), 5428-5448.
(251) Sharma, H.; Kalita, B. K.; Pathak, D.; Sarma, B. Low Molecular Weight Supramolecular Gels as a Crystallization Matrix. *Crystal Growth & Design* **2024**, *24* (1), 17-37.
(252) Hu, B.; Owh, C.; Chee, P. L.; Leow, W. R.; Liu, X.; Wu, Y.-L.; Guo, P.; Loh, X. J.; Chen, X. Supramolecular hydrogels for antimicrobial therapy. *Chem. Soc. Rev.* **2018**, *47* (18), 6917-6929, 10.1039/C8CS00128F.
(253) Riaz, Z.; Baddi, S.; Feng, C.-L. Supramolecular co-assembled hybrid hydrogels for antibacterial therapy. *Supramol. Mater.* **2024**, 100064.

(254) Rizzo, C.; Arrigo, R.; Dintcheva, N. T.; Gallo, G.; Giannici, F.; Noto, R.; Sutera, A.; Vitale, P.; D'Anna, F. Supramolecular Hydro-and Ionogels: A Study of Their Properties and Antibacterial Activity. *Chem. Eur. J.* **2017**, *23* (64), 16297-16311.
(255) Nandi, N.; Gayen, K.; Ghosh, S.; Bhunia, D.; Kirkham, S.; Sen, S. K.; Ghosh, S.; Hamley, I. W.; Banerjee, A. Amphiphilic peptide-based supramolecular, noncytotoxic, stimuli-responsive hydrogels with antibacterial activity. *Biomacromolecules* **2017**, *18* (11), 3621-3629.
(256) Baddi, S.; Dang-i, A. Y.; Huang, T.; Xing, C.; Lin, S.; Feng, C.-L. Chirality-influenced antibacterial activity of methylthiazole-and thiadiazole-based supramolecular biocompatible hydrogels. *Acta Biomater.* **2022**, *141*, 59-69.
(257) Yang, L.; Zhang, C.; Huang, F.; Liu, J.; Zhang, Y.; Yang, C.; Ren, C.; Chu, L.; Liu, B.; Liu, J. Triclosan-based supramolecular hydrogels as nanoantibiotics for enhanced antibacterial activity. *J. Control. Release* **2020**, *324*, 354-365.
(258) Xie, Y.-Y.; Zhang, Y.-W.; Qin, X.-T.; Liu, L.-P.; Wahid, F.; Zhong, C.; Jia, S.-R. Structure-dependent antibacterial activity of amino acid-based supramolecular hydrogels. *Colloids Surf. B* **2020**, *193*, 111099.
(259) Chakraborty, P.; Datta, H. K.; Biswas, P.; Dastidar, P. Supramolecular Synthon Approach in Designing Organic Sulfonates as Supramolecular Gelators: An Easily Accessible Topical Gel with Antibacterial Properties. *Chem. Mater.* **2021**, *33* (7), 2274-2288.
(260) Zheng, F.; Du, W.; Yang, M.; Liu, K.; Zhang, S.; Xu, L.; Wen, Y. Constructing ROS-responsive supramolecular gel with innate antibacterial properties. *Pharmaceutics* **2023**, *15* (8), 2161.
(261) Ghosh, D.; Coulter, S. M.; Laverty, G.; Holland, C.; Doutch, J. J.; Vassalli, M.; Adams, D. J. Metal cross-linked supramolecular gel noodles: structural insights and antibacterial assessment. *Biomacromolecules* **2024**, *25* (5), 3169-3177.
(262) Giuri, D.; Cenciarelli, F.; Tomasini, C. Low-molecular-weight gels from amino acid and peptide derivatives for controlled release and delivery. *J. Pept. Sci.* **2024**, *30* (12), e3643.
(263) Abbas, M.; Ovais, M.; Atiq, A.; Ansari, T. M.; Xing, R.; Spruijt, E.; Yan, X. Tailoring supramolecular short peptide nanomaterials for antibacterial applications. *Coord. Chem. Rev.* **2022**, *460*, 214481.
(264) Simonson, A. W.; Aronson, M. R.; Medina, S. H. Supramolecular peptide assemblies as antimicrobial scaffolds. *Molecules* **2020**, *25* (12), 2751.
(265) Xie, Y.-Y.; Wang, X.-Q.; Sun, M.-Y.; Qin, X.-T.; Su, X.-F.; Ma, X.-F.; Liu, X.-Z.; Zhong, C.; Jia, S.-R. Heterochiral peptide-based biocompatible and injectable supramolecular hydrogel with antibacterial activity. *J. Mater. Sci.* **2022**, *57* (8), 5198-5209.
(266) Zhang, R.; Xu, L.; Dong, C. Antimicrobial peptides: An overview of their structure, function and mechanism of action. *Protein Pept. Lett.* **2022**, *29* (8), 641-650.
(267) Bonafé Allende, J. C.; Ambrosioni, F.; Ruiz Moreno, F. N.; Marin, C.; Romero, V. L.; Virgolini, M. B.; Maletto, B. A.; Jimenez Kairuz, A. F.; Alvarez Igarzabal, C. I.; Picchio, M. L. Pyrogallol-rich supramolecular hydrogels with enzyme-sensitive microdomains for controlled topical delivery of hydrophobic drugs. *Biomater. Adv.* **2025**, *166*, 214075.
(268) Xing, B.; Yu, C.-W.; Chow, K.-H.; Ho, P.-L.; Fu, D.; Xu, B. Hydrophobic Interaction and Hydrogen Bonding Cooperatively Confer a Vancomycin Hydrogel: A Potential Candidate for Biomaterials. *J. Am. Chem. Soc.* **2002**, *124* (50), 14846-14847.
(269) Marinescu, M.; Cinteza, L. O.; Marton, G. I.; Marutescu, L. G.; Chifiriuc, M.-C.; Constantinescu, C. Density functional theory molecular modeling and antimicrobial behaviour of selected 1, 2, 3, 4, 5, 6, 7, 8-octahydroacridine-N (10)-oxides. *Journal of Molecular Structure* **2017**, *1144*, 14-23.

(270) Lan, Y.; Corradini, M. G.; Weiss, R. G.; Raghavan, S. R.; Rogers, M. A. To gel or not to gel: correlating molecular gelation with solvent parameters. *Chem. Soc. Rev.* **2015**, *44* (17), 6035-6058, 10.1039/C5CS00136F.
(271) Adams, D. J.; Morris, K.; Chen, L.; Serpell, L. C.; Bacsa, J.; Day, G. M. The delicate balance between gelation and crystallisation: structural and computational investigations. *Soft Matter* **2010**, *6* (17), 4144-4156, 10.1039/C0SM00409J.
(272) Lan, Y.; Corradini, M. G.; Liu, X.; May, T. E.; Borondics, F.; Weiss, R. G.; Rogers, M. A. Comparing and Correlating Solubility Parameters Governing the Self-Assembly of Molecular Gels Using 1,3:2,4-Dibenzylidene Sorbitol as the Gelator. *Langmuir* **2014**, *30* (47), 14128-14142.
(273) Wang, Y.; Tang, L.; Yu, J. Investigation of Spontaneous Transition from Low-Molecular-Weight Hydrogel into Macroscopic Crystals. *Cryst. Growth Des.* **2008**, *8* (3), 884-889.
(274) Foster, J. A.; Damodaran, K. K.; Maurin, A.; Day, G. M.; Thompson, H. P. G.; Cameron, G. J.; Bernal, J. C.; Steed, J. W. Pharmaceutical polymorph control in a drug-mimetic supramolecular gel. *Chem. Sci.* **2017**, *8* (1), 78-84, 10.1039/C6SC04126D.
(275) Hektisch, H. K.; Dennis, J.; Hanoka, J. I. Crystal growth in gels. *Journal of Physics and Chemistry of Solids* **1965**, *26* (3), 493-496.
(276) Edwards, W.; Smith, D. K. Enantioselective Component Selection in Multicomponent Supramolecular Gels. *J. Am. Chem. Soc.* **2014**, *136* (3), 1116-1124.
(277) Cross, E. R.; Sproules, S.; Schweins, R.; Draper, E. R.; Adams, D. J. Controlled Tuning of the Properties in Optoelectronic Self-Sorted Gels. *J. Am. Chem. Soc.* **2018**, *140* (28), 8667-8670.
(278) Draper, E. R.; Eden, E. G. B.; McDonald, T. O.; Adams, D. J. Spatially resolved multicomponent gels. *Nature Chemistry* **2015**, *7*, 848, Article.
(279) LIESEGANG, R. E. Uber einige eigenschaften von gallerten. *Naturwissensch Wochenschr* **1896**, *11*, 353-362.
(280) Duffus, C.; Camp, P. J.; Alexander, A. J. Spatial control of crystal nucleation in agarose gel. *J. Am. Chem. Soc.* **2009**, *131* (33), 11676-11677.
(281) Daly, R.; Kotova, O.; Boese, M.; Gunnlaugsson, T.; Boland, J. J. Chemical Nano-Gardens: Growth of Salt Nanowires from Supramolecular Self-Assembly Gels. *ACS Nano* **2013**, *7* (6), 4838-4845.
(282) Contreras-Montoya, R.; Álvarez de Cienfuegos, L.; Gavira, J. A.; Steed, J. W. Supramolecular gels: a versatile crystallization toolbox. *Chem. Soc. Rev.* **2024**, 10.1039/D4CS00271G.
(283) Stahly, G. P. Diversity in single-and multiple-component crystals. The search for and prevalence of polymorphs and cocrystals. *Crystal growth & design* **2007**, *7* (6), 1007-1026.
(284) King, K. N.; McNeil, A. J. Streamlined approach to a new gelator: inspiration from solid-state interactions for a mercury-induced gelation. *Chem. Commun.* **2010**, *46* (20), 3511-3513.
(285) Veits, G. K.; Carter, K. K.; Cox, S. J.; McNeil, A. J. Developing a gel-based sensor using crystal morphology prediction. *J. Am. Chem. Soc.* **2016**, *138* (37), 12228-12233.
(286) Rizzo, C.; Andrews, J. L.; Steed, J. W.; D'Anna, F. Carbohydrate-supramolecular gels: Adsorbents for chromium (VI) removal from wastewater. *Journal of colloid and interface science* **2019**, *548*, 184-196.
(287) Biswakarma, D.; Dey, N.; Bhattacharya, S. A biocompatible hydrogel as a template for oxidative decomposition reactions: a chemodosimetric analysis and in vitro imaging of hypochlorite. *Chem. Sci.* **2022**, *13* (8), 2286-2295.

(288) Kuppadakkath, G.; Volkova, I.; Damodaran, K. K. Designing Stimuli-Responsive Supramolecular Gels by Tuning the Non-Covalent Interactions of the Functional Groups. *Gels* **2024**, *10* (9), 584.